The role of the phasin PhaP in promoting polyhydroxybutyrate (PHB) granule formation in *Caulobacter crescentus*

by

Rachael Marie Buckley

B.A. Biological Chemistry, B.A. German, Grinnell College, 2006

Submitted to the Department of Chemistry in Partial Fulfillment
of the Requirements for the Degree of

Doctor of Philosophy in Biological Chemistry
at the
MASSACHUSETTS INSTITUTE OF TECHNOLOGY

September 2013

Signature of Author: _____
Department of Chemistry
August 30, 2013

Certified by: _____
JoAnne Stubbe
Novartis Professor of Chemistry and Professor of Biology
Thesis Supervisor

Accepted by: _____
Robert W. Field
Haslam and Dewey Professor of Chemistry
Chairman, Departmental Committee on Graduate Students

This doctoral thesis has been examined by a Committee of the Departments of Chemistry and Biology as follows:

Elizabeth M. Nolan
Assistant Professor of Chemistry
Pfizer-Laubach Career Development Assistant Professor
Thesis Chair

JoAnne Stubbe
Novartis Professor of Chemistry and Professor of Biology
Thesis Supervisor

Anthony J. Sinskey
Professor of Microbiology and Health Sciences and Technology

To all four of my parents

ACKNOWLEDGEMENTS

I feel honored to be one of the last graduate students to come from JoAnne's lab. While it was not always easy, it was certainly worth the journey. I would not be the scientist or person I am today if I had been in any other lab. JoAnne has a critical mind that is unparalleled and I am grateful for the scientific curiosity tempered with a healthy dose of skepticism and critical skills that she has instilled in me.

Sarah O'Connor was a very supportive thesis chair for my first three years at MIT, and I thank her for her input and advice. I greatly appreciate that Liz Nolan agreed to serve as my thesis chair for my remaining time at MIT, and for the support and guidance she has provided me in that time. Her genuine interest in my project and my development has meant a lot to me. I also had the opportunity to TA for her, and I am very inspired by her impeccable organization and engaging teaching skills. Finally, thank you to Tony Sinskey, whose ability to see science from a different angle was valuable in my development as a student and scientist. I will never forget his shirts, especially that amazing shimmery purple one.

Professor Karen Allen has been a valuable mentor for me throughout our collaboration. Her warm and easy going nature made for fruitful discussions about both scientific and personal matters, and I am very grateful for her guidance throughout my graduate school experience. I only wish our collaboration had been as fruitful as our discussions! Several of Karen's post docs and graduate students have helped me over the years, and I am indebted to Drs. Nick Silvaggi, Kelly Daughtry, Nick Denunzio and Lorenzo Finci, among others, for their help with screening crystals, advice for setting up crystal trays and generally for their commiseration about proteins that refused to crystallize and crystals that refused to diffract.

When I joined the lab two post docs were on the PHB project and their guidance shaped my graduate school experience. Sumit was a great mentor and a great friend, and I value our walks out to the Charles River when we discussed life and experiments and queen bees and everything in between. Thank you for giving me the advice that graduate school is a marathon, not a sprint. It sure was one hell of a marathon for me. You were always on my side and I will never forget that. Ping was initially more of a mystery to me than Sumit was, but now he and I have grown to be very good friends. I am excited to watch his development as a professor at Kansas State, and have found our discussions about science and life to be extremely fulfilling and entertaining! I wish Ping and Sumit all the best, and I do not intend to lose track of them!

I would not be writing this thesis without the companionship over the last six years of the members of the Stubbe lab. I'm not sure that I can express in just a few sentences what Mimi, Ellen and Joey have meant to me. In a different setting we might not all have become friends, and yet here we are. I'm getting teary-eyed just writing this! Our friendship and your support over the years mean so much to me. So many memories are popping into my head right now, but I'm pretty sure you guys have them all in your head like I do, and I don't think MIT will let me spend a dozen pages writing them all down. I treasure your friendship. Kanch, your friendship, companionship and support has meant so much to me in the last few years, and in particular in the last year. Somehow I did not go insane in the last few months of grad school, and I think I owe you a big thanks for that. Our walks to Koch to see our besties Jeff and Eva are among the

many, many happy memories I take with me! I look forward to our fun outings continuing in the future.

To current lab members Henry, Yifeng, Lisa, Mac, Kanch, Wankyu, Olga, Denyce and Leo, thank you for all your support in the last few years. I needed it! I can't wait to hear what big things you all go on to do! Mac, you deserve special thanks and recognition for being the best fixer of all things broken in lab. I have always appreciated the times I have come to you to say "Mac...do you have any experience with instrument X breaking?" and you said "No" then rolled up your sleeves and went to work figuring out what was wrong. Teaching with you was also a fun and extremely valuable experience.

To my past labmates Chia, Jun, Dani, Q, Mo, Xuling, Yimon, Drew, Crystal, Luke, Yan, Ken, Thomas, thank you for teaching me, laughing and commiserating with me, partying with me, and for everything else we did in between. I couldn't have asked for a better lab-family than you guys. Thanks to my undergrads Becca and Gernieve for teaching me as I tried to teach you.

I also need to thank several members of the Sinskey lab for their help and friendship over the years. Chris and Charles were some of my earliest confidants in the PHB subgroup and I have fond memories of those subgroup meetings we held at the Muddy Charles. Even after our formal collaboration ended you were both great informal collaborators and great sources of support. You two are easily the best cloners I have ever known! Jingnan, thank you for carrying on the informal Stubbe-Sinskey collaboration! Your warmth and good nature have meant a lot to me.

A few students of mine require special recognition, in particular Jeremy, Scott, Veena and Rishi from my first year of TAing, and Khizar and Deena from my later adventures in TAing. You all have helped me to realize and remember how much I love teaching and I thank you for that.

I would also like to thank Gang Liu, who made possible about half of my thesis by fixing the instruments that I needed for my various experiments. He is basically a magic-worker. I also appreciate how much I learned from him for teaching me about instruments and how to fix them and for making my PhD considerably easier than it would have been without mister fix-it.

I am so fortunate to have met the best possible group of friends, so thank you to Shay's for bringing us all together and thank you to the Shay's wall for giving us somewhere to sit. In no particular order, Aaron, Bob, Charley, Craig and Julie, Brent and Jenn, Hillary, Amy, Michelle, Kristen and Ryan, Manuel, Dave, David, Jen, Jenni, JK, Ros, Cate, Marie, Rob, Alex, John, Jessica, Paul, Fredie, Alp and Billie, Oz, Whitney, Ilina, Ko, Keller and Steph, Larisa, Brandon and Timnah, Chris and Esme and Penelope, Edward, Dain, Johnny, Ignacio--you guys mean so much to me. Just listing all your names reminds me how very lucky I am to know you all and call you my friends. Charley in particular, your support of both me and Phil while we go through this has been invaluable. I look forward to our house-buying and house-owning adventures!

Thank you to Audra and Lisa for reminding me all throughout that even when things felt pretty hopeless, I was never in this alone! Thank you for helping me to remember that feeling feelings is not so unusual a thing for a human to do.

Laurie has been my best friend since I was 8. It's difficult to express how lucky I feel to have had to have her in my life all this time. Our daily chats kept me sane (or as sane as was possible at times) and I look forward to seeing her more often than has been possible in the last seven years. Mark, thank you for being my constant cheerleader through all of this!

Thank you to Buttons and Bodie, the most amazing cats and my little choochers, for all their "help" keeping my papers warm while I tried to read them. Thanks to Buttons especially for tearing several of my papers to shreds for his own amusement...I'm sure those weren't important anyway. Thanks to Bodie for sitting on my lap and being a little purr factory to help me feel less stressed and to keep my blood pressure down.

Phil, you have seen me at my worst, and yet you still stuck around. We met a little over five years ago at science camp and we have the National and Yuengling and crystallography data to thank for bringing us together. In the last few weeks before I defended my thesis, I got very sick with food poisoning and dehydration, and Phil held my hand and read articles about cats to me while I got an IV to replace the fluids and electrolytes I lost. I think that experience sums up Phil's loyalty, dedication and love very well. Phil, my best scientific discussions have been with you, and thank you for reading everything I wrote and trying your best to convince me it was good. This paragraph couldn't possibly begin to do you justice. Phil is the best guy in the world, and I am incredibly lucky.

My family is made up of pretty much the most awesome people ever, Buckleys, Roemers, and Fagans alike. I'm looking forward to watching Paigey and Daniel grow up, and getting to be more a part of their lives from now on as their Auntie Rach. Thank you to my (at the time of writing) 93-year-old grandma, Gran, who has been very patient in waiting for me to get my PhD so she can tell all of her bridge friends about it.

I am extremely lucky to have had four loving parents to raise me. Thank you for fostering my intellectual and emotional sides as well as a genuine love of the outdoors. None of this would have been possible without your love and support during my 25 years of school. Mom, Gare, Mike and Sylvie, I dedicate this thesis to you.

The role of the phasin PhaP in promoting polyhydroxybutyrate (PHB) granule formation in *Caulobacter crescentus*

by
Rachael Marie Buckley

Submitted to the Department of Chemistry
on August 30, 2013 in Partial Fulfillment of the
Requirements for the Degree of Doctor of Philosophy in
Biological Chemistry

Abstract

Polyhydroxybutyrate (PHB) is a biodegradable polymer produced by many microorganisms when they find themselves limited in an essential nutrient such as nitrogen or phosphorus but in the presence of an abundant carbon source. PHB and other related polymers are of interest because they have valuable properties as elastomers and thermoplastics, and are environmentally-friendly plastics than can potentially replace oil-based polymers. Bacteria package PHB as insoluble granules within the cell, maintaining the amorphous nature of the polymer, which is necessary for its degradation and reutilization when the environment becomes more conducive to growth and division. We are interested in understanding how the bacteria synthesize PHB and how they package it in such a way as to maintain its amorphous (rather than crystalline) nature. Examination of PHB biosynthesis has primarily been carried out in *Ralstonia eutropha*, which accumulates PHB to 80% of its cell dry weight (cdw) under the appropriate growth conditions. However most organisms do not accumulate PHB to such extremes, thus we have focused our efforts on understanding whether what we have learned about PHB biosynthesis in *R. eutropha* is true for organisms that accumulate far less PHB. To that end we have studied PHB accumulation in *Caulobacter crescentus*. Under conditions of nitrogen limitation but with abundant glucose available, C. crescentus accumulates PHB to ~12% of its cdw. We have quantitatively examined the levels of the PHB synthase, the major granule-associated protein PhaP and PHB per cell to gain an understanding of PHB biosynthesis in *C. crescentus*. We have furthermore isolated and characterized the PHB synthase and PhaP, and studied their roles in polymer formation *in vitro*. Our results have led to a model for granule formation in *C. crescentus* and suggest that many aspects of the model for granule formation developed based on studies in *R. eutropha* are true for organisms that accumulate PHB to much lower levels.

Thesis Supervisor: JoAnne Stubbe
Title: Novartis Professor of Chemistry and Professor of Biology

Table of Contents

List of Figures

List of Tables

List of Schemes

List of Abbreviations

$A_{280/260/210/412}$	Absorbance at 280 nm, 260 nm, 210 nm or 412 nm
Ab	*Acinetobacter baumannii*
Ac	*Aeromonas caviae*
AFM	Atomic force microscopy
Amp	Ampicillin
Av	*Allochromatium vinosum*
BSA	Bovine serum albumin
Cc	*Caulobacter crescentus*
cdw	Cell dry weight
cmc	Critical micelle concentration
CoA	Coenzyme A
Cv	Column volumes
cryoET	Cryoelectron tomography
DLS	Dynamic light scattering
DR	Downstream gene region
DTNB	5,5′-dithiobis-(2-nitrobenzoic acid)
EDTA	Ethylenediaminetetraacetic acid
ESI-MS	Electrospray ionization mass spectrometry
eYFP	Enhanced yellow fluorescent protein
GPC	Gel permeation chromatography
HB	Hydroxybutyryl
HBCoA	3-(*R*)-hydroxybutyryl CoA
(HB)n	Oilgomers 3-hydroxybutyrate of length n
HB-NAC	HB-N-acetylcysteamine
Hecameg	Methyl-6-O-(N-heptylcarbamoyl)-α-D-gulcopyranoside
HVCoA	3-(*R*)-hydroxyvaleryl CoA
IF	Internal gene fragment
IPTG	Isopropyl β-D-1-thiogalactopyranoside
Km	Kanamycin
LB	Luria-Bertani broth
LVER	Low viscosity embedding resin
M	Molecular mass
MALDI-TOF	Matrix assisted laser desorption ionization, time-of-flight spectrometry
M_n	Number average molecular weight
M_p	Peak molecular weight
M_w	Weight average molecular weight
NMR	Nuclear magnetic resonance
OD_{600}	Optical density at 600 nm
PBS	Phosphate buffered saline
PCR	Polymerase chain reaction
PDI	Polydispersity
PHAs	Polyhydroxyalkanoates
PHB	Polyhydroxybutyrate
PHB_{High}	Nitrogen limited PHB production medium (0.01% NH_4Cl, 2% fructose)

PYE	Peptone yeast extract
Re	*Ralstonia eutropha*
RT	Room temperature
sDCoA	Saturated trimer CoA – an analog of $(HB)_3$-CoA in which the terminal OH group is replaced with a H
SDS-PAGE	Sodium dodecyl sulfate - polyacrylamide gel electrophoresis
SEC	Size exclusion chromatography
SLS	Static light scattering
Sm	Streptomycin
sTCoA	Saturated trimer CoA – an analog of $(HB)_3$-CoA in which the terminal OH group is replaced with a H
TAE	Tris-acetate-EDTA buffer
TAG	Triacylglycerides
TCA	Trichloroacetic acid
TEM	Transmission electron microscopy
TFA	Trifluoroacetic acid
TFE	2,2,2,-trifluoroethanol
TNB^-	2-nitro-5-thiobenzoate anion
TOPO	Topoisomerase cloning (patented by Invitrogen)
Tris	Tris(hydroxymethyl)-aminoethane
TSB	Tryptic soy broth
UR	Upstream gene region

Chapter 1:

Introduction

1 Introduction

1.1 General relevance of PHAs

1.1.1 Relevance to biodegradable plastics

Polyhydroxyalkanoates (PHAs) are polyoxoesters synthesized by most microorganisms when they are exposed to environments limited in a nutrient such as nitrogen, phosphorus, etc., but with an abundant carbon source (sugar or fatty acid) (*1, 2*). As the polymers are synthesized from soluble CoA monomers, they undergo a phase transition and are deposited as insoluble inclusions, or granules, within the cytoplasm (Figure 1.1A). When the environment is once again conducive to growth and division, the bacteria break down the polymer and use the energy and monomeric precursors for biosynthetic pathways.

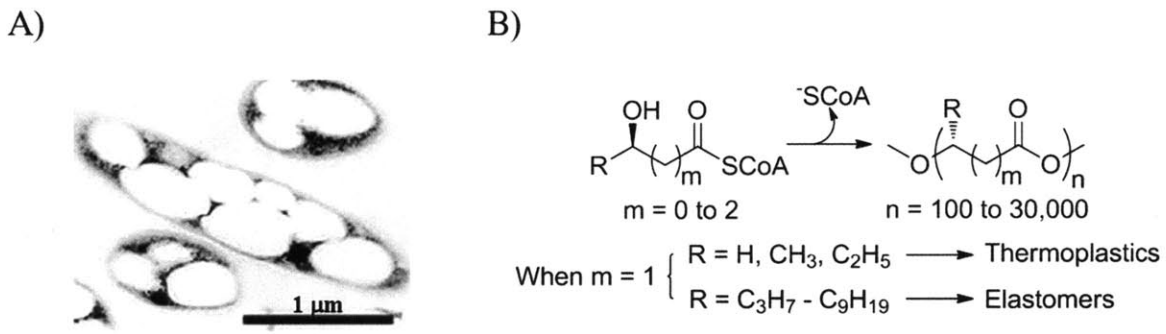

Figure 1.1 General structure and properties of PHAs. A) Transmission electron micrograph of *Ralstonia eutropha* filled with cytoplasmic granules (*1*). B) General scheme of polymerization and properties of PHAs depending on monomeric precursors.

PHAs are of general interest because they are biodegradable polymers from renewable sources. Depending on the structure of the monomeric precursors they can have properties of thermoplastics (R = H, CH_3, C_2H_5) and elastomers (R = C_3H_7 – $C_{13}H_{27}$) (Figure 1.1B) (*3, 4*). Oil-based polymers have enjoyed widespread use in the last century owing to their diverse properties and durability. Unfortunately they are not biodegradable, and in 2010, world-wide manufactured

plastic waste exceeded 31 million tons, 14 million tons of which was generated in the US alone (*5*). This waste accumulates both in landfills and in the ocean (*6*). Thus PHAs are an attractive alternative to environmentally unfriendly oil-based polymers. The commercial development and distribution of PHAs has been undertaken by a number of companies, including Metabolix Inc. (Cambridge, MA), and Proctor and Gamble (Cincinnati, OH). One challenge facing these companies is the engineering of recombinant systems such as bacteria and plants for efficient production of PHAs with varied properties. Unfortunately this process is far from optimal in terms of the levels of PHA accumulated (e.g. <15% cell dry weight, cdw, in plants) and production and polymer extraction costs (*6, 7*). Understanding PHA production at a fundamental level, by studying the mechanism of polymerization and the means by which the bacteria store and utilize PHAs, contributes to the goal of producing PHAs in an economically viable fashion.

1.1.2 Relevance to non-template driven biological polymerizations

PHA biosynthesis is also interesting from a fundamental point of view since it is a paradigm for non-template-driven polymerization reactions. A great deal is known about template-driven biological polymerizations, including the biosynthesis of DNA, RNA and proteins. In contrast relatively little is known about the mechanisms of initiation, elongation and termination of non-template-driven polymerizations (*2*), for example, the synthesis of starch from ADP-glucose (*8*), glycogen from UDP-glucose (*9*), polyphosphate from ATP (*10*) and poly-γ-glutamate from glutamate (*11*). These processes all use soluble monomeric precursors that undergo a phase change to insoluble material as they are polymerized. The insoluble polymer is then deposited inside the cell as granules or inclusions.

1.2 Widespread occurrence of PHA biosynthesis in microorganisms

A wide variety of microorganisms synthesize PHAs, the most common of which is polyhydroxybutyrate (PHB). PHB was first identified in and isolated from *Bacillus* sp. in 1926 by Lemoigne (*12*). Macrae and Wilkinson later identified specific growth conditions under which *B. cereus* and *B. megaterium* accumulated and degraded PHB, and they demonstrated that it was accumulated after logarithmic growth in the stationary phase (*13*). They also concluded, as a result of their experiments, that PHB served as intracellular carbon and energy storage. PHA accumulation has since been documented in numerous bacteria, including cyanobacteria, thermophiles, proteobacteria, and Gram-positive bacteria, as well as in archaea. Table 1.1 summarizes some of the organisms in which PHA accumulation has been studied. It is by no means exhaustive and is intended to give a sense of the range in extent of accumulation of PHAs. In almost all cases, the bacteria in Table 1.1 were cultured in conditions that maximize PHA production.

Table 1.1 Extent of PHA accumulation in various bacteria and archaea.

Organism	PHA content (% cdw)	Carbon source	Reference
Gram-positive bacteria			
Bacillus subtilis DSM10	33.5	Acetate and 3-hydroxybutyrate	(*14*)
Bacillus cereus DSM31	41.4	Acetate and 3-hydroxybutyrate	(*14*)
Micrococcus sp.	35-40	Sucrose	(*15*)
Nocardia carollina	2.4	Glucose	(*16*)
Streptomyces	1-10	Glucose	(*17*)
Cyanobacteria			
Gloeothece sp. PCC6909	6-9	Acetate	(*18*)
Spirulina	2.5	Acetate	(*19*)
Synechocystis PCC6803	4.1	CO_2	(*20*)

Thermophiles			
Chelatococcus sp. MW10	70	Glucose	(*21*)
Synechococcus sp. MA19	20	CO_2	(*22*)
Thermus thermophilus	35-40	Gluconate, octanoate	(*23*)
Proteobacteria			
Azotobacter vinelandii	75	Glucose	(*24*)
Caulobacter crescentus	10-20	Glucose	(*25*)
Ectothiorhodospira shaposhnikovii	1	Bicarbonate	(*26*)
Enterobacter aerogenes	7.3	Glucose	(*27*)
Methylobacterium	30	Methanol, valerate	(*28*)
Paracoccus denitrificans	24	n-pentanol	(*29*)
Pseudomonas stutzeri	7	Glucose	(*27*)
Ralstonia eutropha	80	Fructose	(*1, 2, 30*)
Rhizobium	25-45	Mannitol	(*31*)
Archaea			
Haloarcula hispanica	2.4	Glucose	(*32*)
Haloarcula japonica	0.5	Glucose	(*33*)
Haloferax mediterranei	17	Glucose	(*34*)
Halopiger aswanensis	34	Acetate/butyrate	(*35*)

PHB production by the soil bacterium *Ralstonia eutropha* has been extensively studied. Under conditions of nitrogen limitation with fructose as a carbon source, *R. eutropha* can accumulate polymer up to 80% of its cdw (*1, 2, 30*). Of the organisms whose PHA accumulation has been studied, *R. eutropha* is on the high end of accumulation. While this is interesting from the point of view of producing biodegradable polymers for commercial distribution, it is unlikely that organisms accumulate PHAs to such high levels in the natural environment. In contrast, *Caulobacter crescentus* – the focus of much of the research presented in this thesis – is on the

lower end of PHA accumulation and accumulates considerably less PHB than *R. eutropha*. Thus *C. crescentus*, with our extensive knowledge of this organism's biochemistry and genetics, provides a good model for studying PHA biosynthesis.

1.3 Proteins involved in PHB biosynthesis

1.3.1 Overview of players

This section presents an overview of the protein players in PHB biosynthesis in *R. eutropha* and *C. crescentus*. The proteins, and the various manners in which they were identified and characterized, will be discussed more thoroughly in the following sections. *R. eutropha* produces PHB via the proteins encoded by the *phaCAB* operon (*36, 37*). This operon encodes three proteins: PhaA is a thiolase that catalyzes the condensation of two molecules of acetyl CoA to acetoacetyl CoA (Figure 1.2); PhaB is an NADPH-dependent reductase that reduces acetoacetyl CoA to 3-(*R*)-hydroxybutyryl CoA (HBCoA); and PhaC catalyzes the polymerization of HBCoA monomeric units to generate PHB.

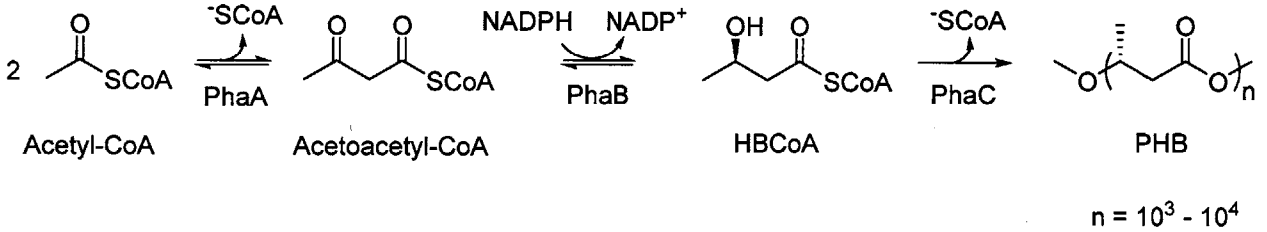

Figure 1.2 Biosynthetic pathway for PHB production.

Several additional gene products are involved in PHB biosynthesis in *R. eutropha* (Figure 1.3A). PhaP1 is the major granule associated phasin protein and its gene is located 58 kbp upstream of *phaCAB (38, 39). phaR* encodes the transcription factor PhaR, which negatively regulates the expression of *phaP1* and autoregulates its own production, and is located

immediately downstream of *phaCAB (40)*. The genes that encode several intracellular PHB depolymerases, collectively called PhaZs, are dispersed throughout the genome (*39*).

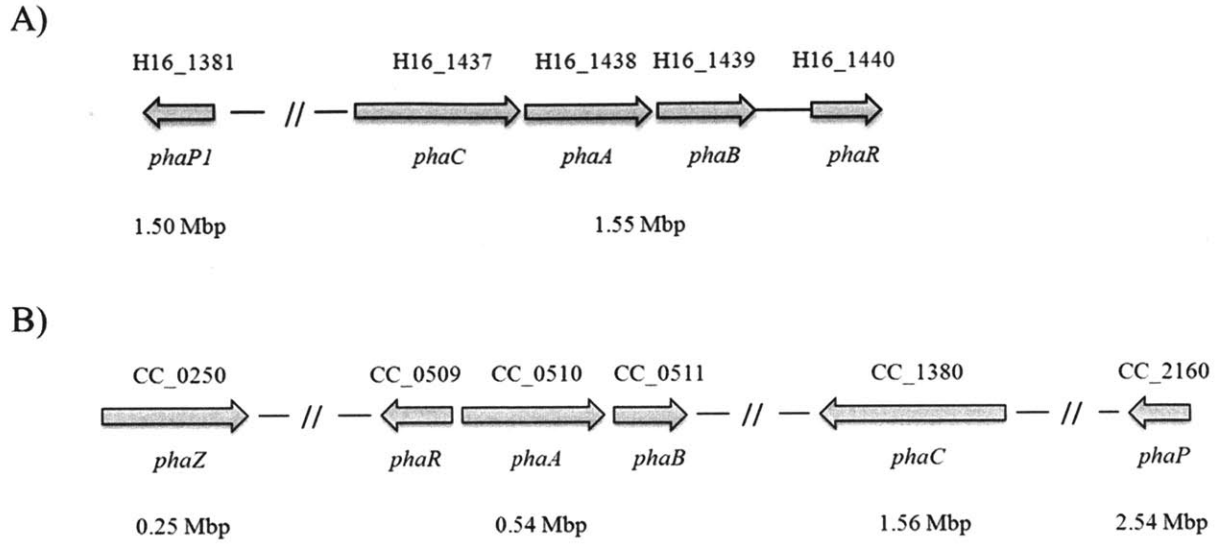

Figure 1.3 Organization of PHB biosynthetic genes in A) *Ralstonia eutropha* and B) *Caulobacter crescentus*. *R. eutropha* has multiple and redundant putative phasins (PhaPs) and depolymerases (PhaZs). The position of the major phasin, *phaP1*, in the *R. eutropha* genome is shown. Thus far we have only identified a single depolymerase (*phaZ*) and a single phasin (*phaP*) in *C. crescentus*.

The research presented in this thesis focuses primarily on the PHB biosynthetic system in *C. crescentus*. In contrast to *R. eutropha*, it appears that *C. crescentus* has a simpler set of PHB biosynthesis proteins. The genes encoding these proteins are annotated based on homology of the protein products to known PHB biosynthetic proteins. Sequence annotation indicates that the organization of the PHB biosynthetic genes in *C. crescentus* differs from that in *R. eutropha* in terms of the organization of the genes within the genome and the number of putative PHB biosynthetic proteins (Figure 1.3B). Although *phaA* and *phaB* in *C. crescentus* are colocalized in the genome as in *R. eutropha*, *phaR* is immediately upstream but transcribed in the opposite direction (*41*). *phaZ* is 300 kbp upstream of *phaAB*, and *phaC* and *phaP* are located ~1 Mbp and ~2 Mbp downstream of *phaAB*, respectively. The putative PhaR has 29% identity with PhaR

from *R. eutropha*. The putative PhaZ has 47% identity with PhaZa1 from *R. eutropha*. Sequencing of the *R. eutropha* genome has thus far revealed six additional PhaP1 homologs that colocalize with PHB granules, but their expression levels are much lower than that of PhaP1 (*42-44*). *R. eutropha* also contains a homolog of PhaC, encoded by *phaC2*, that shares 33% sequence identity with PhaC, but it is not expressed even when *phaC* is deleted (*45*). Preliminary analysis by sequence gazing does not reveal additional phasins in the *C. crescentus* genome, nor have we thus far been able to conclusively identify PhaZ homologs other than that annotated in the genome.

1.3.2 PHA synthases (PhaCs)

1.3.2.1 Overview of synthases

PHA synthases, or PhaCs, are divided into classes I through IV based on their substrate specificities, subunit composition and quaternary structure. Class I and III synthases are short chain polymerases (R = CH_3, CH_2CH_3, Figure 1.1B) and generate PHB from HBCoA or copolymers of HBCoA and 3-(*R*)-hydroxyvaleryl CoA (HVCoA) (*46*). Class I synthases are composed of a single subunit, PhaC, that is typically ~65 kDa. Class III synthases are composed of two 40 kDa subunits, the synthase PhaC and PhaE, a protein of unknown function. *Ralstonia eutropha* and *Allochromatium vinosum* produce the prototypes for the class I and III synthases, respectively. Class II synthases consist of a single subunit PhaC, ~60 kDa, and polymerize long chain 3-hydroxyalkanoates derived from fatty acids, where R = C_3H_7 to $C_{14}H_{29}$ *(47)*. *Pseudomonas aeruginosa* expresses the prototypical class II synthase. Class IV synthases also accept HBCoA and HVCoA as substrates, but have a subunit composition and quaternary structure distinct from the class I and III synthases. They consist of two subunits, PhaC and PhaR (distinct from the transcription factor PhaR discussed below) that are 40 kDa and 20 kDa,

respectively. Members of the genus *Bacillus* produce the prototype of the class IV sythases *(48)*. The vast majority of our mechanistic understanding of PHB polymerization comes from studies carried out on the class I synthase from *R. eutropha* and the class III synthase from *A. vinosum*. These studies will be summarized as a backdrop to the motivation of the studies on *C. crescentus*.

To study the mechanism of polymerization, a rapid and reproducible assay is required. Two different assays for PhaC have been developed (*49*). The first uses 5,5′-dithiobis-(2-nitrobenzoic acid) (DTNB) to measure the release of the product CoA as an indicator of the addition of each new hydroxybutyryl (HB) unit to the growing polymer. The free thiol of CoA reacts with DTNB to liberate the 2-nitro-5-thiobenzoate anion (TNB^-), which has a λ_{max} at 412 nm (ε = 13,600 M^{-1} cm^{-1}). Assays are typically carried out in a discontinuous fashion, as TNB^- has been shown to inhibit PhaC activity (*50*). This assay is the most reliable way to measure activity. A drawback of this assay, however, is that it does not directly measure polymerization, as CoA release may be the result of hydrolysis of substrate as well as polymerization. This becomes an issue when considering the activity of mutant PhaCs and the polymerization of unnatural substrates. A second assay uses [3-^{3}H]-HBCoA and directly measures the products of the polymerization. The reaction is quenched and the [^{3}H]-$(HB)_n$ products are extracted into chloroform and analyzed by scintillation counting (*49*). However, the extraction efficiency of the products into chloroform is dependent on their length, and efficiency drops off as the length increases. The DTNB assay is thus more efficient and reliable to study PhaC activity.

Class I synthases. The class I synthases are coded for by a single gene, *phaC*. *phaC* from *R. eutropha* was first cloned and characterized in 1989 by Peoples and Sinskey (*37*). Successful overexpression, purification and characterization of the synthase, $PhaC_{Re}$, was reported in 1994

by the Sinskey lab in collaboration with our lab (*49*). Initial efforts to purify PhaC were thwarted by its propensity to "stick" to the chromatography resin and glassware. Addition of the non-ionic detergent hecameg (Figure 1.4) at levels substantially below its critical micelle concentration (cmc) overcame this issue for reasons that are still not well understood. In the presence of hecameg, $PhaC_{Re}$ was readily purified to homogeneity. Almost all experiments with $PhaC_{Re}$ described subsequently included hecameg.

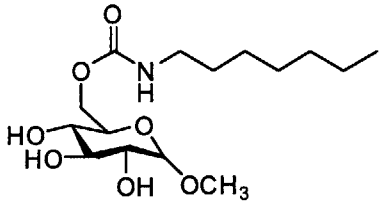

Figure 1.4 Structure of the non-ionic detergent hecameg (methyl-6-O-(N-heptylcarbamoyl).

The specific activity of early preparations of $PhaC_{Re}$ varied between 8 and 40 U/mg (where a unit, U, of activity is one μmol of substrate consumed per min) (*46, 49*). The discrepancy between measurements was attributed to the presence of high-molecular-weight (M_w) aggregates of $PhaC_{Re}$. Once the aggregates were removed by size exclusion chromatography (SEC), the specific activity plateaued at 40 U/mg. $PhaC_{Re}$ purified as an N-terminally hexahistidine-tagged construct has a specific activity is ~40 U/mg at 30 °C (*46, 51*). Removal of the tag does not change the specific activity (*46*). The enzyme exhibits a lag phase in CoA release that is dependent on enzyme concentration (Figure 1.5A). Goodwin and coworkers have measured a K_m of ~110 μM for $PhaC_{Re}$ in the presence of 70% fructose, which they claim eliminates the lag phase. In our hands, however, the experiments could not be reproduced (*46*). Furthermore they monitored the disappearance of the absorbance of the thioester of HBCoA at 236 nm as an indicator for polymerization. Given that the absorption of the adenine moiety of CoA at 260 nm is strong and extends into the 236 nm region, their assay is not very sensitive.

Very recently, Ushimaru and coworkers demonstrated that addition of the detergent Triton X-100 at concentrations well below its cmc to assays of $PhaC_{Re}$ eliminated the lag phase and allowed them to measure a K_m for HBCoA of 321 μM (*52*).

The lag phase in CoA release has many possible explanations. One possibility considered was that $PhaC_{Re}$ exists in two conformational states, only one of which is active, and that a necessity for conversion between the inactive and active states causes the lag phase. SEC revealed that $PhaC_{Re}$ existed as a monomeric form in equilibrium with a dimeric form, and the equilibrium shifts toward dimer upon acylation with artificial substrates, as described below (*49*). A second possibility considered was that the lag phase in $PhaC_{Re}$ activity could be in part due to omission of a suitable primer. Lag phases have been observed in activity assays of glycogen synthase and rubber polymerase when the appropriate primer units are omitted (*53-55*). The origin of the lag phase is discussed in further detail below.

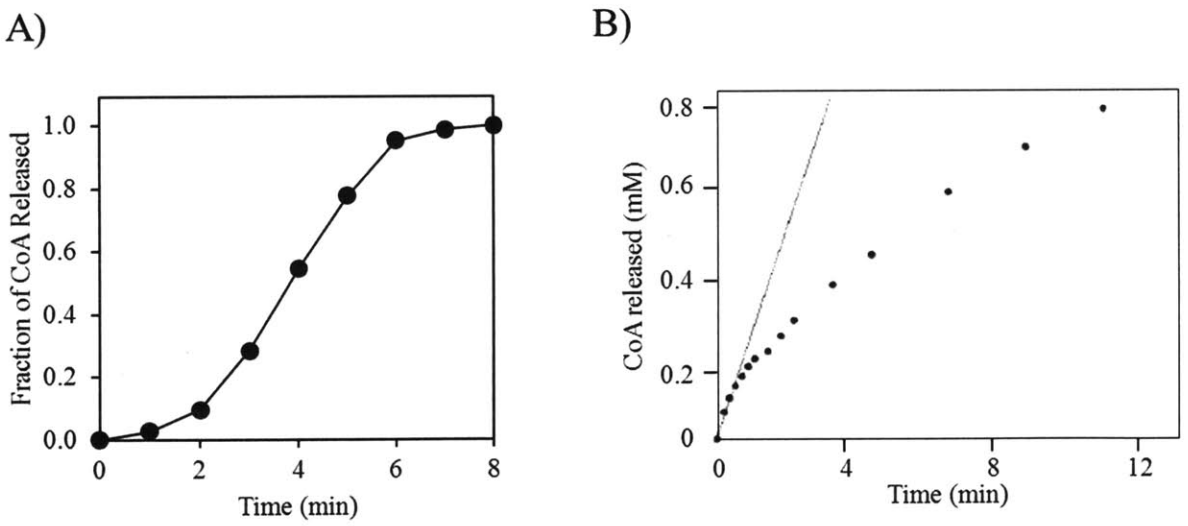

Figure 1.5 Kinetics of class I and class III synthases. A) CoA release from the class I synthase $PhaC_{Re}$ shows a variable lag phase followed by a linear phase. Specific activity of $PhaC_{Re}$ is determined from the linear phase. Adapted from reference (*56*). B) CoA release from the class III synthase $PhaEC_{Av}$ shows a burst phase followed by a slower phase. Specific activity of $PhaEC_{Av}$ is measured from the burst phase. Adapted from reference (*50*).

Class III synthases. Class III synthases are composed of two subunits, PhaC and PhaE. PhaC is the synthase whereas PhaE is of unknown function and is not homologous to any protein in the database. The class III synthase from *A. vinosum*, $PhaEC_{Av}$, was first purified recombinantly from *E. coli* in 1994 by Steinbüchel and coworkers (*57*). PhaE was shown to be essential for optimal activity and the active synthase contains PhaE and PhaC in a 1:1 ratio (*50*). In contrast to $PhaC_{Re}$, $PhaEC_{Av}$ is well-behaved in solution, despite immunogold labeling experiments and transmission electron microscopy (TEM) evidence suggesting that it too is associated with the surface of PHB granules *in vivo (57)*. $PhaEC_{Av}$ is kinetically distinct from $PhaC_{Re}$ and has a rapid phase in CoA release, followed by a slower phase (Figure 1.5B). At 30 °C, the specific activity of $PhaEC_{Av}$, which is determined from the burst phase, is 140 U/mg (*50*). The K_m for HBCoA, again measured from the rate of the burst phase, is 0.13 mM (*46*). By size exclusion chromatography the enzyme is a mixture of dimers and tetramers of PhaEC (*58*).

1.3.2.2 Sequence alignments and threading models of PHA synthases

Threading models for structure prediction of PhaCs. Early mechanistic thinking was guided by analysis of residues conserved among the available sequences of synthases and by comparison with the sequences and structure of lipases. Lipases catalyze the hydrolysis of fatty acyl groups from triacylglycerides (TAG) and as such function at lipid-water interfaces. Similarly, PhaCs are thought to function at the interface of the cytosol and the PHA granule surface. Lipases belong to the α/β-hydrolase family and contain the conserved catalytic residues Ser/(Asp/Glu)/His within the α/β hydrolase domain (*59-61*). The Ser participates in covalent catalysis and is found within a lipase box motif (G-X-S-X-G), and the His deprotonates the Ser to activate it for covalent catalysis. The role of the conserved Asp/Glu is not well understood, as its deletion has little effect on catalytic activity in the case of lipases. Steinbüchel and coworkers

noted in 1992 that PhaCs also contain a lipase box motif in which the active site Ser in lipases is replaced with a conserved Cys (*62*). The mechanistic significance of this was not known at the time.

Subsequently, our lab demonstrated by sequence alignment that $PhaC_{Av}$ has a 45 amino acid stretch with 42% homology to the α/β hydrolase domain of *Pseudomonas* lipase containing the active site (*49, 63*). The essential Ser and His in lipases align with the conserved Cys (C149) located within the lipase box and with a conserved His (H331) in $PhaC_{Av}$. These residues were shown by mutagenesis to be essential to activity (*63*). Furthermore, while two conserved Asp residues were identified, only one (D302) was important to catalysis, as demonstrated by mutagenesis (*63*). Together these observations indicated an important role for these residues that must be taken into account in a mechanistic model. The alignment of $PhaC_{Av}$ with lipase also suggested that $PhaC_{Av}$ was a member of the α/β hydrolase domain family and would therefore likely be structurally similar to lipases within this domain. Using the X-ray structure of *Pseudomonas* lipase as a template, a threading model was generated to predict the structure of the α/β-hydrolase fold domain of $PhaC_{Av}$, as well as the relative locations of the conserved Cys, Asp and His residues (*63*). The model suggested that the active site nucleophile C149 sits in a sharp elbow turn between a β-strand and an α-helix, as is the case with the Ser nucleophile of lipases. H331 is predicted to be located on an adjacent loop, and D302A was predicted to be near the core of the structure in which C149 sits, though no precise distance could be given. The localization of these three residues within the core structure of the modeled synthase further underscored their mechanistic importance. Alignments of class I synthase sequences reveal the corresponding conserved Cys, Asp and His residues, and suggest that the class I enzymes are also members of the α/β hydrolase fold family. A threading model of $PhaC_{Re}$ was also generated

using lipase from *Burkholderia glumae* as a template, predicting the same relative positions of the active site residues (*64*). The numbering of the Cys/Asp/His in $PhaC_{Re}$, $PhaEC_{Av}$, and PhaC from *C. crescentus* ($PhaC_{Cc}$) is given in Table 1.2.

Table 1.2 Numbering of active site residues in $PhaC_{Re}$ and $PhaEC_{Av}$ and $PhaC_{Cc}$.

Class I - $PhaC_{Re}$	Class III - $PhaEC_{Av}$	Class I – $PhaC_{Cc}$
C319	C149	C406
D480	D302	D562
H508	H331	H590

Current analysis of available PhaC sequences. In the decade since the alignments above were done, hundreds of PhaC sequences have been deposited in the database. As of 2012, an alignment of 72 class I synthases selected from a variety of genera and species reveals a total of 39 absolutely conserved residues, including the Cys, Asp, and His residues discussed above. These residues are indicated in the sequence of $PhaC_{Re}$ in Figure 1.6. The active site Cys is the only conserved Cys residue. Five conserved Pro and nine conserved Gly residues likely play important structural roles. Furthermore, six Asp, three Ser, three Asn, and five Trp residues are absolutely conserved.

matgkgaaastqegksqpfkvtpgpfdpatwlewsrqwqgtegnghaaasgipgldalagvkiapaql
gdiqqrymkdfsalwqamaegkaeatgplhdrrfagdawrtnlpyrfaaafyllnaralteladavea
daktrqrirfaisqwvdamspanflatnpeaqrlliesggeslragvrnmmedltrgkisqtdesafe
vgrnvavtegavvfeneyfqllqykpltdkvharpllmvppcinkyyildlqpesslvrhvveqghtv
flvswrnpdasmagstwddyiehaairaievardisgqdkinvlgfcvggtivstalavlaargehpa
asvtllttlldfadtgildvfvdeghvqlreatlgggagapcallrglelantfsflrpndlvwnyvv
dnylkgntpvpfdllfwngdatnlpgpwycwylrhtylqnelkvpgkltvcgvpvdlasidvptyiyg
sredhivpwtaayastallanklrfvlgasghiagvinppaknkrshwtndalpespqqwlagaiehh
gswwpdwtawlagqagakraapanygnaryraiepapgryvkaka

Figure 1.6 Absolutely conserved amino acids in class I synthases. The sequence given is of $PhaC_{Re}$. Residues highlighted in red are absolutely conserved in a sequence alignment of 72 class I synthases. The catalytic Cys, Asp and His residues are additionally underlined.

An alignment of 35 class III PhaCs reveals that, including the active site Cys, Asp and His, there are a total of 14 absolutely conserved residues. These residues are indicated in the primary sequence of $PhaC_{Av}$ in Figure 1.7. Among these residues are D84 and S90, which were recognized over a decade ago as absolutely conserved among the then reported sequences of class III synthases (*50*). D84N and S90A mutants were constructed and had activities that were 3% and 0.75% that of wt, respectively, suggesting they are important, but not essential, to activity (Jia and Stubbe, unpublished results). There are two conserved Pro and four conserved Gly residues, two of which are contained within the lipase box. Finally there are two conserved Trp and one conserved Asn residue.

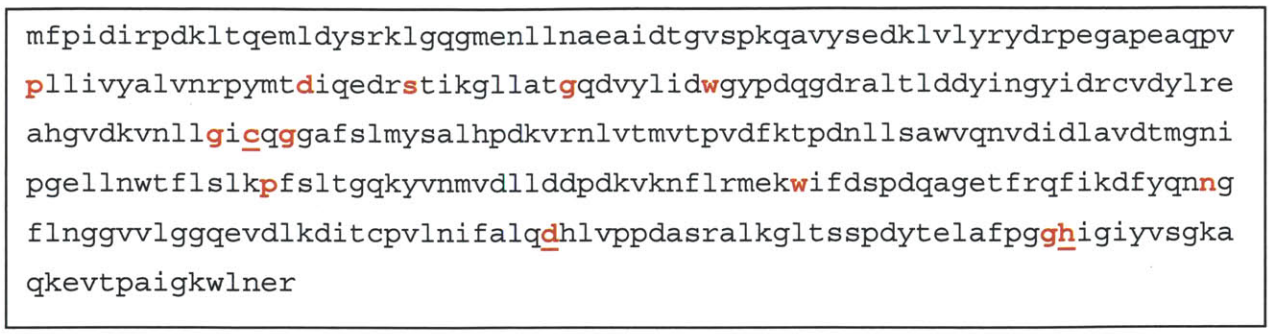

Figure 1.7 Absolutely conserved amino acids in class III synthases. The sequence given is of $PhaC_{Av}$. Residues highlighted in red are absolutely conserved in a sequence alignment of 35 class III synthases. The catalytic Cys, Asp and His residues are additionally underlined.

Several programs are available online that attempt to predict the secondary and tertiary structure of proteins based on the primary sequence. These programs rely on sequence homology of proteins of unknown structure with those of known 3-dimensional structure as well as motifs common to particular known protein folds. Given the vast increase in the number of 3D structures of proteins since the original threading models were generated, it is worth investigating what information an updated threading model might provide. The C-terminal domain of $PhaC_{Re}$ (encompassing residues 230-558, $PhaC_{Re230\text{-}558}$) and the entire $PhaC_{Av}$ sequence were submitted to the online programs Phyre2 (*65*) and SPARKS-X (*66*). The C-terminal domain of $PhaC_{Re}$ was selected because it contains the active site residues Cys/Asp/His and the α/β hydrolase domain. The top hit for $PhaC_{Re230\text{-}558}$ and the second hit for $PhaC_{Av}$ were models generated using the template with protein databank ID 2RAU. 2RAU is a 40 kDa putative lipase in the archaea species *Sulfolobus solfotaricus*, whose structure was solved to 1.85 Å resolution by the Joint Center for Structural Genomics. Its structure has not been published in an accompanying paper. Interestingly, a BLAST search of the sequence of 2RAU against available protein sequences in the database retrieves entries annotated as putative class III PHA synthases in *Acinetobacter*, among other organisms. Closer examination of the sequences of

these putative synthases reveals that the active site Cys of the typical PHB synthase is replaced by a Ser and that there is no *phaE* homolog adjacent to the gene sequence in the genome. However, alignment of the putative PhaC from *Acinetobacter baumanii* ($PhaC_{Ab}$) with $PhaC_{Av}$ reveals that the Ser of $PhaC_{Ab}$ aligns with C149 of $PhaC_{Av}$. Furthermore an Asp and His in $PhaC_{Ab}$ align with D302 and H331 in $PhaC_{Av}$. The two synthases share 24% sequence identity. Thus, it is unclear whether these sequences are unusual PhaCs or lipases. However, these observations led us to believe that 2RAU might serve as a good template for threading models of PhaCs.

The overall folds of the models are shown in Figure 1.8. Loops (in green) are included to give a sense of what percentage of the structure cannot be assigned a secondary structure. The backbones of the models overlay in the regions that have defined secondary structure. In both models, the core of the structure is an α/β hydrolase domain consisting of a β-sheet (composed of six to eight β-strands) surrounded by four α-helices. An additional domain composed of three to four short α-helices is also modeled (above the α/β hydrolase domains in Figure 1.8), but does not contain the active site residues and is primarily loops.

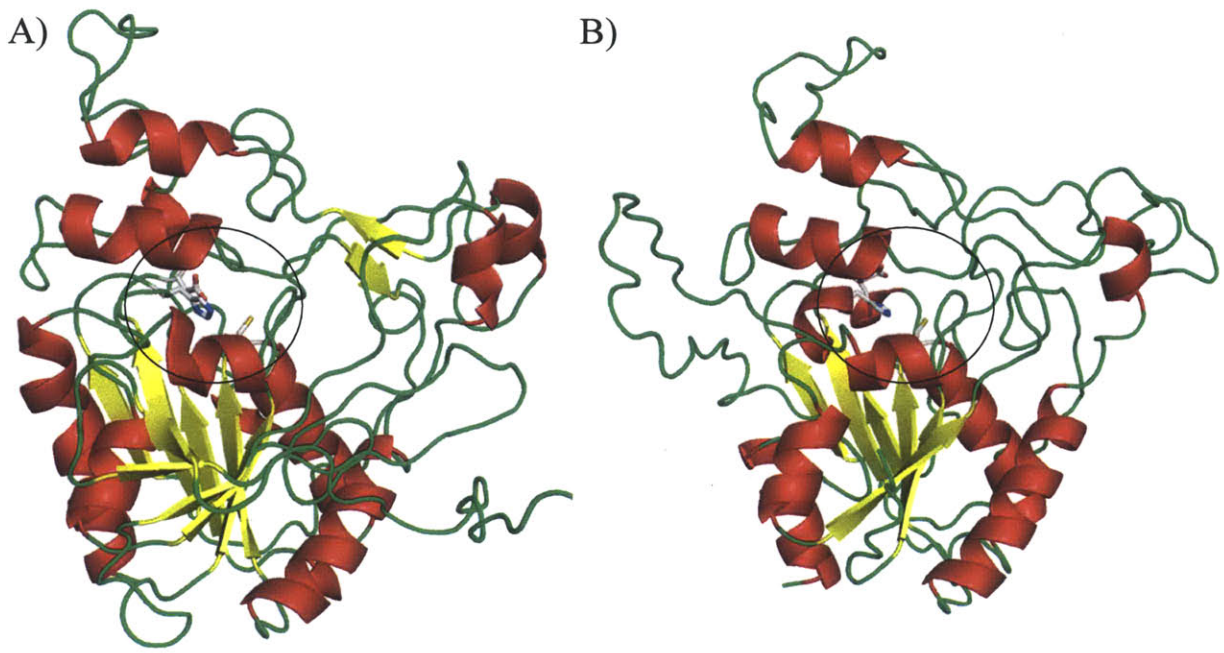

Figure 1.8 Overall structure of models generated for A) $PhaC_{Av}$ and B) $PhaC_{Re230\text{-}558}$ using the program SPARKS-X. The active site Cys, Asp and His are indicated with a black circle.

In both models, the essential Cys (C149/319) involved in covalent catalysis is located on a sharp turn between a β-strand and an α-helix, just as the early threading models predicted. D302/477 and H331/508 are also located on different loops between a β-strand and an α-helix. In both, models the Cys/Asp/His residues of the active site form a triangle with His in the middle. In the model of $PhaC_{Av}$, C149 is 3.6 Å from H331, and D302 is 3.9 Å from H331 (Figure 1.9A). In the model of $PhaC_{Re230\text{-}558}$, C319 is 3.7 Å from H508, and H508 is 4 Å from D477 (Figure 1.9B).

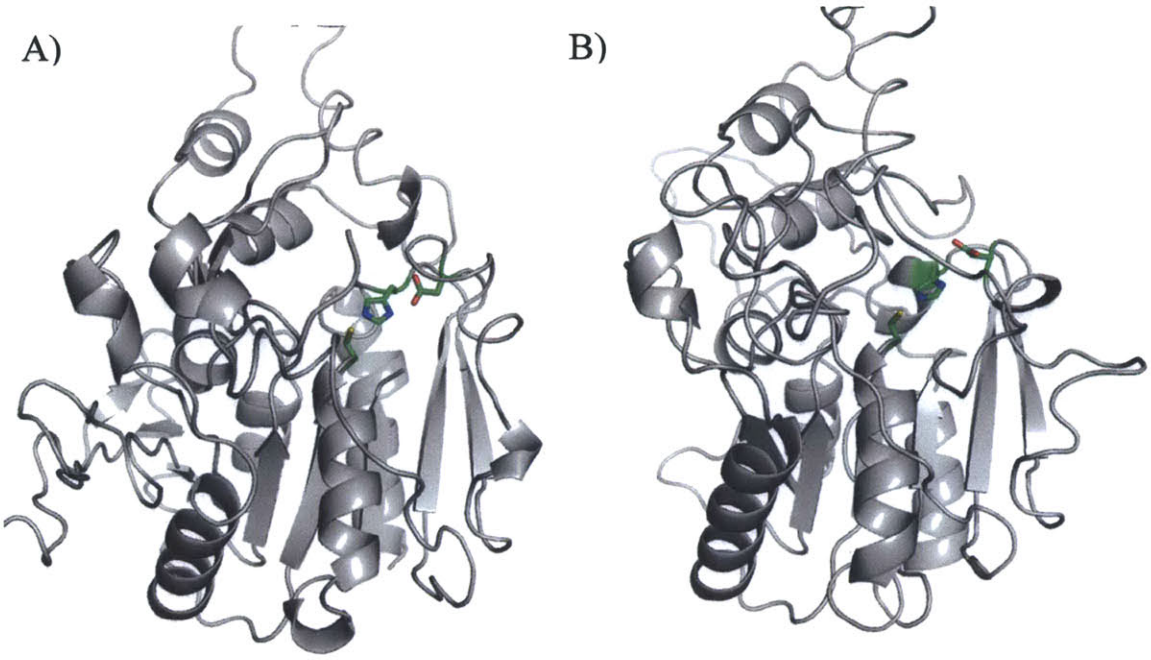

Figure 1.9 Structure models of A) $PhaC_{Av}$ and B) $PhaC_{Re230\text{-}558}$ to indicate the relative locations of the active site residues. The structures are rotated ~90° relative to the structures in Figure 1.8. The active site residues are indicated in green.

The active site in both models lies at the back of a pocket with two channels connecting it to the surface. In the structure of 2RAU, a PEG molecule from the crystallization buffer occupies this site. When the structure of 2RAU is aligned with either synthase, this PEG molecule fits into the synthase active site. Figure 1.10 shows a surface rendering of both structures with PEG molecule docked into the active site to provide a sense of depth. The two views are rotated ~90° from one another and show the two entrances to the active site. The observation of two channels into the active site is intriguing given the presumed necessity for a PHB synthase to have both an entrance to the active site for incoming HBCoA monomers and an exit from the active site for extrusion of growing polymer. However, as this is both a model and representative of a static structure, conformational changes that reshape the putative active site (e.g., upon substrate binding) cannot be ruled out. In the model of $PhaC_{Re230\text{-}558}$, D477 sits at the edge of one of the

entrances into the active site. In the model of $PhaC_{Av}$, D302 is obscured from the surface by an unstructured loop.

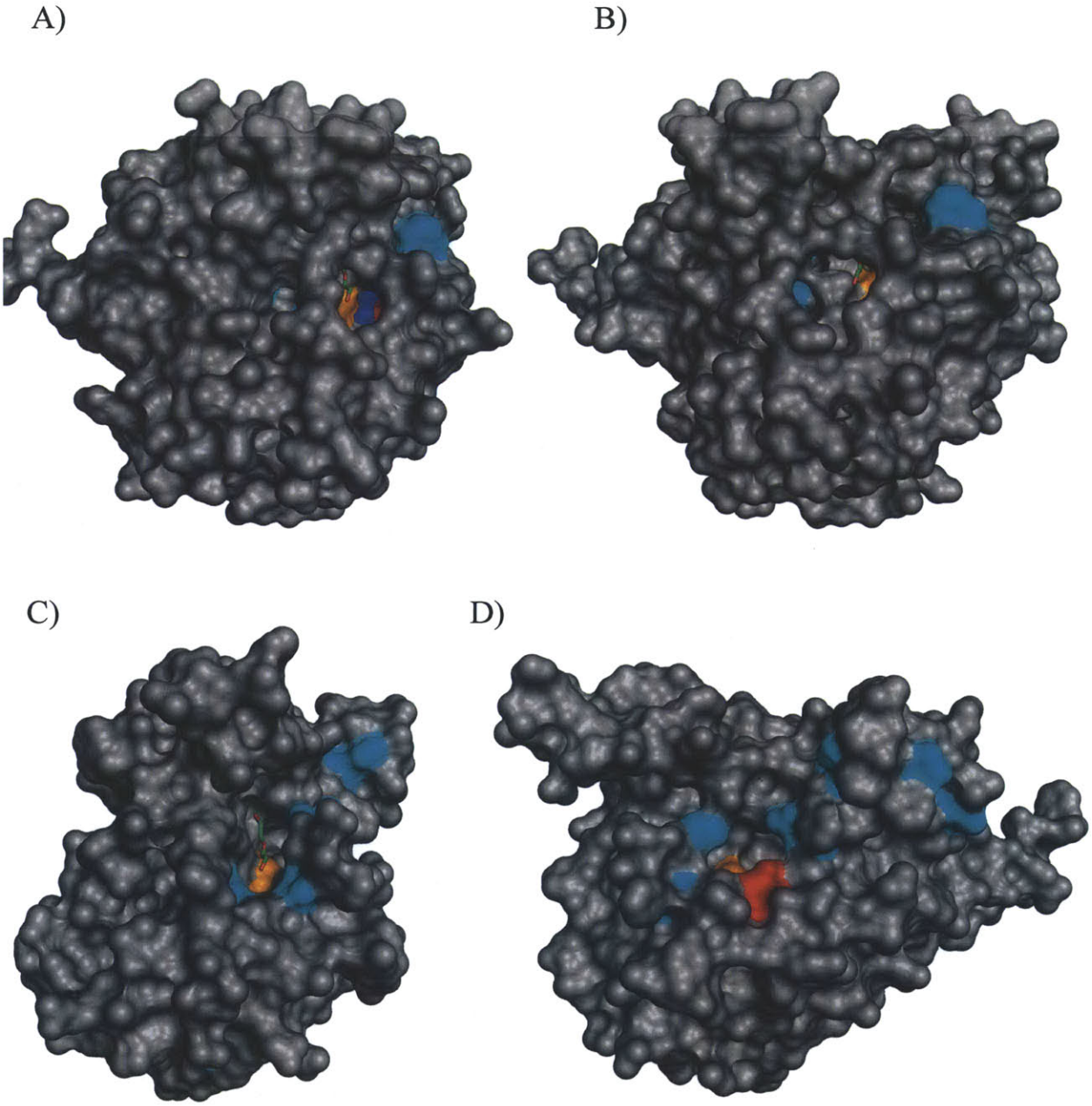

Figure 1.10 Surface rendering of $PhaC_{Av}$ and $PhaC_{Re230-558}$. A) and B) are $PhaC_{Av}$ rotated 90° with respect to one another. C149 is shown in orange, D302 is shown in red and H331 is shown in blue. The absolutely conserved residues are cyan. C) and D) are $PhaC_{Re230-558}$ rotated 90° with respect to one another. C319 is shown in orange, D480 is shown in red and H508 is shown in blue. The absolutely conserved residues are cyan. The PEG molecule (green) is shown docked in the active sites of both structures.

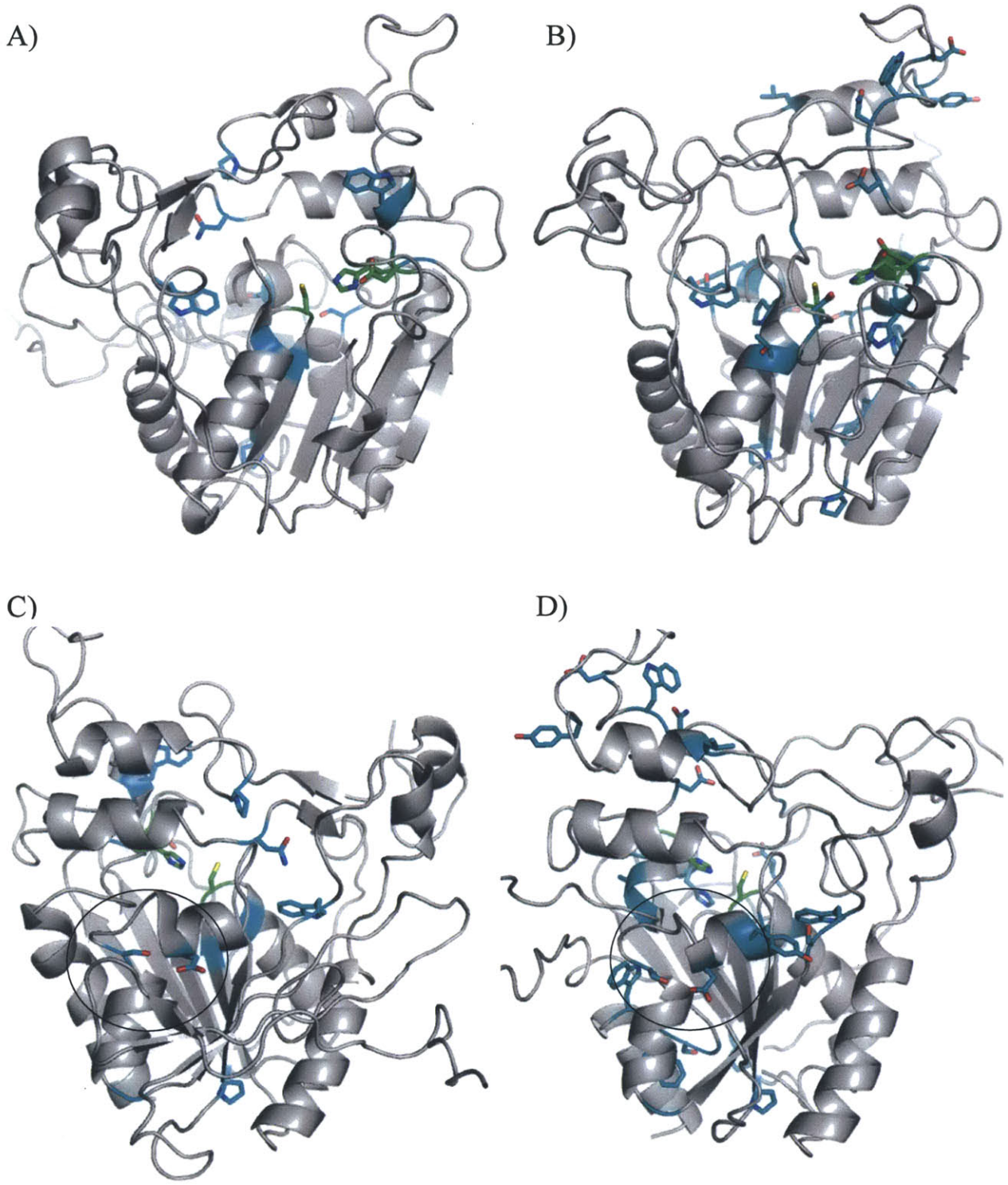

Figure 1.11 Positions of absolutely conserved residues in class I and class III PhaCs. Active site residues are shown in green, and additional absolutely conserved residues are shown in cyan. A) $PhaC_{Av}$ and B) $PhaC_{Re230\text{-}558}$, with active site residues in front. C) $PhaC_{Av}$ and D) $PhaC_{Re230\text{-}558}$ rotated 180° with respect to A and B. The absolutely conserved residues D84 and S90 (in $PhaC_{Av}$) and D254 and S260 (in $PhaC_{Re}$) are indicated in a black circle.

Figures 1.11A and B show the predicted positions of the absolutely conserved residues (cyan) in class I and III synthases, in addition to the active site residues (green). In $PhaC_{Av}$, the absolutely conserved residues D84 and S90, discussed above, are located on the opposite side of the protein to the active site, 14.9 Å and 20.7 Å away from C149, respectively. These two residues are the two most likely candidates, among the conserved residues, for involvement in termination, reinitiation or loading of substrate, as discussed in subsequent sections. From the models, it is difficult to say whether D84 and S90 are involved, as conformational changes may change their positions relative to the active site. Interestingly, when the two models are overlaid, D84 and S90 in $PhaC_{Av}$ overlay with the absolutely conserved residues D254 and S260 in $PhaC_{Re230\text{-}558}$. This observation further suggests that these residues might have an as yet unresolved role in catalysis.

In $PhaC_{Re230\text{-}558}$, five of the six absolutely conserved Asp residues are included in the modeled portion of the protein. D351 and D428 both sit at one entrance to the active site. The three conserved Ser residues in the model are located 15-20 Å from C319. As expected, the conserved Pro residues are located immediately before or after secondary structural elements. Another conserved residue, A510, is modeled in an α-helix following the active site H508. Taguchi *et al.* have proposed that A510 is involved in substrate recognition (*67*). They first examined a conserved residue, Q418, in PhaC1 from *Pseudomonas* sp. 61-3, and demonstrated via directed evolution that its mutation to Leu allowed the synthase to incorporate 36 mol% lactyl CoA into a copolymer of HB and lactyl units (*67*). The wt enzyme, in comparison, polymerizes long-chain 3-hydroxyalkanoates. The authors hypothesized that Q481 plays a role in substrate specificity in PhaC1 from *Pseudomonas*. A510 in $PhaC_{Re}$ aligns with Q481 in PhaC1; thus, the authors investigated the role of A510 in $PhaC_{Re}$. $PhaC_{Re}$ does not normally accept

lactyl-CoA as a substrate (*46*), but mutation of A510 to several different amino acids resulted in a variety of mutant synthases that incorporated lactyl CoA into copolymers of HB an lactyl monomers in varying mol% (*68*). The position of A510 near the active site of $PhaC_{Re}$ in the threading model is consistent with their observations that it plays a role in substrate recognition.

1.3.2.3 Working model for the mechanism of polymerization

Figure 1.12 illustrates two of several possible mechanistic models that could account for the roles of Cys, Asp and His in polymerization. We currently favor the model presented in Figure 1.12B. The evidence that supports this model will be discussed in the following sections. The model proposes that synthases act as a dimer of PhaCs (in the case of class I) or PhaECs (in the case of class III). In both models, the essential Cys residue participates in covalent catalysis with the growing PHB chain. The essential His deprotonates Cys to generate the active thiolate nucleophile, which then attacks the thioester of HBCoA, liberating $^{-}$SCoA and forming an HB-PhaC thioester. At this point, the two mechanisms diverge. In the mechanism shown in Figure 1.12A, the second HBCoA is loaded to the active site Cys of the other PhaC monomer. The catalytically important Asp acts as a general base to deprotonate the hydroxyl group of the second HBCoA, which attacks the HB-PhaC thioester of the first PhaC monomer. The growing chain is transferred to the second PhaC and the elongation process continues. The active site is therefore formed at the interface of the dimer of PhaCs. This mechanism predicts that the growing PHB chain is always covalently attached to the enzyme and that there are no non-covalent intermediates. The second mechanism, presented in Figure 1.12B, proposes that only one PhaC active site in the dimer participates in polymerization. After the first HBCoA unit is loaded onto the active site Cys, a second HBCoA monomer binds non-covalently to the same active site. Asp serves as the general base catalyst to deprotonate the hydroxyl group, which then

attacks the HB-PhaC thioester, temporarily releasing the growing chain from the enzyme. The enzyme rapidly reacylates to continue polymerization. This mechanism predicts that only a single active site Cys of the PhaC dimer is required for catalysis, and that polymerization involves covalent as well as non-covalent intermediates.

In light of the threading models presented above, it seems unlikely that the active site could be formed at the interface of two monomers, given that the active site residues are relatively buried. The active sites of lipases are also buried, and furthermore the lipases thus far characterized are all monomeric (*69, 70*). Thus, the available information we have from structure modeling efforts and analogy to lipases seems to indicate that the mechanism shown in Figure 1.12A is unlikely to be correct.

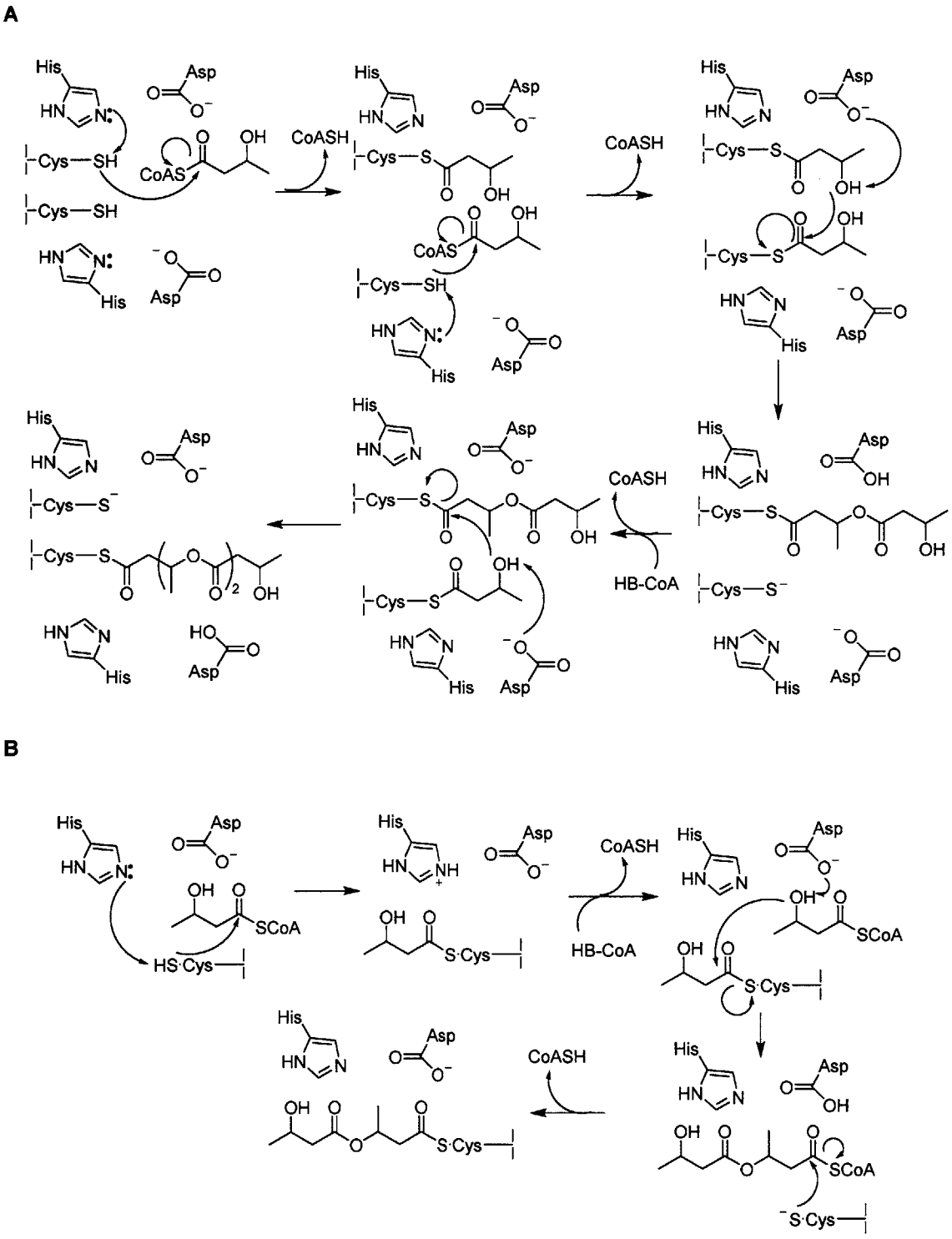

Figure 1.12 Models for the mechanisms of initiation and elongation. The mechanism involves conserved C/D/H residues. We currently favor model B, which proceeds via both covalent and non-covalent intermediates. Adapted from reference (*71*).

1.3.2.4 Evidence for covalent catalysis and efforts to study the initiation process

Priming studies with $PhaC_{Re}$. In the original purification of recombinant $PhaC_{Re}$, Gerngross and coworkers identified C319 by mutagenesis as essential for activity (*49*). In an effort to identify covalent intermediates at early stages in polymerization, they incubated $PhaC_{Re}$ with 10-100 equivalents of [3-^{3}H]-HBCoA and examined the products by sucrose density gradient ultracentrifugation. Fractions throughout the gradient were analyzed for radioactivity by scintillation counting. The radioactivity was associated entirely with a fraction that migrated as large polymer, even when HBCoA was present in small excess over synthase (*49*). Furthermore, only a small amount of synthase was associated with the large polymer, while the majority remained unmodified. These results suggested that the rate of initiation was much slower than the rate of polymerization, resulting in non-uniform loading of the synthase. This approach would therefore not facilitate identification of early intermediates in polymerization; thus, alternative approaches were necessary to obtain evidence for covalent catalysis.

Studies of non-template-dependent polymerization reactions have suggested that often "primers" made from the monomeric building blocks of the polymer are involved in the initiation process (*2*). The use of artificial primers to uniformly load PhaCs allowed for the investigation of early steps in polymerization as well as the identification of covalent intermediates. A series of $(HB)_nCoA$ (n = 2-4) primers and a saturated trimer of HBCoA (sTCoA) (Figure 1.13) were synthesized and examined for their potential to prime $PhaC_{Re}$ (*51*). Incubation of these oligomers with $PhaC_{Re}$ in the absence of HBCoA provided several key insights into the mechanism of polymerization. When $PhaC_{Re}$ was incubated with $(HB)_3CoA$ and sTCoA, the quaternary structure shifted from predominantly monomer to predominantly dimer. Furthermore, the length of the lag phase of CoA release decreased, and the specific activity increased. The data together

led to a model in which a requirement for priming and formation of the $PhaC_{Re}$ dimer was a cause of the lag phase in CoA release (*51*). Incubation of $PhaC_{Re}$ with [^{3}H]-sTCoA revealed that only the dimer fraction contained radiolabel, and that the stoichiometry was one label per dimer of PhaC. These results suggested that the dimer was the predominant active form of the synthase and that one dimer of PhaCs makes a single PHB chain. However, assays of the monomer fraction isolated by SEC reveal that it has the same specific activity as the dimer (*51, 58*). Finally, trypsin digest of $PhaC_{Re}$ reacted with [^{3}H]-sTCoA revealed three peptides containing the radiolabel. These peptides were sequenced by N-terminal degradation and all three contained C319, providing the first evidence for covalent catalysis by the active site Cys (*72*). Subsequent studies further examined priming of $PhaC_{Re}$ with sTCoA (*72*). Incubation of $PhaC_{Re}$ with sTCoA resulted in a burst of CoA release equal to 0.5 equivalents of CoA per monomer of PhaC. This result was consistent with the above experiments that demonstrated that each dimer was labeled with one [^{3}H]-sT and further confirmed that a dimer of PhaCs synthesizes a single PHB chain. Importantly, the radiolabel of [^{3}H]-sTCoA can be chased into polymer when HBCoA is added to the reaction mixture, demonstrating the chemical competence of sTCoA (*51, 72*).

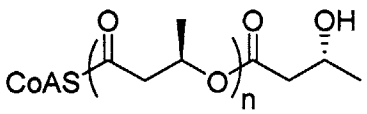

n = 1: $(HB)_2$CoA
n = 2: $(HB)_3$CoA
n = 3: $(HB)_4$CoA

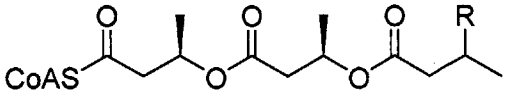

R = H: sTCoA
R = ^{3}H: [^{3}H]-sTCoA

Figure 1.13 Structures of $(HB)_3$CoA (R = OH) and sTCoA (R = H or ^{3}H).

Because $PhaC_{Re}$ is non-uniformly loaded *in vitro*, efforts were made to find a protein factor that might serve the function *in vivo* that artificial primers serve *in vitro*, that is, uniformly

loading the synthase and in the case of $PhaC_{Re}$, decreasing or eliminating the lag phase in activity (*58*). However, recent results from our lab suggest non-uniform loading occurs *in vivo* as well. Incorporation of a Strep2-tagged synthase gene in place of the wt gene under the endogenous promoter in the *R. eutropha* genome allowed $PhaC_{Re}$ to be isolated by affinity chromatography (*73*). It was hoped that rapid isolation of the synthase might allow copurification of a protein factor involved in initiating polymerization, but no factor was found. However, a portion of the Strep2-tagged synthase as isolated was associated with high M_w PHB, while the remainder was unmodified. The PHB-complexed $PhaC_{Re}$ exhibited no lag phase and had a higher specific activity than the recombinant $PhaC_{Re}$. These results suggest that PHB can function as the primer, that $PhaC_{Re}$ is non-uniformly loaded *in vivo*, and that priming is responsible in part for elimination of the lag phase (*73*).

Priming studies with $PhaEC_{Av}$. While $PhaEC_{Av}$ is kinetically distinct from $PhaC_{Re}$, *in vitro* studies with $PhaEC_{Av}$ primed with sTCoA have highlighted the mechanistic similarities between the two synthases. SDS-PAGE and autoradiography analysis of the products of $PhaEC_{Av}$ reacted with 5 and 50 equiv. [1-^{14}C]-HBCoA revealed that a few molecules of $PhaEC_{Av}$ generate large polymer, while the majority of the synthase remains unmodified. Thus, as is the case with $PhaC_{Re}$, the rate of initiation of polymerization by $PhaEC_{Av}$ is also much slower than the rate of elongation (*74, 75*). Incubation of $PhaEC_{Av}$ with sTCoA results in a burst of CoA release corresponding to 0.5 equivalents per PhaEC, again suggesting that a dimer of PhaECs makes a single PHB chain (*63*). Trypsin digest of synthase following incubation with [^{3}H]-sTCoA revealed three radiolabeled peptides. The M_w of the peptides was determined by electrospray ionization mass spectrometry (ESI-MS) and they were sequenced MS/MS methods, revealing that C149 was covalently attached to sT, confirming its role in covalent catalysis (*50*).

Surprisingly, peptides containing C149 labeled with sT elongated by one and two additional HB units were also identified. An explanation for this observation is that sTCoA stored for extended periods of time undergoes slow hydrolysis, and the sTCoA stock therefore contained small amounts of HBCoA. The enzyme was thus serendipitously caught in the act of elongation, providing the most convincing evidence for the involvement of C149 in covalent catalysis (*50*).

Priming studies with PhaC from Aeromonas caviae. Recently Doi and coworkers demonstrated *in vitro* that HBCoA can act as a primer for the class I PhaC from *Aeromonas caviae* ($PhaC_{Ac}$) and that $PhaC_{Ac}$ can be uniformly loaded (*76*). These observations are potentially interesting because this is the first report of a wt PhaC that appears to be uniformly loaded with substrate alone (i.e. without artificial primers). The authors used matrix assisted laser dissorption ionization, time-of-flight (MALDI-TOF) spectrometry, SEC and dynamic light scattering (DLS) to monitor the polymerization reaction and the oligomeric state of $PhaC_{Ac}$. MALDI-TOF demonstrated that when $PhaC_{Ac}$ was reacted with 60 equivalents of HBCoA, the unmodified protein peak disappeared concomitant with appearance of a peak of higher m/z, suggesting all of the synthase is modified with oligomer/polymer. It should be noted that a caveat to using mass spectrometry methods to monitor polymerization reactions is that the ionization efficiencies of the various species are not well understood and may differ depending on oligomer/polymer length. Furthermore, in the figures in their paper, the m/z values of the peaks are illegible, and there is no discussion about whether the m/z values of the various peaks are consistent with $PhaC_{Ac}$ modified with PHB chains of various lengths. The authors further demonstrated by SEC and DLS that reaction with HBCoA shifts the equilibrium from predominantly monomeric to dimeric $PhaC_{Ac}$ (*76*). Again with the amount of detail provided for their DLS experiments, it is difficult to critically evaluate their data. The authors conclude that a

dimer of $PhaC_{Ac}$ is the favored form during catalysis, consistent with our observations that the dimer form of $PhaC_{Re}$ and dimer/tetramer forms of $PhaEC_{Av}$ are active for polymerization. However, a more careful and thorough investigation of priming $PhaC_{Ac}$ with HBCoA is necessary to determine whether this synthase is interesting.

1.3.2.5 Evidence for roles of His and Asp in initiation and elongation

The artificial primer sTCoA was also used to investigate of the role of the conserved His and Asp residues in initiation and elongation in both $PhaC_{Re}$ and $PhaEC_{Av}$. When H508 of $PhaC_{Re}$ was mutated to Gln, incubation with sTCoA resulted in no CoA release, suggesting that His functions to deprotonate the Cys involved in catalysis (*72*). When D480 was mutated to Asn, slow CoA release was observed upon incubation with sTCoA, suggesting that this residue does not play a role in activating C319 for covalent catalysis. Similar experiments were carried out with $PhaEC_{Av}$. When H331 was mutated to Gln, no CoA release was observed upon incubation with sTCoA (*63*). Interestingly, when D302 of $PhaEC_{Av}$ was mutated to Asn, acylation with sTCoA revealed a burst of 0.5 equivalents of CoA per PhaC, and no additional CoA release over 120 min (*63*). This result demonstrated that D302 is not involved in acylation of Cys with sTCoA and suggested that the acylated mutant synthase was stable to hydrolysis. In contrast, following the initial burst of CoA release from priming wt $PhaEC_{Av}$ with sTCoA, CoA release continues at a substantially slower rate, resulting in the production of the sT acid. This result was interpreted to suggest that D302 functions as a general base catalyst to activate water for hydrolysis of the acylated enzyme, and further that its role in polymerization is to deprotonate the hydroxyl group of HBCoA for ester formation.

The mutant D302A-$PhaEC_{Av}$ was used to study elongation *in vitro*. The mutation to Ala slows the rate of elongation to make it more comparable to the rate of initiation. D302A-

$PhaEC_{Av}$ has a specific activity that is 0.012% that of wt. *In vitro* reactions between D302A-$PhaEC_{Av}$ and 5-300 equivalents of [1-^{14}C]-HBCoA allowed for the detection for the first time of $(HB)_n$ intermediates covalently bound to $PhaC_{Av}$ by Western blot analysis using antibodies to $PhaEC_{Av}$ and autoradiography of the dried gel (*74*). Trypsin digest of D302A-$PhaEC_{Av}$ reacted with 50 equiv. HBCoA followed by ESI-MS analysis of the peptides revealed that C149 was modified with HB_n, where n = 3-10. Evidently, mutation of D302 to A allowed for more uniform loading and elongation, supporting the role for D302 in elongation.

1.3.2.6 Evidence for covalent and non-covalent intermediates in elongation

Efforts to form heterodimers to support or eliminate the mechanism in Figure 1.12A. A central question was to distinguish between the mechanisms shown in Figure 1.12A and B. One key distinction is that the mechanism in Figure 1.12A requires the participation of the active site Cys residues from both subunits in polymerization, whereas the mechanism in Figure 1.12B requires a Cys from a single subunit only. In this second model, only one of the two monomers would be active. Zhang and coworkers attempted to reconstitute heterodimers of $PhaC_{Re}$ with one wt subunit and one catalytically inactive C319A mutant subunit (*77*). In their experiments, the specific activity of wt-$PhaC_{Re}$ was first measured. It was then combined in a stoichiometric ratio of 1:1 with C319A-$PhaC_{Re}$ under dilute conditions, which the authors believe promotes dissociation of the synthase entirely into monomers. Solid fructose was then dissolved in the solution for a final concentration of 70% w/v, which the authors claim shifts the equilibrium in favor of dimerization. Their analysis, which we have presented below, is somewhat convoluted. Statistically, the monomers should reform heterodimers in a ratio of 1:2:1 of wt-wt-$PhaC_{Re}$ to wt-C319A-$PhaC_{Re}$ to C319A-C319A-$PhaC_{Re}$. That is, 50% of the wt $PhaC_{Re}$ would reassociate with other wt subunits, whereas the other 50% would associate with C319A subunits. As such, the

specific activity of wt-PhaC$_{Re}$ (measured originally based only on the amount of wt-PhaC$_{Re}$ present in the assay mixture) should either decrease by 50% (if heterodimers are catalytically inactive) or stay the same (if heterodimers are catalytically active). In their experiments, the authors measured a decrease in specific activity of wt-PhaC$_{Re}$ of 50% upon reconstitution of wt-C319A-PhaC$_{Re}$ heterodimers, which they interpreted to suggest that heterodimers are catalytically inactive. They therefore conclude that Cys from each subunit of the dimer is required for polymerization (as in the mechanism in Figure 1.12A).

In principle this is the ideal experiment to address whether one Cys or two is necessary for activity. However Zhang and coworkers failed to consider the complicated equilibria of monomer-dimer interconversion (*77*). A best estimation from the information available in their paper is that their "dilute" conditions that promote monomerization are 3 μM PhaC. We have estimated the monomer/dimer equilibrium to have a K_D of less than 4 μM. Furthermore, in our hands fructose decreased the specific activity of PhaC$_{Re}$, inconsistent with the findings on which Zhang and coworkers based their studies (*1, 58*). Therefore, the conclusions from their studies in our minds remain unresolved.

Efforts to trap non-covalent intermediates. A second distinction between the two mechanisms is that the mechanism in Figure 1.12A predicts only covalent intermediates, whereas the mechanism in Figure 1.12B predicts that transient non-covalent intermediates form during polymerization. Three sets of experiments suggest that the mechanism of elongation proceeds through non-covalent intermediates as outlined in Figure 1.12B. The first set of experiments was *in vitro* polymerization reactions carried out using PhaEC$_{Av}$ and the artificial substrate HB-N-acetylcysteamine (HB-NAC), which revealed that the synthase could polymerize HB-NAC (*78*). The k_{cat} for this reaction was 0.65 s^{-1}, compared to 65 s^{-1} with HBCoA (*46*). The K_m of HB-NAC

was 8.6 mM, 60-fold higher than for HBCoA. The HB-NAC was entirely consumed in the reaction and the polymer generated was ~75 kDa in M_w, compared to ~1,000 kDa for polymer generated from HBCoA. One possible interpretation for the lower M_w resulting from HB-NAC polymerization is that the reaction proceeds through non-covalent intermediates [$(HB)_nNAC$] as in Figure 1.12B (*78*). The partitioning between reacylation of the active site Cys and dissociation in these experiments is, in principle, governed only by the K_Ds of the NAC vs. CoA moieties (which are reflected in their K_ms). Thus dissociation of $(HB)_nNAC$ would occur more readily than $(HB)_nCoA$ and potentially at a lower M_w. An alternative interpretation of these results is that they are suggestive of a model of chain termination by thiolysis. This proposal will be explored below in the section dealing with mechanisms of termination.

In the second set of experiments, the C149S-PhaEC mutant of $PhaEC_{Av}$ was used to detect non-covalent intermediates [$(HB)_nCoA$]. Efforts to detect non-covalent intermediates with wt $PhaEC_{Av}$ by rapid mixing of sT-$PhaEC_{Av}$ with [1-^{14}C]-HBCoA followed by quenching with acid revealed that all of the radioactivity remained associated with the protein, that is, there were no detectable non-covalent intermediates. A failure to detect non-covalent intermediates does not rule out the mechanism in Figure 1.12B, however, because the rate of reacylation of the wt synthase following addition of an HB unit may be too fast to allow detection. Therefore, it was proposed that the mutant C149S-$PhaEC_{Av}$ might allow detection of putative non-covalent intermediates due to a reduced rate of reacylation. The relative rates of reacylation in the wt and C149S enzymes were estimated by measuring the rates of acylation with [^{3}H]-sTCoA. As expected, the rate of reacylation of C149S-$PhaEC_{Av}$ was 170-fold slower than for wt (0.035 s^{-1} vs. 5 s^{-1}). Chemical quench experiments from 1-15 min of C149S-$PhaEC_{Av}$ with [1-^{14}C]-HBCoA allowed detection for the first time of the non-covalent intermediates $(HB)_nCoA$, where n = 2 and

3 (*71*). When the reaction was carried out for 60 min, 50% of the radioactivity was present in $(HB)_2CoA$, indicating that it is a major species formed in the reaction. These results provide evidence to support the mechanism in Figure 1.12B. It should be noted, however, that because the first experiments rely on the use of a substrate analog (HB-NAC) and the second set of experiments relies on a mutant synthase, the relevance of these results to the wt enzyme mechanism remains to be established conclusively.

Reaction of sT-C149S-PhaECAv suggests the enzyme is capable of catalyzing reactions in addition to polymerization. Very recently, chain elongation experiments with $PhaC_{Re}$ and $PhaEC_{Av}$ primed with sTCoA have given unusual results that could be interpreted to suggest the presence of a loading site separate from the active site Cys (Li and Stubbe, unpublished results). For these experiments, an HBCoA analog, $HBCH_2CoA$, was synthesized in which the S atom of the thioester was replaced with a methylene group (Figure 1.14).

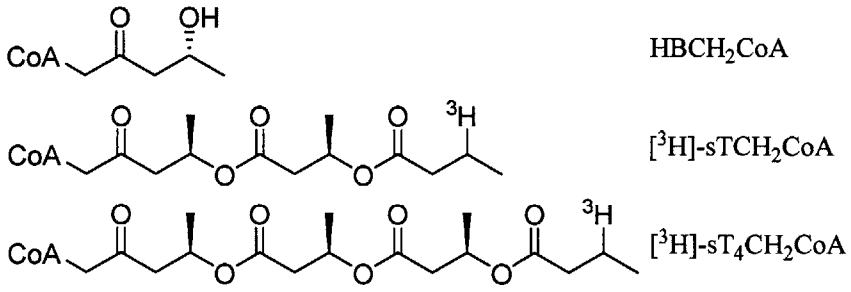

Figure 1.14 Structures of the substrate analog $HBCH_2CoA$ and non-covalent intermediates $[^3H]$-$sTCH_2CoA$ and $[^3H]$-sT_4CH_2CoA.

This analog was designed to function as a chain terminator that would allow the detection of non-covalent intermediates as seen with the C149S-$PhaEC_{Av}$ mutant above. When $PhaEC_{Av}$ was primed with $[^3H]$-sTCoA and then reacted with $HBCH_2CoA$, the major resulting intermediate was $[^3H]$-$sTCH_2CoA$ rather than the expected chain elongation product $[^3H]$-sT_4CH_2CoA (Figure 1.14). A similar result was seen when an identical experiment was carried

out with wt $PhaC_{Re}$. Quantitation of the radioactivity in these experiments is summarized in Table 1.3 and revealed the major product is [^{3}H]-$sTCH_2CoA$.

Table 1.3 Distribution of radioactivity among covalent and non-covalent intermediates from reactions of wt [^{3}H]-sT- $PhaEC_{Av}$ or wt $PhaC_{Re}$ and $HBCH_2CoA$.

Enzyme	[$HBCH_2CoA$]	[^{3}H]-$sTCH_2CoA$	[^{3}H]-sT_4CH_2CoA	[^{3}H]-labeled acids	Protein pellet
Wt [^{3}H]-sT-$PhaC_{Re}$	200 μM	23%	0%	23%	50%
Wt [^{3}H]-sT-$PhaC_{Re}$	5.5 mM	44%	0%	29%	24%
Wt [^{3}H]-sT-$PhaEC_{Av}$	490 μM	16%	6%	31%	37%
Wt [^{3}H]-sT-$PhaEC_{Av}$	10 mM	33%	6%	32%	22%

Similar experiments with C149S-$PhaEC_{Av}$ demonstrated that the same phenomenon is observed when HBCoA is used instead of $HBCH_2CoA$, and with primers other than sTCoA. Thus, the unusual results are neither primer specific nor specific to $HBCH_2CoA$. Furthermore, while priming of C149S-$PhaEC_{Av}$ with sTCoA results in CoA release as detected by DTNB assay (suggesting loading of the entire sT chain onto S149), ESI-MS of the protein immediately following the priming process revealed that the enzyme was acylated with sD, rather than sT. This result was interpreted to suggest that the sT chain may be first loaded to a site distinct from S149, followed by transfer of the sD chain to S149 where polymerization then occurs. This alternative loading site could be either S149 of the other PhaC subunit, or a different amino acid residue, such as another conserved Ser. HB-C149S-$PhaEC_{Av}$ is not detected by ESI-MS, likely due to its rapid hydrolysis following chain transfer. One model to explain these results is shown in Figure 1.15. The relevance of this model to the normal reaction mechanism is as yet unclear. Furthermore, the positions of the conserved residues relative to the active site on the threading

model of $PhaC_{Av}$ reveal no obvious candidates for a loading site. In the threading model of $PhaC_{Re}$, three absolutely conserved residues near the active site include T323, D351 and D428; however, there are no conserved Ser or Cys residues in the vicinity. The results are nonetheless interesting and reveal that synthases are capable of catalyzing unusual chemistry that requires further examination.

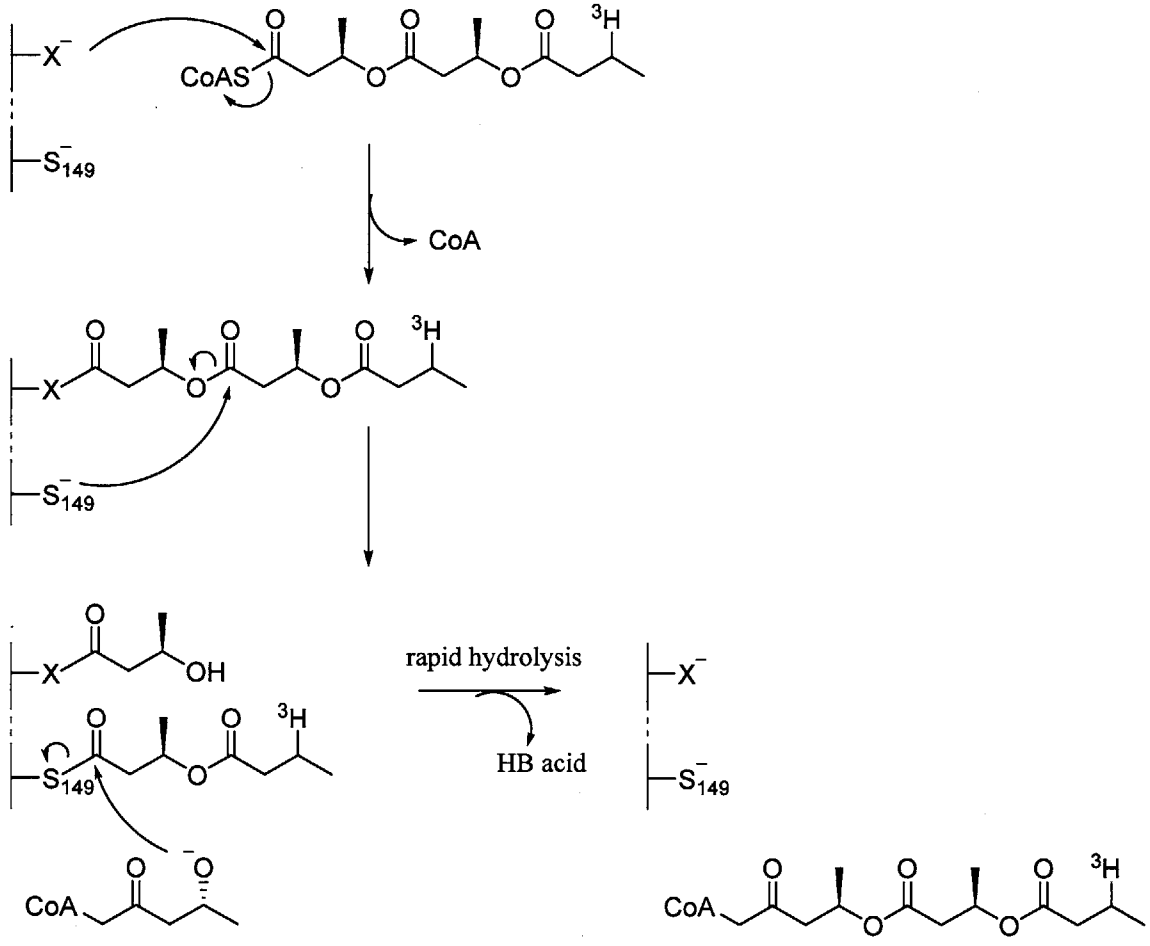

Figure 1.15 Proposed model to explain the unusual phenomenon observed in reactions between sT-PhaCs and the chain terminator $HBCH_2CoA$. X indicates a nucleophile (either C149 of the second PhaC subunit, or another nucleophilic amino acid). S can be either C149 or S149, in the case of the C149S mutant.

1.3.2.7 Experiments investigating the mechanisms of termination and reinitiation

The role of the synthase in termination and investigations into the nature of a putative chain transfer agent. PhaCs generate high M_w PHBs that are remarkably monodisperse, raising the question of how PHB M_w is sensed and what controls termination and reinitiation. Early experiments by Gerngross and coworkers suggested that PHB M_w is a property dictated by the synthase itself, rather than by HBCoA concentration (*79*). They demonstrated that low concentrations of $PhaC_{Re}$ in *in vitro* polymerization reactions resulted in higher M_w PHB than at higher concentrations. Furthermore, increasing the concentration of HBCoA from 0.9-8.9 mM did not affect the M_w of PHB, nor did terminating the reaction prior to complete substrate consumption.

In another study, our lab carried out *in vitro* studies with $PhaEC_{Av}$ to investigate how the synthase might catalyze termination and reinitiation. $PhaEC_{Av}$ was incubated with 70,000 equivalents of HBCoA and the reaction was monitored as a function of time by Western blot using antibodies to $PhaEC_{Av}$ (*75*). These experiments revealed that $PhaC_{Av}$ gradually disappears from its monomeric position on the gel as the reaction progressed, until a PHB chain of 1.8 MDa was synthesized (as judged by separate DTNB assays), after which $PhaC_{Av}$ reappears at its monomeric position. This suggests that $PhaC_{Av}$ is able to terminate and release the completed PHB chain. When a similar reaction was investigated at lower substrate to enzyme ratios, a time-dependent phenomenon was observed by SDS-PAGE and autoradiography: when $PhaEC_{Av}$ was incubated with [1-^{14}C]-HBCoA for extended periods of time, a species thought to be $PhaEC_{Av}$ labeled with 40-100 [^{14}C]-HB units converted to $PhaEC_{Av}$ labeled with 3-10 [^{14}C]-HB units (*75*). These results suggested that $PhaEC_{Av}$ catalyzed termination by hydrolysis of the PHB chain at a position removed from the active site Cys, leaving a primed synthase. The primed synthase is

likely PhaC that is covalently attached to an HB oligomer that is 3-10 HB units long. Hydrolysis could either occur by activation of a water molecule by an amino acid residue such as a conserved Asp, or by chain transfer directly to a nucleophilic residue followed by hydrolysis.

Other *in vivo* studies have suggested that the chain transfer agent may be a compound containing a hydroxyl group. In fermentations of *R. eutropha* under PHB accumulation conditions, the addition of compounds such as polyethylene glycol (*80*), glycerol (*81*) and 1,2-propanediol (*81*) resulted in PHB of a lower M_w than when the compounds were omitted. Furthermore, isolation and characterization of the PHB by NMR revealed that the alcohols were covalently attached to the carboxy terminus of the PHB chains (*81, 82*). These observations lead the authors to conclude that the alcohols served as more efficient chain transfer agents than a putative endogenous chain transfer agent, which they propose could be hydroxybutyrate. It should be noted that hydroxybutyrate as a chain transfer agent is pure speculation on the part of the authors, as this would be difficult to determine *in vivo*. An alternative explanation for the observations with alcohol chain terminators is that these compounds interact with the PHB granules themselves (rather than with the synthase active site) to catalyze transesterification. Thus, the evidence for alcohols serving as chain transfer agents is inconclusive. Finally, the results presented earlier in which $PhaC_{Re}$ was reacted with the substrate analog HB-NAC could also be interpreted as suggesting a mechanism for termination (*78*). In those experiments, the observation that the PHB chains terminated in NAC could be explained by one of two models. In the first model, discussed above, the chain could dissociate from the active site instead of reacylating the enzyme. Alternatively, the enzyme could reacylate with the growing chain, and the CoA liberated from the addition of the last HB unit could reattack either at the thioester of

the acylated enzyme or at an oxoester within the PHB chain. This latter mechanism would account for the observations of primed synthase following termination, as discussed above.

The role of PhaP in PHB chain termination. Finally, *in vivo* studies of *R. eutropha* grown in both rich TSB medium and nitrogen-limited PHB_{high} medium have examined the ratio of molecules of PHB to molecules of $PhaC_{Re}$ by quantitation of PHB amounts, GPC analysis of PHB M_w and Western blots of $PhaC_{Re}$ levels. These experiments demonstrated that PhaC is constitutively expressed in *R. eutropha*, and there are as many as 60-100 PHB chains per PhaC, depending on the growth condition (*56, 83*). This suggests that there are multiple reinitiation events per PhaC, that is, each PhaC makes several PHB chains. Recent studies carried out by our lab suggest that *in vivo* the ratio of PhaP1 to $PhaC_{Re}$ is responsible for determining the M_w of PHB. In a Δ*phaR* strain of *R. eutropha*, which overexpresses PhaP1, the ratio of PhaP1 to $PhaC_{Re}$ is higher than in wt, and the PHB M_w is lower, possibly due to increased chain termination events (*56*).

Working model for termination. Together these studies suggest a model whereby PhaC itself catalyzes termination, but PhaP "triggers" (by an unknown mechanism) the termination event. Termination by PhaC may be catalyzed by direct transfer of the PHB chain to a nucleophilic residue such as an Asp on the PhaC, followed by hydrolysis. Alternatively, termination may be catalyzed by hydrolysis via general base catalysis by PhaC on a water molecule or chain transfer to CoA or a hydroxyl-containing molecule, such as hydroxybutyrate.

1.3.3 Phasins and regulation of phasin expression in *R. eutropha*

1.3.3.1 PhaP1, PhaP2-7 and PhaM

Phasins are the predominant granule-associated proteins and have been identified in numerous organisms by analysis of their genomes and by their association with isolated PHB granules (*84*). Phasins are typically 13-25 kDa in M_w but have very little sequence conservation between organisms, in contrast to other proteins involved in PHB biosynthesis. The most well studied phasin is PhaP1, which is the major phasin in *R. eutropha* and can constitute up to 5% of the total cellular protein content in times of maximum PHB accumulation. PhaP1 was first identified associated with purified granules by Steinbüchel and coworkers in 1995 (*38*). Studies carried out in *R. eutropha* have provided much of the basis of our understanding of the role of phasins in PHB accumulation. TEM using gold-labeled PhaP1 antibodies demonstrated the *in vivo* association of PhaP1 with the surface of granules (*38*). Under nitrogen-limiting conditions, wt *R. eutropha* contains 5-15 granules that are 700-800 nm in diameter (Figure 1.16A) (*85*).

Deletion of *phaP1* of *R. eutropha* results in a strain that accumulated ~2-fold less PHB than the wt strain and the PHB was contained in a single, irregularly shaped granule (Figure 1.16B) (*38, 86*). Overexpression of PhaP1, on the other hand, results in the production of many smaller granules relative to wt (*38, 87*). These results led to the early proposal that PhaP1 controls the size and number of PHB granules and also prevents fusion of granules to control the surface area to volume ratio (*38*). However our recent cryoelectron tomography (cryoET) experiments investigating granule biogenesis in *R. eutropha* grown in medium promoting accumulation of PHB to 80% cdw suggests that in fact the granules are constantly fusing, thus PhaP1 may only function to prevent excessive fusion (*85*).

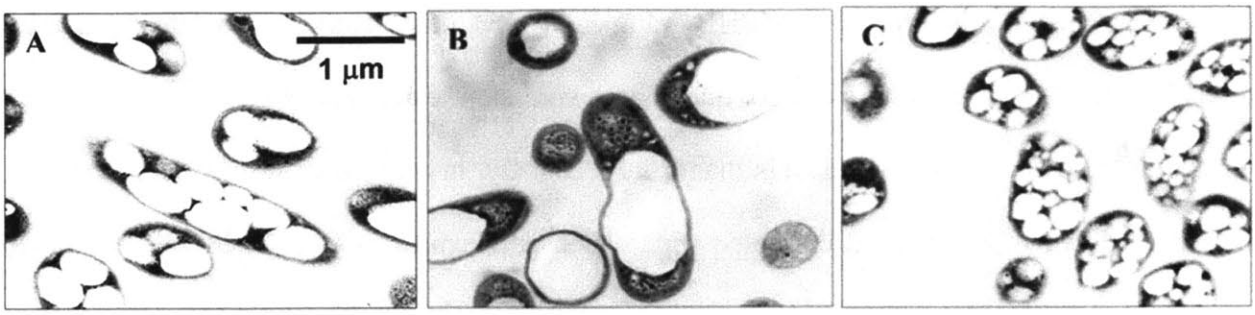

Figure 1.16 TEM of A) wt *R. eutropha*, B) Δ*phaP1* and C) Δ*phaR*, PhaP1 overexpression. Figure adapted from reference (*1*).

Additional evidence for the role of PhaP1 in controlling the number and size of granules was provided by *in vitro* studies of synthesis of PHB granules by $PhaEC_{Av}$ monitored by scanning electron microscopy (*88*). These studies demonstrated that addition of PhaP1 from *R. eutropha* resulted in the synthesis of many smaller granules compared to those synthesized in the absence of PhaP1. From the information provided, we estimate that the concentrations used in their assays were 10 nM $PhaEC_{Av}$ and 250 nM PhaP1. Additionally, Horowitz and Sanders demonstrated by solid-state NMR spectroscopy that PHB in granules *in vivo* is amorphous rather than crystalline (*89*). They proposed that an amphipathic species such as a granule-associated protein could bind the surface to prevent coalescence of smaller granules into larger ones, which otherwise would promote nucleation events that would result in crystalline polymer. Thus, it has been suggested that phasins play a role in preventing crystallization of PHB. Crystallization prevents reutilization of PHB by intracellular depolymerases, which act only on amorphous PHB (as discussed below).

Subsequent to the discovery of PhaP1, several additional phasins were identified in *R. eutropha (39)*. Genome scanning studies carried out by Pötter and coworkers identified three additional phasins based on 40-50% homology to PhaP1, which they called PhaP2, 3 and 4 (*42*). They demonstrated the granule association of PhaP3 and PhaP4 by 2D PAGE of PHB granules.

PhaP2 was shown to bind crystalline PHB granules *in vitro*, though this is tenuous evidence that PhaP2 is a phasin. The authors did not quantitate expression levels, but PhaP3 and 4 are present on the granules at much lower levels than PhaP1. Finally, in a mutant strain of *R. eutropha* in which the *phaP1* promoter is disrupted (but which still expresses low levels of PhaP1), the authors demonstrated an apparent increase in the amount of PhaP3 associated with isolated granules, as judged by Coomassie-stained SDS-PAGE (*42*). Construction of the individual deletion strains of *phaP2*, *phaP3* or *phaP4* had no discernible effect on growth, PHB accumulation or granule size and number.

In efforts to find new players in PHB biosynthesis in *R. eutropha*, Pfeiffer and coworkers screened for protein-protein interactions using $PhaC_{Re}$ and PhaPs 1-4 as bait in two-hybrid assays, and in this way discovered a fifth phasin, PhaP5, that interacted with PhaP2 (*43*). Deletion of *phaP5* revealed that it is also not essential for PHB accumulation. And finally Pfeiffer and coworkers found PhaP6 and PhaP7 by examining the *R. eutropha* genome for proteins containing the "phasin 2 motif," which is a stretch of sequence enriched in hydrophobic residues (*44*). They demonstrated that enhanced yellow fluorescent protein (eYFP) fusion constructs with PhaP1-7 colocalized with PHB granules during PHB production but were diffuse in the cytoplasm in the absence of PHB. Each of these fusion constructs was under the regulation of the *phaCAB* operon promoter, so their actual expression levels in these experiments likely varied greatly from their native expression levels. Deletion of *phaP6* or *phaP7* had no discernible effect on PHB accumulation. Thus, while PhaP2-7 may be granule-associated, their roles (if any) in PHB biosynthesis are not well understood.

One additional granule-associated protein, PhaM, was recently identified by Jendrossek and coworkers by two-hybrid assay using $PhaC_{Re}$ and PhaP5 as bait. Independently, Cho *et al.* in

our lab found PhaM associated with PHB granules in *R. eutropha* (*73, 90*). Studies by the Jendrossek lab demonstrated that deletion of *phaM* results in a strain in which PHB granules are unevenly segregated between daughter cells during division. PhaM contains a Histone-like domain, rich in Ala, Lys and Pro, and non-specifically binds DNA *in vitro*, thus Jendrossek *et al.* suggested that PhaM functions to anchor PHB granules to the nucleoid to promote even distribution between daughter cells during division (*90, 91*). Interestingly, isolation of Strep2-tagged $PhaC_{Re}$ by Cho *et al.* revealed not only high M_w PHB and PhaP1 associated with the synthase, but also DNA and PhaM, consistent with the role proposed by Jendrossek and coworkers (*73*).

1.3.3.2 Structure of PhaP1 and interaction with $PhaC_{Re}$

There is currently no X-ray structure available for any phasin protein. Small angle X-ray scattering studies predicted that PhaP1 is a flat, triangular homotrimer with a side length and height of 80 ± 3 and 26 ± 1 Å, respectively (*92*). In the same study, the authors attempted to identify a particular sequence within PhaP1 that is responsible for binding to PHB. A variety of truncations of PhaP1 were fused to GFP and their PHB binding capacity assayed by fluorescence and co-precipitation with PHB granules *in vitro*. These studies failed to identify a particular portion of the PhaP1 sequence responsible for binding PHB granules. There is also no direct evidence for interactions between $PhaC_{Re}$ and PhaP1 *in vivo* or *in vitro*. Jendrossek and coworkers used two-hybrid screens to identify interaction partners with $PhaC_{Re}$, but PhaP1 was not among the proteins identified (*43, 90*). Furthermore, pull-down studies in our lab confirm that $PhaC_{Re}$ and PhaP1 do not associate *in vitro*, though PhaP1 increases the length of the lag phase and decreases the specific activity of $PhaC_{Re}$ (*56*).

1.3.3.3 Expression levels of PhaP1 in R. eutropha

PHB accumulation in *R. eutropha* has been studied by our lab primarily in two growth conditions: the nutrient rich medium tryptic soy broth (TSB) and the nitrogen-limited medium supplemented with fructose, PHB_{high} (*83, 86, 93, 94*). In TSB, *R. eutropha* transiently accumulates PHB to a maximum of 25% cdw after 4 h, then declines to <5% cdw (Figure 1.17A). In PHB_{high}, *R. eutropha* accumulates PHB from a minimum of 5% to a maximum of 80% of the cdw (Figure 1.17B). We have thus far not identified growth conditions in which *R. eutropha* contains less than ~5% PHB cdw.

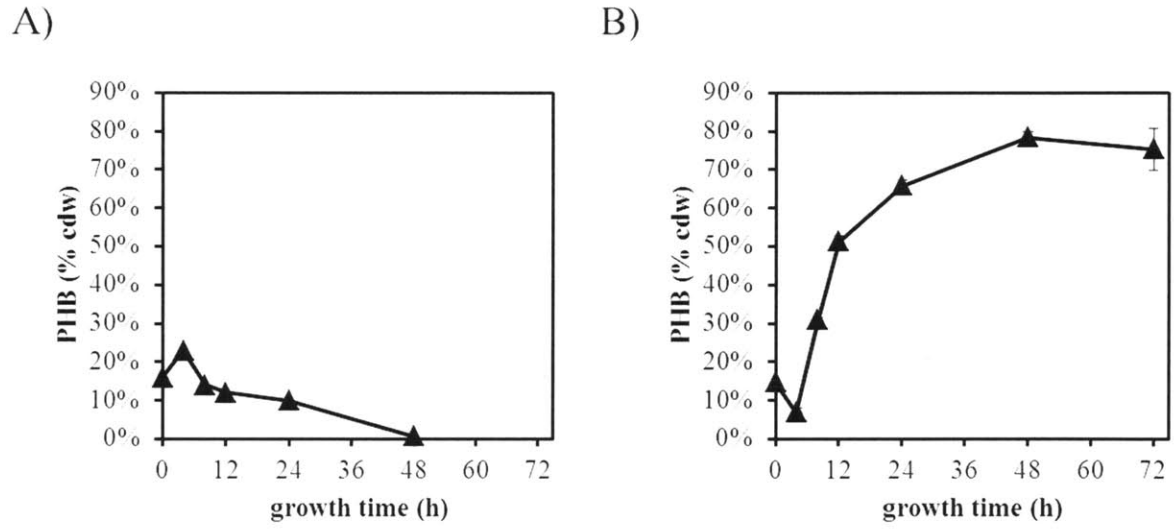

Figure 1.17 PHB content of *R. eutropha* grown in A) TSB medium and B) PHB_{high} medium. A is adapted from (*94*). B is adapted from (*56*).

Analysis of PhaP1 expression levels using antibodies and Western blots carried out in *R. eutropha* grown in these media has provided additional insight into the function of PhaP1. Studies from our lab demonstrated that PhaP1 expression is correlated with PHB accumulation and is dependent on the expression of an active $PhaC_{Re}$ (*86, 95*). Western blots of PhaP1 levels and GPC analysis of the M_w of PHB allowed a quantitative examination of PhaP1 and PHB

levels. In *R. eutropha* grown 4 h in TSB medium there are one or two PhaPs per PHB chain (*83*). After 24 h growth in PHB_{high} medium, the molar ratio of PHB to PhaP is ~2 (He and Stubbe, unpublished data). These observations inspired a more thorough investigation of the PHB to PhaP1 ratio in PHB_{High} medium, which found that this ratio remained between 1-2 throughout growth (*56*).

1.3.3.4 Regulation of PhaP1 expression by PhaR

PhaP expression is thought to be coupled to PHB biosynthesis by the transcription factor PhaR. The working model for regulation by PhaR is given in Figure 1.18. In this model PhaR represses PhaP expression until PHB is produced by the constitutively active PhaC. PHB is proposed to bind PhaR to allow PhaP expression. This model was proposed on the basis of observations made in *Paracoccus denitrificans* and *R. eutropha*, which are discussed below.

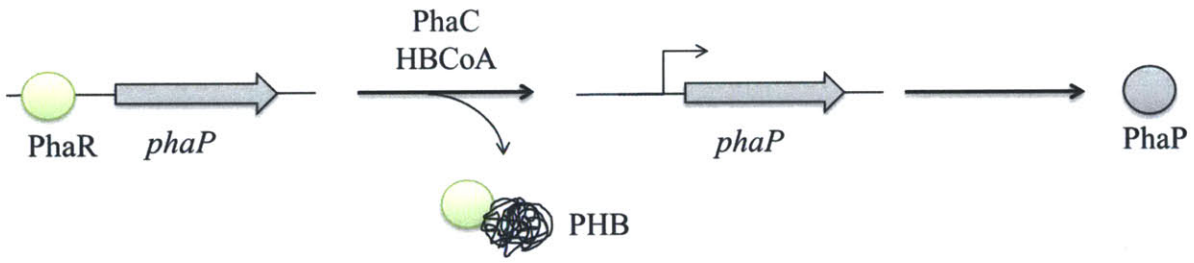

Figure 1.18 Working model for regulation of *phaP* expression by PhaR. PhaR is also thought to regulate its own expression by a manner similar to that illustrated for PhaP. Adapted from reference (*2*).

Studies of PhaR from *P. denitrificans* by Maehara and coworkers provided the first insight into the regulation of phasin expression (*96*). *P. denitrificans* produces PHB via the protein products of the *phaZCPR* operon. Maehara *et al.* noted that *phaR* encoded a protein of unknown function that was conserved in *R. eutropha*, *Allochromatium vinosum*, *Rhizobium meliloti* and *Thiocystis violacea*. They demonstrated by gel mobility shift assays that PhaR bound the intergenic regions of *phaC-phaP* and *phaP-phaR* in the *phaZCPR* operon. It should be noted

however, that gel mobility shift experiments are inherently difficult to conduct, as the association of transcription factors to DNA is particularly sensitive to the concentration of Mg^{2+}. In fact, Maehara and coworkers omitted Mg^{2+} all together from some of their gel shift assays. To examine the effect of PhaR on *phaP* expression, they established a cell free protein expression system in *E. coli* harboring *phaP* on a plasmid, and demonstrated that addition of PhaR repressed expression of *phaP*. Addition of PHB to the cell-free expression system derepressed the transcription of *phaP (97)*. However, as the amount of PHB added to the expression system was increased, PhaP expression decreased, which is inconsistent with the model in Figure 1.18. The authors explained this unexpected result by suggesting that proteins involved in transcription and translation were non-specifically binding to the added PHB, thus decreasing PhaP expression in a manner un-related to PhaR regulation. This underscores the caution that must be taken in over-interpreting the *in vitro* association of proteins to granules, as well as the necessity for *in vivo* studies, such as those described subsequently. Maehara and coworkers were able to demonstrate the presence of PhaR on native PHB granules, isolated by sucrose density gradient ultracentrifugation, by Western blot analysis using antibodies to PhaR. PhaR was also present in the soluble cell fraction of cell lysates (*97*). Again, however, many proteins non-specifically adhere to PHB granules due to their hydrophobic nature.

R. eutropha contains a homolog to *P. denitrificans phaR* just 0.45 kb downstream of the *phaCAB* locus. Our lab has carried out *in vivo* studies in *R. eutropha*, which have contributed several observations about the roles of PhaR and PhaP1 in PHB biosynthesis. Deletion of *phaR* resulted in reduction of PHB accumulation to ~70% the level of the wt strain. Furthermore, PhaP1 expression was uncoupled from PHB accumulation such that PhaP1 levels were constitutively high and not correlated with the amount of PHB in the cell (*40*). PhaP1 expression

was constitutive even in a Δ*phaR*Δ*phaC* double mutant incapable of accumulating any PHB. A Δ*phaP1*Δ*phaR* mutant strain exhibited a more severe defect in PHB accumulation than the Δ*phap1* mutant strain, thus PhaR may play additional roles in PHB accumulation aside from regulation of PhaP1 expression, including but not limited to, regulating its own expression (*40*).

Collectively, the studies described in this section support the working model shown in Figure 1.18. However, as there are no precedents for such a model of regulation in other non-template driven biological polymerizations, the mechanisms of regulation of PHB biosynthesis require additional study. Furthermore, the mechanisms of regulation of PHB biosynthesis may turn out to be organism specific.

1.3.4 PHA depolymerases

The final major players in PHB biosynthesis are the PHB depolymerases, collectively called PhaZs. There are two kinds of depolymerases, namely the extracellular and intracellular depolymerases. Extracellular depolymerases degrade crystalline PHB, which is found in the environment as a result of its release by dead bacteria or as biodegradable commercial goods. Intracellular depolymerases are structurally distinct from extracellular depolymerases and act on amorphous PHB, which is found inside the cell. Intracellular depolymerases are responsible for, among other likely functions, the mobilization of PHB granules inside the cell when the environment is conducive for growth and division (i.e. a limiting nutrient is restored).

Characterization of intracellular PHB depolymerases requires a good assay for activity *in vitro*, which as yet is not available. One issue is that depolymerases only act on amorphous PHB as it is found *in vivo*. Native granules isolated from the organism cannot be used as substrate for *in vitro* assays because intracellular PhaZs co-purify during isolation. Thus artificial, amorphous

granules prepared from crystalline PHB using detergents (*98*), short HB_n oligomers (n = 2-4) or *p*-nitrophenyl esters are used as substrates. In assays that use HB_n oligomers are substrates, hydroxybutyrate (HB) dehydrogenase is used to measure release of HB. However, release of HB is a few steps removed from the first events of depolymerase activity, the release of HB_n oligomers, and is catalyzed by oligomer hydrolases included in assay mixtures. Due to these issues, depolymerases are typically identified by homology to known depolymerases and characterized primarily by *in vivo* genetic experiments.

R. eutropha has at least six intracellular depolymerases, which have been identified by genetic screening methods. The first intracellular depolymerase, now called PhaZa1, was identified by shotgun gene cloning by Saito and coworkers (*99*). They purified PhaZa1 from recombinant *E. coli* for preparation of antibodies, and demonstrated by Western blot analysis that PhaZa1 was associated with PHB granules *in vivo*. A null mutant was still capable of degrading PHB, leading the authors to propose that *R. eutropha* contained multiple depolymerases. Artificial granules were synthesized and used to characterize the *in vitro* activity of PhaZa1, which was found to release primarily HB oligomers as product with a specific activity of ~1 μmol/min/mg (*100*). Studies from our lab identified two additional intracellular depolymerases, PhaZa2 and PhaZa3, based on ~30% sequence identity with PhaZa1. The PHB accumulation and utilization phenotypes of a series of single, double and triple mutant strains of *phaZa1*, *phaZa2* and *phaZa3* were examined (Δ*phaZa1*, Δ*phaZa2*, Δ*phaZa3*, Δ*phaZa12*, Δ*phaZa13*, Δ*phaZa23*, and Δ*phaZa123*) (*101*). These results demonstrated that PhaZa1 and PhaZa2 were sufficient to account for PHB degradation during growth on rich medium and PHB utilization medium, but did not identify a role for PhaZa3. Saito and coworkers identified two HB oligomer hydrolases, PhaZb and PhaZc, as well as a fourth intracellular depolymerase, PhaZd (*100, 102, 103*). PhaZb,

PhaZc, and PhaZd were present in both the cytosolic cell fraction and associated with PHB granules, and individual deletion of any one resulted in higher levels of PHB during accumulation and degradation. These results were interpreted to suggest that these enzymes play a role in PHB utilization.

Several studies under different growth conditions have examined the expression levels of the various depolymerases and oligomer hydrolases in order to gain insight into their roles in PHB biosynthesis and homeostasis. mRNA profiling and Western blot analysis indicates that PhaZa1 is constitutively expressed in both nutrient rich and nitrogen-limited media (*93*). PhaZa2 and PhaZd protein levels increase during PHB accumulation, then decrease during PHA utilization (*83, 93, 100*). Differential expression patterns suggest the various depolymerases have different roles in PHB biosynthesis that are still not well understood. How their activity is regulated to prevent futile cycling, that is, simultaneous synthesis and degradation of PHB, is also unclear. Jendrossek and coworkers demonstrated that native granules isolated from *R. eutropha* can catalyze the formation of HBCoA when exogenous CoA is supplied (*104*). PhaZa1 incubated with artificial granules and CoA also catalyzed the formation of HBCoA, thus the authors suggested that PhaZa1 catalyzes thiolysis rather than hydrolysis to break down PHB. This is an attractive proposal as it explains how cells can avoid futile cycling when PhaC and PhaZs are expressed simultaneously.

1.4 Working model for granule formation

1.4.1 Size, composition and properties of PHB granules

A model that describes the process of granule formation must take into account several properties of the granules. First, soluble monomeric precursors are converted into large insoluble

polymers, which are packaged in granules, via a process that does not expose the cell to the toxic effects of exposed hydrophobic polymer chains. At early stages in granule formation in *R. eutropha* (when the cells contain 5-10% PHB cdw), the granules are small, typically ~100 nm in diameter (*85*). As PHB levels increase, granules fuse and the resulting granules have diameters of 600-700 nm (*85*). Second, the PHB in the granules is amorphous (*89*). How crystallization of PHB, which readily occurs when granules are isolated from bacteria, is prevented during granule formation must be accounted for.

Finally, a suitable model for granule formation must account for the composition of the granule surface. To study the composition of granules, Griebel and coworkers developed a density gradient centrifugation method to isolate PHB granules from *Bacillus megaterium* that minimally disrupted the granule structure (*105*). They determined that the granules were composed of 97-98% PHB, 2% protein and 0.5% lipid by mass. They demonstrated that the isolated granules catalyzed the polymerization of [^{14}C]-HBCoA into polymer, suggesting that the PHB synthase was associated with the granule surface. Western blot analysis and TEM using gold-labeled antibodies have demonstrated that several proteins are associated with the surface of the granules. As discussed above, PhaP1 is the predominant granule-associated protein in *R. eutropha*, and it covers 20-30% of the granule surface during growth in PHB_{high} medium (*38, 56, 85, 92*). PhaC, PhaZs and PhaR are present in much lower levels (*87, 99, 106*). As discussed above, various studies from our lab have demonstrated that in mature granules in *R. eutropha*, there are 1-2 PHB chains per PhaP1 (*56, 83*).

The role that lipids play in the surface structure of PHB granules has been controversial. Isolation of granules, even by "gentle" methods such as ultracentrifugation, can potentially result in the non-specific association of hydrophobic species such as membrane proteins and lipids.

Mayer and Hoppert used TEM to examine the surface of PHB granules in ultrathin sections of *R. eutropha (107)*. They identified a boundary layer with a thickness of 3-4 nm, consistent with a lipid monolayer. Atomic force microscopy (AFM) studies of the surface of PHB granules isolated from lysed *R. eutropha* suggested the presence of a protein-based network layer, proposed to be composed of PhaP1, surrounding the PHB granules. The network layer is in turn covered by a smooth outer layer of unknown composition (*108*). It is important to note that both of these techniques are rather perturbative. In the case of TEM, samples must be dehydrated, stained and embedded in plastic. In the case of the AFM studies, the cells were lysed and the granules were dried on the sample stage. Furthermore, tips used in AFM can cause sample deformation. Recently our lab in collaboration with the Jensen lab examined the granule surface using cryoET (*85*). Sample preparation for cryoET is mild: the cells are flash frozen in liquid ethane, and following imaging, remain viable when thawed. By this method we have demonstrated that the granules are surrounded by a discontinuous, "patchy" layer, inconsistent with the observations by both TEM and AFM.

1.4.2 Previous models to describe granule formation

Three models have been proposed in the literature to describe granule formation *in vivo*. The models described in this section are summarized in Figure 1.19.

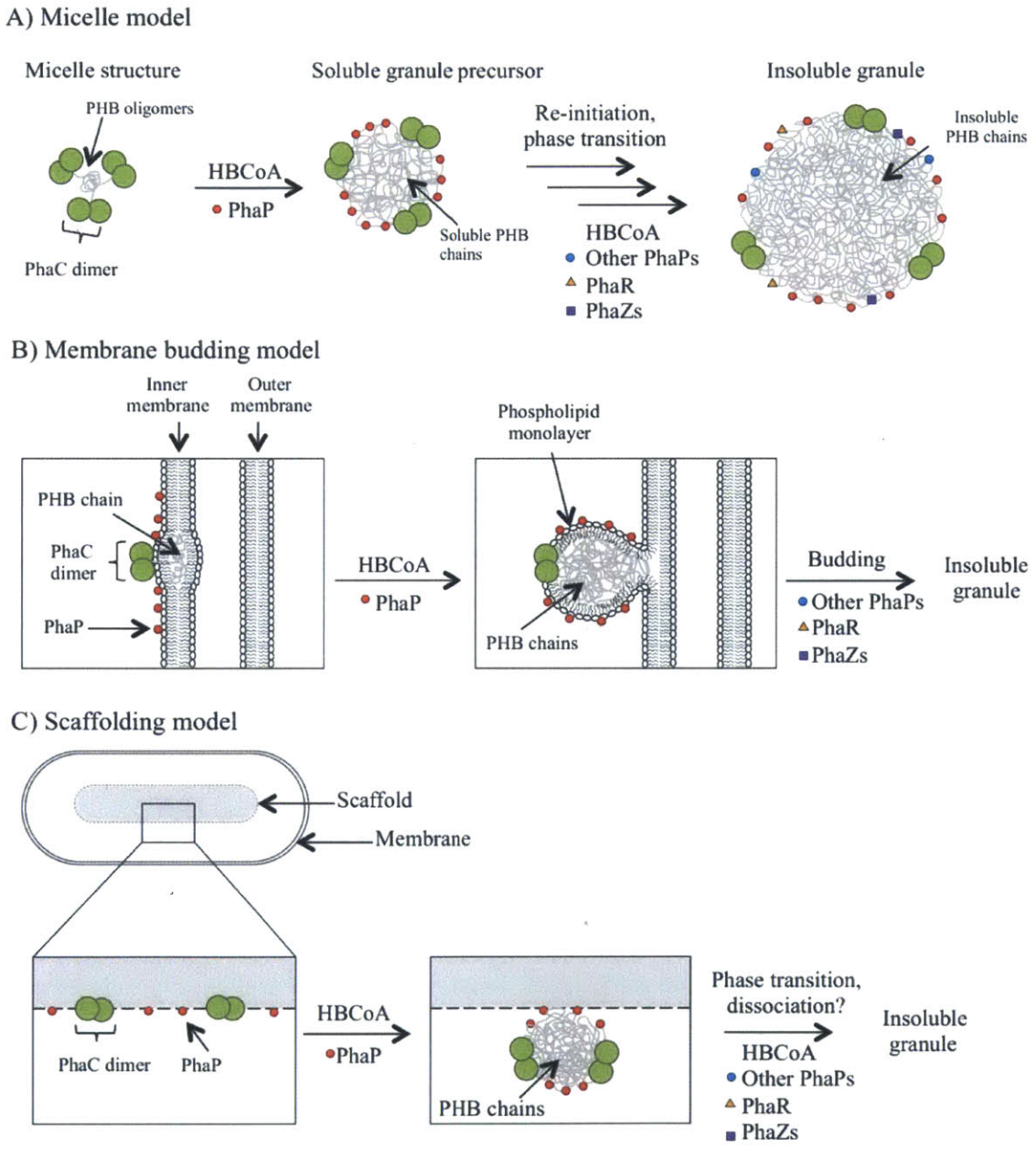

Figure 1.19 Models for granule formation. A) Micelle model. B) Membrane budding model. C) Scaffolding model. Adapted from (*56*).

Micelle model (Figure 1.19A). The micelle model was the earliest model proposed to describe granule formation. The model proposes that granules are formed by random aggregation of granule-nucleating species consisting of short PHB chains, covalently linked to PhaCs and non-covalently associated with PhaP, into micelle structures. As the chains elongate by addition of more HB units, the phase transition from soluble short PHB oligomers to insoluble polymer occurs. As discussed above, various experiments suggest that initiation of polymerization is much slower than elongation both *in vitro* and *in vivo (49, 75)*. This observation seems at odds with a simple micelle model as one would expect that if only a small fraction of PhaCs were synthesizing polymer rapidly, there would not be sufficient time for small PHB chains to aggregate into micelles. Furthermore, analysis of PHB by GPC in *R. eutropha* grown in PHB_{high} reveals that the M_w is high even when the cells contain very little PHB (*56*).

Membrane budding model (Figure 1.19B). An alternative model, the membrane budding model, was proposed by our lab and was based on eukaryotic lipid body biosynthesis (*1, 2*). This model could account for the presence of lipids on the surface of the granules. In this model, PhaP and PhaC are associated with the inner leaflet of the plasma membrane and the growing PHB chains are extruded into the membrane. The chains aggregate and form a granule, which eventually buds off of the membrane. In this model the phase transition occurs in the membrane and the granule is at least partially coated in a monolayer of membrane-derived lipids. A variant of this model specifies that the granules bud from the membrane at the cell poles and the sites of future poles based upon fluorescence imaging studies (*43, 109*). A specific prediction of the membrane budding model is that lipid biosynthesis is upregulated during PHB accumulation to account for the loss of lipid from the membrane. However recent microarray data from the Sinskey lab suggest that the biosynthesis of the major membrane lipids in *R. eutropha,*

phosphatidylethanolamine and phosphatidylglycerol/cardiolipin, is downregulated under conditions that promote PHB accumulation (*110*). These findings are inconsistent with a membrane budding model.

Scaffolding model (Figure 1.19C). A third model, the scaffolding model, was also proposed by our lab on the basis of TEM time course studies of *R. eutropha* grown in PHB_{high}. The images reveal a dark-stained feature along the center axis of the cell. Clustered around this "mediation element" are several tiny (~100 nm in diameter) granules (Figure 1.20A) (*94*). PhaP and PhaC are associated with the scaffold, which was proposed at the time to be composed of DNA, protein or both. The scaffold serves to locally concentrate the PhaC and PhaP to allow for granule nucleation and growth. As the granules grow larger the mediation element is no longer observed, either due to its degradation, or because larger PHB granules obscure it (Figure 1.20D). This model predicts that the granule surface is composed of PhaP and PhaC with no phospholipid component.

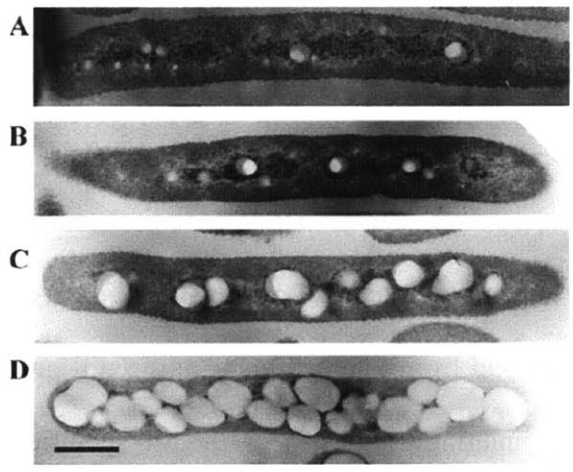

Figure 1.20 TEM of *R. eutropha* showing the dark-stained feature, or "mediation element." The cells were grown in nitrogen limited PHB_p medium for A) 2.5 h, B) 5 h, C) 9 h and D) 24 h. Scale bar is 0.5 μm. Adapted from reference (*94*).

1.4.3 Current working model for granule formation: the modified micelle model

Our recent cryoET data and biochemical studies of $PhaC_{Re}$ isolated for the first time from *R. eutropha* have led us to favor a variation of the micelle model shown in Figure 1.19A, which we call the modified micelle model. This model is diagrammed in Figure 1.21. The primary difference between this model and the original micelle model is that the nucleating species is composed of a dimer of PhaC covalently attached to a PHB chain with several (4-9) PhaPs also associated. This initial "nucleating species" is soluble, which may be due to its high PhaP/PHB ratio. The nucleating species grow as more PHB is synthesized, with PhaC catalyzing termination and reinitiation of new PHB chains. As the nucleating species grow larger and fuse, the ratio of PHB/PhaP reaches 1-2. During growth and fusion of the nucleating species, the phase transition occurs, and the mature granules become insoluble. PhaR, PhaZs and other granule associated proteins attach to the mature granules. The following paragraphs discuss the evidence supporting the modified micelle model.

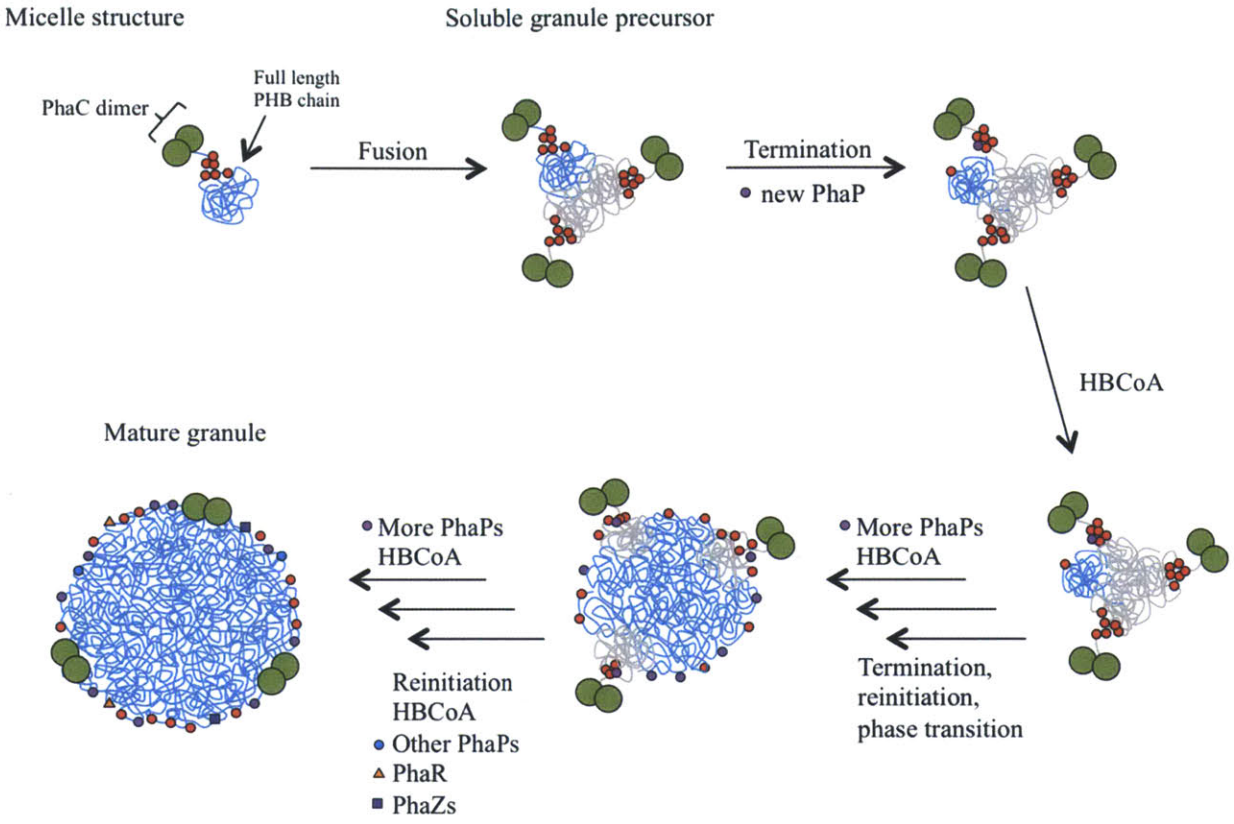

Figure 1.21 Modified micelle model. This model differs from the original micelle model primarily in the composition of the nucleating species. In the modified micelle model, this species contains a PhaC dimer, several PhaPs and full length PHB. Several nucleating species fuse and each completed PHB chain remains associated with a PhaP after termination. As the species fuse the soluble-to-insoluble phase transition occurs and other granule-associated proteins bind. Adapted from reference (*56*).

Evidence for the nucleating species comes from work by our lab in collaboration with the Sinskey lab, which reported the first isolation of $PhaC_{Re}$ from the native organism (*73*). A Strep2-tagged *phaC* was incorporated into the *R. eutropha* genome in place of the wt *phaC* gene. The cells were then grown in TSB medium that promotes the transient accumulation of PHB to a maximum of ~15% PHB cdw after 4 h growth (Figure 1.17A). The affinity-tagged synthase was isolated at the 4 h time point. While the original goal of this experiment was to identify a protein factor responsible for modulating the rates of initiation and elongation such that they are more

evenly matched, no factor was found. Instead, a soluble species containing high M_w PHB, PhaC and PhaP1 was unexpectedly isolated. This is the nucleating species proposed in Figure 1.21 and accounted for 17% of the total PHB in the cells (*73*). Analysis of the M_w of PHB in the soluble and insoluble fractions confirmed that the soluble species is full-length, ~300 kDa under these growth conditions. Western blots of PhaP1 and PhaC levels and analysis of PHB content in the soluble species revealed that the nucleating species contained 1-3 PhaC molecules, 4-9 PhaP1 molecules, and one PHB chain (*73*). The model proposes that the nucleating species fuse as reinitiation events occur and the ratio of PhaP to PHB approaches 1, as observed in the whole cell analysis described in previous sections. The fact that PhaR or other known granule-associated species did not co-purify with the nucleating species suggest that these proteins bind the mature granules. A complication of these experiments that must be considered is that in the engineered strain of $PhaC_{Re}$, StrepII-PhaC was 30-fold overexpressed relative to PhaC in the wt strain, in spite of being under control of the endogenous promoter. Furthermore, in wt *R. eutropha* the PHB M_w is ~1,000 kDa, vs. 300 kDa in the engineered strain.

CryoET experiments carried out by our lab in collaboration with the Jensen lab support a model in which PHB granules initiate and remain cytoplasmic throughout formation, consistent with the modified micelle model (*85*). The distribution within the cytoplasm shows no bias towards localization near the membrane, which argues against a membrane budding model. A membrane budding model would also suggest at least partial coverage of the granule surface with lipids. As discussed above, investigation of the surface of the PHB granules in the cryoET tomographs revealed that the surface was discontinuous, or "patchy." The patches on the surface layer were of low contrast and only ~2 nm thick, too thin to be a lipid mono- or bilayer. In contrast, membranes observed in the tomographs are high contrast and continuous (*85*). CryoET

experiments also revealed the propensity of the granules to fuse as PHB synthesis continues, as evidenced by non-spherical granules that resembled two granules of different radii that had just fused.

While our TEM studies, which led to the scaffolding model for granule formation, did not identify the composition of dark-stained feature, cryoET studies suggested that it is nucleoid. An interesting result of the studies above was the finding that DNA was also associated with the nucleating species. In addition to PhaC and PhaP1, PhaM also co-purified with the nucleating species (*73*). PhaM was subsequently identified by Jendrossek and coworkers and its role characterized as discussed above (*90*). The proposed function of PhaM is to anchor PhaC to the nucleoid to promote even segregation of PHB granules between daughter cells during division (*90, 91, 111*). These findings could be integrated into the modified micelle model to reconcile the present studies with previous studies suggesting the presence of a scaffold. Granule self-assembly from the nucleating species is cytoplasmic and may occur associated with nucleoid as a scaffold.

Together these data convincingly support the modified micelle model for granule formation in *R. eutropha* as shown in Figure 1.21. However, our experiments have been primarily restricted to *R. eutropha*, and as discussed above, growth conditions have not yet been identified in which the cells contain <5% PHB cdw (*94*). In order to look at granule formation in cells containing <5% PHB cdw and to investigate the universality of the mechanism of granule formation, we have investigated PHB biosynthesis in *C. crescentus*, which is described in detail in Chapter 3 of this thesis.

1.5 Lifestyle of *Caulobacter crescentus*

1.5.1 Early isolations and descriptions of *Caulobacter crescentus*

This thesis presents studies focused on characterizing the PHB biosynthetic apparatus in *Caulobacter crescentus*, an oligotrophic, Gram-negative aquatic bacterium that is well-adapted to living in nutrient-poor environments. Some of the first reported strains belonging to the genus *Caulobacter* were isolated from tap water (*111*). The first description of the genus *Caulobacter* was published in 1935 by Henrici and Johnson, who isolated bacteria attached to a microscope slide that had been submerged in lake water (*112*). After extensive rinsing the bacteria remained attached. The authors described the cell morphology as curved with rounded ends, and having a long slender stalk protruding from one end of the cell, with what they designated holdfast material at its distal end. This holdfast material appeared to anchor the cell to the surface of the microscope slide.

Subsequent studies unraveled the dimorphic lifestyle of *Caulobacters*, specifically that of *Caulobacter crescentus*. The stalked cell described in 1935 is one of two cell forms that *C. crescentus* adopts. Each round of cell division produces a sessile stalked cell and a motile flagellated cell, called a swarmer cell (Figure 1.22) (*113-115*). The stalked cell is capable of DNA replication and immediately begins a new round of cell division. The swarmer cell, however, cannot initiate DNA replication and remains for a period of time (the length of which is dependent in part on nutrient availability) in the swarmer stage before differentiating into a stalked cell. As such, *C. crescentus* has been widely studied in the last several decades as a model for differentiation and cell cycle regulation (*113, 114*).

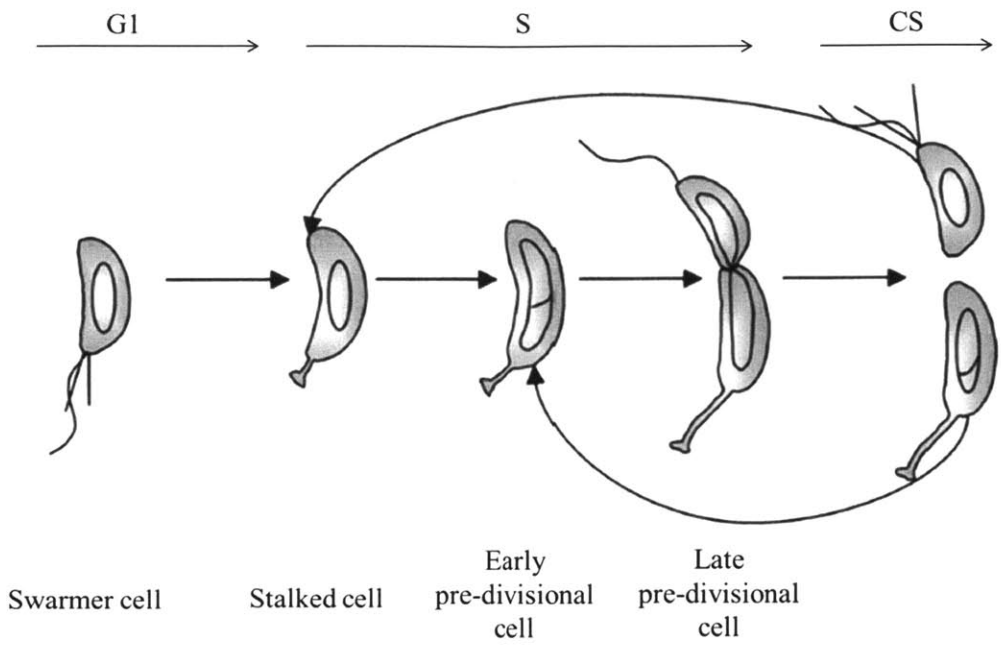

Figure 1.22 Lifecycle of *C. crescentus*. The motile swarmer cell remains for a certain period of time in the G1 phase before differentiating into a sessile stalked cell. The stalked cell is capable of DNA replication and immediately begins a round of cell division. Each stalked cell produces one stalked cell and one swarmer cell which begin the cycle anew. G1, lag phase before DNA replication. S, period of new DNA synthesis. CS, cell separation. Adapted from reference (*114*).

1.5.2 Adaptations to living in nutrient poor environments

As mentioned above, early isolates of the genus *Caulobacter* were obtained from dilute aquatic environments, tap water and even distilled laboratory water (*111, 115*). Enrichment of *Caulobacters* could be achieved by allowing extended growth that resulted in depletion of the medium to nutrient levels that cannot support most strains of bacteria. The remaining viable bacteria that did propagate were typically members of the genus *Caulobacter*. Several strains of *Caulobacter* were initially isolated, characterized and propagated. Of these strains, *Caulobacter crescentus* CB15 became the predominant laboratory strain, characterized by its ability to be synchronized owing to the different densities of stalked and swarmer cells that allowed their separation by centrifugation (*115*). After propagation of CB15 in the laboratory, the strain

spontaneously mutated and lost the ability to be synchronized. The mutation causing this behavior was never identified. However, through careful propagation of individual colonies of *C. crescentus* CB15, a mutant that was still synchronizable was once again identified. This strain, now called *Caulobacter crescentus* NA1000, is the predominant laboratory strain of *C. crescentus* studied today, and is the focus of the studies presented in this thesis.

One of the hallmarks of *C. crescentus* is its ability to thrive under low-nutrient conditions, such as those that promote accumulation of PHAs. This adaptation is achieved in part by its dimorphic lifestyle. Each round of cell division produces one sessile cell and one swarmer cell. The swarmer cells have the ability to disperse and find new nutrient sources. They can then differentiate into stalked cells and enter another round of division. Having one motile daughter cell that disperses from the sessile daughter cell eliminates competition for resources between successive generations and therefore allows greater propagation of the species in otherwise low-nutrient environments.

A second adaptation to nutrient-limited conditions is the stalk, which is an extension of the inner membrane, peptidoglycan and outer membrane of the cell. There are numerous theories as to what role the stalk might play. One hypothesis is that the stalk increases the buoyancy of the cell and keeps the cells near the air-water interface in aquatic environments, essential for an obligate aerobe such as *C. crescentus (115)*. Under conditions of phosphate limitation, the stalk elongates to 10 times its ordinary length. Stalks serve to anchor the cell to a surface, so stalk elongation at times of nutrient limitation would allow the cell to extend farther beyond the surface. This extension would reduce competition between *C. crescentus* and a nascent biofilm also associated with the same surface, for example. The validity of these theories is rather difficult to assess experimentally. However, the role of the stalk in phosphate uptake has been

studied experimentally by electron microscopy (*116, 117*). Elongation of the stalk under phosphate limitation also serves to increase the surface area to volume ratio of the cytoplasm for enhanced nutrient uptake. Brun and coworkers carried out 2D gel electrophoresis of the proteins of the stalk of *C. crescentus* cells grown 3-5 days on minimal medium until phosphate was limiting (*118*). They found that the stalk was devoid of cytoplasmic proteins and enriched in periplasmic and outer membrane proteins. The proteins were identified and many were involved in cell motility and secretion, and inorganic ion uptake and metabolism. These findings are compatible with the hypothesis that the stalk is involved in nutrient uptake.

The sequencing of the *C. crescentus* genome allowed a more thorough genetic analysis of the mechanisms of adaptation to a low-nutrient environment (*41*). *E. coli* and *Vibrio cholera* have OmpF-type outer membrane porin proteins that allow for the passive diffusion of hydrophilic molecules across the outer membrane. *C. crescentus* in contrast does not have OmpF-type porins, and instead has 67 TonB-dependent outer membrane channel proteins. The members of the TonB-dependent channel family catalyze energy-dependent transport of substrates across the outer membrane. *C. crescentus* has more TonB-dependent channels than any other sequenced organism. *Pseudomonas aeruginosa* contains 34 TonB-dependent channels, which is the next highest number after *C. crescentus*. Most organisms contain only ~10 of these channels. Substrates of TonB-dependent channels include ferric ions complexed to siderophores, heme, cobalamin, maltodextrins, etc. (*119-121*). These nutrients are actively pumped by the channels across the outer membrane using the electrochemical potential of the cytoplasmic membrane (*122*). TonB-dependent channels have high affinity for their substrates, and in fact the energy input is used for release of tightly-bound substrate. Once the nutrients are pumped across

the outer membrane, they passively diffuse into the cytoplasm via lower-affinity cytoplasmic membrane transporters.

In addition to mechanisms for enhancing the uptake of nutrients in the environment, the *C. crescentus* genome contains a proportionally large number of genes related to sensing and responding to environmental cues including nutrient availability. Approximately 2.5% of the nearly 4,000 genes in the *C. crescentus* genome are dedicated to swarmer cell motility and nutrient sensing. These include several genes whose predicted products are involved in chemotaxis, 16 chemoreceptors, and genes involved in flagellar assembly or movement (*41*). All of these adaptations make *C. crescentus* well-suited for thriving in low-nutrient environments such as those that promote PHB accumulation.

1.5.3 Previous studies of PHB production in *C. crescentus*

Compared to *R. eutropha*, little is known about PHB accumulation in *C. crescentus*. Early descriptions of *C. crescentus*, such as those reported by Poindexter, noted that TEM analysis revealed white inclusions consistent with PHB granules in cells grown in 0.2% peptone, 0.1% yeast extract supplemented with $MgSO_4$ and $CaCl_2$ (PYE medium) (*115*). As discussed above, phosphate limitation results in elongation of the stalk. Phosphate limitation is also known to induce PHB accumulation, and thus researchers investigating stalk elongation by various microscopy methods also observed PHB granules (*115, 118, 123*). Some examples of the micrographs are provided in Figure 1.23.

PHB granules of ~100 nm in diameter have also been observed in cryoET experiments carried out by the Jensen lab focused on examining filament bundles in *C. crescentus* in log phase cells grown in M2 salts supplemented with glucose. An example of these PHB granules is

shown in Figure 1.23C, revealing that the granules are adjacent to but not associated with the cell membrane. In one image, the granule appeared to be associated with a filament bundle in this picture, hence our interest in using this organism to study the scaffolding model. Closer examination by Dr. Morgan Beeby in the Jensen group revealed this is not the case.

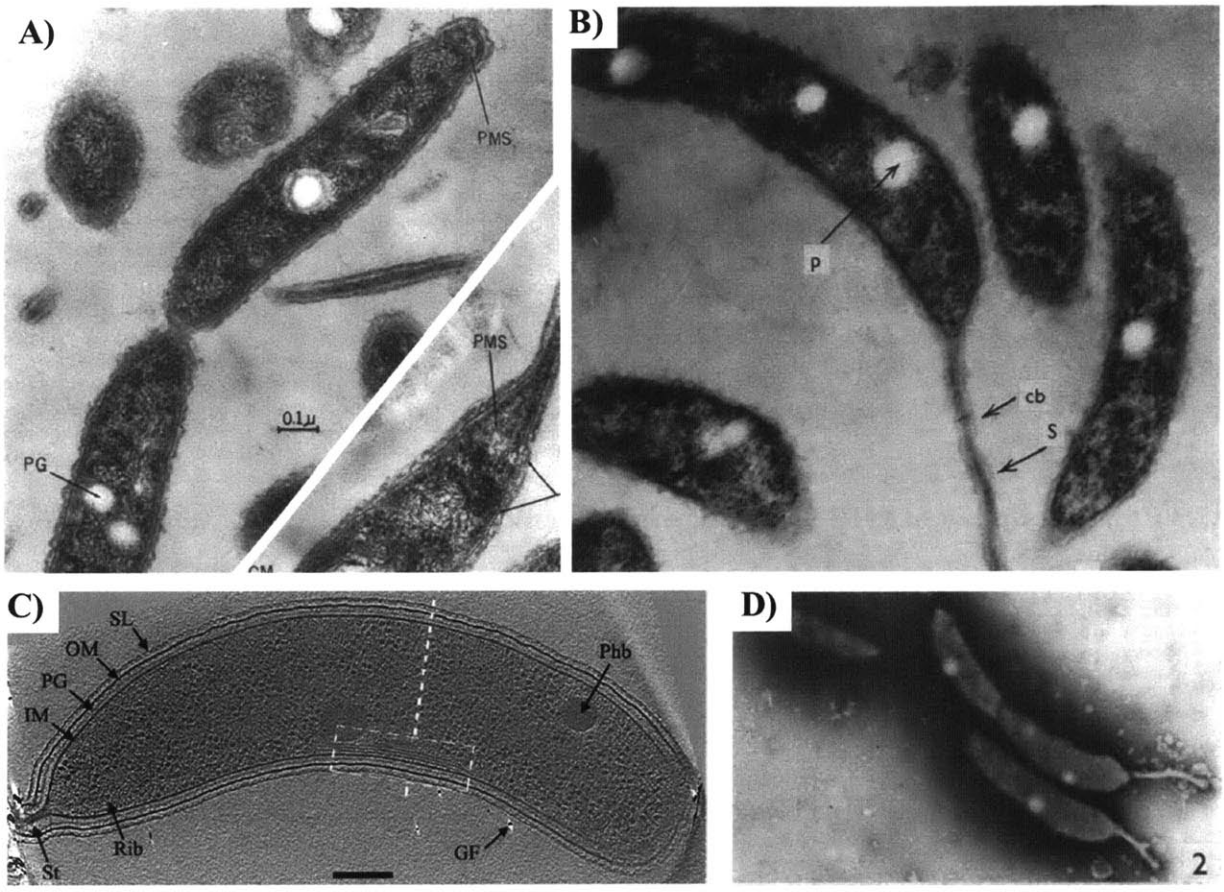

Figure 1.23 Sample micrographs of *C. crescentus* grown in various media in which PHB granules have been observed. A) Thin section TEM of *C. crescentus* grown in PYE medium, PG, PHB granule; PMS, polar membrane structure. Adapted from reference (*115*). B) Thin section TEM of *C. crescentus* grown in PYE medium. P, PHB granule; cb, cross-band in wall of stalk; S, stalk. Adapted from reference (*123*) C). CryoET of *C. crescentus* grown in M2 minimal salts supplemented with glucose IM, internal membrane; PG, peptidoglycan; OM, outer membrane; SL, S-layer; St, stalk; Rib, ribosome; GF, gold filament; Phb, PHB granule. Adapted from reference (*124*). D) Whole cell TEM *C. crescentus* grown in PYE medium, adapted from reference (*123*).

In an effort to broaden understanding of PHB production in various bacteria, Qi and Rehm examined the ability of *C. crescentus* to accumulate PHB in cells grown in PYE medium with $CaCl_2$ omitted, supplemented with 1% glucose as a carbon source *(25)*. The rationale for their selection of growth medium was likely based on the observation by Poindexter that PHB accumulation decreases with increasing Ca^{2+} availability (*117*). Presumably these conditions were selected because Ca^{2+} is thought to facilitate phosphate uptake; thus, limitation of Ca^{2+} in the growth medium might indirectly result in phosphate limitation. The authors reported a time course study over 100 h in which they recorded the growth and the extent of PHB accumulation. After 40 h the cells accumulated a maximum of 18% PHB cdw. At this time, they isolated the PHB and measured a M_w of ~550 kDa with a polydispersity of 1.6. They also performed a preliminary characterization of the PHB synthase of *C. crescentus*.

C. crescentus contains a class I PhaC, which is annotated as a 65 kDa synthase in the database. However, Qi and coworkers examined the gene sequence upstream of *phaC* and identified an alternative start codon. This protein product would have a M_w of 73 kDa, 8 kDa larger than the 65 kDa typical of class I synthases. Excluding the predicted 8 kDa N-terminal region in PhaC, PhaC from *C. crescentus* has 37% sequence identity with $PhaC_{Re}$, leading the authors to hypothesize that antibodies raised against $PhaC_{Re}$ would cross-react with PhaC in *C. crescentus*. SDS-PAGE of crude cell extracts from *C. crescentus* were blotted and analyzed with $PhaC_{Re}$ antibodies, revealing a band that migrated at ~75 kDa, higher than the $PhaC_{Re}$ standard (Figure 1.24). The authors also demonstrated that the 73 kDa synthase can be expressed recombinantly and is active in crude extracts of *E. coli (25)*. Since this initial report there have been no additional reports characterizing PHB accumulation in *C. crescentus* or the unusual class I synthase.

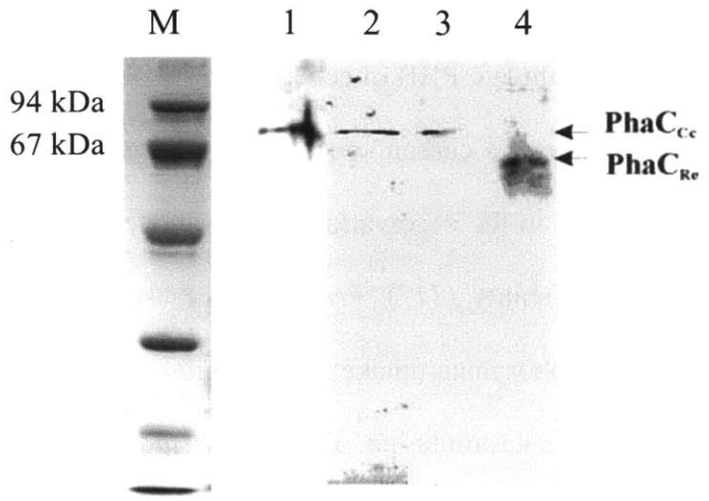

Figure 1.24 Western blot analysis of PhaC from *C. crescentus* and PhaC$_{Re}$ using antibodies to PhaC$_{Re}$. M, M_w markers. Lane 1, crude extract of *R. eutropha* H16 harboring a plasmid containing *phaC* from *C. crescentus*. Lane 2, crude extract of *E. coli* harboring a plasmid containing *phaC* from *C. crescentus*. Lane 3, crude extracts of wt *C. crescentus*. Lane 4, PhaC$_{Re}$ standard. Adapted from reference (*25*).

1.6 Preview of future chapters

The majority of the studies in this thesis are focused on characterization of the PHB biosynthetic apparatus in *C. crescentus*, which is an attractive system to study because it is genetically tractable and conditions for its growth have been well established (*115*). Furthermore, *C. crescentus* has served as a model for studying bacterial two-component signaling systems such as those used to sense and respond to nutrient levels in the environment (*125, 126*).

Chapter 2 presents the cloning and characterization of the class I synthase from *C. crescentus*. We were initially interested in PhaC$_{Cc}$ as a promising candidate for crystallization. In contrast to PhaC$_{Re}$, PhaC$_{Cc}$ is extremely soluble and well-behaved in solution. Although we were unable to crystallize PhaC$_{Cc}$, characterization of the synthase *in vitro* has given us some insight into PHB biosynthesis in *C. crescentus* and mechanisms of polymerization by PhaCs. PhaC$_{Cc}$ is a 73 kDa protein containing an unusual N-terminal domain, enriched in Ala, Pro and Lys residues,

which has no homology to other proteins in the database. The truncated $PhaC_{Cc}$ originally annotated in the genome was also isolated with the N-terminal domain removed, and has a specific activity that is 50-fold lower than that of the full length synthase. *C. crescentus* contains a 15 kDa phasin, PhaP, which we have also characterized. *In vitro* assays containing $PhaC_{Cc}$ and PhaP reveal that the inclusion of PhaP enhances the turnover of HBCoA and increases the specific activity of $PhaC_{Cc}$. We propose a model for *in vitro* granule assembly in which PhaP helps to package the growing granule in such a way as to prevent its collapse onto $PhaC_{Cc}$, which would hinder turnover. Priming studies using sTCoA in combination with size exclusion chromatography suggest that a dimer of $PhaC_{Cc}$ synthesizes two PHB chains, which is distinct from $PhaC_{Re}$ and $PhaEC_{Av}$. These studies also unexpectedly reveal that $PhaC_{Cc}$ is capable of catalyzing thiolysis of a PHB chain, which may give insight into a mechanism of termination that leaves the synthase primed with a single HB unit.

Chapter 3 presents characterization of PHB biogenesis in *C. crescentus* grown in M2 minimal medium that is limited in nitrogen and supplemented with 1% glucose as the sole carbon source (PHB_p medium). Whereas *R. eutropha* grown in nitrogen-limited medium accumulates upwards of 80% PHB cdw, *C. crescentus* accumulates considerably less, only ~10% PHB cdw. These two organisms represent opposite ends of the spectrum of PHA accumulation among the organisms thus far studied. Maximizing PHA accumulation is attractive from a commercial point of view, but it is unlikely that organisms in their natural environments produce PHB to the extent that *R. eutropha* does in the laboratory. Many important observations regarding the roles of PhaC, PhaP1 and PhaZs in PHB biogenesis have been made in *R. eutropha*. Our studies in *C. crescentus* address the question of which of the observations made in *R. eutropha* are more general aspects of PHB accumulating organisms.

Isolation of PHB granules from *C. crescentus* grown in PHB_p medium allowed the identification of granule-associated proteins including PhaP, a putative PhaR and a PhaZ homolog. Antibodies were generated to PhaP and PhaC, which were expressed and purified as described in Chapter 2. At the earliest time points in PHB accumulation, ~10% of the PHB in the cells is in the soluble fraction, and this PHB is full length compared to the M_w of PHB throughout growth. Western blot analysis of PhaP, PhaC and PHB levels during PHB granule initiation and accumulation revealed that PhaP increases concomitant with PHB, that the molecular ratio is 1-2 PHB chains per PhaP, and that PhaC is constitutively expressed throughout growth. A Δ*phaP* deletion strain was constructed to further examine the role of PhaP. This strain was shown to accumulate only 1% PHB cdw under the same growth conditions as the wt strain. PhaC is initially expressed at the same levels as in wt, but as the cells continue to grow, PhaC is degraded. The M_w and PDI of PHB in the wt strain and the two mutant strains Δ*phaP* and Δ*phaR* (in which PhaP is overexpressed) are the same, suggesting that PhaC alone controls termination. From our findings we propose a model for granule formation in *C. crescentus* in which the nucleating granule species contains soluble full-length PHB, PhaC and ~1 PhaP chain per PHB. As PHB accumulates, these species fuse and granules continue to grow. PhaC catalyzes termination, and a PhaP remains associated with each terminated chain to maintain its amorphous state and package it into the growing granule. A newly synthesized PhaP molecule replaces the one lost to the terminated chain, maintaining the ratio of 1-2 PHB chains per PhaP. This model is similar to what we have proposed in *R. eutropha* as well, with a few minor differences.

Chapter 4 summarizes our efforts to crystallize a PHB synthase that were done in collaboration with the Allen lab at Boston University. As yet, no X-ray structure is available for

a PHA synthase of any class. Thus, our early efforts were focused on cloning several synthases from different organisms in the hopes that one would be more amenable to crystallization. Several crystallization conditions were also identified and pursued for a truncated construct of $PhaEC_{Av}$ that was originally cloned, purified and crystallized by Dr. Paul Hubbard in the Drennan lab. However we were unable to obtain crystals that diffracted higher than 4.5 Å. Furthermore, conditions were identified in which $PhaC_{Cc}\Delta N$ could be crystallized in a form that diffracted to 2 Å; however, crystal growth took upwards of one year and could not be reproduced. Finally, Chapter 5 presents additional experiments, including preliminary efforts to examine the structure of a truncated construct of the class III synthase $PhaEC_{Av}$ by electron microscopy, TEM studies of the distribution of PHB granules at early time points between stalked and swarmer cells, *in vitro* studies of the truncated $PhaC_{Cc}\Delta N$ construct, and efforts to prepare and characterize mutant heterodimers of $PhaC_{Cc}$.

1.7 References

1. Stubbe, J., Tian, J. (2003) Polyhydroxyalkanoate (PHA) homeostasis: the role of the PHA synthase, *Nat. Prod. Rep. 20*, 445-457.
2. Stubbe, J., Tian, J., He, A., Sinskey, A.J., Lawrence, A.G., Liu, P. (2005) Nontemplate-dependent polymerization processes: Polyhydroxyalkanoate synthases as a paradigm, *Annu. Rev. Biochem. 74*, 433-480.
3. Steinbüchel, A., and Valentin, H. E. (1995) Diversity of bacterial polyhydroxyalkanoic acids, *FEMS Microbiol. Lett. 128*, 219-228.
4. Sudesh, K., Abe, H., and Doi, Y. (2000) Synthesis, structure and properties of polyhydroxyalkanoates: biological polyesters, *Prog. Polym. Sci. 25*, 1503-1555.

5. EPA. (2012) Environmental Protection Agency: Wastes-resource conservation-common wastes and materials.

6. Keshavarz, T., and Roy, I. (2010) Polyhydroxyalkanoates: bioplastics with a green agenda, *Curr. Opin. Microbiol. 13*, 321-326.

7. Snell, K. D., and Peoples, O. P. (2009) PHA bioplastic: A value-added coproduct for biomass biorefineries, *Biofuels, Bioprod. Biorefin. 3*, 456-467.

8. Smith, A. M. (2001) The biosynthesis of starch granules, *Biomacromolecules 2*, 335-341.

9. Ball, S. G., and Morell, M. K. (2003) From bacterial glycogen to starch: understanding the biogenesis of the plant starch granule. , *Annu. Rev. Plant Biol. 54*, 207-233.

10. Rao, N. N., Gomez-Garcia, M. R., and Kornberg, A. (2009) Inorganic polyphosphate: essential for growth and survival, *Annu. Rev. Biochem. 78*, 605-647.

11. Candela, T., and Fouet, A. (2006) Poly-gamma-glutamate in bacteria, *Mol. Microbiol. 60*, 1091-1098.

12. Lemoigne, M. (1926) Produits de deshydration et de polymerisation de l' acide b-oxybutyrique., *Bulletin de la societe de chimie biologique 8*, 770-782.

13. Macrae, R. M., and Wilkinson, J. F. (1958) Poly-beta-hyroxybutyrate metabolism in washed suspensions of *Bacillus cereus* and *Bacillus megaterium*, *J. Gen. Microbiol. 19*, 210-222.

14. Chen, G. Q., Konig, K. H., and Lafferty, R. M. (1991) Occurrence of poly-D(-)-3-hydroxyalkanoates in the genus *Bacillus*, *FEMS Microbiol. Lett. 68*, 173-176.

15. Vijayendra, S. V., Veeramani, S., and Smala, T. R. (2009) Optimization of polyhydroxybutyrate production by a beta-carotene producing strain of *Micrococcus* sp., *J. Food Sci. 45*, 506-509.

16. Valentin, H. F., and Dennis, D. (1996) Metabolic pathway for poly(3-hydroxybutyrate-co-3-hydroxyvalerate) formation in *Nocardia corallina*: inactivation of mutB by chromosomal integration of a kanamycin resistance gene, *Appl. Environ. Microbiol. 62*, 372-379.

17. Verma, S., Bhatia, Y., Valappil, S. P., and Roy, I. (2002) A possible role of poly-3-hydroxybutyric acid in antibiotic production in *Streptomyces*, *Arch. Microbiol. 179*, 66-69.

18. Stal, L. (1992) Poly(hydroxyalkanoate) in cyanobacteria: an overview, *FEMS Microbiol. Lett. 103*, 169-180.

19. Vincenzini, M., Sili, C., de Philippis, R., Ena, A., and Materassi, R. (1990) Occurrence of poly-beta-hydroxybutyrate in *Spirulina* species, *J. Bacteriol. 172*, 2791-2792.

20. Wu, G. F., Wu, Q. Y., and Shen, Z. Y. (2001) Accumulation of poly-beta-hydroxybutyrate in cyanobacterium *Synechocystis* sp. PCC6803, *Bioresour. Technol. 76*, 85-90.

21. Ibrahim, M. H., and Steinbüchel, A. (2010) High-cell-density cyclic fed-batch fermentation of a poly(3-hydroxybutyrate)-accumulating thermophile, *Chelatococcus* sp. strain MW10, *Appl. Environ. Microbiol. 76*, 7890-7895.

22. Miyake, M., Erata, M., and Asada, Y. (1996) A thermophilic cyanobacterium, *Synechococcus* sp. MA19, capable of accumulating poly-beta-hydroxybutyrate, *J. Ferment. Bioeng. 82*, 512-514.

23. Pantazaki, A. A., Tambaka, M. G., Langlois, V., Guerin, P., and Kyriakidis, D. A. (2003) Polyhydroxyalkanoate (PHA) biosynthesis in *Thermus thermophilus*: purification and biochemical properties of PHA synthase, *Mol. Cell. Biochem. 254*, 173-183.

24. Page, W. J., Manchak, J., and Rudy, B. (1992) Formation of poly(hydroxybutyrate-co-hydroxyvalerate) by *Azotobacter vinelandii* UWD, *Appl. Environ. Microbiol. 58*, 2866-2873.

25. Qi, Q., and Rehm, B.A. . (2001) Polyhydroxybutyrate biosynthesis in *Caulobacter crescentus*: molecular characterization of the polyhydroxybutyrate synthase., *Microbiology 147*, 3353-3358.

26. Zhang, S., Kolvek, S., Goodwin, S., and Lenz, R. W. (2004) Poly(hydroxyalkanoic acid) biosynthesis in *Ectothiorhodospira shaposhnikovii*: characterization and reactivity of a type III PHA synthase, *Biomacromolecules 5*, 40-48.

27. Porwal, S., Kumar, T., Lal, S., Rani, A., Kumar, S., Cheema, S., Purohit, H. J., Sharma, R., Singh Patel, S. K., and Kalia, V. C. (2008) Hydrogen and polyhydroxybutyrate producing abilities of microbes from diverse habitats by dark fermentative process, *Bioresour. Technol. 99*, 5444-5451.

28. Bourque, D., Ouellette, B., Andre, G., and Groleau, D. (1992) Production of poly-beta-hydroxybutyrate from methanol - characterization of a new isolate of *Methylobacterium extorquens*, *Appl. Microbiol. and Biotechnol. 37*, 7-12.

29. Yamane, T., Chen, X., and Ueda, S. (1996) Growth-associated production of poly(3-hydroxyvalerate) from n-pentanol by a methylotrophic bacterium, *Paracoccus denitrificans*, *Appl. Environ. Microbiol. 62*, 380-384.

30. Anderson, A. J., and Dawes, E. A. (1990) Occurrence, metabolism, metabolic role, and industrial uses of bacterial polyhydroxyalkanoates, *Microbiol. Rev. 54*, 450-472.

31. Lakshman, K., and Shamala, T. R. (2003) Enhanced biosynthesis of polyhydroxyalkanoates in a mutant strain of *Rhizobium meliloti*, *Biotechnol. Lett. 25*, 115-119.

32. Fernandez-Castillo, R., Rodriguez-Valera, F., Gonzalez-Ramos, J., and Ruiz-Berraquero, F. (1986) Accumulation of poly (beta-hydroxybutyrate) by Halobacteria, *Appl. Environ. Microbiol. 51*, 214-216.

33. Nicolaus, B., Lama, L., Esposito, E., Manca, M. C., Improta, R., Bellitti, M. R., Duckworth, A. W., Grant, W. D., and Gambacorta, A. (1999) *Haloarcula* spp able to biosynthesize exo- and endopolymers, *J. Indust. Microbiol. Biotechnol. 23*, 489-496.

34. Huang, T. Y., Duan, K. J., Huang, S. Y., and Chen, C. W. (2006) Production of polyhydroxyalkanoates from inexpensive extruded rice bran and starch by *Haloferax mediterranei*, *J. Indust. Microbiol. Biotechnol. 33*, 701-706.

35. Hezayen, F. F., Rehm, B. H. A., Eberhardt, R., and Steinbüchel, A. (2000) Polymer production by two newly isolated extremely halophilic archaea: application of a novel corrosion-resistant bioreactor, *Appl. Microbiol. Biotechnol. 54*, 319-325.

36. Peoples, O. P., and Sinskey, A. J. (1989) Poly-beta-hydroxybutyrate biosynthesis in *Alcaligenes eutrophus* H16. Characterization of the genes encoding beta-ketothiolase and acetoacetyl-CoA reductase, *J. Biol. Chem. 264*, 15293-15297.

37. Peoples, O. P., and Sinskey, A. J. (1989) Poly-beta-hydroxybutyrate (PHB) biosynthesis in *Alcaligenes eutrophus* H16. Identification and characterization of the PHB polymerase gene (*phbC*), *J. Biol. Chem. 264*, 15298-15303.

38. Wieczorek, R., Pries, A., Steinbüchel, A., and Mayer, F. (1995) Analysis of a 24-kilodalton protein associated with the polyhydroxyalkanoic acid granules in *Alcaligenes eutrophus*, *J. Bacteriol. 177*, 2425-2435.

39. Pohlmann, A., Fricke, W. F., Reinecke, F., Kusian, B., Liesegang, H., Cramm, R., Eitinger, T., Ewering, C., Potter, M., Schwartz, E., Strittmatter, A., Voss, I., Gottschalk, G., Steinbüchel, A., Friedrich, B., and Bowien, B. (2006) Genome sequence of the bioplastic-producing " Knallgas" bacterium *Ralstonia eutropha* H16 *Nature Biotechnol. 24*, 1257-1262.

40. York, G. M., Stubbe, J., and Sinskey, A. J. (2002) The *Ralstonia eutropha* PhaR protein couples synthesis of the PhaP phasin to the presence of polyhydroxybutyrate in cells and promotes polyhydroxybutyrate production, *J. Bacteriol. 184*, 59-66.

41. Nierman, W. C., Feldblyum, T. V., Laub, M. T., Paulsen, I. T., Nelson, K. E., Eisen, J., Heidelberg, J. F., Alley, M. R. K., Ohta, N., Maddock, J. R., Potocka, I., Nelson, W. C., Newton, A., Stephens, C., Phadke, N. D., Ely, B., DeBoy, R. T., Dodson, R. J., Durkin, A. S., Gwinn, M. L., Haft, D. H., Kolonay, J. F., Smit, J., Craven, M. B., Khouri, H., Shetty, J., Berry, K., Utterback, T., Tran, K., Wolf, A., Vamathevan, J., Ermolaeva, M., White, O., Salzberg, S. L., Venter, J. C., Shapiro, L., and Fraser, C. M. (2001) Complete genome sequence of *Caulobacter crescentus*, *Proc. Nat. Acad. Sci. 98*, 4136-4141.

42. Pötter, M., Müller, H., Reinecke, F., Wieczorek, R., Fricke, F., Bowien, B., Friedrich, B., and Steinbüchel, A. (2004) The complex structure of polyhydroxybutyrate (PHB) granules: four orthologous and paralogous phasins occur in *Ralstonia eutropha* *Microbiol. 150*, 2301-2311.

43. Pfeiffer, D., and Jendrossek, D. (2011) Interaction between poly(3-hydroxybutyrate) granule-associated proteins as revealed by two-hybrid analysis and identification of a new phasin in *Ralstonia eutropha* H16, *Microbiol. 157*, 2795-2807.

44. Pfeiffer, D., and Jendrossek, D. (2012) Localization of poly(3-Hydroxybutyrate) (PHB) granule-associated proteins during PHB granule formation and identification of two new phasins, PhaP6 and PhaP7, in *Ralstonia eutropha* H16, *J. Bacteriol. 194*, 5909-5921.

45. Peplinski, K., Ehrenreich, A., Doring, C., Bomeke, M., Reinecke, F., Hutmacher, C., and Steinbüchel, A. (2001) Genome-wide transcriptome analyses of the 'Knallgas' bacterium *Ralstonia eutropha* H16 with regard to polyhydroxyalkanoate metabolism, *Microbiol. 156*, 2136-2152.

46. Yuan, W., Jia, Y., Tian, J., Snell, K. D., Muh, U., Sinskey, A. J., Lambalot, R. H., Walsh, C. T., and Stubbe, J. (2001) Class I and III polyhydroxyalkanoate synthases from *Ralstonia eutropha* and *Allochromatium vinosum*: characterization and substrate specificity studies, *Arch. Biochem. Biophys. 394*, 87-98.

47. Rehm, B. H. (2003) Polyester synthases: natural catalysts for plastics, *Biochem. J. 376*, 15-33.

48. Valappil, S. P., Boccaccini, A. R., Bucke, C., and Roy, I. (2007) Polyhydroxyalkanoates in Gram-positive bacteria: insights from the genera *Bacillus* and *Streptomyces*, *Antonie Van Leeuwenhoek 91*, 1-17.

49. Gerngross, T. U., Snell, K. D., Peoples, O. P., Sinskey, A. J., Csuhai, E., Masamune, S., and Stubbe, J. (1994) Overexpression and purification of the soluble polyhydroxyalkanoate synthase from *Alcaligenes eutrophus*: evidence for a required posttranslational modification for catalytic activity, *Biochemistry 33*, 9311-9320.

50. Müh, U., Sinskey, A.J., Kirby, D.P., Lane, W.S., Stubbe, J. (1999) PHA Synthase from *Chromatium vinosum*: cysteine 149 is Involved in covalent catalysis, *Biochemistry 38*, 826-837.

51. Wodzinska, J., Snell, K. D., Rhomberg, A., Sinskey, A. J., Biemann, K., and Stubbe, J. (1996) Polyhydroxybutyrate synthase: evidence for covalent catalysis, *J. Amer. Chem. Soc. 118*, 6319-6320.

52. Ushimaru, K., Sangiambut, S., Thomson, N., Sivaniah, E., and Tsuge, T. (2013) New insights into activation and substrate recognition of polyhydroxyalkanoate synthase from *Ralstonia eutropha*, *Appl. Microbiol. Biotechnol. 97*, 1175-1182.

53. Smythe, C., and Cohen, P. (1991) The discovery of glycogenin and the priming mechanism for glycogen biogenesis, *Eur. J. Biochem. 200*, 625-631.

54. Light, D. R., and Dennis, M. S. (1989) Purification of a prenyltransferase that elongates cis-polyisoprene rubber from the latex of *Hevea brasiliensis*, *J. Biol. Chem. 264*, 18589-18597.

55. Light, D. R., Lazarus, R. A., and Dennis, M. S. (1989) Rubber elongation by farnesyl pyrophosphate synthases involves a novel switch in enzyme stereospecificity, *J. Biol. Chem. 264*, 18598-18607.

56. Cho, M. (2012) Studies on the mechanism of polyhydroxybutyrate (PHB) granule formation in *Ralstonia eutropha* H16, in *Chemistry*, p 346, Massachusetts Institute of Technology, Cambridge.

57. Liebergesell, M., Sonomoto, K., Madkour, M., Mayer, F., and Steinbüchel, A. (1994) Purification and characterization of the poly(hydroxyalkanoic acid) synthase from

Chromatium vinosum and localization of the enzyme at the surface of poly(hydroxyalkanoic acid) granules, *Eur. J. Biochem. 226*, 71-80.

58. Tian, J. (2005) Mechanistic investigation of polyhydroxybutyrate (PHB) synthases and elucidation of PHB biosynthesis and degradation process in *Wautersia eutropha* H16, in *Chemistry*, p 345, Massachusetts Institute of Technology, Cambridge.

59. Karlsson, M., Contreras, J. A., Hellman, U., Tornqvist, H., and Holm, C. (1997) cDNA cloning, tissue distribution, and identification of the catalytic triad of monoglyceride lipase. Evolutionary relationship to esterases, lysophospholipases, and haloperoxidases, *J. Biol. Chem. 272*, 27218-27223.

60. Brumlik, M. J., and Buckley, J. T. (1996) Identification of the catalytic triad of the lipase/acyltransferase from *Aeromonas hydrophila*, *J. Bacteriol. 178*, 2060-2064.

61. Frenken, L. G., Egmond, M. R., Batenburg, A. M., Bos, J. W., Visser, C., and Verrips, C. T. (1992) Cloning of the *Pseudomonas glumae* lipase gene and determination of the active site residues, *Appl. Environ. Microbiol. 58*, 3787-3791.

62. Liebergesell, M., and Steinbüchel, A. (1992) Cloning and nucleotide sequences of genes relevant for biosynthesis of poly(3-hydroxybutyric acid) in *Chromatium vinosum* strain D, *Eur. J. Biochem. 209*, 135-150.

63. Jia, Y., Kappock, T. J., Frick, T., Sinskey, A. J., and Stubbe, J. (2000) Lipases provide a new mechanistic model for polyhydroxybutyrate (PHB) synthases: characterization of the functional residues in *Chromatium vinosum* PHB synthase, *Biochemistry 39*, 3927-3936.

64. Rehm, B. H., Antonio, R. V., Spiekermann, P., Amara, A. A., and Steinbüchel, A. (2002) Molecular characterization of the poly(3-hydroxybutyrate) (PHB) synthase from

Ralstonia eutropha: in vitro evolution, site-specific mutagenesis and development of a PHB synthase protein model, *Biochim. Biophys. Acta 1594*, 178-190.

65. Kelley, L. A., and Sternberg, M. J. (2009) Protein structure prediction on the Web: a case study using the Phyre server, *Nat. Protoc. 4*, 363-371.

66. Yang, Y., Faraggi, E., Zhao, H., and Zhou, Y. (2011) Improving protein fold recognition and template-based modeling by employing probabilistic-based matching between predicted one-dimensional structural properties of query and corresponding native properties of templates, *Bioinformatics (Oxford, England) 27*, 2076-2082.

67. Taguchi, S., Yamada, M., Matsumoto, K., Tajima, K., Satoh, Y., Munekata, M., Ohno, K., Kohda, K., Shimamura, T., Kambe, H., and Obata, S. (2008) A microbial factory for lactate-based polyesters using a lactate-polymerizing enzyme, *Proc. Natl. Acad. Sci. 105*, 17323-17327.

68. Ochi, A., Matsumoto, K., Ooba, T., Sakai, K., Tsuge, T., and Taguchi, S. (2012) Engineering of class I lactate-polymerizing polyhydroxyalkanoate synthases from *Ralstonia eutropha* that synthesize lactate-based polyester with a block nature, *Appl. Microbiol. Biotechnol. 97*, 3441-3447.

69. Pleiss, J., Fischer, M., and Schmid, R. D. (1998) Anatomy of lipase binding sites: the scissie fatty acid binding site, *Chem. Phys. Lipids 93*, 67-80.

70. Lang, D., Hofmann, B., Haalck, L., Hecht, H., Spener, F., Schmid, R. D., and Schomburg, D. (1996) Crystal structure of a bacterial lipase from Chromobacterium viscosum ATCC 6918 refined at 1.6 Å resolution, *J. Mol. Biol. 259*, 704-717.

71. Li, P., Chakraborty, S., and Stubbe, J. (2009) Detection of covalent and noncovalent intermediates in the polymerization reaction catalyzed by a C149S class III polyhydroxybutyrate synthase, *Biochemistry 48*, 9202-9211.

72. Jia, Y., Yuan, W., Wodzinska, J., Park, J., Sinskey, A.J., Stubbe, J. (2001) Mechanistic studies on class I polyhydroxybutyrate (PHB) synthase from *Ralstonia eutropha*: class I and III synthases share a similar catalytic mechanism., *Biochemistry 40*, 1011-1019.

73. Cho, M., Brigham, C. J., Sinskey, A. J., and Stubbe, J. (2012) Purification of polyhydroxybutyrate synthase from its native organism, *Ralstonia eutropha*: implications for the initiation and elongation of polymer formation in vivo, *Biochemistry 51*, 2276-2288.

74. Tian, J., Sinskey, A. J., and Stubbe, J. (2005) Detection of intermediates from the polymerization reaction catalyzed by a D302A mutant of class III polyhydroxyalkanoate (PHA) synthase, *Biochemistry 44*, 1495-1503.

75. Tian, J., Sinskey, A. J., and Stubbe, J. (2005) Class III polyhydroxybutyrate synthase: involvement in chain termination and reinitiation, *Biochemistry 44*, 8369-8377.

76. Numata, K., Motoda, Y., Watanabe, S., Tochio, N., Kigawa, T., and Doi, Y. (2012) Active intermediates of polyhydroxyalkanoate synthase from *Aeromonas caviae* in polymerization reaction, *Biomacromolecules 13*, 3450-3455.

77. Zhang, S. M., Kolvek, S., Lenz, R. W., and Goodwin, S. (2003) Mechanism of the polymerization reaction initiated and catalyzed by the polyhydroxybutyrate synthase of *Ralstonia eutropha*, *Biomacromolecules 4*, 504-509.

78. Lawrence, A. G., Choi, J., Rha, C., Stubbe, J., and Sinskey, A. J. (2005) In vitro analysis of the chain termination reaction in the synthesis of poly-(R)-beta-hydroxybutyrate by the class III synthase from *Allochromatium vinosum*, *Biomacromolecules 6*, 2113-2119.

79. Gerngross, T. U., and Martin, D. P. (1995) Enzyme-catalyzed synthesis of poly[(R)-(-)-3-hydroxybutyrate]: formation of macroscopic granules in vitro, *Proc. Natl. Acad. Sci. 92*, 6279-6283.

80. Shi, F. Y., Ashby, R., and Gross, R. A. (1996) Use of poly(ethylene glycol)s to regulate poly(3-hydroxybutyrate) molecular weight during *Alcaligenes eutrophus* cultivations, *Macromol. 29*, 7753-7758.

81. Madden, L. A., Anderson, A. J., Shah, D. T., and Asrar, J. (1999) Chain termination in polyhydroxyalkanoate synthesis: involvement of exogenous hydroxy-compounds as chain transfer agents, *Int. J. Biol. Macromol. 25*, 43-53.

82. Shi, F. Y., Gross, R. A., and Rutherford, D. R. (1996) Microbial polyester synthesis: Effects of poly(ethylene glycol) on product composition, repeat unit sequence, and end group structure, *Macromol. 29*, 10-17.

83. Tian, J., He, A., Lawrence, A. G., Liu, P., Watson, N., Sinskey, A. J., and Stubbe, J. (2005) Analysis of transient polyhydroxybutyrate production in *Wautersia eutropha* H16 by quantitative Western analysis and transmission electron microscopy, *J. Bacteriol. 187*, 3825-3832.

84. Wieczorek, R., Steinbüchel, A., and Schmidt, B. (1996) Occurrence of polyhydroxyalkanoic acid granule-associated proteins related to the *Alcaligenes eutrophus* H16 GA24 protein in other bacteria, *FEMS Microbiol. Lett. 135*, 23-30.

85. Beeby, M., Cho, M., Stubbe, J., and Jensen, G. J. (2012) Growth and localization of polyhydroxybutyrate granules in *Ralstonia eutropha*, *J. Bacteriol. 194*, 1092-1099.

86. York, G. M., Stubbe, J., and Sinskey, A. J. (2001) New insight into the role of the PhaP phasin of *Ralstonia eutropha* in promoting synthesis of polyhydroxybutyrate, *J. Bacteriol. 183*, 2394-2397.

87. Pötter, M., Madkour, M. H., Mayer, F., and Steinbüchel, A. (2002) Regulation of phasin expression and polyhydroxyalkanoate (PHA) granule formation in *Ralstonia eutropha* H16, *Microbiol. 148*, 2413-2426.

88. Jossek, R., Reichelt, R., and Steinbüchel, A. (1998) In vitro biosynthesis of poly(3-hydroxybutyric acid) by using purified poly(hydroxyalkanoic acid) synthase of *Chromatium vinosum*, *Appl. Microbiol. Biotechnol. 49*, 258-266.

89. Shaw, G. L., Melby, M. K., Horowitz, D. M., Keeler, J., and Sanders, J. K. M. (1994) Nuclear magnetic resonance relaxation studies of poly(hydroxybutyrate) in whole cells and in artificial granules, *Int. J. Biol. Macromol. 16*, 59-63.

90. Pfeiffer, D., Wahl, A., and Jendrossek, D. (2011) Identification of a multifunctional protein, PhaM, that determines number, surface to volume ratio, subcellular localization and distribution to daughter cells of poly(3-hydroxybutyrate), PHB, granules in *Ralstonia eutropha* H16, *Mol. Microbiol. 82*, 936-951.

91. Wahl, A., Schuth, N., Pfeiffer, D., Nussberger, S., and Jendrossek, D. (2012) PHB granules are attached to the nucleoid via PhaM in *Ralstonia eutropha*, *BMC Microbiol. 12*, 262-282.

92. Neumann, L., Spinozzi, F., Sinibaldi, R., Rustichelli, F., Potter, M., and Steinbüchel, A. (2008) Binding of the major phasin, PhaP1, from *Ralstonia eutropha* H16 to poly(3-hydroxybutyrate) granules, *J. Bacteriol. 190*, 2911-2919.

93. Lawrence, A. G., Schoenheit, J., He, A., Tian, J., Liu, P., Stubbe, J., and Sinskey, A. J. (2005) Transcriptional analysis of *Ralstonia eutropha* genes related to poly-(R)-3-hydroxybutyrate homeostasis during batch fermentation, *Appl. Microbiol. Biotechnol. 68*, 663-672.

94. Tian, J., Sinskey, A. J., and Stubbe, J. (2005) Kinetic studies of polyhydroxybutyrate granule formation in *Wautersia eutropha* H16 by transmission electron microscopy, *J. Bacteriol. 187*, 3814-3824.

95. York, G. M., Junker, B. H., Stubbe, J. A., and Sinskey, A. J. (2001) Accumulation of the PhaP phasin of *Ralstonia eutropha* is dependent on production of polyhydroxybutyrate in cells, *J. Bacteriol. 183*, 4217-4226.

96. Maehara, A., Doi, Y., Nishiyama, T., Takagi, Y., Ueda, S., Nakano, H., and Yamane, T. (2001) PhaR, a protein of unknown function conserved among short-chain-length polyhydroxyalkanoic acids producing bacteria, is a DNA-binding protein and represses *Paracoccus denitrificans phaP* expression in vitro, *FEMS Microbiol. Lett. 200*, 9-15.

97. Maehara, A., Taguchi, S., Nishiyama, T., Yamane, T., and Doi, Y. (2002) A repressor protein, PhaR, regulates polyhydroxyalkanoate (PHA) synthesis via its direct interaction with PHA, *J. Bacteriol. 184*, 3992-4002.

98. Horowitz, D. M., and Sanders, J. K. M. (1994) Amorphous, biomimetic granules of polyhydroxybutyrate - preparation, characterization, and biological implications, *J. Amer. Chem. Soc. 116*, 2695-2702.

99. Saegusa, H., Shiraki, M., Kanai, C., and Saito, T. (2001) Cloning of an intracellular poly[D(-)-3-hydroxybutyrate] depolymerase gene from *Ralstonia eutropha* H16 and characterization of the gene product, *J. Bacteriol. 183*, 94-100.

100. Abe, T., Kobayashi, T., and Saito, T. (2005) Properties of a novel intracellular poly(3-hydroxybutyrate) depolymerase with high specific activity (PhaZd) in *Wautersia eutropha* H16, *J. Bacteriol. 187*, 6982-6990.

101. York, G. M., Lupberger, J., Tian, J., Lawrence, A. G., Stubbe, J., and Sinskey, A. J. (2003) *Ralstonia eutropha* H16 encodes two and possibly three intracellular Poly[D-(-)-3-hydroxybutyrate] depolymerase genes, *J. Bacteriol. 185*, 3788-3794.

102. Kobayashi, T., Shiraki, M., Abe, T., Sugiyama, A., and Saito, T. (2003) Purification and properties of an intracellular 3-hydroxybutyrate-oligomer hydrolase (PhaZ2) in *Ralstonia eutropha* H16 and its identification as a novel intracellular poly(3-hydroxybutyrate) depolymerase, *J. Bacteriol. 185*, 3485-3490.

103. Kobayashi, T., Uchino, K., Abe, T., Yamazaki, Y., and Saito, T. (2005) Novel intracellular 3-hydroxybutyrate-oligomer hydrolase in *Wautersia eutropha* H16, *J. Bacteriol. 187*, 5129-5135.

104. Uchino, K., Saito, T., Gebauer, B., and Jendrossek, D. (2007) Isolated poly(3-hydroxybutyrate) (PHB) granules are complex bacterial organelles catalyzing formation of PHB from acetyl coenzyme A (CoA) and degradation of PHB to acetyl-CoA, *J. Bacteriol. 189*, 8250-8256.

105. Griebel, R., Smith, Z., and Merrick, J. M. (1968) Metabolism of poly-beta-hydroxybutyrate .I. Purification, composition and properties of native poly-beta-hydroxybutyrate granules from *Bacillus megaterium*, *Biochemistry 7*, 3676-3681.

106. Gerngross, T. U., Reilly, P., Stubbe, J., Sinskey, A. J., and Peoples, O. P. (1993) Immunocytochemical analysis of poly-beta-hydroxybutyrate (PHB) synthase in *Alcaligenes eutrophus* H16: localization of the synthase enzyme at the surface of PHB granules, *J. Bacteriol. 175*, 5289-5293.

107. Mayer, F., and Hoppert, M. (1997) Determination of the thickness of the boundary layer surrounding bacterial PHA inclusion bodies, and implications for models describing the molecular architecture of this layer, *J. Basic Microbiol. 37*, 45-52.

108. Dennis, D., Sein, V., Martinez, E., and Augustine, B. (2008) PhaP is involved in the formation of a network on the surface of polyhydroxyalkanoate inclusions in *Cupriavidus necator* H16, *J. Bacteriol. 190*, 555-563.

109. Jendrossek, D. (2005) Fluorescence microscopical investigation of poly(3-hydroxybutyrate) granule formation in bacteria, *Biomacromolecules 6*, 598-603.

110. Brigham, C. J., Budde, C. F., Holder, J. W., Zeng, Q. D., Mahan, A. E., Rha, C., and Sinskey, A. J. (2010) Elucidation of beta-Oxidation Pathways in *Ralstonia eutropha* H16 by Examination of Global Gene Expression, *J. Bacteriol. 192*, 5454-5464.

111. Houwink, A. L. (1951) *Caulobacter* versus *Bacillus* spec. div., *Nature 168*, 654-655.

112. Henrici, A. T., and Johnson, D. E. (1935) Studies of freshwater bacteria II. Stalked bacteria, a new order of schizomycetes, *J. Bacteriol. 30*, 61-93.

113. Laub, M. T., Shapiro, L., and McAdams, H. H. (2007) Systems biology of *Caulobacter*, *Annu. Rev. Genet. 41*, 429-441.

114. Ausmees, N., and Jacobs-Wagner, C. (2003) Spatial and temporal control of differentiation and cell cycle progression in *Caulobacter crescentus*, *Annu. Rev. Microbiol. 57*, 225-247.

115. Poindexter, J. S. (1964) Biological properties and classification of *Caulobacter* group, *Bacteriol. Rev. 28*, 231-293.

116. Schmidt, J. M., and Stanier, R. Y. (1966) The development of cellular stalks in bacteria, *J. Cell Biol. 28*, 423-436.

117. Poindexter, J. S. (1984) The role of calcium in stalk development and in phosphate acquisition in *Caulobacter crescentus*, *Arch. Microbiol. 138*, 140-152.

118. Brun, Y. V., and Shapiro, L. (1992) A temporally controlled sigma-factor is required for polar morphogenesis and normal cell division in *Caulobacter*, *Genes Dev. 6*, 2395-2408.

119. Andrews, S. C., Robinson, A. K., and Rodriguez-Quinones, F. (2003) Bacterial iron homeostasis, *FEMS Microbiol. Rev. 27*, 215-237.

120. Braun, V., Hantke, K., and Koster, W., (Eds.) (1998) *Bacterial ion transport: mechanisms, genetics and regulation*, Marcel Dekker, New York.

121. Postle, K., and Kadner, R. J. (2003) Touch and go: tying TonB to transport, *Mol Microbiol 49*, 869-882.

122. White, J. C., Di Girolamo, P. M., Fu, M. L., Preston, Y. A., and Bradbeer, C. (1973) Transport of vitamin B12 in *Escherichia coli*. Location and properties of the initial B12-binding site. , *J. Biol. Chem. 248*, 3978-3986.

123. Schmidt, J. M. (1968) Stalk elongation in mutants of Caulobacter crescentus, *J. Gen. Microbiol. 53*, 291-298.

124. Briegel, A., Dias, D. P., Li, Z., Jensen, R. B., Frangakis, A. S., and Jensen, G. J. (2006) Multiple large filament bundles observed in *Caulobacter crescentus* by electron cryotomography, *Mol. Microbiol. 62*, 5-14.

125. Laub, M. T., and Goulian, M. (2007) Specificity in two-component signal transduction pathways, *Annu. Rev. Genet. 41*, 121-145.

126. Shapiro, L., and Losick, R. (2000) Dynamic spatial regulation in the bacterial cell, *Cell 100*, 89-98.

Chapter 2:

Characterization of the class I PHB synthase from *Caulobacter crescentus*

2. Characterization of the class I PHB synthase from *Caulobacter crescentus*

2.1 Introduction

Class I and class III PHA synthases catalyze the polymerization of (*R*)-3-hydroxybutyryl CoA (HBCoA) to make polyhydroxybutyrate (PHB) (*1, 2*). The class I synthases are composed of a single subunit PhaC, that is typically 65 kDa in molecular weight (M_w), and are typified by the synthase from *Ralstonia eutropha* ($PhaC_{Re}$). The class III synthases are composed of two subunits, PhaC and PhaE, both ~40 kDa in M_w, and are typified by PhaEC from *Allochromatium vinosum* ($PhaEC_{Av}$). In the class III enzymes, PhaC is the synthase whereas PhaE is of unknown function but is essential for activity. The class I and III synthases appear to share a common mechanism for polymerization (*3-5*). As discussed in Chapter 1, polymerization occurs via covalent catalysis at an active site Cys (C319 in $PhaC_{Re}$ and C149 in $PhaEC_{Av}$), and involves the participation of a conserved His residue (H508 in $PhaC_{Re}$ and H331 in $PhaEC_{Av}$), which deprotonates Cys to generate the active thiolate (*3, 5, 6*).

The two mechanistic models shown in Figure 2.1 have been the primary working models for polymerization by class I and III synthases in the last decade. A number of observations with both $PhaC_{Re}$ and $PhaEC_{Av}$ have led to the development of these two models. First, $PhaC_{Re}$ is a mixture of monomers and dimers in solution, and $PhaEC_{Av}$ is a mixture of dimers and tetramers of PhaEC in solution. Use of the artificial primer sTCoA, which is a terminally saturated $(HB)_3CoA$ analog (Figure 2.2), demonstrated that incubation of both synthases with sTCoA results in acylation with sT at a stoichiometry of one per dimer (*3-5*). Thus, in both models a dimer of synthases is proposed to generate a single PHB chain. The model in Figure 2.1A was proposed based on analogy to fatty acid synthases (*7*) and involves the participation of two thiols. These two thiols are proposed to be the active site Cys residues of each monomer; thus,

the active site is formed at the interface of the monomers. Polymerization involves attack by the active site Cys of one monomer on HBCoA, to release CoA. A second HBCoA unit is then loaded onto the Cys residue of the other monomer. A conserved Asp residue (D480 in $PhaC_{Re}$, D302 in $PhaEC_{Av}$) is proposed to deprotonate the 3-OH of one HB unit, which attacks the HB-PhaC thioester on the other subunit resulting in transfer of the growing chain to a single subunit. A third HBCoA unit is then loaded onto the "empty" subunit, and polymerization continues. In the model shown in Figure 2.1B, which is based on the model proposed for some type III polyketide synthases (*8*), the second HBCoA monomer non-covalently binds and ester bond formation occurs by attack at the enzyme-HB thioester to temporarily release the growing chain from the enzyme. Cys then rapidly reattacks the growing chain, releasing the second CoA. A major distinction between the models in Figure 2.1A and B is that the former predicts no non-covalent intermediates, whereas the latter predicts the involvement of transient non-covalent intermediates. The evidence for the various aspects of the models as well as attempts to distinguish between the two will be described below.

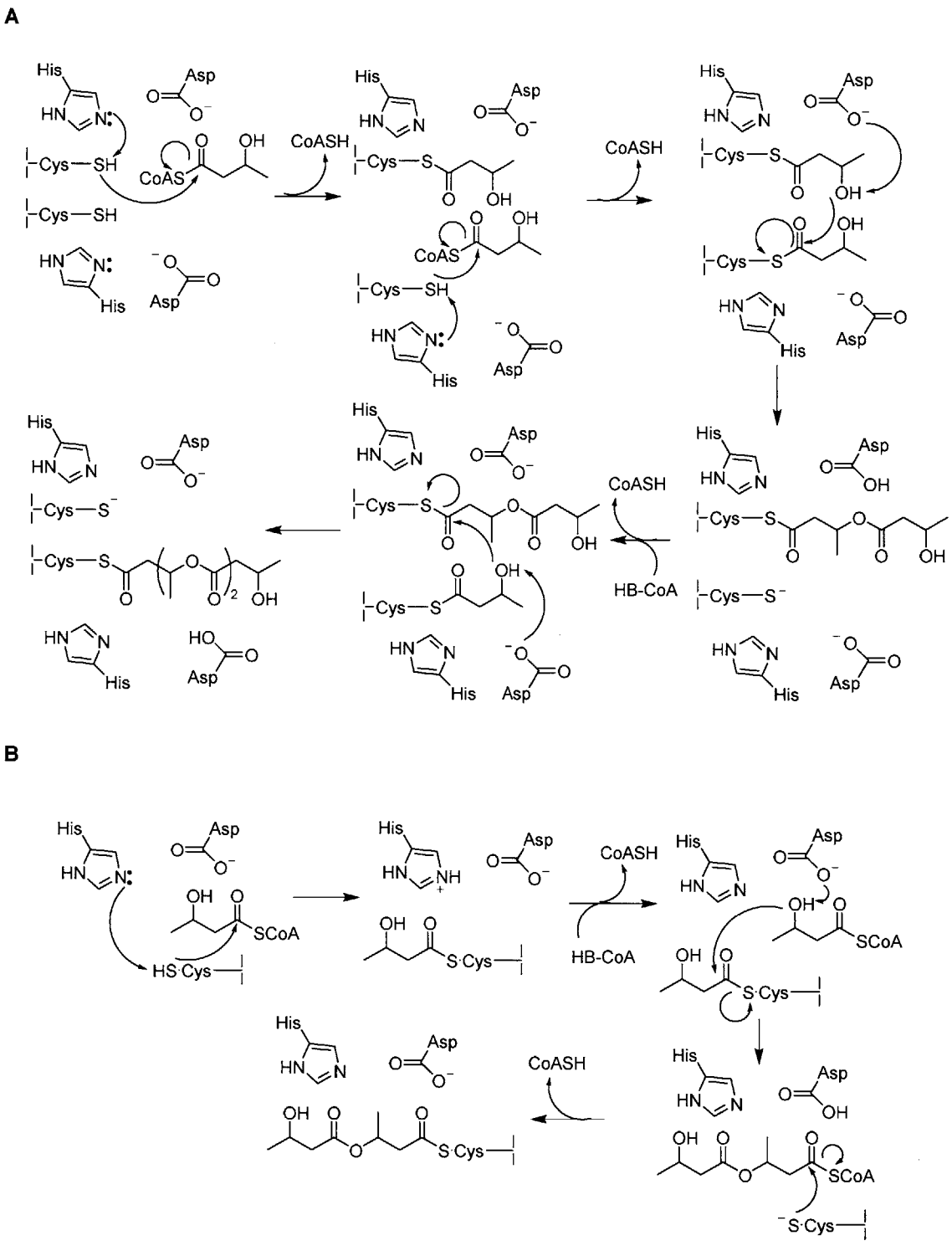

Figure 2.1 Working model for the mechanism of polymerization by PhaCs. A) Mechanistic model based on analogy to fatty acid synthase involving the participating of two Cys residues. B) Mechanistic model based on analogy to some type III polyketide synthases, involving the participation of a single Cys residue.

Studies of the mechanisms of initiation, elongation and termination of PHB polymerization have proved challenging due to a number of peculiarities associated with $PhaC_{Re}$ and $PhaEC_{Av}$. In the present work, we report the isolation and characterization of a class I synthase from *Caulobacter crescentus*, $PhaC_{Cc}$. We were initially interested in $PhaC_{Cc}$ as a candidate for crystallography (Chapter 4), as currently no structure for a PHA synthase has been solved. However, initial purifications revealed that $PhaC_{Cc}$ was well-behaved in solution, prompting us to explore whether it could provide insight into the mechanism of polymerization that have previously been difficult to study in $PhaEC_{Av}$ and $PhaC_{Re}$.

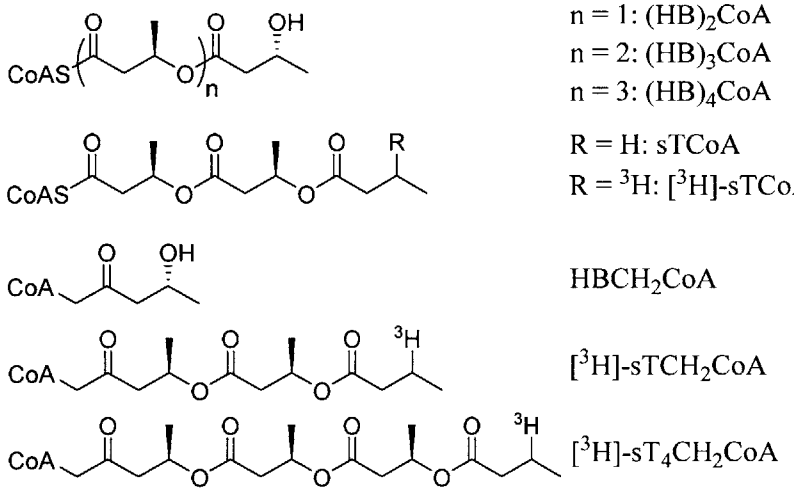

n = 1: $(HB)_2CoA$
n = 2: $(HB)_3CoA$
n = 3: $(HB)_4CoA$

R = H: sTCoA
R = ^3H: [^3H]-sTCoA

$HBCH_2CoA$

[^3H]-$sTCH_2CoA$

[^3H]-sT_4CH_2CoA

Figure 2.2 Structures of synthetic primers, substrate analogs and non-covalent products discussed in this Chapter.

Studies of the initiation of polymerization have been carried out primarily *in vitro* on recombinant synthases. Early attempts to purify overexpressed $PhaC_{Re}$ failed because it non-specifically bound the chromatography resin and glassware. It was not until the non-ionic detergent hecameg was found to bind to a hydrophobic surface of $PhaC_{Re}$ and prevent non-specific binding that our lab in collaboration with the Sinskey lab reported the first successful purification of $PhaC_{Re}$ (*6*). Analysis of CoA release to monitor polymer formation revealed a lag

phase that is variable and dependent on concentration of the synthase. Lag phases in activity can have many possible causes. For example, lag phases have been observed in glycogen synthase when the appropriate initiating primer unit is omitted (*9*). Thus, artificial primers, short oligomers of HBCoA (HB_nCoA, where n = 2-4) and sTCoA (Figure 2.2), were investigated for their effect on the lag phase of $PhaC_{Re}$. Incubation with these molecules resulted in acylation of the active site Cys, which in turn shifted the monomer/dimer equilibrium of $PhaC_{Re}$ towards the dimeric form. In addition, the length of the lag phase of CoA release decreased and the specific activity, measured by the linear part of CoA released subsequent to the lag phase, increased (*3*). This observation suggests that a requirement for priming is at least in part responsible for the observed lag phase, but also raises the question as to what is the relevant primer *in vivo*.

Several studies have addressed the identity of the native primer. Self-priming with HBCoA cannot be studied directly because for both $PhaC_{Re}$ and $PhaEC_{Av}$, the rate of initiation of polymerization is much slower than the rate of elongation. As a consequence, even in the presence of just a few equivalents of HBCoA, a few molecules of PhaC make high M_w polymer whereas the remainder of the PhaC is unmodified (*6, 10, 11*). Recently, Doi and coworkers reported the characterization of the class I synthase from *Aeromonas caviae*, $PhaC_{Ac}$ (*12*). They incubated $PhaC_{Ac}$ with just five equiv. HBCoA and demonstrated by size exclusion chromatography (SEC) that, upon incubation with HBCoA, $PhaC_{Ac}$ shifted from predominantly monomeric to predominantly dimeric. There was no apparent loss of material due to precipitation, though the fraction of aggregated material (that eluted in the void volume) increased. These results suggested that $PhaC_{Ac}$ was uniformly self-priming with HBCoA alone, and that priming shifted the equilibrium towards dimeric PhaC. This result is potentially very

interesting; unfortunately the overall characterization of the enzyme is very poor, thus a more careful examination of priming of $PhaC_{Ac}$ is necessary.

Kudo and coworkers have alternatively proposed that the TCA cycle intermediate succinyl CoA serves as the primer (*13*). They extracted PHB from *R. eutropha* and partially hydrolyzed it in a suspension of chloroform and aqueous HCl into fragments were small enough (800-2500 Da) for end-group analysis by NMR and electrospray ionization mass spectrometry (ESI-MS). From their analysis, they conclude that a fraction of the hydrolytic fragments contained a succinyl group at one end. They propose these fragments represent the end of the polymer synthesized first, and that succinyl CoA is the starter unit. However, attempts in our group to prime $PhaC_{Re}$ by incubation with succinyl CoA did not result in CoA release (Cho and Stubbe, unpublished), though it should be noted that succinyl CoA readily forms succinic anhydride in solution. Thus the nature of the priming unit in PHB biosynthesis remains unclear.

The issue of the slow rate of initiation presents a challenge for studying elongation, as synthase cannot be uniformly loaded in order to study the early steps in polymer elongation. A key mechanistic question initially was to distinguish between the two mechanisms in Figure 2.1 by trapping the putative non-covalent intermediates in Figure 2.1B. To look for non-covalent intermediates, wt $PhaEC_{Av}$ was acylated with sTCoA then incubated with HBCoA (*14*). The reaction was quenched in acid at various time points, the precipitated protein was removed by centrifugation, and the supernatant was examined by HPLC. No non-covalent intermediates could be trapped with wt $PhaEC_{Av}$. However, our inability to observe non-covalent intermediates could mean either that the mechanism in Figure 2.1B is incorrect, or that non-covalent intermediates do form, but the rate of reacylation is too fast to be able to capture them. Thus these experiments failed to distinguish between the two mechanisms. We have recently reported

the trapping of the non-covalent intermediates $(HB)_2CoA$ and $(HB)_3CoA$ from the reaction of the mutant C149S-$PhaEC_{Av}$ with HBCoA (*14*). Mutation of the active site Cys to Ser slowed the rate of reacylation ~150-fold and allowed observation for the first time of non-covalent intermediates of polymerization. However, the caveat remains that mutation of the active site Cys could alter the mechanism of elongation, thus the relevance to the wt mechanism is not unequivocally established.

Efforts have also been made to trap non-covalent intermediates by first priming wt $PhaC_{Re}$ and $PhaEC_{Av}$ with [^{3}H]-sTCoA, then reacting the primed synthase with the chain terminator $HBCH_2CoA$ (Figure 2.2). In principle, if polymerization occurs via the mechanism in Figure 2.1B, then $HBCH_2CoA$ would bind the primed enzyme and attack the [^{3}H]-sT-PhaC thioester, resulting in the formation of [^{3}H]-sT_4CH_2CoA (Figure 2.2). Unexpectedly, the major product of the reaction is [^{3}H]-$sTCH_2CoA$, though a small amount of [^{3}H]-sT_4CH_2CoA is formed as well. A similar phenomenon was observed when the primers $(HB)_2CoA$ and $(HB)_3CoA$ were used in place of sTCoA. While these observations suggest that polymerization occurs via non-covalent intermediates (with the caveat that artificial primers were necessary to observe them), it also raises the issue of unusual, and potentially off-pathway, chemistry taking place in the reaction between PhaCs and artificial primers. A model that could explain the results involves the loading of [^{3}H]-sT first onto an amino acid distinct from the active site Cys, followed by transfer of a saturated dimer unit ([^{3}H]-sD) to the active site Cys. $HBCH_2CoA$ could then bind the active site and attack [^{3}H]-sD-PhaC to produce the observed product [^{3}H]-$sTCH_2CoA$. Whether there is a loading site and the relevance of such a site to the wt enzyme is not clear. These unusual results further underscore the necessity for caution when using substrate analogs

such as artificial primers, but reveal that PhaCs are capable of catalyzing chemistry in addition to the polymerization reaction.

In addition to the chemistry of elongation, the process involves physical steps of packaging of the polymer as the phase transition from soluble to insoluble occurs. Granule assembly *in vivo* involves several proteins in addition to the synthase that become associated with the granule surface as PHB accumulates. Of these, the most predominant are the phasins (PhaPs), which are low M_w proteins that are thought to play a role in determining granule size and number (*15-17*). Several studies have suggested that phasins play an important role in granule assembly. *In vitro*, granules can assemble from synthase and HBCoA alone. However Steinbüchel and coworkers demonstrated by phase contrast as well as scanning electron microscopy that granules synthesized *in vitro* by $PhaEC_{Av}$ are smaller when PhaP1 from *R. eutropha* is included (*18*). Their images are convincing and suggest that phasins influence the process of elongation and granule packing. However, from the level of detail provided in the paper the mole ratio of $PhaEC_{Av}$ to PhaP1 cannot be determined. Assays of $PhaC_{Re}$ in the presence of increasing equivalents of PhaP1 (the major phasin in *R. eutropha*) reveal that PhaP1 increases the length of the lag phase and decreases the specific activity of the enzyme without changing the M_w of the PHB produced. These results were interpreted to suggest that PhaP1 slows the rate of polymerization in order to allow for folding of the nascent PHB chain (*19*).

Finally, when a PHB chain has reached a certain M_w, the chain must be terminated in order to free the PhaC active site for additional polymerization. It has long been known that termination and reinitiation occur *in vivo* (*20*). Recently we have shown in *R. eutropha* that the ratio of PHB chains to $PhaC_{Re}$ increases ~15-fold, from 6 to 87, as the amount of PHB in the cells increases from 5% to 80% cdw, suggesting that there are many termination and reinitiation

events per synthase during PHB accumulation (*19*). PhaCs are thought to catalyze termination, and several species have been proposed to serve as chain transfer agents, including hydroxybutyrate (*21*), CoA (*22*) and a nucleophilic water molecule (*11, 20, 23*). The idea that hydroxybutyrate may function in termination comes from the observation that including compounds such as polyethylene glycol (*24*), glycerol (*21*) and 1,2-propanediol (*21*) in fermentations of *R. eutropha* resulted in PHB of a lower M_w than when these compounds were omitted. Furthermore, the polymer was isolated and characterized by NMR, revealing that the alcohols were attached to the carboxy terminus of the PHB chains, and suggesting that they served as more efficient chain transfer agent than the natural agent, which may be water or hydroxybutyrate. However, an alternative explanation for the observed decrease in M_w is that the alcohols undergo transesterification with the PHB after it is synthesized, rather than specifically interacting with the PhaC active site during polymerization. Thus, the significance of these observations is unclear.

Alternatively, CoA could catalyze termination. Our lab has demonstrated that polymer produced from the substrate analog HB-N-acetylcysteamine (HB-NAC) terminates in NAC (*25*). One possible interpretation of this observation is that in the natural system, CoA serves as the chain transfer agent; however, this has not been demonstrated with HBCoA. Our lab has also previously demonstrated that the synthase catalyzes termination to leave an HB_n (where n = 3-10) primer unit attached to PhaC (*11, 26*). Thus, a plausible model for termination involves the PhaC either activating a water molecule and catalyzing hydrolysis of the PHB chain or catalyzing thiolysis by CoA liberated during the addition of the final HB unit. Finally, the M_w of PHB produced by the *R. eutropha* mutant strains Δ*phaP1* and Δ*phaR* (in which PhaP1 is overexpressed) is lower than that in wt, and in Δ*phaP1* the PDI is higher. These results suggest

that while $PhaC_{Re}$ catalyzes termination, the ratio of PhaP1 to PhaC somehow influences termination in *R. eutropha*, thereby determining the M_w and PDI of the PHB (*19*).

Studies of the mechanisms of initiation, elongation and termination carried out with $PhaEC_{Av}$ and $PhaC_{Re}$ have provided a good deal of insight into PHB biosynthesis. However there have been several challenges associated with studying these enzymes, as described above. In this Chapter, we present the isolation and characterization of the class I synthase $PhaC_{Cc}$ in order to gain additional insight into the mechanism of polymerization. $PhaC_{Cc}$ was originally cloned and purified as a candidate for crystallography studies. In contrast to $PhaC_{Re}$, $PhaC_{Cc}$ was found to be soluble and well-behaved in solution, supporting our efforts to pursue crystallization but also prompting us to investigate whether mechanistic studies could further shed light on our understanding of the polymerization process.

Our studies demonstrate that like $PhaC_{Re}$ and $PhaEC_{Av}$, the rate of initiation by $PhaC_{Cc}$ is much slower than the rate of elongation. Priming $PhaC_{Cc}$ with sTCoA uniformly loads the synthase, but the rate of hydrolysis of the acylated enzyme appears to be rapid and consequently large polymer is still produced. We have also isolated the phasin PhaP, which we identified in studies presented in Chapter 3, and demonstrate that it plays a role in interacting with the growing PHB chain, likely to facilitate *in vitro* granule formation. Finally, studies with the artificial primer sTCoA have revealed additional unusual chemistry suggesting that $PhaC_{Cc}$ can catalyze thiolysis with CoA. These results may provide insight into a possible mechanism for termination by thiolysis via CoA at an internal ester bond leaving $PhaC_{Cc}$ primed with an HB unit.

2.2 Materials and Methods

2.2.1 Materials

All chemicals were obtained at the highest purity available from Sigma-Aldrich (St. Louis, MO) unless otherwise specified. (*R/S*)-[1-^{14}C]-HBCoA was obtained from American Radiolabeled Chemicals, Inc. and diluted with (*R*)-HBCoA synthesized by Dr. Ping Li following the method of Yuan *et al. (27)*. The compounds sTCoA and [^{3}H]-sTCoA were synthesized by Dr. Ping Li according to the method of Jia *et al.* (*4*). Oligonucleotide primers used in this study were obtained from Integrated DNA Technologies (Coralville, IA) and are listed in Table 2.1. Restriction enzymes were purchased from New England Biolabs (Beverly, MA), GoTaq DNA polymerase was purchased from Promega (Fitchburg, WI), and PfuII Turbo and Pfx polymerases were purchased from Stratagene (La Jolla, CA). The plasmids used in this study are listed in Table 2.2. Scintillation fluid was obtained from Perkin Ellmer.

2.2.2 Construction of expression vectors encoding N-terminally tagged PhaC$_{Cc}$s

Genomic DNA was isolated from 1 mL of saturated overnight *C. crescentus* culture grown in PYE using the GenElute Bacterial Genomic Kit (Sigma-Aldrich, St. Louis, MO) according to the manufacturer's protocol for Gram-negative bacteria.

For the construction of pRBhis$_6$phaCΔN and pRBhis$_6$phaC, *phaCΔN* and *phaC* were amplified from ~200 ng of genomic DNA using PfuII Turbo polymerase. For *phaCΔN*, the primers phaCΔNfw/phaCΔNrev were used to insert a 5′ BamHI restriction site and a 3′ NheI restriction site. For *phaC*, the primers phaCfw/phaCrev were used to insert a BamHI restriction site at the 5′ end of *phaC* and an NheI restriction site at the 3′ end of *phaC*. An annealing temperature of 55 °C and an extension temperature of 72 °C for 1 min were used for both

reactions. The amplified products *phaCΔN* and phaC were digested with BamHI and NheI, then ligated into pET28a (Novagen) digested with the same enzymes at an insert to vector ratio of 5:1. The ligation reactions were transformed into *E. coli* XL10 Gold cells, and colonies were screened by colony PCR using GoTaq polymerase and the primers phaCΔNfw/phaCΔNrev or phaCfw/phaCrev for pRBhis$_6$phaCΔN and pRBhis$_6$phaC, respectively. For each plasmid, one colony containing insert was sent for sequencing at MIT Biopolymers Laboratory.

Table 2.1 Primers used in Chapter 2.

Name	Sequence[a]
phaCΔNfw	5′ - GATATAGCTAGCGTCGAGACCCTCTCGGCGAAT - 3′
phaCΔNrev	5′ - GATATAGGATCCTCAGGGTTGTGACTTTACCAGCAC - 3′
phaCfw	5′ - GATATAGCTAGCATGGCCACGGCGAA - 3′
phaCrev	5′ – GATATAGGATCCTCAGGGTTGTGACTTTACCAGCAC - 3′
phaPfw	5′ - GATATACATATGGCCGCGGCCGAAAACCTGAAGACCAC - 3′
phaPrev	5′ - GATATAAAGCTTTTAGCGGGCGGCCTGGAACTTTTCGAC - 3′
phaC406Afw	5′ - GCGTCAACACCGTAGGCTACGCCATCGGCGGCACCCTG CT - 3′
phaC406Arev	5′ - AGCAGGGTGCCGCCGATGGCGTAGCCTACGGTGTTGAC GC - 3′
phaC406Sfw	5′ - CCGTAGGCTACTCCATCGGCGGCACCC - 3′
phaC406Srev	5′ - GGGTGCCGCCGATGGAGTAGCCTACGG - 3′
phaCD562Nfw	5′ - GTGCAGTCCTCGAAGGACAACCACATCGCG - 3′
phaCD562Nrev	5′ - CGCGATGTGGTTGTCCTTCGAGGACTGCAC - 3′
phaCH590Qfw	5′ - CCATGGCCGGTTCGGGTCAGATCGCGGGCGTGATCAACC - 3′
phaCH590Qrev	5′ - GGTTGATCACGCCCGCGATCTGACCCGAACCGGCCATGG- 3′

[a]Restriction sites and mutated codons are underlined.

Table 2.2 Plasmids used in Chapter 2.

Plasmid	Description	Reference
pRBphaC_{Cc}	*phaC_{Cc}* inserted into pET28a between NheI and BamHI restriction sites; encodes N-terminal His_6-tag and the linker SSGLVPRGSHMAS containing a thrombin site (underlined).	This work
pRBphaC_{Cc}-C406A	Same as pRBphaC_{Cc}, with point mutation C406A	This work
pRBphaC_{Cc}-C406S	Same as pRBphaC_{Cc}, with point mutation C406S	This work
pRBphaC_{Cc}-D562N	Same as pRBphaC_{Cc}, with point mutation D562N	This work
pRBphaC_{Cc}-H590Q	Same as pRBphaC_{Cc}, with point mutation H590Q	This work
pRBphaC_{Cc}ΔN	*phaC_{Cc}ΔN* inserted into pET28a between NheI and BamHI restriction sites; encodes N-terminal His_6-tag and the linker SSGLVPRGSHMAS containing a thrombin site (underlined).	This work
pRBphaP	*phaP* inserted into pET28a between NdeI and HindIII restriction sites; encodes N-terminal His_6-tag and the linker SSGLVPRGSH containing a thrombin site (underlined).	This work

2.2.3 Expression and purification of PhaC_{Cc}s

PhaC_{Cc}ΔN and PhaC_{Cc} were expressed in *E. coli* BL21(DE3) cells (Stratagene) from plasmids pRBphaC_{Cc}ΔN and pRBphaC_{Cc}, respectively. Cultures (2 L LB supplemented with 50 μg/mL kanamycin [Km] in 6 L flasks) were inoculated with 5 mL saturated overnight LB cultures and grown at 37 °C to OD_{600} = 0.6. The cultures were then cooled rapidly on ice to ~18 °C and induced with 0.4 mM isopropyl β-D-1-thiogalactopyranoside (IPTG). The cells were grown an additional 3-4 h at 18 °C, then harvested by centrifugation at 3,500 x*g* for 10 min. Cells were flash frozen in liquid nitrogen and stored at -80 °C until use. A typical yield was 2 g wet cell paste per L.

All purification steps were carried out at 4 °C. PhaC_{Cc}ΔN and PhaC_{Cc} were purified by identical methods. In the purification of PhaC_{Cc}, all steps included 1 tablet of protease inhibitor cocktail (Roche) per 50 mL of buffer. Cells were resuspended in 3-5 mL/g of wet cell paste in lysis buffer containing: 50 mM NaH_2PO_4, 300 mM NaCl, 10 mM imidazole, pH 8.0. The cells

were lysed by two passes through a French pressure cell at 14,000 psi. The insoluble cell debris was removed by centrifugation at 17,000 x*g* for 20 min. The soluble fraction was equilibrated with 1 mL of Ni-NTA resin (Qiagen) per 5 mL of soluble extract for 30 min by gentle stirring. The slurry was loaded into a column and the resin allowed to settle, then the flowthrough was collected. The column was washed with 20 column volumes (cv) of lysis buffer followed by 10 cv of lysis buffer with 50 mM imidazole. $PhaC_{Cc}$ and $PhaC_{Cc}\Delta N$ were eluted by batch elution with lysis buffer with 250 mM imidazole. For $PhaC_{Cc}$, the elution fractions containing protein were combined and concentrated to ~200-300 μM (~10-20 mg/mL). $PhaC_{Cc}$ was then exchanged into 20 mM Hepes pH 7.5, 200 mM NaCl, and stored at 4 °C or flash frozen and stored at -80 °C. $PhaC_{Cc}\Delta N$ was concentrated to 0.5-1 mM (~30-60 mg/mL), flash frozen in liquid nitrogen and stored at -80 °C. Typical yields for $PhaC_{Cc}$ and $PhaC_{Cc}\Delta N$ were 3 mg and 10 mg per g of cells, and had specific activities of 50 and 1 U/mg, respectively.

2.2.4 Protein quantitation

Protein concentration was determined by A_{280} (ε = 103,270 M^{-1} cm^{-1} for $PhaC_{Cc}\Delta N$; ε = 103,630 M^{-1} cm^{-1} for $PhaC_{Cc}$; ε = 8,250 M^{-1} cm^{-1} for PhaP) or Bradford assay using BSA as a standard (*28*). The extinction coefficients were determined using the Peptide Property Calculator from Northwestern University (http://www.basic.northwestern.edu/biotools/proteincalc.html) and the concentrations determined using the calculated values were consistent with concentrations determined using the Bradford assay. For heterogeneous mixtures of proteins, total concentration was determined by Bradford assay.

2.2.5 Enzyme assays

All assays are carried out at 30 °C. A typical assay contained in a final volume of 170 µL: 20 mM Hepes pH 7.5, 20 mM NaCl, 1 mM HBCoA and 500 nM $PhaC_{Cc}\Delta N$, 25 nM $PhaC_{Cc}$ or 50-100 µM $PhaC_{Cc}$ mutant ($PhaC_{Cc}$-C406A, -C406S, -D562N, or -H590Q). The reaction was initiated by addition of enzyme. At various time points, 20 µL aliquots were withdrawn and quenched in 50 µL ice-cold 10% trichloroacetic acid (TCA). The samples were centrifuged 5 min at 14,000 x*g* to remove precipitated protein, and 68 µL was removed and added to 262 µL of 0.25 mM 5,5′-dithiobis-(2-nitrobenzoic acid (DTNB) in 0.5 M KH_2PO_4, pH 7.8. The reactions were incubated for 5 min and A_{412} of each sample was measured. Specific activity was calculated from the rate of the first linear phase and is given in U/mg, where one unit is one µmol substrate consumed per min. Data were fit to a sigmoidal function using Equation 2.1.

Equation 2.1 $$y = \frac{Ax^n}{K^n + x^n}$$

To determine the kinetic parameters for HBCoA, the concentration of HBCoA was varied from 0.05 to 6 mM with 50 nM $PhaC_{Cc}$. The data were fit to the Michaelis-Menten equation, equation 2.2, and the Hill equation, Equation 2.3

Equation 2.2 $$v = \frac{V_{max}[S]}{K_M + [S]}$$

Equation 2.3 $$v = \frac{V_{\max}[S]^n}{K^n + [S]^n}$$

2.2.6 Stability of purified $PhaC_{Cc}$ upon storage at 4 °C and -80 °C

The specific activity of freshly-purified $PhaC_{Cc}$ was compared to $PhaC_{Cc}$ stored for one week at 4 °C in 20 mM Hepes pH 7.5, 200 mM NaCl with and without 20% glycerol or for one

week at -80 °C in 20 mM Hepes pH 7.5, 200 mM NaCl with and without 20% glycerol. The activity was measured as described above.

2.2.7 Construction of active site mutants of $PhaC_{Cc}$

The mutants $PhaC_{Cc}$-C406S, -D562N and -H590Q were generated from the template pRBhis$_6$phaC using the primers phaCC406Sfw/phaCC406Srev, phaCD562Nfw/phaCD562Nrev and phaCH590Qfw/phaCH590Qrev, respectively (Table 2.1). The reactions contained 50 ng pRBhis$_6$phaC as template and 1 μM of each primer and PfuII Turbo polymerase, and were carried out using an annealing temperature of 55 °C for 30 s and an extension temperature of 68 °C for 7 min. All sequences and mutations were confirmed by sequencing at MIT Biopolymers Laboratory.

Attempts to generate the active site C406A mutant synthase by conventional mutagenesis methods were unsuccessful. Therefore, this mutant was generated by the primer overlap extension method (*29*). This method is briefly outlined in Figure 2.3. The PCR products described below are named following the scheme in Figure 2.3. For the construction of pRBhis$_6$phaC-C406A, the 5′ region of *phaC* was amplified using *GoTaq* polymerase and the primers phaCfw and phaCC406Arev (product his$_6$AB), and the 3′ region was amplified using *GoTaq* polymerase and the primers phaCC406Afw and phaCrev (product his$_6$CD) (Table 2.1). An annealing temperature of 55 °C and extension temperature of 72 °C for 1 min were used. phaCfw introduced an NheI restriction site at the 5′ end of his$_6$AB and phaCrev introduced a BamHI restriction site at the 3′ end of his$_6$CD.

The amplified PCR products were purified and the relative concentrations estimated by densitometry analysis by ethidium bromide staining in a 1% agarose gel. Based on this analysis,

products his_6AB and his_6CD were combined in a 1:1 ratio. These products then served as the templates for a second set of PCR reactions. his_6AB and his_6CD were amplified using *GoTaq* polymerase and the primers phaCfw and phaCrev. This PCR reaction "stitched" together the two template pieces, producing the products his_6AD corresponding to *his_6-phaC-C406A*. *his_6-phaC-C406A* was subcloned into pCR2.1 TOPO by the manufacturer's protocol, then excised using the appropriate restriction enzymes. Using T4 DNA ligase, *his_6-phaC-C406A* was then ligated into pET28a (Novagen) between the NheI and BamHI restriction sites.

The resulting plasmid, pRBhis_6phaC-C406A was sequenced at MIT Biopolymers Laboratory and found to contain a single base pair insertion at the site of the mutation. Therefore a final round of mutagenesis using PfuII polymerase and the primers phaCC406Afw and phaCC406Afw was carried out to remove the insertion using an annealing temperature of 55 °C and an extension temperature of 68 °C. The sequence was confirmed by sequencing at the MIT Biopolymers Laboratory.

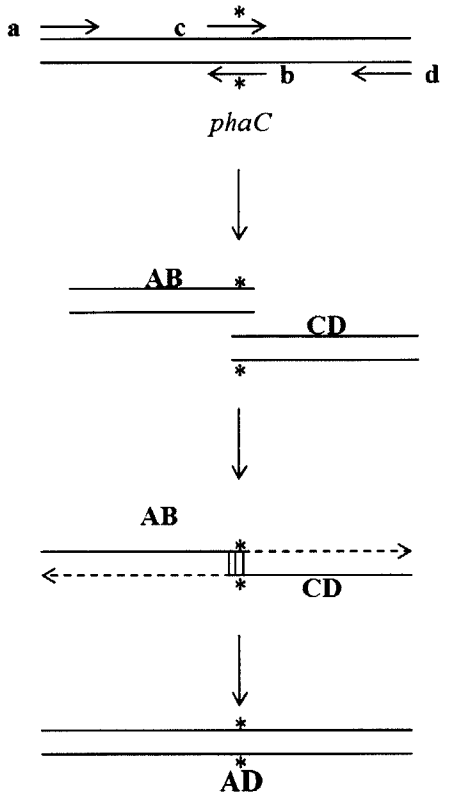

Figure 2.3 Schematic of primer overlap extension method of mutagenesis adapted from (*29*). Site-directed mutagenesis is accomplished using primers b and c, which contain the mutation (*), and primers a and d, which anneal to the 5′ and 3′ ends of the gene, respectively. The first PCR reaction produces fragments AB and CD. PCR products AB and CD, which overlap at the site of the mutation, are then used as template for the second PCR reaction. AB and CD hybridize at the site of the mutation and PCR using primers a and d generates the full length product AD.

2.2.8 Determination of the quaternary structure of $PhaC_{Cc}$ by size exclusion chromatography (SEC)

$PhaC_{Cc}$ (100 μL, 1-100 μM) and $PhaC_{Cc}\Delta N$ (1-50 μM) were injected onto a Superdex 200 10/300 GL analytical column (M_w range = 10,000-600,000 Da, GE Healthcare, Piscataway, NJ) attached to an Akta Purifier FPLC (GE Healthcare, Piscataway, NJ) at 4 °C. The eluent was 20 mM Hepes pH 7.5, 200 mM NaCl and the flow rate was 0.25 mL/min. A_{280} and A_{260} were monitored. Retention volumes (times) were compared with the retention volumes (times) of M_w

standards (GE Healthcare): thyroglobulin (M_w = 669 kDa, retention volume, time = 8.5 mL, 34 min); ferritin (440 KDa, 10.0 mL, 40 min); aldolase (158 kDa, 12.3 mL, 49.2 min); conalbumin (75 kDa, 13.9 mL, 55.6 min); ovalbumin (44 kDa, 58.8 min). The void volume of the column (7.22 mL, 28.9 min) was measured by injecting 100 µL of a 1 mg/mL solution of Blue Dextran (GE Healthcare). To prepare the standard curve, the partition coefficient (K_{av}) of each sample was calculated using Equation 2.4.

Equation 2.4

$$K_{av} = \frac{V_e - V_0}{V_c - V_0}$$

V_e is the retention volume measured for a given standard, V_0 is the void volume, and V_c is the column bed volume (24 mL). A plot of K_{av} vs. logM_w was prepared from the K_{av} values of the standards generating the standard curve and the M_w determined using this curve.

To measure the recovery of $PhaC_{Cc}$ from the column, the protein peak was collected and concentrated to ~3 mL using a Centricon YM30 spin concentrator with a molecular weight cutoff of 30,000 Da (Millipore, Billerica, MA).

2.2.9 Stoichiometry of acylation and rate of hydrolysis of acylated $PhaC_{Cc}$ generated from sTCoA

The stoichiometry of acylation of $PhaC_{Cc}$ was measured using the DTNB assay to monitor CoA release. The reaction was carried out at 30 °C and contained in a final volume of 110 µL: 20 mM Hepes pH 7.5, 20 mM NaCl, 50 µM $PhaC_{Cc}$ and 500 µM sTCoA. At various time points, 20 µL aliquots were withdrawn and quenched in 50 µL ice cold 10% TCA. The samples were analyzed by the discontinuous DTNB assay described above at time points from 10 s to 5 min.

2.2.10 Stability of [^{3}H]-sT-PhaC$_{Cc}$ by Sephadex G50 chromatography

2.2.10.1 Separation in 20 mM Hepes, pH 7.5, 200 mM NaCl.

In a final volume of 75 µL at 30 °C, the reaction contained: 50 µM PhaC$_{Cc}$ (3.75 nmol) and 500 µM [^{3}H]-sTCoA (specific activity 1900 cpm/nmol) in 20 mM Hepes pH 7.5, 200 mM NaCl. The reaction was initiated by addition of enzyme and then immediately loaded onto a 10 mL Sephadex G50 column (7 mm x 300 mm). The column was eluted with 20 mM Hepes pH 7.5, 200 mM NaCl at 0.6 mL/min. The eluent was collected in 25 x 80 µL fractions, 70 x 40 µL fractions, then 95 x 80 µL fractions in 96-well plates. The A_{280} and A_{260} of each fraction was measured and then the fractions were added to 900 µL H_2O and 9 mL scintillation fluid. Each well was washed with an additional 120 µL H_2O, and added to the mix.

2.2.10.2 Separation in 20 mM KH_2PO_4, pH 4.5, 2 M urea

The reaction was carried out at 30 °C. In a final volume of 50 µL, the reaction contained: 50 µM PhaC$_{Cc}$ (2.5 nmol) and 500 µM [^{3}H]-sTCoA (specific activity 1300 cpm/nmol) in 20 mM Hepes pH 7.5, 200 mM NaCl. The reaction was initiated by addition of enzyme and was immediately loaded onto a 10 mL Sephadex G50 column (7 mm x 300 mm) and eluted with 20 mM KH_2PO_4 pH 4.5, 2 M urea at 0.3 mL/min. The eluent was collected in 160 x 100 µL fractions in 96-well plates and analyzed as described above.

2.2.11 Separation in 20 mM Hepes, pH 7.5, 200 mM NaCl following reaction of sT-PhaC with 5 equiv. HBCoA

In a final volume of 50 µL at 30 °C, the reaction contained: 200 µM PhaC$_{Cc}$ (3.75 nmol) and 500 µM [^{3}H]-sTCoA (specific activity 1300 cpm/nmol) in 20 mM Hepes pH 7.5, 200 mM NaCl. The reaction was initiated by addition of enzyme, and after ~10 s was chased with 1 mM

HBCoA, then loaded onto a 10 mL Sephadex G50 column (7 mm x 300 mm, 10 mL) and eluted with 20 mM Hepes pH 7.5, 200 mM NaCl at 0.6 mL/min. The eluent was collected in 190 x 100 µL fractions in 96-well plates and analyzed as described above.

2.3.12 Analysis of small molecule products of the reaction of sTCoA with $PhaC_{Cc}$ by HPLC

In a final volume of 500 µL at 30 °C, the reaction contained: 50 µM $PhaC_{Cc}$ and 500 µM [^{3}H]-sTCoA (specific activity = 147 cpm/nmol) in 20 mM Hepes pH 7.5, 20 mM NaCl. Aliquots (50 µL) were withdrawn from 5 s to 5 min and quenched in 20 µL ice-cold 10% TCA. The samples were centrifuged at 4 °C for 10 min at 20,000 x*g* to pellet the precipitated protein. The supernatant was removed and the pellets were washed with 50 µL ice cold H_2O, and the wash combined with the supernatant. The combined wash and supernatant were adjusted to pH ~5 by addition of 12 µL 1 M NaOH. One hundred µL of each sample was injected onto a nucleoside-nucleotide column (Alltech, 7 µm, 4.6 mm x 250 mm) attached to a Waters HPLC equipped with a diode array detector. The elution protocol used 20 mM KP_i pH 4.7 (solvent A) and methanol (solvent B) and a linear gradient from 5% to 70% solvent B from 0-60 min. Fractions (1 mL) were collected, and 900 µL from each fraction was combined with 9 mL scintillation fluid (Perkin Ellmer) and counted for 10 min. The rate of sTCoA consumption and new product formation were fit to Equations 2.5 and 2.6.

Equation 2.5 $$y = y_0 + Ae^{-x/t}$$

where 1/t is the rate constant of sTCoA consumption. To calculate the rate of sDCoA formation, the total nmol of sDCoA present in the reaction was determined by the total radioactivity in the peak. To determine the rate constant *k*, the data were fit to Equation 2.6.

Equation 2.6 $$y = A_1 - A_2e^{-kx}$$

2.2.13 Identification of small molecule products of the reaction of sTCoA with $PhaC_{Cc}$ by matrix assisted laser desorption mass spectrometry time of flight analysis (MALDI-TOF)

In a final volume of 50 μL, the reaction contained: 50 μM $PhaC_{Cc}$ and 500 μM sTCoA in 20 mM Hepes pH 7.5, 20 mM NaCl. The sample was then treated and analyzed by HPLC identically to the time points described above. The peaks were collected from the HPLC, shell frozen in liquid N_2 and lyophilized. The samples were solubilized in 100 μL H_2O and submitted for MALDI-TOF analysis at MIT Biopolymers. Ten μL of each sample was desalted using a Zip-tip (C18, Millipore, Billerica, MA) and eluted with 50% acetonitrile, 0.1% trifluoroacetic acid (TFA) and then combined 1:1 with matrix (α-cyano-4-hydroxycynammic acid) and analyzed.

To quantitate products containing no radioactivity, a standard curve using known amounts of HBCoA was prepared. Samples (100 μL containing 10-250 nmol) were injected onto the HPLC and analyzed by A_{260}. The peaks were integrated and peak areas were plotted against nmol HBCoA to generate a standard curve. The amount of sTCoA was quantitated by A_{260} as well because the peak overlapped with a peak containing radioactivity but no A_{260}.

2.2.14 Gel permeation chromatography (GPC) analysis of the M_w of PHB produced by reaction of $PhaC_{Cc}$ and sT-$PhaC_{Cc}$ reacted with HBCoA

The M_w and PDI of PHB produced by $PhaC_{Cc}$ *in vitro* under three different reaction conditions was determined.

PHB in a typical assay (reaction 1). The reaction contained in a final volume of 100 μL: 50 nM $PhaC_{Cc}$ and 1 mM [1-^{14}C]-HBCoA (specific activity 175 cpm/nmol (*R*)-HBCoA), 20 mM

Hepes pH 7.5, 20 mM NaCl. The reaction was carried out 30 min at 30 °C, at which time all the substrate was consumed.

*PHB produced by reaction of [^{3}H]-sT-PhaC with HBCoA to determine whether sTCoA is chemically competent for polymerization (reaction **2**).* In a final volume of 12.5 μL at 30 °C, $PhaC_{Cc}$ (50 μM) was reacted with 500 μM [^{3}H]-sTCoA (specific activity = 5700 cpm/nmol) for 10 s at room temperature (RT) in 20 mM Hepes pH 7.5, 20 mM NaCl. Ten μL of this reaction was then added to 990 μL 20 mM Hepes pH 7.5, 20 mM NaCl to dilute $PhaC_{Cc}$ and unreacted [^{3}H]-sTCoA, and 100 μL was diluted into 1 mM HBCoA in 1 mL 20 mM Hepes pH 7.5, 20 mM NaCl to give a final concentration of 50 nM $PhaC_{Cc}$. The reaction was carried out for 30 min at 30 °C.

*PHB produced by reaction of sT-PhaC with [1-^{14}C]-HBCoA (reaction **3**).* This reaction was identical to reaction 2, except that unlabeled sTCoA and [1-^{14}C]-HBCoA (specific activity 175 cpm/nmol (*R*)-HBCoA) were used.

GPC analysis of PHB produced. The three reaction mixtures were transferred to borosilicate tubes (16 x 125 mm), shell frozen and lyophilized to dryness. A magnetic stir-bar was added to each tube, the tubes were capped with rubber septa, and each septum was pierced with a glass Pasteur pipette, which functioned as a make-shift reflux condensor. $CHCl_3$ (2 mL) was added to each tube, which were refluxed for 48 h at 70 °C. The tubes were then cooled, centrifuged at 4 °C for 10 min at 3,000 x*g* to pellet the insoluble material, and the chloroform was carefully removed with a Pasteur pipette and stored at -20 °C until analysis. The insoluble material was refluxed an additional 48 h in 2 mL fresh chloroform at 70 °C, after which the insoluble material was once again pelleted by centrifugation. This chloroform extract was combined with the material from the first extraction. The samples were then filtered to remove

remaining insoluble material using a glass syringe (0.5 mL) fitted with a 0.4 μm PTFE filter (13 mm). The filters were washed with 3 mL fresh chloroform, which was added to the filtrate. Reactions **1** and **3** were concentrated to 500 μL and reaction 2 was concentrated to 250 μL by evaporating excess chloroform under a stream of air. To determine recovery, 25 μL of the extracted material was placed in a scintillation vial and the chloroform was evaporated under a stream of air. The radioactivity in each sample was analyzed by liquid scintillation counting.

Each sample (100 μL) was then injected onto a 2 x 300 x 7.5 mm Plgel Olexis column (Varian, Palo Alto, CA) connected to a Waters 515/2487 HPLC and eluted at a flow rate of 1 mL/min with chloroform at 30 °C. Fractions (1 mL) were collected, and each fraction was placed in a scintillation vial and the chloroform was evaporated under a stream of air. Fractions were mixed with 9 mL of scintillation fluid, vigorously vortexed, and analyzed by scintillation counting. Isopropanol (retention time, 21 min) was added to each sample as an internal standard (at 1 μL per 120 μL of sample) to normalize product retention times. Molecular weights were determined by comparison to a set of polystyrene standards (Varian) of the M_w (retention time): 3.1 kDa (17.8 min), 10 kDa (17 min), 73 kDa (15.4 min), 205 kDa (14.8 min), 490 kDa (13.9 min), 1800 kDa (12.9 min), 5000 kDa (12.4 min). The M_w and PDI of each sample were determined using the standard curve polynomial generated by PSS WinGPC Unity software with the above standards. The preparation of the standard curve is described in detail in section 3.2.11 of Chapter 3. Retention volumes were plotted against radioactivity and M_w, M_n and PDI were determined using Equations 3.6, 3.7 and 3.8, and the adjusted calibration curve in section 3.2.11. Radioactivity was substituted for refractive index intensity (I_V).

2.2.15 Activity of $PhaC_{Cc}$ following acylation with sTCoA

In a final volume of 10 μL at 30 °C, $PhaC_{Cc}$ (50 μM) was reacted with 500 μM sTCoA. After ~10 s, the reaction was diluted with 590 μL 20 mM Hepes pH 7.5, 20 mM NaCl, and 10 μL was withdrawn and added to an assay mixture. The assay mixture contained, in a final volume of 170 μL: 50 nM $PhaC_{Cc}$ (some portion of which is acylated with sT), ~0.5 μM sTCoA and 1 mM HBCoA. At various time points, 20 μL aliquots were withdrawn, quenched in 50 μL ice cold 10% TCA and analyzed by the discontinuous DTNB assay as described above.

2.2.16 Examination of the uniformity of loading of reaction of $PhaC_{Cc}$ with HBCoA

2.2.16.1 SDS-PAGE and autoradiography analysis

In a final volume of 22 μL, $PhaC_{Cc}$ (4 μM) was reacted with 5 and 50 equiv. of [1-^{14}C]-HBCoA (88,000 cpm total per reaction) at 30 °C. At 10 and 30 s, 10 μL aliquots were withdrawn and quenched in 10 μL Laemmli buffer (without reducing agent) and the samples were not boiled. A $PhaC_{Cc}$ standard and the 20 μL samples were quickly loaded onto a 10% SDS-PAGE gel and run at 150 V for 1 h on ice. The gel was stained for 15 min in fresh Coomassie stain, then destained for 15 min in fast destain. The gel was rinsed 3 x 5 min in H_2O, then immediately dried. The gel was then exposed to a low energy phosphor screen (Molecular Dynamics) for 12 h. The phosphor screen was scanned using the Storm Imaging System and analyzed using ImageQuant TL software (Amersham Biosciences). Densitometry analysis was performed using ImageJ Software (*30*).

2.2.16.2 GPC analysis

In a final volume of 100 μL the reaction contained: 4 μM $PhaC_{Cc}$ and 200 μM [1-^{14}C]-HBCoA (specific activity 175 cpm/nmol (*R*)-HBCoA) in 20 mM Hepes pH 7.5, 20 mM NaCl.

The reaction was carried out for 5 min at 30 °C to allow for complete substrate consumption. Proteinase K (50 μg) (Sigma-Aldrich) was added to the reaction and incubated 30 min at 37 °C to digest $PhaC_{Cc}$. The reaction was transferred to a borosilicate tube (16 mm x 125 mm), flash frozen and lyophilized to dryness. PHB was extracted as described in section 2.2.13. The extracted PHB was concentrated to 250 μL by evaporating chloroform under a stream of air. A sample (100 μL) was analyzed by GPC as described in section 2.2.13.

2.2.17 Examination of the uniformity of loading of reaction of $PhaC_{Cc}$ primed with sTCoA and then reacted with HBCoA

In a final volume of 22 μL, $PhaC_{Cc}$ (4 μM) was reacted with 500 μM sTCoA for ~10 s at 30 °C and the reaction was chased with 5 or 50 equiv. [1-^{14}C]-HBCoA (85,000 cpm total per reaction) for 30 s. The reactions were quenched by the addition of 22 μL Laemmli buffer without reducing agent and the samples were not boiled. Twenty μL of each sample was loaded immediately onto one half of a 10% SDS-PAGE gel for Coomassie staining and onto the other half for autoradiography. $PhaC_{Cc}$ standards were also loaded to each half of the gel and the gel was run on ice for 1 h at 150 V. The gel was then carefully cut in half. One half was stained for 15 min in fresh Coomassie stain, then destained for 15 min in fast destain. The gel was rinsed 3 x 5 min in H_2O, then imaged. The other half was immediately dried and exposed to a low energy phosphor screen for 12 h and scanned as above. A standard curve of the log(M_w) of four protein standards and the $PhaC_{Cc}$ control was prepared by measuring (in mm) the distance traveled by each protein standard from the top of the separating gel.

2.2.18 Analysis of $PhaC_{Cc}$ migrating with [^{14}C]-PHB by SDS-PAGE, Western blot and silver stain analysis

In a final volume of 22 μL, $PhaC_{Cc}$ (4 μM) was pre-incubated 30 s at RT with 0 or 500 μM sTCoA, then 50 equiv. of [1-^{14}C]-HBCoA (85,000 cpm) was added for a final volume of 22 μL. The reactions were quenched after 10 s with an equal volume of Laemmli buffer without reducing agent and the reactions were not boiled. Each sample was split into two 10 μL fractions, which were loaded onto two separate 10% SDS-PAGE gels. The gels were run on ice for 1 h at 150 V. One gel was stained for 15 min in fresh Coomassie stain, and destained for 15 min in fast destain. The gel was rinsed 3 x 5 min in H_2O, then imaged. The second gel was rinsed in for 30 min in 25 mM Tris base pH 8.3, 192 mM glycine, 0.01% SDS (w/v), 15% methanol (v/v) (Western blot transfer buffer). The protein samples were then wet transferred onto a PVDF membrane (Immun-Blot, Bio-Rad) in Western transfer buffer for 80 min at 100 V on ice. The membranes were then blocked in blocking buffer containing 3% milk (w/v) in Tris-acetate-EDTA (TAE) buffer with 0.1% Tween-20 (v/v). The primary rabbit antibodies for PhaC were used without further purification. Blots were incubated with anti-PhaC antibody (1:2000 diluted) in blocking buffer for 1 h at RT, then rinsed 3x for 5 min in 50 mL phosphate buffered saline (PBS). For the secondary antibody, goat anti-rabbit antibody conjugated with horseradish peroxidase (Thermo Scientific, Rockford, Ill.) was used at a 1:2000 dilution in blocking buffer. The blots were incubated in secondary antibody for 1 h at RT, then rinsed 3x for 5 min in 50 mL PBS. The blots were developed using SuperSignal® West Femto Maximum Sensitivity Substrate (Thermo Scientific) and imaged using a BioRadChemiDoc XRS imager.

2.2.19 Cloning, expression and purification of PhaP

For construction of the plasmid pRBhis$_6$phaP, *phaP* was amplified from ~200 ng of genomic DNA using *Taq* polymerase and the primers phaPfw/phaPrev (Table 2.1) to introduce a 5′ NdeI restriction site and a 3′ HindIII restriction site, respectively. The amplified PCR product was digested with NdeI and HindIII and ligated overnight at RT with pET28a vector digested with the same restriction enzymes at an insert to vector ratio of 5:1. The ligation reaction was transformed into *E. coli* XL10 Gold cells, and colonies were screened by colony PCR using GoTaq polymerase and the primers phaPfw/phaPrev (Table 2.1). One colony containing insert was sent for sequencing at the MIT Biopolymers Laboratory.

pRBPhaP was transformed into *E. coli* BL21(DE3) cells. Cultures (2 L LB supplemented with 50 μg/mL Km in 6 L flasks) were inoculated with 5 mL saturated overnight culture and grown at 37 °C to OD_{600} = 0.6. The cultures were then cooled on ice to ~18 °C and expression was induced by addition of 0.4 mM IPTG. The cells were grown 3-4 h at 18 °C and harvested by centrifugation. Cells (typically 2 g per L of culture) were flash frozen in liquid nitrogen and stored at -80 °C until use.

All purification steps were carried out at 4 °C. Cells were resuspended in 3-5 mL/g of wet cell paste in lysis buffer containing: 50 mM NaH_2PO_4, 300 mM NaCl, 10 mM imidazole, pH 8.0. The cells were lysed by two passes through a French pressure cell at 14,000 psi. The insoluble cell debris was removed by centrifugation at 17,000 x*g* for 20 min. The soluble fraction was equilibrated with 1 mL of Ni-NTA resin (Qiagen) per 5 mL of soluble extract for 30 min by gentle stirring. The slurry was loaded into a column and the resin allowed to settle, then the flowthrough was collected by gravity flow. The column was washed with 20 cv of lysis buffer followed by 10 cv of lysis buffer with 50 mM imidazole. PhaP was eluted with 5 cvs lysis buffer

containing 250 mM imidazole. The fractions containing PhaP (determined by A_{280}) were combined and exchanged into 50 mM Tris pH 7.6, 10 mM NaCl and combined with 0.25 mL Q Sepharose resin per mg of protein. Under these conditions, PhaP does not bind to the column. The flowthrough containing PhaP was thus collected and concentrated to 200 μM (3 mg/mL). Subsequent to purification, the His_6 affinity tag was removed by treatment with three units of thrombin (Roche) per mg of PhaP for 12 h at 4 °C. A typical yield was 5 mg PhaP per g of cells.

2.2.20 Determination of oligomeric state of PhaP by SEC

PhaP (100 μL of 180 μM) was injected onto a Superdex 200 10/300 GL column (M_w range = 10,000-600,000 Da, GE Healthcare, Piscataway, NJ) attached to an Akta Purifier FPLC (GE Healthcare, Piscataway, NJ) at 4 °C. The eluent was 20 mM Hepes pH 7.5, 200 mM NaCl and the flow rate was 0.25 mL/min. A_{280} and A_{260} was monitored. Retention times were compared with the retention times of the M_w standards described in section 2.2.9.

2.2.21 Effect of PhaP, BSA and hecameg on $PhaC_{Cc}$ activity

In a final volume of 170 μL, the reaction mixture contained: 20 mM Hepes pH 7.5, 20 mM NaCl, 0.76 mM HBCoA, 25 nM $PhaC_{Cc}$ and 25 nM to 12.5 μM PhaP or 25 nM BSA. PhaP or BSA and HBCoA were preincubated at 30 °C for 5 min, then reaction was initiated by addition of $PhaC_{Cc}$. At various time points, 20 μL aliquots were withdrawn and quenched in 50 μL 10% TCA. Time points were analyzed as described above using the discontinuous DTNB assay. A similar reaction was carried out with $PhaC_{Cc}\Delta N$. In a final volume of 170 μL, the reaction mixture contained: 20 mM Hepes pH 7.5, 20 mM NaCl, 500 nM $PhaC_{Cc}\Delta N$, 500 nM untagged-PhaP and 0.76 mM HBCoA.

2.2.22 Pull-down of PhaP with $PhaC_{Cc}\Delta N$ and $PhaC_{Cc}$

A final volume of 1 mL contained 20 mM Hepes pH 7.5, 20 mM NaCl, 10 μM $PhaC_{Cc}\Delta N$ or $PhaC_{Cc}$ and 10 μM untagged-PhaP and was incubated for 10 min at 4 °C. The mixture was then incubated with 0.2 mL Ni-NTA agarose resin, loaded into a column (0.5 x 1.2 cm) and the flow through collected. The column was washed with 4 x 1 mL fractions of 20 mM Hepes pH 7.5, 20 mM NaCl, 10 mM imidazole and the washes collected. The protein was eluted with four 1 mL fractions of 20 mM Hepes pH 7.5, 20 mM NaCl, 250 mM imidazole. Fifteen μL of each fraction was combined with 10 μL Laemmli buffer and analyzed by 15% SDS-PAGE. A control reaction containing only 10 μM untagged-PhaP was carried out identically to assess non-specific binding to the Ni-NTA resin.

2.2.23 Examination of the effect of PhaP on the uniformity of loading of $PhaC_{Cc}$ by SDS-PAGE and autoradiography

A final volume of 22 μL contained: $PhaC_{Cc}$ (4 μM) pre-incubated 5 min at RT with 4 μM PhaP, and the reaction was chased with 5 or 50 equiv. of [1-^{14}C]-HBCoA (85,000 cpm total per reaction). The reactions were quenched by the addition of 22 μL Laemmli buffer without reducing agent and the samples were not boiled. The samples were then processed as described in section 2.2.16.1.

2.3 Results

2.3.1 Expression and purification of $PhaC_{Cc}$ and $PhaC_{Cc}\Delta N$

PhaC from *C. crescentus* is annotated in the NCBI database as a 65 kDa synthase (accession number NP_420193) with the start methionine indicated with an arrow in Figure 2.4. In 2001, however, Qi and coworkers suggested that the start codon had been misassigned and that PhaC was actually a 73 kDa synthase containing an unusual N-terminal domain rich in proline, alanine and lysine residues that contains no homology to any protein in the database (*31*). This proposal was based on cross-reactivity between antibodies raised to $PhaC_{Re}$ and a 73 kDa band with which it reacted in *C. crescentus* crude extracts. Alignment of $PhaC_{Re}$ with the longer PhaC from *C. crescentus* shows that the two share 37% sequence identity, and that the majority of the putative N-terminal domain does not align with $PhaC_{Re}$ (Figure 2.4). Secondary structure prediction programs such as Jpred and CFSSP (Chou and Fassman Secondary Structure Prediction Server) gave no insight about the N-terminal domain.

To investigate which annotation was correct, we cloned, expressed and purified both constructs of PhaC. The portion of *phaC* that encodes the truncated 65 kDa $PhaC_{Cc}$ construct (*phaCΔN*) was cloned into pET28a to encode an N-terminal His_6-tag with no linker, and with $(G_4S)_n$ linkers where n = 1, 2 and 3. Expression and small-scale purification of these proteins revealed no benefit to having $(G_4S)_n$ linkers, and we therefore proceeded with the construct with no additional linker between the His_6-tag and the N-terminus of PhaC. The full length *phaC* was cloned into pET28a to encode a His_6-tag with a spacer between the tag and the start of *phaC* that encodes the following amino acid sequence: SSGLVPRGSHMAS. The underlined portion of the linker is a thrombin cleavage site.

Figure 2.4 Alignment of $PhaC_{Re}$ with $PhaC_{Cc}$. The arrow indicates the start Met as annotated in the database used for $PhaC_{Cc}\Delta N$. Red boxes highlight the active site residues. The synthases share 37% identity.

Expression of both full-length $PhaC_{Cc}$ and $PhaC_{Cc}\Delta N$ at 37 °C resulted in little protein in the soluble fraction, thus expression of both proteins was carried out at 18 °C. Typical growths of $PhaC_{Cc}$ and $PhaC_{Cc}\Delta N$ yielded 2 g cells per L of culture and typical purifications yielded about 10 mg protein per g of cells in the case of $PhaC_{Cc}\Delta N$ and 3 mg protein per g cells in the case of $PhaC_{Cc}$. During purification, a large fraction of both $PhaC_{Cc}\Delta N$ and $PhaC_{Cc}$ was lost in the 50 mM imidazole wash (Figure 2.5A, lane 6 and Figure 2.5B, lane 8); however, in both cases the specific activity of this fraction was considerably lower than that of the final protein (0.09 vs. 1 U/mg in Table 2.3, 8.5 vs. 50 U/mg in Table 2.4) despite the proteins being comparably pure by SDS-PAGE. It is possible that the protein that elutes in the 50 mM imidazole wash is aggregated protein. Furthermore when the 50 mM imidazole wash is assayed, it is diluted into buffer so the assay contains ~2 mM imidazole, which may negatively affect activity. In a single step, both proteins can be purified to 95% homogeneity as judged by 10% SDS-PAGE (Figure 2.5A, lane 7 and Figure 2.5B, lane 9) and the pure protein is free of DNA contamination. Unlike $PhaC_{Re}$, successful purification of both $PhaC_{Cc}$ constructs does not require additives such as the detergent hecameg.

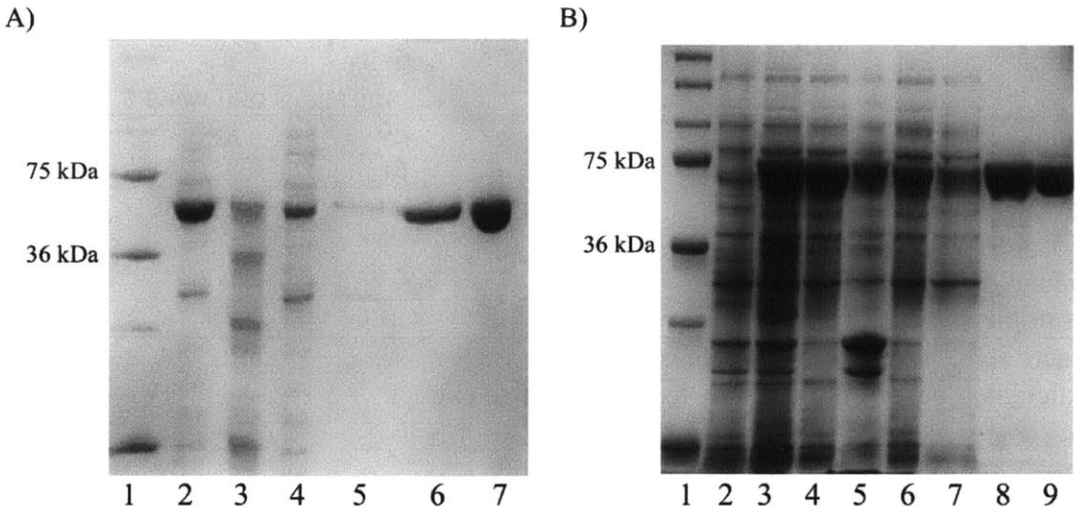

Figure 2.5 Typical 10% SDS-PAGE purification gel of $PhaC_{Cc}\Delta N$ and $PhaC_{Cc}$. A) Purification gel of $PhaC_{Cc}\Delta N$. Lane 1, M_w standards. Lane 2, soluble cell-free extract. Lane 3, insoluble cell-free extract. Lane 4, Ni-NTA agarose flowthrough. Lane 5, 10 mM imidazole wash. Lane 6, 50 mM imidazole wash. Lane 7, final purified $PhaC_{Cc}\Delta N$, eluted with 250 mM imidazole. B) Purification gel of $PhaC_{Cc}$. Lane 1, M_w standards. Lane 2, whole cell pre-induction sample. Lane 3, whole cell post-induction sample. Lane 4, soluble cell-free extract. Lane 5, insoluble cell-free extract. Lane 6, Ni-NTA agarose flowthrough. Lane 7, 10 mM imidazole wash. Lane 8, 50 mM imidazole wash. Lane 9, final purified $PhaC_{Cc}$, eluted with 250 mM imidazole.

Table 2.3 Purification of truncated $PhaC_{Cc}\Delta N$.

Purification step	Volume (mL)	Protein (mg)	Activity (U^a/mg)	Total units	% yield[b]
Crude soluble extract	8	87	0.3	24	100
Crude insoluble extract	6.5	93	0.09	8.1	n/a
Ni-NTA flowthrough	14	63	0.1	6.3	26
10 mM imidazole wash	42.5	6.7	0.04	0.3	1.2
50 mM imidazole wash	25	5.6	0.09	0.5	2.1
Pure sample	0.75	14	1	14	60

[a]One unit of activity is one μmol CoA released per min.
[b]% yield is calculated based on total units in crude soluble extract.

Table 2.4 Purification of full length $PhaC_{Cc}$.

Purification step	Volume (mL)	Protein (mg)	Activity (U^a/mg)	Total units	% yield[b]
Crude soluble extract	11	180	4.9	880	100
Crude insoluble extract	30	18	14	250	n/a
Ni-NTA flowthrough	10	120	1.4	170	20
10 mM imidazole wash	40	28	0.9	25	2.8
50 mM imidazole wash	24	12	8.5	100	11
Pure sample	1.0	11	50	550	63

[a]One unit of activity is one μmol CoA released per min.
[b]% yield is calculated based on total units in crude soluble extract.

2.3.2 $PhaC_{Cc}$ has 50-fold higher activity than $PhaC_{Cc}\Delta N$

A DTNB assay is used to measure the activity of all PhaCs by monitoring CoA release. Incubation of $PhaC_{Cc}\Delta N$ (500 nM) with HBCoA gives the results shown in Figure 2.6A. These studies reveal sigmoidal kinetics, with a lag phase in CoA release followed by a roughly linear phase in CoA release. The time points from 2.5 to 10 min in Figure 2.6A were used to measure the specific activity of 0.5-1.5 U/mg at 30 °C. A similar lag phase has been reported for $PhaC_{Re}$ (*3, 6*). Full length $PhaC_{Cc}$ was assayed using the same protocol and the results are shown in Figure 2.6B. The specific activity is ~50 U/mg. As can be seen in the inset in Figure 2.6B, there is no clear linear portion of the curve, so specific activities are determined by fitting the assay data at < 2 min to a linear function. The difference in activity between the 73 kDa and 65 kDa PhaC suggests that the gene has been misannotated and that the full length protein is 73 kDa. Support for this conclusion is provided by Western blots using antibodies to his-tagged $PhaC_{Cc}\Delta N$, which identified a band in crude extracts of *C. crescentus* that migrates at ~75 kDa (section 3.3.4 of Chapter 3).

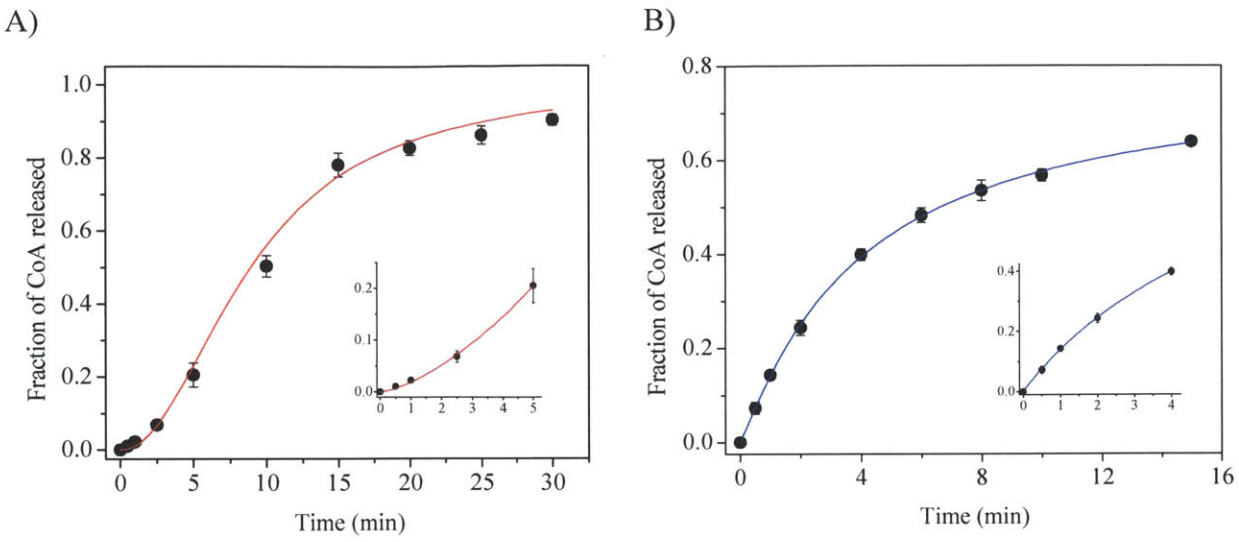

Figure 2.6 Time course of CoA release catalyzed by $PhaC_{Cc}\Delta N$ and $PhaC_{Cc}$. A) The assay was carried out at 30 °C and contained 0.76 mM HBCoA and 500 nM $PhaC_{Cc}\Delta N$. The inset is an expansion of the first 5 min. Data are fit to Equation 2.1 in section 2.2.5. **B)** The reaction mixture contained 25 nM $PhaC_{Cc}$ and 0.76 mM HBCoA. The inset is an expansion of the first 4 min. The data are fit to Equation 2.1. Assays were done in triplicate and the error bars are standard deviation from the mean.

Notably, full-length $PhaC_{Cc}$ has no lag phase in activity. The origin of the lag phase in $PhaC_{Cc}\Delta N$ is not understood, although we have previously proposed with $PhaC_{Re}$ that it might be associated with a requirement for dimerization and/or priming of the synthase for polymerization. Consistent with the lack of requirement for hecameg or another detergent in purification buffers, the presence of 0.05% hecameg in the assay buffer had no effect on the activity of $PhaC_{Cc}$ (Figure 2.7).

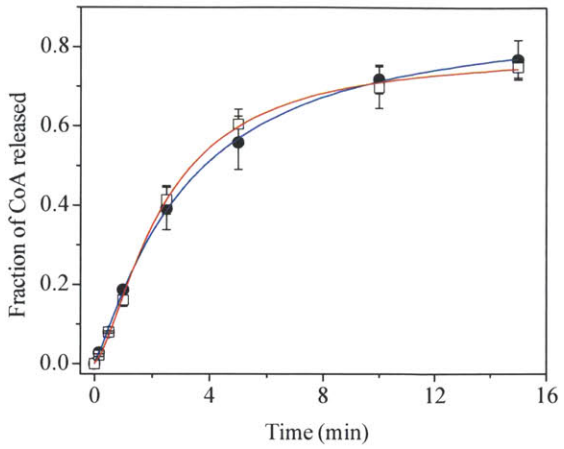

Figure 2.7 Effect of 0.05% hecameg on $PhaC_{Cc}$ activity. A) Time course of CoA release from assays containing 25 nM $PhaC_{Cc}$ and 0% (●, blue) or 0.05% (□, red) hecameg. The data are fit to Equation 2.1.

2.3.3 Full length $PhaC_{Cc}$ is stable during storage at 4 °C and -80 °C

Because the full length $PhaC_{Cc}$ appears to be the relevant synthase *in vivo*, we went on to further characterize its kinetics. In order to assess the stability of $PhaC_{Cc}$ activity upon storage, aliquots were stored with and without 20% glycerol at 4 °C and -80 °C, and assayed after one week. Even after one week at 4 °C, the activity remained the same as the freshly purified sample (Figure 2.8A). The presence of glycerol did not have an appreciable effect on the activity upon storage at 4 °C or -80 °C (Figure 2.8B). Therefore, $PhaC_{Cc}$ was stored in 20 mM Hepes pH 7.5, 200 mM NaCl at -80 °C for prolonged storage.

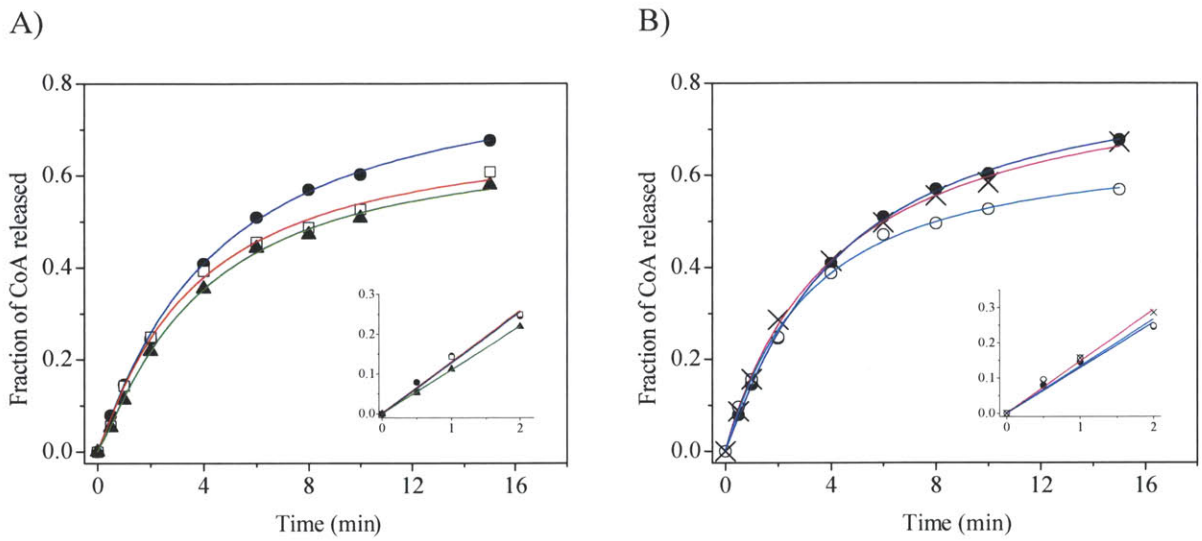

Figure 2.8 Time course of CoA release from $PhaC_{Cc}$ stored at 4 °C and -80 °C. The reactions were carried out at 30 °C and contained 0.76 mM HBCoA. A) Assays of $PhaC_{Cc}$ (25 nM) that was freshly purified (●, blue), or stored at 4 °C for 6 days in the absence (□, red) and presence (▲, green) of 20% glycerol. B) Assays of $PhaC_{Cc}$ (25 nM) that was freshly purified (●, blue), or stored for 6 days at -80 °C in the absence (○, cyan) and presence (×, magenta) of 20% glycerol. All assays are fit to Equation 2.3. The insets show the first 2 min of CoA release fit to a linear function, from which the specific activity is calculated.

2.3.4 Kinetic parameters of full-length $PhaC_{Cc}$

The kinetic parameters for full-length $PhaC_{Cc}$ (designated $PhaC_{Cc}$ subsequently) were next determined in 20 mM Hepes buffer, pH 7.5, and the results shown in Figure 2.9A fit to the Michaelis-Menten equation, and in Figure 2.9B fit to the Hill equation. Though both equations provide good fits, the Hill equation provides a slightly better fit (R^2 = 0.96 for the Michaelis-Menten equation vs. R^2 = 0.99 for the Hill equation), suggesting that the kinetics of full-length $PhaC_{Cc}$ exhibit some cooperativity. The Michaelis-Menten equation gives a k_{cat} of 84 s^{-1}, a K_M of 0.35 mM and a k_{cat}/K_M 2.6 x 10^5 $M^{-1}s^{-1}$. The Hill equation gives a k_{cat} of 75 s^{-1}, a K_M of 0.29 mM and a k_{cat}/K_M of 2.6 x 10^5 $M^{-1}s^{-1}$. The Hill coefficient n is 1.5. Cooperativity as a function of substrate concentration has also recently been reported with the class I synthase from *Aeromonas caviae* ($PhaC_{Ac}$), and similar analysis gave a Hill coefficient of 2.6 (*12*). At HBCoA

concentrations of 0.75-1 mM $PhaC_{Cc}$ has nearly maximum activity, and subsequent assays were performed at these concentrations.

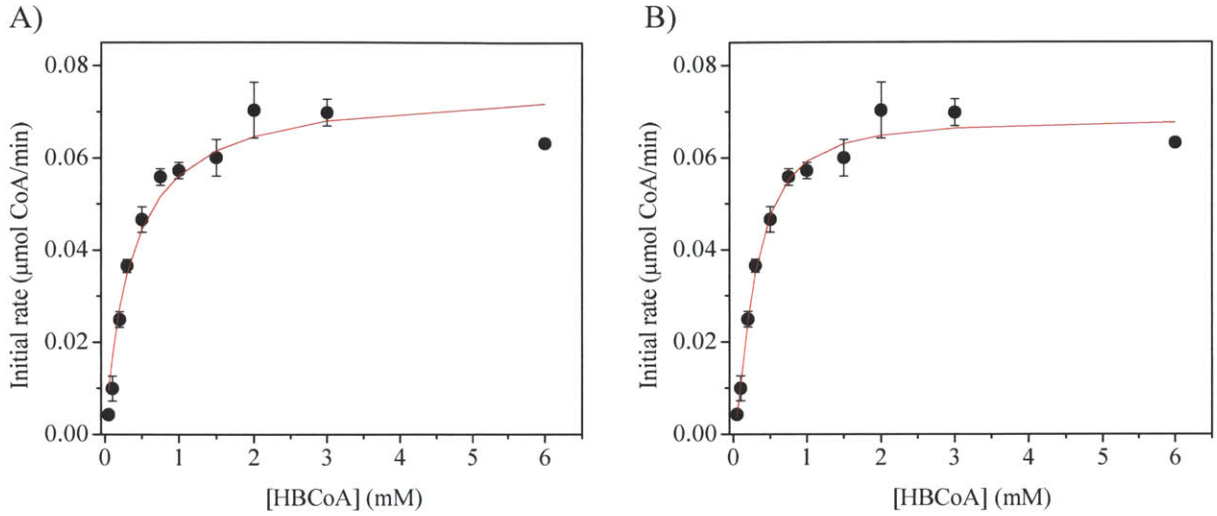

Figure 2.9 Specific activity of $PhaC_{Cc}$ as a function of [HBCoA]. The reactions were carried out at 30 ˚C and contained 50 nM $PhaC_{Cc}$ and 0.05-6 mM HBCoA. The data were fit to A) the Michaelis-Menten equation (Equation 2.2) and B) the Hill equation (Equation 2.3). The error bars represent the standard deviation from the mean of at least three assays.

2.3.5 Characterization of active site mutants of $PhaC_{Cc}$ reveals C406, D562 and H590 are involved in catalysis

Previous work from our lab identified the active site residues C319, D480 and H508 in $PhaC_{Re}$ and their involvement in catalysis (*3, 4, 6*). C319 is located within the "lipase box" motif (G-X-C-X-G) and has been shown in $PhaC_{Re}$ to be involved in covalent catalysis (*3, 6*). H508 is proposed to generate the active thiolate by deprotonating C319, and D480 is thought to be involved in activating the hydroxyl group of the incoming HBCoA monomer for nucleophilic attack on the acylated enzyme (*4*). The sequence alignment of $PhaC_{Re}$ with $PhaC_{Cc}$ shows the corresponding residues to be C406, D562 and H590 in $PhaC_{Cc}$ (Figure 2.4, red boxes). The active site mutants $PhaC_{Cc}$-C406A, -C406S and -D562N were therefore prepared to determine whether these residues were also important to $PhaC_{Cc}$ activity. The mutants were expressed and

purified identically to wt $PhaC_{Cc}$ and assayed for activity (Figure 2.10 and Table 2.5). $PhaC_{Cc}$-C406S and -D562N have specific activities of 0.002 and 0.006 U/mg, respectively. $PhaC_{Cc}$-C406A and $PhaC_{Cc}$-H590Q had activities of 0.0002 U/mg, which is the lower limit of detection for the assay. As expected, the C406A mutant is inactive, consistent with its involvement in covalent catalysis.

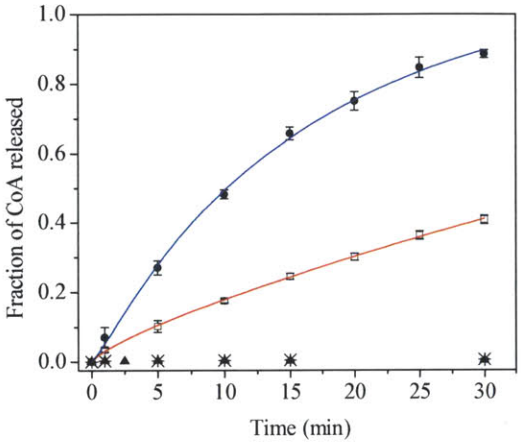

Figure 2.10 Time course of CoA release catalyzed by mutant $PhaC_{Cc}$s. The reactions were carried out at 30 °C and contained 1 mM HBCoA and 100 μM $PhaC_{Cc}$-D562N (•), 100 μM $PhaC_{Cc}$-C406S (□), 50 μM $PhaC_{Cc}$-C406A (▲), and 50 μM $PhaC_{Cc}$-H590Q (✳).The data for $PhaC_{Cc}$-D562N and $PhaC_{Cc}$-C406S are fit to Equation 2.3. Error bars represent the standard deviation from the mean of three experiments.

Table 2.5 Activities of mutants of full length $PhaC_{Cc}$ and $PhaC_{Re}$.

	$PhaC_{Cc}$		$PhaC_{Re}$ [a]	
Construct	SA (U/mg)	% of wt	SA (U/mg)	% of wt
wt	50	100	20	100
C406A[b]	0.0002	0.0004	<0.0001	<0.0005
C406S	0.002	0.004	n/a[c]	n/a
D562N	0.006	0.012	0.0008	0.004
H590Q	0.0002	0.0004	n/a	n/a

[a]Values taken from reference (*4*), in which the relative specific activities were measured.
[b]Numbering is from $PhaC_{Cc}$
[c]not available in reference

2.3.6 Size exclusion chromatography (SEC) suggests that $PhaC_{Cc}$ resides in predominantly a single oligomeric state

$PhaC_{Re}$ is a mixture of monomeric and dimeric forms in solution with a K_D of ~4 μM. The active form is predominantly the dimer of PhaCs, which synthesizes a single PHB chain (*3, 10*). In the case of $PhaC_{Ac}$ the equilibrium shifts towards dimeric state upon incubation with HBCoA (*12*). The class III synthase $PhaEC_{Av}$ is a mixture of dimers and tetramers of PhaEC, both of which are active. In this system as well the PhaC appears to make a single PHB chain per dimer of PhaECs (*5*). The unusual stoichiometry of PHB chains/PhaC has important mechanistic implications. We therefore wanted to determine if the oligomeric state of $PhaC_{Cc}$ and the number of PHB chains per $PhaC_{Cc}$ fit this model. SEC as 4 °C was used to examine its M_w, and the elution profile and resulting standard curve are shown in Figure 2.11.

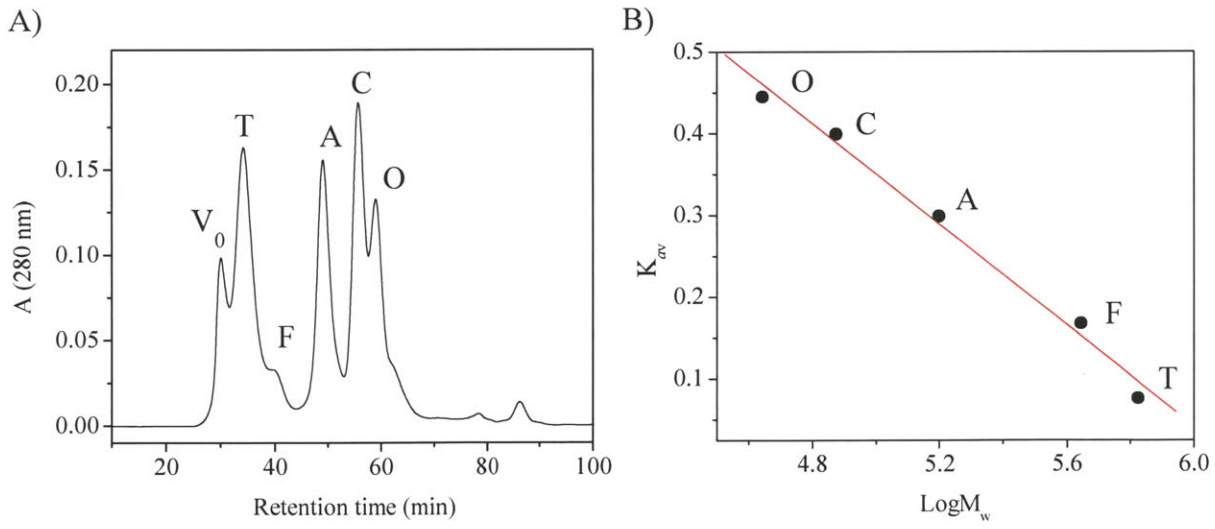

Figure 2.11 Size exclusion chromatography standards. A) A_{280} trace of protein standards. V_0, void volume. T, thyroglobulin. F, ferritin. A, aldolase. C, conalbumin. O, ovalbumin. B) Standard curve prepared plotting the gel phase distribution coefficient (K_{av}) of each standard vs. its $logM_w$.

To examine the quaternary structure of $PhaC_{Cc}$, (100 μL of 1, 25 or 100 μM) was analyzed and the retention time of the major peak at each concentration is ~43.8 min (Figure

2.12). Using the standard curve, the molecular weight is 240 kDa based on the standard curve. The subunit molecular weight of $PhaC_{Cc}$ is 75 kDa, and if the protein is assumed to be globular it may be a trimeric. At 1 μM and 25 μM, a second shoulder peak is observed that elutes with a retention time of between 49-50 min. The M_w of this peak according to the standard curve is ~130 kDa, which would be consistent with a dimer of PhaCs.

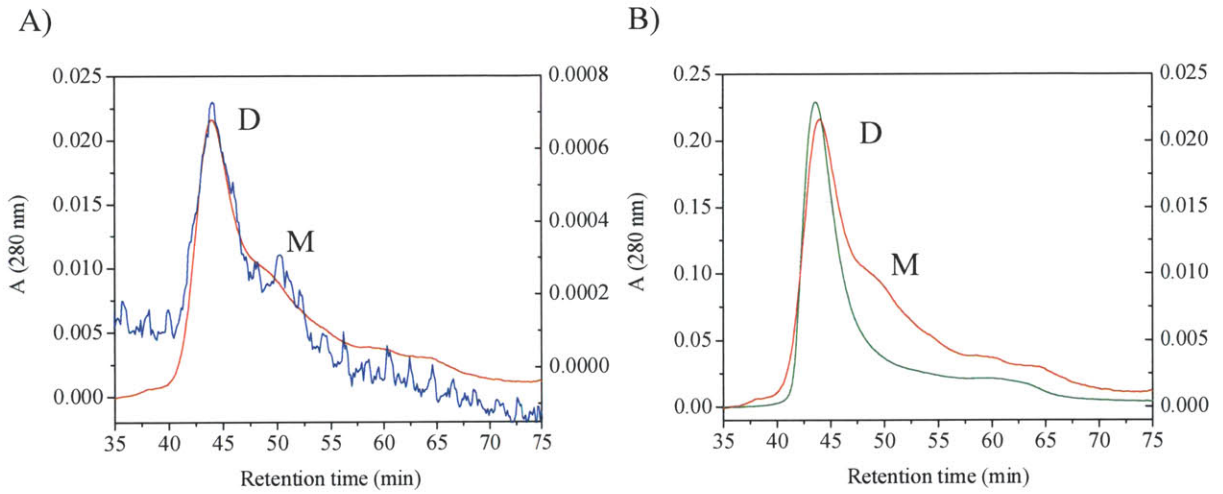

Figure 2.12 Representative SEC traces of $PhaC_{Cc}$. Samples (100 μL) were injected onto a GE Healthcare Superdex 200 10/300 GL column at 4 ˚C and eluted at 0.25 mL/min with 50 mM KH_2PO_4, pH 7.5, 150 mM NaCl. A) A_{280} trace of 1 μM (blue, right Y-axis) and 25 μM (red, left Y-axis) $PhaC_{Cc}$. B) A_{280} trace of 25 μM (red) (right Y-axis) and 100 μM (green) (left Y-axis) $PhaC_{Cc}$. In both panels, the traces at each [PhaC] are plotted on two Y-axes that are adjusted for scale.

We also analyzed the quaternary structure of $PhaC_{Cc}\Delta N$ to determine whether the N-terminal domain has an effect on oligomerization. At a concentration of 50 μM, $PhaC_{Cc}\Delta N$ elutes as three peaks (Figure 2.13A, black trace). The predominant peak elutes with a retention time of ~49 min and has a M_w of 165 kDa based on the standard curve. A dimer has a calculated M_w of 134 kDa. A smaller feature (53 min) has a M_w of 90 kDa and is likely a monomer of $Pha_{Cc}\Delta N$, which has a calculated M_w of 67 kDa. Finally a third small feature elutes at ~40.6 min and has a M_w of 370 kDa. This peak could correspond to either a pentamer (P) of PhaCs (M_w of

335 kDa) or a hexamer (H) of PhaCs (M_w = 400 kDa). The distribution of oligomeric species from 1-25 μM was also examined (Figure 2.13B). Analysis of peak heights suggests that the dimer to monomer ratio does not change with concentration. Together the results suggest that $PhaC_{Cc}\Delta N$ exists predominantly as a dimer in solution. Taking into account structural modeling efforts with $PhaC_{Cc}$ presented in Chapter 4 that model the N-terminal 8 kDa as a separate domain from the rest of the protein, it is possible that like $PhaC_{Cc}\Delta N$, $PhaC_{Cc}$ is also a mixture of dimeric and monomeric PhaCs, but has an unusual shape due to the N-terminal domain.

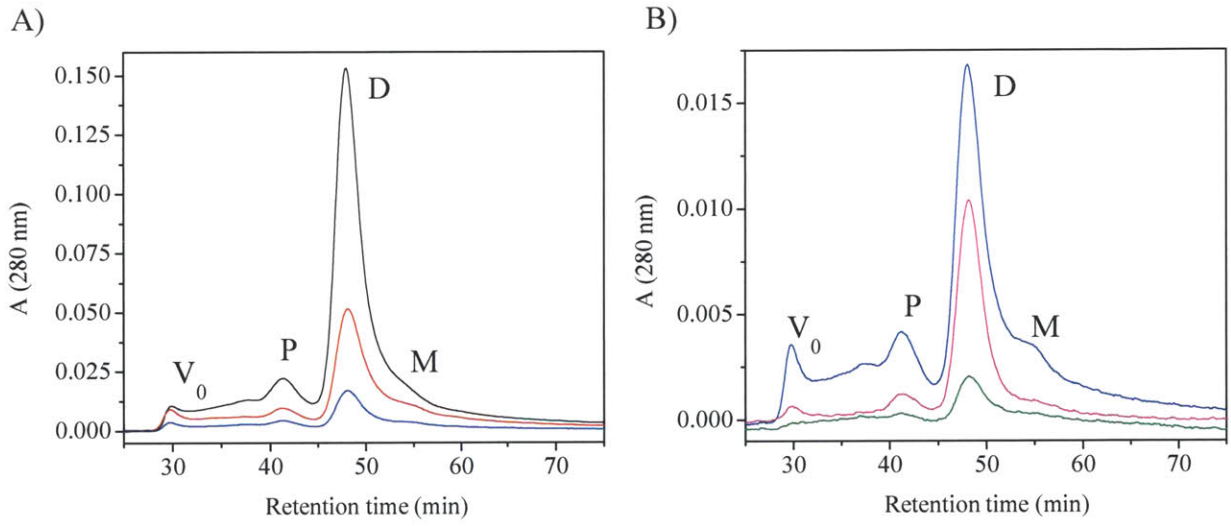

Figure 2.13 Representative SEC traces of $PhaC_{Cc}\Delta N$. Samples (100 μL) were injected onto a GE Healthcare Superdex 200 10/300 GL column at 4 °C and eluted at 0.25 mL/min with 20 mM Hepes, pH 7.5, 200 mM NaCl. A_{280} was monitored. A) A_{280} traces of 50 μM (black), 25 μM (red), and 10 μM (blue) $PhaC_{Cc}\Delta N$. B) A_{280} traces of10 μM (blue), 5 μM (magenta) and 1 μM (green) $PhaC_{Cc}\Delta N$.

Because the peak areas were lower than expected given the concentrations of $PhaC_{Cc}$ injected onto the column, the recovery of $PhaC_{Cc}$ from the column was measured. A second sample (100 μL of 100 μM, 0.75 mg) was injected and the protein peak was collected, concentrated and the amount of $PhaC_{Cc}$ recovered was measured by A_{280}. Of the 0.75 mg of $PhaC_{Cc}$ injected onto the column, ~0.3 mg was recovered, suggesting that more than half of the

$PhaC_{Cc}$ was precipitating. We do not observe aggregate protein eluting in the void volume (28-29 min). With prolonged use the column back pressure increased, suggesting that the protein was precipitated on the filter at the top of the column.

2.3.7 Reaction of $PhaC_{Cc}$ with sTCoA: analysis of CoA release suggests one sT per PhaC monomer

SEC suggested that the oligomeric state of $PhaC_{Cc}$ was distinct from that of $PhaC_{Re}$, which is a mixture of monomer and dimer species in solution. Furthermore, $PhaC_{Cc}$ does not require hecameg for purification and does not have a lag phase in activity. The stoichiometry of PHB synthesis was previously shown to be one PHB chain per dimer for both $PhaC_{Re}$ and $PhaEC_{Av}$ (*3-5, 32*). In the case of $PhaC_{Re}$, incubation with sTCoA prior to addition of HBCoA shortened the lag phase and increased the specific activity of the enzyme (*3*). Furthermore the acylated enzyme is stable to hydrolysis, allowing its isolation and quantitation of sT bound.

To examine the similarities and differences with other PhaCs, we quantitated CoA release by incubation of $PhaC_{Cc}$ with 10 equiv. sTCoA. The results are shown in Figure 2.14. These experiments showed a burst of CoA release corresponding to ~1 per monomer of $PhaC_{Cc}$. This stoichiometry is distinct from previous observations, and suggested that $PhaC_{Cc}$ can be uniformly loaded, which could facilitate studies of polymer elongation. The burst of CoA release is followed by continued slow CoA release at a rate of 0.2 min^{-1}, which proceeds at 1/24,000 of the turnover rate (Figure 2.14).

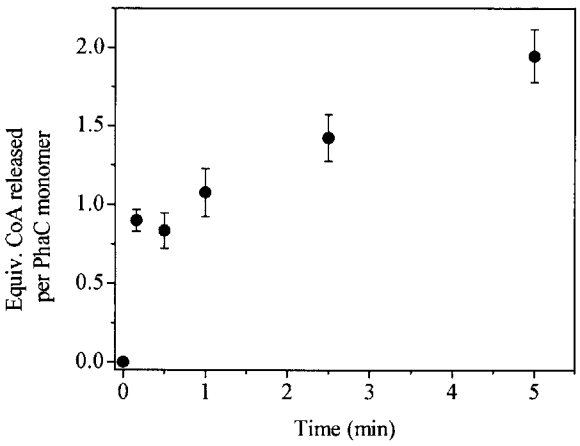

Figure 2.14 Reaction of $PhaC_{Cc}$ with sTCoA monitored by DTNB assay. The reaction contained 50 μM $PhaC_{Cc}$ and 500 μM sTCoA and was carried out at 30 °C. Error bars represent the standard deviation from the mean of three experiments. Equivalents of CoA released are given per PhaC monomer. CoA release occurs from 10 s to 5 min at 0.2 min^{-1}.

2.3.8 Sephadex G50 analysis of $PhaC_{Cc}$ reacted with [^{3}H]-sTCoA reveals 0.2 equiv. of [^{3}H]-sT per PhaC

We next determined the amount of acylated enzyme that could be isolated by gel filtration at 4 °C. If the rate of CoA release measured in the previous experiment is indicative of the rate of hydrolysis of the acylated enzyme, then we would predict that the acylated enzyme has a half-life of 3.5 min at 30 °C. Assuming that a decrease in temperature of 10 °C results in a 2-fold decrease in the rate of hydrolysis, we would predict that the half-life would be ~15 min at 4 °C. This analysis suggests that $PhaC_{Cc}$ acylated with one equiv. of sT could be readily isolated. To investigate whether this was the case, $PhaC_{Cc}$ (50 μM) was incubated with 10 equiv. [^{3}H]-sTCoA for 30 s at 30 °C, then placed on a Sephadex G50 column at 4 °C to separate [^{3}H]-sT-$PhaC_{Cc}$ from unreacted [^{3}H]-sTCoA. The eluent was collected in fractions and analyzed for radioactivity to examine the stoichiometry of labeling (Figure 2.15). The recovery of radioactivity was 95%. $PhaC_{Cc}$ eluted at 6.3 min and was associated with only 0.19 equiv. of [^{3}H]-sT. The remaining radioactivity was associated with the peak that eluted after ~10 min,

which includes unreacted [^{3}H]-sTCoA, [^{3}H]-sT acid and other small molecule products. An identical control reaction containing $PhaC_{Cc}$-C406A was carried out to determine whether the active site Cys was essential for observing association of [^{3}H]-sT with the synthase. The recovery of radioactivity was 94% and no radioactivity was associated with the synthase (data not shown), suggesting that wt $PhaC_{Cc}$ is covalently labeled with [^{3}H]-sT.

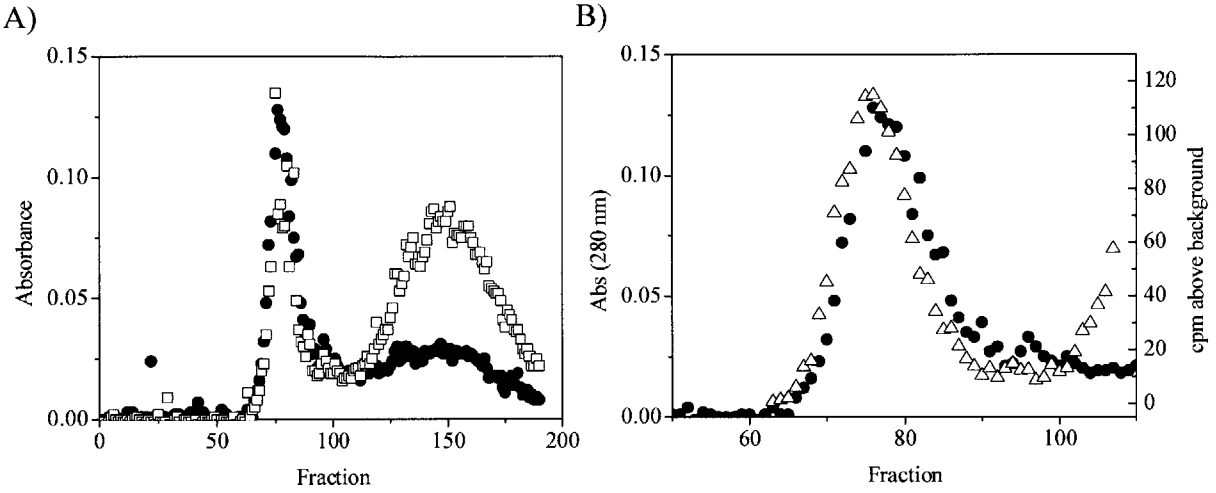

Figure 2.15 Acylation of $PhaC_{Cc}$ with [^{3}H]-sTCoA followed by separation by Sephadex G50 chromatography. The reaction contained 50 μM $PhaC_{Cc}$ and 500 μM [^{3}H]-sTCoA (specific activity = 1300 cpm/nmol). A) Elution profile showing A_{280} (●) and A_{260} (□), indicating $PhaC_{Cc}$ (fractions 65-100) and unreacted sTCoA and free CoA (fractions 100-200). B) Expansion of A_{280} elution profile (●) between fractions 40-120, overlaid with cpm measured for each fraction (Δ).

In an effort to stabilize the acylated enzyme, the same experiment was carried out except that sT-$PhaC_{Cc}$ was eluted from the Sephadex G50 column equilibrated in 20 mM KH_2PO_4, pH 4.7, 2 M urea. This buffer was chosen because thioester linkages are susceptible to hydrolysis under basic conditions, but moderately stable to hydrolysis between pH 2-6 (*33*). The urea was added to partially denature $PhaC_{Cc}$ to limit enzyme-catalyzed hydrolysis. The recovery of radioactivity was 90%. $PhaC_{Cc}$ eluted after ~8.3 min and the fractions that contained synthase were analyzed by scintillation counting, revealing only 0.11 equiv. [^{3}H]-sT associated with $PhaC_{Cc}$ (Figure 2.16). This result was unanticipated given that the thioester should be more

stable to hydrolysis under mildly acidic conditions. The remaining radioactivity was found in small molecules and eluted after 17 min.

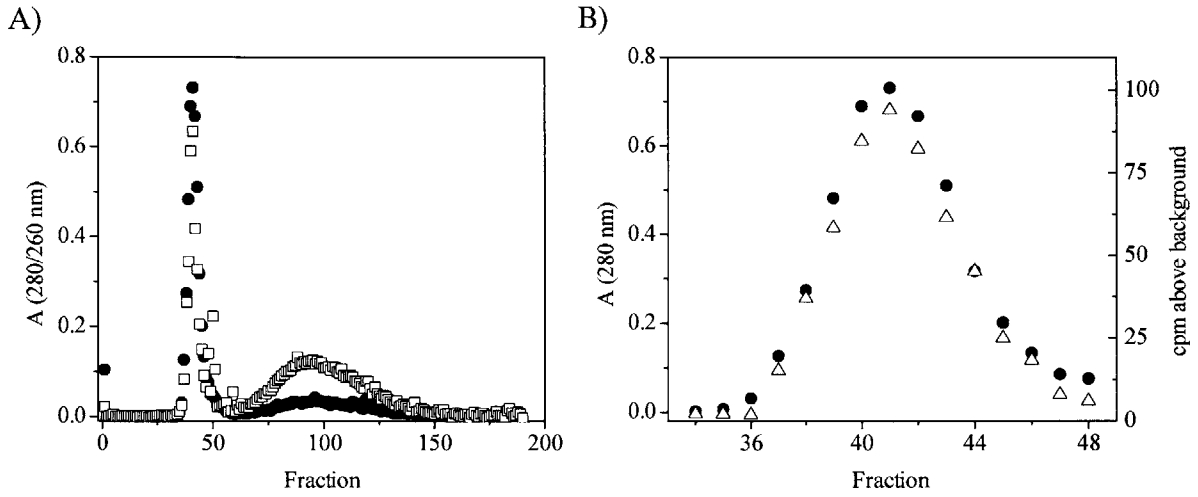

Figure 2.16 Reaction of $PhaC_{Cc}$ with [^{3}H]-sTCoA followed by separation by Sephadex G50 chromatography. The reaction was carried out at 30 °C and contained 50 μM $PhaC_{Cc}$ and 500 μM [^{3}H]-sTCoA. The specific activity of the [^{3}H]-sTCoA was 1300 cpm/nmol. After ~10 s of incubation the reaction was placed on a Sephadex G50 column at 4 °C and eluted with 20 mM KH_2PO_4, pH 4.7, 2 M urea. A) The elution profile showing A_{280} (●) and A_{260} (□), indicating $PhaC_{Cc}$ (fractions 20-40) and [^{3}H]-sTCoA (fractions 45-100). B) Expansion of the peak containing $PhaC_{Cc}$, with A_{280} (●) and cpm (Δ) overlaid.

Finally, we investigated whether reaction of [^{3}H]-sT-$PhaC_{Cc}$ with 5 equiv. HBCoA would stabilize the acylation by extending the PHB chain. The hypothesis was that a longer chain could potentially close the active site, slowing the rate of hydrolysis. For these experiments, the concentration of $PhaC_{Cc}$ was higher than in previous experiments to ensure that the enzyme was saturated with HBCoA. $PhaC_{Cc}$ (200 μM) was reacted with 500 μM [^{3}H]-sTCoA for ~10 s at 30 °C, followed by addition of 5 equiv. HBCoA and the mixture was placed on a Sephadex G50 column at 4 °C after ~10 s of reaction. The column was eluted in 20 mM Hepes pH 7.5, 200 mM NaCl (Figure 2.17). The recovery of radioactivity from the column was 92%. $PhaC_{Cc}$ eluted at 7.5 min and the protein-containing fractions were analyzed by scintillation counting. Only 0.04 equiv. [^{3}H]-sT per monomer of $PhaC_{Cc}$ were associated with the synthase, ~5-fold less than when

HBCoA is omitted. Again, this result was unexpected and suggested that the reaction of $PhaC_{Cc}$ with [^{3}H]-sTCoA might be more complicated than anticipated, and that rapid hydrolysis of the acylated enzyme is not the reason for our inability to isolate $PhaC_{Cc}$ labeled with 1 equiv. [^{3}H]-sT.

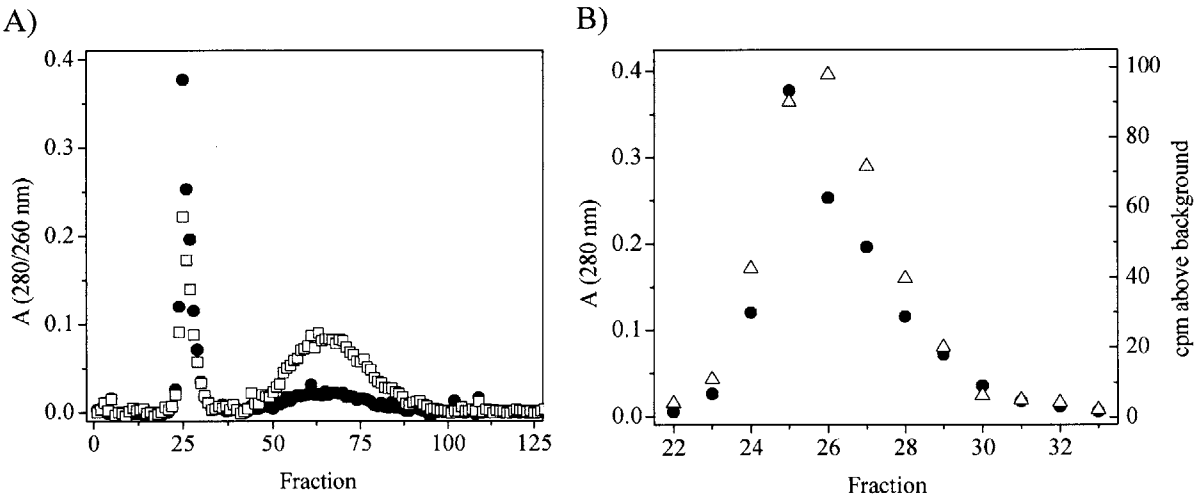

Figure 2.17 Elution profile of [^{3}H]-sT-$PhaC_{Cc}$ reacted with 5 equiv. of HBCoA. $PhaC_{Cc}$ (200 μM) was reacted with 500 μM sTCoA, and chased with 1 mM HBCoA. A) Elution profile showing A_{280} (●) and A_{260} (□), indicating $PhaC_{Cc}$ (fractions 40-60) and [^{3}H]-sTCoA or [^{3}H]-small molecules (fractions 70-150). B) A_{280} elution profile (●) overlaid with cpm measured for each fraction (Δ).

2.3.9 sTCoA undergoes chemistry subsequent to acylation of $PhaC_{Cc}$

Our inability to isolate uniformly acylated [^{3}H]-$PhaC_{Cc}$ in spite of attempts to stabilize the acylated enzyme by reducing the temperature and pH, and by extending the acylated chain, suggested that another factor besides instability of the acylated enzyme was thwarting our efforts. To determine whether additional reaction(s) besides acylation to produce CoA and sT-$PhaC_{Cc}$ occurred, the small molecule products of this reaction were isolated and examined by HPLC and their retention times compared to a set of authentic standards, which included CoA, HBCoA, sTCoA and the terminally-saturated tetramer CoA, sT_4CoA. $PhaC_{Cc}$ (25 nmol) was incubated with [^{3}H]-sTCoA (250 nmol, specific activity = 146 cpm/nmol) and aliquots of the

reaction were quenched with 10% TCA at time points from 10 s to 5 min. Each aliquot was centrifuged to pellet the precipitated protein and the supernatant was removed. The protein pellet was washed once with H_2O and the wash was added to the supernatant. The radioactivity associated with the precipitated protein was analyzed by scintillation counting from 10 s to 5 min, revealing changes with time, with a maximum of 0.9 equiv. [^{3}H]-sT-PhaC$_{Cc}$ at 0.75 min (Table 2.6).

Table 2.6 Equivalents of [^{3}H]-sT associated with PhaC$_{Cc}$ following incubation for the indicated lengths of time.

Time (min)	Equiv. [^{3}H]-sT per PhaC
0.16	0.73
0.5	0.70
0.75	0.88
1	0.69
2	0.81
3	0.61
5	0.56

To examine the small molecule products, the pH of the supernatant/wash was adjusted to pH ~5 by addition of 1 M ice-cold NaOH with rapid mixing to avoid local high concentrations of base. The samples were analyzed by HPLC and fractions were collected. The recovery of radioactivity for each time point was 95-100%. As a control, [^{3}H]-sTCoA was injected onto the HPLC and fractions were collected and analyzed by scintillation counting to detect additional radioactive species present as breakdown products due to storage of the starting material (Figure 2.18A). The results show that a radioactive species lacking A_{260} that migrates with a retention time of 37 min is present in the starting material.

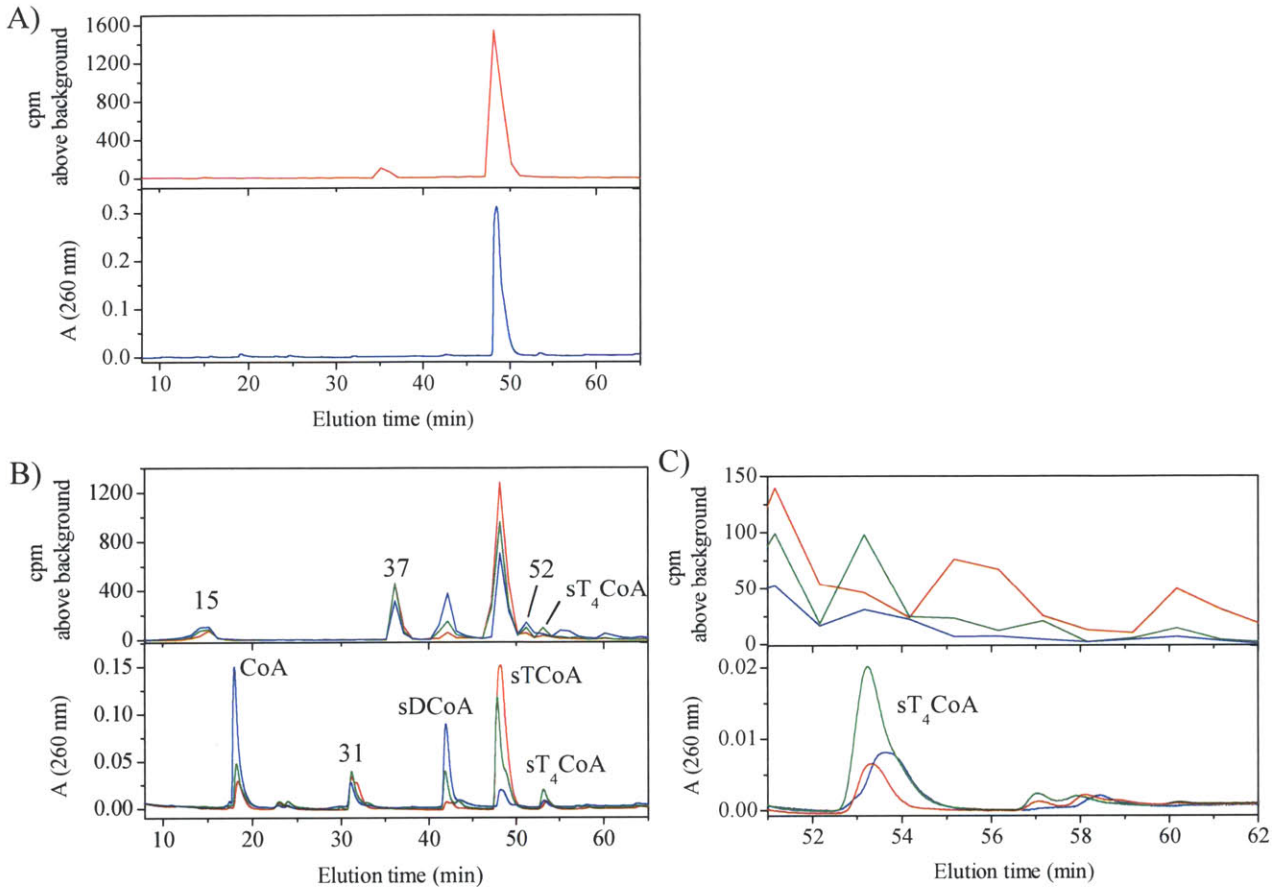

Figure 2.18 HPLC traces of $PhaC_{Cc}$ incubated with [^{3}H]-sTCoA. A) Control of [^{3}H]-sTCoA prior to reaction with $PhaC_{Cc}$. The peak with an elution time of 47 min is [^{3}H]-sTCoA. An additional radioactive peak containing no A_{260} elutes at ~37 min. B) Small molecule products of $PhaC_{Cc}$ incubated with [^{3}H]-sTCoA. The reaction was carried out at 30 °C and contained 50 μM $PhaC_{Cc}$ and 500 μM [^{3}H]-sTCoA (specific activity 146 cpm/nmol). Aliquots of the reaction were analyzed after 10 s (red), 45 s (green) and 5 min (blue) incubation. C) Expansion of small peaks with later elution times from panel B. The species in panels B and C are labeled as they are referred to in the text.

Table 2.7 Amounts (nmol) of small molecule species produced by the reaction of $PhaC_{Cc}$ with [^{3}H]-sTCoA from 10 s to 5 min[a].

Time point	15 min[c]	CoA[b] 18 min	31 min[c]	sDCoA[b,c] 43 min	sTCoA[b] 47 min	52 min[b]	sT_4CoA[b,c] 54 min	56-65 min[c]
0	0	0	0	0	250	0	0	0
0.16	13	25	40	7	179	7	6	0
0.5	17	-	-	18	-	10	14	4
0.75	22	35	25	26	105	11	13	8
1	25	38	47	28	75	11	14	8
2	25	63	31	54	49	15	12	20
3	30	74	28	57	29	18	7	26
5	27	99	17	55	16	17	4	32

[a]The amounts were determined on individual aliquots, but are reported normalized to the entire reaction. The A_{260} trace for the 0.5 min time point was not obtained due to a malfunction with (likely a bubble inside of) the diode array detector. Therefore the amounts of CoA, the species at 31 min, sTCoA and sT_4CoA (all determined from A_{260}) are not given.
[b]Amount was determined by A_{260}.
[c]Amount was determined by radioactivity.

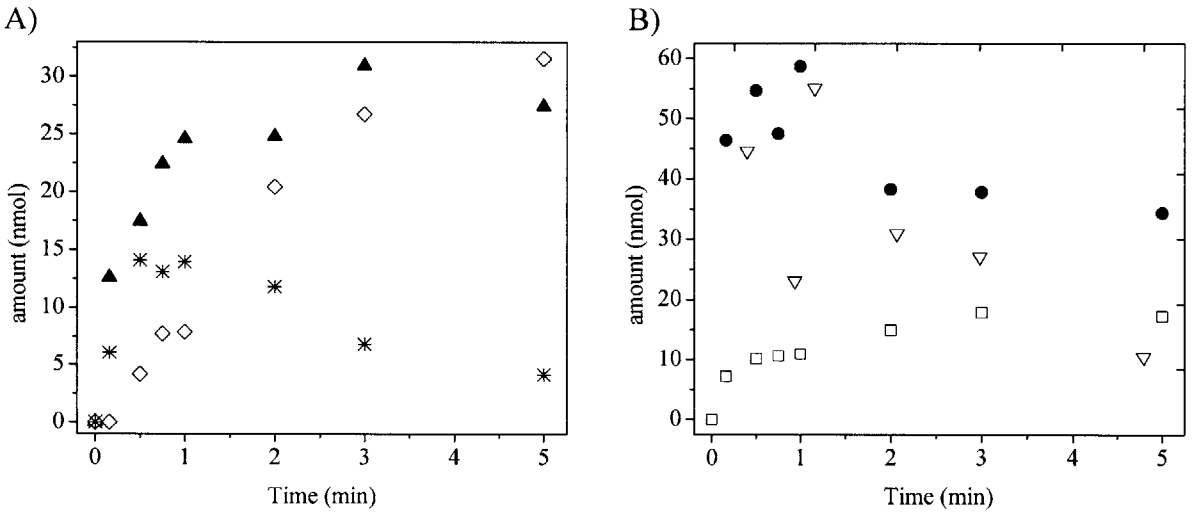

Figure 2.19 Changes in the amounts of the species in Table 2.7 as the reaction progresses. A) Changes in the amounts of the species at 15 min (▲), 54 min (sT_4CoA) (◇) and 56-65 min (✳). B) Changes in the amounts of the species at 31 min (▽), 37 min (●) and 52 min (□).

Figure 2.18B shows overlays of the A_{260} trace and radioactivity of the time points taken after 10 s, 45 s and 5 min incubation of [^{3}H]-sTCoA with $PhaC_{Cc}$, with the major products labeled as they will be referred to in this section. The amounts of each species, shown in Table 2.7, were determined by radioactivity and/or A_{260} using a standard curve prepared from HBCoA (5-250 nmol, 50 μM-2.5 mM). Figure 2.19 shows the changes in concentration of some of these species. After 10 s, the amount of CoA (elution time 18 min), determined by A_{260}, was 24.8 nmol, equal to one equiv. per PhaC. This result suggests $PhaC_{Cc}$ reacts with [^{3}H]-sTCoA to produce a burst of CoA and [^{3}H]-sT-PhaC, and is consistent with the DTNB assays of $PhaC_{Cc}$ reacted with sTCoA, which also indicate a burst of one equiv. CoA release after 10 s (section 2.3.8). Additional CoA release occurs from 10 s to 5 min with a k_{obs} of 0.6 min^{-1} (Figure 2.20A), similar to the rate constant measured by the DTNB assay (0.2 min^{-1}). The peak with a retention time of 47 min is [^{3}H]-sTCoA. The amount of [^{3}H]-sTCoA decreases from 10 s to 5 min at a rate of 1.4 min^{-1} (Figure 2.20B). It should be noted that after the 45 s time point, the amount of [^{3}H]-sTCoA determined by radioactivity no longer correlated with that calculated by A_{260}, as the former consistently indicated higher amounts of [^{3}H]-sTCoA than the latter. This result was interpreted to indicate that one or more species (possibly [^{3}H]-HB_n acid) was formed that co-eluted with [^{3}H]-sTCoA. Therefore, the concentration of [^{3}H]-sTCoA was determined by A_{260}, providing the results shown in Figure 2.20B.

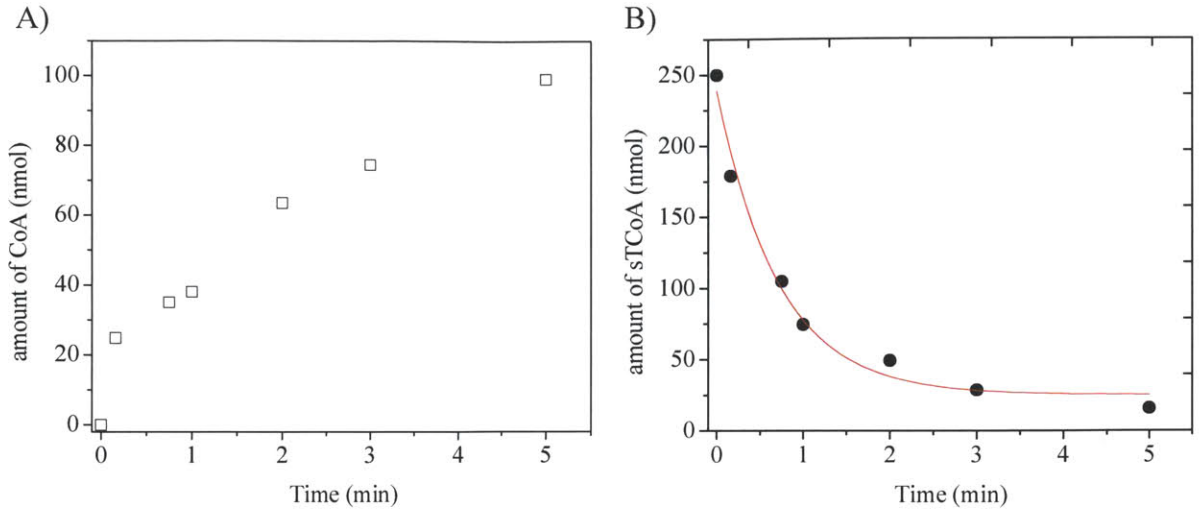

Figure 2.20 Changes in the amount of A) CoA and B) [^{3}H]-sTCoA during incubation of PhaC$_{Cc}$ with [^{3}H]-sTCoA. In a final volume of 500 µL, the reaction contained 50 µM PhaC$_{Cc}$ (25 nmol) and 500 µM [^{3}H]-sTCoA (250 nmol). The amount of CoA and [^{3}H]-sTCoA was determined by comparison of the A_{260} peak area to a standard curve prepared from HBCoA. The data for [^{3}H]-sTCoA consumption were fit to Equation 2.5 to give a rate of disappearance of 1.4 min^{-1}.

After 10 s, quantitation of [^{3}H]-sTCoA by A_{260} and radioactivity indicates that ~180 nmol unreacted [^{3}H]-sTCoA remains of the initial 250 nmol. Considering that only 25 nmol CoA was released in the burst, this result suggested that an additional ~45 nmol [^{3}H]-sTCoA has been consumed in reactions other than the acylation reaction that produces CoA and [^{3}H]-sT-PhaC$_{Cc}$. One species that migrates with a retention time of 31 min has A_{260} but contains no radioactivity, and changes little in the course of the reaction (Figure 2.19B). Radioactive species migrating with retention times of 15 min, 37 min, 43 min, 52 min and 54 min are also formed. The peak at 37 min is present in the control. The peak at 43 min represents the major small molecule product and increases over the course of the reaction.

To identify this major product (43 min), the identical reaction was carried out in which PhaC$_{Cc}$ and unlabeled sTCoA were incubated 5 min at 30 °C. The small molecules were analyzed by HPLC and the peak at 43 min was collected, lyophilized to dryness and analyzed by

MALDI-TOF. The MALDI-TOF (positive mode) data revealed that the sample had a m/z of 924.8, consistent with the expected m/z of a singly protonated saturated dimer CoA (sDCoA) (Figure 2.21A and B). Analysis of the amount of sDCoA by radioactivity and A_{260} yields the same results and revealed that sDCoA is produced with a rate constant of 1 min^{-1} and that its production stops after 2 min (Figure 2.21C). The rate constant measured is considerably slower than the turnover number of the enzyme of 4800 min^{-1}; howeve, it is similar to the rate constant for the consumption of sTCoA.

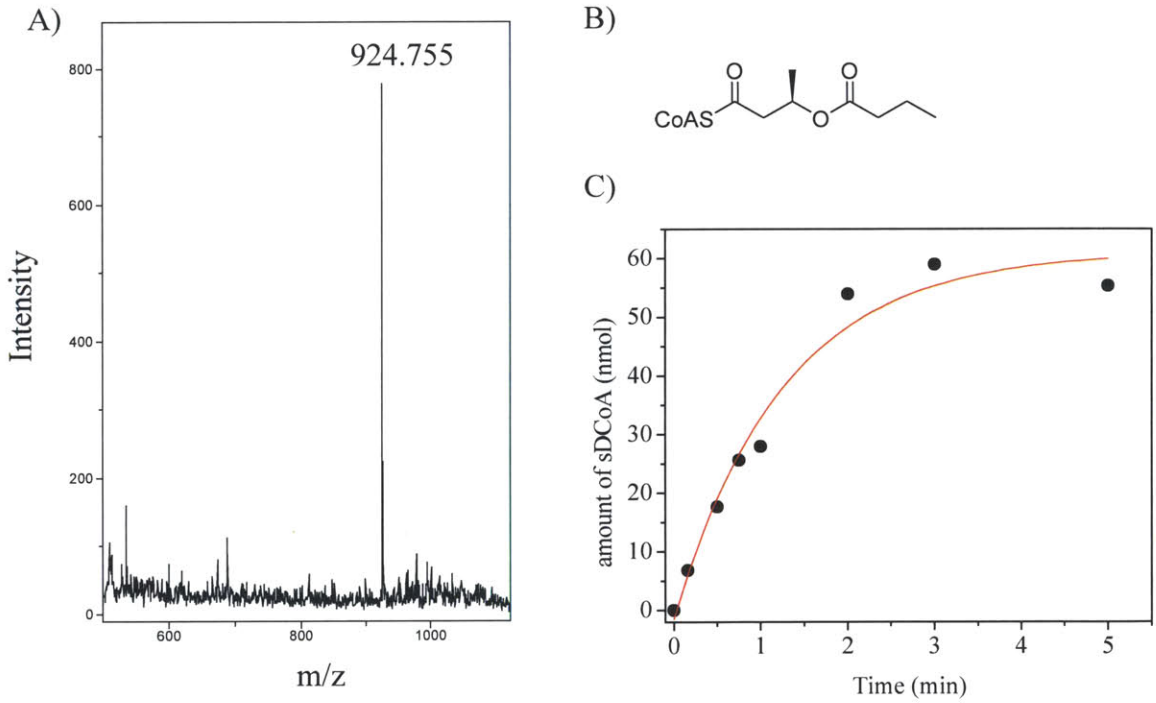

Figure 2.21 MALDI-TOF analysis and rate of formation of sTCoA. A) MALDI-TOF of sDCoA (elution time 43 min) in positive mode. The calculated M_w of is 923.71, and the major peak has a m/z of 924.75, consistent with $[M+H]^+$. B) Structure of sDCoA. C) Rate of formation of sDCoA. The amount of sDCoA present in the reaction was determined by both A_{260} and radioactivity, giving consistent results. The data were fit to Equation 2.6, giving k_{obs} of 1 min^{-1} for the formation of sDCoA. This reaction was carried out once.

One mechanism that could account for the formation of sDCoA and for the slow rate of CoA release is shown in Scheme 2.1. In this mechanism, $PhaC_{Cc}$ is acylated with [^{3}H]-sT and

CoA remains non-covalently bound. This species is referred to as [^{3}H]-sT-PhaC•CoA. CoA can dissociate from this species, leaving [^{3}H]-sT-PhaC. The rate constant measured for this process is 0.2-0.6 min^{-1}, a range provided by the results of the DTNB assays discussed in section 2.3.8 and the experiments described in this section. Alternatively, [^{3}H]-sT-PhaC•CoA can undergo a reaction in which the thiolate of CoA attacks the indicated ester of sT to generate HB-PhaC and sDCoA. This reaction occurs with a rate constant of 1 min^{-1}, measured from the rate of formation of sDCoA. It should be noted that, in order for the measured rates to be indicative of CoA release and sDCoA formation, the rates of hydrolysis of HB-PhaC and [^{3}H]-sT-PhaC would have to be faster than 1 min^{-1}, as these steps would be necessary to free up the enzyme active site for reaction with additional [^{3}H]-sTCoA.

The fact that PhaC$_{Cc}$ can catalyze thiolysis via CoA to generate sDCoA and putative HB-PhaC may be suggestive of a possible mechanism of termination. While it must be cautioned that sTCoA is not the natural substrate and that the reactions observed could be off pathway, previous studies have suggested that the thiol N-acetylcysteamine can serve as chain transfer (or chain termination) agent *in vitro (25)*. Thus the k_{obs} for the formation of sDCoA of 1 min^{-1} may be indicative of the rate constant for chain termination. Taking into account the rate of polymerization of 4800 min^{-1}, then one would expect that a PhaC$_{Cc}$ molecule would on average synthesize a PHB chain of ~5000 HB units before a termination event would occur. This would correspond to PHB of a M_w of 400-450 kDa. This M_w is similar to that of PHB extracted from *C. crescentus*, which has a M_w of 350-400 kDa (Chapter 3).

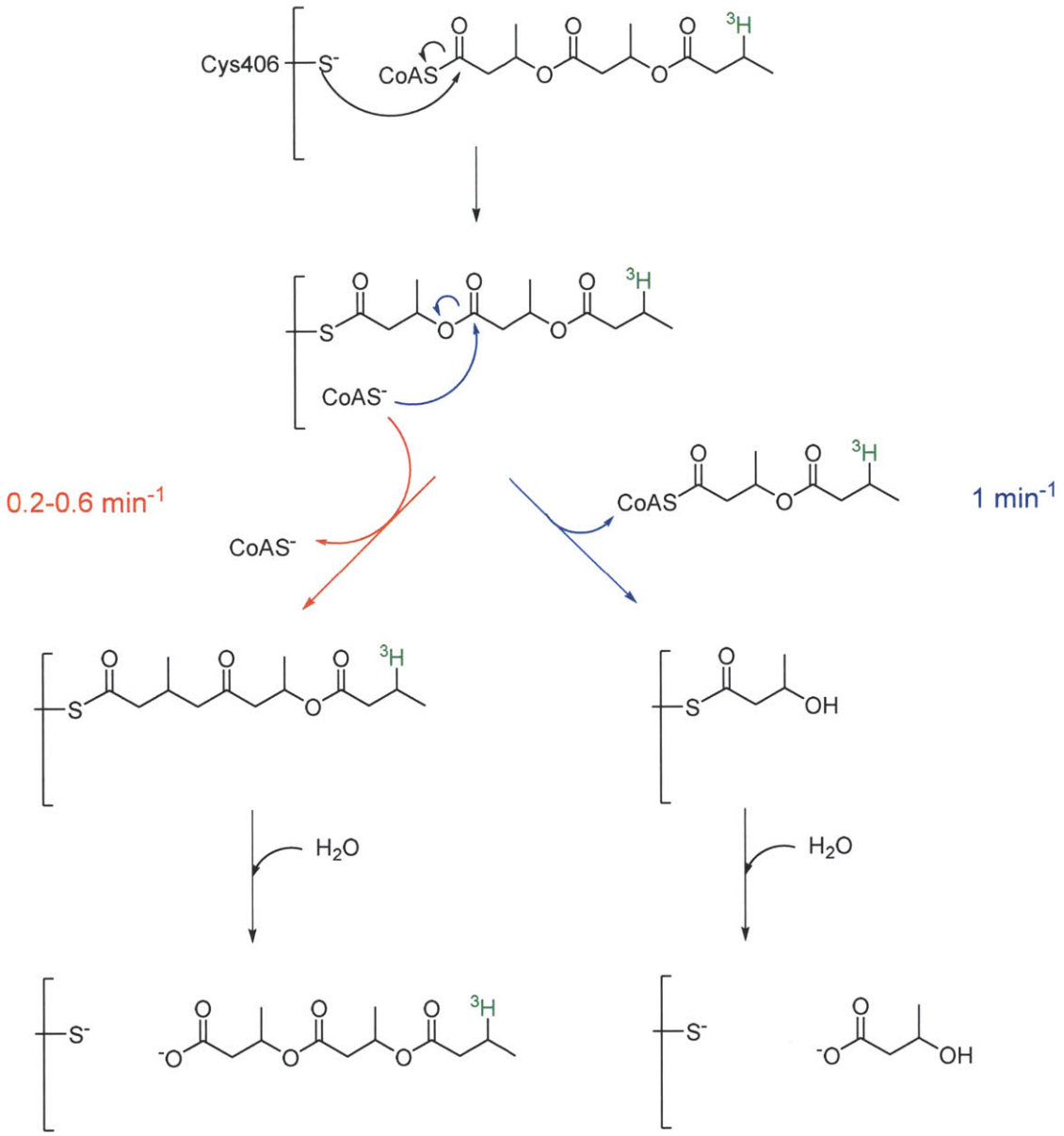

Scheme 2.1 Proposed mechanism for formation of [^{3}H]-sDCoA. PhaC$_{Cc}$ first reacts with [^{3}H]-sTCoA to form [^{3}H]-sT-PhaC•CoA, where CoA remains bound to the enzyme active site. This species can then either lose CoA (red pathway), or CoA can attack the indicated ester bond to form [^{3}H]-sDCoA and HB-PhaC (blue pathway).

We next wished to conclusively identify the radioactive species that has a retention time of 54 min, as its migration was consistent with an sT$_4$CoA standard. A very small peak with the same elution time is present in the control (Figure 2.18A), but contains no radioactivity. This peak was collected and submitted for MALDI-TOF analysis, which confirmed that it contains

sT_4CoA, in addition to two other peaks which we could not identify based on their m/z values. In negative mode analysis, sT_4CoA has a predicted m/z of 1094.89 for the singly deprotonated species (Figure 2.22). It accumulates to ~13 nmol, then declines as the reaction progresses. sT_4CoA is likely yet another product of a side reaction of $PhaC_{Cc}$ with sTCoA. A mechanism which could account for this product is shown in Scheme 2.2, which involves attack by $PhaC_{Cc}$ at an internal oxoester rather than the thioester of sTCoA to form HBCoA and sD-$PhaC_{Cc}$. The formation of HBCoA in this model is necessary to account for the amount of sT_4CoA formed, as there is not sufficient contaminating HBCoA in the [^{3}H]-sTCoA stock to account for sT_4CoA formed via chain elongation. HBCoA could dissociate from the enzyme and attack the thioester of sT-$PhaC_{Cc}$ to elongate the chain by one unit. Several additional species form as the reaction progresses. These species have later elution times (after 54 min) and appear in small amounts, and most contain radioactivity but have no detectable A_{260}. These species may be [^{3}H]-HB_n acids. In summary, the reaction of $PhaC_{Cc}$ is more complicated than originally anticipated and involves the formation of several products in addition to the predicted sT-$PhaC_{Cc}$ species.

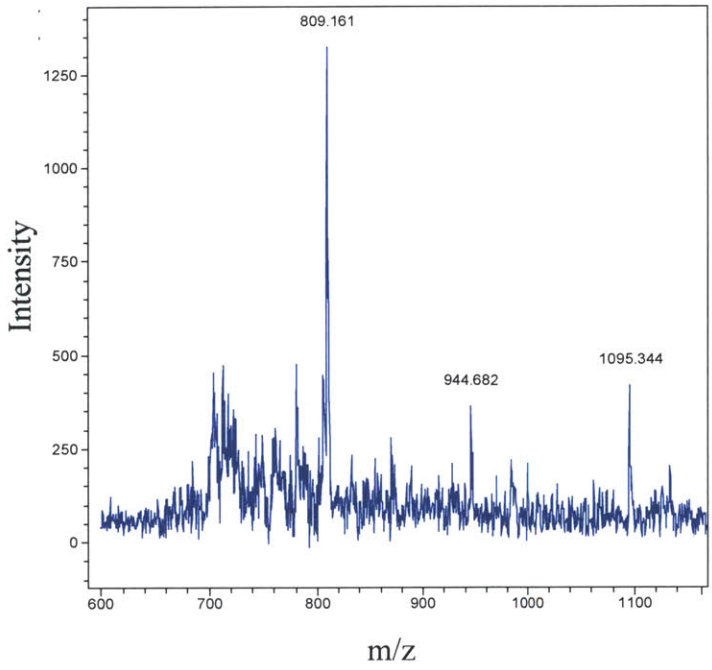

Figure 2.22 Negative mode MALDI-TOF spectrum of the peak with an elution time of ~54 min. sT_4CoA has a predicted M_w of 1095.9. The sample contained a peak with a m/z of 1095.3, consistent with the predicted m/z of the $[M-H]^-$ species of sT_4CoA (1094.9).

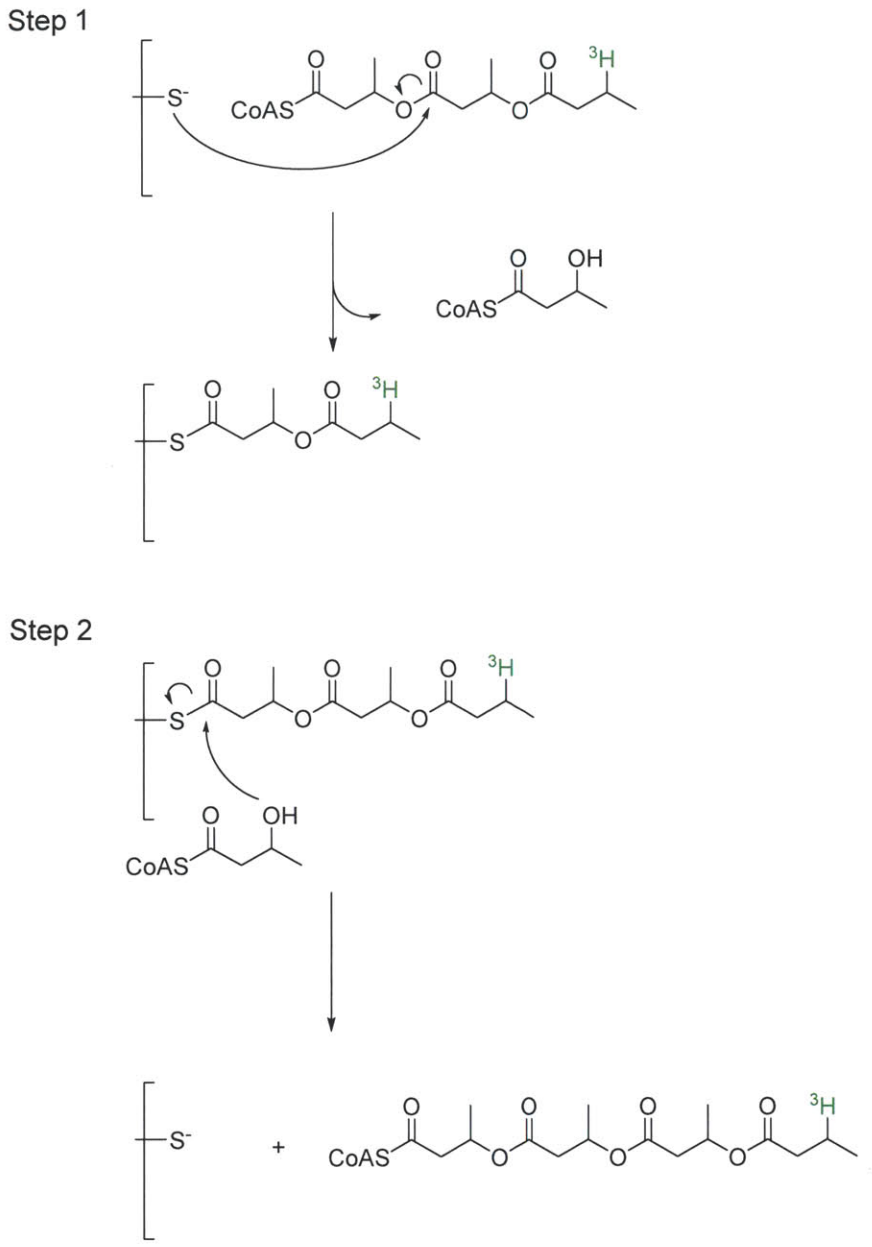

Scheme 2.2 Possible mechanism for the formation of [^{3}H]-sT$_4$CoA. In the first step, HBCoA is formed from the reaction of PhaC$_{Cc}$ with [^{3}H]-sTCoA in which the Cys attacks at the indicated oxoester rather than the CoA thioester. HBCoA then dissociates from the active site. In the second step, HBCoA formed from Step 1 attacks the thioester of [^{3}H]-sT-PhaC$_{Cc}$ as indicated to form [^{3}H]-sT$_4$CoA.

2.3.10 GPC analysis of the reaction products of $PhaC_{Cc}$ and sT-$PhaC_{Cc}$ incubated with [1-^{14}C]-HBCoA: sTCoA is chemically competent for polymerization

To investigate the M_w of PHB produced *in vitro* and determine whether it is consistent with the M_w predicted by a rate of chain termination of 1 min^{-1}, PHB produced *in vitro* was extracted into chloroform for analysis by GPC. Given the low refractive index of PHB and the experimental limitations on the amount of polymer that can be generated *in vitro*, it is necessary to prepare PHB from radiolabeled substrates in order to monitor its elution. These experiments also allowed us to examine the chemical competence of [^{3}H]-sT to produce [^{3}H]-PHB.

Three types of reactions were carried out. In the first reaction, unprimed $PhaC_{Cc}$ (50 nM) was reacted 30 min with 1 mM [1-^{14}C]-HBCoA and the PHB was extracted into chloroform for GPC analysis. [1-^{14}C]-HBCoA is typically prepared by diluting [1-^{14}C]-(*R*/*S*)-HBCoA with unlabeled (*R*)-HBCoA. As a result, 50% of the radioactivity in a given sample is (*S*)-HBCoA. Therefore, 50% of the total radioactivity present in an experiment should not be incorporated into PHB due to very low concentrations and that (*S*)-HBCoA has previously been shown not to be a substrate for PhaCs. The PHB eluted from the GPC column with a retention time of 12.7 min (Figure 2.23). Using the adjusted calibration curve prepared as described in section 3.2.11 (Chapter 3), the M_w and PDI of the polymer were calculated to be 680 kDa (~8,000 HBs) with a PDI of 12 (Table 2.8). Small molecules eluted between 21 and 23 min. For this reaction, the total recovery of [1-^{14}C]-(*R*)-HBCoA was ~100% (Table A2.1 in the Appendix to this Chapter). A small amount of [1-^{14}C]-(*S*)-HBCoA was apparently also incorporated into polymer (~40 pmol) (Table A2.2). However, assays of $PhaC_{Cc}$ with racemic (*R*/*S*)-HBCoA suggested that (*S*)-HBCoA is not a substrate for $PhaC_{Cc}$ (not shown). One possible explanation for the incorporation of (*S*)-HBCoA into polymer is that it undergoes non-enzymatic transesterification with the polymer

during the extraction of polymer into chloroform. Alternatively, in our assays, we may not have been able to measure the consumption of a small amount of (*S*)-HBCoA because of the limit of detection by the DTNB assay.

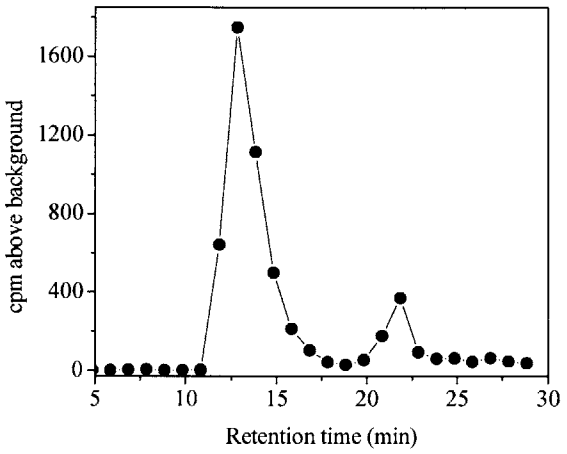

Figure 2.23 GPC trace of PHB extracted from polymerization of [1-^{14}C]-HBCoA by PhaC$_{Cc}$. The reaction contained 50 nM PhaC$_{Cc}$ and 1 mM [1-^{14}C]-HBCoA (specific activity = 175 cpm/nmol [1-^{14}C]-(*R*)-HBCoA). The polymer elutes with a retention time of 12.9 min. The small molecules elute with retention times between 21-23 min. The experiment was performed once.

Table 2.8 M_w and PDI of PHB extracted from *in vitro* reactions of unprimed and primed PhaC$_{Cc}$ with HBCoA.

Reaction	[PhaC$_{Cc}$] (μM)	[HBCoA] (μM)	sTCoA[a]	M_w (kDa)	PDI[b]
1	0.05	1000*	no	680	12
2	0.05	1000	yes*	440	35
3	0.05	1000*	yes	530	9.8
4	4	20*	no	28	15
5	4	200*	no	64	4.5

*denotes the species containing the radiolabel

[a]the concentration of sTCoA in the final reaction is not provided because it is diluted 1000-fold from the initial reaction and is present in the assay as a mixture of free sTCoA and acylated sT-PhaC$_{Cc}$.

[b]the PDIs measured in these experiments are considerably higher than that of PHB extracted from *C. crescentus*. This is likely due to the fact that because fractions are collected to make the measurements. Smaller fractions afford more precise measurements, but for practical purposes the fractions are not extremely small.

In the second reaction, $PhaC_{Cc}$ was first primed with [^{3}H]-sTCoA then diluted 1000-fold (to a final concentration of 50 nM) into an assay mixture containing 1 mM HBCoA, and incubated for 30 min. The PHB was then extracted into chloroform and analyzed by GPC as above (Figure 2.24). The total recovery of radioactivity was 78%, which includes the radioactivity extracted into chloroform and the radioactivity that remained associated with the chloroform-insoluble material (Table A2.1). PHB eluted with a retention time of 13.7 min, and the radioactivity associated with the PHB peak (210 cpm in the entire sample) corresponded to 0.036 nmol of [^{3}H]-sT incorporated into polymer (Table A2.2). The reaction contained 0.05 nmol of $PhaC_{Cc}$, so the stoichiometry of incorporation of [^{3}H]-sT into polymer was 0.73 per PhaC. The M_w of the polymer was ~440 kDa (~5,000 HBs) and the PDI was 35 (Table 2.8). The small molecules eluted as a large peak after 19 min and likely include unreacted [^{3}H]-sTCoA and the additional species observed in the previous section.

The PDI of the polymer peak is extremely high because the radioactivity of the peak is very low and the peak is broad. The M_n of the sample, which is the sum of the M_w of each chain divided by the total number of chains, is much lower than the M_w, because the calculation for M_w takes into account the M_w of a chain in determining the M_w of the entire sample (that is, high M_w chains are weighted more heavily in the calculation), whereas M_n is simply the numerical average. Therefore PDI, which is M_w/M_n, is much higher when M_n is considerably smaller than M_w.

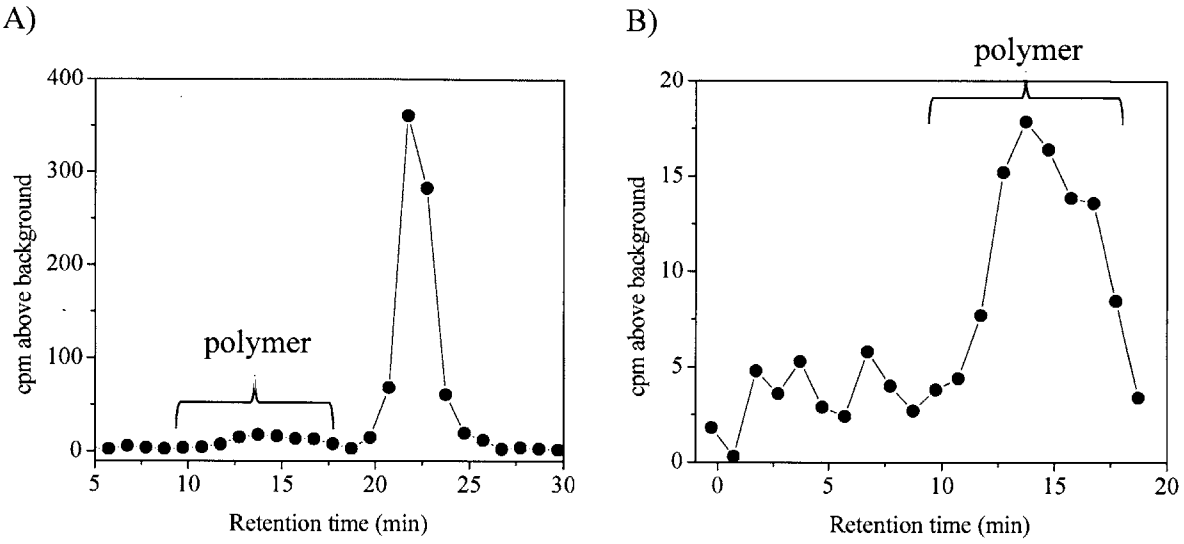

Figure 2.24 GPC trace of PHB extracted from polymerization of HBCoA by $PhaC_{Cc}$ primed with [^{3}H]-sTCoA. The final reaction contained 50 nM $PhaC_{Cc}$, some portion of which was acylated with [^{3}H]-sTCoA, and 1 mM HBCoA. A) Full elution profile of extracted material. Polymer (the low, broad peak) elutes with a retention time of ~13.7 min, and small molecules elute after 19 min. B) Expansion of the polymer peak from A. The experiment was carried out once. The error of each measured fraction in the polymer peak is ~8%.

In order to confirm the results of the reaction of [^{3}H]-sT-$PhaC_{Cc}$ with HBCoA, a third reaction was carried out in which $PhaC_{Cc}$ was primed with sTCoA, then the mixture was diluted 1000-fold into 1 mM [1-^{14}C]-HBCoA (specific activity = 175 cpm/nmol [1-^{14}C]-(*R*)-HBCoA). In this reaction, [1-^{14}C]-HBCoA instead of [^{3}H]-sTCoA (available at low specific activity) facilitated PHB quantitation and analysis. The resulting polymer was extracted into chloroform and analyzed by GPC (Figure 2.25). The reaction contained a total of 35,000 cpm [1-^{14}C]-(*R*/*S*)-HBCoA, of which 29,200 cpm (85%) was extracted into chloroform, while 4,400 cpm remained with the material that was insoluble in chloroform. The total recovery of radioactivity was therefore 98% (Table A2.1). Of the chloroform extracted material, ~85% was in large polymer that eluted at 12.7 min, whereas the remaining radioactivity was associated with small molecules that eluted in two peaks after 19 min (Table A2.2). We again see incorporation of more than 50% of the total radioactivity in polymer, analysis of which indicates that ~40 pmol of [1-^{14}C]-(*S*)-

HBCoA was incorporated into polymer. The M_w of the polymer was 530 kDa (~6,000 HBs) with a PDI of 9.8. The M_w measured in this experiment was slightly higher than that measured in the previous reaction and the PDI was considerably lower, likely because of the higher radioactivity in the polymer peak.

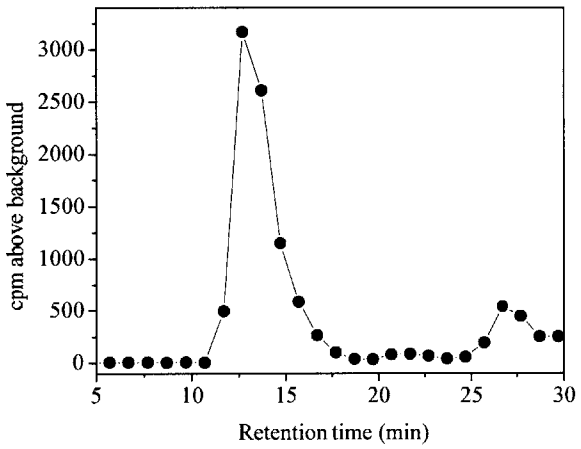

Figure 2.25 GPC trace of PHB extracted from polymerization of [1-^{14}C]-HBCoA by PhaC$_{Cc}$ primed with sTCoA. The final reaction contained 50 nM PhaC$_{Cc}$, some portion of which was acylated with sTCoA, and 1 mM [1-^{14}C]-HBCoA (specific activity = 175 cpm/nmol [1-^{14}C]-(R)-HBCoA. The polymer peak eluted with a retention time of 12.7 min, and the small molecules eluted in two peaks after 19 min. The experiment was done once.

The reactions described in this section contained 20,000 equiv. of HBCoA relative to PhaC$_{Cc}$. Therefore the observed M_ws are lower than would be expected for uniform loading (i.e. one chain per monomer) if no termination occurred, as this would result in polymer of M_w ~1.7 MDa. These results thus suggest that termination occurs *in vitro* in the absence of factors other than PhaC$_{Cc}$. Previous studies of PhaEC$_{Av}$ also suggested the class III synthase was capable of catalyzing termination *in vitro*, suggesting this is a common feature of PHB synthases (*11*). Furthermore, the M_ws measured that correspond to PHB chains of 5,000-8,000 HB units are consistent with the rate constant of thiolysis by CoA (measured in the previous section by sDCoA formation) being 1 min^{-1}.

2.2.11 Priming with sTCoA increases the specific activity of $PhaC_{Cc}$ ~2-fold

The results discussed in the preceding sections suggest that the reaction between sTCoA and $PhaC_{Cc}$ produces at least two species of acylated $PhaC_{Cc}$, namely sT-PhaC and HB-PhaC. We therefore further explored sTCoA as a primer for polymerization by measuring the activity of $PhaC_{Cc}$ following acylation with sTCoA. $PhaC_{Cc}$ was reacted with 10 equiv. sTCoA for ~10 s at 30 °C, and the reaction was diluted 70-fold by the addition of buffer. An aliquot of the diluted reaction was added to an assay mixture containing 1 mM HBCoA and the CoA release was monitored by DTNB assay (Figure 2.26). In the final assay, the concentrations of $PhaC_{Cc}$ was 50 nM and sTCoA at 0.5 μM as a mixture of sTCoA and sT-$PhaC_{Cc}$. The results indicated that priming has only a small effect on activity, increasing it about 2-fold relative to the unprimed enzyme, from 42 U/mg to 72 U/mg. Together with the results demonstrating the chemical competence of sTCoA, these studies demonstrate that sTCoA can serve as a primer for $PhaC_{Cc}$, and that priming has a small but measurable effect on the activity of $PhaC_{Cc}$. In the case of $PhaC_{Re}$, which has a lag phase in CoA release that precedes the linear phase, priming with sTCoA decreases the length of the lag phase and increases the activity 3-fold (*3*).

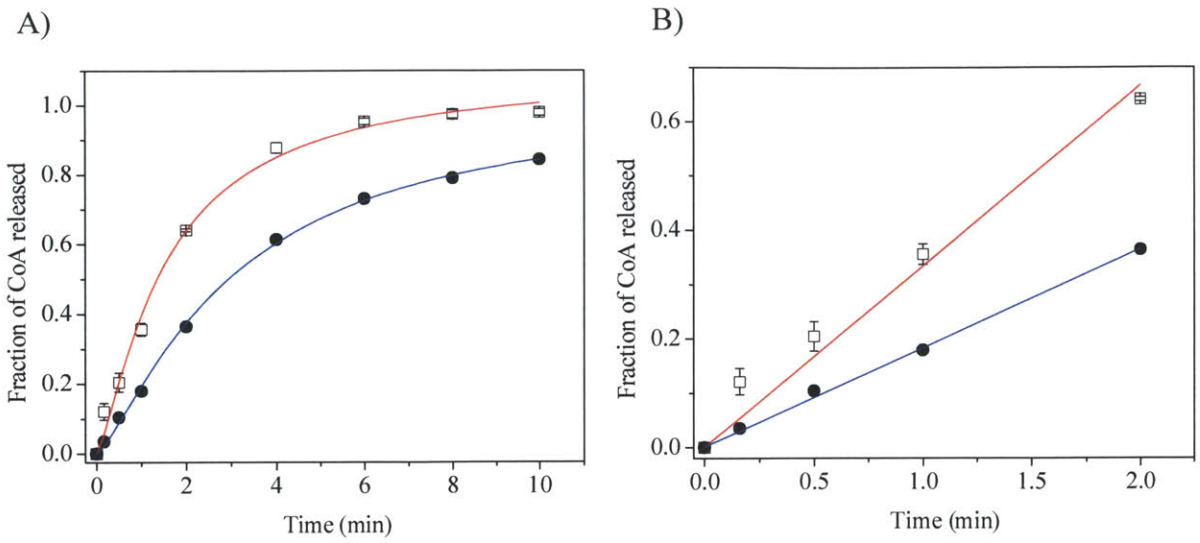

Figure 2.26 Effect of priming with sTCoA on the activity of $PhaC_{Cc}$. A) The reactions contained 50 nM $PhaC_{Cc}$ reacted with either 1 mM HBCoA (●, blue), or $PhaC_{Cc}$ reacted first with 500 μM sTCoA then diluted to a final concentration of 50 nM $PhaC_{Cc}$ and 0.5 μM sTCoA in 1 mM HBCoA (□, red). The data are fit to Equation 2.3. B) Expansion of the early time points. The data are fit with a linear function to calculate specific activity. Error bars represent standard deviation from the mean of three experiments.

2.3.12 Reaction of $PhaC_{Cc}$ and sT-$PhaC_{Cc}$ incubated with [1-^{14}C]-HBCoA analyzed by SDS-PAGE/autoradiography

2.3.12.1 Reaction of $PhaC_{Cc}$ with 5 or 50 equiv. [1-^{14}C]-HBCoA: the rate of initiation is slower than the rate of elongation

The observation that $PhaC_{Cc}$ can at least initially be uniformly loaded by reaction with sTCoA led us to consider whether the same is true when HBCoA is present in only a small excess over $PhaC_{Cc}$. A difficulty we have previously encountered in studying the elongation process of polymerization is that, because the rate of elongation in $PhaC_{Re}$ and $PhaEC_{Av}$ is much faster than the rate of initiation, even in the presence of just a few equivalents of HBCoA, high M_w polymer is generated (*6, 10*). This phenomenon has been shown by SDS-PAGE and autoradiography analysis of the polymerization products of PhaCs incubated with [1-^{14}C]-HBCoA. While this is not an ideal method for examination of PHB products, as we do not fully

understand the migratory properties of different chain lengths of PHB in the denaturing gel, it does provide a sense of the distribution of oligomeric and polymeric products. To investigate the uniformity of loading with a small excess of HBCoA, $PhaC_{Cc}$ (4 μM) was reacted with 5 or 50 equiv. [1-^{14}C]-HBCoA, and the products were examined by SDS-PAGE and autoradiography (Figure 2.27). These experiments required a higher concentration of $PhaC_{Cc}$ than in previous experiments to allow detection of $PhaC_{Cc}$ by SDS-PAGE and Coomassie staining. This method allows visualization of changes in the migration of $PhaC_{Cc}$ relative to the control with no HBCoA, and potentially the detection of small [^{14}C]-HB oligomers associated with synthase.

If $PhaC_{Cc}$ were uniformly loaded with 5 equiv. HBCoA, one might expect to observe radioactivity associated with the synthase by autoradiography, but little or no shift in the migration of $PhaC_{Cc}$. If $PhaC_{Cc}$ were uniformly loaded with 50 equiv. HBCoA, then one might expect to see by SDS-PAGE that $PhaC_{Cc}$ migrates more slowly than the control, as a chain of 50 HBs would increase the M_w by ~4.3 kDa. Autoradiography would further demonstrate that the radioactivity is associated with $PhaC_{Cc}$. Again, however, it must be noted that the migratory properties of such species in SDS-PAGE are difficult to predict.

SDS-PAGE with Coomassie staining shows that the majority of the synthase is unmodified when reacted with both 5 and 50 equiv. HBCoA (Figure 2.27A). By autoradiography, a single predominant species (species II) is observed in the reactions of $PhaC_{Cc}$ with both 5 and 50 equiv. HBCoA (Figure 2.27B). Species II migrates through the stacking gel to the interface of the stacking and separating gels. We interpret this species to be high M_w PHB that does not enter the gel due to its M_w, hydrophobicity, shape, precipitation, or all of the above. A small amount of radioactivity is also associated with species I, which remains in the well. In all lanes there is no detectable radioactivity associated with the synthase, even after exposure for

2 days (not shown). Together these results suggest that $PhaC_{Cc}$ is not uniformly loaded when reacted with 5 or 50 equiv. [1-^{14}C]-HBCoA.

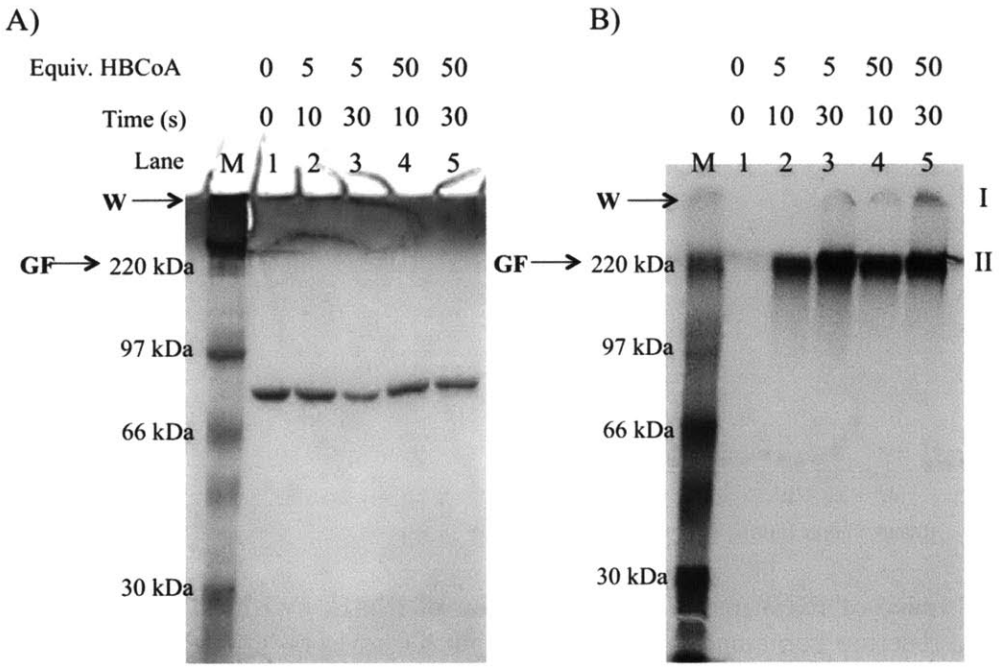

Figure 2.27 SDS-PAGE (10%) monitoring PHB formation from 5 or 50 equivalents of [1-^{14}C]-HBCoA incubated with $PhaC_{Cc}$. Both reactions contain ~85,000 cpm total. Lanes 1-5 are the same in both panels. A) Lanes 1-5, Coomassie stain of $PhaC_{Cc}$ with indicated equiv. of [1-^{14}C]-HBCoA and reaction times. B) Autoradiography of the gel in panel A. Lane 1, 3 μg of $PhaC_{Cc}$. Lanes 2 and 3, $PhaC_{Cc}$ (3 μg per lane) with indicated equiv. of [1-^{14}C]-HBCoA (specific activity = 2 x 10^5 cpm/nmol) and reaction times. Lanes 4 and 5, $PhaC_{Cc}$ (3 μg per lane) with indicated equiv. of [1-^{14}C]-HBCoA (specific activity = 2 x 10^4 cpm/nmol). W, wells. GF, gel front. The 30 kDa markers near the bottom of the gels do not line up because after imaging of the Coomassie stain and prior to autoradiography, the gel was dried, causing it to crack and contract slightly at the bottom.

In order to confirm that species II is high M_w polymer, and to determine its M_w and PDI, $PhaC_{Cc}$ (4 μM) was reacted with 5 or 50 equiv. [1-^{14}C]-HBCoA, and the resulting polymer was extracted into chloroform for GPC analysis (Figure 2.28). For both reactions, the total extraction efficiency was ~100% (Table A2.1). PHB produced from incubation of $PhaC_{Cc}$ with 5 equiv. HBCoA had a M_w of 28 kDa (325 HB monomers) and a PDI of 15, and that produced from incubation of $PhaC_{Cc}$ with 50 equiv. had a M_w of 64 kDa (750 HB monomers) and a PDI of 4.5

(Table 2.8). These results indicate that the rate of elongation is faster than the rate of initiation and the synthase is not uniformly loaded when reacted with 5 or 50 equiv. HBCoA. Furthermore, our interpretation of species II as high M_w PHB is correct.

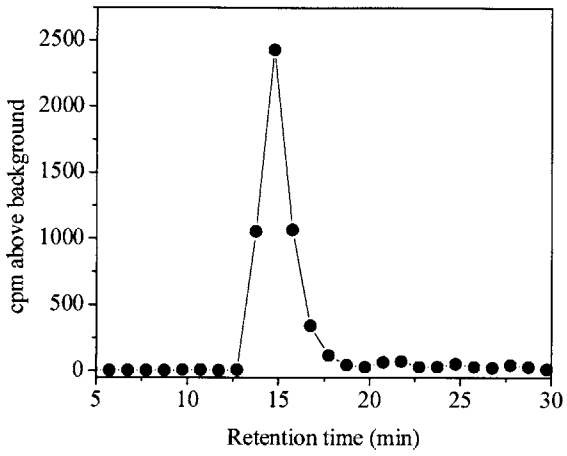

Figure 2.28 GPC trace of PHB produced by reaction of $PhaC_{Cc}$ with 50 equivalents of [1-^{14}C]-HBCoA. The reaction contained 4 μM $PhaC_{Cc}$ and 200 μM [1-^{14}C]-HBCoA. The specific activity of the [1-^{14}C]-HBCoA was 175 cpm/nmol (*R*)-HBCoA. PHB was extracted into chloroform by two rounds of refluxing at 70 °C for 48 h. The reaction was carried out once.

2.3.12.2 Reaction of sT-$PhaC_{Cc}$ with 5 or 50 equiv. [1-^{14}C]-HBCoA: priming with sTCoA increases the distribution of radioactive species

We next investigated whether priming with sTCoA affected the uniformity of loading in the presence of 5 and 50 equiv. [1-^{14}C]-HBCoA. We have previously established that incubation of wt $PhaEC_{Av}$ with sTCoA resulted in enzyme labeled with 0.5 equiv. sT (*5*). When the enzyme was rapidly denatured, digested with trypsin and examined by mass spectrometry, three peptides were isolated containing the active site Cys covalently labeled with sT and a sT chain that had been extended by one and two HB units. $PhaEC_{Av}$ was thus caught in the act of elongation due to the presence of a small amount of HBCoA in the sTCoA as the result of breakdown during storage. This observation suggested that priming bypassed the slow rate of initiation to allow

more uniform elongation by just a few HB units. To investigate the effect of sTCoA on our ability to observe small [^{14}C]-HB oligomer species associated with synthase that might suggest uniform loading, $PhaC_{Cc}$ (4 μM) was incubated with 10 equiv. sTCoA for ~10 s, then chased with 5 or 50 equiv. of [1-^{14}C]-HBCoA. The products of the reaction were analyzed by SDS-PAGE and autoradiography (Figure 2.29). Again SDS-PAGE with Coomassie staining reveals no difference in the migration of $PhaC_{Cc}$ compared to the control (Figure 2.29A). However, autoradiography revealed that priming with sTCoA prior to reaction with [1-^{14}C]-HBCoA changed the distribution of radioactive species. Figure 2.29B shows four distinct radioactive species, species I-IV, and two broad regions of "smeared" radioactivity, regions i and ii.

Species I (in the wells) and species II (at the gel front) are present with and without priming with sTCoA. Species III is present only when $PhaC_{Cc}$ is acylated with sTCoA and migrates just above the unmodified synthase. In lane 2 of Figure 2.29B, species III migrates with an apparent M_w of 89 kDa, 14 kDa larger than unmodified $PhaC_{Cc}$. This species could correspond to $PhaC_{Cc}$ modified with a 160mer of PHB, but represents only a small fraction of total synthase as we detect no $PhaC_{Cc}$ by Coomassie staining. Finally, species IV, present in lane 2 migrates at the position of $PhaC_{Cc}$, and is likely $PhaC_{Cc}$ associated with small PHB oligomers. We have previously interpreted such a species to be $(HB)_n$ where n = 3-10 (*11*). This species is only detectable when $PhaC_{Cc}$ is reacted with 50 equiv. of [1-^{14}C]-HBCoA, even though the reaction contains the same total cpm as the reaction with just 5 equiv. of [1-^{14}C]-HBCoA. Together, the results suggest that acylation with sTCoA affects the distribution of radioactive species *in vitro*. To quantitate the distribution of radioactivity, we performed densitometry analysis to determine what percentage of total radioactivity each species accounted for. This analysis revealed that the radioactivity present in species III and IV accounts for 15-20% of the

total radioactivity in the reactions containing both 5 and 50 equiv. [1-^{14}C]-HBCoA. In contrast, when $PhaC_{Cc}$ is not primed with sTCoA, there is no detectable radioactivity associated with species III and IV. This suggests that priming with sTCoA increases the uniformity of loading, allowing for the detection of small $(HB)_n$ species associated with synthase. The distribution of radioactivity is provided in Figure A2.1 in the appendix to this Chapter.

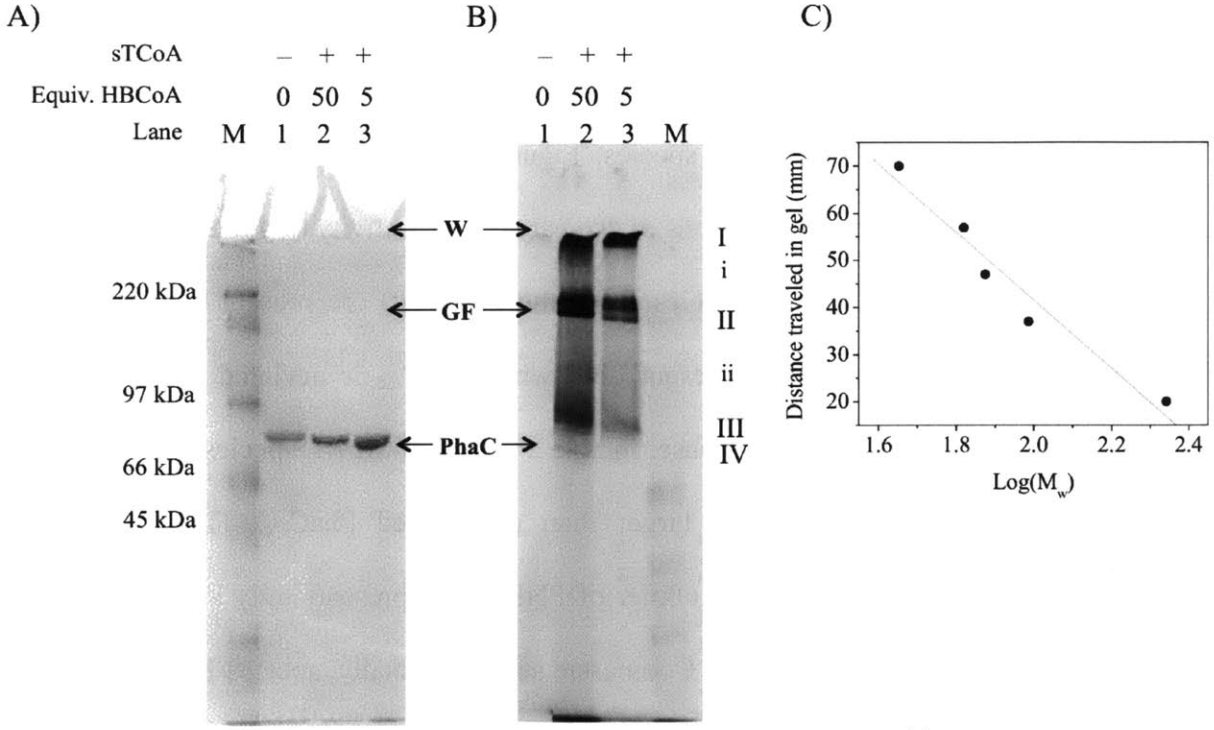

Figure 2.29 SDS-PAGE (10%) analysis of the polymerization of [1-^{14}C]-HBCoA by $PhaC_{Cc}$. A) Coomassie stained gel. M, molecular weight standards. Lanes 1-3 are as described for panel B. B) Autoradiography of gel in panel A. Lane 1, control reaction containing 3 μg of $PhaC_{Cc}$. Lane 2, $PhaC_{Cc}$ (3 μg) reacted with 10 equiv. of sTCoA for 1 min, then chased with 50 equiv. of [1-^{14}C]-HBCoA (specific activity = 2 x 10^4 cpm/nmol). Lane 3, $PhaC_{Cc}$ (3 μg) reacted with 10 equiv. of sTCoA for 1 min, then chased with 5 equiv. of [1-^{14}C]-HBCoA (specific activity = 2 x 10^5 cpm/nmol). M, molecular weight standards. C) Standard curve prepared from migration (in mm) of the indicated M_w standards and $PhaC_{Cc}$ standard in the gel. This standard curve was used to estimate the M_w of species III. W, wells. GF, gel front.

2.3.13 SDS-PAGE and Western blot analysis indicates that small amounts of $PhaC_{Cc}$ are associated with [^{14}C]-PHB species

$PhaC_{Cc}$ cannot be detected associated with the radioactive species in the experiments above in Figure 2.29, presumably because of non-uniform loading of $PhaC_{Cc}$ and the insensitivity of Coomassie staining methods. In order to determine whether the radioactive species observed in Figures 2.25 and 2.27 contain $PhaC_{Cc}$, two reactions were carried out and analyzed by the more sensitive methods of Western blot analysis using antibodies raised to $PhaC_{Cc}\Delta N$ and silver staining. In the first reaction, $PhaC_{Cc}$ was reacted with 50 equiv. of [1-^{14}C]-HBCoA, and in the second reaction $PhaC_{Cc}$ was first acylated with sTCoA, then chased with 50 equiv. of [1-^{14}C]-HBCoA. Both reactions were carried out at RT then quenched by addition of Laemmli buffer, and immediately loaded onto two SDS-PAGE gels and run on ice. One gel was stained with Coomassie stain and the second was transferred to a PVDF membrane for Western blot analysis. Furthermore, the material that did not transfer from the SDS-PAGE gel to the Western blot membrane was analyzed by silver staining of the gel, which can detect as little as 0.25 ng of protein.

These experiments indicate that, although the majority of the synthase remains unmodified, the radioactive species observed in Figure 2.29B are in fact associated with small amounts of $PhaC_{Cc}$. The amount of $PhaC_{Cc}$ associated with the radioactive species II increases substantially when the enzyme is first acylated with sTCoA (Figure 2.30A-C, lanes 3 and 4). Even the relatively insensitive Coomassie stain detects a small amount of protein, which does not enter the separating gel, migrating at the position of radioactive species II (Figure 2.30A, lane 4). This species is only observed when the enzyme is acylated with sTCoA prior to reaction, suggesting that priming increases the population of $PhaC_{Cc}$ that generates high M_w polymer. By

Western blot, a more sensitive method of detection, two distinct $PhaC_{Cc}$ bands can be seen at this position (Figure 2.30B, lane 4). The samples in lanes 3 and 4 in Figure 2.30 are extremely overloaded for Western blot detection; thus, many non-specific bands not visible by SDS-PAGE nevertheless cross-react with the anti-$PhaC_{Cc}$ antibodies. However, comparison of lanes 3 and 4 in panel B again confirms that the two distinct bands in species II are only observed when the synthase is first acylated with sTCoA prior to reaction with [1-^{14}C]-HBCoA.

A silver stain of the SDS-PAGE gel following blotting to a PVDF membrane for Western blot analysis reveals that the transfer of protein species is not complete (Figure 2.30C). The transfer appears quite poor in regions of the gel where we expect PHB to be migrating, based on experiments in the previous section. Interestingly, a sharp band in lane 4 of panel C migrates at the position of radioactive species II. This band is likely the same band observed in lane 4 of panel A, which does not transfer completely to the PVDF membrane, potentially due to its association with PHB. Additionally, the radioactive smear in region ii contains protein that also does not transfer to the PVDF membrane (Figure 2.30C, lane 4). This could be $PhaC_{Cc}$ associated with varying sizes of polymer, or with polymer of varying structures. It should be noted that part of the gel containing the smear in region ii broke during imaging. A large portion of the radioactivity in both the reactions with and without pre-acylation with sTCoA is associated with what we interpret to be large polymer that does not enter the gel (species I). These experiments demonstrate that acylation of $PhaC_{Cc}$ with sTCoA prior to the polymerization reaction results in a broader distribution of $PhaC_{Cc}$ species associated with polymer than without priming. This distribution is distinct from what is observed when the enzyme is not pre-acylated with sTCoA, suggesting that sTCoA increases the uniformity of loading of $PhaC_{Cc}$.

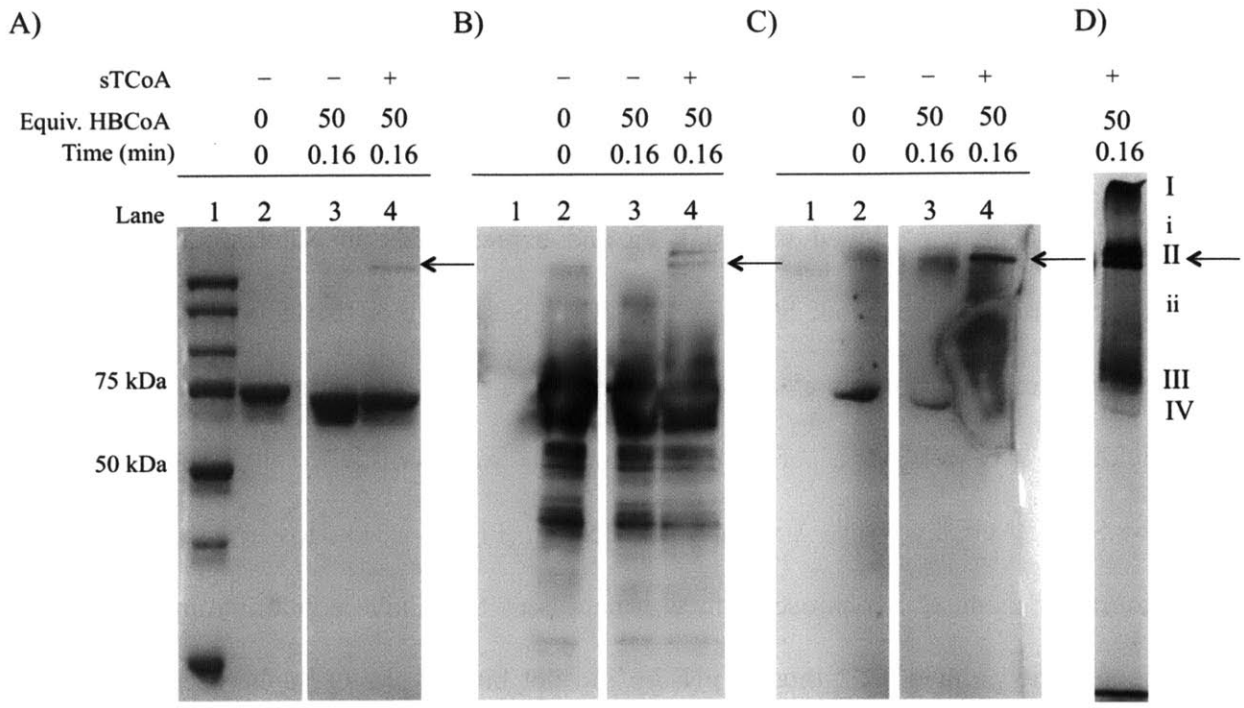

Figure 2.30 SDS-PAGE (10%), Western blot and silver stain analysis of $PhaC_{Cc}$ species from *in vitro* polymerizations. A) Coomassie stain and B) anti-PhaC Western blot of 10% SDS-PAGE analysis of reaction species. C) Silver stain of SDS-PAGE gel following transfer of proteins to PVDF membrane for Western blot analysis. Lanes 1-4 in panels A, B and C are the same. Lane 1, molecular weight standards. Lane 2, $PhaC_{Cc}$ standard (3 μg). Lanes 3, 4 μM $PhaC_{Cc}$ (3 μg) reacted with 200 μM HBCoA. Lane 4, 4 μM $PhaC_{Cc}$ (3 μg) reacted with 500 μM sTCoA, then chased with 200 μM HBCoA. D) Autoradiograph of reaction containing 4 μM $PhaC_{Cc}$ (3 μg) reacted with 500 μM sTCoA then chased with 200 μM HBCoA. Panel D is taken from Figure 2.29 and included for comparison. The arrows indicate the gel front and the position of Species II.

2.3.14 Expression and purification of His_6-PhaP

In Chapter 4, we present studies in which we identified the major granule associated protein in *C. crescentus*, the phasin PhaP, and in which the *in vivo* role of PhaP was investigated in cultures of *C. crescentus* grown in nitrogen-limited medium. These experiments indicated that PhaP is a 15 kDa protein that is the predominant granule-associated protein under our growth conditions. Furthermore, PhaP plays an important role in promoting PHB accumulation, as the Δ*phaP* mutant strain of *C. crescentus* (harboring a clean deletion of *phaP*) accumulates PHB to

only 10% that of the levels in the wt strain. We were therefore interested in studying the effect of PhaP *in vitro* on the activity of PhaC to determine whether reduced PHB accumulation in the Δ*phaP* mutant could be explained in terms of an effect on the activity of $PhaC_{Cc}$. Toward this end, the *phaP* gene was cloned into pET28a and expressed as an N-terminally His_6-tagged construct containing the sequence SSGLVPRGSHMA between the His_6 tag and PhaP, where the underlined portion is a thrombin cleavage site. Growth of *E. coli* harboring the plasmid encoding *phaP* yielded 2 g of cell paste per L of culture. PhaP was purified to >95% homogeneity as judged by SDS-PAGE by Ni-NTA affinity purification (Figure 2.31). However, anion exchange chromatography using Q Sepharose resin was necessary to remove contaminating DNA. PhaP has an isoelectric point of 7.8, thus at pH 7.6 did not bind to the Q Sepharose resin. This pI facilitated separation from contaminating DNA, which binds strongly to the resin. The purification yield was 5 mg PhaP per g of cells. Incubation with thrombin cleaved the His_6 tag completely, as judged by 15% SDS-PAGE (Figure 2.31, compare lanes 10 and 11) and Western blot analysis using antibodies to his-tagged PhaP (not shown).

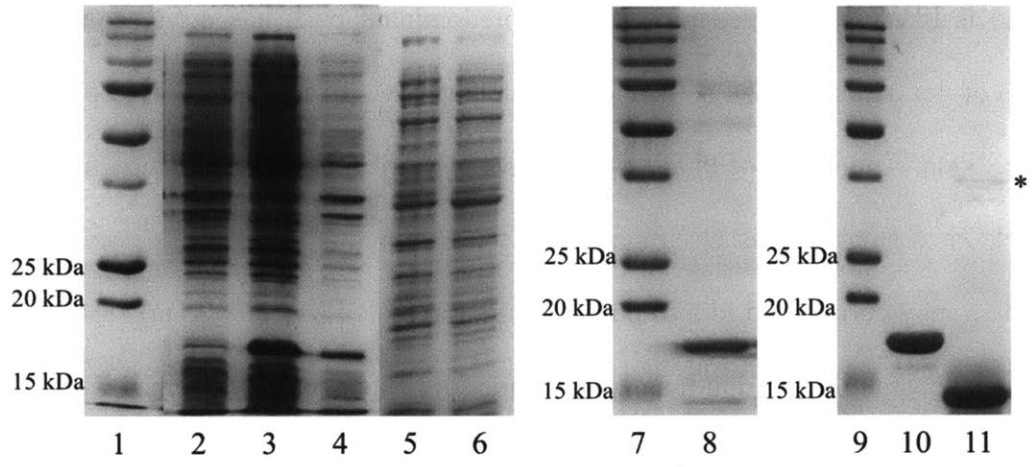

Figure 2.31 SDS-PAGE (15%) purification gel of His_6-PhaP. Lanes 1, 7 and 9, M_w standards. Lane 2, whole-cell pre-induction sample. Lane 3, soluble cell-free extract. Lane 4, insoluble cell-free extract. Lane 5, Ni-NTA agarose flowthrough. Lane 6, Ni-NTA agarose 10 mM imidazole wash. Lane 8, post Ni-NTA column, eluted with 250 mM imidazole. Lane 10, Q Sepharose flowthrough (final purified His_6-PhaP). Lane 11, PhaP after cleavage of His_6 tag with thrombin. The asterisk indicates the position of thrombin.

2.3.15 SEC of PhaP indicates that it is a tetramer or pentamer in solution

As discussed in Chapters 1 and 4, the nucleating granule species *in vivo* (i.e., the PHB granule precursor) is proposed, on the basis of observations made in *R. eutropha*, to consist of a dimer of PhaCs covalently attached to a high M_w PHB chain, with 4-9 PhaPs associated (*19, 34*). Small angle X-ray scattering studies of PhaP1 from *R. eutropha* indicated that it is a homotrimer, with the subunits arranged in a flat triangular shape (*15*). Atomic force microscopy studies of granules isolated from *R. eutropha* have been interpreted to suggest that PhaP1 forms a semi-regular network of PhaP1 molecules arranged to form pores, or sites of ingress from the surface of the granule to the PHB core (*35*). The oligomeric state of phasins can likely provide insight into its role *in vivo* in promoting PHB accumulation.

To determine the oligomeric state of PhaP, PhaP (100 µL of 180 µM) was examined by SEC at 4 °C in 20 mM Hepes pH 7.5, 200 mM NaCl, using a Superdex 10/300 GL size exclusion column with an elution flow rate of 0.25 mL/min (Figure 2.32). A peak eluting in the void

volume (V_0) is likely aggregated protein. The predominant peak has a M_w consistent with a tetramer (T) or pentamer (P) of PhaPs and the calculated M_w of this peak based on the standard curve was 68 kDa. A tetramer of PhaPs would have a M_w of 60 kDa and a pentamer would have a M_w of 75 kDa. A smaller peak eluting after the tetramer/pentamer peak has a calculated M_w of 35 kDa, which may correspond to a dimer of PhaPs (predicted M_w = 30 kDa). Thus, PhaP from *C. crescentus* appears to be predominantly a tetramer or pentamer of PhaPs, if it is assumed to be globular.

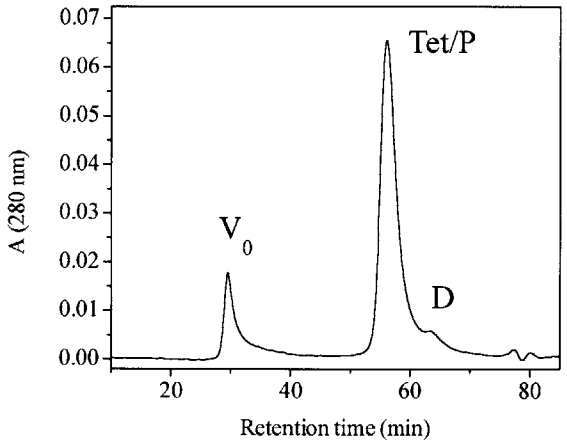

Figure 2.32 Representative SEC trace of PhaP. Samples (100 µL of 180 µM) were injected onto a GE Healthcare Superdex 200 10/300 GL column at 4 °C and eluted at 0.25 mL/min with 20 mM Hepes pH 7.5, 200 mM NaCl.

2.3.16 PhaP and BSA increase HBCoA turnover in assays of $PhaC_{Cc}$

Given that the deletion of *phaP* in *C. crescentus* dramatically reduces its PHB accumulation capability, we were interested in understanding what effect PhaP has on the activity of $PhaC_{Cc}$ *in vitro*. In a preliminary set of experiments, assays were carried out in the presence of one mole equivalent of PhaP to $PhaC_{Cc}$ (on a per monomer basis). In these assays the concentration of $PhaC_{Cc}$ was 25 nM, as at higher concentrations of $PhaC_{Cc}$, the effect observed by including PhaP in the assay was less pronounced. Under these conditions, the inclusion of one

equivalent of PhaP facilitates complete turnover of HBCoA by $PhaC_{Cc}$ in 15 min, whereas $PhaC_{Cc}$ alone only turns over ~60% of the HBCoA (Figure 2.33).

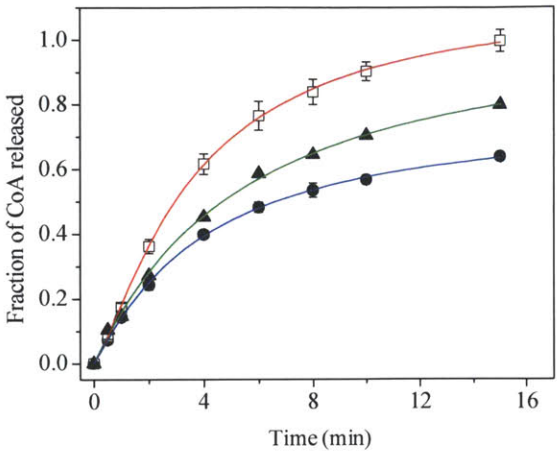

Figure 2.33 Effect of PhaP and BSA on full length $PhaC_{Cc}$ activity. The assays contained 0.76 mM HBCoA, 25 nM $PhaC_{Cc}$ alone (●, blue) or in the presence of 1 mole equivalent of PhaP (□, red) or BSA (▲, green). The data are fit to Equation 2.1. Error bars represent the standard deviation from the mean of three experiments.

Bovine serum albumin (BSA) has been shown to bind to PHB granules *in vitro* (*36*). Niamsiri and coworkers demonstrated that BSA can promote the formation of PHB granules on a surface to which $PhaC_{Re}$ has been immobilized via an N-terminal His_6 tag (*37*). Addition of BSA to the reaction resulted in larger granules and higher total substrate turnover. The authors proposed these observations are the result of BSA interacting with the hydrophobic polymer to prevent hydrophobic collapse. They proposed that this interaction would allow greater substrate access to PhaC, by preventing the growing chain from blocking the active site. Jossek *et al.* have also observed an increase in turnover of HBCoA in assays of $PhaEC_{Av}$ as a result of the inclusion of BSA and PhaP1 from *R. eutropha* (*38*). We therefore investigated the effect of BSA on $PhaC_{Cc}$ turnover, to determine whether it mediated a similar effect as PhaP, as this could give us insight into how PhaP enhances turnover. $PhaC_{Cc}$ was assayed in the presence of one equivalent

of BSA and the results demonstrated that its inclusion affords more extensive turnover of HBCoA in the slow phase, allowing for consumption of ~80% of the HBCoA. As discussed above, high M_w polymer is produced *in vitro*, therefore PhaP and BSA could be playing a similar role to that proposed by Niamsiri *et al.* in stabilizing the nascent PHB granule.

Interestingly, the opposite effect is seen in assays of $PhaC_{Re}$ in the presence of PhaP1. Previous studies by Mimi Cho showed that increasing amounts of PhaP1 increased the length of the lag phase and decreased the specific activity of $PhaC_{Re}$ (*19*). The PHB produced in the presence of PhaP1 migrated faster through an SDS-agarose gel than PHB produced in the absence of PhaP1. However, analysis of the PHB by GPC demonstrated that PhaP1 did not affect the M_w. These results together were interpreted to suggest that PhaP1 increased the lag phase and slowed the overall reaction rate in order to promote folding of the nascent polymer as it emerged from $PhaC_{Re}$. Thus, while the observed effects on the activity of phasins on $PhaC_{Cc}$ and $PhaC_{Re}$ are opposite, they may still be serving the same role in packaging of the polymer and assisting in *in vitro* granule assembly.

In Chapter 3, we demonstrate that the ratio of PhaP/PhaC increases during PHB accumulation from 35 to 500. To determine the effect of increasing equivalents of PhaP on HBCoA consumption and specific activity *in vitro*, assays were carried out in the presence of 0-500 equivalents of PhaP (Figure 2.34). From zero to 50 equivalents of PhaP the specific activity of $PhaC_{Cc}$ increases from 43 U/mg to 125 U/mg. Increasing the equivalents of PhaP to 500 gives no further increase in specific activity (Table 2.9).

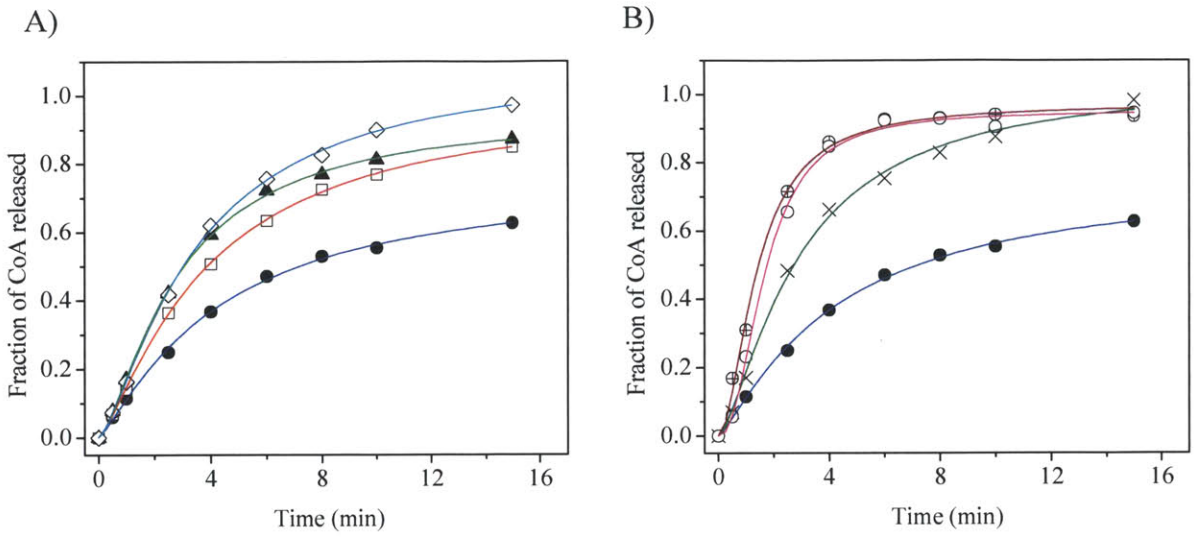

Figure 2.34 Effect of increasing ratio of PhaP to $PhaC_{Cc}$ on HBCoA consumption *in vitro*. The data are fit to a sigmoidal function. A) The assays contained 0.76 mM HBCoA, 25 nM $PhaC_{Cc}$ alone (●, blue) or in the presence of 1 (□, red), 2 (▲, green), or 5 (◊, cyan) equivalents of PhaP. B) The assays contained 0.76 mM HBCoA, 25 nM $PhaC_{Cc}$ alone (●, blue) or in the presence of 10 (×, dark green), 50 (○, magenta) or 500 (⊕, dark red) equivalents of PhaP. The data are fit to Equation 2.1.

Table 2.9 Rate of CoA release and specific activity of $PhaC_{Cc}$ in the presence of varying equivalents of PhaP.

Equivalents PhaP	Rate (μmol/min)	Specific Activity (U/mg)
0	0.0125	43
1	0.0187	65
2	0.217	75
5	0.215	74
10	0.251	87
50	0.361	125
100	0.385	133
500	0.377	130

We next compared the effects of PhaP on turnover at two concentrations of HBCoA (300 μM and 750 μM) and two concentrations of $PhaC_{Cc}$ (25 nM and 50 nM) to determine whether either of these parameters influenced the observed effect of PhaP. The K_M for HBCoA is ~300 μM, hence this concentration was selected for comparison. For these experiments, we selected 50 equiv. of PhaP relative to $PhaC_{Cc}$ (on a monomer basis) because the results of the previous section indicated that, under the reaction conditions, at this ratio the maximum specific activity of $PhaC_{Cc}$ was achieved (Table 2.9). As shown in Figure 2.35A, when the concentration of HBCoA is 300 μM, doubling the concentration of $PhaC_{Cc}$ from 25 nM (red) to 50 nM (blue) has the same effect as including 50 equiv. of PhaP (green), in that under both conditions the HBCoA is completely turned over. However, increasing the concentration of HBCoA to 750 μM lessens the effect of doubling the concentration of $PhaC_{Cc}$ on the total fraction of substrate consumed (Figure 2.35B). When the assay contains 50 nM (blue) instead of 25 nM $PhaC_{Cc}$ (red), the fraction of total CoA consumed only increased from 50 to 75% in the experimental time frame. However, inclusion of PhaP to an assay containing 25 nM $PhaC_{Cc}$ (green) facilitated complete turnover of the substrate. Therefore, the effect of PhaP becomes more pronounced at higher concentrations of HBCoA, an important factor in understanding the role of PhaP in enhancing turnover, as will be discussed below. The fact that all of the substrate is consumed in the assays containing 300 μM HBCoA also suggests that the slowing of turnover in assays containing higher [HBCoA] is due to accumulation of PHB rather than the [HBCoA] dropping far below its K_m.

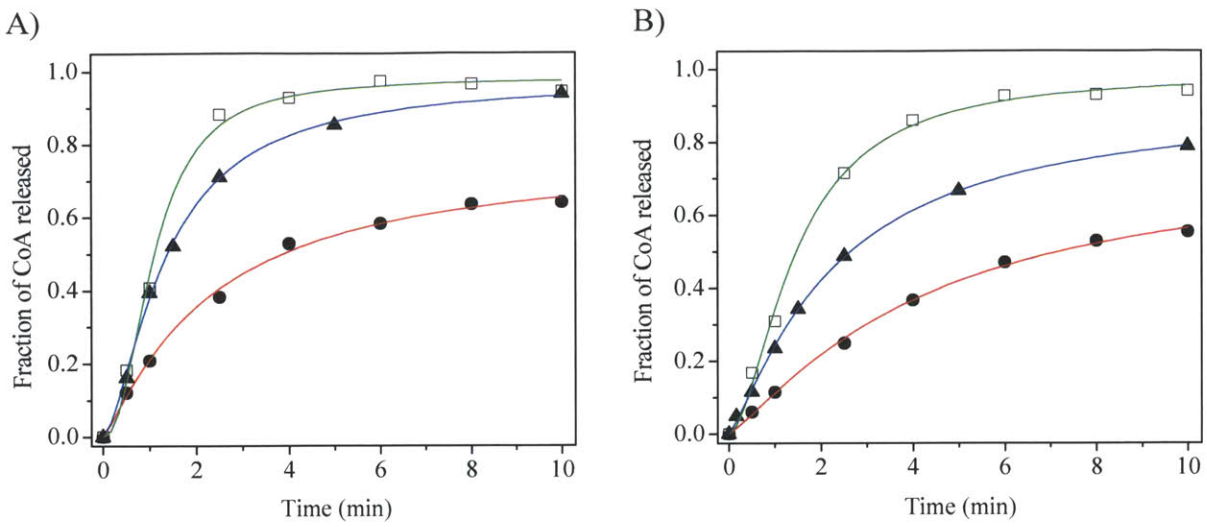

Figure 2.35 Effect of varying the concentration of $PhaC_{Cc}$ and HBCoA on turnover in the presence of PhaP. A) Assays carried out at an HBCoA concentration of 300 μM. The assays contained 25 nM $PhaC_{Cc}$ (●, red), 25 nM $PhaC_{Cc}$ and 25 nM PhaP (□, green), or 50 nM $PhaC_{Cc}$ (▲, blue). B) Assays carried out at an HBCoA concentration of 750 μM. The assays contained 25 nM $PhaC_{Cc}$ (●, red), 25 nM $PhaC_{Cc}$ and 25 nM PhaP (□, green), or 50 nM $PhaC_{Cc}$ (▲, blue).

2.3.17 PhaP also increases HBCoA consumption in assays of $PhaC_{Cc}\Delta N$

The observation that the corresponding PhaPs have opposite effects on the activities of $PhaC_{Re}$ and $PhaC_{Cc}$ raises the possibility that the unusual N-terminal domain of $PhaC_{Cc}$ mediates the effect of PhaP. We therefore tested the effect of PhaP on $PhaC_{Cc}\Delta N$ activity. The presence of one equiv. of PhaP in the assay mixture of $PhaC_{Cc}\Delta N$ led to the same effect as with $PhaC_{Cc}$ (Figure 2.36). The substrate is turned over completely in the presence of one equiv. of PhaP whereas in its absence, only ~60% of the substrate is consumed within the same timescale. This result suggests that the N-terminal domain of $PhaC_{Cc}$ is not necessary to mediate the effect of PhaP on PhaC activity.

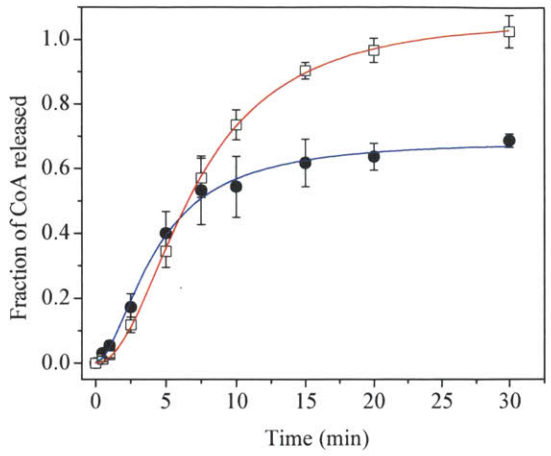

Figure 2.36 Time course of CoA release from PhaC$_{Cc}$ΔN in the presence of one equivalent of untagged-PhaP. The assays contained 0.75 mM HBCoA, 500 nM PhaC$_{Cc}$ΔN and 0 nM PhaP (●, blue) or 500 nM PhaP (□, red). Error bars are standard deviation from the mean of three experiments. The data are fit to Equation 2.1.

2.3.18 Full length PhaC$_{Cc}$ and PhaP interact in solution

The observation that the addition of PhaP to the assay mixture increased the consumption of HBCoA led us to investigate whether PhaC$_{Cc}$ΔN and PhaC$_{Cc}$ interact with PhaP *in vitro*. Taking advantage of the affinity tag on PhaC$_{Cc}$, PhaP was incubated for 10 min at 4 °C with either PhaC$_{Cc}$ΔN or PhaC$_{Cc}$ in a 1:1 ratio (at 10 μM each protein), and the mixture was equilibrated with Ni-NTA resin and loaded onto a column. When PhaP was incubated with PhaC$_{Cc}$, neither the flowthrough nor the washes contained either protein (Figure 2.37A, lanes 2-6). When the column was eluted with 250 mM imidazole, PhaP and PhaC$_{Cc}$ both elute (Figure 2.37A, lanes 7-10). In contrast, when PhaC$_{Cc}$ΔN was incubated with PhaP and the proteins added to 250 μL of Ni-NTA resin, PhaP came out in the flowthrough and wash fractions (Figure 2.37B, lanes 2-4). The control reaction containing only PhaP demonstrates that PhaP itself does not bind the column and in the absence of PhaC$_{Cc}$ comes out in the wash fractions (Figure 2.37C, lanes 2-6). These results suggest that PhaC$_{Cc}$ and PhaP form a complex *in vitro*, but PhaC$_{Cc}$ΔN and PhaP

either do not or interact more weakly; thus, the N-terminal domain of PhaC may mediate interaction with PhaP. However, the observation that PhaP has the same effect on the turnover of substrate by both proteins indicates that the interaction between the proteins is not necessary, and therefore PhaP is likely interacting with the nascent PHB chain to facilitate polymerization.

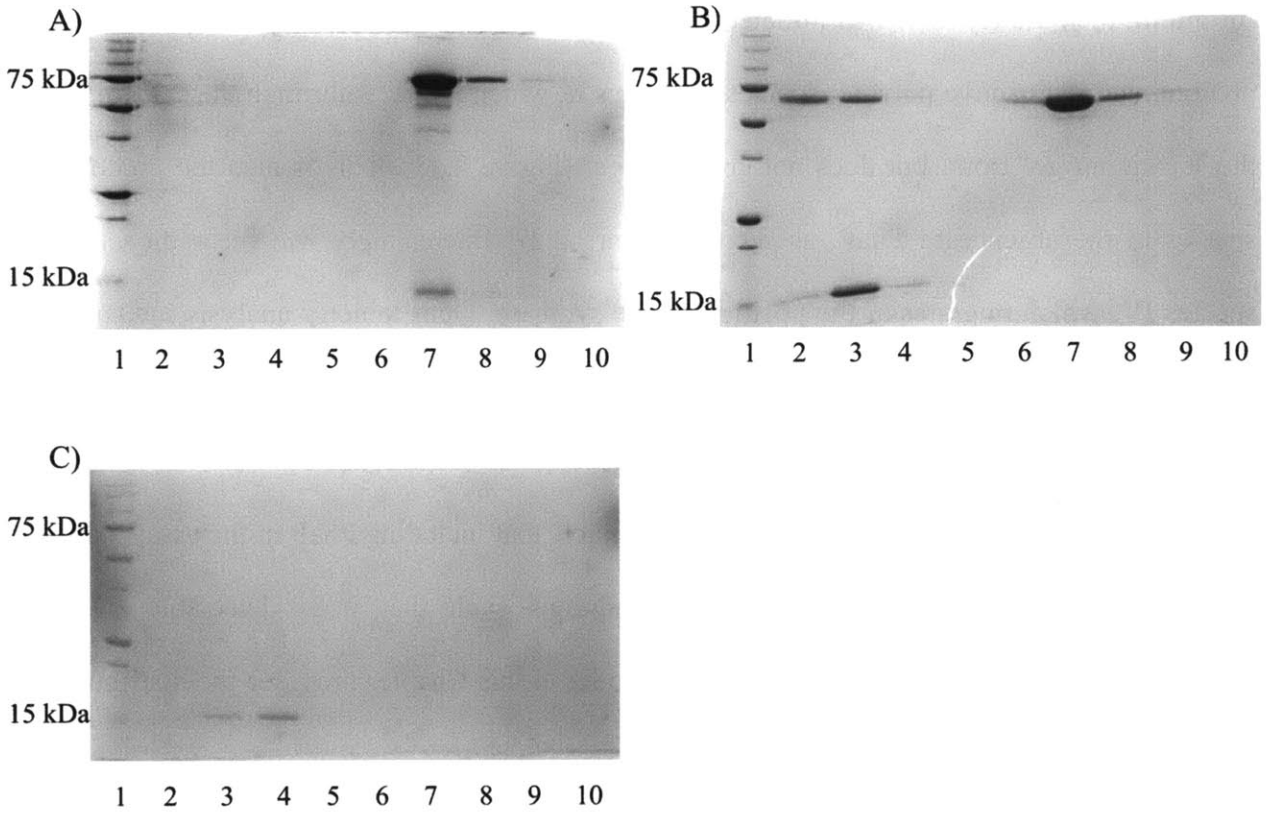

Figure 2.37 SDS-PAGE (15%) analysis of pull-down assay of PhaP with $PhaC_{Cc}$. A) Pull-down of PhaP with $PhaC_{Cc}$ (10 μM each). Lane 1, M_w markers. Lane 2, flowthrough. Lanes 3-6, 10 mM imidazole wash fractions. Lanes 7-10, 250 mM imidazole elution fractions. B) Pull-down of PhaP with $PhaC_{Cc}\Delta N$ (10 μM each). Lane 1, M_w markers. Lane 2, flowthrough. Lanes 3-6, 10 mM imidazole wash fractions. Lanes 7-10, 250 mM imidazole elution fractions. C) Control containing 10 μM PhaP. Lane 1, M_w markers. Lane 2, flowthrough. Lanes 3-6, 10 mM imidazole wash fractions. Lanes 7-10, 250 mM imidazole elution fractions.

2.3.19 Including PhaP in assays of $PhaC_{Cc}$ results in a small amount of [^{14}C]-HB_n associated with $PhaC_{Cc}$

Finally, we examined the effect of PhaP on the uniformity of loading of $PhaC_{Cc}$ by HBCoA using SDS-PAGE and autoradiography assay. PhaP and $PhaC_{Cc}$ were incubated at RT for 5 min, then the reaction was initiated by the addition of 20 or 200 μM [1-^{14}C]-HBCoA. The predominant radioactive polymer species is species II, which migrates through the stacking gel to the separating gel front, but does not enter the gel (Figure 2.38). This is also the predominant species in the absence of PhaP, as seen in Figure 2.27. Interestingly, we see radioactivity in species IV, which migrates at the position of the synthase. Densitometry analysis indicates that this species accounts for 3% of the total radioactivity in lane 2 (Figure 2.38). As demonstrated in experiments discussed above, this species is not observed in the absence of PhaP, but is observed when $PhaC_{Cc}$ is first primed with sTCoA. It is possible that including PhaP in the assay stabilizes this species sufficiently under the assay conditions such that it is detectable by SDS-PAGE/autoradiography. Figure A2.1 in the appendix to this Chapter provides the distribution of radioactive species in Figure 2.38.

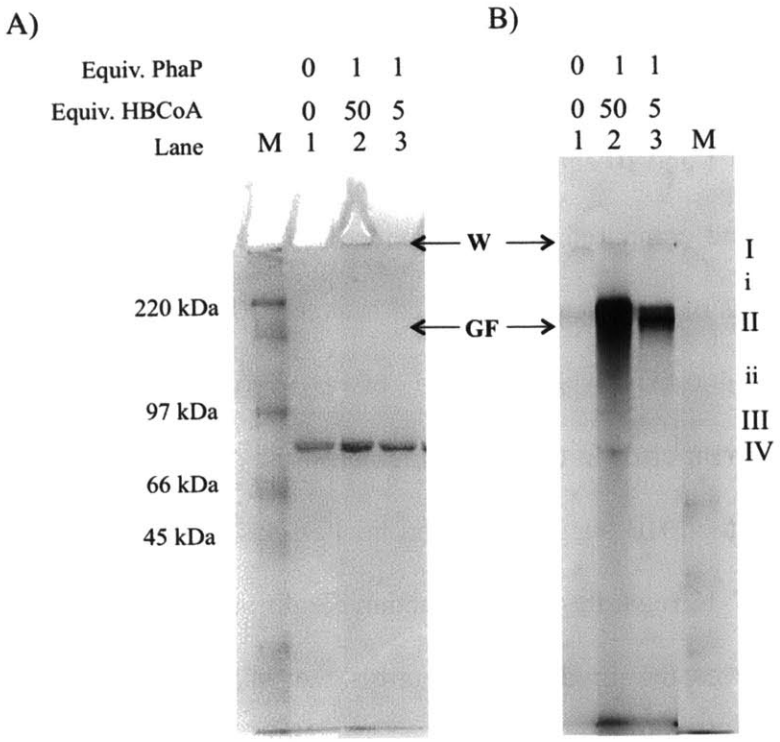

Figure 2.38 SDS-PAGE (10%) analysis of the polymerization of [1-^{14}C]-HBCoA by PhaC$_{Cc}$ in the presence of PhaP. A) Coomassie stained gel. M, molecular weight standards. Lanes 1-3 are as described for panel B. B) Autoradiography of gel in panel A. Lane 1, control reaction containing 3 μg of PhaC$_{Cc}$. Lane 2, PhaC$_{Cc}$ (3 μg) incubated with one equiv. PhaP for 1 min, then reacted with 50 equiv. of [1-^{14}C]-HBCoA (specific activity = 2 x 10^4 cpm/nmol). Lane 3, PhaC$_{Cc}$ (3 μg) incubated with one equivalent PhaP for 1 min, then reacted with 5 equiv. of [1-^{14}C]-HBCoA (specific activity = 2 x 10^5 cpm/nmol). M, molecular weight standards. Molecular weights were estimated using the standard curve in Figure 2.29C.

2.3.20 PhaP does not change the M_w of PHB produced by PhaC$_{Cc}$ *in vitro*

Analysis of the M_w and PDI of PHB produced by wt *R. eutropha* and the mutant strains Δ*phaP1* and Δ*phaR* (which overexpresses PhaP1) demonstrated that the PHB in both mutant strains has a lower M_w than in wt, and the PDI is higher in Δ*phaP1* (*19*). These results suggested that PhaP1 plays a role in triggering termination, and therefore in part dictates M_w and PDI of the polymer. Studies presented in Chapter 3 of this thesis suggest that the same is not true in *C. crescentus*: PHB extracted from the wt strain and the two mutant strains Δ*phaP* and Δ*phaR* has

nearly the same M_w and PDI. In order to confirm that PhaP does not affect the M_w and PDI of PHB produced by $PhaC_{Cc}$ *in vitro*, reactions were carried out in which $PhaC_{Cc}$ was reacted with 20,000 equiv. HBCoA in the presence of 1 and 10 equiv. PhaP. The resulting PHB was extracted into chloroform for analysis by GPC and compared to PHB produced in the absence of PhaP (Figure 2.39). The extraction efficiencies of these reactions varied between 90-95% and the M_w of the PHB produced was between 250-400 kDa, whereas the M_w of PHB produced when PhaP is omitted is ~660 kDa. Due to the inherent error in these measurements, the M_ws are likely the same or very similar. Again, the M_w of the PHB suggests that termination has occurred *in vitro*. Furthermore, the PDI remains between 7-12 regardless of the reaction conditions. Together these results suggest that PhaC alone catalyzes termination and controls the M_w and PDI of the polymer. It should be noted that the PDI values of PHB extracted from *C. crescentus* are typically ~2, considerably lower than the PDI of PHB produced *in vitro*. This difference could be due to the fact that measurements of *in vitro* produced PHB are made by collecting and analyzing fractions for radioactivity. The smaller the fraction, the more precise the measurements are, particularly at the beginning and end of a peak. However, for practical purposes, extremely small fractions were not collected. Alternatively, PHB produced *in vivo* could inherently have a lower PDI as a result of conditions *in vivo* that cannot be mimicked *in vitro*, such as the concentration of HBCoA, the presence of other protein factors, or perhaps even the quaternary structure of PhaC and PhaP on the surface of granules.

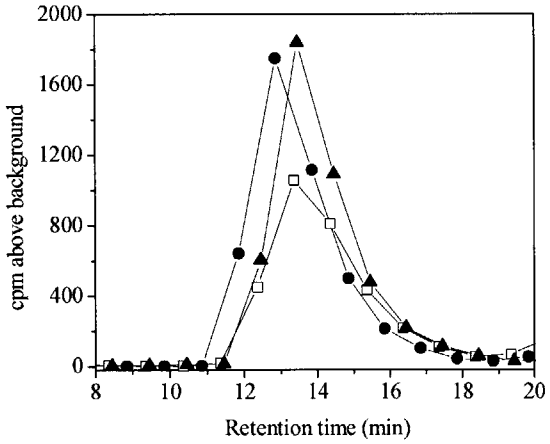

Figure 2.39 GPC trace of PHB extracted from reactions containing $PhaC_{Cc}$, PhaP and HBCoA. The reactions contained 50 nM $PhaC_{Cc}$, 1 mM HBCoA and 0 nM (●), 50 nM (□) or 500 nM PhaP (▲) and were carried out for 30 min at 30 °C.

2.4 Discussion

In this Chapter we demonstrate that full length $PhaC_{Cc}$ is 73 kDa and has an activity that is 50-fold higher than $PhaC_{Cc}\Delta N$. Kinetic studies on $PhaC_{Cc}$ revealed that it does not exhibit a lag phase in CoA release and is very soluble in comparison with the prototypical class I synthase $PhaC_{Re}$. We therefore pursued *in vitro* studies into the mechanism of polymerization in the hopes that it might provide new insight.

We first examined the priming process by acylation of $PhaC_{Cc}$ with sTCoA, which demonstrated that, in contrast to $PhaC_{Re}$ and $PhaEC_{Av}$, $PhaC_{Cc}$ generates one PHB chain per monomer. This observation initially led us to investigate whether the elongation process could be monitored with this synthase. However, as is the case with $PhaC_{Re}$ and $PhaEC_{Av}$, the rate of initiation with $PhaC_{Cc}$ is much slower than the rate of elongation, preventing us from studying the early steps in the elongation process. When $PhaC_{Cc}$ is incubated with 5 equiv. of HBCoA, high M_w PHB is produced and most of the $PhaC_{Cc}$ is unmodified. Thus, non-uniformity of loading appears to be a common feature of PHB synthases examined in detail to date (*6, 10*).

Affinity purification of a StrepII-tagged $PhaC_{Re}$ from an engineered mutant strain of *R. eutropha* revealed that a fraction of the total synthase *in vivo* is associated with high M_w PHB, while the rest is unmodified (*34*). This result suggests that the synthase *in vivo* is non-uniformly loaded as well, raising the possibility that non-uniform loading is an inherent and necessary feature of PhaCs. One possibility is that non-uniform loading ensures that high M_w polymer is synthesized *in vivo* regardless of the concentration of HBCoA. In both *R. eutropha* and *C. crescentus*, even when the cells contain very little PHB, the M_w of the PHB is high (*19*). This feature of PHB biosynthesis may be necessary to ensure that the PHB is properly packaged into granules or contained within granule precursors (discussed in Chapter 3), which may require that the PHB is full length. Our SDS-PAGE/autoradiography experiments investigating the products of the reactions of $PhaC_{Cc}$ and sT-$PhaC_{Cc}$ with [1-^{14}C]-HBCoA suggested that priming with sTCoA increases the uniformity of loading, such that 20% of the radioactivity was associated with smaller $(HB)_n$ species. However, the relevance of the artificial primers to the in vivo reaction is still unclear.

While we cannot study the mechanism of elongation due to the issue of non-uniform loading, we have studied the role of PhaP from *C. crescentus* in the physical process of elongation and granule assembly. Our results have led us to propose the model shown in Figure 2.40 for the involvement of PhaP in *in vitro* granule assembly. In this model, PhaP associates with $PhaC_{Cc}$ in the absence of HBCoA (species **1**). Next, HBCoA is added at a large excess over $PhaC_{Cc}$ and PHB synthesis begins. PhaP acts as a chaperone, interacting with the growing PHB chain as it emerges from the $PhaC_{Cc}$ active site (species **2**). As the polymer forms *in vitro*, if there is sufficient PhaP present, PhaP can also coat the growing granule (species **3**) to further prevent non-specific "sticking" of $PhaC_{Cc}$ to the hydrophobic surface, which could disrupt its

activity. In the absence of PhaP, we propose the growing PHB granule collapses onto $PhaC_{Cc}$, shown as species **3** in Figure 2.40B, hindering further turnover by blocking access of HBCoA to the active site. As more substrate is consumed, a phase or structural transition occurs, and granules may fuse as they grow larger (species **4**). $PhaC_{Cc}$ catalyzes termination and reinitiation *in vitro* in both the presence and absence of PhaP, and termination may occur via thiolysis at an oxoester of the PHB chain, rather than at the HB_n-PhaC thioester, leaving a primed synthase. The evidence for this model, presented in the following paragraphs, comes from experiments described in this Chapter and in Chapter 3, as well as what we and others have observed for *in vitro* reactions with $PhaC_{Re}$ and $PhaEC_{Av}$.

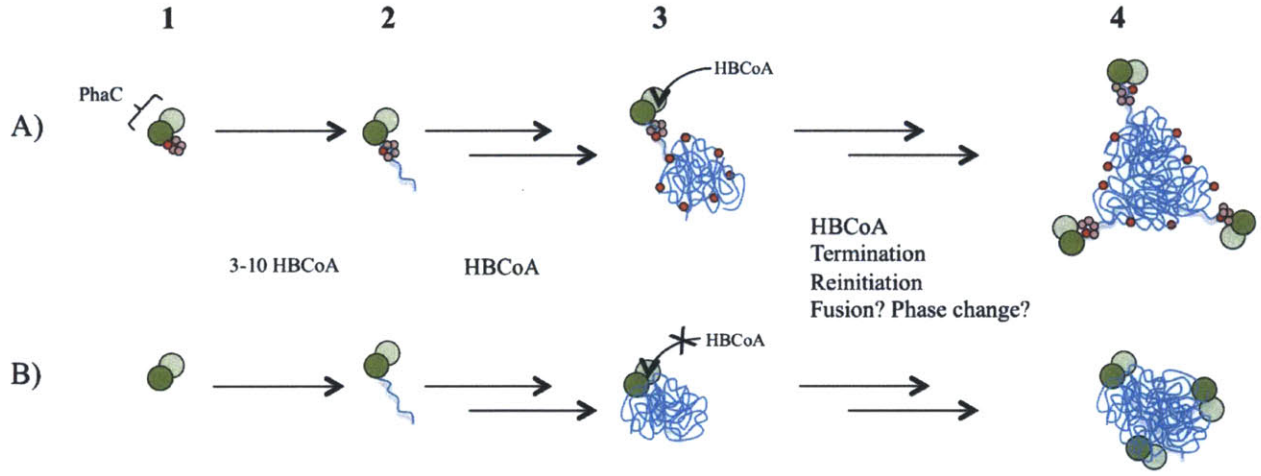

Figure 2.40 Working models for the role of PhaP in promoting *in vitro* granule assembly. A) Formation of granules in the presence of PhaP. Prior to addition of HBCoA, PhaC and PhaP interact in solution (species **1**). The stoichiometry of this interaction is not known, but because PhaP is thought to be a tetramer or pentamer at physiological concentrations, it is depicted as such. When HBCoA is added, PhaC starts to synthesize a PHB chain, and PhaP acts as a chaperone to facilitate the egress of the growing chain from the active site (species **2**). As more HBCoA is added to the growing polymer, excess PhaP in the assay mixture can associate with the surface of a nascent granule (species **3**). We propose that this species is ~170 HB units long, and still soluble. The association of PhaP allows access of HBCoA to the active site of PhaC. Finally, when the PHB reaches ~22 kDa in M_w a phase change occurs to produce the insoluble granule, which can potentially fuse with other granules in the assay mixture (species **4**). B) Formation of granules in the absence of PhaP. The main distinction between this model and the model in panel A is that when the polymer reaches a certain M_w, it collapses back onto PhaC (as shown in species 3), hindering further turnover.

The model begins with $PhaC_{Cc}$ and PhaP in the absence of HBCoA. SEC experiments suggest that $PhaC_{Cc}$ is a mixture of two oligomeric species at low concentrations. These species have M_w that are most consistent with a trimer of $PhaC_{Cc}$. However, SEC experiments examining the quaternary structure of $PhaC_{Cc}\Delta N$ demonstrated that the truncated synthase is a mixture of two species, with the major species having a M_w consistent with a dimer. Thus, we believe that $PhaC_{Cc}$ may be a dimer with an unusual shape that could come from the N-terminal domain. This domain likely has an extended or unusual structure due to the presence of a proline rich region, including six consecutive Pro residues that are immediately followed by the sequence PPFPPF. Unfortunately, attempts to model this domain using secondary structure prediction software provided no structural insight. Because material is lost during our SEC experiments, additional experiments are required to fully understand the quaternary structure of $PhaC_{Cc}$, including for example analytical ultracentrifugation studies. Regardless of its quaternary structure, our studies of the acylation of $PhaC_{Cc}$ with sTCoA suggest that a dimer of synthases makes two PHB chains. For clarity, only a single chain is depicted in Figure 2.40. We furthermore propose that in the absence of HBCoA, PhaP associates with $PhaC_{Cc}$. This proposal is based on pull-down assays, which demonstrated this association *in vitro*. It should be noted that we do not have evidence for the stoichiometry of the interaction depicted in Figure 2.40; however, based on SEC of PhaP, at the concentrations used in our pull-down assays, PhaP is a tetramer or pentamer.

Our model next depicts an early stage in the polymerization process, after a short PHB chain of 3-10 units has been synthesized. PhaP associates with this chain, facilitating its egress from the active site of $PhaC_{Cc}$. We predict that this species is an intermediate in polymerization based on a variety of experiments. First, SDS-PAGE/autoradiography experiments of $PhaC_{Cc}$ primed with sTCoA then reacted with [1-^{14}C]-HBCoA reveal a [^{14}C]-HB_n species migrating at

the position of $PhaC_{Cc}$. Because the association of [^{14}C]-HB_n does not alter the apparent migration properties of $PhaC_{Cc}$ in the SDS gel, n is likely small. In similar experiments carried out with the mutant enzyme D302A-$PhaEC_{Av}$, [^{14}C]-HB_n species observed by SDS-PAGE/autoradiography with migratory properties similar to those observed in the experiments in the present work were analyzed by trypsin digest of the enzyme followed by ESI-MS (*26*). These experiments revealed peptides containing C149 that had been modified with $(HB)_n$, where n =3-10. It is by analogy to these experiments that we propose that $(HB)_{3-10}$-$PhaC_{Cc}$ is an intermediate in polymerization. This species was not observed without priming of $PhaC_{Cc}$ with sTCoA prior to incubation with [1-^{14}C]-HBCoA, which could be due to the fact that under these experimental conditions, most of the substrate is converted into large polymer due to the rapid elongation process. Alternatively, [^{14}C]-HB_{3-10}-$PhaC_{Cc}$ species may be present only in very small amounts and therefore not detectable due to the specific activity of the [1-^{14}C]-HBCoA. Interestingly, inclusion of PhaP in the assay mixture results in an increase in the amount of the $(HB)_{3-10}$-$PhaC_{Cc}$ species, which may suggest that interaction of PhaP with this species stabilizes it sufficiently to hydrolysis to allow its accumulation and thus detection by SDS-PAGE.

Evidence that PhaP interacts with the growing PHB chain comes from assays carried out with $PhaC_{Cc}$ and $PhaC_{Cc}\Delta N$. Including PhaP in the assay mixture increases the extent of HBCoA turnover catalyzed by both synthases. The significance of this observation will be addressed further below. Pull-down assays indicate, however, that under our reaction conditions, $PhaC_{Cc}\Delta N$ and PhaP do not interact, whereas $PhaC_{Cc}$ and PhaP do. This could mean either that the N-terminal domain of $PhaC_{Cc}$ mediates this interaction, or that the K_D of the interaction between PhaP and $PhaC_{Cc}\Delta N$ is higher than that of $PhaC_{Cc}$. Thus, the effect mediated by including PhaP in the assay mixtures of both synthases is likely due to interaction of PhaP with

the PHB chain rather than with the synthase. The proposal that PhaPs carry out their various roles in polymerization via interaction with the PHB chain rather than with the synthase is also consistent with observations made with PhaP1 from *R. eutropha*. In wt *R. eutropha*, a ratio of 1-2 PHB chains per PhaP1 *in vivo* is maintained throughout cell growth and PHB accumulation (*19, 39*) (He and Stubbe, unpublished data). When $phaC_{Re}$ is replaced with $phaEC_{Av}$ in an engineered mutant strain of *R. eutropha*, the same molecular ratio is maintained (*19*), indicating that the ratio is not "synthase-specific" and suggesting that it is maintained by an interaction between PHB and PhaP1. Furthermore, pull-down assays between PhaP1 and $PhaC_{Re}$ indicate that the two proteins do not interact in solution, yet including PhaP1 in assays of $PhaC_{Re}$ increases the length of the lag phase, decreases the specific activity of the synthase, and alters the structure of the resulting polymer (judged based on its migratory properties through an SDS-agarose gel matrix) (*19*). Though the effects on the activities of $PhaC_{Re}$ and $PhaC_{Cc}$ are opposite with their respective phasins, in both cases the phasins appear to exert their effects via interaction with the PHB.

As polymerization continues in our model, the PHB chain begins to fold over on itself, forming a small amorphous granule. We propose that an additional intermediate in the polymerization process is HB_n-PhaC where n = ~170. This species was also observed by SDS-PAGE/autoradiography experiments examining the reaction of sT-$PhaC_{Cc}$ with [1-^{14}C]-HBCoA (Figure 2.29). Its identity was inferred based on the fact that a [^{14}C]-HB-containing species was observed to migrate slower than unmodified $PhaC_{Cc}$ with a predicted M_w of ~14 kDa larger than $PhaC_{Cc}$, which would correspond to $PhaC_{Cc}$ modified with ~170 HB units. A few things are interesting about this observation. The first is that this species migrates into the separating gel rather than precipitating at the top of the gel, suggesting that it is sufficiently soluble to migrate through SDS-PAGE, though, as noted above, we do not fully understand how various HB_n

species migrate in SDS-PAGE. GPC analysis of the M_w of the PHB formed from the reaction of unprimed $PhaC_{Cc}$ with [1-^{14}C]-HBCoA that does not enter the separating gel but precipitates at the top reveals that it is ~22 kDa. Together, these results suggest that within the 14 kDa and 22 kDa range in M_ws, the PHB undergoes some sort of structural and/or phase change that prevents it from migrating into the SDS-PAGE separating gel. The observation of the HB_{170}-$PhaC_{Cc}$ species is also interesting because when C149S-$PhaEC_{Av}$ is reacted with HBCoA and analyzed by ESI-MS, similar species including HB_{75}-C149S-PhaC, HB_{105}-C149S-PhaC and HB_{238}-C149S-PhaC have been observed (Li and Stubbe, unpublished data). Thus similar intermediates are observed with these two enzymes, suggesting that some feature of its structure facilitates its detection by our methods of analysis.

Our model proposes that PhaP associates with this species to package it in such a way as to prevent it from collapsing onto $PhaC_{Cc}$ and hindering access of HBCoA and thus further turnover. As briefly mentioned above, when HBCoA is present at a sufficiently high concentration (0.75-1 mM) in our assays, the rate of the reaction slows as the substrate is turned over, and appears to stop before complete substrate consumption. This effect can be alleviated by reducing the concentration of HBCoA, which facilitates complete turnover of substrate. This result suggests that the decrease in turnover is due to accumulation of PHB in the assay mixture rather than the concentration of HBCoA falling below its K_m as is it consumed. The slowing of turnover can also be alleviated by including PhaP, suggesting that PhaP associates with the forming PHB granules to prevent non-specific aggregation that hinders turnover. The species that form in the presence and absence of PhaP are illustrated as species **3** in Figure 2.40A and B. This feature of our model is similar to the model proposed by Niamsiri and coworkers, who studied the role of BSA in promoting the formation of PHB granules by $PhaC_{Re}$ that was

immobilized to a gold surface (*37*). They convincingly demonstrated by AFM that BSA promotes the formation of larger granules and more complete substrate consumption than occurs in its absence. Niamsiri *et al.* furthermore presented fluorescence confocal microscopy images, which they interpret as demonstrating that BSA is found throughout the granule, rather than just on its surface (*37*). Unfortunately, from the images provided, it is difficult to critically evaluate the data, and we have no evidence that PhaP is found inside the granule rather than just on its surface. In fact, our electron microscopy studies using immunogold labeling of antibodies to PhaP1 suggest that it is only on the surface of granules in *R. eutropha* (*1, 2*).

The role of PhaP in preventing granule collapse to maintain the activity of $PhaC_{Cc}$ and access of HBCoA to the active site is consistent with observations we have made *in vivo* as well, as described in Chapter 3. Our *in vivo* studies demonstrate that the Δ*phaP* mutant strain of *C. crescentus* only accumulates PHB to ~1% of its cdw, whereas the wt strain accumulates PHB to ~12% of its cdw. Analysis of the activity of $PhaC_{Cc}$ in crude cell extracts of wt and Δ*phaP* demonstrates that in the wt strain, $PhaC_{Cc}$ has higher activity and catalyzes more extensive turnover of exogenous HBCoA than $PhaC_{Cc}$ in Δ*phaP*. Furthermore, in Δ*phaP* the expression levels of $PhaC_{Cc}$ decrease as a function of growth time. We have interpreted these results to suggest that in the absence of PhaP *in vivo*, the PHB aggregates in such a way as to hinder further turnover, and that $PhaC_{Cc}$ may be degraded as a result of unfolding or precipitating on the exposed surface of the hydrophobic granule. Thus, we have observed PhaP playing a similar function in promoting granule assembly both *in vivo* and *in vitro*.

We finally propose in our model that $PhaC_{Cc}$ catalyzes termination, and unexpected results with the artificial primer sTCoA suggest that termination might occur by thiolysis to leave a primed synthase. It has been previously demonstrated that synthases are capable of catalyzing

termination (*11, 40*). Our GPC experiments examining the M_w of PHB produced by $PhaC_{Cc}$ demonstrate that the M_w is lower than would be expected assuming each PhaC makes one PHB chain. This result suggests that termination and reinitiation of polymerization are occurring in the presence of just $PhaC_{Cc}$ and HBCoA. The working model for termination is that the synthase either activates a water molecule for hydrolysis of the PHB chain, or that a nucleophilic amino acid residue on PhaC first attacks the chain to catalyze transfer from the active site Cys, followed by rapid hydrolysis (*11*). In both cases, the enzyme is proposed to terminate the chain at 3-10 HB units removed from the Cys residue, leaving a primed synthase.

In the present studies, we unexpectedly found that when $PhaC_{Cc}$ is incubated with sTCoA, it catalyzes side reactions in addition to the expected acylation reaction. The major side reaction is the formation of sDCoA, which we propose happens by the thiolysis mechanism shown in Scheme 2.1, in which CoA from the most recently added HB unit reattacks at an internal oxoester. sDCoA forms at a rate of 1 min^{-1}, whereas the rate of polymerization is ~5,000 min^{-1}. Given the differences in these rates, one would expect that if the rate of thiolysis is in fact indicative of termination, then the typical PHB chain length would be ~5,000 HB units long. Consistent with this expectation, both *in vitro* and *in vivo*, we see PHB that is 3,000-6,000 HB units long. Thus, a mechanism for controlling chain termination might be the relative rates of polymerization versus thiolysis by CoA.

It is becoming clear from our studies that synthases catalyze unusual chemistry in addition to the chemistry of polymerization. As described in the introduction, incubation of wt $PhaC_{Re}$ and $PhaEC_{Av}$ with sTCoA followed by addition of the chain terminator $HBCH_2CoA$ results in the formation of a major product that is one HB unit shorter than the product predicted by the mechanisms in Figure 2.1 (Li and Stubbe, unpublished data). Because these and the

present observations have been made with artificial primers, it is not yet clear whether they are relevant to the normal reaction pathway. However, the fact that $PhaC_{Cc}$ is capable of catalyzing thiolysis to leave PhaC primed with an HB unit is attractive in terms of our working model for termination. We have also re-examined the reaction of $PhaEC_{Av}$ with sTCoA and found that this reaction also results in the formation of a small amount of sDCoA (Figure A2.2, in the Appendix to this Chapter), suggesting that this chemistry might be general to synthases. Therefore, we propose a modification to the model for termination that PhaCs catalyze chain termination by thiolysis using CoA, leaving a primed synthase that is ready to synthesize the next PHB chain.

The results presented in this Chapter demonstrate that some of the peculiarities that make PHB synthases difficult to study, such as the issue of non-uniform loading, are likely general features of PHB synthases. However, in our studies of the new class I synthase from $PhaC_{Cc}$, we have gained insight into the role of PhaP in promoting granule assembly, as well as into a possible mechanism for termination by thiolysis. The issue of initiation of PHB formation remains unresolved, largely because of the challenge of non-uniform loading. Recent studies suggest that PhaC from *Aeromonas caviae* may be useful for examining the mechanism of priming, as this synthase appears to uniformly load when incubated with just a few equiv. of HBCoA (*12*). However a more thorough and careful examination of this synthase than what has thus far been carried out is necessary. In summary, PhaCs are difficult to study mechanistically due to the issues described in this Chapter, and ultimately our understanding of PHB polymerization may come from studies carried out on synthases isolated from a variety of sources. The studies presented in this Chapter add a few more insights into the puzzle of PHB biosynthesis.

2.5 Acknowledgement

We thank Ping Li for synthesizing HBCoA and sTCoA, and Ping Li, Mimi Cho and Phil Snyder for helpful discussions.

2.6 Appendix

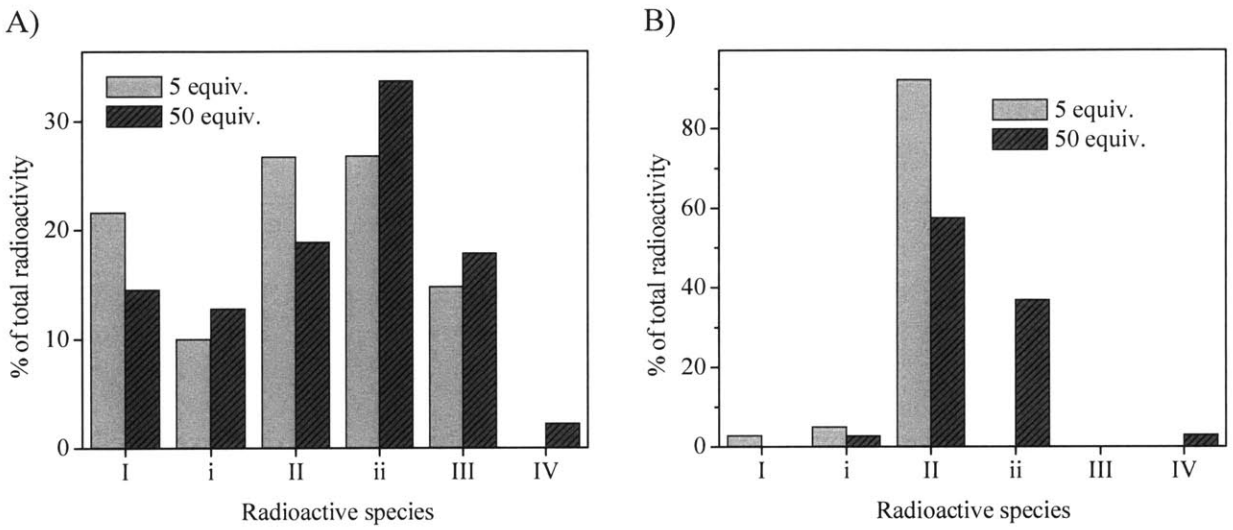

Figure A2.1 Distribution of radioactivity in species observed by SDS-PAGE/autoradiography analysis of $PhaC_{Cc}$ reacted with [1-^{14}C]-HBCoA. Analysis was performed using ImageJ Software (*30*). A) Distribution of radioactivity from Figure 2.29B. B) Distribution of radioactivity from Figure 2.38B.

Table A2.1 Inventory of radioactivity.

	Initial radioactivity		Radioactivity after extraction into chloroform			Radioactivity analyzed by GPC	
Reaction	Total cpm (*R/S*)	Total cpm (*R*)	cpm in washes[a]	cpm extracted	% extraction (*R*)[b]	cpm injected onto column	cpm recovered from column (%)
1	13,700	6,850	2,480	11,600	100[c]	5,800	5,480 (95)
2	2,850[d]	--	120	2,110	78	1050	920 (88)
3	35,000	17,500	7,300	24,700	100[c]	4,950	5,000 (100[c])
4	35,000	17,500	4,400	29,200	100[c]	11,700	10,200 (87)
5	13,700	6,850	2,400	6,100	90	2,440	2,590 (100[c])

[a]wash fractions were collected from the material that remained associated with the tube in which samples were refluxed

[b]the % extraction is determined on the basis of the total nmol of [1-^{14}C]-(*R*)-HBCoA extracted into chloroform; in reactions 1 and 3, in which the cpm extracted is greater than the total cpm of [1-^{14}C]-(*R*)-HBCoA in the reaction, the assumption is made that 100% of the [1-^{14}C]-(*R*)-HBCoA was extracted in addition to some portion of the [1-^{14}C]-(*S*)-HBCoA.

[c]in some cases, recoveries were >100%, which is likely due to error associated with the difficulties of pipetting exact amounts of chloroform

[d]the *R/S* distinction does not apply to [^{3}H]-sTCoA

Table A2.2 Distribution of extracted radioactivity between polymer and small molecules.

	Distribution of extracted radioactivity		
Reaction[a]	Total cpm extracted	cpm in PHB (% of total)	cpm in small molecules (% of total)
1	11,600	12,600 (100[b])	0 (0)
2	2,110	210 (10)	1,900 (90)
3	24,700	21,600 (87)	3,100 (13)
4	29,200	25,100 (85)	4,500 (15)
5	6,100	6,420 (100[b])	0 (0)

[a]the reaction numbering used is the same as in Table 2.8

[b]in some cases, recoveries were >100%, which is likely due to error associated with the difficulties of pipetting exact amounts of chloroform

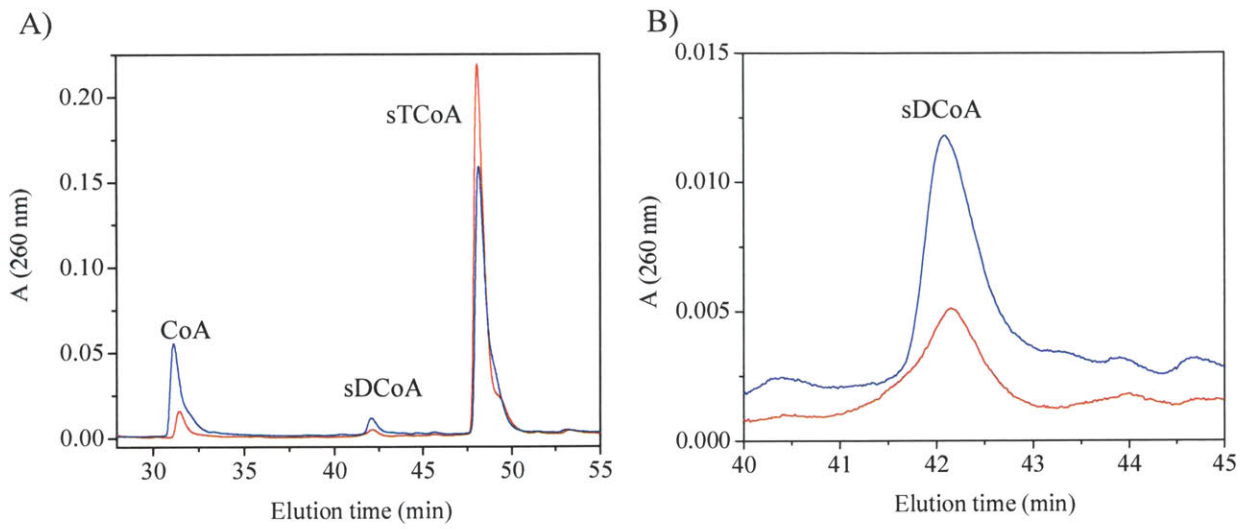

Figure A2.2 Small molecule products of the reaction of $PhaEC_{Av}$ and sTCoA. The reaction contained 50 μM $PhaEC_{Av}$ and 500 μM sTCoA, and was carried out for 10 min (red) and 60 min (blue) at 30 ˚C. The samples were worked up as described in section 2.3.12. A) A_{260} trace, showing a peak at 31 min (also observed in the reaction with sTCoA and $PhaC_{Cc}$), the increase in the peak at 43 min (sDCoA) and a decrease in the peak at 47 min (sTCoA). B) Expansion of the region around the peak corresponding to sDCoA.

2.7 References

1. Stubbe, J., Tian, J. (2003) Polyhydroxyalkanoate (PHA) homeostasis: the role of the PHA synthase, *Nat. Prod. Rep. 20*, 445-457.

2. Stubbe, J., Tian, J., He, A., Sinskey, A.J., Lawrence, A.G., Liu, P. (2005) Nontemplate-dependent polymerization processes: Polyhydroxyalkanoate synthases as a paradigm, *Annu. Rev. Biochem. 74*, 433-480.

3. Wodzinska, J., Snell, K. D., Rhomberg, A., Sinskey, A. J., Biemann, K., and Stubbe, J. (1996) Polyhydroxybutyrate synthase: evidence for covalent catalysis, *J. Amer. Chem. Soc. 118*, 6319-6320.

4. Jia, Y., Yuan, W., Wodzinska, J., Park, J., Sinskey, A.J., Stubbe, J. (2001) Mechanistic studies on class I polyhydroxybutyrate (PHB) synthase from *Ralstonia eutropha*: class I and III synthases share a similar catalytic mechanism., *Biochemistry 40*, 1011-1019.

5. Jia, Y., Kappock, T. J., Frick, T., Sinskey, A. J., and Stubbe, J. (2000) Lipases provide a new mechanistic model for polyhydroxybutyrate (PHB) synthases: characterization of the functional residues in *Chromatium vinosum* PHB synthase, *Biochemistry 39*, 3927-3936.

6. Gerngross, T. U., Snell, K. D., Peoples, O. P., Sinskey, A. J., Csuhai, E., Masamune, S., and Stubbe, J. (1994) Overexpression and purification of the soluble polyhydroxyalkanoate synthase from *Alcaligenes eutrophus*: evidence for a required posttranslational modification for catalytic activity, *Biochemistry 33*, 9311-9320.

7. Smith, S. (1994) The animal fatty acid synthase: one gene, one polypeptide, seven enzymes, *FASEB J. 8*, 1248-1259.

8. Austin, M. B., and Noel, J. P. (2003) The chalcone synthase superfamily of type III polyketide synthases, *Nat. Prod. Rep. 20*, 79-110.

9. Smythe, C., and Cohen, P. (1991) The discovery of glycogenin and the priming mechanism for glycogen biogenesis, *Eur. J. Biochem. 200*, 625-631.

10. Tian, J. (2005) Mechanistic investigation of polyhydroxybutyrate (PHB) synthases and elucidation of PHB biosynthesis and degradation process in *Wautersia eutropha* H16, in *Chemistry*, p 345, Massachusetts Institute of Technology, Cambridge.

11. Tian, J., Sinskey, A. J., and Stubbe, J. (2005) Class III polyhydroxybutyrate synthase: involvement in chain termination and reinitiation, *Biochemistry 44*, 8369-8377.

12. Numata, K., Motoda, Y., Watanabe, S., Tochio, N., Kigawa, T., and Doi, Y. (2012) Active intermediates of polyhydroxyalkanoate synthase from *Aeromonas caviae* in polymerization reaction, *Biomacromolecules 13*, 3450-3455.

13. Yamanaka, K., Kimura, Y., Aoki, T., and Kudo, T. (2009) End-group analysis of bacterially produced poly(3-hydroxybutyrate): discovery of succinate as the polymerization starter, *Macromolecules 42*, 4038-4046.

14. Li, P., Chakraborty, S., and Stubbe, J. (2009) Detection of covalent and noncovalent intermediates in the polymerization reaction catalyzed by a C149S class III polyhydroxybutyrate synthase, *Biochemistry 48*, 9202-9211.

15. Neumann, L., Spinozzi, F., Sinibaldi, R., Rustichelli, F., Potter, M., and Steinbüchel, A. (2008) Binding of the major phasin, PhaP1, from *Ralstonia eutropha* H16 to poly(3-hydroxybutyrate) granules, *J. Bacteriol. 190*, 2911-2919.

16. Wieczorek, R., Pries, A., Steinbüchel, A., and Mayer, F. (1995) Analysis of a 24-kilodalton protein associated with the polyhydroxyalkanoic acid granules in *Alcaligenes eutrophus*, *J. Bacteriol. 177*, 2425-2435.

17. York, G. M., Stubbe, J., and Sinskey, A. J. (2001) New insight into the role of the PhaP phasin of *Ralstonia eutropha* in promoting synthesis of polyhydroxybutyrate, *J. Bacteriol. 183*, 2394-2397.

18. Jossek, R., Reichelt, R., and Steinbüchel, A. (1998) In vitro biosynthesis of poly(3-hydroxybutyric acid) by using purified poly(hydroxyalkanoic acid) synthase of *Chromatium vinosum*, *Appl. Microbiol. Biotechnol. 49*, 258-266.

19. Cho, M. (2012) Studies on the mechanism of polyhydroxybutyrate (PHB) granule formation in *Ralstonia eutropha* H16, in *Chemistry*, p 346, Massachusetts Institute of Technology, Cambridge.

20. Kawaguchi, Y., and Doi, Y. (1992) Kinetics and mechanism of synthesis and degradation of poly(3-hydroxybutyrate) in *Alcaligenes eutrophus*, *Macromolecules 25*, 2324-2329.

21. Madden, L. A., Anderson, A. J., Shah, D. T., and Asrar, J. (1999) Chain termination in polyhydroxyalkanoate synthesis: involvement of exogenous hydroxy-compounds as chain transfer agents, *Int. J. Biol. Macromol. 25*, 43-53.

22. Kurja, J., Zirkzee, H. F., de Koning, G. M., and Maxwell, I. A. (1995) A new kinetic model for the accumulation of poly(3-hydroxybutyrate) in *Alcaligenes eutrophus*, 1. Granule growth, *Macromol. Theory Simul. 4*, 839-855.

23. Kusaka, S., Abe, H., Lee, S. Y., and Doi, Y. (1997) Molecular mass of poly[(R)-3-hydroxybutyric acid] produced in a recombinant *Escherichia coli*, *Appl. Microbiol. Biotechnol. 47*, 140-143.

24. Shi, F. Y., Ashby, R., and Gross, R. A. (1996) Use of poly(ethylene glycol)s to regulate poly(3-hydroxybutyrate) molecular weight during *Alcaligenes eutrophus* cultivations, *Macromol. 29*, 7753-7758.

25. Lawrence, A. G., Choi, J., Rha, C., Stubbe, J., and Sinskey, A. J. (2005) In vitro analysis of the chain termination reaction in the synthesis of poly-(R)-beta-hydroxybutyrate by the class III synthase from *Allochromatium vinosum*, *Biomacromolecules 6*, 2113-2119.

26. Tian, J., Sinskey, A. J., and Stubbe, J. (2005) Detection of intermediates from the polymerization reaction catalyzed by a D302A mutant of class III polyhydroxyalkanoate (PHA) synthase, *Biochemistry 44*, 1495-1503.

27. Yuan, W., Jia, Y., Tian, J., Snell, K. D., Muh, U., Sinskey, A. J., Lambalot, R. H., Walsh, C. T., and Stubbe, J. (2001) Class I and III polyhydroxyalkanoate synthases from *Ralstonia eutropha* and *Allochromatium vinosum*: characterization and substrate specificity studies, *Arch. Biochem. Biophys. 394*, 87-98.

28. Bradford, M. M. (1976) Rapid and sensitive method for quantitation of microgram quantities of protein utilizing principle of protein-dye binding, *Anal. Biochem. 72*, 248-254.

29. Heckman, K. L., and Pease, L. R. (2007) Gene splicing and mutagenesis by PCR-driven overlap extension, *Nat. Protoc. 2*, 924-932.

30. Schneider, C. A., Rasband, W. S., and Eliceiri, K. W. (2012) NIH Image to ImageJ: 25 years of image analysis, *Nature Methods 9*, 671-675.

31. Qi, Q., and Rehm, B.A. . (2001) Polyhydroxybutyrate biosynthesis in *Caulobacter crescentus*: molecular characterization of thc polyhydroxybutyrate synthase., *Microbiology 147*, 3353-3358.

32. Müh, U., Sinskey, A.J., Kirby, D.P., Lane, W.S., Stubbe, J. (1999) PHA Synthase from *Chromatium vinosum*: cysteine 149 is Involved in covalent catalysis, *Biochemistry 38*, 826-837.

33. Bracher, P. J., Snyder, P. W., Bohall, B. R., and Whitesides, G. M. (2011) The relative rates of thiol-thioester exchange and hydrolysis for alkyl and aryl thioalkanoates in water, *Orig. Life Evol. Biosph. 41*, 399-412.

34. Cho, M., Brigham, C. J., Sinskey, A. J., and Stubbe, J. (2012) Purification of polyhydroxybutyrate synthase from its native organism, *Ralstonia eutropha*: implications for the initiation and elongation of polymer formation in vivo, *Biochemistry 51*, 2276-2288.

35. Dennis, D., Sein, V., Martinez, E., and Augustine, B. (2008) PhaP is involved in the formation of a network on the surface of polyhydroxyalkanoate inclusions in *Cupriavidus necator* H16, *J. Bacteriol. 190*, 555-563.

36. Horowitz, D. M., and Sanders, J. K. M. (1995) Biomimetic, amorphous granules of polyhydroxybutyrate: composition, mobility, and stabilization *in vitro* by proteins. , *Can. J. Microbiol. 41*, 115-123.

37. Niamsiri, N., Bergkvist, M., Delamarre, S. C., Cady, N. C., Coates, G. W., Ober, C. K., and Batt, C. A. (2007) Insight in the role of bovine serum albumin for promoting the in situ surface growth of polyhydroxybutyrate (PHB) on patterned surfaces via enzymatic surface-initiated polymerization, *Colloids Surf B Biointerfaces 60*, 68-79.

38. Jossek, R., Reichelt, R., and Steinbüchel, A. (1998) In vitro biosynthesis of poly(3-hydroxybutyric acid) by using purified poly(hydroxyalkanoic acid) synthase of *Chromatium vinosum*, *Appl. Microbiol. and Biotechnol. 49*, 258-266.

39. Tian, J., He, A., Lawrence, A. G., Liu, P., Watson, N., Sinskey, A. J., and Stubbe, J. (2005) Analysis of transient polyhydroxybutyrate production in *Wautersia eutropha* H16 by quantitative Western analysis and transmission electron microscopy, *J. Bacteriol. 187*, 3825-3832.

40. Gerngross, T. U., and Martin, D. P. (1995) Enzyme-catalyzed synthesis of poly[(R)-(-)-3-hydroxybutyrate]: formation of macroscopic granules in vitro, *Proc. Natl. Acad. Sci. 92*, 6279-6283.

Chapter 3:

The role of PhaP in promoting PHB accumulation in *Caulobacter crescentus* in nitrogen-limited medium

3 The role of PhaP in promoting PHB accumulation in *Caulobacter crescentus* in nitrogen-limited medium

3.1 Introduction

In Chapter 2, we reported the isolation and characterization of PhaC from *Caulobacter crescentus* ($PhaC_{Cc}$) as well as its phasin, PhaP. *In vitro* assays revealed that the kinetics of $PhaC_{Cc}$ are biphasic and have an initial burst phase followed by a slower phase. Under certain reaction conditions, the inclusion of PhaP can increase the length of the burst phase and increase the total consumption of substrate from ~70% (in the absence of PhaP) to 100%. The observation that PhaP increases the extent of HBCoA turnover *in vitro* suggests that it may play a key role in PHB biosynthesis *in vivo* as well. The goal of the current work was to investigate the role of PhaP in PHB biosynthesis in *C. crescentus*. To that end, growth conditions that promote PHB accumulation have been developed and PhaP expression levels under these conditions measured as a function of PHB accumulation. The effect of deletion of *phaP* on the PHB content of cells, the molecular weight (M_w) and polydispersity (PDI) of the PHB, and the granule size and shape has been examined. The role of a putative regulator of PhaP expression, PhaR, is also investigated.

Phasins are the major PHA-granule associated proteins. They share little sequence similarity, but have the general features that they are typically small (13-25 kDa), amphiphilic proteins that are associated with the PHA granule surface and can constitute a high fraction of the total cellular protein during PHA accumulation (*1*). Phasins can be identified in sequence searches by the phasin2 motif, which is not a particular amino acid sequence but instead a region enriched in hydrophobic residues. Phasins are thought to play an important role in PHA granule biogenesis, yet only the role of PhaP1 from *R. eutropha* has been thoroughly studied. When

limited in nitrogen but with an abundance of fructose available (referred to as PHB_{high} growth conditions), *R. eutropha* accumulates PHB up to 80% of its cell dry weight (cdw). Under these conditions PhaP1 constitutes up to 5% of the total protein content of the cell (*2, 3*). PhaP1 expression is strictly correlated with PHB accumulation and the ratio of PHB chains to PhaP is 1-2 throughout growth. Its deletion results in accumulation of only 40% PHB cdw, and that PHB is packaged in a single irregularly shaped granule, as opposed to the 5-15 spherical granules accumulated in the wt strain (*3-6*). PhaP is also thought to dictate polymer termination and thereby its M_w and PDI. If PhaP is absent or if it is overexpressed during PHB accumulation the polymer M_w is lower, suggesting uncontrolled termination. The PDI also increases in the absence of PhaP (*7*).

Dozens of organisms have putative transcriptional regulators of phasin expression, collectively referred to as PhaRs. The functional assignments are made primarily based upon i) homology to known PhaRs, such as that from *R. eutropha*, ii) association with PHB granules, and iii) their locations within the genome relative to other PHB biosynthetic genes. The role of PhaR in PHB biosynthesis has been convincingly demonstrated in *R. eutropha* and to a lesser extent in *Paracoccus denitrificans (5, 8, 9)*. In *R. eutropha*, deletion of *phaR* results in a strain that constitutively overexpresses PhaP1 and accumulates PHB in more and smaller granules than the wt strain (*5, 8*). This result, in combination with the results from deletion of *phaP1*, suggests that PhaP1 determines the size and number of PHB granules in *R. eutropha*. PhaR homologs in some α-proteobacteria (a group that includes *C. crescentus*) such as *Rhizobium etli* and *Sinorhizobium meliloti* contain a PhaR homolog called AniA. Studies have suggested that AniA plays a role in regulation of the expression of many genes involved in directing carbon flux through various biosynthetic pathways, including PHB biosynthesis (*10, 11*). *Pseudomonas*

oleovorans expresses PhaF, which is a granule-associated protein thought to be involved in regulation of the PHA synthase PhaC1 and PhaI, a phasin-type protein (*12, 13*). Thus, regulation of PHB accumulation appears to vary by organism (*14*).

A great deal has been learned from studying the role of PhaP1 in PHB accumulation in *R. eutropha* and its regulation by PhaR. However, the generality of these functions in PHB accumulating organisms has not been thoroughly studied. Furthermore, when an essential nutrient (nitrogen, phosphate, O_2, etc.) is limiting, *R. eutropha* accumulates PHB to ~80% cdw, which is likely much higher than the levels to which it is accumulated in the "natural" environment. We have investigated PHB accumulation in *C. crescentus* in nitrogen-limited conditions to determine if the roles of PhaP1 and PhaR in *R. eutropha* are general to PHB accumulating organisms. *C. crescentus* has long been known to accumulate PHB (*15*), but the first characterization of its accumulation as a function of growth was not reported until 2001 (*16*). In that study, Qi and Rehm grew *C. crescentus* in rich medium lacking Ca^{2+} and supplemented with 1% glucose. Under these conditions, *C. crescentus* accumulated PHB to ~18% of its cdw. They showed that antibodies to $PhaC_{Re}$ cross-reacted with PhaC from *C. crescentus* ($PhaC_{Cc}$), and in Western blots using these antibodies $PhaC_{Cc}$ appeared to be 73 kDa, 8 kDa larger than $PhaC_{Re}$ (65 kDa) (*16*). Since that study, there have been no additional publications reporting the investigation of PHB biosynthesis in *C. crescentus*.

Our efforts have been to characterize the PHB biosynthetic proteins of *C. crescentus*. As a starting point, a protocol for growth on nitrogen-limited defined minimal medium supplemented with 1% glucose (PHB production, or PHB_p, medium) was developed. We have identified putative biosynthetic proteins PhaP and PhaR as granule-associated, and constructed the precise deletion strains of *C. crescentus*, Δ*phaP* and Δ*phaR*. Antibodies to recombinantly

purified $PhaC_{Cc}$ and PhaP were generated. The levels of PHB, PhaP and $PhaC_{Cc}$ were measured in the two mutant strains and the wt strain during a growth in nitrogen-limited medium supplemented with glucose, in order to develop a model for the role of PhaP in promoting PHB accumulation in *C. crescentus*. The results show that while $PhaC_{Cc}$ is constitutively expressed, the expression levels of PhaP are correlated with PHB accumulation. Quantitative analysis demonstrated that the ratio of PHB chains to PhaP remains between 1-2 throughout growth, similar to the ratio measured in *R. eutropha* (He and Stubbe, unpublished data)*(7, 17)*. Deletion of *phaP* results in severe attenuation of PHB accumulation. We have examined the role of PhaR in regulating PhaP expression and find that in the mutant strain Δ*phaR*, PhaP levels are upregulated but still correlated with PHB levels, suggesting that the mechanism of regulation of PhaP expression in *C. crescentus* is distinct from that in *R. eutropha*. Finally, transmission electron microscopy (TEM) is a tool we and others have previously used to examine biogenesis of granules in *R. eutropha*. TEMs of wt *C. crescentus* and the two mutant strains provided some insight into the role of PhaP, suggesting that PhaP helps to control the size and number of PHB granules in *C. crescentus*. This role is similar to what has been proposed for *R. eutropha (3)*.

In summary, our results suggest that some of the observations made in *R. eutropha*, such as the molar ratio of PhaP to PHB and the correlation of PhaP expression with PHB levels, are common features of PHB producing organisms regardless of the extent to which PHB is accumulated. However, the mode of regulation of the expression of PHB biosynthetic proteins and their correlation with PHB levels are distinct in *C. crescentus*, reinforcing the notion that regulation mechanisms are organism specific.

3.2 Materials and Methods

3.2.1 Materials

All chemicals were purchased from Sigma-Aldrich (St. Louis, MO) at the highest purity available, unless otherwise noted, and used without further purification. Restriction enzymes were purchased from New England Biolabs (Beverly, MA) and *Taq* DNA polymerase was purchased from Promega (Fitchburg, WI). Oligonucleotide primers were purchased from Integrated DNA Technologies (Coralville, IA) and are listed in Table 3.1. Strains and plasmids are listed in Table 3.2. The relative concentrations of vectors and inserts used for ligation reactions were determined by densitometry analysis of ethidium bromide stained 1% agarose gels. Glutaraldehyde (15% solution), OsO_4, uranyl acetate, propylene oxide, low viscosity embedding resin (LVER, containing vinyl-4-cyclohexene dioxide, diglycidyl ether polypropylene glycol, nonenyl succinic anhydride, and dimethylamino ethanol combined in proportions as per the manufacturer's protocol), flat silicone embedding molds and 200-mesh nickel grids coated with carbon Formvar were purchased from Electron Microscopy Sciences (Hattfield, PA).

Table 3.1 Primers and oligonucleotides used in this study.

Name	Sequence[a]
phaPURfw	5′-GATATAGGATCCGAGGTAAGCCTGGCGAACATGAAGCGACGTC CGTCATTTGAACTGG-3′
phaPURrev	5′-GATATACATATGCAGCTCGACCTTCCGCCCCGCCTCCTTTCCTCC CCAGGAGACTCCCC-3′
phaPDRfw	5′-GATATACATATGGGCCTGCTCCAGGCGCGCTCACCGGCGCGTCT GTGACATCAGAACTTGAAGG-3′
phaPDRrev	5′-GATATAGGATCCGATCGAGATCTGGCCCGAGATGTGGACCAGG CTTCCGGAGCGTACG-3′
phaRURfw	5′-GATATAGGATCCCGGCGGCTTCGATGACGGCCTTGCCCAGTTC-3′
phaRURrev	5′-GATATACATATGTTCGTTCCCTAGAAGCGGTTACGTCCGCTTTTC GCATCGCACTATCGCG-3′
phaRDRfw	5′-GATATACATATGCCAAGCCGATCCAGCCGTTCTTAACCGTCCTG GCCCTAGG-3′
phaRDRrev	5′-GATATGGGATCCCCGTGCCAAGATAGGTCGATCTGGCCGTGTCC AGCAC-3′
phaCfw	5′-GATATAGCTAGCATGGCCACGGCGAA-3′
phaCrev	5′-GATATAGGATCCTCAGGGTTGTGACTTTACCAGCAC-3′
phaCIntfw	5′-GATATAGGATCCCCGCTGCTGATCTTCCCGCCGTGGATCAACGT GG-3′
phaCIntrev	5′-GATATAGGATCCCTGACGAAGAACGACCAGATCAGGTCGTTAC CGCGCAGGGCG-3′
phaRIntfw[b]	5′-GCCAACCGCCGCCTCTACAACACGGCATCCTCTTCGTACGTCAC CC-3′
phaRIntrev[b]	5′-CGCATCCTCGGGACGGACATAGGCGAAGGGCGAGAACATCTTC ATCGCC-3′
phaRExtfw[b]	5′-CGACCACCACCTTGGCCGAGCCGTCGGCAATCTGCTGG-3′
phaRExtrev[b]	5′-CGTCGCGTGGAACCAGGGCGTCGAAGGGGATCGATCGGACC-3′
phaZfw[b]	5′-GATATACATATGCTCTACGCCCTGCACGAGGCGGCCTATTAC-3′
phaZrev[b]	5′-GATATAAAGCTTTCAGACTTCCTCGCCGAAGTTCGGGTCGC-3′

[a]Restriction sites underlined.
[b]Used only for sequencing purposes.

Table 3.2 Plasmids used in this study.

Strain	Genotype	Reference
Caulobacter crescentus		
CB15N	Wild type	
CB1002	CB15N, Δ*phaP*	This study
CB1003	CB15N, Δ*phaR*	This study
CB1005	CB15N, *phaC:km*; *phaC* is disrupted by insertion of pJQ200mp18Km encoding *kmR* in the middle of *phaC*	This study

Plasmid	Description	Reference
pJQ200mp18Km		(*18*)
pRB02	pJQ200mp18Km containing *phaP* deletion allele; deletion allele consists of 300 bp 5′ upstream and 3′ downstream region fragments flanking *phaP* joined by an NdeI site, and is inserted into a BamHI site in the multiple cloning region	This study
pRB03	pJQ200mp18Km containing *phaR* deletion allele; deletion allele consists of 300 bp 5′ upstream and 3′ downstream region fragments flanking *phaR* joined by an NdeI site, and is inserted into a BamHI site in the multiple cloning region	This study
pRB05	pJQ200mp18Km containing *phaC* insertion allele; insertion allele consists of an internal 500 bp fragment of *phaC*, and is inserted into the BamHI site in the multiple cloning region	This study

3.2.2 Media and growth conditions

C. crescentus (a gift of Prof. Michael Laub) and three mutant strains (Δ*phaP*, Δ*phaR*, *phaC*:km) were cultivated in PYE (peptone-yeast extract, 0.2% Bacto peptone [Difco], 0.1% yeast extract [Difco], 1 mM $MgSO_4$, and 0.5 mM $CaCl_2$) or in modified M2 minimal salts (6.1 mM Na_2HPO_4, 3.9 mM KH_2PO_4, 4.7 mM NH_4Cl, 0.5 mM $CaCl_2$, 10 μM $FeSO_4$) with 1% glucose. Modified M2 minimal medium supplemented with 1% glucose will be referred to as the PHB_p (PHB production) growth medium. All growths were carried out at 30 °C with shaking at 220 rpm. A single colony from a PYE/agar plate was grown 15-18 h (to saturation, OD_{600} = 1.4) in 50 mL PYE in a 500 mL baffled flask. This culture is the "saturated overnight culture." A

second 50 mL PYE culture in a 500 mL flask, the "starter culture," was inoculated with 2.5 mL of the saturated overnight culture. This starter culture was grown 4-5 h until OD_{600} = 0.15 (early log phase), then 25 mL was used to inoculate 500 mL PHB_p cultures in 4 L baffled flasks.

3.2.3 Isolation and purification of PHB granules by ultracentrifugation

PHB granules were isolated from 500 mL wt *C. crescentus* grown 24 h in PHB_p by a modification of a previously reported protocol (*19*). Cells (~1 g wet weight) were harvested by centrifugation for 20 min at 10,000 x*g* and the cell pellet was resuspended in 3 mL granule isolation buffer (50 mM Tris, 1 mM EDTA, pH 8.0). The cells were lysed by two passes through the French pressure cell at 14,000 psi. The insoluble fraction (containing PHB granules) was pelleted by centrifugation for 20 min at 4 °C and 20,000 x*g*. The soluble supernatant was decanted and the insoluble fraction was resuspended in 3 mL of granule isolation buffer. Resuspended PHB granules (3 mL per glycerol gradient) were purified from other insoluble material by ultracentrifugation over a glycerol density gradient at 21,000 rpm for 2 h at 4 °C in a Beckman L8-70M Ultracentrifuge equipped with an SW 41 rotor. The glycerol gradient was composed of the following: 2 mL each of 90% glycerol, 80% glycerol, 70% glycerol and 40% glycerol prepared in granule isolation buffer. The glycerol solutions were prepared using volumetric flasks. The gradient was prepared in Ultra-Clear Centrifuge Tubes (14 x 89 mm) (Beckman Instruments, Palo Alto, CA). The 40% glycerol layer was added first to the centrifuge tube. Using a syringe equipped with a blunt-ended cannula needle, the layers were added one at a time in order of increasing density by slowly dispensing each layer below the less dense layers. The layers were of sufficiently different density such that mixing of layers could be prevented by slow and careful dispensing. The density gradients were prepared immediately before use.

Following centrifugation, a syringe equipped with an 18½ gauge needle was used to pierce the side of the centrifuge tube to extract the materials that sedimented at the density layer interfaces. The extracted samples were pelleted by centrifugation for 10 min at 14,000 x*g* at room temperature (RT), and the glycerol supernatant was discarded. Each sample was resuspended in 100 µL Laemmli buffer (*20*) to give a final concentration of ~2-5 mg/mL protein. For identification of granule-associated proteins, samples were resolved by 15% SDS-PAGE and blotted to PVDF membranes (Immun-Blot, Bio-Rad) for 80 min at 100 V on ice in a Criterion wet blotting apparatus (Bio-Rad). The blotting buffer contained 25 mM Tris base, 192 mM glycine, 0.01% SDS (w/v) and 15% methanol (v/v). The blots were stained with Coomassie stain, and select protein bands of interest were carefully excised with clean razor blades and submitted to the Tufts Proteomics Core Facility for N-terminal sequencing by Edman degradation.

3.2.4 Protein purification and generation of antibodies

Expression and purification of the N-terminally $(His)_6$-tagged proteins $PhaC_{Cc}\Delta N$, $PhaC_{Cc}$ and PhaP were carried out as described in section 2.2.4 of this thesis. $PhaC_{Cc}\Delta N$ is a truncated construct of $PhaC_{Cc}$ in which the N-terminal 8 kDa domain (85 amino acids) is deleted. $PhaC_{Cc}\Delta N$ and PhaP (~1 mg each) were sent for preparation of antibodies by Covance (Princeton, NJ).

3.2.5 Homologous recombination to construct the *phaC* disruption strain *phaC*:km

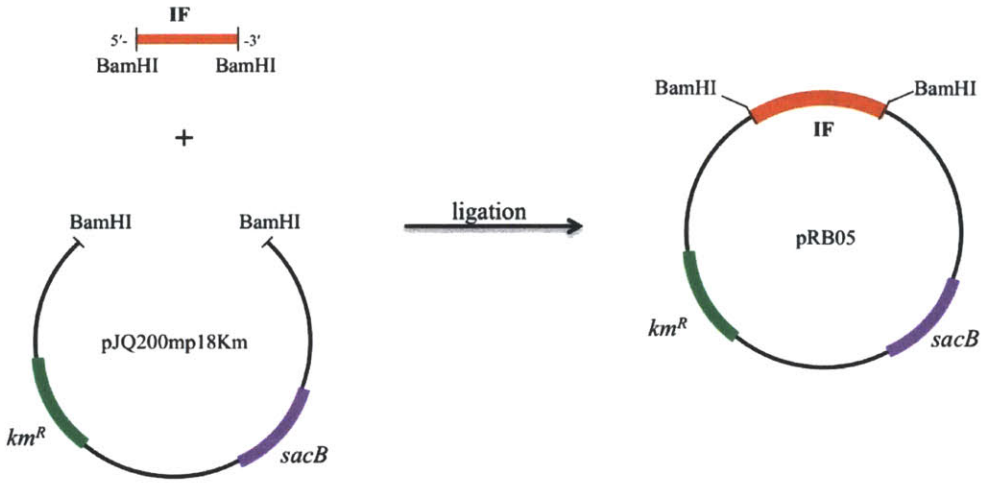

Figure 3.1 Cloning of pRB05. A 0.5 kb internal fragment (IF) of *phaC* was amplified using primers that inserted BamHI restriction sites on both ends of the fragment. The IF and parent plasmid pJQ200mp18km were digested with BamHI then ligated together to generate the plasmid pRB05.

Construction of the homologous recombination plasmid pRB05. For reasons that are unclear, the clean deletion strain Δ*phaC* could not be prepared by the precise deletion methods described below that were used to prepare Δ*phaP* and Δ*phaR*. Therefore a disruption mutant strain was constructed in which the homologous recombination plasmid pRB05 was inserted in the middle of *phaC*, conferring kanamycin (*21*) resistance. pRB05 was prepared from pJQ200mp18Km, which encodes km resistance (km^R) as a marker for successful gene disruption (Table 3.2) (Figure 3.1) (*18*). pRB05 contains a 0.5 kb internal fragment of *phaC* which undergoes recombination with *phaC* in the genome to insert pRB05. The resulting mutant strain is referred to as *phaC*:km. To construct pRB05, a 0.5 kb internal fragment of *phaC* (consisting of bp 976-1474 of *phaC*) was amplified using GoTaq polymerase and the primers phaCIntfw/phaCIntrev (Table 3.1), which insert BamHI sites to the 5′ and 3′ ends of the amplified product. The *phaC* internal fragment and parent plasmid pJQ200mp18Km were

digested with BamHI and the ligation was carried out overnight with T4 DNA ligase at RT at an insert to vector ratio of 5:1 to generate pRB05. The ligation reaction was transformed into *E. coli* XL10 Gold cells and plated on LB/agar containing 50 μg/mL km. Twenty-four colonies were screened by colony PCR using the primers phaCIntfw/phaCIntrev (Table 3.1). Six colonies containing the insert were grown overnight in 5 mL LB containing 50 μg/mL km, and the plasmids were isolated and submitted for sequencing at the MIT Biopolymers Laboratory.

Homologous recombination to prepare the phaC:*km strain.* pRB05 was introduced into wt *C. crescentus* (250 μL cells of OD_{600} = 20 in PYE) by electroporation at RT for 1 s at 1.5 V (τ = 5 msec) using a Bio-Rad *E. coli* Pulser. Following electroporation, 1 mL of PYE was added to the reaction and it was incubated for 2 h at 30 °C with gentle rotation. The transformation reaction was centrifuged at 4 °C for 10 min at 10,000 x*g* to pellet the cells and the supernantant was decanted. The cells were resuspended in 100 μL fresh PYE and plated on PYE/agar supplemented with 25 μg/mL km to select for incorporation of pRB05 into the genome. Eleven km resistant colonies were screened by colony PCR using two reactions. The first reaction was a positive control using the primers phaZfw/phaZrev to amplify the putative *phaZ*, with an expected size of 1.3 kb. The second reaction used the primers phaCfw/phaCrev, with an expected product size of 2 kb (if *phaC* is intact) or no product if *phaC* is disrupted, because the inserted sequence would be >10 kb and likely not successfully amplified. All eleven km resistant colonies screened contained the *phaC* disruption. The disruption was further confirmed by Western blot analysis, which failed to detect $PhaC_{Cc}$. The cells also did not produce PHB when grown 24 h in PHB_p medium.

3.2.6 Homologous recombination to construct the Δ*phaP* and Δ*phaR* mutant strains

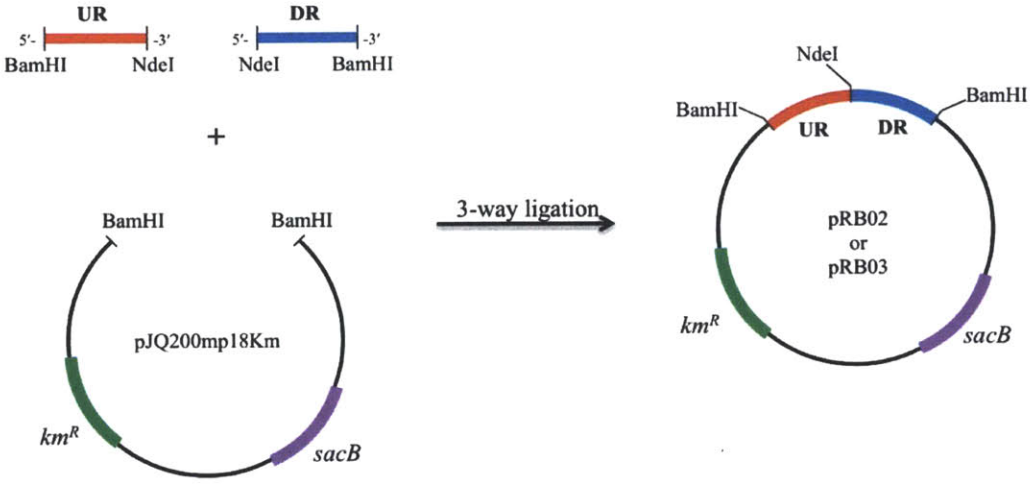

Figure 3.2 Cloning of pRB02 and pRB03. Upstream region (UR) and downstream region (DR) fragments (0.3 kb each) of sequence flanking *phaP* or *phaR* were amplified using primers to insert the indicated restriction sites. The UR and DR fragments of *phaP* or *phaR* were digested with NdeI and BamHI and parent plasmid pJQ200mp18km was digested with BamHI. The UR and DR of *phaP* and the UR and DR of *phaR* were ligated into pJQ200mp18km to generate pRB02 and pRB03, respectively.

Construction of homologous recombination plasmids pRB02 and pRB03. pRB02 and pRB03, derivatives of the parent plasmid pJQ200mp18Km, were used to construct the precise deletion strains Δ*phaP* and Δ*phaR*, respectively. pJQ200mp18Km encodes kanamycin resistance (km^R) and sucrose sensitivity (*sacB*) selection markers for homologous recombination. pRB02 contains a 0.3 kb region located immediately upstream of *phaP* ligated adjacent to a 0.3 kb region located immediately downstream of *phaP*. Similarly, pRB03 contains a 0.3 kb region located immediately upstream of *phaR* ligated adjacent to a 0.3 kb region located immediately downstream of *phaR*. These plasmids are diagrammed in Figure 3.2.

For construction of pRB02, 0.3 kb fragments of the upstream region (UR) and downstream region (DR) immediately adjacent to the *phaP* open reading frame were amplified separately from *C. crescentus* by colony PCR. To amplify the UR and insert BamHI and NdeI

restriction sites on the 5′ and 3′ ends, respectively, the primers phaPURfw/phaPURrev and GoTaq polymerase were used (Table 3.1). To amplify the DR and insert NdeI and BamHI restriction sites on the 5′ and 3′ ends, respectively, the primers phaPDRfw/phaPDRrev and GoTaq polymerase were used. The UR and DR PCR products were purified and digested with NdeI and BamHI. The digested UR and DR fragments were then combined with BamHI-digested pJQ200mp18Km in a ratio of 5:5:1 (UR:DR:pJQ200mp18Km) and ligated using T4 DNA ligase.

For construction of pRB03, 0.3 kb UR and DR fragments of the putative *phaR* open reading frame were amplified and inserted into pJQ200mp18Km by a method identical to that used for pRB02, except that the primers used were phaRURfw/phaRURrev (Table 3.1).

The ligation reactions to generate pRB02 and pRB03 were transformed into *E. coli* XL10 Gold cells and plated on LB/agar containing 50 μg/mL km. Twenty-four colonies of each transformation were screened by colony PCR using the primers phaPURfw/phaPDRrev (for pRB02) and phaRURfw/phaRDRrev (for pRB03). Six colonies containing insert were grown overnight in 5 mL LB containing 50 μg/mL km, and the plasmids were isolated and submitted for sequencing at the MIT Biopolymers Laboratory.

*Homologous recombination to prepare the Δ*phaP *and Δ*phaR *strains.* pRB02 and pRB03 (500 ng) were introduced into wt *C. crescentus* (250 μL cells of OD_{600} = ~20 in PYE) by electroporation at RT 1.5 V for 1 s (τ = 5 msec) using a Bio-Rad *E. coli* Pulser. Immediately following electroporation, 1 mL of PYE was added and the cells were grown 2 h at 30 °C with gentle rotation. The transformation reactions were centrifuged at 4 °C for 10 min at 10,000 x*g*, the supernatant was decanted and the cells were resuspended in 100 μL PYE and plated on PYE/agar supplemented with 25 μg/mL km to select for the first recombination event (insertion of the plasmid into the genome). After two days growth at 30 °C, the km resistant colonies were

grown overnight at 30 °C in 5 mL PYE in 125 mL flasks with shaking at 220 rpm to allow excision of the plasmid from the genome (with or without the gene of interest). Five μL of the overnight cultures was plated on PYE/agar supplemented with 3% w/v sucrose to select for excision of the plasmid. The plates were incubated for two days at 30 °C. Each sucrose insensitive colony was then streaked out twice, once onto PYE/agar containing 25 μg/mL km and once onto PYE/agar containing 3% sucrose. The colonies that were sucrose insensitive and km sensitive had successfully excised the plasmid from their genome.

Screening of km sensitive/sucrose insensitive colonies to identify mutant strains. Colonies that were both km sensitive and sucrose insensitive were then screened by PCR to confirm the mutations. Eight Δ*phaP* transconjugants were screened to confirm excision of *phaP* from the genome. A wt *C. crescentus* colony was also included as a control. Each colony was screened by three different PCR reactions. The first reaction was a positive control using the primers phaCfw/phaCrev, which amplified *phaC* (expected product size 2 kb). The second reaction used the primers phaPfw/phaPrev to amplify *phaP*, with expected product sizes of 0.42 kb if *phaP* is present, or no product if *phaP* is excised. The third reaction used the primers phaPURfw/phaPDRrev, which anneal 0.3 kb upstream and 0.3 kb downstream of *phaP* and amplify the sequence between. In this reaction, if *phaP* is present the expected product size is 1 kb, whereas if *phaP* is deleted, the expected product size is 0.6 kb. One colony of the eight screened contained the products of the expected sizes for a Δ*phaP* transconjugant.

Eleven Δ*phaR* transconjugants were screened to confirm excision of *phaR* from the genome. A wt *C. crescentus* colony was also included as a control. Each colony was screened by three different PCR reactions to confirm excision of *phaR*. The first reaction was a positive control using the primers phaCfw/phaCrev, which amplified *phaC* (expected product size 2 kb).

The second reaction used the primers phaRIntfw/phaRIntrev, which anneal to internal portions of *phaR*. If *phaR* is intact, the expected product size is 0.4 kb (an internal fragment of *phaR*), and if *phaR* is excised no product is expected. The third reaction used the primers phaRExtfw/phaRExtrev, which anneal 0.3 kb upstream and 0.3 kb downstream of *phaR*. If *phaR* is intact, the expected product size is 1.2 kb. If *phaR* is excised, the expected product size is 0.6 kb. The reaction containing the primers phaRExtfw and phaRExtrev produced inconclusive results in wt *C. crescentus* as the reaction failed to amplify a band. However, in a single Δ*phaR* transconjugant of the eleven screened, a 0.6 kb fragment was amplified using primers phaRExtfw/phaRExtrev, and no product resulted from the reaction using the primers phaRIntfw/phaRIntrev. These observations suggested that *phaR* had been excised in this colony. To confirm this expectation, the 0.6 kb PCR product amplified using the primers phaRExtfw/phaRExtrev was ligated into pCR-TOPO 2.1 (Invitrogen) following the manufacturer's protocols. The ligation product was transformed into *E. coli* TOP10 cells for amplification, and the sequencing analysis at MIT Biopolymers confirmed the excision of *phaR*.

3.2.7 Preparation of samples for PHB quantitation and Western blot analysis

Aliquots of cells were withdrawn from PHB_p cultures of wt, Δ*phaP* and Δ*phaR* at various time points for preparation of Western blot and crotonate analysis. For the 0 h time points, 40 mL of PYE "starter" culture (grown 4-5 h to OD_{600} = 0.15) was withdrawn. For the 7.5 and 10 h time points, 30 mL of PHB_p culture was withdrawn. For the remaining time points, 25 mL of PHB_p culture was withdrawn. Aliquots were centrifuged at 4 °C for 10 min at 5,000 x*g* to pellet the cells. Cell pellets were rinsed by resuspension in 15 mL ice cold ddH_2O and pelleted again by centrifugation at 4 °C for 10 min at 5,000 x*g*. The pellets were then resuspended in 0.75-1 mL of

ddH_2O and the OD_{600} of the suspension was determined from a 1:50 dilution in ddH_2O. The number of cells in the suspension was calculated using the conversion factor that an OD_{600} of 1 corresponds to 1.1 x 10^6 cells/μL. This conversion factor was determined by preparing 10^6-, 10^7- and 10^8-fold dilutions of a saturated overnight PYE culture, plating 100 μL of each concentration in triplicate on PYE/agar, and counting the colonies after 2 days of growth at 30 °C. The cell suspensions were then lysed by sonication using a VirSonic100 Sonicator (SP Industries, Warminster, PA) set to a power setting of 3-4. Each sample was sonicated on ice by 30 x 1 s pulses separated by 1 s pauses to prevent overheating.

For Western samples, 150 μL of the lysed suspension was combined with 150 μL Laemmli buffer (*20*) and the samples were frozen in liquid nitrogen and stored at -80 °C until use (within two weeks). For crotonate samples, the remaining lysate was added to pre-weighed borosilicate vials (16 x 125 mm) (Corning, Corning, NY) then dried overnight in a 120 °C oven.

3.2.8 Crotonate assay analysis of PHB content in cell samples

Following overnight drying, the dry weight of each crotonate sample (typically 10-20 mg) was determined and the samples were boiled in 1 mL concentrated H_2SO_4 for 30 min for analysis of PHB content by the crotonic acid assay (*22*). Samples or dilutions of samples (25 μL), containing 2.5-250 μg of PHB, were injected onto a Bio-Rad Aminex HPX-87H organic acid column connected to a Waters 515/2487 HPLC and eluted with 5 mM H_2SO_4 at a flow rate of 0.5 mL/min at 50 °C with monitoring of absorption at 210 nm. The temperature was controlled by a Waters Column Heater. The retention time for crotonic acid was 33 min. A standard curve of PHB (2.5-250 μg) versus peak area was generated from commercially available PHB (Fluka).

3.2.9 Quantitative Western blot analysis to measure PhaP and PhaC expression levels

For PhaP Western blots, gels were loaded such that each lane contained approximately ~7.5 x 10^7 cells. To prepare samples for the standard curve, 7.5 x 10^7 Δ*phaP* cells were spiked with recombinant PhaP (25-300 ng). Each time point was measured in triplicate from three different cultures. For PhaC Western blots, gels were loaded such that each lane contained ~7 x 10^7 cells and the standard curve (1-10 ng) was prepared from recombinant His_6-PhaC. The standard curve was not spiked with the *phaC*:km mutant strain.

Samples were resolved by 10% (for PhaC Western blots) or 15% (for PhaP Western blots) Criterion precast SDS-PAGE gels (Bio-Rad). Samples were blotted onto PVDF membranes (Immun-Blot, Bio-Rad) for 80 min at 100 V on ice in a Criterion wet blotting apparatus (Bio-Rad). The blotting buffer contained 25 mM Tris base, 192 mM glycine, 0.01% SDS (w/v) and 15% methanol (v/v). The blots were then blocked in blocking buffer containing 3% milk (w/v) in Tris-acetate-EDTA (TAE) buffer with 0.1% Tween-20 (v/v). The primary rabbit antibodies for PhaP and PhaC were used without further purification. Blots were incubated with anti-PhaP antibody (1:5000 diluted) or anti-PhaC antibody (1:2000 diluted) in blocking buffer for 1 h at RT, then rinsed 3 x 5 min in 50 mL phosphate buffered saline (PBS).

For PhaP Westerns, the secondary antibody was goat anti-rabbit antibody conjugated with horseradish peroxidase (Thermo Scientific, Rockford, Ill.), used at a 1:2000 dilution in blocking buffer. For PhaC Western blots the secondary antibody was also goat anti-rabbit conjugated with horseradish peroxidase, but from a different supplier (Santa Cruz Biotechnology, Santa Cruz, CA). The blots were incubated in secondary antibody for 1 h at RT, then rinsed 3 x 5 min in 50 mL PBS. The blots were developed using SuperSignal® West Femto Maximum Sensitivity Substrate (Thermo Scientific) and imaged using a BioRadChemiDoc XRS

imager. Signals were analyzed using the Quantity-One® software and quantitated by comparison to the standard curves.

The rationale for using two different antibodies was based on the observation from preliminary Western blots that the secondary antibody from Santa Cruz Biotechnology was more sensitive than the secondary antibody from Thermo Scientific. While the secondary antibody from Thermo Scientific was sufficiently sensitive to detect PhaP, PhaC was more difficult to detect and required the higher sensitivity secondary antibody from Santa Cruz Biotechnology.

3.2.10 Gel permeation chromatography (GPC) analysis of PHB molecular weight.

Preparation of samples for extraction of PHB into chloroform. Samples of varying volumes were withdrawn from PHB_p cultures at various time points. The volume was dependent on the predicted PHB content as determined by crotonic acid analysis. For a given time point, measurements were made from three samples taken from three individual cultures. For wt cells at 0 h, 500 mL PYE "starter" cultures were centrifuged at 10,000 x*g* for 20 min at 4 °C to pellet the cells. To accumulate enough cell mass, nine separate 500 mL cultures were grown in three separate growths. The three cultures in each growth were combined into one GPC sample. For wt cells at 10 h, 500 mL PHB_p culture was centrifuged to pellet the cells. For wt 20 h and 40 h samples, 200 mL PHB_p culture was centrifuged at 4 °C for 20 min at 10,000 x*g* to pellet the cells. The cell pellets were resuspended in 5-10 mL ddH_2O and transferred to 50 mL Falcon tubes. The samples were frozen in liquid nitrogen and lyophilized to dryness. For the 0 h and 10 h samples, the lyophilized cells (70 mg) were divided into ~20 mg portions, which were placed into borosilicate tubes (16 mm x 125 mm) for extraction into chloroform. For the 20 h and 40 h time

points, 20 mg cells was removed and placed into a borosilicate tube for extraction into chloroform.

For Δ*phaP* cells, 500 mL PHB_p culture grown 24 h was centrifuged at 10,000 x*g* for 20 min at 4 °C to pellet the cells. The supernatant was decanted and the samples were resuspended in 5 mL ice cold ddH_2O, transferred to 50 mL Falcon tubes and frozen in liquid nitrogen and lyophilized to dryness. The resulting lyophilized cell masses (~200 mg) were divided into 20 mg portions, which were transferred to borosilicate tubes (16 mm x 125 mm) for extraction into chloroform. For Δ*phaR* cells, 200 mL PHB_p culture grown 24 h was centrifuged at 10,000 x*g* for 20 min at 4 °C to pellet the cells. The cell pellets were resuspended in ~10 mL ice cold ddH_2O and transferred to 50 mL Falcon tubes. The samples were frozen in liquid nitrogen and lyophilized to dryness. From the lyophilized cell mass, a single 20 mg portion was transferred into a borosilicate tube for extraction into chloroform.

Extraction of PHB by refluxing in chloroform. One magnetic stir bar was added to each sample, the tubes were capped with rubber septa and each septum was pierced with a glass Pasteur pipette. This set-up was designed to function as a makeshift condenser such that upwards of 30 individual samples could be prepared at a time. PHB was extracted by refluxing in chloroform at 70 °C for 48 h with stirring. Care was taken to thoroughly resuspend the lyophilized material in the chloroform by disrupting clumps with a spatula and vigorous stirring. After extraction, the cell debris was removed by filtration using a glass syringe fitted with a 13 mm syringe filter with a 0.45 μm PTFE membrane (Perkin Elmer, Hopkinton, MA). Each filter was washed with 3-5 mL fresh chloroform, which was added to the filtrate. Excess chloroform was evaporated under a stream of air to bring the samples to a final concentration of ~3 mg/mL as determined by crotonic acid assay. The volume of the final sample varied between 200 μL and

2 mL. The extraction efficiency was determined by crotonic acid assay of 25-100 μL of the extracted material. Typical efficiencies were 30-40%.

Analysis of PHB M_w and PDI by GPC. Samples (100 μL) were injected onto a 2 x 300 x 7.5 mm Plgel Olexis column (VWR, Rador, PA) connected to an HPLC with a refractive index detector (Waters, Milford, MA) and eluted at a flow rate of 1 mL/min with chloroform at 30 °C. The temperature was controlled with a Waters Column Heater. Isopropanol (retention time, 21 min) was used as an internal standard at 1% v/v in each sample to adjust sample peak retention times. The retention times of the eluted material were compared to a set of polystyrene standards (Varian) of molecular weights (retention time): 3.1 kDa (17.8 min), 10 kDa (17 min), 73 kDa (15.4 min), 205 kDa (14.8 min), 490 kDa (13.9 min), 1800 kDa (12.9 min), 5000 kDa (12.4 min). The M_w and PDI of each sample was determined using the PSS WinGPC Unity software (Polymer Standards Service, GmbH, Mainz, Germany) and a standard curve prepared as described in section 3.2.11 from the polystyrene standards.

Calculation of the M_w and PDI of a sample using the adjusted calibration curve. For a given sample, the data are exported as a .cdf file, which is the file format supported by the PSS WinGPC Unity software. For data analysis, the first step is to adjust the retention time of isopropanol to 21 min. The retention time of isopropanol can vary between 21 – 21.5 min. The second step is to import the adjusted calibration curve, prepared as described below. The third step is to manually select the peak of interest using the cursor, and the software automatically applies the adjusted calibration curve to generate the M_w, M_n, PDI and other values of interest.

3.2.11 Preparation of an accurate calibration curve to calculate the M_w and PDI of PHB extracted from *C. crescentus*

Determination of the absolute M_w of PHB by static light scattering (SLS). SLS experiments were carried out by Dr. Mimi Cho in order to determine the M_w of a PHB standard. This M_w was used to adjust the calibration curve prepared using polystyrene standards as described below, in order to account for differences in peak broadening and migration between PHB and polystyrene. In SLS, the M_w of a polymer is determined using the Rayleigh equation (Equation 3.1).

Equation 3.1

$$\frac{KC}{R_\theta} = (\frac{1}{M_w} + 2A_2C)P_\theta$$

The Rayleigh equation relates the ratio of scattered light to incident light (R_θ) of a sample to its M_w. K is the optical constant, C is the sample concentration, A_2 is the 2nd virial coefficient related to solute/solvent interaction, and P_θ is the angular dependence of the scattering intensity (*23, 24*). For the purposes of SLS, the particle size is assumed to be smaller than the wavelength of incident light and the concentration of sample is sufficiently dilute to prevent multiple photon scattering. These assumptions allow P_θ to be approximated as one, simplifying the Rayleigh equation to Equation 3.2.

Equation 3.2

$$\frac{KC}{R_\theta} = \frac{1}{M_w} + 2A_2C$$

A Debye plot of KC/R_θ versus C is generated by measuring R_θ at various sample concentrations. Equation 3.2 is the linear function that describes the Debye plot, in which the y-intercept is the M_w of the polymer sample and the slope is A_2. R_θ values are determined in the SLS experiment using Equation 3.3.

Equation 3.3

$$R_\theta = \frac{I_A n_o^2}{I_T n_T^2} R_T$$

In Equation 3.3, I_A is the scattering intensity of the solute, I_T is the scattering intensity of toluene (the reference standard), n_o is the refractive index of the solvent, n_T is the refractive index of toluene (1.50), and R_T is the Rayleigh ratio of toluene (1.35×10^{-5}) (*23*).

K in Equation 3.2 is the optical constant and is determined using Equation 3.4, where λ is the wavelength of incident light, N_A is Avogadro's number, n_o is the refractive index of the solvent, and dn/dC is the differential refractive index of the solute.

Equation 3.4

$$K = \frac{2\pi^2}{\lambda^4 N_A}(n_o \frac{dn}{dC})^2$$

For SLS experiments, PHB was extracted into chloroform from *R. eutropha* grown 24 h in PHB_{high}, then 100 µL of a 3 mg/mL solution of extracted PHB was injected onto the GPC column as described in the previous section. The peak containing PHB (retention time 10-15 min) was collected and the sample was dried under a stream of air. The residue was then dissolved in 2,2,2,-trifluoroethanol (TFE) to ~2 mg/mL and the solution was filtered through a 4 mm glass syringe fitted with a 0.2 µm PTFE membrane (VWR). To determine the exact concentration of the sample, an aliquot was removed for crotonate analysis. Dilutions of the PHB solution (0.05-0.2 mg/mL) were prepared in TFE for analysis by SLS. SLS experiments were carried out on a Malvern Zetasizer ZS instrument (Malvern, Worcestershire, UK) with a 633 nm laser. The refractive index of the solvent TFE (n_o) is 1.291 (*25*). The differential refractive index of PHB was previously determined to be 0.150 mL/g (*26, 27*). Two different SLS experiments were carried out from two different GPC purifications of PHB and the M_w was 990 kDa ± 50 kDa.

Generation of the calibration curve. The calibration curve correlates retention times with the known peak molecular weight (*28*) of the polystyrene standards described in section 3.2.10. The $\log M_p$ of the standards were plotted against their retention times using the PSS WinGPC Unity software. The data were fit to a 2nd degree polynomial ($\log M_p = AV^2 + BV + C$), where A, B and C are constants and V is the retention volume. The absolute M_w of PHB determined by SLS was then used to adjust the calibration curve to account for differences in peak broadening and migration between PHB and polystyrene. This adjustment was done using Equations 3.5 and 3.6.

Equation 3.5

$$\log M_{PHB} = \frac{1}{1+a}(\log\frac{1}{K}) + \frac{1}{1+a}\log M_{polystyrene}$$

Equation 3.6

$$M_w = \frac{\sum_{v=1}^{N}[(M_{PHB})_v * I_v]}{\sum_{v=1}^{N} I_v}$$

Equation 3.5 is the Mark-Houwink relation, which relates the molecular masses of two different polymers (PHB and polystyrene in our experiments). K and a are relative intrinsic viscosity parameters (*29*) and $\log M_{polystyrene}$ is the 2nd degree polynomial described above. Equation 3.6 is the mathematical definition of M_w and I_V is the differential refractive index signal from GPC and $(M_{PHB})_V$ is the molecular mass of PHB at a given retention volume (V).

The PSS WinGPC Unity software finds values for K and a that satisfy both equations. The values I_V and V come from the SLS experiments with the PHB standard and the GPC trace of the PHB standard, respectively. When satisfactory values for K and a have been obtained, the software reports a function of $\log M_{PHB}$ versus V, also a 2nd degree polynomial. This function is the adjusted calibration curve that was used to obtain the M_w and PDI values for all GPC

samples described in this chapter. Equations 3.7 and 3.8 are applied by the program to calculate the number average molecular weight (M_n) and PDI, respectively.

Equation 3.7

$$M_n = \frac{\sum_{v=1}^{N} I_v}{\sum_{v=1}^{N} [I_v / (M_{PHB})_v]}$$

Equation 3.8

$$PDI = \frac{M_w}{M_n}$$

3.2.12 Quantitation of PHB and PhaP in the soluble fractions of wt *C. crescentus* grown in PYE

Two 500 mL PYE cultures in 4 L baffled flasks were inoculated by the same protocol as described in section 3.2.2. The cultures were grown at 30 °C for 15 h with shaking at 220 rpm. The cells were then pelleted by centrifugation for 10 min at 10,000 x*g* at 4 °C. The supernatant was decanted and the cells were resuspended in ~40 mL of cold 20 mM Hepes pH 7.5, 20 mM NaCl. The cells were lysed by two passes at 4 °C through the French pressure cell at 14,000 psi. For one culture, the lysate was transferred to a 50 mL pear-shaped flask, shell frozen in liquid nitrogen and lyophilized. The resulting cell material was refluxed in 20 mL chloroform with stirring for 48 h at 70 °C for GPC analysis. The sample was prepared and analyzed as described above. For the other culture, Western blot and crotonate samples were prepared from the whole cell lysate and analyzed as described above. The soluble and insoluble fractions were then separated by centrifugation at 4 °C for 20 min at 30,000 x*g*. The soluble fraction was decanted and set aside. The insoluble fraction was resuspended in 20 mM Hepes pH 7.5, 20 mM NaCl to a volume equal to that of the soluble fraction. Samples for crotonate and Western blot analysis

were prepared and analyzed as described above. The remaining soluble and insoluble fractions were transferred to individual 50 mL pear-shaped flasks and refluxed in ~20 mL chloroform for 48 h at 70 °C for GPC analysis. The samples were then prepared and analyzed as described above.

3.2.13 Error propagation in calculation of mole ratios of PhaP, PhaC and PHB

The errors (standard deviation from the mean) of measurements of PhaP and PHB levels were propagated to calculate the error for mole ratios of PHB to PhaP. The following equation for error propagation for uncertainties in products and quotients was used:

Equation 3.9

$$\delta q = q\sqrt{(\frac{\delta x}{x})^2 + (\frac{\delta y}{y})^2}$$

The uncertainty in the ratio q (δq) is equal to the square root of the sum of the squares of the fractional uncertainties in x and y (PhaP and PHB concentrations, respectively) times the ratio q (*30*).

Because multiple measurements are made in order to calculate the mole ratios, there are several sources of error. These include cell counting, PHB measurement (which can be a significant source of error when the cells contain very little PHB), quantitation of protein levels by Western blot, and M_w determination of PHB by GPC. In particular for measurement of PHB M_w, extraction efficiencies were often quite low due to the samples containing very small amounts of PHB. However, it should be noted that mole ratios are independent of cell counting and thus have inherently lower error.

3.2.14 Activity assays to compare PhaC activity in wt and Δ*phaP* crude cell lysates

The specific activity of PhaC was measured in crude cell lysates of wt or Δ*phaP* cells grown in PYE medium. The inoculation protocol was as described in section 3.2.2, except that 200 mL PYE cultures (instead of PHB_p cultures) in 2 L baffled flasks were inoculated at a dilution of 1:25. The PYE cultures were grown at 30 °C with shaking at 220 rpm until OD_{600} = ~0.75, at which point the cells were pelleted by centrifugation at 10,000 x*g* for 15 min at 4 °C. The cell pellets (~0.5 g) were resuspended in 10 mL of 20 mM Hepes pH 7.5, 200 mM NaCl then lysed by passage twice through the French pressure cell at 14,000 psi. The crude lysates were immediately assayed in triplicate at 30 °C. The crude lysates were not subject to centrifugation; thus, assays measured the activity in both the soluble and insoluble fractions. It should be noted that the final assays were not cloudy and did not appear to contain particulate matter from the insoluble fraction. The assays contained in a final volume of 210 µL: 40 µL lysate (~110 µg total protein) and 1 mM HBCoA in 20 mM Hepes pH 7.5, 20 mM NaCl. At various time points 20 µL aliquots were withdrawn and quenched in 50 µL ice cold 10% trichloroacetic acid (TCA). Each sample was centrifuged to pellet precipitated protein, and 68 µL was withdrawn and added to 262 µL 0.25 mM 5-5'-dithiobis-(2-nitrobenzoic acid) (DTNB) in 0.5 M K_2HPO_4, pH 7.8. The A_{412} of each sample was measured. To calculate specific activity, the amount of PhaC in each sample was determined to be 14 ng by Western blot analysis carried out as described in section 3.2.8. The samples for Western blots were prepared by combining crude lysate with one volume of Laemmli buffer, then boiling for 15 min at 100 °C.

3.2.15 Transmission electron microscopy (TEM)

3.2.15.1 Fixation

The methods for preparation of TEM samples were adapted from (*31*). To prepare a typical sample, 25 mL of cell culture grown in PHB_p medium was combined 1:1 with 25 mL fixative containing 2% (v/v) glutaraldehyde, 3% (w/v) paraformaldehyde, 5% (w/v) sucrose in 0.1 M sodium cacodylate, pH 7.4. Samples were mixed with gentle rocking for 1 min, then centrifuged for 10 min at 7000 x*g* at 4 °C. The cell pellets were resuspended in 10 mL fresh fixative and incubated for 1 h at 4 °C with gentle rocking. After fixation, the cell pellets were washed three times in 1 mL of 0.1 M sodium cacodylate pH 7.4 by centrifugation at 7000 x*g* at 4 °C. After fixation and for the rest of the sample preparation, the cell pellets were hard and did not readily dissociate into individual cells or clumps of cells. The pellets were therefore "dislodged" with a toothpick from the bottom of the sample tube into the various solutions and broken apart. The cell pellets were then dislodged into 1 mL of 1% OsO_4 solution in Veronal-acetate buffer (0.24% (w/v) sodium acetate, 0.58% (w/v) sodium barbitol, 0.02 N HCl) and incubated for 1 h at RT with gentle rotation. Samples were centrifuged for 5 min at 14,000 x*g*, and the supernatant was removed. One mL Kellenberger uranyl acetate stain (0.5% uranyl acetate in Veronal acetate buffer) was then added to each sample, and the pellets were dislodged and broken apart, then incubated overnight for additional staining.

3.2.15.2 Dehydration

Following uranyl acetate staining, the uranyl acetate was removed and the pellets were dehydrated by incubation in increasing concentrations of ethanol. The pellets were dislodged into 1.5 mL 50% (v/v) ethanol in ddH_2O and rotated gently on a nutating mixer at RT for 10 min, then centrifuged 1 min at 14,000 x*g* and the supernatant decanted. This process was repeated

with 70%, 90% and 95% ethanol, and repeated three times with 100% ethanol. The pellets were then dislodged into 1 mL of a mixture of 50% (v/v) ethanol, 50% (v/v) propylene oxide for 5 min, then 100% propylene oxide for 5 min. Finally the pellets were dislodged into 1 mL of a mixture of 50% (v/v) propylene oxide, 50% (v/v) low viscosity embedding resin (*23*) and incubated overnight at RT.

3.2.15.3 Embedding

The pellets were transferred into 1.5 mL 100% LVER, placed under vacuum at RT for 4 h, then exchanged into fresh 100% LVER. This process was repeated three times. After the final incubation in LVER the samples were centrifuged 1 min at 14,000 x*g* and then LVER was removed. The pellets were then placed on a clear surface (typically a plastic petri dish) and cut into smaller pieces (~1-2 mm) using a toothpick. Several pieces of each sample were then embedded in flat silicone molds in ~250 µL fresh 100% LVER. The samples were cured for 48 h at 60 °C.

3.2.15.4 Sectioning and microscopy

Sectioning and imaging were carried out at the W.M. Keck Microscopy Facility at the Whitehead Institute (Cambridge, MA). Sectioning was performed by Dr. Mimi Cho. Sections (70-80 nm thick) were cut from each beam capsule using a Reichert Ultracut E Ultramicrotome equipped with a Diatome diamond knife. Sections were scooped up by 200-mesh Formvar coated nickel grids. Samples were then imaged using an FEI Technai Spirit Transmission Electron Microscope at 80 kV at the W.M. Keck Microscopy Facility at the Whitehead Institute for Biomedical Research. To estimate the bias of granules in 9 h wt cultures towards the perimeter of the cells, a total of 322 granules from 220 cells were examined. The cells were selected from 18 micrographs collected from three separate growths and had a long axis of >1 µm parallel to

the plane of the micrograph, which accounted for 25-30% of the total cells in each micrograph. A line was drawn carefully down the center of the cell, and the distance of each granule from this line was measured to determine whether the granules were located closer to the edge of the cell or the center. To determine the distribution in numbers of granules per cell in 9 h wt cultures, the same cells with an axis of >1 μm were examined. The same analysis of numbers of granules per cell was carried out on selected cells in 24 h wt cultures (177 cells from 10 micrographs), 24 h Δ*phaP* cultures (276 cells from 13 micrographs) and 24 h Δ*phaR* cultures (182 cells from 10 micrographs). The diameter of granules was measured in mm and converted into nm using the scale bar. While measuring an accurate diameter of granules requires serial slicing and tomography, measuring the range of diameters of hundreds of granules can provide a range in which the typical granule falls.

3.3 Results

3.3.1 Growth of wt *C. crescentus* in nitrogen-limited medium

In order to characterize PHB accumulation in *C. crescentus*, it was first necessary to identify suitable and reproducible growth conditions. Several media have been reported in the literature for growth of *C. crescentus* (*32*). The most common rich medium used in the laboratory is PYE, which contains 0.2% peptone, 0.1% yeast extract, 0.5 mM $CaCl_2$ and 1 mM $MgSO_4$. At peptone concentrations higher than 0.5%, cells become unusually elongated, thus PYE is suitable for growth of *C. crescentus* because it is low in nutrients compared to typical rich media (*15*). Several minimal media have also been reported for growth of *C. crescentus* *(32)*. Growth in M2 minimal medium was first reported by Johnson and Ely in 1976 and is now the most common medium for growth of cultures on defined minimal medium (*33*). *C.*

crescentus can utilize a variety of compounds as its sole carbon source, the most common of which in laboratory cultures is glucose. These guidelines as well as previous studies discussed below informed our preliminary examinations of growth conditions.

Two preliminary growths were carried out. The first growth reproduced the results of Qi and coworkers, who reported PHB accumulation in *C. crescentus* to ~18% cdw after 60 h growth at 30 °C in PYE medium lacking Ca^{2+} and supplemented with 1% glucose, referred to as PYE(-) medium (*16*). Their rationale for choosing PYE(-) was not clear from the paper; however' earlier studies suggested a role for Ca^{2+} in phosphate uptake into the cell. Therefore, Ca^{2+} starvation may indirectly cause phosphate limitation (*34*). To reproduce their results, 50 mL PYE cultures in 500 mL baffled flasks were grown to saturation (~15 h, OD_{600} = 1.4) and the cells pelleted and washed with 0.85% saline. PYE(-) cultures (grown in duplicate in 2.8 L baffled flasks) were inoculated with the washed cells and grown 24 h. The two cultures reached a final OD_{600} = 4.3 and contained 18 and 24% PHB cdw.

The second set of preliminary growth conditions reproduced the results of Dr. Chris Brigham (Sinskey lab at MIT), who reported PHB accumulation to ~19% cdw in a modified M2 salts minimal medium supplemented with 1% glucose, referred to as modified M2G (Brigham, unpublished data). In this media the concentration of NH_4Cl was reduced to 2.3 mM, 25% of the concentration in the standard growth conditions. Modified M2G medium was adapted from growth conditions previously used to study gene expression in *C. crescentus* during nitrogen limitation (*35*). To reproduce Brigham's results, 50 mL PYE cultures in 500 mL baffled flasks were grown to saturation, pelleted and washed in 0.85% saline. The washed cells were then used to inoculate 2 x 1 L modified M2G cultures in 2.8 L flasks. The cultures were grown 24 h and at this time were saturated at an OD_{600} = 0.7. The two cultures contained 6.5 and 16% PHB cdw.

These preliminary studies suggested that while Brigham's results in M2G could be reproduced to induce PHB accumulation, the growth protocol did not produce consistent results between two cultures. Furthermore, while Qi and Rehm's PYE(-) protocol afforded greater cell masses for a given culture volume, the exact nature of nutrient limitation was not clear in this medium. Therefore, even though modified M2G medium resulted in lower cell masses, it was pursued in our studies, and will henceforth be referred to as PHB_p (PHB production) medium.

Initial attempts to conduct time course studies of growth and PHB production in wt cells grown in PHB_p medium were complicated by the fact that the cultures had long and variable lag phases of 4-12 h preceding logarithmic growth. It was therefore necessary to develop an inoculation protocol in which reproducible lag phases in growth could be achieved. In this protocol, which is outlined in Figure 3.3, single colonies grown on PYE/agar plates were used to inoculate 50 mL PYE cultures in 500 mL baffled flasks, which were grown overnight to saturation. A second set of 50 mL PYE "starter cultures" was then inoculated with 2 mL of the saturated overnight culture, and grown to early log phase (OD_{600} = 0.15, 4-5 h post inoculation). Finally, 500 mL PHB_p cultures in 4 L baffled flasks were inoculated directly with 25 mL of starter culture (without first rinsing cells in saline to remove PYE).

Several aspects of this protocol contribute to the reproducibility of growth. First, oxygen limitation can lead to filamentous cells and irregularities in cell division (*32*), therefore cultures were always grown in baffled flasks with 7-10x volume in head space relative to the culture volume. Second, inoculation of minimal medium with saturated cultures in stationary phase can lead to the long and variable lag phases observed in preliminary growths, thus PHB_p cultures were always inoculated with PYE starter cultures in early log phase. And finally, 500 mL PHB_p cultures were inoculated with 25 mL of PYE culture directly (i.e. without first washing the cells

with saline) to provide a small amount of "carryover" nutrients in the minimal medium. As a result of these modifications to the growth protocol, a reproducible lag phase of ~5 h and subsequent growth were achieved.

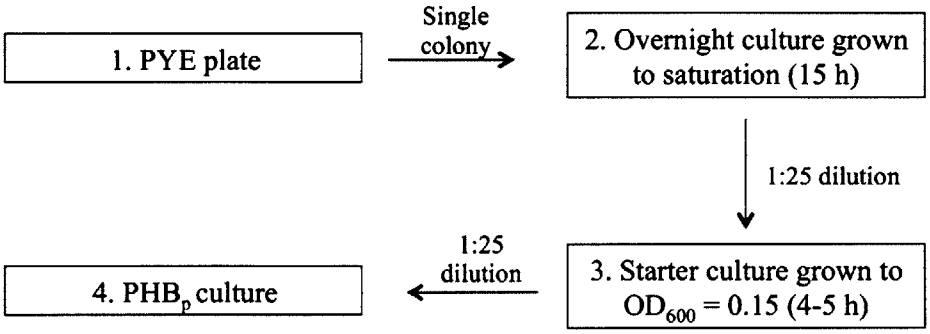

Figure 3.3 Schematic of growth protocol. All growth in liquid media was carried out at 30 °C with shaking at 220 rpm. Individual colonies grown 2 days at 30 °C on PYE/agar plates were used to inoculate 50 mL liquid PYE cultures in 500 mL baffled flasks. These cultures were then grown overnight to saturation. Two mL of overnight culture was then used to inoculate 50 mL liquid PYE starter cultures in 500 mL baffled flasks. These starter cultures were grown 4-5 h until they reached an OD_{600} = 0.15. The starter cultures were then diluted 1:25 into 500 mL of PHB_p growth medium in 4 L baffled flasks for growth and PHB accumulation.

Having optimized the growth conditions, the growth and PHB levels in wt *C. crescentus* grown in PHB_p medium were measured in three separate cultures. Following a 5 h lag phase, the cultures grew with a doubling time of 3 h until OD_{600} = 0.6 (after 15 h), then continued to grow more slowly (Figure 3.4). After prolonged growth in minimal medium, nutrients are depleted and *C. crescentus* growth slows and the duration of the swarmer stage increases (*35*). This is reflected in the slowed growth from 15 h to 36 h. By 36 h the cultures reach an OD_{600} = 1.0, and little to no additional growth is observed to 72 h.

Samples were taken between 0-72 h to analyze PHB content of the cells by the crotonic acid assay. PHB accumulates during both the log phase (5-15 h) and the later slow growth phase (15-36 h). The amount of PHB in the cells increases from 1 ± 0.2% cdw at 0 h to 11 ± 1.8% after 36 h (Figure 3.4). Interestingly, at the early time points the cells contained at least 5x less PHB

than *R. eutropha* contains at its minimum, allowing us in this system to monitor PHB production at the granule initiation phase. From 36 h to 72 h, the cells did not accumulate additional PHB. In these growths the cells accumulated less PHB than in the preliminary growths reproducing Brigham's results. The discrepancy between PHB levels might reflect the fact that the flasks used in the preliminary growths had a smaller head space. Thus, the cultures were likely inadvertently O_2-limited in addition to being limited in nitrogen, which may have resulted in higher PHB levels.

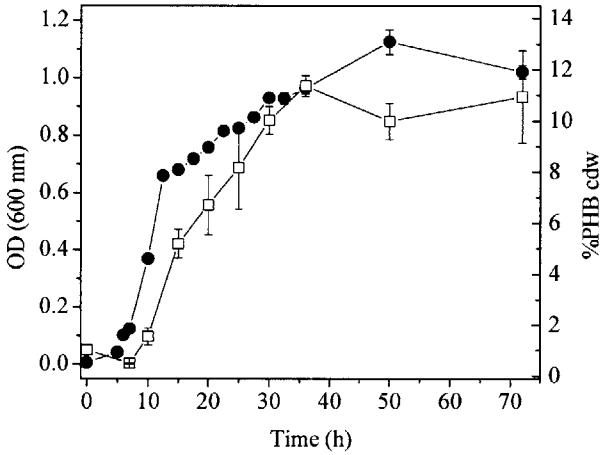

Figure 3.4 Growth and analysis of PHB levels in wt *C. crescentus* grown in PHB_p growth conditions. The OD_{600} (•) and amount of PHB (% cdw) (□) were measured at the indicated growth times. Error bars are standard deviation from the mean of samples from three different cultures.

3.3.2 Isolation of granules allowed identification of granule-associated proteins

Granules from the above growth conditions were isolated by glycerol density gradient ultracentrifugation to determine if proteins involved in granule biogenesis could be identified. Identification of proteins associated with PHB granules can be problematic and the method of granule isolation must be carefully considered. Isolation methods that are too harsh might promote dissociation of important factors, precluding their identification. On the other hand, gentler isolation methods can result in the non-specific co-purification of proteins that are not

involved in granule biosynthesis. This problem is especially an issue when considering the hydrophobic nature of PHB granules, which tends to promote non-specific adsorption of proteins. Therefore, granule-association alone does not necessarily indicate a protein is involved in PHB biosynthesis.

In spite of these complications, granule association of proteins that are homologs to known PHB biosynthetic proteins can be informative. A putative phasin (PhaP), intracellular depolymerase (PhaZ), and homolog of PhaR from *R. eutropha* are annotated in the *C. crescentus* genome. This annotation is based on their sequence similarity to homologs in other organisms. However, these proteins have not been previously characterized. Phasins, PhaRs and depolymerases have been shown to be granule associated in several organisms (*1, 3, 36-38*). Therefore, to determine whether any or all of these proteins are present on granules in *C. crescentus*, they were isolated from wt cultures grown in both PYE(-) and PHB_p medium. The results from a culture grown 24 h in PHB_p medium are shown in Figure 3.5, but they are representative of results achieved in both growth conditions. All purification steps were carried out at 4 °C. The cells were first lysed by French pressure cell, then the granules were purified from the insoluble lysate fraction by ultracentrifugation over a glycerol density gradient. Three bands, at the interfaces of the 40% and 70% glycerol layers, the 70% and 80% glycerol layers, and the 80% and 90% glycerol layers (Figure 3.5A), were collected individually with syringes. The proteins were resolved by 15% SDS-PAGE then transferred to a PVDF membrane, which was stained with Coomassie to visualize the proteins (Figure 3.5B). Several protein bands in the material from the 40%/70% glycerol interface (Figure 3.5B, lane 3) were excised and sent for sequencing by N-terminal Edman degradation. These bands are indicated with asterisks in Figure

3.5B. The results were compared to sequences found in the *Caulobacter crescentus* CB15 genome (*39*).

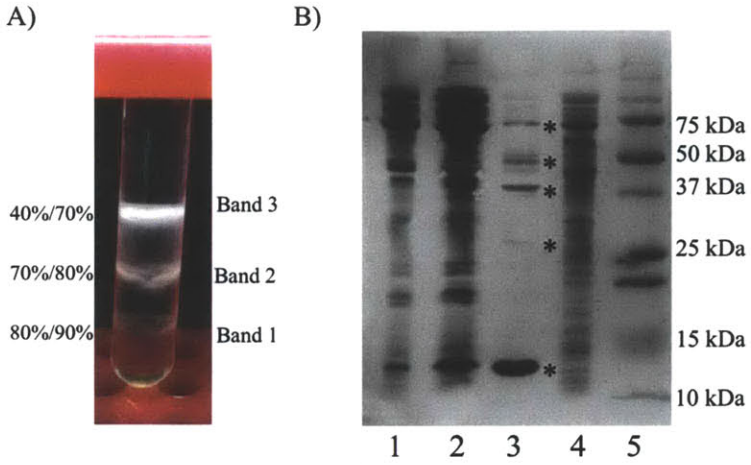

Figure 3.5 Granule isolation by glycerol density gradient ultracentrifugation and SDS-PAGE (15%) analysis of proteins associated with isolated PHB granules. Granules were isolated from cultures following 24 h growth in PHB_p medium. A) Glycerol density gradient ultracentrifugation to isolate PHB granules from insoluble cell material. The gradient of 40%, 70%, 80% and 90% glycerol was prepared in 100 mM Tris, 1 mM EDTA, pH 8.0. The interfaces of these layers are represented next to the gradient as 40%/70%, for example. B) SDS PAGE (15%) analysis of granule-associated proteins isolated from the different interfaces of the gradient in A. Lane 1, protein content of band 1. Lane 2, protein content of band 2. Lane 3, protein content of band 3. The asterisks indicate the bands sent for sequencing. Lane 4, soluble cell-free extract. Lane 5, molecular weight standards.

The protein migrating just below the 15 kDa protein marker present in all three samples was noticeably enriched in the topmost, whitest band (Band 3) that sedimented at the interface of the 40% to 70% glycerol layers (Lane 3, Figure 3.5B). The band was excised and sent for sequencing, and the 5 N-terminal amino acids of the protein were AAAEN. This sequence is present in the database in CC_2160 (accession number NP_490263), annotated as "PHB-granule associated protein, phasin." The sequence AAAEN is found at position 49 of CC_2160, which is annotated as a 20 kDa protein of 191 amino acids. However the protein as isolated attached to PHB granules migrates as a ~15 kDa protein (Figure 3.5B). Furthermore, Western blot analysis of this protein, discussed below, confirms that it is ~15 kDa in whole cells. The annotation

appears to be incorrect in the database with methionine 48 being the correct translational start site for the protein. This protein will be referred to as PhaP in the remainder of this thesis. A BLAST search using the PhaP amino acid sequence does not identify additional phasin-like proteins in the *C. crescentus* genome. Furthermore, BLAST searches using the sequences of PhaP1, 2, 3, 4 and 5 from *R. eutropha* neither identifies PhaP nor any additional phasin candidates (*3, 40, 41*). This is perhaps not surprising, because PhaP1 and PhaP share only 22% sequence identity and differ in M_w by 5 kDa. The phasins from *Azospirillum* sp. B510 and *Sinorhizobium meliloti* are both ~15 kDa in M_w and share 37% and 39% sequence identity with PhaP from *C. crescentus*, respectively. A BLAST search using the sequence of these phasins identifies PhaP but no additional phasin candidates. Thus, it is likely that *C. crescentus* has only a single phasin, which we have identified by its granule association. Recently, an additional PHB granule-associated protein, PhaM, was identified in *R. eutropha* (*42*). The authors proposed that PhaM is responsible for associating PHB granules with the nucleoid in order to promote even segregation of granules between daughter cells during division. Neither SDS-PAGE analysis nor BLAST using PhaM from *R. eutropha* identified a homologous protein in *C. crescentus*. In fact, homologs of PhaM are absent from all sequenced α-proteobacteria genomes (including *C. crescentus*) and seem to be exclusive to the β-proteobacteria.

The faint band at ~25 kDa was also analyzed and contained the sequence SENPE. This sequence is found in the listing CC_0509 (accession number NP_419328), annotated as a 23.8 kDa "hypothetical protein" containing a "PHB/PHA accumulation regulator DNA-binding domain." This protein has 29% sequence identity to PhaR from *R. eutropha* and will be referred to as PhaR in the rest of this thesis. The corresponding gene *phaR* is located in the *C. crescentus* genome immediately upstream of genes whose products are annotated as PhaA and PhaB, the

putative β-ketothiolase and NADPH-dependent reductase, respectively, required to make (*R*)-HBCoA, in the PHB biosynthetic pathway. The association of PhaR with PHB granules and its homology to PhaR from *R. eutropha* suggests a role in PHB biosynthesis, which we have explored in these studies.

The strong band at ~37 kDa contained the sequence MVSFLT and was identified as an uncharacterized, conserved protein. This protein has 23% homology to a protein from *Oceanicola batsensis* annotated as NADH:ubiquinone oxidoreductase 41 kDa complex I subunit. The observation that it co-purifies with granules may be due to its membrane association rather than specific granule association. This band is a major granule-associated protein in granule isolations from PYE(-) cultures as well (data not shown). This finding illustrates the caution that must be taken when interpreting results from granule isolation experiments.

A band at ~50 kDa was excised and submitted for Edman sequencing revealing the amino acids MLYAL. This sequence is found starting at position 8 in the listing CC_0250 (accession number NP_419069), which is annotated as a 48 kDa "polyhydroxyalkanoate depolymerase, intracellular." As is the case with the PhaP sequence, the listing in the database may have identified the incorrect start methionine in CC_0250. The observation that this protein is associated with the PHB granule supports the annotation as a PHB depolymerase, as it is known in several other systems that depolymerases are constitutively expressed and associated with PHB granules (*14*). Furthermore CC_0250 shares 45% homology with PhaZa1 from *R. eutropha*. A BLAST search using the CC_0250 sequence does not retrieve other putative PHB depolymerases, nor does use of any of the *R. eutropha* depolymerases (PhaZal, PhaZa2, PhaZa3, PhaZd) as search vehicles in BLAST reveal any additional depolymerases. Using the 78 kDa *R. eutropha* oligomer hydrolase PhaZb as a BLAST template does not reveal a homolog in *C.*

crescentus. However, using the oligomer hydrolase PhaZc for BLAST reveals that *C. crescentus* contains several proteins containing α/β hydrolase domains that are 30-40 kDa in M_w. None of these has been characterized so their involvement in PHB biosynthesis is unknown. Finally, an additional putative depolymerase, CC_0847 (accession number NP_419664.1), was identified using the sequence of a protein annotated as an extracellular depolymerase in *Pseudomonas stutzeri* (accession number ACG63775) as a search vehicle in BLAST. CC_0847 is annotated as a 35 kDa "hypothetical protein" containing an esterase lipase domain and an LqpC domain, which contains the lipase box (GxSxG) that is characteristic of intracellular PHB depolymerases.

Sequencing of the band that migrates at ~75 kDa gave DDQKA, which is found beginning at position 23 in a protein annotated as a 70 kDa outer membrane cobalamin receptor protein. As with the 37 kDa protein described above, this protein is likely present in the granule-containing fraction resulting from contamination with membrane material.

Compared to *R. eutropha*, which has at least five phasins, up to seven intracellular depolymerases, and two 3-hydroxybutyrate oligomer hydrolases, *C. crescentus* appears to use a "simpler" set of PHB biosynthetic proteins, having only a single phasin and one intracellular depolymerase as well as an additional putative depolymerase.

3.3.3 Construction of *phaC*:km, Δ*phaP*, Δ*phaR* strains

In order to investigate the role of PhaP in PHB accumulation, three mutant strains were constructed. The strain *phaC*:km, a disruption strain in which a km resistance marker is inserted in the middle of *phaC*, was constructed because several attempts to generate the clean deletion strain of *phaC* were unsuccessful. The clean deletion strains Δ*phaP* and Δ*phaR* were successfully prepared. The mutations of all strains were confirmed by PCR screening and/or

sequencing, and Western blot analysis of *phaC*:km and Δ*phaP* with anti-PhaC and anti-PhaP antibodies, respectively, further confirmed the deletions.

3.3.4 Generation and characterization of antibodies against PhaC and PhaP

Antibodies to PhaP and $PhaC_{Cc}$ were generated from purified recombinant PhaP and $PhaC_{Cc}$ and used for Western blot analysis of expression levels of PhaP and PhaC during PHB accumulation. $(His)_6$-tagged $PhaC_{Cc}\Delta N$ and PhaP were expressed recombinantly in *E. coli*, purified by Ni-affinity chromatography as described in Chapter 2, and sent for generation of rabbit polyclonal antibodies. Antibodies were used without further purification.

We first characterized the antibodies to $PhaC_{Cc}$ to determine the M_w of $PhaC_{Cc}$ *in vivo*. As discussed above, studies by Qi and coworkers led them to conclude that *C. crescentus* expresses a 73 kDa class I synthase based on cross-reactivity between anti-$PhaC_{Re}$ antibodies and a band migrating at ~75 kDa in *C. crescentus* crude extracts (*16*). However, the cross-reactivity between their $PhaC_{Re}$ antibodies and $PhaC_{Cc}$ was poor and it is difficult to draw a strong conclusion from their data (see section 1.5.3). Our antibodies to $PhaC_{Cc}$ were not very sensitive and PhaC is present at low amounts in the cells (discussed below). At a dilution of 1:2000, the PhaC antibody cross-reacted with several bands. Western blot analysis of wt cells in comparison with *phaC*:km cells however, identified a strong band that migrated at the position of a His_6-PhaC standard (75 kDa) that was not present in *phaC*:km (Figure 3.6). Its position relative to the 75 kDa His_6-PhaC standard suggests that the synthase is in fact the longer 73 kDa protein. This conclusion is supported by *in vitro* assays of $PhaC_{Cc}$ and His_6-$PhaC_{Cc}\Delta N$ in Chapter 2, in which the former was shown to have 50-fold higher activity than the latter.

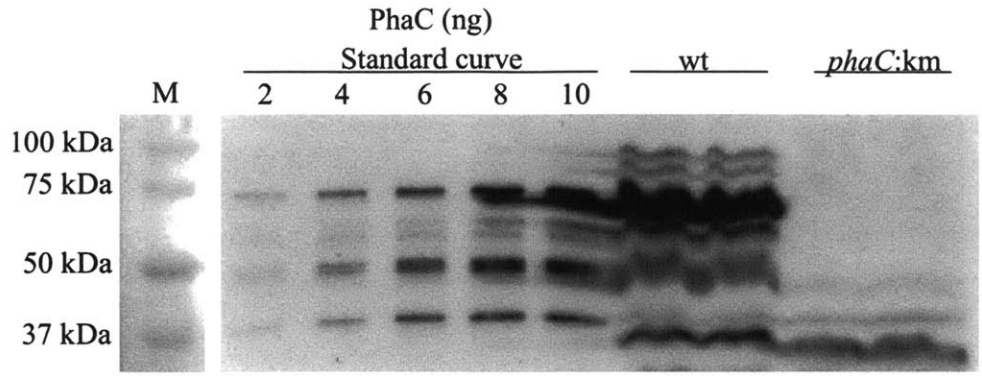

Figure 3.6 Anti-PhaC Western blots of wt and *phaC*:km. Each lane contains 3 x 10^8 cells. Samples (two of each) were taken from a single culture of each strain grown 24 h in PHB_p. The standard curve was prepared from recombinantly purified His_6-PhaC.

Preliminary PhaP Western blots revealed that antibodies to PhaP were highly specific and did not cross-react with other bands in whole cell samples of *C. crescentus*. They were used without further purification at a dilution of 1:5000.

3.3.5 The M_w of PHB is high throughout growth in PHB_p

We next wished to quantitatively characterize levels and changes in levels of PHB, PhaP and PhaC during growth in PHB_p. The M_w and PDI of PHB in wt cells at various points in PHB accumulation were first examined. PHB from cells grown 5 h in PYE (starter culture, 0 h time point in Figure 3.4) and 10 h, 20 h and 40 h in PHB_p medium was extracted into chloroform for GPC analysis. The extraction efficiencies varied from 20-55% (Table 3.3). Several issues affect the extraction efficiency. Cells grown 0 h or 10 h in PHB_p contain only ~1% PHB cdw, and extraction of very small amounts of material from large cell mass typically results in low recovery. To increase yield, each of the lyophilized cell samples from 0 h and 10 h time points (~70 mg per sample) were split into 20 mg fractions, which were individually refluxed in chloroform. The PHB extracted from all fractions of a given sample was then combined for GPC analysis. This approach improved the extraction efficiency considerably: when PHB was

extracted from 70 mg lyophilized cells, the recovery was typically ~10% (data not shown), while in 20 mg fractions the recovery increased to 30-50% (Table 3.3).

The M_w and PDI were determined by comparison to a standard curve generated from polystyrene standards. Each time point was measured in triplicate from three individual cultures. The GPC analysis indicates that the M_w of PHB is ~325 kDa throughout growth. Even at very early time points in PHB_p growth conditions, when PHB is only ~1% cdw, the M_w of the PHB is high and the PDI is ~2 (Figure 3.7). This result is similar to what was previously reported in *R. eutropha* in cells that contain only 5% PHB: its M_w is ~700 kDa, compared to ~1,000 kDa when the cells contain 80% PHB cdw (*7*). As observed with *R. eutropha*, the elongation rate *in vivo* appears to be much faster than the initiation rate, giving rise to full length polymer even at the earliest time points. Furthermore, the similarities of the M_w of PHB throughout the time course suggest a built in mechanism for chain termination. The PDI remains ~2 from 0-20 h, but PHB extracted from cells grown 40 h has a higher PDI of ~4.5.

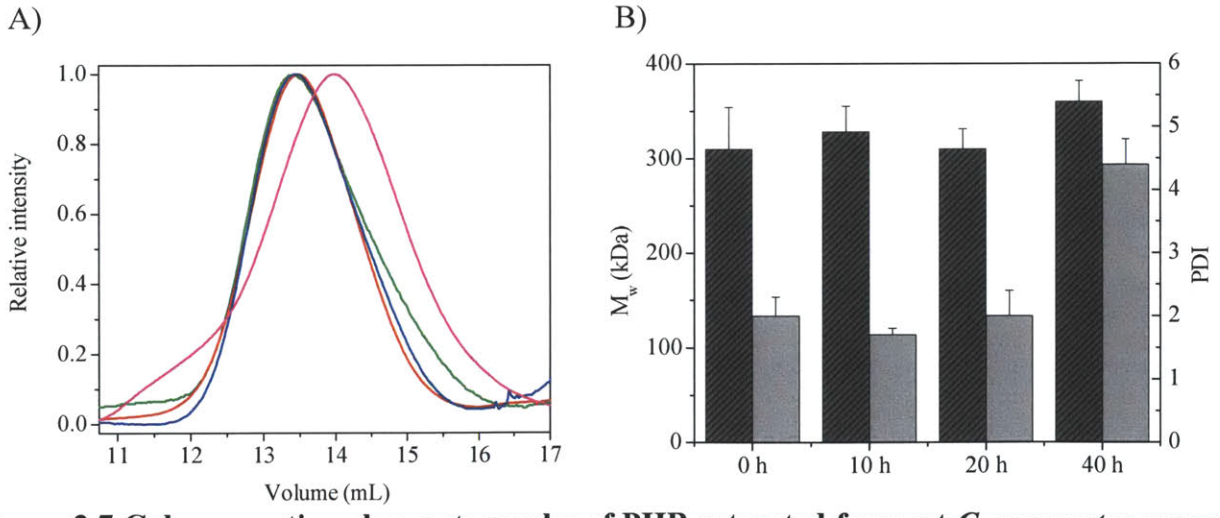

Figure 3.7 Gel permeation chromatography of PHB extracted from wt *C. crescentus* grown in PHB_p conditions. A) Overlay of representative GPC traces of PHB extracted from *C. crescentus* grown in PHB_p medium at the following time points: 0 h (green), 10 h (red), 20 h (blue), 40 h (magenta), B) M_w (striped) and PDI (gray) of PHB from 0-40 h. Error bars are the standard deviation from the mean of three separate samples, each taken from a different culture.

Table 3.3 Percent PHB extracted from lyophilized *C. crescentus*.

Strain	Growth time (h)	%PHB extracted[a]	M_w	PDI
wt	0	53 ± 11	310 ± 44	2.0 ± 0.3
	10	31 ± 7	330 ± 27	2.0 ± 0.4
	20	55 ± 10	310 ± 21	2.0 ± 0.4
	40	36 ± 6	360 ± 22	4.4 ± 0.4
Δ*phaP*	24	26 ± 6	430 ± 28	2.1 ± 0.6
Δ*phaR*	24	21 ± 3	270 ± 21	1.8 ± 0.2

[a]Extraction efficiency was determined by crotonic acid assay.
Error bars are the standard deviation from the mean of extraction from three samples, each taken from a different culture. The values for the individual samples are provided in Table A3.1 in the Appendix.

3.3.6 Molecules per cell of PHB, PhaC and PhaP in wt *C. crescentus* as a function of growth

Comparison of the concentrations of PHB, PhaC and PhaP per cell can provide insight into the roles of PhaC and PhaP in PHB accumulation. To determine concentrations per cell, it was first necessary to establish a method for determining the number of cells in a given sample. This was done by normalization of cell concentrations based on OD_{600}. Typically, cells of a known OD_{600} were serially diluted and the cells counted by plating on PYE/agar. Subsequently, an $OD_{600} = 1$ was assumed to be 1.1×10^6 cells/μL. Because the maximum concentration of PHB accumulated was ~10% cdw, it was assumed that it does not contribute to OD_{600} (*43*). Knowing the concentration of cells and the concentrations of PHB, PhaC and PhaP during growth on PHB_p medium from 0-72 h, the number of molecules of each species per cell was calculated.

From the mass of PHB per cdw and its M_w, the number of molecules of PHB per cell was calculated and was found to increase ~10-fold from 14,000 ± 160 PHB chains per cell at 0 h to 150,000 ± 25,000 chains per cell at 72 h post inoculation (Figure 3.8). The M_w of PHB in *R. eutropha* is ~700 kDa when the cells contain 5% cdw of PHB, which corresponds to ~14,000 molecules per cell (*7*).

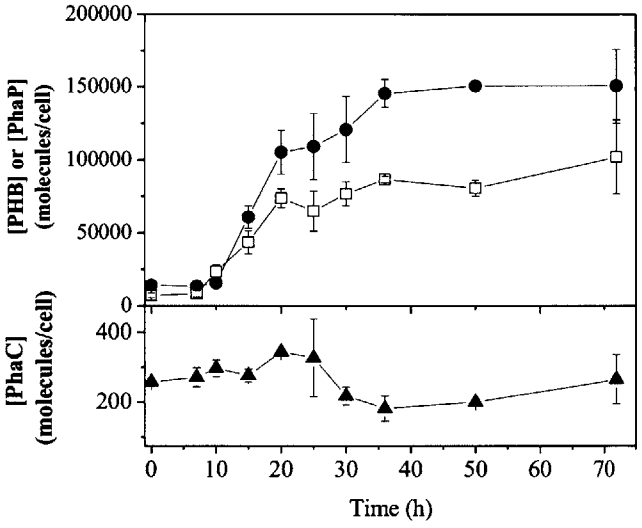

Figure 3.8 Concentrations of PhaC (▲), PhaP (□) and PHB (●) in wt PHB_p cultures. The numbers were calculated from quantitative Western blot analysis of PhaP and PhaC levels and from GPC analysis of PHB molecular weight. The M_w of PHB used to calculate the ratios was 325 kDa. Each measurement was made in triplicate. The error bars reflect the standard deviation from the mean of these measurements. The data for the individual replicates are included in Table A3.2 as an appendix to this Chapter.

Regardless of growth conditions or PHB content, PhaC in *R. eutropha* is constitutively expressed at 2,000-6,000 molecules per cell (*7, 44*). To investigate whether the same is true in *C. crescentus*, the expression levels of $PhaC_{Cc}$ in the wt strain were examined by Western blot analysis (Figure 3.9). The results indicate that throughout growth, PhaC levels remain between 200-400 molecules/cell (Figure 3.8). Thus, while the levels of PhaC in *C. crescentus* are about one order of magnitude lower than in *R. eutropha*, they also remain constant through PHB accumulation.

In order to investigate whether PhaP expression levels correlate with PHB levels in *C. crescentus*, as is the case in *R. eutropha*, Western blot analysis of PhaP levels was carried out (Figure 3.10). From 0-72 h PhaP levels increase from 7,000 ± 1,500 molecules per cell at 0 h to 103,000 ± 25,000 molecules/cell at 72 h, about a 15-fold change (Figure 3.8A). In *R. eutropha*,

PhaP levels increase ~16-fold from 11,000 to 180,000 molecules per cell (*7*). In contrast with PhaC levels, absolute PhaP concentrations in the two organisms are very similar.

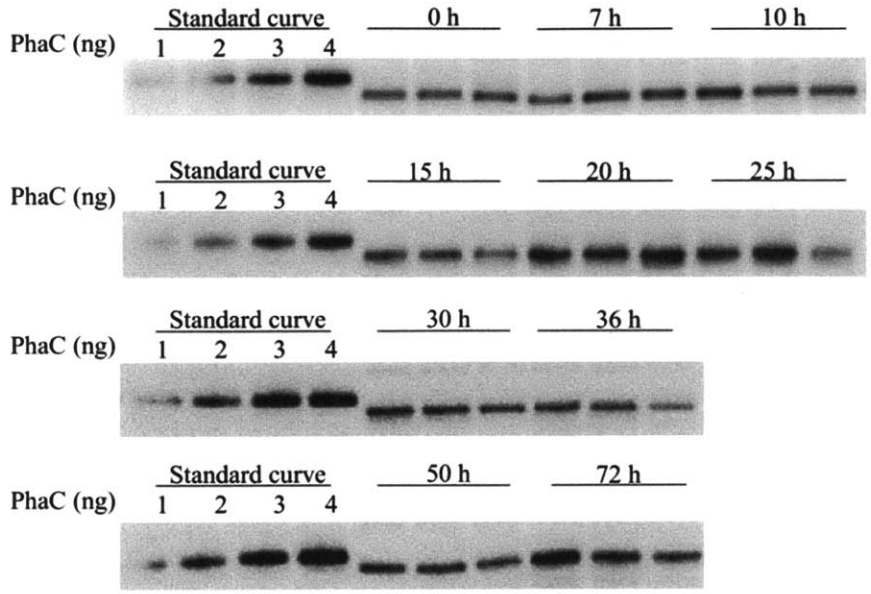

Figure 3.9 Anti-PhaC Western blot of wt *C. crescentus* grown in PHB_p medium. All sample lanes contain 1.9 x 10^8 cells. It should be noted that the standard curve in this figure is prepared from His_6-PhaC (75 kDa), thus it migrates at a slightly higher M_w than PhaC (73 kDa) in the samples. Furthermore the standards are not spiked with an equal number of *phaC*:km cells. Samples were taken at each time point from three individual cultures.

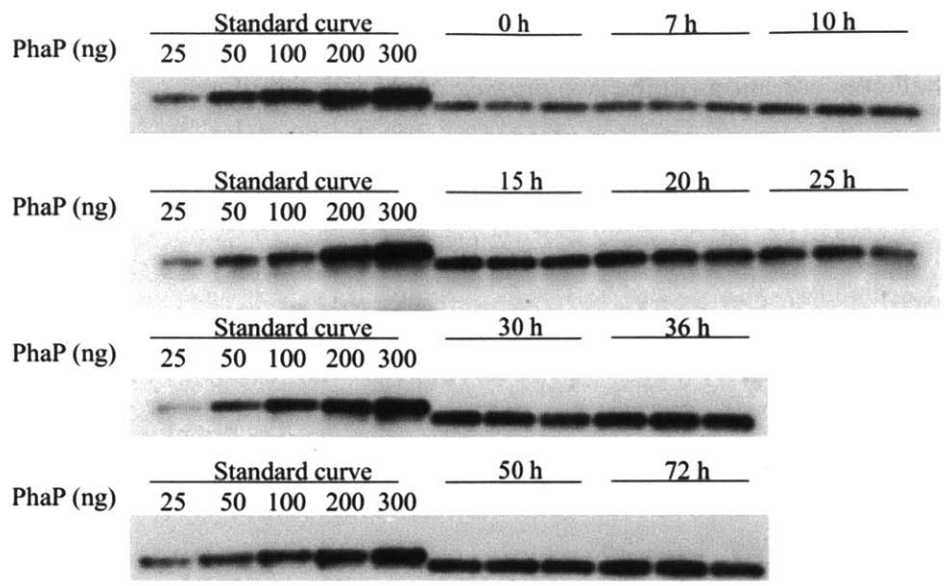

Figure 3.10 Anti-PhaP Western blots of wt *C. crescentus* grown in PHB_p. The standard curve was prepared from recombinantly purified PhaP and each lane of the standard curve contains 7.5 x 10^7 cells of Δ*phaP*. Each sample lane contains ~7.5 x 10^7 cells. Samples were taken at each time point from three individual cultures.

3.3.7 Mole ratios of PhaC and PhaP to moles of PHB in PHB_p

Having determined the molecules of PHB, $PhaC_{Cc}$ and PhaP per cell, the mole ratios of PHB/PhaP and PHB/PhaC throughout growth were calculated. The mole ratio of PHB to PhaP provides insight into the *in vivo* role of PhaP in granule biogenesis in *C. crescentus*. This ratio remains between 1-2 throughout growth in PHB_p, indicating that PhaP plays an important mechanistic role in PHB production (Figure 3.11). This striking ratio has also been observed in *R. eutropha* grown in both rich and nitrogen-limited media, further strengthening the argument that this stoichiometry is mechanistically important to understanding the role of PhaP in granule formation (*7, 17*) (He and Stubbe, unpublished data). This role will be addressed in more detail in the Discussion section. Because there are ~300 PhaCs per cell throughout PHB accumulation, the moles of PHB/PhaC increases ~10-fold from 50 to 500, indicating that multiple termination

and reinitiation events occur throughout growth (Figure 3.11). This is similar to what we have observed in *R. eutropha*, in which the mole ratio of PHB/PhaC increases ~15-fold from 6-87 (*7*).

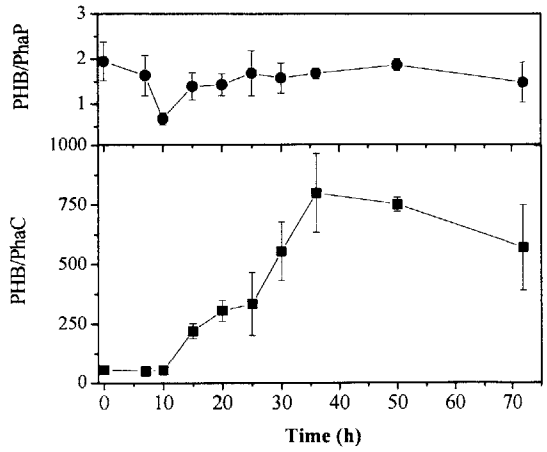

Figure 3.11 Mole ratios of PHB/PhaP and PHB/PhaC in wt *C. crescentus* grown in PHB_p. Error bars are propagated from the uncertainties in Figure 3.10.

3.3.8 PHB and PhaP are present in the soluble cell fraction in wt *C. crescentus* starter cultures

The modified micelle model for granule formation, currently our favored model, proposes that the species that nucleates granule formation is a soluble, cytoplasmic species containing PhaC, PhaP and full length PHB. We therefore wished to determine whether a portion of the PHB in starter cultures of wt *C. crescentus* is in the soluble cell fraction. To obtain sufficient cell mass, two cultures were grown 15 h until early stationary phase, and the cells were pelleted and resuspended in buffer. One culture was lysed, shell frozen and lyophilized, then the PHB was extracted into chloroform to prepare a sample for GPC analysis. The second culture was lysed, and whole cell samples for crotonate and Western blot were taken from the lysate. The soluble and insoluble fractions were subsequently separated by centrifugation, the insoluble

fraction was resuspended in buffer to a volume equal that of the soluble fraction, and samples were analyzed from each fraction by crotonate assay and Western blot using PhaP antibodies. Additionally, to determine the M_w of the PHB in both fractions, the remaining soluble and insoluble material was shell frozen and lyophilized, and the PHB was extracted into chloroform for GPC analysis. Scheme 2.1 shows a flow chart for the analysis of samples from the second culture.

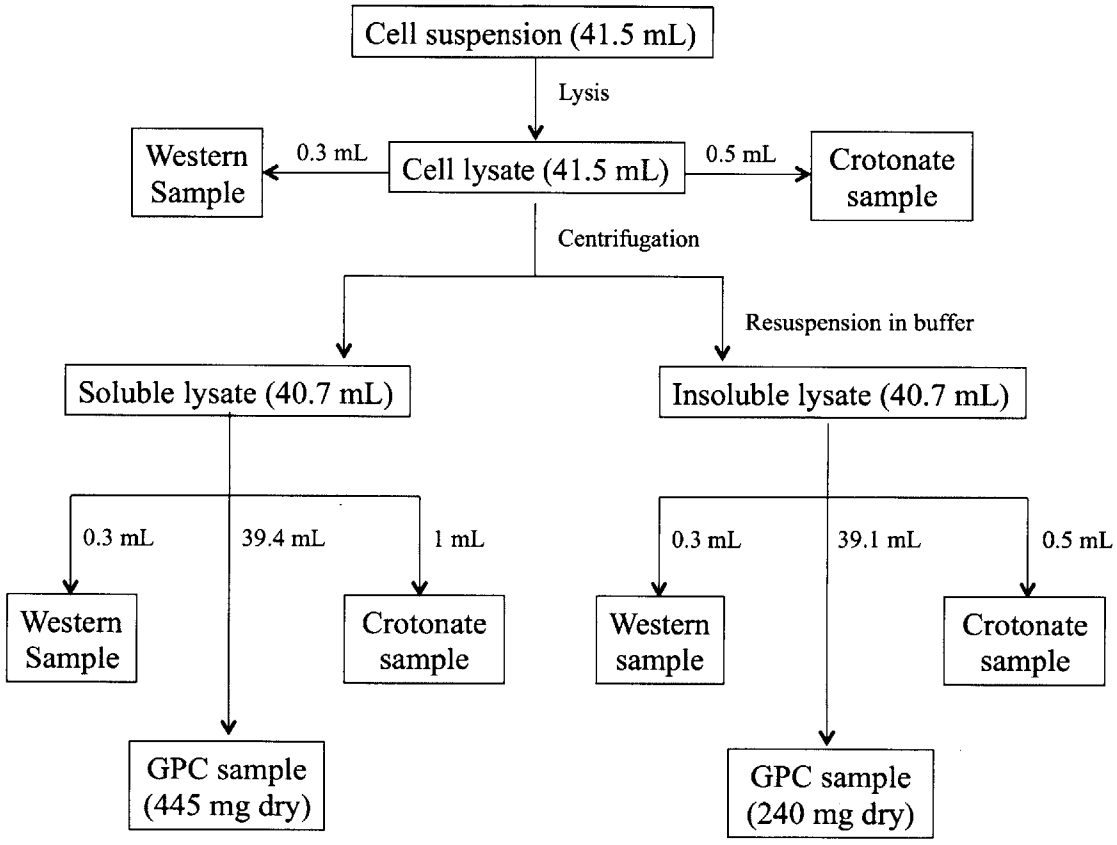

Scheme 3.1 Flow chart for crotonate, Western blot and GPC analysis of samples from whole cell, soluble and insoluble fractions of wt *C. crescentus*. Cells were grown 15 h in PYE then pelleted and lysed. Samples were taken for crotonate, Western blot and GPC analysis from the whole cell, soluble and insoluble cell fractions.

GPC analysis of the PHB in the whole cell sample from the first culture revealed that its M_w was 180 kDa with a PDI of 2.2 (Figure 3.12) (Table 3.4), slightly lower than the M_w of PHB

from the time point taken 9 h after inoculation into PHB_p medium. Crotonate analysis of PHB content of the whole cell lysate of the second culture revealed that whole cells contained 2% PHB cdw. Analysis of the soluble and insoluble fractions individually indicated that they contained 0.2% and 3.4% PHB by dry weight. As a percentage of the total PHB (by mass) in the cells, the soluble fraction contained ~7%, compared to ~90% in the insoluble fraction (Table 3.5). This result is similar to the percentage of total PHB present in the soluble fraction of the *R. eutropha* strain from which soluble PHB was isolated, which accounts for 10% of the total PHB in the cells by mass (*38*).

Table 3.4 M_w and PDI of PHB extracted from whole cell, soluble and insoluble fractions of wt *C. crescentus* grown 15 h in PYE. The measurements were made once from a single sample.

Cell fraction	%PHB extracted	M_w	PDI
Whole cell	40	180	2.2
soluble	33	196	2.0
insoluble	63	190	2.3

To compare the M_w of PHB in the soluble and insoluble fractions, and determine whether the soluble PHB was full length, it was extracted into chloroform for GPC and compared to the M_w of PHB in whole cells. The M_w of the PHB in the soluble and insoluble fraction were 196 kDa with a PDI of 2.0, and 180 kDa with a PDI of 2.2, respectively. Again, due to low quantities of PHB in all samples, extraction efficiencies were low (Table 3.4). However, the data suggest that the M_w of PHB in PYE starter cultures is lower than that in cultures accumulating PHB, and furthermore that the soluble fraction of cells at this time point contains PHB.

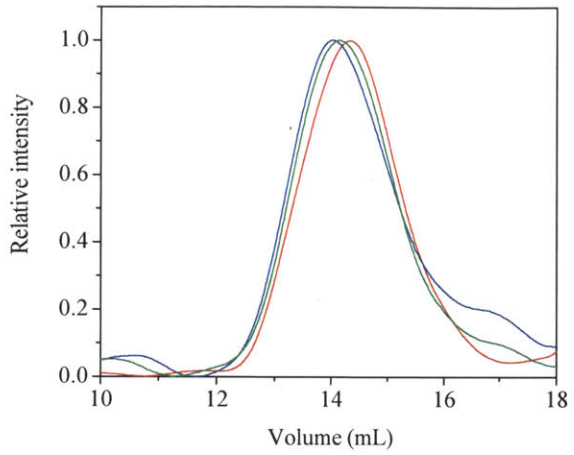

Figure 3.12 Gel permeation chromatography of PHB extracted from the whole cell (red), soluble (blue) and insoluble (green) fractions of *C. crescentus*. PHB was extracted from cells grown 15 h in PYE then lysed by French press.

Table 3.5 Summary of PhaP and PHB content of the whole cell, soluble and insoluble fractions of *C. crescentus* grown in PYE.

	Volume	PhaP (nmol)	% total PhaP	PHB (nmol)	% total PHB	Ratio of PHB:PhaP
Whole cell	41.5	40 +/- 3.8	100	63	100	1.6:1
Soluble fraction	41.5	4.8 +/- 0.7	12	4.1	6.5	0.9:1
Insoluble fraction	41.5	32 +/- 1.3	80	62	89	1.9:1

The soluble nucleating species isolated from *R. eutropha* contained an enrichment of PhaP molecules per PHB chain compared to the whole cell and insoluble fraction (*38*). We therefore examined the PhaP content in whole cell, soluble, and insoluble fractions by quantitative Western blot analysis (Figure 3.13). Using these data in combination with the mass of PHB in the cells and its M_w, the molar ratio of PHB to PhaP was calculated. The molar ratio of PHB to PhaP was 1.7:1 in whole cells, 0.8:1 in the soluble fraction, and 2:1 in the insoluble fraction (Table 3.5). While we have been able to isolate *C. crescentus* from growth conditions in

which it contains very little PHB, we are unable to measure an increase in PhaP relative to PHB chains at this early time point, as is suggested by observations in *R. eutropha* (*38*).

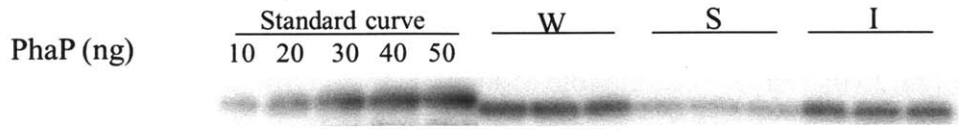

Figure 3.13 Quantitative Western blot analysis of PhaP content of whole cell (W), soluble (S) and insoluble (I) cell fractions of 15 h PYE starter cultures. The standard curve was prepared from recombinantly purified PhaP and each lane of the standard curve contains 7.5 x 10^7 cells of Δ*phaP*. Samples were taken in triplicate from one culture.

3.3.9 Deletion of *phaP* results in decreased PHB production compared to the wt strain

Growth and PHB accumulation in Δ*phaP* cultures was examined in triplicate to gain further insight into the role of PhaP in PHB biosynthesis in *C. crescentus* (Figure 3.14). In PHB_p medium Δ*phaP* accumulates PHB from 0.5 to 1.5% cdw, 10- to 20-fold lower than the wt strain under the same growth conditions. The cultures saturate at an OD_{600} = ~0.75, slightly lower than wt cells. In *R. eutropha*, deletion of *phaP1* results in decreased accumulation of PHB by 50% relative to the wt strain. In addition the PHB had lower M_w and higher PDI, 740 kDa with a PDI of 3.3, than in the wt strain. In order to determine whether deletion of *phaP* in *C. crescentus* affected the M_w and PDI of the PHB, Δ*phaP* was grown 24 h and the PHB was extracted into chloroform for GPC analysis. The M_w from three different cultures was 430 ± 28 kDa and the PDI was 2.1 ± 0.6 (Table 3.3). These values are very similar to those for the wt strain, indicating that the behavior of PhaP from *C. crescentus* has some distinct features relative to that of PhaP1 in *R. eutropha*.

Due to the fact that Δ*phaP* makes very low levels of PHB, it was necessary to isolate PHB from large masses of cells. Extraction efficiency decreases as the mass of cells increases,

thus the samples were divided into 20 mg portions of cells for extraction. The efficiency was still quite low, 20-30% of the expected quantity of PHB as predicted by crotonate assay analysis of whole cells (Table 3.3). It is possible that PHB of a particular M_w and PDI is preferentially extracted, a caveat that must be considered when interpreting the data. However, if the extracted material is indicative of all PHB chains, then the role of PhaP in chain termination is minimal in *C. crescentus*.

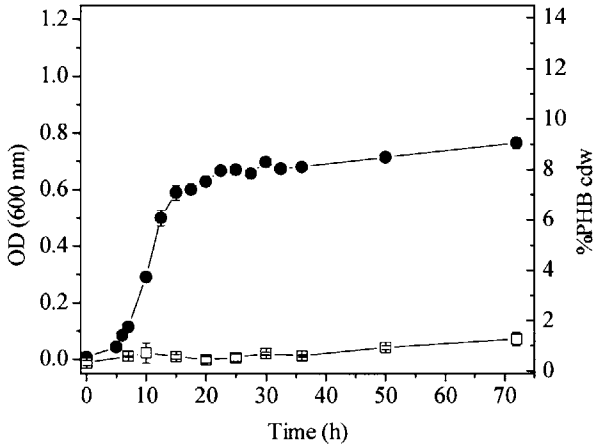

Figure 3.14 Growth and analysis of PHB levels in *C. crescentus* Δ*phaP* grown in PHB_p growth conditions. The OD_{600} (●) and amount of PHB (% cdw) (□) were measured at the indicated growth times. Error bars represent the standard deviation from the average of three growths.

3.3.10 Molecules of PHB and PhaC per cell in the Δ*phaP* mutant strain

If we make the assumption that the M_w of PHB in Δ*phaP* remains the same throughout growth, as is the case with the wt strain, then we can calculate the molecules of PHB per cell in Δ*phaP* as a function of growth. At 0 h in PHB_p medium the cells contain 5,100 ± 300 PHB chains per cell, and the concentration of PHB increases ~3-fold to 14,600 ± 1,300 after 72 h growth (Figure 3.15A) (Table A3.4).

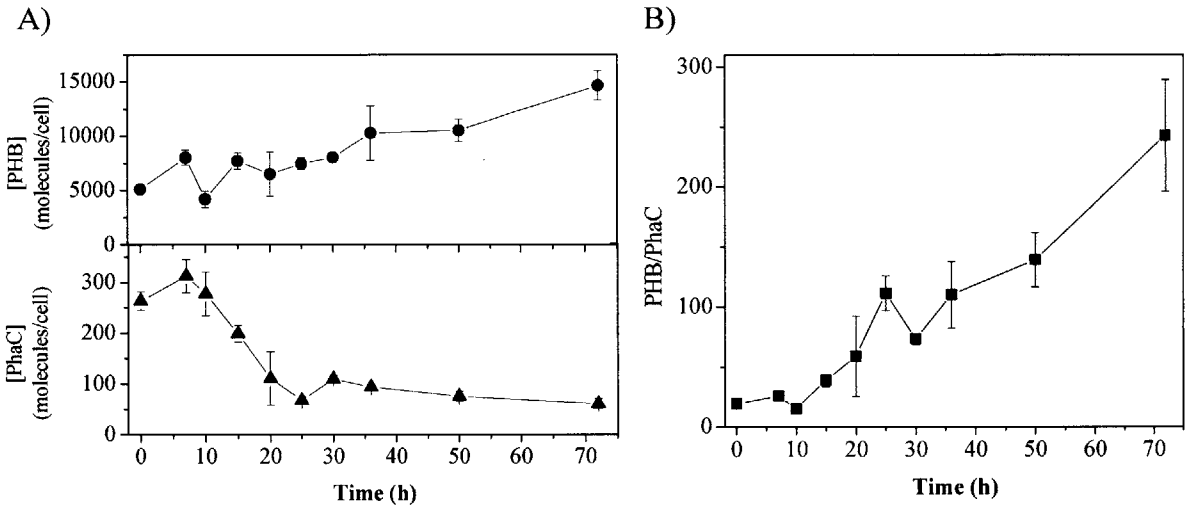

Figure 3.15 Quantitative analysis of PHB and PhaC levels in Δ*phaP* PHB_p cultures. A) Concentrations of PHB (●) and PhaC (▲) per cell. Values were calculated from quantitative Western blot analysis of PhaC levels and crotonate analysis of PHB levels from 0-72 h. The M_w of PHB used to calculate PHB molecules/cell (430 kDa) was determined by GPC from the average M_w of PHB extracted from three cultures grown 24 h in PHB_p. B) Mole ratio of PHB/PhaC. The error bars are propagated from the uncertainties in A. The data for the individual replicates are provided in Table A3.4 as an appendix to this Chapter.

To investigate whether reduced PHB accumulation in Δ*phaP* is the result of lower PhaC expression, PhaC levels during growth in PHB_p were determined by Western blot (Figure 3.16). The amount of PhaC per cell from 0-15 h was 200-300 molecules. However, after 15 h the amount of PhaC per cell steadily declined to ~60 molecules per cell at 72 h. Thus, while PhaC levels were initially similar to those in the wt strain, PhaC levels appeared to decrease with time. This observation raised the possibility that PhaC might be degraded in Δ*phaP* because it is inactivated as a function of polymerization due to the formation of unfolded hydrophobic polymer, as is suggested in assays presented in Chapter 2.

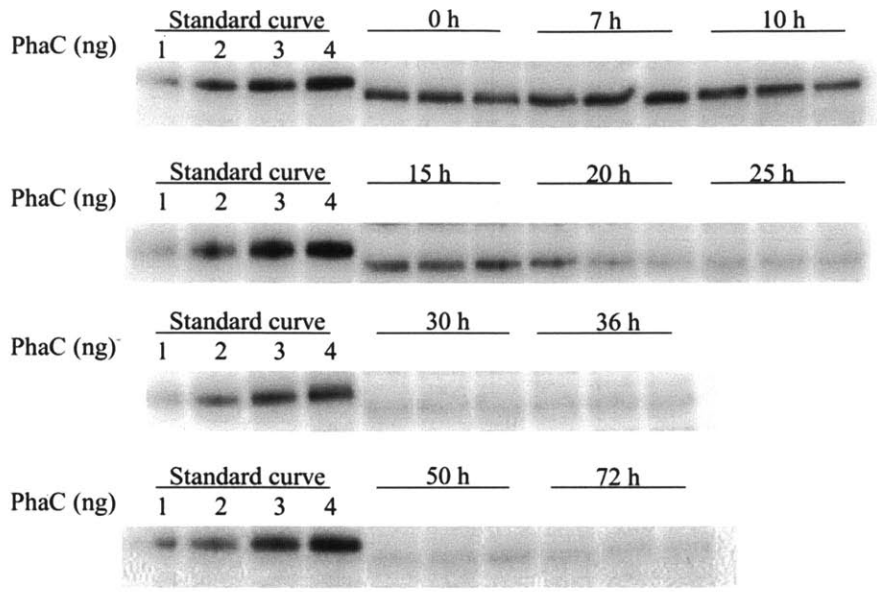

Figure 3.16 Western blot of $PhaC_{Cc}$ in Δ*phaP* cells grown 0-72 h in PHB_p. The standard curve is prepared from recombinant $PhaC_{Cc}$ and is not spiked with the disruption mutant *phaC*:km. Each lane contains ~7.5 x 10^7 cells. Samples were taken at each time point from three individual cultures.

3.3.11 *In vitro* assays of crude cell lysates of wt and Δ*phaP* cultures suggest that presence of PhaP enhances consumption of HBCoA

To investigate whether reduced accumulation of PHB by the strain Δ*phaP* is a result of inactivation of PhaC due to the presence of PHB that is not associated with PhaP, the activity of PhaC was measured in crude cell lysates of wt and Δ*phaP* grown to OD_{600} = 0.75 PYE. PYE growth conditions were selected over PHB_p medium because PHB levels are low and cell density is comparably high in PYE. In this experiment, wt cells contained 0.2% cdw and Δ*phaP* contained 0.1% PHB cdw, within error of one another. To achieve comparable cell density in cultures grown in PHB_p medium, the wt strain would contain ~10% PHB cdw whereas Δ*phaP* would contain only 0.5-1.5% PHB. This 10- to 20-fold difference in PHB levels might interfere with PhaC activity measurements by increasing the activity of PhaC in wt due to association with

PHB granules (or priming with PHB) instead of the presence of PhaP, thus PYE growth conditions were selected for this experiment.

To prepare assay samples, wt and Δ*phaP* cells were pelleted, resuspended in buffer and lysed by passage through the French pressure cell at 4 °C. The amount of PhaC in each strain was determined by quantitative Western blot analysis (Figure 3.17A). The wt strain and Δ*phaP* both contained ~200 molecules of PhaC/cell, consistent with the above findings that PhaC levels in the two strains are initially similar, but that levels in Δ*phaP* decrease during growth in PHB_p. CoA release by PhaC in samples of wt and Δ*phaP* lysate containing 14 ng PhaC was measured using the discontinuous DTNB assay (Figure 3.17B). Both the biphasic kinetics and the effect of PhaP seen in experiments on the recombinant proteins (Chapter 2) are observed with the native proteins as well. *In vitro* experiments using recombinant proteins have demonstrated that the presence of PhaP increases both the specific activity of PhaC and the overall turnover of HBCoA. This effect is clear in the crude cell extract assays of native PhaC in the wt and Δ*phaP* strains as well. PhaC in wt cell lysate turns over 50% more HBCoA than in Δ*phaP* cells under these experimental conditions, despite both containing the same amount of PhaC. This result suggests that lower PHB accumulation in Δ*phaP* may also be the result of the positive effect that PhaP has on the extent of the polymerization reaction by PhaC. Furthermore, we have interpreted the results of the *in vitro* assays with PhaP to suggest that PhaP promotes folding of the PHB chain that allows access of the soluble HBCoA to the active site of PhaC as the insoluble polymer grows. Therefore, one explanation for the decrease in PhaC levels is that in the absence of PhaP, PhaC might unfold due to association with the hydrophobic polymer, leading to its degradation by proteolytic machinery.

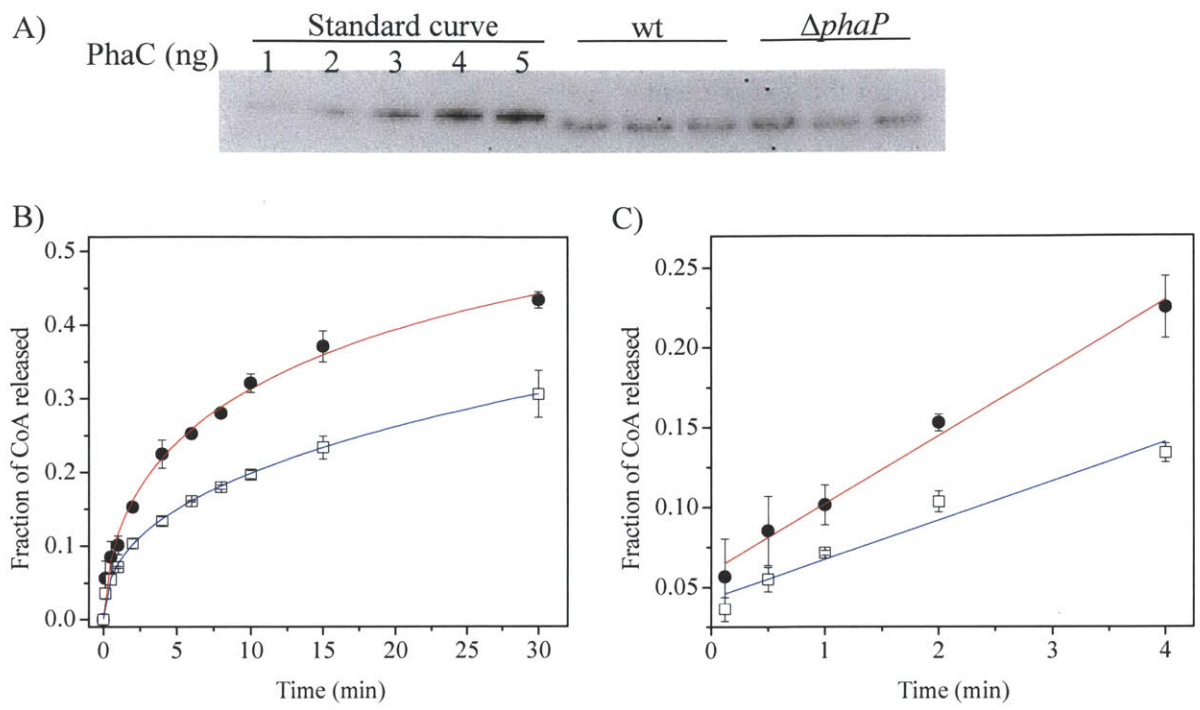

Figure 3.17 Specific activity of $PhaC_{Cc}$ in crude lysates of wt and Δ*phaP* cells. A) Anti-PhaC Western blot to measure amount of PhaC in wt and Δ*phaP* cell lysate samples. B) CoA release by PhaC in wt (●, red trace) and Δ*phaP* (□, blue trace) lysates. The reactions contained 40 µL lysate (~110 µg total protein, 14 ng $PhaC_{Cc}$) and 1 mM HBCoA. Data are fit to the sigmoidal function given in section 3.2.13. C) Expansion of early time points in B. Error bars represent the standard deviation from the average of three assays.

3.3.12 Deletion of *phaR* results in decreased PHB accumulation relative to wt

C. crescentus contains a putative homolog of PhaR, which was identified in this work as a granule-associated protein. To examine whether deletion of *phaR* has an effect on growth and PHB accumulation, Δ*phaR* was grown 0-72 h in PHB_p medium. The growth of Δ*phaR* was very similar to the wt strain, showing a logarithmic growth phase between 5-15 h with a doubling time of ~3 h, followed by a period of slower growth. After 30 h, Δ*phaR* accumulated ~7% PHB cdw, slightly less than wt grown in the same conditions (Figure 3.18). The amount of PHB did not increase significantly from 30-72 h. After 24 h growth in PHB_{high} medium, wt *R. eutropha* accumulates 66% PHB cdw, whereas Δ*phaR* accumulates just 45% PHB cdw. Thus, in

both organisms, deletion of *phaR* results in accumulation of PHB to 70% that of wt levels. To determine the M_w and PDI of the PHB, cultures were grown 24 h in PHB_p and the PHB was extracted into chloroform for GPC analysis. The M_w was 270 ± 21 kDa, slightly lower than wt, but the PDI was 2.2 ± 0.6, similar to wt.

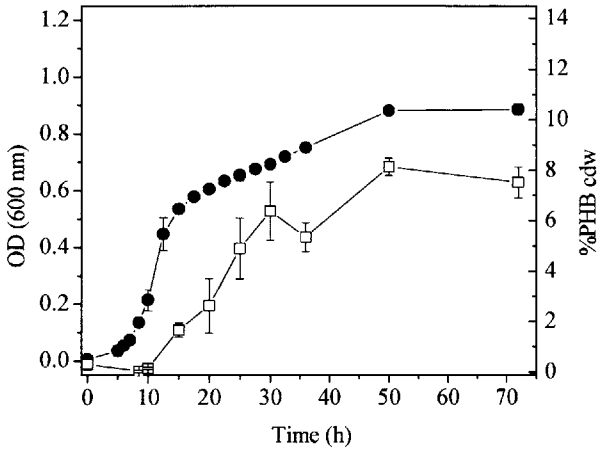

Figure 3.18 Growth and analysis of PHB levels in *C. crescentus* Δ*phaR* grown in PHB_p growth conditions. The OD_{600} (●) and amount of PHB per cell (□) were measured at the indicated growth times. The error bars represent the standard deviation from the mean of three different cultures.

3.3.13 Molecules of PHB, PhaP and PhaC per cell in the Δ*phaR* mutant strain

Again, if we make the assumption that the M_w of PHB in Δ*phaR* remains the same throughout growth, then we can calculate the molecules of PHB per cell. At 0 h in PHB_p medium Δ*phaR* cells contain 4,300 ± 1,100 PHB chains per cell (Figure 3.19). The amount of PHB increases to 246,000 ± 18,000 chains per cell after 72 h growth (Table A3.6).

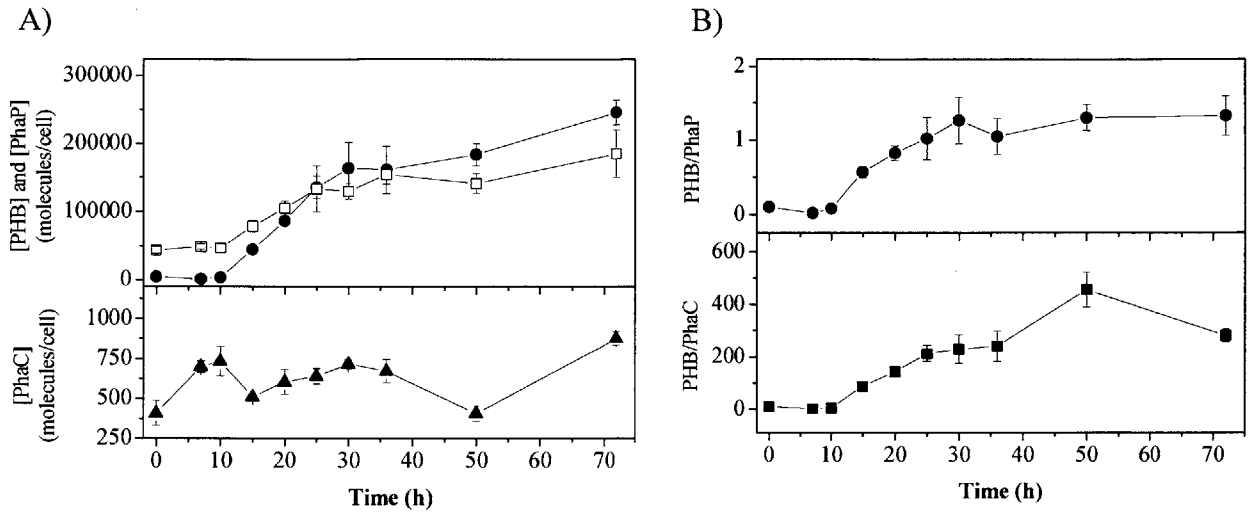

Figure 3.19 Quantitative analysis of PhaP and PHB levels in *C. crescentus* Δ*phaR* grown in PHB_p conditions. A) Molecules of PhaC (▲), PHB (●) and PhaP (□) per cell. B) The molar ratio of PHB to PhaP and PHB/PhaC as a function of growth time. The error bars in A represent standard deviation from the mean of three samples from three different cultures. The error bars in B are propagated from the uncertainties in A. The M_w of PHB used to calculate molecules per cell and the PHB:PhaP ratio above was 270 kDa, determined from a single measurement of PHB produced by *ΔphaR* after 24 h in PHB_p. The data are given in Table A3.6 as an appendix to this Chapter.

In *R. eutropha*, PhaR acts as a negative regulator of *phaP* expression, and its deletion results in constitutive overexpression of PhaP and reduced PHB accumulation (70% that of wt). Qualitative Northern blot studies suggest that PhaF, a regulatory protein involved in PHA biosynthesis in *P. oleovorans*, controls transcription of *phaC1* in addition to the gene for the phasin *phaI* (*12, 13*). To understand the role of PhaR in *C. crescentus*, PhaP and PhaC levels were investigated in the Δ*phaR* strain. Western blots of PhaC expression levels in Δ*phaR* show a difference from the wt strain (Figure 3.20). In Δ*phaR*, the expression of PhaC was higher than in the wt strain and varied between 400 ± 80 and 880 ± 40 molecules per cell (Figure 3.19). This feature is distinct from what is seen in the Δ*phaR* strain of *R. eutropha*, in which PhaC levels are constitutive but lower than in wt, and is instead similar to the role of PhaF in *P. oleovorans*. Analysis of PhaP levels show that the concentration of PhaP in Δ*phaR* is ~6-fold higher than in

the wt strain at 0 h, and ~2-fold higher at later time points (36-72 h) (Figures 3.19 and 3.21). In the Δ*phaR* mutant of *R. eutropha*, PhaP1 is constitutively overexpressed and its levels do not change with increasing PHB. However, in the Δ*phaR* strain of *C. crescentus*, PhaP is overexpressed but its levels still increase 4-fold with increasing PHB, from 44,000 ± 5,000 molecules per cell at 0 h to 185,000 ± 35,000 molecules per cell at 72 h post inoculation (Figure 3.19). The results suggest that PhaR plays a role in controlling PhaP expression level but not in coupling it to PHB accumulation, and that it also plays a role in controlling PhaC expression levels.

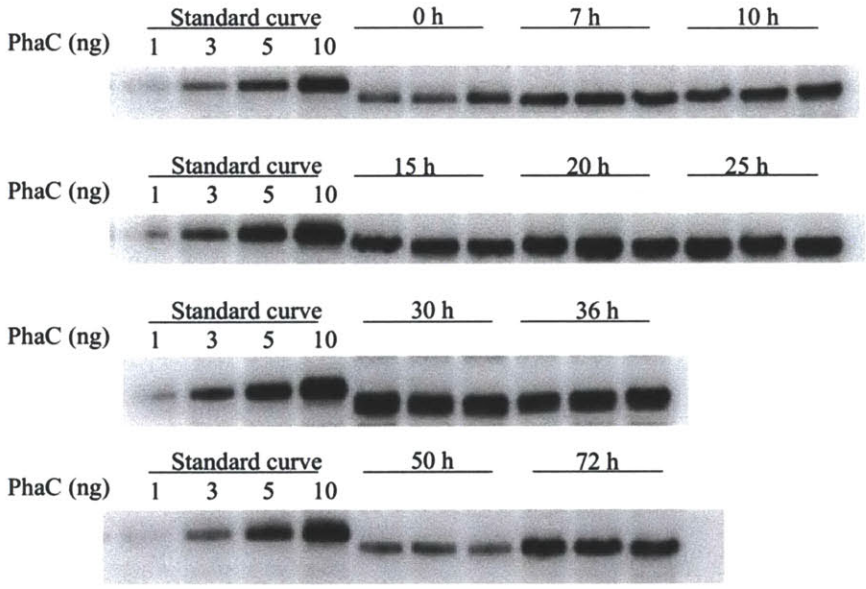

Figure 3.20 Western blot analysis of PhaC levels in Δ*phaR* grown in PHB_p medium. The standard curve is prepared from recombinant $PhaC_{Cc}$ and is not spiked with the disruption mutant *phaC*:km. Each sample lane contains ~7.5 x 10^7 cells. Samples were taken at each time point from three individual cultures. All samples intensities were within the standard curve.

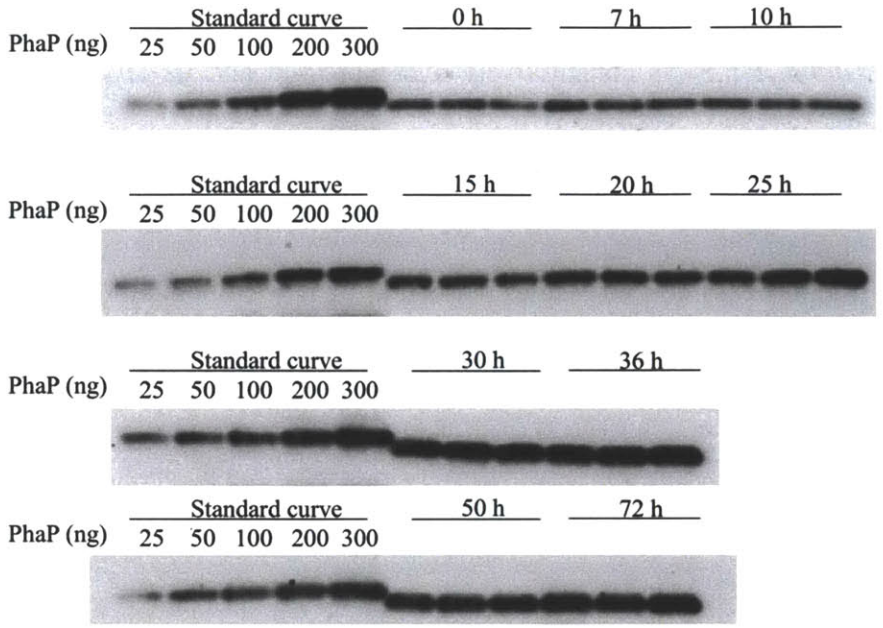

Figure 3.21 Western blot analysis of PhaP levels in Δ*phaR* grown in PHB_p medium. The standard curve was prepared from recombinantly purified PhaP and each lane of the standard curve contains 7.5 x 10^7 cells of Δ*phaP*. Each sample lane contains ~7.5 x 10^7 cells. Samples were taken at each time point from three individual cultures.

At early time points, the ratio of PHB to PhaP is 1:10. At later time points, this ratio decreases to 1-2, similar to the ratio observed in the wt strain (Figure 3.19B). The observation that, despite the differences in concentrations of PhaP and PHB in Δ*phaR* compared to wt, the ratio of PHB to PhaP is ultimately 1-2 further underscores the significance of this ratio to understanding the role of PhaP in PHB accumulation.

3.3.14 Electron microscopy visualization of granule formation in wt, Δ*phaP* and Δ*phaR* strains

To examine early granule localization and further explore the role of PhaP in PHB biogenesis in *C. crescentus*, wt, Δ*phaP* and Δ*phaR* cells were grown in PHB_p medium and samples were prepared for TEM analysis. *R. eutropha*, contains at minimum 5-10% PHB cdw at

early time points in PHB biogenesis in the growth conditions employed (*7, 17, 44*). TEMs of *R. eutropha* cells containing 5% PHB cdw revealed that tiny granules were localized adjacent to the nucleoid along the long axis of the cell (*17, 31*). *C. crescentus* offers a unique opportunity to examine very early granules when PHB is present at only 1% cdw. TEMs at 9 h of *C. crescentus* grown in PHB_p containing ~1% PHB cdw reveal that early putative granules are small, with diameters between 50-100 nm (Figure 3.22A). It should be noted that serial slices would be necessary to quantitate and statistically analyze the size and number of granules. However, the fact that only small granules are seen in all randomly sectioned slices suggests that there are no larger granules present in the cell. The number of granules per cell was determined by counting granules from 220 cells in 18 micrographs (from three separate growths). Of these cells, 50% contained 0-1 granules, 30% contained 2 granules, and 20% contained 3-6 granules (Table 3.6). Figure 3.22 shows representative cells containing 3-6 granules in order to emphasize the localization of early granules to the perimeter of the cell. In the 220 cells whose granules were counted, ~85% of the granules are located closer to the membrane than to the center of the cell. A "dark-stained feature" like that observed by Tian *et al.* that is now believed to be nucleoid is not evident in these samples (*17*). However, there are no nucleoid-free regions in the cytoplasm of *C. crescentus (45)*. Thus, is it likely that nucleoid exclusion of early granules is the cause of their localization near the cell membrane. From these data we cannot determine whether the granules are nucleoid associated. After 12 h growth in PHB_p the PHB content increased to ~3% cdw. At this stage the cells contain a mixture of large (200-250 nm in diameter) and small (50-100 nm in diameter) granules (Figure 3.22B).

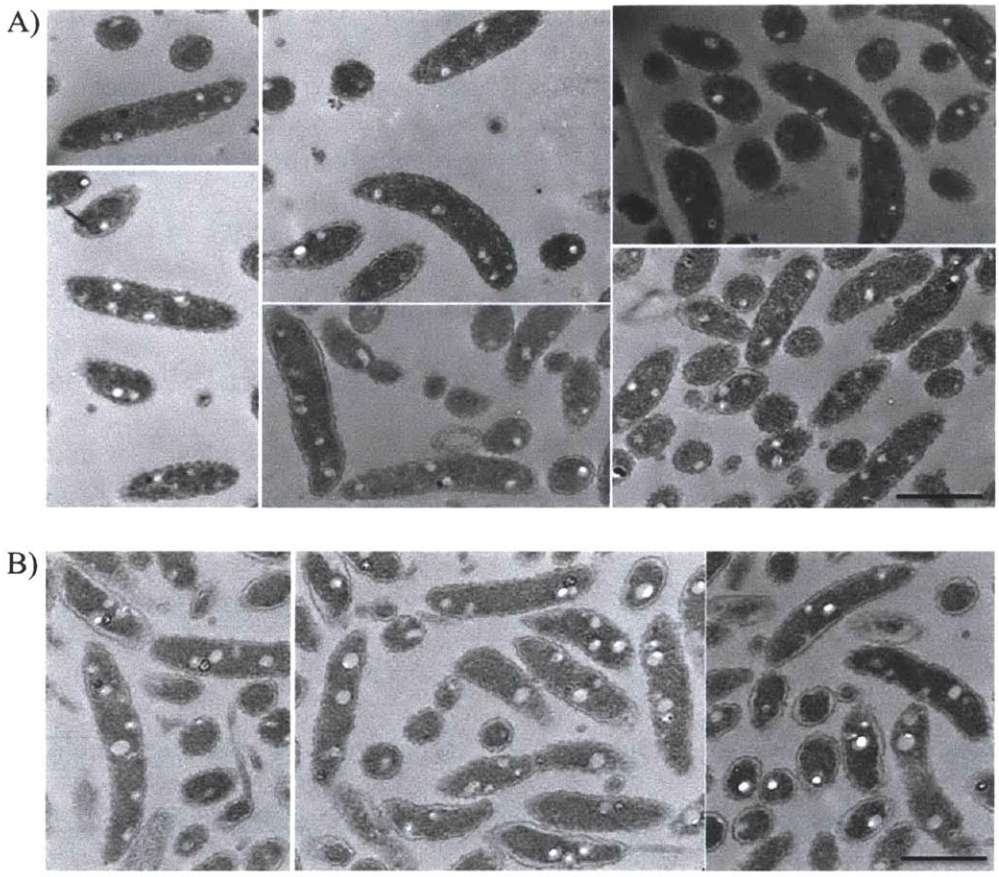

Figure 3.22 Representative electron micrographs of granules at A) 9 h and B) 12 h growth in PHB_p. The cells from this growth contain 1% PHB at 9 h and 3% PHB at 12 h growth. The bar represents 1 μm.

Table 3.6 Granule counting in wt, Δ*phaP* and Δ*phaR* cultures grown in PHB_p.

	% of cells containing a given number of granules[a]			
Number of granules	wt (9 h)[b]	wt (24 h)[c]	Δ*phaP*	Δ*phaR*
0	20	10	27	4
1	24	31	54	12
2	28	32	17	27
3	18	17	1.5	29
4	6	6	0.5	14
5	3	3	0	10
6	1	1	0	3
7+	0	0	0	1

[a]The number of cells containing a particular number of granules is given as a percentage of the total number of cells that were counted.
[b]For the 9 h wt culture, granules in 220 cells were counted.
[c]For 24 h cultures, granules in 177 wt cells, 276 Δ*phaP* cells and 182 Δ*phaR* cells were counted.

Cultures of the wt strain grown 24 h in PHB_p medium were also examined by TEM (Figure 3.22). Cells whose long axis was parallel to the plane of the micrographs (>1 μm in length in the micrographs) were examined to determine the average number of granules per cell. Of 177 cells from ten micrographs, 90% contained 0-3 visible granules, while the remaining 10% contained 4-6 granules. This distribution is summarized in Table 3.4. The granules vary in size from 100-300 nm in diameter. At this stage, the cells appear elongated relative to those in early PHB_p cultures (Figure 3.23). The outer layer of the cells is wavier than in the cells in Figure 3.16, which may be caused by the dehydration and embedding process being more disruptive to cells grown for extended periods on nitrogen-limited medium, as has been proposed in aged nitrogen-limited cultures of *R. eutropha* (*46*). The irregular looking morphology compared to the younger cultures in Figure 3.17 may also be due to extended growth in nutrient limited medium (*32, 47*).

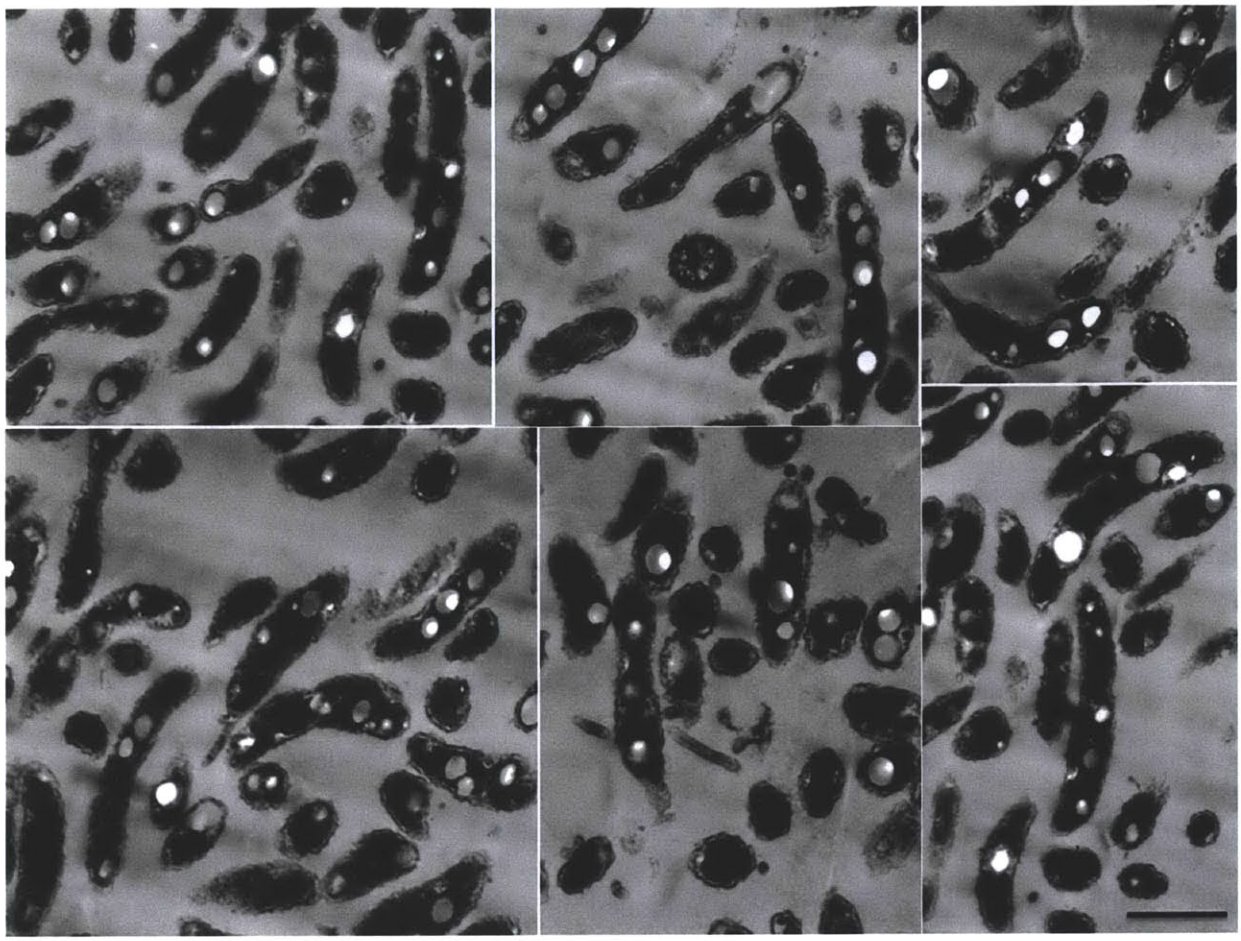

Figure 3.23 Electron micrographs of wt grown 24 h in PHB_p medium. The cells accumulate PHB to 10-12% cdw under these growth conditions. The above panels are representative images, and additional micrographs can be found in the appendix of this thesis. The bar represents 1 μm.

TEMs of Δ*phaP* cultures grown 24 h in PHB_p medium reveal that these cells contain PHB in a single granule that is similar in shape to those found in wt after 24 h growth. The granules in Δ*phaP* at this time are 50-150 mm in diameter, smaller than in the wt strain after 24 h (Figure 3.24). The Δ*phaP* cultures contain 1% PHB cdw, thus a more informative comparison might be with the 9 h wt cultures in Figure 3.20A, which also contain ~1% PHB cdw. In contrast to Δ*phaP*, a majority of wt cells contain many small granules at this stage. Of 276 Δ*phaP* cells from 13 different micrographs, 80% contained 0-1 visible granules per cell. The morphology of Δ*phaP* cells at this stage resembles the younger cultures in Figure 3.20 rather than the irregular morphology of the cells in Figure 3.23.

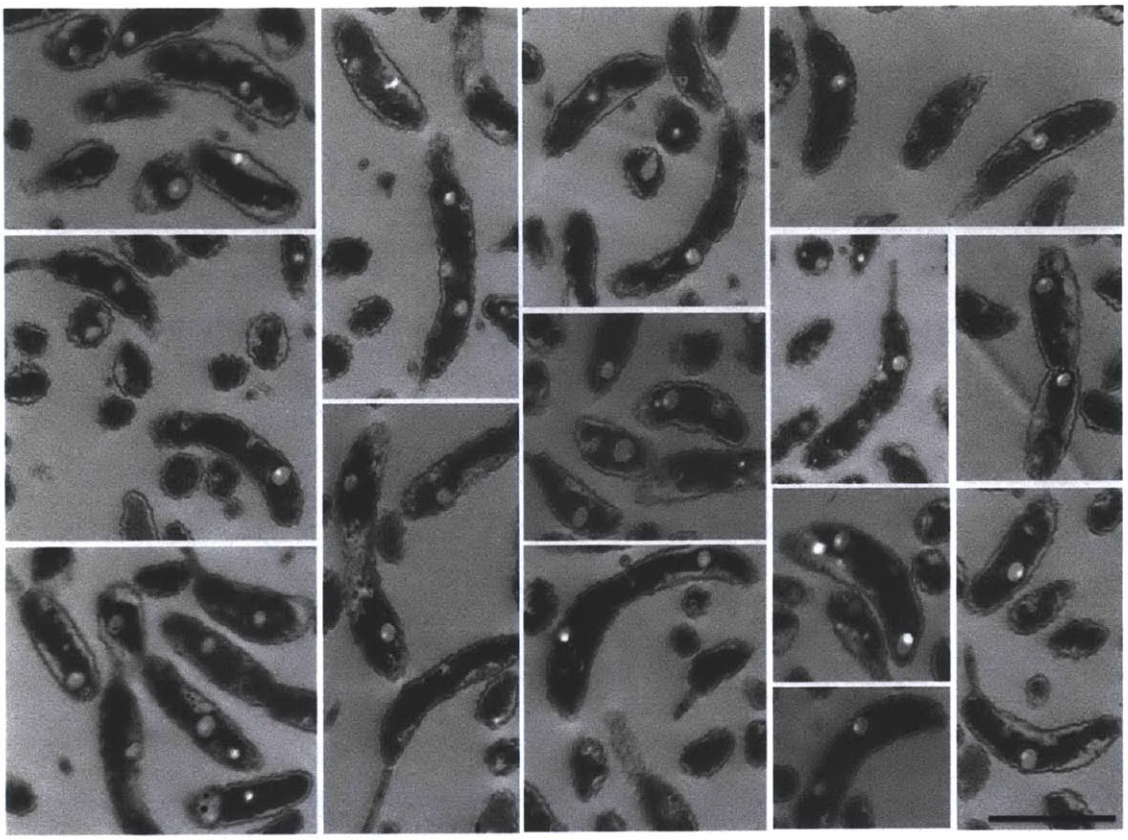

Figure 3.24 Electron micrographs of *ΔphaP* grown 24 h in PHB_p medium. The cells accumulate PHB to ~1% cdw under these growth conditions. The above panels are representative images, and additional micrographs can be found in the Appendix of this thesis. The bar represents 1 μm.

Finally, TEM of Δ*phaR* cultures grown 24 h in PHB_p medium suggests that deletion of *phaR* results in the production of more granules per cell, despite lower overall PHB content compared to wt. The granules of 182 cells in ten micrographs whose long axes were parallel to the plane of the micrograph were counted. Of these cells, 30% contained 3 granules and another ~30% contained 4-7 granules. In comparison, micrographs of the wt strain discussed above indicated that only ~10% of wt cells contained 4-6 granules, and none contained 7 or more granules. It should be noted that Figure 3.25 shows Δ*phaR* cells that are representative of the population of cells containing 3-7 granules (which accounted for 60% of the cells), however 15% of the cells contained 0-1 granule (Table 3.6).

Together the analysis of the wt strain and the two mutant strains by TEM suggests that PhaP plays a role in determining the number and size of granules in *C. crescentus*, as has been proposed for PhaP1 in *R. eutropha*.

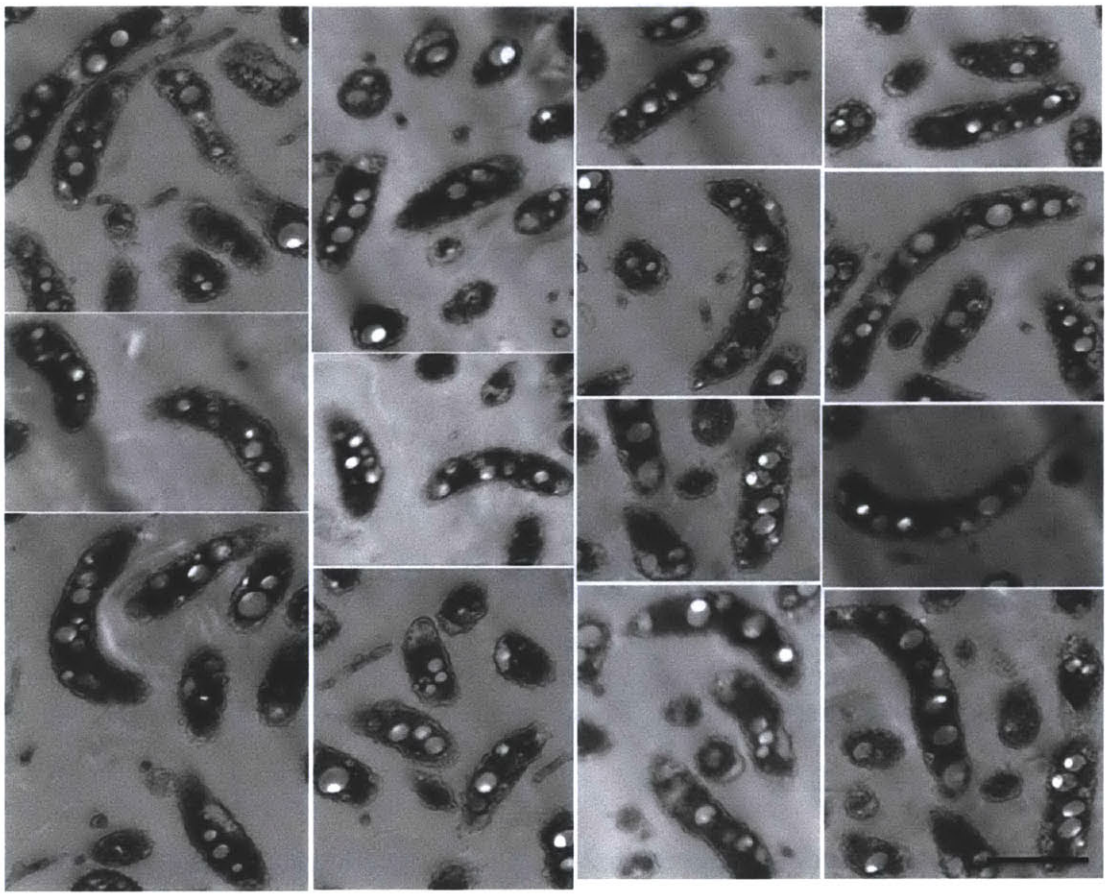

Figure 3.25 Electron micrographs of *ΔphaR* grown 24 h in PHB_p medium. The cells accumulate PHB to 7-8% cdw under these growth conditions. The above panels are representative images, and additional micrographs can be found in the appendix of this thesis. The bar represents 1 μm.

3.4 Discussion

The studies presented in this Chapter outline our efforts to understand the mechanism of PHB granule formation in *C. crescentus*, as well as the role of the predominant granule-associated protein PhaP in promoting PHB accumulation. Most of our understanding of PHB biosynthesis has come from studies carried out in *R. eutropha*, which accumulates PHB to 80% of its cdw when the cells are limited in nitrogen but in the presence of an abundant carbon source. These studies have been extremely informative; however, most organisms do not accumulate PHB to such extreme levels. We were therefore interested in investigating whether paradigms of granule formation and the roles of the PHB biosynthetic proteins that were established based on studies in *R. eutropha* were also true for an organism that accumulates far less PHB. We have investigated PHB accumulation in *C. crescentus*, which we have shown accumulates PHB to just 12% of its cdw when nitrogen is a limiting nutrient but a carbon source is abundant. PhaC and the granule-associated proteins, PhaP, PhaR and PhaZ were identified. To examine the roles of PhaP and PhaC in granule biogenesis, antibodies were generated and their expression levels throughout growth were examined by Western blot analysis. The deletion mutants Δ*phaP* and Δ*phaR* were generated to determine the effect on the amount of PHB and its M_w and PDI, and on PhaP and PhaC expression levels. Together, these studies provided a quantitative picture of the concentrations of PHB, PhaC and PhaP during PHB accumulation in *C. crescentus*. The results are discussed in the context of what is known in *R. eutropha*, and a model for granule initiation and growth in *C. crescentus* is proposed.

PhaC synthesizes PHB from the soluble, monomeric substrate HBCoA to generate high M_w polymer. As the polymer grows, a phase transition occurs from soluble precursors to insoluble, amorphous polymer. During the process of granule growth, several additional proteins

including phasins (PhaPs), depolymerases (PhaZs), and the transcription factor PhaR, become associated with the granule. The proteins are found on the surface of the granule, suggesting they associate after the granule is formed. Of these proteins, phasins are the predominant component, while the other proteins are thought to be present at much lower levels. A key question in probing the mechanism of granule formation is how the transition from soluble monomeric precursors to insoluble polymer occurs without subjecting the cell to the stress of large regions of exposed hydrophobic PHB. Understanding the structure of the mature granule is key to understanding how granule formation occurs.

Several studies have been undertaken to examine the composition of mature granules. In *R. eutropha*, mature PHB granules are typically 200-500 nm in diameter and at maximum PHB accumulation, the cells contain 5-15 granules (*6*). The phasin PhaP1 is the predominant granule-associated protein (*3, 4*). Based on studies examining the surface area of granules, and the size and number of PhaP1 molecules per cell, PhaP1 has been calculated to cover 22-54% of the surface of granules (*7, 17*). Dennis and coworkers examined the surface of isolated granules by atomic force microscopy (AFM) and observed a lattice-like network covering the granules, which they interpreted as being composed of PhaP1 (*48*). In their studies the lattice covered the entire granule. However, the calculations of surface coverage by PhaP1 as well as recent cryoET data discussed below, suggest that the granules have only partial or "patchy" surface coverage. Importantly, cryoET is a non-perturbative method, whereas AFM has many drawbacks including sample preparation that involves lysing cells, drying of isolated granules, and the potential for mechanical deformation from the AFM tip. Thus the AFM observation of full surface coverage by Dennis *et al.* may be the result of an artifact from sample preparation and imaging.

Early studies of PHB granules isolated from *Bacillus megaterium* revealed that they are 97-98% PHB, 2% protein and 0.5% lipid (*19*). This observation led to speculation that granules could be partly coated with a lipid bilayer or monolayer. EM evidence from various groups rovided conflicting results as to the thickness of the putative surface layer, which some claimed was consistent with a monolayer and others with a bilayer (*49-52*). Thus, no concrete evidence for a lipid coating has been obtained, and in fact more recent data suggests that lipid coating is unlikely. First, use of cryoET to examine the surface of granules in *R. eutropha* revealed that they contain a "patchy," discontinuous surface that is ~2 nm thick and less dense than the inner and outer membrane bilayers (*6*). A thickness of 2 nm is too thin to be a lipid monolayer and is instead consistent with a proteinaceous layer. Given relative abundances of proteins on the surface of granules in *R. eutropha*, this is likely composed predominantly of PhaP1. Second, microarray studies of mRNA transcripts in *R. eutropha* grown under PHB accumulation conditions revealed that the expression of enzymes involved in the biosynthesis of cardiolipin and phosphatidylethanolamine (the major cell membrane phospholipids in *R. eutropha*) decreases (*53*). This finding is inconsistent with a model in which the cells would need to synthesize large amounts of lipids to coat growing PHB granules. Together the results suggest that in *R. eutropha* the surface of the granules is composed of "patches" of proteinaceous rafts composed of PhaP1 and likely other PHB biosynthetic proteins including PhaC, PhaZs and PhaR, and that no continuous lipid monolayer is present, and a bilayer is clearly ruled out due to size.

CryoET data, in addition to providing information about the surface composition of mature granules as discussed above, have also given insight into the localization of early granules and their growth and fusion throughout PHB accumulation (*6*). The localization of

granules has implications on their mechanism of formation, and cryoET has conclusively demonstrated that early granules form in the cytoplasm, and do not bud from the cell membrane and/or poles, as has been previously reported. Early EM experiments carried out in our lab suggested that early granules formed around a dark-stained scaffolding structure, whose identity was at the time unknown. CryoET suggests that this structure was in fact nucleoid, rather than for example a scaffolding protein (*6*). Furthermore, cryoET revealed that throughout PHB accumulation, there is continual granule nucleation and growth, as well as fusion of mature granules into larger ones. The observation that granules fuse lends further support to the idea that the surface of granules is patchy rather than continuous, with hydrophobic surfaces allowing fusion.

Conditions have not been identified in which *R. eutropha* contains no PHB. Thus our understanding of how mature granules form from soluble precursors is based on fortuitous observations made in an engineered mutant strain of *R. eutropha* containing a StrepII-tagged PhaC in place of the wt PhaC (*38*). In this strain, when the cells contain 5% PHB cdw, affinity purification of the synthase reveals that a fraction is associated with high M_w PHB and PhaP1, and that this species is soluble. The stoichiometry in this fraction is 2 PhaCs, 1 PHB chain and 4-9 PhaP1s, which is proposed to be indicative of a soluble nucleating species (a granule precursor). Whereas whole cell measurements of the ratio of molecules of PHB to PhaP reveal that it is 1-2 throughout PHB accumulation, PhaP1 appears to be enriched relative to PHB in the nucleating species, which led to the proposal that PhaP1 plays a role in maintaining the solubility of the nucleating species. Furthermore, this species did not contain PhaR or PhaZs, suggesting that they become associated at a later point in granule formation. From these data, a model for PHB granule formation was proposed in which the soluble nucleating species contain just PhaC,

PhaP1 and HBCoA. These species then fuse as PHB accumulation continues, and following fusion of the nucleating species, a phase transition occurs from soluble to insoluble polymer and other granule-associated proteins bind the mature granules (*38*).

Based on our studies of PHB accumulation in *C. crescentus*, we propose a model for granule formation that is very similar to that in *R. eutropha*, with a few distinctions (Figure 3.26). In this model, at early time points in granule formation, the cells contain mostly insoluble PHB with a small population of soluble PHB. Both the soluble and insoluble fractions contain PHB with a M_w of ~200 kDa, and 1-2 PHB chains per PhaP. The insoluble species arise from the fusion of these soluble species. PhaP plays a role in maintaining the structure and solubility of these species. When the cells find themselves limited in an essential nutrient but with an abundant carbon source, PHB begins to accumulate and the soluble species fuse and grow. PhaC alone dictates termination and reinitiation, controlling the M_w and PDI of the PHB. As the amount of PHB in the cells increases, the ratio of PHB chains to PhaP remains between 1-2. The model proposes that the ratio is maintained because each terminated chain remains with a PHB chain to maintain its structure and to prevent it from occluding the PhaC active site, thereby allowing further turnover. PhaP serves to "fold" each PHB chain as it is being synthesized to prevent it from collapsing onto PhaC, thereby obscuring the active site and preventing turnover. The mature granule comprises PHB, PhaP, PhaC as well as PhaZ and PhaR. The evidence for this model, as well as the features that are distinct from what is proposed in *R. eutropha*, are discussed below.

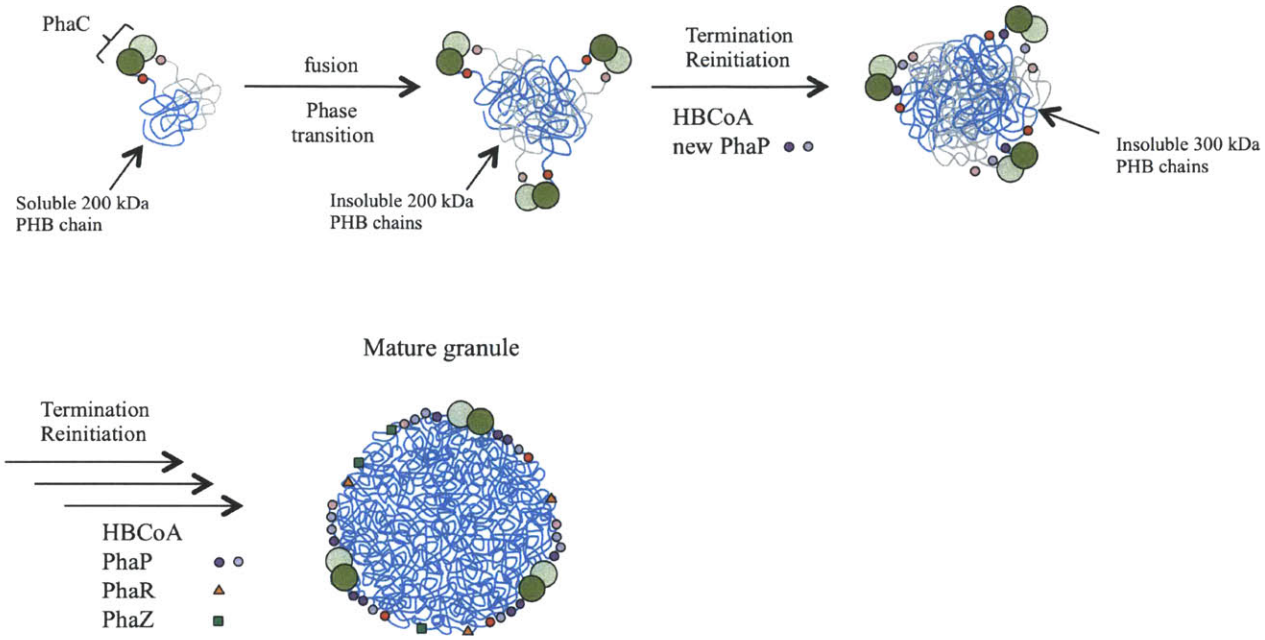

Figure 3.26 Model for granule initiation and formation in *C. crescentus*. The initial nucleating species is composed of PhaC (green spheres), PHB and PhaP (red spheres), where PhaP and PHB are present in a 1:1 ratio. As PHB accumulation begins, the soluble species fuse and undergo a phase transition to form early granules. As PHB synthesis progresses, PhaC catalyzes termination and reinitiation. Each terminated chain remains associated with one PhaP, which is replaced by a newly synthesized PhaP (purple spheres) to maintain the ratio of 1-2 PHB chains per PhaP.

PhaC is depicted as a dimer with each monomer synthesizing a PHB chain. This species is proposed on the basis of experiments described in Chapter 2 in which acylation with the artificial primer sTCoA (a terminally saturated trimer of HBCoA) suggests a stoichiometry of one chain per monomer. Furthermore, size exclusion chromatography experiments suggest that PhaC may be a dimer with an unusual shape. In Figure 3.26 the second monomer and its respective PHB chain and PhaP are depicted in a lighter shade for clarity.

The identity of the soluble nucleating granule species is supported by a number of observations in this Chapter and in Chapter 2, and also by comparison to the putative nucleating species in *R. eutropha*. In nutrient rich PYE broth, *C. crescentus* contains 0.5-2% PHB cdw, and

~10% of this PHB is soluble, while the remaining PHB is in insoluble granules. PHB granules are nearly always present in *C. crescentus* cells grown in PYE imaged by a variety of methods including cryoET (*54*), whole cell TEM (*55*), and thin section TEM (*15, 55*). The soluble species contains high M_w PHB and ~1 PHB chain per PhaP, and the insoluble species contains high M_w PHB and 1-2 PHB chains per PhaP. We propose that the granules arise from the fusion of these soluble species. The observation that the nucleating species contains high M_w PHB that is soluble is similar to the model proposed for *R. eutropha*. However, in *R. eutropha* the nucleating species is proposed to contain 4-9 PhaPs per PHB chain, enriched relative to the 1-2 PHBs per PhaP present in the bulk whole cell measurement. There are several possible explanations for this difference. First, the soluble species in *R. eutropha* was isolated from a mutant strain in which the wt *phaC* gene was replaced with a gene encoding a StrepII-tagged PhaC (*56*). In this strain, StrepII-PhaC was upregulated 30-fold relative to PhaC in the wt strain despite being under control of the endogenous promoter, and the M_w of the PHB was ~1/3 that of PHB in the wt strain. Thus the enrichment of PhaP1 in the soluble species could be an artifact of the strain. Alternatively, if the nucleating species in wt *R. eutropha* is the same as that in the StrepII-PhaC strain, then the nucleating species in *R. eutropha* and *C. crescentus* could simply have different compositions due to differences in the properties of the PHB. In wt *R. eutropha* the PHB is between 700-1000 kDa throughout growth, ~3-fold higher than that in *C. crescentus*. The enrichment of PhaP1 in the nucleating species in *R. eutropha* is proposed to play a role in maintaining the solubility and structure of the PHB (*38*). The fact that the soluble PHB species in *C. crescentus* contains just one PhaP per PHB chain may reflect the fact that fewer PhaPs are required to maintain the structure and solubility of PHB of a lower M_w. Finally, measurements made at very early time points in PHB accumulation in *C. crescentus* have inherently higher

error due to the fact that we are measuring very small amounts of PHB and PhaP. Therefore, we cannot rule out that PhaP levels are enriched relative to PHB at early time points, but that we simply cannot make this measurement accurately given the error.

Several experiments have given insight into the function of PhaP in the synthesis of granules. In Chapter 2, we present results suggesting that just one equivalent of PhaP relative to PhaC in *in vitro* assays facilitates an increase in specific activity of PhaC and in overall turnover of HBCoA. Under these assay conditions (high ratio of HBCoA to PhaC), PhaC is assumed to be relatively uniformly loaded, thus at least at early stages in polymerization, the ratio of PHB chains to PhaP is ~1:1. Additionally, pull-down assays of PhaC and the N-terminally truncated $PhaC_{Cc}\Delta N$ with PhaP indicate that only full length PhaC and PhaP interact *in vitro*, yet PhaP mediates the same effect on activity and substrate consumption with both synthases. This suggests that PhaP interacts with the growing PHB chain rather than with PhaC. Finally, in this Chapter we demonstrated in activity assays of crude cell lysates from both wt and Δ*phaP C. crescentus* grown in PYE that the specific activity of PhaC and its overall turnover of exogenously added HBCoA are increased in the wt strain relative to Δ*phaP*. We interpret these results together to suggest that PhaP associates with the PHB chain to package it in such a way as to maintain its solubility, at least in the region around the PhaC active site, so as to prevent collapse of hydrophobic polymer onto PhaC and thereby allow access of soluble HBCoA.

A "folding" or "packing" function of PhaP is consistent with what has been proposed in several systems. Steinbüchel and coworkers noted, by phase contrast and scanning electron microscopy, that granules produced *in vitro* by PhaEC from *Allochromatium vinosum* were smaller in the presence of PhaP1 from *R. eutropha* than in its absence (*57*). Niamsiri *et al.* demonstrated that addition of BSA to a reaction containing HBCoA and PhaC from *R. eutropha*

immobilized on a surface resulted in the formation of larger granules and more complete substrate turnover (*58*). BSA has long been known to bind PHB (*3, 5, 8*), and they suggested that in their experiments, BSA was playing a role in folding the nascent granule to prevent it from obscuring the PhaC active site, similar to what we have proposed for PhaP in *C. crescentus*. A folding function is also consistent with our TEM results, which suggest that PhaP plays a role in *C. crescentus* in determining the number and size of granules. While we have not performed stereology or tomography to examine the exact size, volume and number of granules, generally we see that Δ*phaR* contains more and smaller granules than wt. In Δ*phaP*, which contains 1% PHB cdw, a comparison of the sizes of granules to those in wt cells also containing 1% PHB reveals that Δ*phaP* contains fewer and larger granules than wt. In *R. eutropha* wt, Δ*phaP1* and Δ*phaR* strains, the same trends in granule size and number are observed (*45, 59*). Finally, our finding that Δ*phaP* cannot accumulate more than 1% PHB cdw can be explained by a model in which PHB misfolds and/or crystallizes in the absence of PhaP, which could lead to the active site of PhaC being obscured, or simply to the precipitation of PhaC on the exposed hydrophobic granule. Precipitation or unfolding of PhaC could lead to its degradation by the proteolytic machinery in the cell, which would be consistent with our observation that PhaC levels decrease as a function of growth time in Δ*phaP*.

Our observation that early granules form near the perimeter of the cell in *C. crescentus* seems to suggest they might bud from the membrane, as has alternatively been proposed as a mechanism for granule formation. This result would contradict a model in which the nucleating species is soluble; however, we think the membrane budding model is still not supported, for three reasons. First, the nucleoid of *C. crescentus* has previously been shown to occupy the majority of the cytosol (Figure 3.27) (*54, 60*). Thus, the appearance of early granules near the

cell membrane may be due to nucleoid exclusion. Second, investigation of cryoET images of *C. crescentus* from the Jensen lab have fortuitously provided high resolution images of PHB granules that are ~100 nm in diameter, similar to what we see in wt cells after 9 h growth in PHB_p medium (Figure 2.22A). In their micrographs the granules are near the membrane but are very clearly not budding from it (*59*). Finally, if granules were budding from the membrane, one would expect that lipids derived from the membrane would associate with the granule surface and cause the PHB granules to be insoluble. Our observation that 10% of the PHB is in the soluble fraction at early time points suggests that lipids are not associated.

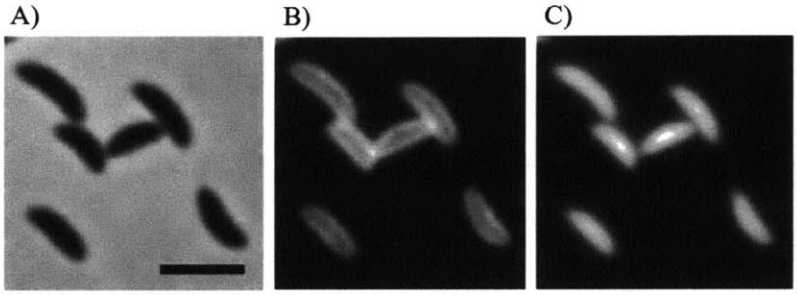

Figure 3.27 Phase contrast and fluorescence microscopy images of *C. crescentus*. A) Phase contrast image. B) Fluorescent image of FM4-64 cytoplasmic membrane dye signal. C) Fluorescent image of DAPI nucleoid dye signal. The DAPI signal overlays with the phase contrast image in panel A, suggesting that there are no nucleoid-free regions in *C. crescentus*. Furthermore the DAPI stain is even throughout the cell. The scale bar is 2 μm. Figure is adapted from (*7*).

Our model continues with the fusion of soluble species, which occurs as more PHB is accumulated, leading to the formation of granules. After each PHB chain is completed, PhaC catalyzes termination. In Chapter 2, we propose this is controlled by the relative rates of polymerization and termination by thiolysis. In *C. crescentus*, our observation that PHB in the wt strain, in Δ*phaP* and in Δ*phaR* are similar in M_w and PDI suggests that PhaP does not play a role in "triggering" termination, as is thought to be the case in *R. eutropha* (*7*). Extraction efficiencies in preparing GPC samples are low, however, therefore we are making the assumption that the

extracted material is representative of the total PHB content of the cells. It has long been proposed that PhaCs alone are capable of catalyzing termination (*61, 62*). However in the Δ*phaP1* and Δ*phaR* strains of *R. eutropha*, the M_w of PHB is lower and in Δ*phaP1* the PDI is higher than that in the wt strain. This suggests that PhaP1 plays a role in triggering termination, and that an increase or decrease in the amount of PhaP1 in the cells leads to uncontrolled termination and thereby higher PDI (*7*). This does not appear to be the case in *C. crescentus*. In Chapter 2, analysis of the M_w and PDI of PHB produced *in vitro* by PhaC in the presence and absence of PhaP indicate that 1) PhaC catalyzes termination, as the M_w is lower than would be expected for uniform loading without termination and 2) that the inclusion of PhaP (1-10 equiv.) does not greatly change the M_w and PDI. Furthermore, the range of M_ws of PHB measured *in vitro* are very similar to those measured *in vivo*, 300-600 kDa in the former and 200-400 kDa in the latter. Together with the results *in vivo* with mutant strains, these findings suggest that PhaC catalyzes termination and dictates M_w and PDI in *C. crescentus*.

The ratio of 1-2 PHB chains per PhaP is maintained throughout PHB biosynthesis, as is the case in *R. eutropha*. One way in which this ratio can be maintained is if a PhaP remains associated with each terminated PHB chain, while a newly synthesized PhaP takes its place to facilitate folding of the newly initiated PHB chain. This model is identical to what has been proposed in *R. eutropha* (*6*). Such a model would predict that as PHB accumulation occurs, PhaPs associated with terminated chains would spread outwards from PhaC on the surface of the granule, which could explain the observation by cryoET of proteinaceous "rafts" on the surface of granules in *R. eutropha (6)*. However, as we have not yet examined the surface of PHB granules in *C. crescentus*, we are speculating for the time being as to the nature of their surface.

In *C. crescentus*, the mature granules consist of at least PHB, PhaP, PhaC, PhaZ and PhaR, as revealed by our analysis of the proteins associated with isolated granules. We have examined the role of PhaR in *C. crescentus*, and have demonstrated that deletion of *phaR* results in an overall increase in PhaP expression, but that it is still correlated with PHB accumulation. Deletion of *phaR* also results in increased expression of PhaC. The role of PhaR in PHB biosynthesis in *C. crescentus* remains to be further explored, as is the means of coupling PhaP expression with PHB accumulation. However, it appears to be distinct from the role of PhaR in *R. eutropha*, further suggesting that the regulation of PHB biosynthesis is likely to be distinct in each organism.

The results presented in this Chapter indicate that some aspects of PHB biosynthesis are general to organisms such as *C. crescentus*, which accumulates just 10% PHB cdw in PHB_p medium, and *R. eutropha*, which can accumulate up to 80% PHB cdw. Our studies in *C. crescentus* demonstrate that many of these findings, in particular the striking ratio of one PhaP per PHB chain in mature granules, are more general features of PHB biosynthesis regardless of the extent of PHB accumulation. The results also further underscore the importance of PhaP in granule formation and, in *C. crescentus*, PhaC activity. While the details of the role of PhaPs in PHB biosynthesis appear to be distinct, the overall role in promoting PHB biosynthesis by maintaining the structure of granules appears to be conserved. Finally, aspects of the regulation of PHB biosynthesis remain poorly understood, and *C. crescentus* may prove to be an ideal model for studying regulation because it has a simpler set of PHB biosynthetic genes and because it already serves as a model for studying signal response and cell cycle regulation.

3.5 Acknowledgment

We thank Prof. Michael Laub for supplying us with wt *C. crescentus*, and Barrett Perchuck, Dr. Kasia Gora and Dr. Chris Brigham for help with trouble shooting cloning and growths. We also thank Mimi Cho for slicing TEM samples and for helpful discussions, and Jingnan Lu and Halim Yusof for help with GPC experiments and helpful discussions.

3.6 Appendix

Table A3.1 Extraction efficiency, M_w and PDI of PHB extracted from wt cultures. PHB was extracted from three different wt cultures grown from 0-40 h in PHB_p.

Time (h)	Extraction efficiency (%)[a]	M_w (kDa)	PDI
0	55	347	1.6
	62	314	2.2
	41	260	2.2
10	25	344	1.7
	29	342	1.8
	39	297	2.5
20	46	284	2.5
	65	325	1.8
	53	312	1.8
40	40	330	4.8
	29	370	4.1
	40	367	4.3

[a]Extraction efficiency was determined by crotonate analysis.

Table A3.2 Molecules per cell of PHB, PhaP and PhaC and molar ratios of PHB/PhaP and PHB/PhaC in wt *C. crescentus*.

Time point (h)	PHB (molecules/cell)	PhaP (molecules/cell)	PhaC (molecules per cell)	Ratio PHB/PhaP	Ratio PHB/PhaC
0	14,000 ± 1,160	7,200 ± 1,500	260 ± 10	1.9 ± 0.4	54 ± 4.9
7	13,400 ± 520	8,200 ± 2,300	270 ± 30	1.6 ± 0.5	49 ± 5.4
10	15,600 ± 640	23,400 ± 4,700	300 ± 20	0.7 ± 0.1	53 ± 4.7
15	60,600 ± 7,680	43,500 ± 7,900	280 ± 20	1.4 ± 0.2	220 ± 31
20	105,000 ± 15,000	73,600 ± 6,400	340 ± 10	1.4 ± 0.2	310 ± 44
25	109,100 ± 22,700	64,900 ± 13,600	330 ± 110	1.7 ± 0.5	330 ± 130
30	121,000 ± 22,700	76,700 ± 8,200	220 ± 30	1.6 ± 0.4	550 ± 120
36	146,000 ± 9,600	86,700 ± 2,200	180 ± 40	1.7 ± 0.1	800 ± 170
50	151,000 ± 1,850	80,700 ± 5,500	200 ± 10	1.9 ± 0.1	750 ± 30
72	151,000 ± 25,500	102,000 ± 25,300	260 ± 70	1.5 ± 0.4	570 ± 180

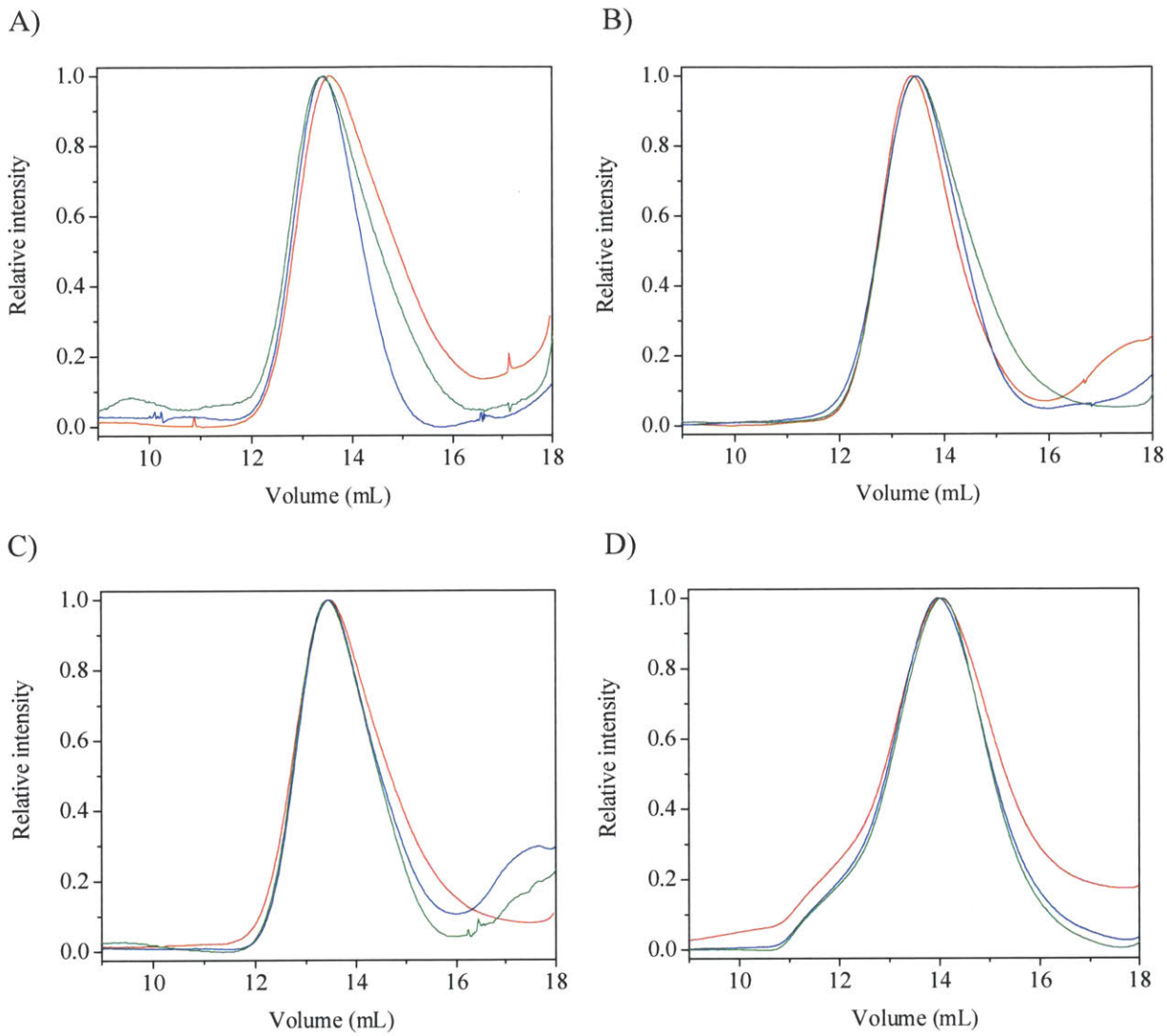

Figure A3.1 Gel permeation chromatography of PHB extracted from wt *C. crescentus*. Cultures were grown 0-40 h in PHB_p medium, and the PHB was extracted into chloroform by refluxing at 70 ˚C for 48 h. PHB was extracted from three separate cultures at A) 0 h, B) 10 h, C) 20 h and D) 40 h post inoculation into PHB_p.

Table A3.3 Extraction efficiency, M_w and PDI of PHB extracted from Δ*phaP* cultures. PHB was extracted from three different Δ*phaP* cultures grown 24 h in PHB_p.

	Extraction efficiency (%)[a]	M_W (kDa)	PDI
1	20	429	2.7
2	31	407	1.9
3	27	463	1.6

[a]Extraction efficiency was determined by crotonate analysis.

Table A3.4 Molecules per cell of PHB and PhaC and molar ratio of PHB/PhaC in Δ*phaP C. crescentus*.

Time point (h)	PHB (molecules/cell)	*PhaP (molecules/cell)*	PhaC (molecules per cell)	*Ratio PHB/PhaP*	Ratio PHB/PhaC
0	5,080 ± 300		260 ± 10		20 ± 1.8
7	8,000 ± 700		270 ± 30		26 ± 3.5
10	4,180 ± 750		300 ± 20		15 ± 3.6
15	7,670 ± 760		280 ± 20		39 ± 5.1
20	6,470 ± 2,020		340 ± 10		59 ± 34
25	7,430 ± 530		330 ± 110		110 ± 14
30	8,010 ± 60		220 ± 30		73 ± 4.5
36	10,200 ± 2,500		180 ± 40		110 ± 28
50	10,500 ± 1,040		200 ± 10		140 ± 23
72	14,600 ± 1,320		260 ± 70		240 ± 47

Table A3.5 Extraction efficiency, M_w and PDI of PHB extracted from Δ*phaR* cultures. PHB was extracted from three different Δ*phaP* cultures grown 24 h in PHB_p.

	Extraction efficiency (%)[a]	M_w (kDa)	PDI
1	19	297	1.8
2	24	260	1.6
3	21	260	1.9

[a]Extraction efficiency was determined by crotonate analysis.

Table A3.6 Molecules per cell of PHB, PhaP and PhaC and molar ratios of PHB/PhaP and PHB/PhaC in *ΔphaR C. crescentus*.

Time point (h)	PHB (molecules/cell)	PhaP (molecules/cell)	PhaC (molecules per cell)	Ratio PHB/PhaP	Ratio PHB/PhaC
0	4,260 ± 1,130	43,500 ± 4,880	410 ± 78	0.1 ± 0.03	10 ± 3.4
7	810 ± 590	48,500 ± 3,880	700 ± 35	0.02 ± 0.01	1.2 ± 0.9
10	3,430 ± 640	46,500 ± 6,520	730 ± 92	0.07 ± 0.02	4.7 ± 1.0
15	44,500 ± 4,150	78,500 ± 8,000	510 ± 15	0.6 ± 0.08	87 ± 8.6
20	86,300 ± 4,730	105,000 ± 11,100	600 ± 80	0.8 ± 0.1	140 ± 21
25	136,000 ± 16,400	133,000 ± 33,800	640 ± 49	1.0 ± 0.3	210 ± 30
30	164,000 ± 38,000	130,000 ± 11,600	710 ± 28	1.3 ± 0.3	230 ± 54
36	161,000 ± 34,800	154,000 ± 13,800	670 ± 73	1.0 ± 0.2	240 ± 58
50	184,000 ± 16,100	141,000 ± 14,400	400 ± 48	1.3 ± 0.2	450 ± 67
72	246,000 ± 18,000	185,000 ± 34,700	880 ± 43	1.3 ± 0.3	280 ± 25

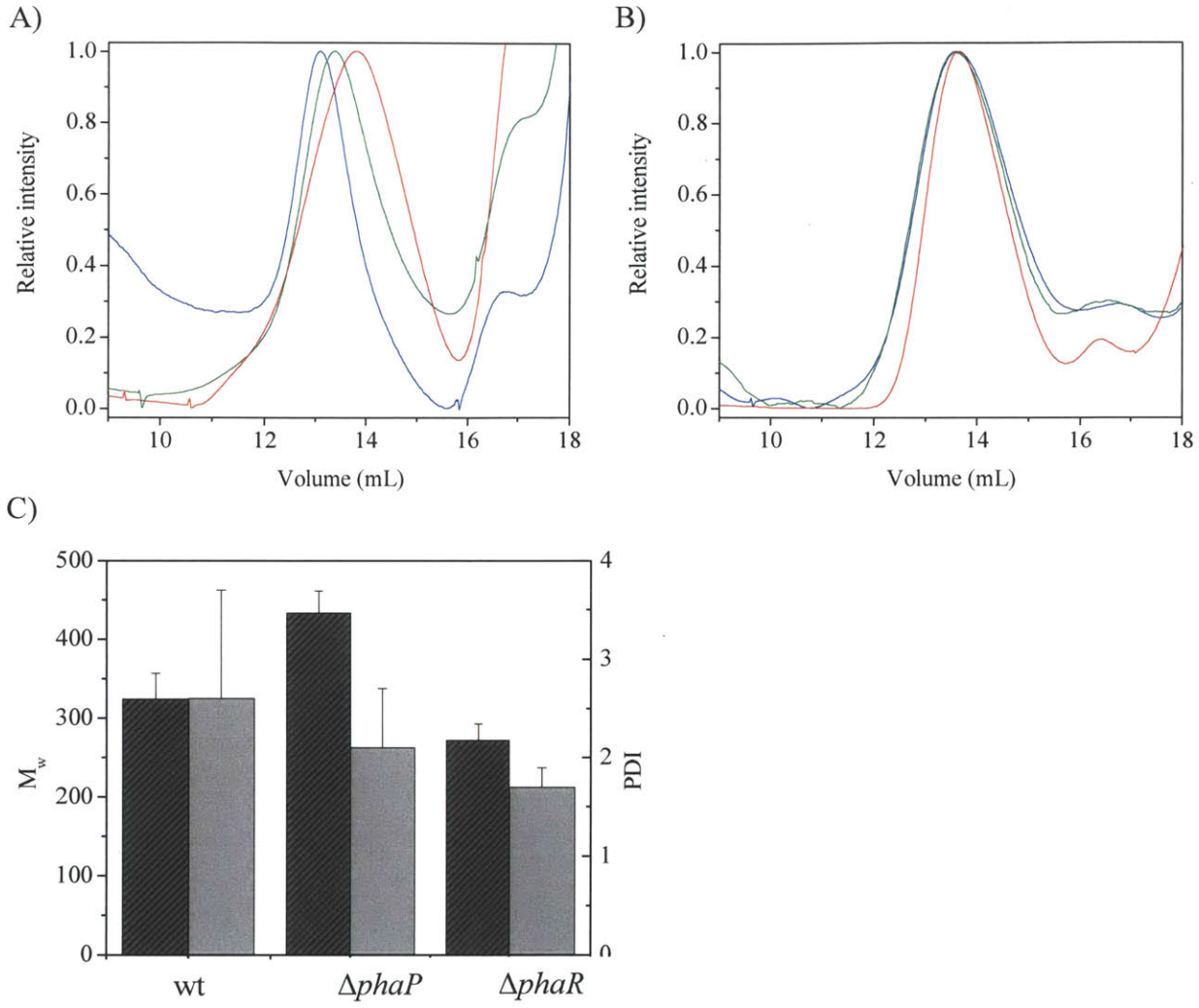

Figure A3.2 Gel permeation chromatography of PHB extracted from wt, Δ*phaP* and Δ*phaR* strains. A) Overlay of traces of PHB extracted from three Δ*phaP* cultures grown 24 h in PHB_p medium. B) Overlay of traces of PHB extracted from three Δ*phaR* cultures grown 24 h in PHB_p medium. C) Comparison of M_w (striped) and PDI (gray) of PHB extracted from wt, Δ*phaP* and Δ*phaR* cultures.

3.7 References

1. Wieczorek, R., Steinbüchel, A., and Schmidt, B. (1996) Occurrence of polyhydroxyalkanoic acid granule-associated proteins related to the *Alcaligenes eutrophus* H16 GA24 protein in other bacteria, *FEMS Microbiol. Lett. 135*, 23-30.
2. Stubbe, J., Tian, J. (2003) Polyhydroxyalkanoate (PHA) homeostasis: the role of the PHA synthase, *Nat. Prod. Rep. 20*, 445-457.
3. Wieczorek, R., Pries, A., Steinbüchel, A., and Mayer, F. (1995) Analysis of a 24-kilodalton protein associated with the polyhydroxyalkanoic acid granules in *Alcaligenes eutrophus*, *J. Bacteriol. 177*, 2425-2435.
4. York, G. M., Stubbe, J., and Sinskey, A. J. (2001) New insight into the role of the PhaP phasin of *Ralstonia eutropha* in promoting synthesis of polyhydroxybutyrate, *J. Bacteriol. 183*, 2394-2397.
5. Pötter, M., Madkour, M. H., Mayer, F., and Steinbüchel, A. (2002) Regulation of phasin expression and polyhydroxyalkanoate (PHA) granule formation in *Ralstonia eutropha* H16, *Microbiol. 148*, 2413-2426.
6. Beeby, M., Cho, M., Stubbe, J., and Jensen, G. J. (2012) Growth and localization of polyhydroxybutyrate granules in *Ralstonia eutropha*, *J. Bacteriol. 194*, 1092-1099.
7. Cho, M. (2012) Studies on the mechanism of polyhydroxybutyrate (PHB) granule formation in *Ralstonia eutropha* H16, in *Chemistry*, p 346, Massachusetts Institute of Technology, Cambridge.
8. York, G. M., Stubbe, J., and Sinskey, A. J. (2002) The *Ralstonia eutropha* PhaR protein couples synthesis of the PhaP phasin to the presence of polyhydroxybutyrate in cells and promotes polyhydroxybutyrate production, *J. Bacteriol. 184*, 59-66.

9. Maehara, A., Doi, Y., Nishiyama, T., Takagi, Y., Ueda, S., Nakano, H., and Yamane, T. (2001) PhaR, a protein of unknown function conserved among short-chain-length polyhydroxyalkanoic acids producing bacteria, is a DNA-binding protein and represses *Paracoccus denitrificans phaP* expression in vitro, *FEMS Microbiol. Lett. 200*, 9-15.

10. Encarnacion, S., del Carmen Vargas, M., Dunn, M. F., Davalos, A., Mendoza, G., Mora, Y., and Mora, J. (2002) AniA regulates reserve polymer accumulation and global protein expression in *Rhizobium etli*, *J. Bacteriol. 184*, 2287-2295.

11. Povolo, S., and Casella, S. (2000) A critical role for *aniA* in energy-carbon flux and symbiotic nitrogen fixation in *Sinorhizobium meliloti*, *Arch. Microbiol. 174*, 42-49.

12. Prieto, M. A., Buhler, B., Jung, K., Witholt, B., and Kessler, B. (1999) PhaF, a polyhydroxyalkanoate-granule-associated protein of *Pseudomonas oleovorans* GPo1 involved in the regulatory expression system for *pha* genes, *J. Bacteriol. 181*, 858-868.

13. Hoffmann, N., and Rehm, B. H. (2004) Regulation of polyhydroxyalkanoate biosynthesis in *Pseudomonas putida* and *Pseudomonas aeruginosa*, *FEMS Microbiol. Lett. 237*, 1-7.

14. Stubbe, J., Tian, J., He, A., Sinskey, A.J., Lawrence, A.G., Liu, P. (2005) Nontemplate-dependent polymerization processes: Polyhydroxyalkanoate synthases as a paradigm, *Annu. Rev. Biochem. 74*, 433-480.

15. Poindexter, J. S. (1964) Biological properties and classification of *Caulobacter* group, *Bacteriol. Rev. 28*, 231-293.

16. Qi, Q., and Rehm, B.A. . (2001) Polyhydroxybutyrate biosynthesis in *Caulobacter crescentus*: molecular characterization of the polyhydroxybutyrate synthase., *Microbiology 147*, 3353-3358.

17. Tian, J., He, A., Lawrence, A. G., Liu, P., Watson, N., Sinskey, A. J., and Stubbe, J. (2005) Analysis of transient polyhydroxybutyrate production in *Wautersia eutropha* H16 by quantitative Western analysis and transmission electron microscopy, *J. Bacteriol. 187*, 3825-3832.

18. Quandt, J., and Hynes, M. F. (1993) Versatile suicide vectors which allow direct selection for gene replacement in gram-negative bacteria, *Gene 127*, 15-21.

19. Griebel, R., Smith, Z., and Merrick, J. M. (1968) Metabolism of poly-beta-hydroxybutyrate .I. Purification, composition and properties of native poly-beta-hydroxybutyrate granules from *Bacillus megaterium*, *Biochemistry 7*, 3676-3681.

20. Laemmli, U. K. (1970) Cleavage of structural proteins during the assembly of the head of bacteriophage T4, *Nature 227*, 680-685.

21. Heckman, K. L., and Pease, L. R. (2007) Gene splicing and mutagenesis by PCR-driven overlap extension, *Nat. Protoc. 2*, 924-932.

22. Karr, D. B., Waters, J. K., and Emerich, D. W. (1983) Analysis of poly-beta-hydroxybutyrate in *Rhizobium japonicum* bacteroids by ion-exclusion high-pressure liquid chromatography and UV detection, *Appl. Environ. Microbiol. 46*, 1339-1344.

23. Malvern (2004) *Zetasizer nano series user manual*, Worcestershire, UK.

24. Slotboom, D. J., Duurkens, R. H., Olieman, K., and Erkens, G. B. (2008) Static light scattering to characterize membrane proteins in detergent solution, *Methods 46*, 73-82.

25. Haynes, W. M., (Ed.) (2012) *CRC handbook of chemistry and physics*, 92nd ed., CRC Press, Boca Raton, FL.

26. Akita, S., Einaga, Y., Miyaki, Y., and Fujita, H. (1976) Solution properties of poly(D-β–hydroxybutyrate). 1. Biosynthesis and characterization, *Macromolecules 9*, 774-780.

27. Miyaki, Y., Einaga, Y., Hirosye, T., and Fujita, H. (1977) Solution properties of poly(D-β-hydroxybutyate). 2. Light scattering and viscosity in trifluoroethanol and behavior of highly expanded polymer coils, *Macromolecules 10*, 1356-1364.

28. Nicolaus, B., Lama, L., Esposito, E., Manca, M. C., Improta, R., Bellitti, M. R., Duckworth, A. W., Grant, W. D., and Gambacorta, A. (1999) *Haloarcula* spp able to biosynthesize exo- and endopolymers, *J. Indust. Microbiol. Biotechnol. 23*, 489-496.

29. Striegel, A. M., Yau, W. W., Kirkland, J. J., and Bly, D. D. (2009) *Modern size-exclusion liquid chromatography: practice of gel filtration and gel permeation chromatography*, 2nd ed., Wiley, Hoboken, NJ.

30. Taylor, J. R. (1997) *An introduction to error analysis: the study of uncertainties in physical measurements*, 2nd ed., University Science Books, Sausalito, CA.

31. Tian, J., Sinskey, A. J., and Stubbe, J. (2005) Kinetic studies of polyhydroxybutyrate granule formation in *Wautersia eutropha* H16 by transmission electron microscopy, *J. Bacteriol. 187*, 3814-3824.

32. Poindexter, J. S. (1981) The *Caulobacters* - ubiquitous unusual bacteria, *Microbiol. Rev. 45*, 123-179.

33. Johnson, R. C., and Ely, B. (1976) Isolation of spontaneously derived mutants of *Caulobacter crescentus*, *Genetics 86*, 25-32.

34. Poindexter, J. S. (1984) The role of calcium in stalk development and in phosphate acquisition in *Caulobacter crescentus*, *Arch. Microbiol. 138*, 140-152.

35. England, J. C., Perchuk, B. S., Laub, M. T., and Gober, J. W. (2010) Global regulation of gene expression and cell differentiation in *Caulobacter crescentus* in response to nutrient availability, *J. Bacteriol. 192*, 819-833.

36. Saegusa, H., Shiraki, M., Kanai, C., and Saito, T. (2001) Cloning of an intracellular poly[D(-)-3-hydroxybutyrate] depolymerase gene from *Ralstonia eutropha* H16 and characterization of the gene product, *J. Bacteriol. 183*, 94-100.

37. Maehara, A., Taguchi, S., Nishiyama, T., Yamane, T., and Doi, Y. (2002) A repressor protein, PhaR, regulates polyhydroxyalkanoate (PHA) synthesis via its direct interaction with PHA, *J. Bacteriol. 184*, 3992-4002.

38. Cho, M., Brigham, C. J., Sinskey, A. J., and Stubbe, J. (2012) Purification of polyhydroxybutyrate synthase from its native organism, *Ralstonia eutropha*: implications for the initiation and elongation of polymer formation in vivo, *Biochemistry 51*, 2276-2288.

39. Marks, M. E., Castro-Rojas, C. M., Teiling, C., Du, L., Kapatral, V., Walunas, T. L., and Crosson, S. (2010) The genetic basis of laboratory adaptation in *Caulobacter crescentus*, *J. Bacteriol. 192*, 3678-3688.

40. Pötter, M., Müller, H., Reinecke, F., Wieczorek, R., Fricke, F., Bowien, B., Friedrich, B., and Steinbüchel, A. (2004) The complex structure of polyhydroxybutyrate (PHB) granules: four orthologous and paralogous phasins occur in *Ralstonia eutropha* *Microbiol. 150*, 2301-2311.

41. Pfeiffer, D., and Jendrossek, D. (2011) Interaction between poly(3-hydroxybutyrate) granule-associated proteins as revealed by two-hybrid analysis and identification of a new phasin in *Ralstonia eutropha* H16, *Microbiol. 157*, 2795-2807.

42. Pfeiffer, D., Wahl, A., and Jendrossek, D. (2011) Identification of a multifunctional protein, PhaM, that determines number, surface to volume ratio, subcellular localization

and distribution to daughter cells of poly(3-hydroxybutyrate), PHB, granules in *Ralstonia eutropha* H16, *Mol. Microbiol. 82*, 936-951.

43. Repaske, R., and Mayer, R. (1976) Dense autotrophic cultures of *Alcaligenes eutrophus*, *Appl. Environ. Microbiol. 32*, 592-597.

44. Lawrence, A. G., Schoenheit, J., He, A., Tian, J., Liu, P., Stubbe, J., and Sinskey, A. J. (2005) Transcriptional analysis of *Ralstonia eutropha* genes related to poly-(R)-3-hydroxybutyrate homeostasis during batch fermentation, *Appl. Microbiol. Biotechnol. 68*, 663-672.

45. Jensen, R. B., and Shapiro, L. (1999) The *Caulobacter crescentus* smc gene is required for cell cycle progression and chromosome segregation, *Proc. Nat. Acad. Sci. 96*, 10661-10666.

46. Wahl, A., Schuth, N., Pfeiffer, D., Nussberger, S., and Jendrossek, D. (2012) PHB granules are attached to the nucleoid via PhaM in *Ralstonia eutropha*, *BMC Microbiol. 12*, 262-282.

47. Felzenberg, E. R., Yang, G. A., Hagenzieker, J. G., and Poindexter, J. S. (1996) Physiologic, morphologic and behavioral responses of perpetual cultures of *Caulobacter crescentus* to carbon, nitrogen and phosphorus limitations, *J. Indust. Microbiol. 17*, 235-252.

48. Dennis, D., Sein, V., Martinez, E., and Augustine, B. (2008) PhaP is involved in the formation of a network on the surface of polyhydroxyalkanoate inclusions in *Cupriavidus necator* H16, *J. Bacteriol. 190*, 555-563.

49. Mayer, F., and Hoppert, M. (1997) Determination of the thickness of the boundary layer surrounding bacterial PHA inclusion bodies, and implications for models describing the molecular architecture of this layer, *J. Basic Microbiol. 37*, 45-52.

50. Boatman, E. S. (1964) Observations on the fine structure of spheroplasts of Rhodospirillum rubrum, *J. Cell Biol. 20*, 297-311.

51. Wang, W. S., and Lundgren, D. G. (1969) Poly-beta-hydroxybutyrate in the chemolithotrophic bacterium *Ferrobacillus ferrooxidans*, *J. Bacteriol. 97*, 947-950.

52. Jensen, T. E., and Sicko, L. M. (1971) Fine structure of poly-beta-hydroxybutyric acid granules in a blue-green alga, *Chlorogloea fritschii*, *J. Bacteriol. 106*, 683-686.

53. Brigham, C. J., Budde, C. F., Holder, J. W., Zeng, Q. D., Mahan, A. E., Rha, C., and Sinskey, A. J. (2010) Elucidation of beta-Oxidation Pathways in *Ralstonia eutropha* H16 by Examination of Global Gene Expression, *J. Bacteriol. 192*, 5454-5464.

54. Briegel, A., Dias, D. P., Li, Z., Jensen, R. B., Frangakis, A. S., and Jensen, G. J. (2006) Multiple large filament bundles observed in *Caulobacter crescentus* by electron cryotomography, *Mol. Microbiol. 62*, 5-14.

55. Schmidt, J. M. (1968) Stalk elongation in mutants of Caulobacter crescentus, *J. Gen. Microbiol. 53*, 291-298.

56. Jossek, R., Reichelt, R., and Steinbüchel, A. (1998) In vitro biosynthesis of poly(3-hydroxybutyric acid) by using purified poly(hydroxyalkanoic acid) synthase of *Chromatium vinosum*, *Appl. Microbiol. Biotechnol. 49*, 258-266.

57. Niamsiri, N., Bergkvist, M., Delamarre, S. C., Cady, N. C., Coates, G. W., Ober, C. K., and Batt, C. A. (2007) Insight in the role of bovine serum albumin for promoting the in

situ surface growth of polyhydroxybutyrate (PHB) on patterned surfaces via enzymatic surface-initiated polymerization, *Colloids Surf B Biointerfaces 60*, 68-79.

58. Horowitz, D. M., and Sanders, J. K. M. (1995) Biomimetic, amorphous granules of polyhydroxybutyrate: composition, mobility, and stabilization *in vitro* by proteins. , *Can. J. Microbiol. 41*, 115-123.

59. Jensen, R. B. (2006) Coordination between chromosome replication, segregation, and cell division in *Caulobacter crescentus*, *J Bacteriol. 188*, 2244-2253.

60. Briegel, A., Ding, H. J., Li, Z., Werner, J., Gitai, Z., Dias, D. P., Jensen, R. B., and Jensen, G. J. (2008) Location and architecture of the Caulobacter crescentus chemoreceptor array, *Molecular Microbiology 69*, 30-41.

61. Gerngross, T. U., and Martin, D. P. (1995) Enzyme-catalyzed synthesis of poly[(R)-(-)-3-hydroxybutyrate]: formation of macroscopic granules in vitro, *Proc. Natl. Acad. Sci. 92*, 6279-6283.

62. Tian, J., Sinskey, A. J., and Stubbe, J. (2005) Class III polyhydroxybutyrate synthase: involvement in chain termination and reinitiation, *Biochemistry 44*, 8369-8377.

Chapter 4:

Efforts to crystallize class I and class III PHB synthases

4 Efforts to crystallize class I and class III PHB synthases

4.1 Introduction

This Chapter describes our efforts to crystallize both class I and class III synthases. These studies were conducted in collaboration with Prof. Karen Allen in the Boston University Department of Chemistry. Our lab has collaborated with the Ellenberger and Drennan laboratories over the past 20 years in ongoing efforts to obtain a crystal structure of the class III synthase from *Allochromatium vinosum*, $PhaEC_{Av}$ and the class I synthase from *Ralstonia eutropha*, $PhaC_{Re}$. Crystals could be readily obtained in many conditions, but they either did not diffract or diffracted to poor resolution (7 Å or worse). Thus, our efforts to obtain high resolution structures of $PhaEC_{Av}$ and $PhaC_{Re}$ have thus far been unsuccessful.

One possible cause of disorder within a crystal lattice can be thermally labile regions of proteins, that is, regions that are flexible enough to disrupt the crystal lattice. In an effort to identify disordered regions of $PhaEC_{Av}$ that might prevent tight packing in a crystal lattice, limited proteolysis experiments were carried out. In these experiments, Geoff Stamper from the Drennan Lab treated $PhaEC_{Av}$ with a small amount of chymotrypsin, and assayed the resulting protein mixtures for activity. He found that PhaE could be cleaved at two chymotrypsin cleavage sites, one site 27 residues and a second site 35 residues from the C-terminus of PhaE, with minimal effect on activity. Paul Hubbard, a former post doc in the Drennan Lab, cloned the *phaEΔ27* construct in the pCDF1 vector with an N-terminal His_6-tag, and separately cloned *phaC* in the pET24a vector. He co-expressed and purified PhaEΔ27 and PhaC, in a 1:1 ratio (as judged by SDS-PAGE). We have previously expressed wt $PhaEC_{Av}$ from a single vector containing *phaEC* and have observed that the two proteins also co-purify in a nearly 1:1 ratio (*1, 2*). Hubbard identified several conditions in which $PhaE\Delta27C_{Av}$ crystallized. The condition he

pursued most extensively was condition 59 of the Index Screen from Hampton Research. This condition contained 0.02 M $MgCl_2 \cdot 6H_2O$, 0.1 M Hepes pH 7.5 and 22% w/v poly(acrylic acid sodium salt) 5,100. The original crystals only diffracted to >7 Å, thus he made several attempts to improve resolution by grid screening around the initial condition. Unfortunately he was unable to improve the resolution beyond 7 Å.

Hubbard provided us with the PhaEΔ27C_{Av} construct, and our efforts to crystallize it are described in this Chapter. We have crystallized it both in the presence and absence of the inhibitor $HBCH_2CoA$, which is an analog of HBCoA in which the S of the thioester is replaced with a methylene group (Figure 4.1). We also prepared a similar PhaEΔ35C_{Av} construct, in which PhaE has an N-terminal His_6-tag and its 35 C-terminal residues are deleted. PhaEΔ35C_{Av} was also extensively screened for crystallization conditions, and like full-length PhaEC_{Av} and PhaEΔ27C_{Av}, PhaEΔ35C_{Av} could be readily crystallized but at best diffracted to only 6.3 Å.

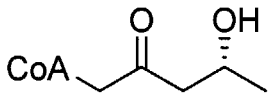

Figure 4.1 Structure of the HBCoA analog $HBCH_2CoA$.

Another approach was taken to obtain a crystal structure of a class I and/or III PHB synthase. As discussed in Chapter 1, the database contains hundreds of sequences of class I and III synthases from various organisms. A common approach, when crystallization of a protein of interest is not successful, is to investigate homologs. To this end, we cloned class III synthases from *Thiococcus pfennigii*, *Xanthamonas campestris*, *Arthrospira maxima*, *Xanthomonas oryzaea*, and *Synechocystis* PCC 8603 and class I synthases from *Caulobacter crescentus*, *Sphingopyxis alaskensis*, *Leptothrix cholodnii*, *Magnetospirillum magneticum*. In this Chapter, we focus on the synthase from *C. crescentus* as well as a truncated construct in which the 85

N-terminal residues are removed ($PhaC_{Cc}$ and $PhaC_{Cc}\Delta N$, respectively) and on the PhaCs from *L. cholodnii* and *S. alaskensis* ($PhaC_{Lc}$ and $PhaC_{Sa}$, respectively). These synthases are well-behaved in solution and can readily be purified to >95% homogeneity. Most effort was put into the crystallization of PhaC from *C. crescentus*, which is described in detail in this Chapter.

Unfortunately, we were ultimately not successful in our efforts to obtain a crystal structure. This Chapter is intended to describe our most promising leads and what techniques were employed in following these leads, and to provide recommendations for future crystallization efforts.

4.2 Materials and Methods

4.2.1 Materials

All chemicals were obtained at the highest purity available from Sigma-Aldrich (St. Louis, MO) unless otherwise specified. All crystallography screens, siliconized glass coverslips and 24-well crystallography trays were purchased from Hampton Research (Aliso Viejo, CA). (*R*)-HBCoA was synthesized by Dr. Ping Li following the method of Yuan *et al. (3)*. Oligonucleotide primers were obtained from Integrated DNA Technologies (Coralville, IA) and are listed in Table 4.1. Restriction enzymes were purchased from New England Biolabs (Beverly, MA), GoTaq DNA polymerase and T4 DNA ligase were purchased from Promega (Fitchburg, WI) and PfuII Ultra polymerase was purchased from Stratagene (La Jolla, CA). The plasmids used in this study are listed in Table 4.2.

Table 4.1 Primers and oligonucleotides used in this study.

Name	Sequence[a]
phaEΔ35fw	5′-*CGCGTCGCAGCCCTG*TAAAAGCTTGCGGCC-3′
phaEΔ35rev	5′-GGCCGCAAGCTTTT*ACAGGGCTGCGACGCG*-3′
phaCSafw	5′-GCTAGCACCGATATGGGCGAGGACAAGAGCAGCGGCGCGGCGA ATCC-3′
phaCSarev	5′-GGATCCTTACCGCTGTTTGACGTAGCGGCCGGGGGCGTCCTCG-3′
phaCLcfw	5′-GTACCATATGAGCGCATTCCTCGGGCAGATGCCTGGGTTGGCCG GCC-3′
phaCLcrev	5′-GTACAAGCTTTCAGACTTTCTGCTTGACGTAACGACCGGGTGCC GGC-3′
phaCMmfw	5′-GTATAATAAGCTAGCGCCGAGCAGACGGGC-3′
phaCMmrev	5′-CAACTGGGATCCTTACACCGCCTTGAC-3′
phaCAmfw	5′-CATATGATGTTACCTTTCGCCTTACAAATGGGTTTAGAAGACTTA ACCCAGG AATATGCAGACCTCACCG-3′
phaCAmrev	5′-GGATCCTCACTCTCGCACTTTTAACCAATCAACAATGGTTGGGGG TAGGTCTCGCTGTAC-3′
phaEAmfw	5′-CATATGGAAAACGAAACAAATCCGTGGAACGAAATGGCCAATCA ATGGGTAAACACCTGGACTC-3′
phaEAmrev	5′-GGATCCTCAACTTACTTCTTGAATTGACTCGGGTTTGGGTGAAGAT GCTGTCATGGTGGATATCTG-3′
phaCSynfw	5′-CATATGATGTTGCCTTTTTTTGCTCAGGTGGGGTTAGAAGAAAAT CTCCATGAAACCCTAG-3′
phaCSynrev	5′-GGATCCTCACTGTCGTTCCGATAGCCAATGGGCGATC-3′
phaESynfw	5′- GCTAGCAAGTTACTTTATTGGATTTAGTCCC-3′
phaESynrev	5′- GCTAGCTTAGCCTGGGTTTGCTTCTGTTTCTCCC-3′
phaECTpfw	5′-GATATAGGATCCT*GGCGGCGGCGGCTCTGGCGGCGGCGGCTCT*AA CGATACGGCCAACAAGAC-3′
phaECTprev	5′-GATATAGCGGCCGCTCAGGCGCG-3′
phaCTpfw	5′-GATATACATATGATGTCCCCATTCCCGATCGACATCCGGCCCGAC AAG-3′
phaCTprev	5′-GATATAGGATCCTCAGCCGCGTTCGTTCAGCCAGCGGC-3′
phaETpfw	5′-GATATACATATGAACGATACGGCCAACAAGACCAGCGACTGGGT CGACATCC-3′
phaETprev	5′-GATATAGGATCCTCACTGGCCGGTGGTGGGCTTGGTGGTCTTG-3′
phaECXcfw	5′-GATATACATATG*GGCGGCGGCGGCTCTGGCGGCGGCGGCTCT*ACA ACCAGCGGTTCGG-3′
phaECXcrev	5′-GATATA-GAGCTC-TCAACCGTTGCCGCCAC-3′
phaCXofw	5′-CATATGAAGGGCCCATTGGGGTTCAGCGCCGAAGACC-3′
phaCXorev	5′-GGATCCTCAGGCATTGCCGCCACGTTCCTGCAGCCAG-3′
phaEXofw	5′-GCTAGCATGGCAAGCAGCGGTTCGGACAACGGCAACTTCGACG-3′
phaEXorev	5′-AAGCTTTCATGCCTGCGCTCCACGTTTTTTACCTGCGGGGGGTG TG-3′

[a]Restriction sites are underlined

Table 4.2 Commercial vectors and plasmids used in this study.

Commercial vector	Description	Source
pET24a	Expression vector, under control of lac operator, T7 promoter; contains f1 origin and encodes kanamycin (Km) resistance	Novagen
pCDF1	Expression vector, under control of lac operator, T7 promoter; contains CDF origin and encodes streptomycin (Sm) resistance; encodes N-terminal His_6-tag and the linker VGTGSNDDDDKSP with an enterokinase cleavage site underlined	Novagen
pET28a	Expression vector, under control of lac operator, T7 promoter; contains f1 origin and encodes kanamycin resistance; encodes N-terminal $(His)_6$-tag and a thrombin cleavage site (SSGLVPRGDSH)	Novagen
pET3a	Expression vector, under control of lac operator, T7 promoter; contains f1 origin and encodes ampicillin (Amp) resistance	Novagen
pTrc99	Expression vector, under control of arabinose promoter; contains F1 origin and encodes Amp resistance	Invitrogen
pET52b	Expression vector, under control of lac operator, T7 promoter; contains F1 origin; encodes N-terminal StrepII-tag (WSHPQFEK) and the linker GALEGALEVLFQGPGYQDP, with a rhinovirus protease cleavage site underlined; encodes Amp resistance	Novagen
Plasmid	**Description**	**Reference**
$pPhaC_{Av}$[a]	pET24a containing *phaC*$_{Av}$ inserted between NdeI and XhoI restriction sites	Hubbard, Drennan, unpublished
$pPhaE\Delta27_{Av}$[a]	pCDF1 containing *phaEΔ27*, which is *phaE* from *A. vinosum* truncated on the C-terminus by 27 amino acids; *phaEΔ27* is inserted between BamHI and HindIII restriction sites and contains an N-terminal His_6-tag and the linker VGTGSNDDDDKSP	Hubbard, Drennan, unpublished
$pPhaE\Delta35_{Av}$	pCDF1 containing *phaEΔ35*, which is *phaE* from *A. vinosum* truncated on the C-terminus by 35 amino acids; *phaEΔ35* is inserted between BamHI and HindIII restriction sites and contains an N-terminal His_6-tag and the linker VGTGSNDDDDKSP	This work
$pPhaC_{Sa}$	pET28a containing *phaC*$_{Sa}$, inserted between NheI and BamHI restriction sites; encodes N-terminal His_6-tag with the linker SSGLVPRGDSH	This work
$pPhaC_{Lc}$	pET28a containing *phaC*$_{Lc}$, inserted between NdeI and HindIII restriction sites; encodes N-terminal	This work

	$(His)_6$-tag with the linker SSGLVPRGDSH	
$pPhaC_{Mm}$[b]	pET28a containing *phaC*$_{Mm}$, inserted between NheI and BamHI restriction sites; encodes N-terminal $(His)_6$-tag with the linker SSGLVPRGDSH	This work
$pPhaC_{Am}$	pET3a containing *phaC*$_{Am}$ inserted between NdeI and BamHI restriction sites	This work
$pPhaE_{Am}$	pET28a containing *phaE*$_{Am}$ inserted between NdeI and BamHI restriction sites; encodes N-terminal $(His)_6$-tag with the linker SSGLVPRGDSH	This work
$pPhaC_{Syn}$	pET3a containing *phaC*$_{Syn}$ inserted between NdeI and BamHI restriction sites	This work
$pPhaE_{Syn}$	pET28a containing *phaE*$_{Syn}$, inserted into an NheI restriction site; encodes N-terminal $(His)_6$-tag and the linker SSGLVPRGDSH	This work
pFS91	pTrc99a containing *phaEC*$_{Tp}$; *phaE* and *phaC* are separated by 40 non-coding base pairs	Budde, Sinskey, unpublished
$pPhaEC_{Tp}$	pET52b containing *phaEC*$_{Tp}$ inserted between BamHI and NotI restriction sites; encodes N-terminal StrepII-tag and contains $(G_4S)_2$ linker	This work
$pPhaC_{Tp}$	pET3a containing *phaC*$_{Tp}$ inserted between NdeI and BamHI restriction sites	This work
$pPhaE_{Tp}$	pET28a containing *phaE*$_{Tp}$, inserted between NdeI and BamHI restriction sites; encodes N-terminal $(His)_6$-tag and the linker SSGLVPRGDSH	This work
$pPhaEC_{Xc}$	pET52b containing *phaEC*$_{Xc}$ inserted between NdeI and BamHI restriction sites; encodes N-terminal StrepII-tag and contains $(G_4S)_2$ linker	This work
$pPhaC_{Xo}$	pET3a containing *phaC*$_{Xo}$ inserted between NdeI and BamHI restriction sites	This work
$pPhaE_{Xo}$	pET28a containing *phaE*$_{Xo}$, inserted between NheI and HindIII restriction sites; encodes N-terminal $(His)_6$-tag and the linker SSGLVPRGDSH	This work

[a]plasmids were a gift of Paul Hubbard
[b]plasmid was generated by Elizabeth Min

4.2.2 Construction of the expression plasmid pPhaEΔ35 from pPhaEΔ27 by mutagenesis

The plasmid pPhaEΔ35 was generated from the parent plasmid pPhaEΔ27, which was a gift of Paul Hubbard from the Drennan Lab. Using pPhaEΔ27 as a template, eight additional C-terminal residues were removed in a single mutagenesis step using the primers phaEΔ35fw and phaEΔ35rev (Table 4.1) to generate pPhaEΔ35. The italicized portions of the primers anneal to

the 3′ end of *phaE* immediately upstream of the fragment to be deleted by mutagenesis. The regular font portions anneal to the region immediately downstream of the fragment to be deleted. Mutagenesis was carried out using PfuII polymerase and 1 μM each primer; the annealing temperature was 55 °C and the extension time and temperature were 7 min at 68 °C. The product was transformed into *E. coli* XL10Gold cells, which were plated onto LB/agar supplemented with 50 μg/mL streptomycin (Sm). Plasmid was isolated and the gene was sequenced at MIT Biopolymers to confirm the desired construct.

4.2.3 Expression and purification of PhaEΔ27C and PhaEΔ35C

For expression of PhaEΔ27C_{Av} and PhaEΔ35C_{Av}, *E. coli* BL21(DE3) Gold cells were co-transformed with pPhaEΔ27$_{Av}$/pPhaC$_{Av}$ or pPhaEΔ35$_{Av}$/pPhaC$_{Av}$, respectively, for co-expression of PhaE_{Av} and PhaC_{Av}. In a typical growth, 2 L cultures (LB supplemented with 50 μg/mL sm and 50 μg/mL Km) in 6 L flasks were inoculated at a dilution of 1:200 with saturated overnight cultures harboring pPhaEΔ27$_{Av}$/pPhaC$_{Av}$ or pPhaEΔ35$_{Av}$/pPhaC$_{Av}$. The cultures were grown at 37 °C with shaking at 220 rpm until they reached and OD_{600} = 0.6. The cultures were then cooled on ice to ~25 °C and induced with 0.4 mM IPTG and grown an additional 3-4 h at 25 °C with shaking at 220 rpm. The cells were then pelleted by centrifugation at 4,000 x*g* for 10 min at 4 °C. The cell pellets were flash frozen in liquid nitrogen and stored at -80 °C until required. A growth typically yielded 2-3 g cell paste per L of culture.

PhaEΔ27C_{Av} or PhaEΔ35C_{Av} were co-purified using Ni-NTA chromatography. Only PhaE in each construct contained the His_6-tag, and the association between PhaE and PhaC facilitated co-purification in a 1:1 ratio. The cells (typically ~10 g) were resuspended in 3-5 mL lysis buffer (50 mM NaH_2PO_4, 300 mM NaCl, 10 mM imidazole, pH 8.0) and lysed by two

passes through the French pressure cell at 14,000 psi. The insoluble cell debris was removed by centrifugation at 4 °C for 20 min at 20,000 x*g*. The soluble supernatant was combined with Ni-NTA resin (1 mL resin per 10 mg protein) and incubated with gentle stirring for 30 min at 4 °C. The slurry was loaded onto a column and the resin allowed to settle. The flowthrough was collected by gravity flow. The column was washed with 20 column volumes (cv) lysis buffer, then the protein was eluted with 5 cv lysis buffer with 250 mM imidazole. The protein containing fractions were combined and concentrated to 3-5 mL, then exchanged into 50 mM sodium cacodylate pH 7.5, 20 mM NaCl by two rounds of dialysis for 4 h against 1 L buffer at 4 °C. The typical yield from purification of both PhaEΔ27C_{Av} and PhaEΔ35C_{Av} was approximately 10 mg/g of cells. The proteins were concentrated to ~20 mg/mL and aliquots of 30 μL, 50 μL and 100 μL were flash frozen in liquid nitrogen and stored at -80 °C.

4.2.4 Activity assays of PhaEC_{Av} constructs

Activities were measured at 30 °C using the 5,5′-dithiobis-(2-nitrobenzoic acid (DTNB) assay described in Chapter 2, section 2.2.5. In a final volume of 100-200 μL, a typical assay of PhaEΔ27C_{Av} or PhaEΔ35C_{Av} contained 15-20 nM synthase and 0.75 mM HBCoA. At various time points, 20 μL aliquots were withdrawn and added to 50 μL 10% ice cold trichloroacetic acid (TCA). The samples were centrifuged 5 min at 14,000 x*g* to remove precipitated protein, and 68 μL was withdrawn and added to 362 μL 0.25 mM DTNB in 0.5 M KH_2PO_4, pH 7.8. A_{412} (ε = 13,600 $M^{-1}cm^{-1}$) was measured. The assay data are fit to a sigmoidal function whose equation is given in Equation 4.1.

Equation 4.1 $$y = A\frac{x^n}{k^n + x^n}$$

4.2.5 Determination of the oligomeric states of PhaEΔ27C_{Av} and PhaEΔ35C_{Av} by size exclusion chromatography (SEC)

The oligomeric states of PhaEΔ27C_{Av} and PhaEΔ35C_{Av} were examined by SEC using a Bio-Sil SEC 400-5 column (Bio-Rad, 300 x 7.8 mm, M_w range 20,000–1,000,000 Da) connected to a Waters 515/2487 HPLC and the elution monitored at 260 and 280 nm. The samples (20 μL of a 5 mg/mL solution) were injected onto the column and eluted at room temperature (RT) at a flow rate of 1.0 mL/min with 50 mM sodium cacodylate, pH 7.5, 200 mM NaCl. The M_w of each sample was determined by comparison with a set of standards (Bio-Rad) of retention times (M_w): thyroglobulin, 9.2 min (670 kDa); γ-globulin, 11.5 min (158 kDa); ovalbumin, 12.2 min (44 kDa); myoglobin, 13.1 min (17 kDa); B_{12}, 13.9 min (1.35 kDa).

4.2.6 General procedures for setting up crystallization trials

Crystallization conditions are described in greater detail in the Results section. Generally, for initial screening of crystallization conditions, PhaEΔ27C_{Av} and PhaEΔ35C_{Av} were ~20 mg/mL in 50 mM sodium cacodylate pH 7.5, 20 mM NaCl, and PhaC_{Cc}ΔN was 30-60 mg/mL in 20 mM Hepes pH 7.5, 20 mM NaCl. Prior to setting up trays, proteins were centrifuged at 4 °C for 10 min at 14,000 x*g* to remove insoluble contaminants such as dust or precipitated protein. Crystallization conditions were screened by the hanging drop method in 24-well trays using siliconized glass cover slips. The wells contained 500 μL mother liquor and the hanging drop typically consisted of 1 μL protein and 1 μL mother liquor. All proteins were examined in the following screens (Hampton Research, Aliso Viejo, CA): Crystal Screens I and II (98 conditions); Index Screen (96 conditions); PEG/Ion Screens I and II (96 conditions); PEGR_x

Screens I and II (96 conditions); SaltR$_x$ Screens I and II (96 conditions). Trays were incubated at 4 °C, 18 °C, 23 °C and 37 °C, as indicated in the text.

Samples of PhaEΔ27C$_{Av}$ (20 mg/mL) and PhaC$_{Cc}$ΔN (65 mg/mL) were also submitted to the Hauptman-Woodward Medical Research Institute (Buffalo, NY) for high throughput screening using the microbatch-under-oil method of crystallization. In this method, 1536-well trays are set up such that each well contains 0.2 μL protein solution and 0.2 μL crystallization solution (a different solution in each well) covered by a drop of Parrafin oil (EMD Chemicals, Inc, Darmstadt, Germany). Slow vapor diffusion from the protein/crystallization solution drop through the Parrafin oil increases the concentration of protein and precipitant in the drop over time, which can potentially facilitate crystal formation. The crystallization solutions used in these experiments can be found at http://www.hwi.buffalo.edu/faculty_research/crystallization.html.

4.2.7 In-house screening of crystals for diffraction

Crystals were screened in the Boston University Department of Chemistry using a Bruker AXS Proteum-R instrument, equipped with a kappa four circle goniometer, MICROSTAR rotating anode X-ray source and PLATINUM135 CCD area detector for single crystal X-ray diffraction. Crystals were screened either at RT (wet mounts) or frozen in a stream of nitrogen (cryo mounts). For wet mounts, single crystals were looped and a small amount of the well solution (5-10 μL) was pipetted into the tip of a cylindrical plastic sheath with one sealed end, which was then placed over the loop holding the crystal (Figure 4.2). The sheath was sealed to the loop using vacuum grease. The well solution in the tip of the plastic sheath prevents the crystal from drying out during screening. For cryo mounts, single crystals were looped from their original drop and gently placed in a 5 μL drop of a cryoprotectant solution (e.g. Paratone-N, PEG

400, isopropanol). The crystal was released from the loop and gently agitated in the cryoprotectant to remove excess water from the crystal. The crystal was then looped again and quickly mounted onto the goniometer head and frozen in a cryostream of nitrogen.

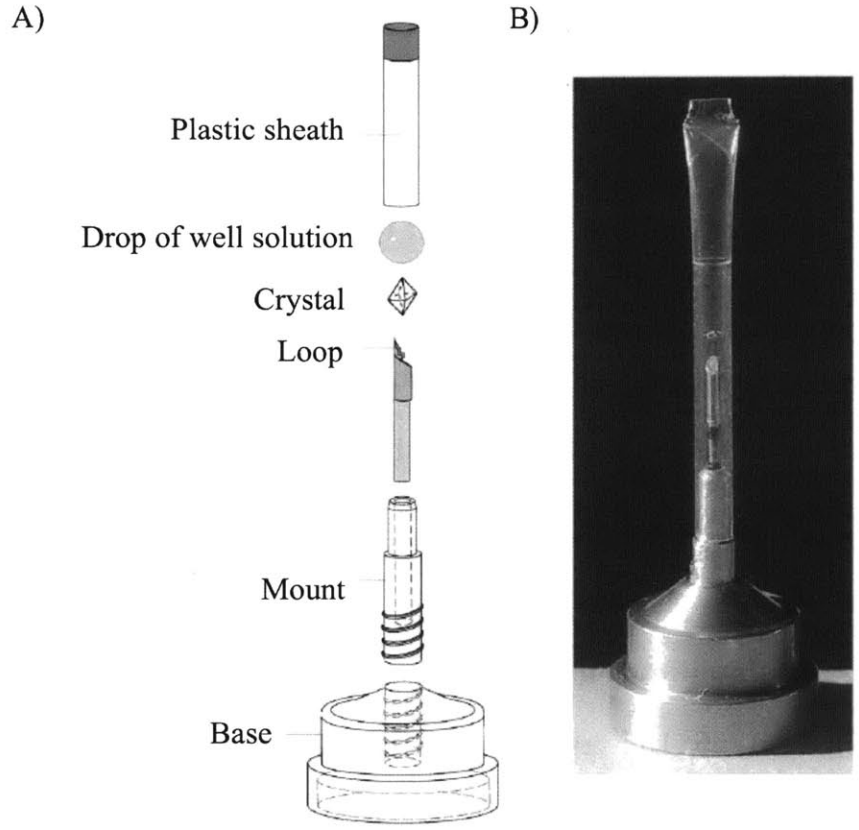

Figure 4.2 Diagram of a room temperature (wet) mount for screening crystals for diffraction. A) Illustration of components for a wet mount set-up. B) Picture of sealed wet mount. Figure was adapted from (*4*).

4.2.8 Construction of the expression plasmid pPhaC$_{Sa}$

The gene for the class I synthase from *Sphingopyxis alaskensis* (*phaC*$_{Sa}$) was cloned into the expression vector pET28a for overexpression and purification. A glycerol stock of *S. alaskensis* was generously provided by the Sinskey lab in the MIT Department of Biology. The cells were streaked onto LB/agar without antibiotics and grown overnight at 37 °C. *phaC*$_{Sa}$ (1.8 kb) was amplified by colony PCR on single colonies using GoTaq polymerase and the primers

phaCSafw/phaCSarev (Table 4.1). phaCSafw inserted an NheI restriction site on the 5′ end of *phaC*$_{Sa}$, and phaCSarev inserted a BamHI restriction site at the 3′ end of *phaC*$_{Sa}$. The PCR product was digested with NheI and BamHI and ligated overnight at RT into pET28a digested with the same restriction enzymes at a vector to insert ratio of 1:5. The ligation product was transformed into *E. coli* XL10 Gold cells, which were grown overnight at 37 °C on LB/agar supplemented with 50 μg/mL Km. Plasmids were isolated and the gene sequenced at the MIT Biopolymers Facility.

4.2.9 Construction of the expression plasmid pPhaC$_{Lc}$

The gene for the class I synthase from *Leptothrix cholodnii* (*phaC*$_{Lc}$) was cloned into pET28a for expression and purification. Genomic DNA from *L. cholodnii* was generously provided from the Emerson lab at the Bigelow Laboratory for Ocean Sciences in East Boothbay, Maine. *phaC*$_{Lc}$ (1.8 kb) was amplified from 50 ng of genomic DNA using GoTaq polymerase and the primers phaCLcfw/phaCLcrev (Table 4.1). phaCLcfw inserted an NdeI restriction site on the 5′ end of *phaC*$_{Lc}$, and phaCLcrev inserted a HindIII restriction site at the 3′ end of *phaC*$_{Lc}$. The PCR product was digested with NdeI and HindIII and ligated overnight at RT into pET28a digested with the same restriction enzymes at a vector to insert ratio of 1:5. The ligation product was transformed into *E. coli* XL10 Gold cells, which were grown overnight at 37 °C on LB/agar supplemented with 50 μg/mL Km. Six colonies were grown to saturation and the plasmids were isolated and the sequences confirmed by the MIT Biopolymers Facility.

4.2.10 Expression and purification of $PhaC_{Sa}$ and $PhaC_{Lc}$

Expression and purification of $PhaC_{Sa}$ and $PhaC_{Lc}$ were carried out exactly as described for $PhaC_{Cc}$ and $PhaC_{Cc}\Delta N$ in Chapter 2. Purification yielded 5 mg $PhaC_{Sa}$ per g of cell paste, and 1 mg of $PhaC_{Lc}$ per g of cell paste. The proteins were purified to >95% purity as judged by 10% SDS-PAGE.

4.2.11 Activity assays of $PhaC_{Sa}$ and $PhaC_{Lc}$

For $PhaC_{Sa}$, in a final volume of 80 μL, a typical assay contained 53 nM synthase and 0.75 mM HBCoA, and the temperature was varied from 10-40 °C. For $PhaC_{Lc}$, in a final volume of 90 μL a typical assay contained 100 nM synthase and 0.75 mM HBCoA and the temperature was varied from 15-40 °C. Prior to the assay, the enzymes were incubated for 5 min at the assay temperature. At various time points, 10 μL aliquots were withdrawn from 0-10 min and added to 25 μL 10% TCA. The samples were centrifuged 5 min at 14,000 x*g* to remove precipitated protein, and 33 μL was withdrawn and added to 117 μL 0.25 mM DTNB in 0.5 M KH_2PO_4, pH 7.8. The A_{412} of each sample was measured. The specific activities were calculated from the linear portion of the assays. The data were fit to a sigmoidal function whose equation is given in Equation 1.

4.2.12 Construction of the expression plasmid $pPhaC_{Mm}$

The gene for the class I synthase from *Magnetospirillum magneticum* (*$phaC_{Mm}$*) was cloned into pET28a for expression and purification. Genomic DNA from *M. magneticum* was generously provided from the Komeili laboratory in the Department of Plant and Microbial Biology at UC Berkeley. *$phaC_{Mm}$* (1.8 kb) was amplified from 50 ng of genomic DNA using

GoTaq polymerase and the primers phaCMmfw/phaCMmrev (Table 4.1). phaCMmfw inserted an NheI restriction site on the 5′ end of $phaC_{Mm}$, and phaCMmrev inserted a BamHI restriction site at the 3′ end of $phaC_{Mm}$. The PCR product was digested with NheI and BamHI and ligated overnight at RT into pET28a digested with the same restriction enzymes at a vector to insert ratio of 1:5. The ligation product was transformed into *E. coli* XL10 Gold cells, which were grown overnight at 37 °C on LB/agar supplemented with 50 μg/mL Km. Plasmids were isolated and the sequences confirmed by the MIT Biopolymers Facility.

4.2.13 General strategy for cloning and expression of class III synthases

Cloning of the class III synthases described in this section followed a general strategy in which *phaE* and *phaC* were cloned into separate expression vectors. The *phaEs* were cloned into pET28a, which encoded an N-terminal $(His)_6$-tag and Km resistance. The *phaCs* were cloned into pET3a, which encoded Amp resistance but no tag. The two plasmids were co-transformed into *E. coli* and maintained by Km/Amp selection. Expression, purification and characterization of the various synthases were successful to varying degrees, but they were generally more poorly behaved in solution than the class I synthases described above, and were thus not pursued extensively for crystallization.

4.2.14 Cloning of $pPhaE_{Am}$ and $pPhaC_{Am}$ and expression of $PhaEC_{Am}$

Construction of the expression plasmids $pPhaE_{Am}$ and $pPhaC_{Am}$. Arthrospira maxima (10 mL of liquid culture) was a generous gift of the Dismukes Laboratory from the Department of Chemistry and Chemical Biology at Princeton. For amplification of *phaE* and *phaC*, the genomic DNA from *A. maxima* was first isolated from 1 mL of the liquid culture using the GenElute

Bacterial Genomic DNA Kit (Sigma-Aldrich) by the manufacturer's protocol. *phaE*$_{Am}$ was amplified from 50 ng genomic DNA using PfuII Ultra polymerase and the primers phaEAmfw/phaEAmrev. phaEAmfw inserted an NdeI restriction at the 5′ end of *phaE* and phaEAmrev inserted a BamHI restriction site at the 3′ end of *phaE*. The amplified PCR product was digested using NdeI/BamHI and was ligated overnight at RT into pET28a digested with the same enzymes at an insert to vector ratio of 5:1. *phaC* was amplified using the primers phaCAmfw/phaCAmrev. phaCAmfw inserted an NdeI restriction site at the 5′ end of *phaC* and phaCAmrev inserted a BamHI restriction site at the 3′ end of *phaC*. The amplified PCR product was then digested with NdeI/BamHI and ligated at RT overnight into pET3a digested with the same restriction enzymes at an insert to vector ratio of 5:1. The ligation products were individually transformed into *E. coli* XL10Gold, which were grown overnight at 37 °C on LB/agar supplemented with 50 μg/mL Km (for pPhaE$_{Am}$) or 100 μg/mL Amp (pPhaC$_{Am}$). Single colonies were grown to saturation and the plasmids were isolated and sent for sequencing at the MIT Biopolymers Facility.

Expression of PhaEC$_{Am}$. All culture medium was supplemented with 50 μg/mL Km and 100 μg/mL Amp. A single colony of *E. coli* BL21(DE3) Gold containing pPhaE$_{Am}$ and pPhaC$_{Am}$ was used to inoculate 5 mL of LB in a 15 mL culture tube. Cells were grown overnight at 37 °C. The culture was then used to inoculate three separate 500 mL LB cultures in 2 L baffled flasks at dilutions of 1:200. The cultures were grown at 37 °C with shaking at 220 rpm until OD_{600} = 0.6. Of the three cultures, two were cooled to ~18 °C on ice, induced with 0.4 mM IPTG and grown an additional 4 h at 18 °C. The third culture was induced with 0.4 mM IPTG and grown an additional 4 h at 37 °C. The cells were harvested by centrifugation at 4,000 x*g* for 10 min at 4 °C.

The culture grown at 37 °C following induction yielded ~3 g of cell paste, whereas the cultures grown at 18 °C following induction yielded ~1 g of cell paste each.

Solubility and activity of $PhaEC_{Am}$ in crude lysate. To test for the solubility of $PhaEC_{Am}$, the cell pellets from the culture induced at 37 °C and from one culture induced at 18 °C were resuspended in 3 mL per g of cells lysis buffer containing 50 mM NaH_2PO_4, 300 mM NaCl, 10 mM imidazole pH 8.0. The cell pellet from the third culture that had also been induced at 18 °C was resuspended in lysis buffer containing the detergent 0.1% n-octyl-β-D-glucopyranoside. The cells were lysed by two passages through the French pressure cell at 14,000 psi. The soluble and insoluble lysate fractions were separated by centrifugation at 4 °C for 20 min at 20,000 x*g*. The soluble fractions were decanted into separate tubes and the insoluble fractions were resuspended in lysis buffer to a volume equal to that of the corresponding soluble fraction. To prepare samples for SDS-PAGE, soluble and insoluble lysate were combined 1:1 with Laemmli buffer and boiled for ten min. Samples (10 μL) were analyzed by 12% SDS-PAGE.

Activity assays contained in a final volume of 110 μL: 10 μL of a 1:25 dilution of soluble or insoluble lysate and 0.75 mM HBCoA in 20 mM Hepes pH 7.5, 20 mM NaCl. At various time points, 20 μL aliquots were withdrawn and quenched in 50 μL ice cold 10% TCA. The samples were briefly centrifuged to remove precipitated protein and 68 μL was withdrawn and added to 262 μL 0.25 mM DTNB in 0.5 M KH_2PO_4, pH 7.8. The A_{412} of each sample was measured. Protein concentration was determined by the Bradford method using a BSA standard.

4.2.15 Cloning of $pPhaE_{Syn}$ and $pPhaC_{Syn}$ and expression and purification of $PhaEC_{Syn}$

Construction of the expression plasmids $pPhaE_{Syn}$ and $pPhaC_{Syn}$. Genomic DNA from *Synechocystis* PCC 6803 was a gift from the Stephanopolous Laboratory in the Department of

Chemical Engineering at MIT. *phaE*$_{Syn}$ was amplified from 50 ng genomic DNA using PfuII Ultra polymerase and the primers phaESynfw/phaESynrev. phaESynfw inserted an NheI restriction at the 5′ end of *phaE* and phaESynrev inserted an NheI restriction site at the 3′ end of *phaE*. The amplified PCR product was digested with NheI and was ligated overnight at RT into pET28a digested with NheI at an insert to vector ratio of 5:1. *phaC* was amplified using the primers phaCSynfw/phaCSynrev. phaCSynfw inserted an NdeI restriction site at the 5′ end of *phaC* and phaCSynrev inserted a BamHI restriction site at the 3′ end of *phaC*. The amplified PCR product was then digested with NdeI/BamHI and ligated at RT overnight into pET3a digested with the same restriction enzymes at an insert to vector ratio of 5:1. The ligation products were individually transformed into *E. coli* XL10Gold, which were grown overnight at 37 °C on LB/agar supplemented with 50 μg/mL Km (for pPhaE$_{Syn}$) or 100 μg/mL Amp (pPhaC$_{Syn}$). Single colonies were grown to saturation and the plasmids were isolated and sent for sequencing at the MIT Biopolymers Facility.

Expression and purification of PhaEC$_{Syn}$. All culture medium was supplemented with 50 μg/mL Km and 100 μg/mL Amp. A single colony of *E. coli* BL21(DE3)Gold containing pPhaE$_{Syn}$ and pPhaC$_{Syn}$ was used to inoculate 5 mL of LB in a 15 mL culture tube. Cells were grown overnight at 37 °C and 0.5 mL was used to inoculate a 100 mL LB culture in a 500 mL flash, which was grown 16 h to saturation. Four 2 L LB culture in 6 L baffled flasks were inoculated with the overnight culture at a dilution of 1:200. The cultures were grown until they reached an OD_{600} = 0.6 and were cooled on ice to ~18 °C. Expression of PhaEC$_{Syn}$ was induced with 0.4 mM IPTG and the culture was grown an additional 4 h at 18 °C. The cells were harvested by centrifugation at 4 °C for 10 min at 4,000 x*g*. The cell pellet (~17 g) was flash frozen in liquid nitrogen and stored until use.

All purification steps were carried out at 4 °C. The cell pellet was resuspended in 3 mL per g of cells in lysis buffer containing 50 mM NaH_2PO_4, 300 mM NaCl, 10 mM imidazole pH 8.0. The cells were lysed by two passes through the French pressure cell at 14,000 psi and the insoluble debris removed by centrifugation for 20 min at 20,000 x*g*. The soluble fraction was combined with Ni-NTA resin (~1 mL per g of cells) and incubated for 30 min with gentle rocking. The slurry was loaded into a column (3.5 cm x 5.5 cm) and the flowthrough collected. The column was washed with 20 cv lysis buffer and 10 cv lysis buffer containing 50 mM imidazole. The protein was eluted with 5 cv lysis buffer containing 250 mM imidazole and concentrated to ~12 mL. The protein was then exchanged into 50 mM tris pH 7.6, 10 mM NaCl, 5% glycerol by Sephadex G25 (200 mL, 5 cm x 300 cm). The protein was centrifuged for 10 min at 14,000 x*g* to remove precipitated protein, and the supernatant was loaded onto a Q Sepharose anion exchange column (30 mL, 3.5 cm x 7 cm). The column was washed with 2 cv 50 mM Tris pH 7.6, 10 mM NaCl, 5% glycerol and the protein was eluted with 300 mL of a linear gradient of 0-500 mM NaCl in 50 mM Tris pH 7.6, 5% glycerol. Finally, the protein was exchanged into 20 mM Hepes pH 7.5, 20 mM NaCl by Sephadex G25 chromatography (25 mL, 1 cm x 30 cm). The final protein was concentrated to 9 mg/mL, centrifuged 10 min at 14,000 x*g* to remove precipitated protein, and flash frozen in 50 µL aliquots and stored at -80 °C until use.

Assay of $PhaEC_{Syn}$ activity. Protein concentration was determined by A_{280} (ε = 114,910 $M^{-1}cm^{-1}$ for PhaEC) or by the Bradford method. Activity was measured by discontinuous DTNB assay. For crude lysate, the assay contained in a final volume of 110 µL: 10 µL of a 1:100 dilution of soluble extract (0.0015 mg protein total), 0.75 mM HBCoA in 20 mM Hepes pH 7.5, 20 mM NaCl. For the purified protein, the assays contained in a final volume of 130 µL: 100 nM $PhaEC_{Syn}$, 0.75 mM HBCoA in 20 mM Hepes pH 7.5, 20 mM NaCl. At time points from 0-10

min, 20 μL aliquots were withdrawn and quenched in 50 μL ice cold 10% TCA. The samples were centrifuged 5 min at 14,000 x*g* to remove precipitated protein and 68 μL aliquots were withdrawn and added to 262 μL 0.25 mM DTNB in 0.5 M KH_2PO_4, pH 7.8. The A_{412} of each sample was measured.

4.2.16 Construction of the plasmids pPhaEC$_{Tp}$, pPhaE$_{Tp}$ and pPhaC$_{Tp}$ and expression and purification of PhaEC$_{Tp}$

Construction of the expression plasmid pPhaEC$_{Tp}$. pFS91 was a gift of the Sinskey lab in the Department of Biology at MIT. pSF91 contains *phaEC$_{Tp}$*, including the 40 non-coding base pairs between the two coding regions. *phaEC$_{Tp}$* was amplified from 100 ng pFS91 using the primers phaECTpfw/phaECTprev (Table 4.1). The primer phaECTpfw inserted a BamHI site and on the 5′ end of *phaEC$_{Tp}$* and encoded a $(G_4S)_2$ linker (shown in italics in Table 4.1) between the StrepII-tag and the 5′ end of phaEC$_{Tp}$. The primer phaECTprev inserted a NotI site at the 3′ end of *phaEC$_{Tp}$*. The PCR product was digested with BamHI and NotI and ligated overnight at RT at an insert to vector ratio of 5:1 into pET52b digested with BamHI and NotI. The ligation product was transformed into *E. coli* XL10Gold cells and grown overnight on LB/agar supplemented with 100 μg/mL Amp. Plasmid was isolated from individual colonies and the sequence of pPhaEC$_{Tp}$ was confirmed by sequencing at MIT Biopolymers Facility.

Construction of the expression plasmids pPhaE$_{Tp}$ and pPhaC$_{Tp}$. phaE$_{Tp}$ was amplified from 100 ng pSF91 using PfuII Ultra polymerase and the primers phaETpfw/phaETprev. phaETpfw inserted an NheI restriction at the 5′ end of *phaE* and phaETprev inserted an NheI restriction site at the 3′ end of *phaE*. The amplified PCR product was digested NheI and was ligated overnight at RT into pET28a digested with NheI at an insert to vector ratio of 5:1. *phaC*

was amplified using the primers phaCTpfw/phaCTprev. phaCTpfw inserted an NdeI restriction site at the 5′ end of *phaC* and phaCTprev inserted a BamHI restriction site at the 3′ end of *phaC*. The amplified PCR product was digested with NdeI/BamHI and ligated at RT overnight into pET3a digested with the same restriction enzymes at an insert to vector ratio of 5:1. The ligation products were individually transformed into *E. coli* XL10Gold cells, which were grown overnight at 37 °C on LB/agar supplemented with 50 μg/mL Km (for pPhaE$_{Tp}$) or 100 μg/mL Amp (pPhaC$_{Tp}$). Single colonies were grown to saturation and the plasmids were isolated and sent for sequencing at the MIT Biopolymers Facility.

Expression of PhaEC$_{Tp}$ from pPhaEC$_{Tp}$. All culture medium was supplemented with 100 μg/mL Amp. A single colony of *E. coli* BL21(DE3) containing pPhaEC$_{Tp}$ was used to inoculate a 5 mL culture in a 15 mL culture tube and grown overnight at 37 °C. The entire culture was used to inoculate a 1 L LB culture in a 2.8 L flask, which was grown at 37 °C until OD_{600} = 0.6. The culture was cooled on ice to ~18 °C then induced with 0.4 mM IPTG. The cells were grown an additional 4 h at 18 °C, then harvested by centrifugation at 4 °C for 10 min at 4,000 x*g*. The cells (~1 g) were frozen in liquid nitrogen and stored at -80 °C until use.

Expression from pPhaE$_{Tp}$/pPhaC$_{Tp}$ and purification of PhaEC$_{Tp}$. All culture medium was supplemented with 50 μg/mL Km and 100 μg/mL Amp. Single colonies of *E. coli* BL21(DE3) containing pPhaE$_{Tp}$ and pPhaC$_{Tp}$ were used to inoculate 5 mL cultures in 15 mL culture tubes. The cultures were grown overnight, then used to inoculate 2 L cultures in 6 L flasks at a dilution of 1:200. The cultures were grown with shaking at 220 rpm at 37 °C until they reached an OD_{600} = 0.6. The cultures were rapidly cooled on ice to ~18 °C and expression of PhaEC$_{Tp}$ was induced with 0.4 mM IPTG. The cells were grown an additional 4 h at 18 °C, then the cells were

harvested by centrifugation at 4,000 x*g* at 4 °C for 10 min. The cells were flash frozen in liquid nitrogen and stored at -80 °C until use. A typical growth yielded 2 g cells per L of culture.

All purification steps were carried out at 4 °C. Cells were resuspended in 3 mL lysis buffer (50 mM NaH_2PO_4, 300 mM NaCl, 10 mM imidazole, pH 8.0) per g of cell paste. When noted in the Results section, the buffers also contained the detergents hecameg or octyl-β-D-glucopyranoside (0.1% or 1%). The cells were lysed by two passes through the French pressure cell at 14,000 psi and the insoluble fraction removed by centrifugation for 10 min at 4 °C and 30,000 x*g*. The soluble fraction was incubated with stirring for 30 min at 4 °C with Ni-NTA affinity resin pre-equilibrated with lysis buffer (~1 mL resin per 3 mL soluble crude extract). The resin was loaded into a column and the flowthrough was collected. The column was washed with 15 cv lysis buffer then eluted with 5 cv of lysis buffer with 250 mM imidazole. The eluent was collected in fractions and the fractions containing protein were combined and concentrated and exchanged into 50 mM Tris pH 7.6, 5% glycerol using Sephadex G25. The protein was then applied to a Q sepharose column (~1 mL resin per 3 mL protein). The column was washed with two cv 50 mM Tris pH 7.6, 5% glycerol, then the protein was eluted with 20 cvs of a linear gradient from 0-500 mM NaCl. The eluent was collected in 0.5 mL fractions, and the fractions containing $PhaEC_{Tp}$ were combined, concentrated, and exchange into 20 mM Hepes pH 7.5, 20 mM NaCl by Sephadex G25. The final protein was concentrated to ~5 mg/mL, flash frozen in liquid N_2, and stored in aliquots at -80 °C. A typical yield was about 1 mg $PhaEC_{Tp}$ per g cells.

Assay of $PhaEC_{Tp}$ activity. Protein concentration was determined by A_{280} using ε = 118,070 $M^{-1}cm^{-1}$ for PhaEC. $PhaEC_{Tp}$ was assayed by the discontinuous DTNB assay. In a final volume of 110 µL, a typical assay contained: 10 or 50 nM $PhaEC_{Tp}$ and 0.75 mM HBCoA in 20 mM Hepes pH 7.5, 20 mM NaCl. When noted in the Results section, the assays also

contained the detergents hecameg or octyl-β-D-glucopyranoside (0.1% or 1%). At various time points, 20 μL aliquots were withdrawn and quenched in 50 μL ice cold 10% TCA. The samples were centrifuged at 4 °C for 10 min at 14,000 x*g* to remove precipitated protein, and 68 μL was withdrawn and added to 262 μL 0.25 mM DTNB in 0.5 M KH_2PO_4, pH 7.8. The A_{412} of each sample was measured.

4.2.17 Cloning of pPhaE$_{Xc}$ and pPhaC$_{Xc}$ and expression and purification of PhaEC$_{Xc}$

Construction of the expression plasmid pPhaEC$_{Xc}$. Genomic DNA from *Xanthomonas campestris* was a gift of the Leach lab in the Department of Bioagricultural Sciences and Pest Management at Colorado State University. *phaEC$_{Xc}$* was amplified from 50 ng genomic DNA using PfuII Ultra polymerase and the primers phaECXcfw and phaECXcrev (Table 4.1). phaECXcfw inserted an NdeI site on the 5′ end of *phaE* and encoded a $(G_4S)_2$ linker between a StrepII-tag and the N-terminus of PhaE. phaECXcrev inserted a BamHI restriction site on the 3′ end of *phaC*. The amplified PCR product was digested with NdeI/BamHI and ligated at RT overnight into pET52b digested with the same restriction enzymes at an insert to vector ratio of 5:1. The ligation product was transformed into *E. coli* XL10Gold cells, which were grown overnight at 37 °C on LB/agar supplemented with 100 μg/mL Amp. Single colonies were grown to saturation and the plasmids were isolated and sent for sequencing at the MIT Biopolymers Facility.

Expression and solubility of PhaEC$_{Xc}$. All culture medium was supplemented with 100 μg/mL Amp. A single colony of *E. coli* BL21(DE3) Gold containing pPhaEC$_{Xc}$ was used to inoculate 5 mL of LB in a 15 mL culture tube and grown overnight at 37 °C. The culture was then used to inoculate two separate 1 L LB cultures in 2.8 L baffled flasks at dilutions of 1:200.

The cultures were grown at 37 °C with shaking at 220 rpm until OD_{600} = 0.6. One culture was induced with 0.4 mM IPTG, then grown an additional 4 h at 37 °C. The second culture was cooled on ice to ~18 °C, induced with 0.4 mM IPTG and grown an additional 4 h at 18 °C. The cells were harvested by centrifugation at 4,000 x*g* for 10 min at 4 °C. The culture induced at 37 °C yielded ~3 g of cell paste, and the culture induced at 18 °C yielded ~1 g of cell paste. To test the solubility of PhaECXc, the cell pellets were resuspended in 3 mL 100 mM Tris HCl, pH 8.0, 150 mM NaCl, 1 mM EDTA per g of cells. The cells were lysed by two passes through the French pressure cell auut 4 °C and 14,000 psi. The insoluble fraction was removed by centrifugation for 20 min at 20,000 x*g*, and samples were prepared from each fraction for analysis by 10% SDS-PAGE.

4.2.18 Cloning of pPhaE$_{Xo}$ and pPhaC$_{Xo}$ and expression and purification of PhaEC$_{Xo}$

Construction of the expression plasmids pPhaE$_{Xo}$ and pPhaC$_{Xo}$. Genomic DNA from *X. oryzae pv. oryzae* was a gift of the Leach lab in the Department of Bioagricultural Sciences and Pest Management at Colorado State University. *phaE$_{Xo}$* was amplified from 50 ng genomic DNA using PfuII Ultra polymerase and the primers phaEXofw/phaEXorev (Table 4.1). phaEXofw inserted an NdeI restriction at the 5′ end of *phaE* and phaEXorev inserted an BamHI restriction site at the 3′ end of *phaE*. The amplified PCR product was digested NdeI and BamHI was ligated overnight at RT into pET28a digested with the same enzymes at an insert to vector ratio of 5:1.

ñ · ° · ñ · ñ ㅁ

phaCXofw inserted an NheI restriction site at the 5′ end of *phaC* and phaCXorev inserted a HindIII restriction site at the 3′ end of *phaC*. The amplified PCR product was digested with NheI/HindIII and ligated at RT overnight into pET3a digested with the same restriction enzymes

at an insert to vector ratio of 5:1. The ligation products were individually transformed into *E. coli* XL10Gold cells, which were grown overnight at 37 °C on LB/agar supplemented with 50 μg/mL Km (for $pPhaE_{Xo}$) or 100 μg/mL amp ($pPhaC_{Xo}$). Single colonies were grown to saturation and the plasmids were isolated and sent for sequencing at the MIT Biopolymers Facility.

Expression and solubility of $PhaEC_{Xo}$. All culture medium was supplemented with 50 μg/mL Km and 100 μg/mL Amp. A single colony of *E. coli* BL21(DE3) Gold containing $pPhaE_{Xo}$ and $pPhaC_{Xo}$ was used to inoculate 5 mL of LB in a 15 mL culture tube. Cells were grown overnight at 37 °C. The culture was then used to inoculate three separate 1 L LB cultures in 2.8 L baffled flasks at dilutions of 1:200. The cultures were grown at 37 °C with shaking at 220 rpm until OD_{600} = 0.6. Of the three cultures, two were cooled to ~18 °C on ice, induced with 0.4 mM IPTG and grown an additional 4 h at 18 °C. The third culture was induced with 0.4 mM IPTG and grown an additional 4 h at 37 °C. The cells were harvested by centrifugation at 4,000 xg for 10 min at 4 °C. The culture grown at 37 °C following induction yielded ~3 g of cell paste, whereas the cultures grown at 18 °C following induction yielded ~1 g of cell paste each.

4.3 Results

4.3.1 Cloning and purification of $PhaE\Delta27C_{Av}$ and $PhaE\Delta35C_{Av}$

The full length construct $PhaEC_{Av}$ was the focus of crystallization efforts for over a decade. $PhaEC_{Av}$ has a noteworthy tendency to crystallize in many conditions; however, the diffraction of these crystals was never greater than ~7 Å (J. Jia, Year End Report 1999). The original motivation behind constructing the truncated $PhaEC_{Av}$ constructs came from limited proteolysis experiments carried out by Geoff Stamper that identified the C-terminal end of PhaE as "floppy" as it could be cleaved with chymotrypsin at two positions 27 and 35 residues from

the C-terminus. Thermally labile ends of proteins can potentially prevent close packing of protein molecules within a crystal lattice and therefore limit diffraction. Tian and York prepared plasmids encoding PhaC and the truncated PhaEs that corresponded to the cleavage sites identified by limited proteolysis and demonstrated that these proteins retained activity that was ~50-75% of full length $PhaEC_{Av}$ (J. Tian, Year End Report 2001).

For crystallography purposes, Paul Hubbard generated the construct $PhaE\Delta27C_{Av}$, which encodes $PhaE\Delta27$ with an N-terminal His_6-tag in the plasmid pCDF1 and untagged-$PhaC_{Av}$ in pET24a, so that large quantities of reproducibly pure protein could be obtained rapidly. As with the full length $PhaEC_{Av}$, $PhaE\Delta27C_{Av}$ crystallized in many conditions, but unfortunately these crystals also did not diffract to higher than 7 Å resolution. In an effort to continue to identify and refine conditions for the crystallization of $PhaE\Delta27C_{Av}$ we obtained the plasmid constructs for $PhaE\Delta27_{Av}$ and $PhaC_{Av}$. We also prepared the plasmid encoding the truncated construct $PhaE\Delta35_{Av}$ (also containing an N-terminal His_6-tag on PhaE) to mimic the second cleavage site identified by Geoff Stamper. $PhaE\Delta27_{Av}$ and $PhaE\Delta35_{Av}$ were co-expressed individually with $PhaC_{Av}$, and $PhaEC_{Av}$s were purified to >95% homogeneity (as judged by SDS-PAGE) in a single step (Figure 4.3). The yield was high, typically ~10-15 mg protein per g cell paste.

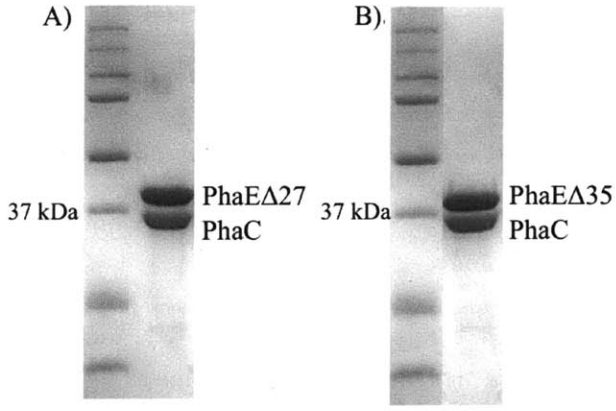

Figure 4.3 SDS-PAGE (12%) of purified truncated $PhaEC_{Av}$ constructs. A) $PhaE\Delta27C_{Av}$ and B) $PhaE\Delta35C_{Av}$.

4.3.2 PhaEΔ27C_{Av} and PhaEΔ35C_{Av} have ~66% the specific activity of full length PhaEC_{Av}

The specific activity of full length PhaEC_{Av} is 150 U/mg at 30 ˚C (*5*). PhaEΔ27C_{Av} and PhaEΔ35C_{Av} both have a specific activity of ~100 U/mg at 30 ˚C, and their kinetics resemble those of full length PhaEC_{Av}, in which a burst phase in CoA release is followed by a slower phase (Figure 4.4). The specific activity is measured from the burst phase.

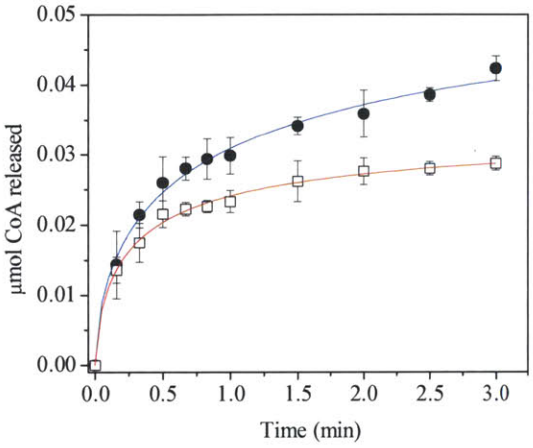

Figure 4.4 Representative assays of PhaEΔ27C_{Av} and PhaEΔ35C_{Av}. Assays contained 15 nM PhaEΔ27C_{Av} (●, blue) or 20 nM PhaEΔ35C_{Av} (□, red). Error bars are the standard deviation from the mean of three experiments. Data are fit Equation 2.1. For PhaEΔ27C_{Av}, $R^2 = 0.98$ and $\chi^2 = 1.3 \times 10^{-6}$. For PhaEΔ35$C_{Av}$, $R^2 = 0.98$ and $\chi^2 = 3.4 \times 10^{-7}$.

4.3.3 PhaEΔ27C_{Av} and PhaEΔ35C_{Av} are mixtures of dimers and tetramers of PhaEC *in vitro*

In order to further characterize both truncated constructs, the oligomeric state was examined. Both constructs (20 µL of 5 mg/mL solutions) were examined by SEC at RT. Their M_w were determined by comparison to a standard curve prepared using protein standards with M_w of 1.35 kDa to 670 kDa.. PhaEΔ27C_{Av} is also a mixture of two oligomeric forms (Figure 4.5A). The calculated M_w are 200 kDa and 380 kDa, likely corresponding to a dimer and

tetramer of PhaEΔ27C$_{Av}$, as the predicted M_w of the dimer and tetramer are ~160 kDa and 320 kDa, respectively. Full length PhaEC$_{Av}$ is a mixture of dimers and tetramers of PhaEC in solution (*6*). The predominant form of PhaEΔ27C$_{Av}$ appears to be the tetramer, similar to full length PhaEC$_{Av}$. In contrast PhaEΔ35C$_{Av}$ is predominantly a single species with a calculated M_w of 350 kDa (Figure 4.5B), suggesting that it is a tetramer of PhaEΔ35C (predicted M_w ~320 kDa).

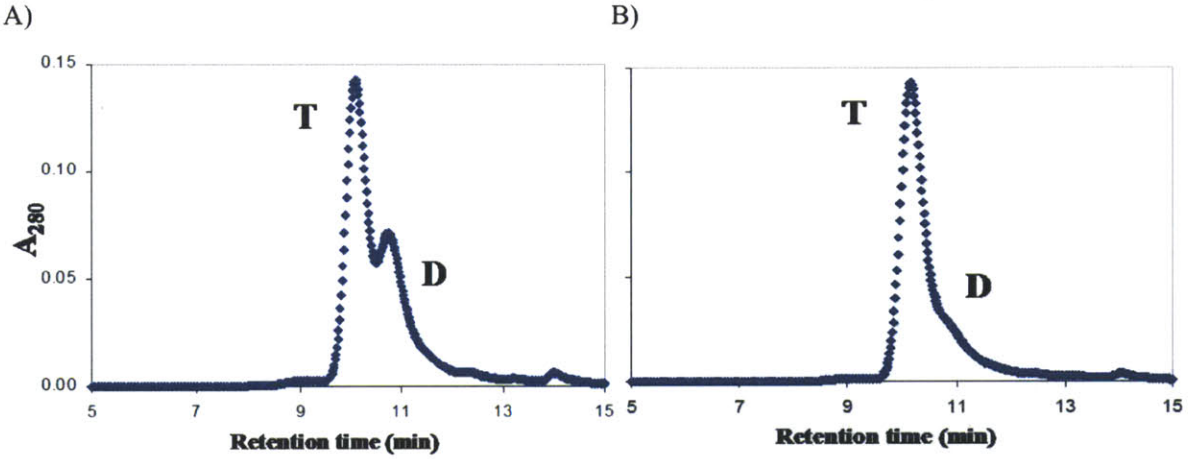

Figure 4.5 SEC of PhaEΔ27C$_{Av}$ and PhaEΔ35C$_{Av}$. The oligomeric states of A) PhaEΔ27C$_{Av}$ (20 µL of 5 mg/mL) and B) PhaEΔ35C$_{Av}$ (20 µL of 5 mg/mL) were examined by SEC at RT using a Bio-Sil SEC 400-5 column (Bio-Rad). Proteins were eluted at a flow rate of 1 mL/min with 50 mM sodium cacodylate, pH 7.5, 200 mM NaCl.

4.3.4 PhaEΔ27C$_{Av}$ crystallizes in many conditions but the crystals only diffract to >7 Å

PhaEΔ27C$_{Av}$ crystallizes in dozens of conditions containing a variety of precipitants (PEGs of various sizes, salts), additives (salts, small molecules such as ethanol) and buffers. Some of these conditions will be briefly presented. A few of these conditions will be discussed in detail in this section and the following, focusing on those that were most thoroughly pursued.

Crystals of PhaEΔ27C$_{Av}$ obtained from the Hauptman-Woodward screen. PhaEΔ27C$_{Av}$ (18 mg/mL) was sent to the Hauptman-Woodward Institute for screening of 1536 crystallization conditions by the microbatch-under-oil method. Crystals of PhaEΔ27C$_{Av}$ formed in dozens of

conditions in the Hauptmann-Woodward screen. A selection of these crystallization conditions is shown in Table 4.3. The diameter of the wells in the images in Table 4.3 is 900 μm.

Table 4.3 Crystals of PhaEΔ27C_{Av} that formed in the Hauptman-Woodward screen.

Condition	Buffer	Precipitant	Additive	Crystal[a]
1	0.1 M ammonium sulfate, 0.1 M sodium acetate, pH 5.0	24% PEG (polyethylene glycol) 20,000	n/a	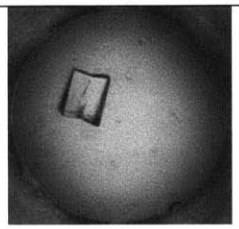
2	0.1 M potassium phosphate dibasic, 0.1 M CAPS pH 10.0	20% PEG 1000	n/a	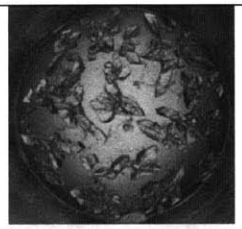
3	0.1 M potassium phosphate-tribasic, 0.1 M sodium acetate, pH 5.0	20% PEG 8000	n/a	
4	0.1 M bis-Tris propane, pH 7.0	40% PEG 400	0.1 M magnesium sulfate heptahydrate	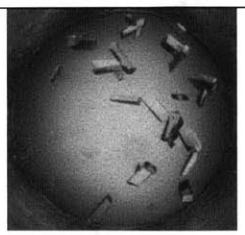
5	0.05 M Hepes pH 6.8	12.5% PEG 3350	0.08% w/v Ala-ala 0.08% w/v Gly-asp 0.08% w/v Gly-gly 0.08% w/v Gly-phe 0.08% w/v Gly-ser 0.08% w/v Ser-tyr	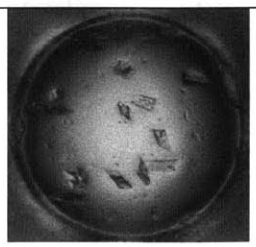

6	0.1 M MES, pH 6.0	40% PEG 400	0.1 M ammonium chloride	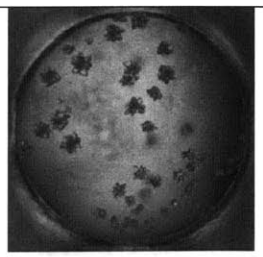
7	0.2 M Potassium thiocyanate, pH 7.0	20% w/v PEG 3350	n/a	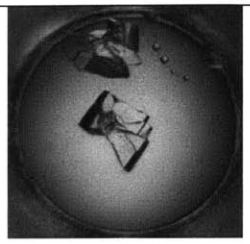
8	3.5 M sodium formate pH 7.0	n/a	n/a	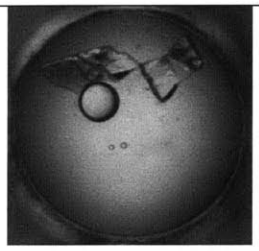
9	0.1 M bis-tris pH 6.5	20% PEG monomethyl ether (MME) 5000	n/a	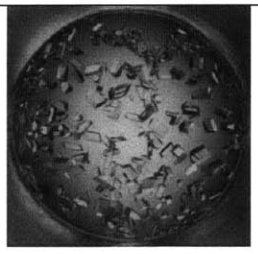
10	0.1 M Tris pH 8.5	1.0 M magnesium sulfate hydrate	n/a	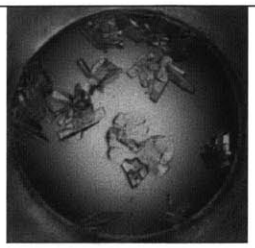
11	0.1 M ammonium phosphate-monobasic, 0.1 M Hepes pH 7.5	12% PEG 20,000	n/a	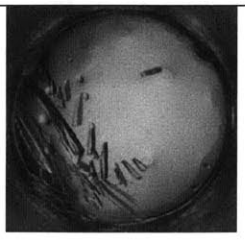

12	0.1 M CAPS pH 10.0	12% PEG 20,000	0.1 M ammonium bromide	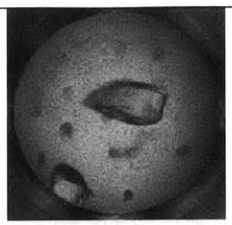
13	0.1 M MES pH 6.0	40% PEG 4000	0.1 M manganese sulfate monohydrate	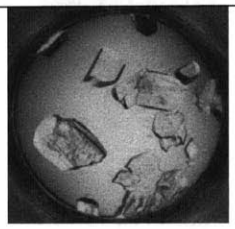
14	8% tacsimate pH 5.0	20% PEG 3350	n/a	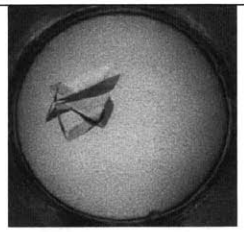
15	0.1 M sodium citrate tribasic dihydrate, pH 5.6	1.0 M ammonium phosphate monobasic	n/a	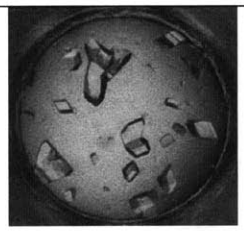

[a]the diameter of the wells in the images is 900 μm.

The crystals in conditions 2 and 3 are examples of a very common morphology of PhaEΔ27C_{Av} crystals produced in a wide variety of conditions. Conditions 2 and 3 in Table 4.3 are buffered at extremes of pH (pH 10 and pH 5, respectively). However, as discussed below, this crystal morphology forms in a wide range of pHs. In our hands, crystals of the fern/dendrite morphology (for example, in condition 3) never diffract, and grid screening around the conditions by varying pH and precipitant concentration does not improve morphology or diffraction. We attempted to reproduce conditions 1, 3, 9, 14 and 15 from the Hauptman-

Woodward screen (Table 4.3). Of these, condition 9 was most extensively pursued because the crystals were reproducible and the pH was near neutral (pH 6.5). Screens were set up using both the hanging drop and microbatch-under-oil method. In the microbatch-under-oil method, 1-2 μL of protein (18 mg/mL) was mixed with 1-2 μL of crystallization solution at the bottom of a well of a 96-well plate, and the drop was covered with light mineral oil. The ratio of protein to precipitant and the final volume of the protein drop were varied. The crystals shown in Figure 4.5 were obtained using the hanging drop method with a protein to precipitant ratio of 1:1. The crystals indicated with arrows in Figure 4.6 were screened for diffraction at RT, but diffracted to 9.5 Å at best.

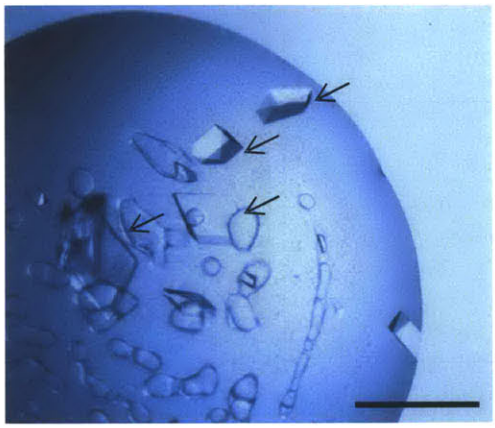

Figure 4.6 Crystals grown in Hauptman-Woodward condition 9. The arrows indicate the crystals that were screened for diffraction at RT using the wet mount method. The scale bar is 500 μm.

Crystallization conditions identified by screening by the hanging drop method. Several conditions from commercially available screens were identified in which PhaEΔ27C_{Av} crystallized. These conditions are summarized in Table 4.4.

Table 4.4 Conditions that promoted crystallization of PhaEΔ27C_{Av} (20 mg/mL).

Screen (condition number)	Condition	Crystal form	Diffraction?
Index (73)	0.1 M Tris pH 8.5, 0.2 M NaCl, 25% w/v PEG 3350	Irregular plate, some dendrite/ferns, 200-300 μm	not screened
Index (92)	0.1 M magnesium formate dehydrate, 15% w/v Polyethylene glycol 3,350	Some diamonds, cuboids, 50-100 μm	no
PEG/Ion (1)	0.2 M NaF, 20% PEG 3350, pH 7.3	Dendrites/ferns, 100-500 μm	no
PEG/Ion (4)*	0.2 M LiCl, 20% PEG 3350, pH 6.8	Dendrites/ferns, 100-500 μm	no
PEG/Ion (6)	0.2 M NaCl, 20% PEG 3350, pH 6.9	Dendrites/ferns, 100-500 μm	no
PEG/Ion (13)	0.2 M sodium thiocyanate, 20% PEG 3350, pH 6.9	Dendrites/ferns, 100-500 μm	not screened
PEG/Ion (15)	0.2 M lithium nitrate, 20% PEG 3350, pH 7.1	Dendrites/ferns, 100-500 μm	not screened
PEG/Ion (17)	0.2 M sodium nitrate, 20% PEG 3350, pH 6.8	Dendrites/ferns, 100-500 μm	not screened
PEG/Ion (18)*	0.2 M potassium nitrate, 20% PEG 3350, pH 6.8	Dendrites/ferns, 100-500 μm	no
PEG/Ion (21)	0.2 M sodium formate, 20% PEG 3350, pH 7.2	Dendrites/ferns, 100-500 μm	not screened
PEG/Ion (22)	0.2 M potassium formate, 20% PEG 3350, pH 7.3	Dendrites/ferns, 100-500 μm	not screened
PEG/Ion (27)	0.2 M sodium acetate, 20% PEG 3350, pH 8.0	Jagged cuboid, 200 x 300 μm	no
PEG/Ion (29)	0.2 M potassium acetate, 20% PEG 3350, pH 8.1	Jagged cuboid, 200 x 300 μm	no
PPC Screen (21)	0.1 M sodium cacodylate pH 6.0, 10% MPEG 5000, 10% 2-Propanol	Long, jagged plate, 750 μm	not screened
PPC Screen (26)	0.1 M calcium acetate, 0.1 M HEPES pH 7.5, 10% PEG 6000	Single irregularly shaped boulder, 200 μm	not screened
PPC Screen (35)	0.1 M magnesium acetate, 0.1 M Tris pH 8.5, 12% PEG 8000	Small ferns/dendrites, 50-100 μm	not screened

*condition was further grid screened, as described in the text.

Several crystals from the conditions listed in Table 4.4 were screened for diffraction at RT and at -196 °C using Paratone N and PEG 400 as cryoprotectants. The crystals that formed with PEG 3350 as a precipitant (conditions 1, 4, 6, 13, 15, 17, 18, 21, and 22 in the PEG/ion

screen) were all of the fern/dendrite morphology but were never of diffraction quality. The conditions PEG/ion 4 and 18 (indicated with an asterisk in Table 4.4) were further refined by grid screening, in which the concentration of additive (lithium chloride or potassium nitrate) and PEG 3350 were iteratively varied. The crystals that formed in these grid screens were of the same morphology as the parent conditions (listed in Table 4.4) and also did not diffract.

In an effort to obtain crystals of higher quality, PhaEΔ27C_{Av} was co-crystallized with the HBCoA analog $HBCH_2CoA$, in which the S of the thioester in HBCoA is replaced with a methylene group (Figure 4.1). $HBCH_2CoA$ has previously been shown to be an inhibitor of the full length PhaEC_{Av} (P. Li and J. Stubbe, unpublished data). The strategy was to co-crystalize PhaEΔ27C_{Av} with a saturating concentration of $HBCH_2CoA$ to potentially "lock" the enzyme into a tighter conformation that could promote higher quality diffraction. PhaEΔ27C_{Av} (18 mg/mL, 225 μM) was incubated with 4.5 mM $HBCH_2CoA$ and crystal trays were set up by the standard hanging drop method to screen the commercially available conditions. The conditions listed in Table 4.5 were identified as promoting crystallization. We decided to focus on condition 26 from the PPC Screen (0.1 M calcium acetate, 0.1 M Hepes, pH 7.5, 10% PEG 6000) because the crystal forms of PhaEΔ27C_{Av} in the presence and absence of 4.5 mM $HBCH_2CoA$ were different from one another (Figure 4.7A and B), suggesting that $HBCH_2CoA$ was bound to PhaEΔ27C_{Av}. The initial crystals identified in Table 4.5 did not diffract. Therefore, the condition was replicated in order to generate many additional crystals that could be screened for diffraction (Figure 4.7C and D). The crystals were screened for diffraction at RT; however, they diffracted at best to 7.5 Å.

Table 4.5 Conditions that promoted crystallization of PhaEΔ27C_{Av} (20 mg/mL) in the presence of 4.5 mM $HBCH_2CoA$.

Screen (condition number)	Condition	Crystal form	Diffraction?
Index (46)	0.1 M BIS-TRIS pH 6.5, 20% w/v PEG MME 5,000	Small, irregular boulders, 50-150 μm	not screened
Index (67)	0.2 M ammonium sulfate, 0.1 M BIS-TRIS pH 6.5, 25% w/v PEG 3,350	Long thin spears, 150 μm Larger chunks, 200-300 μm	not screened
PPC Screen (1)	0.1 M calcium acetate, 0.1 M HEPES pH 7.0, 20% PEG 400	Irregular dendrites, 50-150 μm	no
PPC Screen (26)	0.1 M calcium acetate, 0.1 M HEPES pH 7.5, 10% PEG 6000	Jagged, diamond-shaped, 250 μm	no

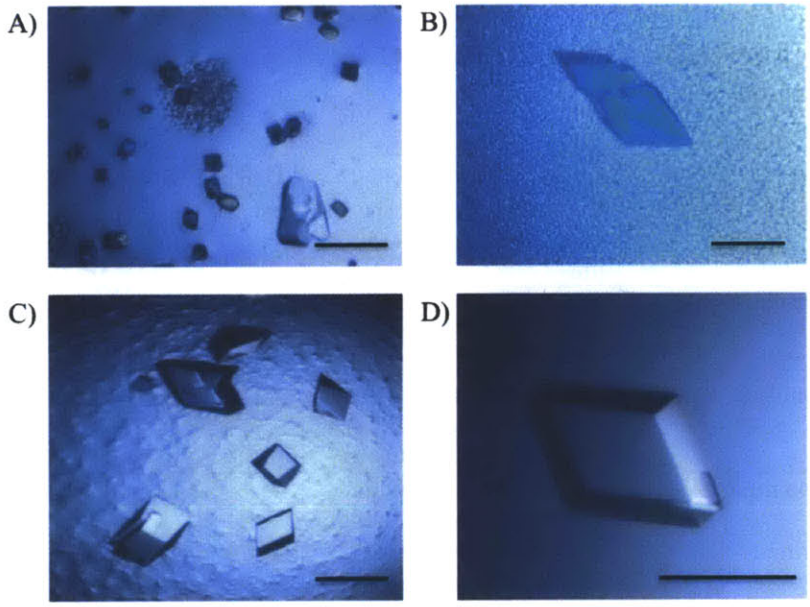

Figure 4.7 Crystals of PhaEΔ27C_{Av} grown in 0.1 M calcium acetate, 0.1 M Hepes, pH 7.5, 10% PEG 6000. A) PhaEΔ27C_{Av} (18 mg/mL). The small diamond triangles are likely salt crystals. The larger irregular boulder is a protein crystal. B) PhaEΔ27C_{Av} (18 mg/mL) co-crystallized with 4.5 mM $HBCH_2CoA$ obtained from the original screen. C) and D) are also crystals of PhaEΔ27C_{Av} (18 mg/mL) co-crystallized with 4.5 mM $HBCH_2CoA$ obtained from attempts to reproduce the conditions in B. The scale bars are 200 μm.

4.3.5 Addition of osmolytes improved the diffraction of crystals of PhaEΔ27C_{Av} co-crystalized with $HBCH_2CoA$ to 4.5 Å

In order to improve diffraction of the crystals described in the preceding section (condition 26 of the PPC screen), 96 different additives were screened in combination with condition 26. The additives were part of the commercially available Additive Screen (Hampton-Research, Aliso Viejo, CA). The results from this screen are shown in Table 4.6. In the majority of conditions, no crystals formed. However, crystals grew in about ~20% of the additives (Table 4.6). Several of these crystals were screened for diffraction.

Table 4.6 Additives that promoted crystallization of PhaEΔ27C_{Av} with 4.5 mM $HBCH_2CoA$ in condition 26 from the PPC Screen.

Additive number	Additive	Crystal form	Diffraction?
3	0.01 M calcium chloride dihydrate	Irregular geometric shapes with flat faces, 150-350 μm	not screened
26	0.01 M L-proline	Diamonds, geometric shapes with flat faces, 50-100 μm	7 Å
27	0.01 M phenol	Diamonds, cubes, geometric shapes with flat faces shapes, 100-300 μm	not screened
29	0.01 M sodium bromide	Large boulders, 500 μm, smaller diamonds, 100 μm	no
36	0.01 M taurine	Large boulders, 250 μm, smaller diamonds and geometric shapes, 50-100 μm	A few spots at 5.4 Å, most at 6 Å
37	0.01 M betaine hydrochloride	Diamonds, 50-100 μm, other geometric shapes, 100 μm	not screened
39	0.01 M spermine tetrahydrochloride	Single diamond plate, 150 μm	not screened
41	0.01 M sarcosine	Diamonds and other geometric shapes, 100-250 μm	A few spots at 4.5 Å, most at 6 Å
43	0.1 M guanidine HCl	Long, jagged rods, 500 μm	9 Å
44	0.01 M urea	Larger boulders, 250 μm, diamonds and other geometric shapes, 100-200 μm	16 Å

49	0.01 M ethylenediaminetetraacetic acid disodium salt dihydrate	Flat, connected array of jagged diamond plates, adhered to coverslip, 1500 μm	not screened
50	0.5% w/v polyvinylpyrrolidone K15	Diamonds, 50-100 μm	7.5 Å
53	1% w/v PEG 3350	Long, thin slivers, 300 μm	no
75	3% v/v (+/-)-2-methyl-2,4-pentanediol	Irregular boulders and diamonds, 150-250 μm	not screened
76	5% v/v PEG 400	Diamonds and other geometric shapes, 100-250 μm	8.2 Å
80	4% v/v polypropylene glycol P 400	Large irregular boulder, 600 μm, smaller irregular shapes, 250 μm	not screened
82	3% v/v ethanol	Many small diamonds, 30-50 μm	not screened
83	3% v/v 2-propanol	Long, thin slivers, 100-300 μm	no
86	4% v/v tert-butanol	Small geometric shapes, 100-200 μm	not screened

In almost all cases, more crystals formed in the presence of the additives listed in Table 4.6 than in the original condition, and these crystals tended to have sharper faces than those formed in the original condition. Several of these crystals were screened for diffraction. The osmolytes taurine and sarcosine, which have been previously shown to improve diffraction quality of crystals of several proteins (*7*), produced the most encouraging results. Many crystals from each additive were screened and these crystals diffracted to ~6 Å, with one to 4.5 Å (Figure 4.8). Though not yet in the range of atomic resolution necessary for structure solving of an enzyme of unknown structure, these results were promising. Therefore, extensive screening around these two conditions was carried out. The variables that were iteratively changed included the concentrations of calcium acetate (0.05 to 0.2 M, PEG 6000 (5 to 20%) and the buffer pH (from 6.8 to 7.8). The M_w of PEG was varied from 400-8,000 and a range of concentrations of taurine or sarcosine were also examined. However, the resulting conditions either failed to produce crystals or produced crystals of lesser quality than the original crystals.

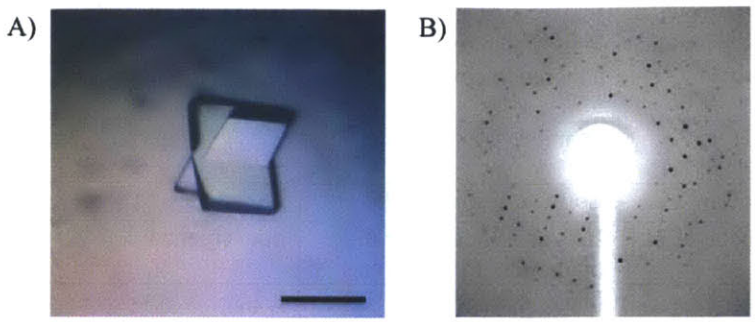

Figure 4.8 Diffraction from a crystal of PhaEΔ27C_{Av} bound $HBCH_2CoA$. A) A crystal of PhaEΔ27C_{Av} (18 mg/mL) co-crystallized with 4.5 mM $HBCH_2CoA$ in 0.1 M calcium acetate, 0.1 M Hepes, pH 7.5, 10% PEG 6000, 0.01 M sarcosine. The scale bar is 200 μm. B) A diffraction pattern produced from the crystal in A. The highest resolution diffraction obtained from this crystal was 4.5 Å.

4.3.6 PhaEΔ35C_{Av} crystallizes in many conditions but the crystals also diffract to >7 Å

We also explored crystallization of the truncated construct PhaEΔ35C_{Av}. As discussed above, this construct was generated based on the results of limited proteolysis experiments carried out by Geoff Stamper that identified an accessible chymotrypsin cleavage site on the C-terminus of PhaE. The observation that PhaEΔ35C_{Av} was primarily a tetramer in solution (as opposed to a mixture of dimers and tetramers as is the case with PhaEΔ27C_{Av}) suggested that this construct was homogeneous in solution and therefore might crystallize in a tighter and thus higher quality form. Several conditions were screened to identify conditions in which PhaEΔ35C_{Av} crystallized. PhaEΔ35C_{Av} (18 mg/mL, 225 μM) was screened with and without 4.5 mM $HBCH_2CoA$. The results are summarized in Tables 4.7 and 4.8.

Table 4.7 Conditions that promoted crystallization of PhaEΔ35C_{Av} (18 mg/mL).

Screen (condition number)	Condition	Crystal form	Diffraction?
Index (46)	0.1 M BIS-TRIS pH 6.5, 20% w/v PEG MME 5,000	Irregular, rounded boulders, 50-200 μm	not screened
Index (90)	0.2 M Sodium formate, 20% w/v PEG 3350	Irregular, rounded boulders, 50-200 μm	not screened

Table 4.8 Conditions that promoted crystallization of PhaEΔ35C_{Av} (18 mg/mL) in the presence of 4.5 mM $HBCH_2CoA$.

Screen (condition number)	Condition	Crystal form	Diffraction?
Index (80)	0.2 M ammonium acetate, 0.1 M HEPES pH 7.5, 25% w/v PEG 3350	Jagged/dendrite clusters, 100-300 μm	not screened
Index (87)	0.2 M sodium malonate pH 7.0, 20% w/v PEG 3350	Cluster of plates, 350 μm	not screened
Index (95)	0.1 M potassium thiocyanate, 30% w/v PEG MME 2000	Several small, rounded shapes, 50-100 μm	not screened
PPC Screen (18)	0.1 M HEPES pH 7.0, 15% PEG 4000, 10% 2-propanol	Many thin diamond plates, 100-300 μm	Dissolved when removed from 18 °C room; not screened
PPC Screen (21)	0.1 M sodium cacodylate pH 6.0, 10% MPEG 5000, 10% 2-propanol	Long, thin slivers, 500-700 μm	not screened
PPC Screen (30)	0.1 M sodium chloride, 0.1 M sodium cacodylate pH 6.0, 12% PEG 8000	A few irregular chunks, 50-100 μm	not screened
PPC Screen (35)	0.1 M magnesium acetate, 0.1 M Tris pH 8.5, 12% PEG 8000	Several small, boulders with irregular surfaces, 50-100 μm	not screened

Condition 18 from the PPC screen (Table 4.7) was pursued. The original crystals dissolved upon transferring them from 18 °C to RT. Therefore a screen was carried out at 18 °C to examine 96 different additives, 8 of which produced crystals. These crystals were stable when transferred from the 18 °C room to RT for screening and were screened for diffraction. However, at best the diffraction was ~6.3 Å (Table 4.9).

Table 4.9 Effects of additives on the diffraction of crystals of PhaEΔ35C_{Av} (18 mg/mL) with $HBCH_2CoA$ in 0.1 M Hepes pH 7.0, 15% PEG 4000, 10% 2-propanol.

Additive number	Additive	Crystal form	Diffraction?
2	3% dioxane	Thin, triangular plates, 200-300 μm	no
9	4% acetonitrile	Thin, triangular plates, 200-300 μm	10 Å
18	4% 1,1,1,3,3,3,-heexafluoro-2-propanol	Thin, triangular plates, 200-300 μm	7.5 Å
27	0.01 M sodium bromide	Thin, triangular plates, 200-300 μm	6.5 Å
48	0.01 M urea	Thin, triangular plates, 200-300 μm	6.25 Å
53	0.01 M betaine chloride	Thin, triangular plates, 200-300 μm	7.5 Å
77	0.015 mM CYMAL-7	Thin, triangular plates, 200-300 μm	7.0 Å
89	0.033 mM n-tridecyl-β-D-maltopyranoside	Long, jagged spears, 200-300 μm	7.5 Å

4.3.7 A single crystal of PhaC$_{Cc}$ΔN that diffracted to 3 Å was obtained

In addition to our crystallization efforts with the class III synthases, crystallization of the class I synthase from *C. crescentus* was extensively examined. *C. crescentus* contains an unusual 73 kDa class I synthase, PhaC$_{Cc}$, whose purification and characterization are discussed in depth in Chapter 2. The synthase differs from the more typical class I synthases (such as PhaC$_{Re}$) by an 85 amino acid N-terminal domain that is rich in Lys, Ala and Pro residues. This domain has no homology to any protein in the database. Our original efforts to crystallize the synthase from *C. crescentus*, however, focused on a truncated construct of PhaC$_{Cc}$ lacking this 85 amino acid N-terminal domain, PhaC$_{Cc}$ΔN. PhaC$_{Cc}$ΔN has a specific activity that is 50-fold lower than the full length PhaC$_{Cc}$. This truncated version of PhaC$_{Cc}$ is how the synthase is (incorrectly) annotated in the database.

$PhaC_{Cc}\Delta N$ was readily purified as an N-terminally $(His)_6$-tagged construct. Despite sharing 37% identity with $PhaC_{Re}$, purified $PhaC_{Cc}\Delta N$ was extremely soluble (up to at least 85 mg/mL, 1.3 mM) and its purification did not require hecameg, as is required for $PhaC_{Re}$. These observations led us to believe that $PhaC_{Cc}\Delta N$ could be a good candidate for crystallization. Thousands of crystallization conditions were therefore screened using a variety of concentrations of $PhaC_{Cc}\Delta N$ (18 mg/mL, 30 mg/mL, 60 mg/mL, 85 mg/mL) and at various temperatures (4 °C, 18 °C, 37 °C). Only a single crystal was obtained, and this crystal formed sometime between 6-12 months after the tray was initially set up (Figure 4.9A). The original crystallization condition was from the commercial screen $PEGR_x$ (condition 18) and contained 60 mg/mL $PhaC_{Cc}\Delta N$ in 0.1 M Hepes, pH 7.5 and 30% PEG 1000. However, because the crystal grew after prolonged incubation, water from the well solution had slowly evaporated and therefore the well solution was more concentrated than the initial condition. The volume of the well solution was ~260 μL, therefore the concentrations of the components were roughly twice that of the original condition. This presented a problem in reproducing the crystallization conditions, as discussed below.

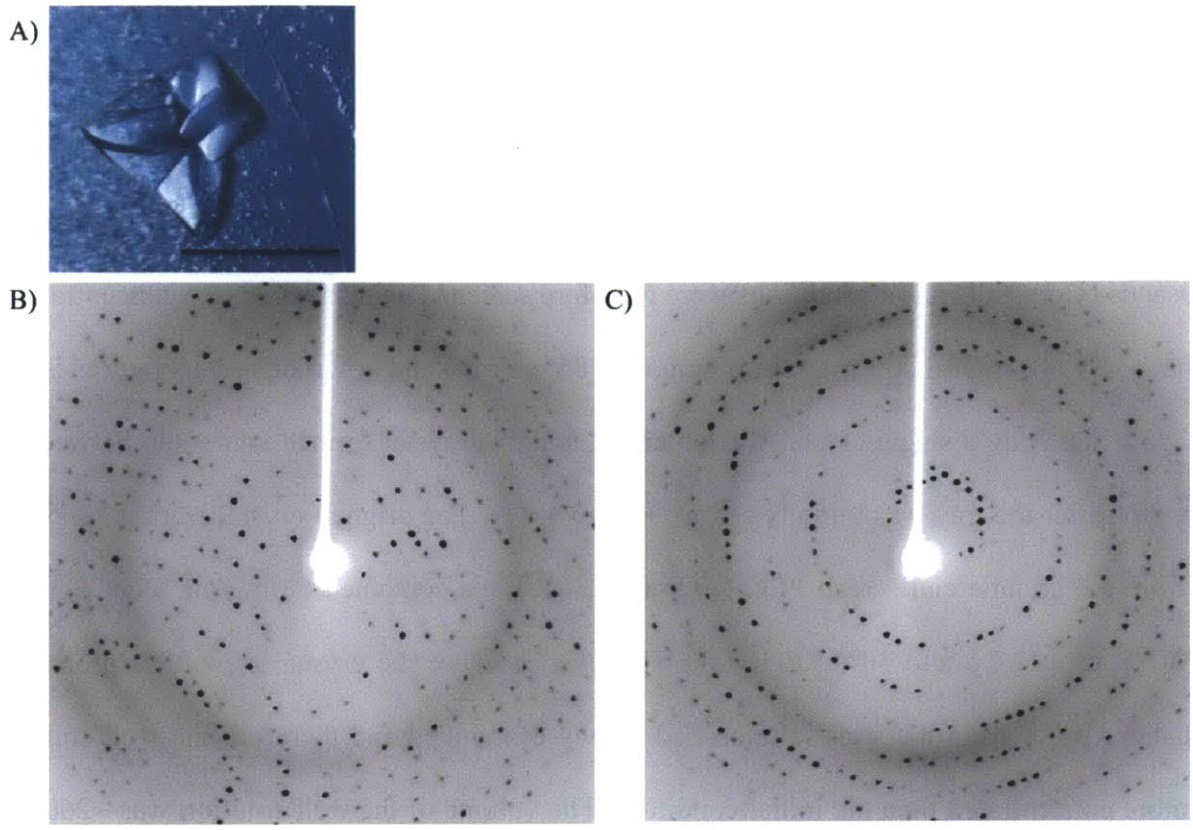

Figure 4.9 Initial data collection from a crystal of PhaC$_{Cc}$ΔN. A) A single crystal of PhaC$_{Cc}$ΔN (60 mg/mL) that formed after ~1 year in 0.1 M Hepes, pH 7.5 and 30% PEG 1000. The scale bar is 200 μm. B) A diffraction image collected at φ = 0°. B) A diffraction image collected at φ = 90°. The highest resolution was ~2 Å.

The crystal from condition 18 was screened for diffraction to confirm that the crystal was protein and that it diffracted. We decided to screen the whole crystal for diffraction at RT as opposed to freezing it in a cryoprotectant. Because we had only one crystal, screening cryoprotectants was too risky as many crystals fall apart or dissolve in the search process. Furthermore, the crystal was not broken into several smaller pieces for screening of cryoprotectants because breaking the crystal could potentially disrupt the crystal lattice and thereby degrade the quality of diffraction. The crystal was initially screened at RT from φ = 0° and 90° (where the φ angle refers to the rotation of the crystal about its axis in the X-ray beam)

(Figure 4.9B and C). The initial screens revealed that it diffracted to ~2 Å. At RT crystals sustain radiation damage in the course of data collection that ultimately destroys the crystal. Thus, to reduce the level of radiation damage and to maximize the amount of data that could be collected at RT, an 88% complete dataset was collected at 3.1 Å resolution by collecting frames (diffraction patterns) at 1° intervals. The data (108 images) were indexed using the SAINT software and were 88% complete overall and 95% in the highest resolution shell (3.1-3.3 Å) (*8*). The dimensions of the unit cell were $\alpha = \beta = 104.2$ Å, $\gamma = 232.7$ Å and the angles of the vertexes were $a = b = 90°$, $c = 120°$. R32 was the lowest symmetry space group that fit the observed reflections without assuming twinning or non-crystallographic symmetry. Using the SAINT software, the solvent content was predicted to be ~33% with one full length molecule in the unit cell. There is most likely one monomer in the asymmetric unit, and the two-fold axis may result from two monomers forming a dimer interface at the edge of the unit cell. The data were merged and scaled using the CCP4i software (*9*).

In order to solve the phases, we attempted molecular replacement using structural models generated from a variety of structure prediction programs. The input models were chosen either from i) homologous proteins present in the PDB, or ii) the results of secondary/tertiary structural prediction software. Table 4.10 lists the programs used to prepare threading models and/or predicted structures, a description of the general methods used by each program and, where applicable, the template (a protein of known structure) used for structure prediction. For the majority of these programs, one simply inputs the sequence of the protein (or region therefore) of interest, and the software searches the database to find homologous proteins of known structure. Using these structures, the programs then generate a structural model of the protein of interest and also provide the xyz coordinates for the positions of every atom modeled. For molecular

replacement purposes, these coordinates were used as input for the PHASER software along with the experimental hkl values.

Unfortunately our molecular replacement efforts using the coordinates from models to search for solutions did not yield acceptable structural models from the experimental data. Structure prediction programs of PhaCs consistently model the α/β hydrolase core domain as a β-sheet (4-7 β-strands) surrounded by 3-5 α-helices. However the modeled region (which contained the α/β hydrolase domain) spans only ~50% of the residues of $PhaC_{Cc}\Delta N$. Solving the phases by this method likely failed because the models used for molecular replacement did not constitute enough of the overall structure.

Table 4.10 Programs used for preparation of structural models for use in molecular replacement.

Program	Template(s)	Method/Notes
LOMETS	1zd4 (human epoxide hydrolase) 1k8q (dog gastric lipase) 1s8o (human epoxide hydrolase)	Models predicted α/β hydrolase folds
EsyPred3D	1tah (*Bacillus glumae* lipase)	1tah template was specified; threading model generated from residues 232-356, containing α/β hydrolase fold
EsyPred3D	1zoi (*Pseudomonas putida* esterase)	No template specified; program selected 1zoi, modeled residues 232-505, containing α/β hydrolase fold
SWISS-MODEL	1tah (*Bacillus glumae* lipase)	Modeled residues 231-505 in PhaC as containing α/β hydrolase fold
I-Tasser	Several	Program models fragments of sequence individually from several templates; modeled entire sequence as two domains (α/β hydrolase fold and an a-helical domain)

4.3.8 Attempts to reproduce the crystal of $PhaC_{Cc}\Delta N$ were unsuccessful

In addition to efforts to solve the structure by molecular replacement, our primary focus was to reproduce the original crystal using a variety of methods. To first determine whether the

protein in the crystal was full length or was truncated by proteolysis, 1 μL from a similar crystallization condition was combined with 60 μL Laemmli buffer and 10 μL of the sample was analyzed by 10% SDS-PAGE (Figure 4.10). We analyzed a sample from a similar condition rather than the drop that contained the crystal to minimize disruption of the original drop. Furthermore the crystal itself was not analyzed because it was saved for streak seeding and microseeding experiments, which are described below. The drop analyzed by SDS-PAGE came from condition 3 of the $PEGR_x$ screen, which consisted of 0.1 M Hepes pH 7.5, and 42% PEG 200. The results indicated that condition 3 contained full length protein that migrates the same as the $PhaC_{Cc}\Delta N$ standard, and suggests that the single crystal obtained in the similar $PEGR_x$ condition 18 consists of full length $PhaC_{Cc}\Delta N$.

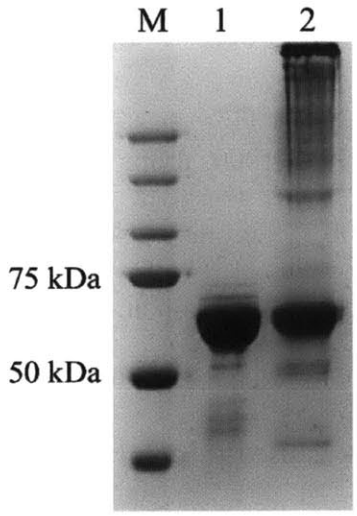

Figure 4.10 SDS-PAGE (10%) of $PhaC_{Cc}\Delta N$. M, molecular weight standards. Lane 1, $PhaC_{Cc}\Delta N$ standard. Lane 2, $PhaC_{Cc}\Delta N$ from ~1 year-old drop from a crystallization screen condition containing 0.1 M Hepes pH 7.5, and 42% PEG 200.

Several factors complicated our attempts to reproduce the crystallization conditions. Because the crystal was found nearly a year after the original tray was set up, protein from the same purification was no longer available. Thus, fresh protein from subsequent purifications was

used. Many trays were set up under conditions identical to the original set-up: 1 μL of 0.1 M Hepes pH 7.5, 30% PEG 1000 and 1 μL 60 mg/mL $PhaC_{Cc}\Delta N$. Under these conditions, the protein immediately precipitated, as was observed with the original drop that yielded the crystal. These results suggested that the crystal formed after slow re-solubilization over the course of the year. In attempting to reproduce the crystallization conditions, several factors were varied to mimic the slow increase in concentration of the precipitant and protein over time. Holding the crystallization conditions constant (0.1 M Hepes pH 7.5, 30% PEG 1000), the concentration of $PhaC_{Cc}\Delta N$ was varied from 10-60 mg/mL, and the temperature was varied (4 °C, 18 °C, RT, and 37 °C). Alternatively grid screens with $PhaC_{Cc}\Delta N$ at 10 mg/mL, 30 mg/mL and 60 mg/mL were carried out in which the pH was varied from 7.0-7.6 in 0.2 unit increments, and PEG was varied from 5-30% in 5% increments. The ratio of protein to crystallization solution was also varied from 1:1, 1:2 and 2:1.

To mimic the slow increase in the concentration of PEG 1000, drops were also set up over wells containing 0.1 M Hepes pH 7.5 and 10% PEG 1000. After one week of equilibration, the cover slip (on which the drop was mounted) was placed over a well containing 0.1 M Hepes pH 7.5 and 15% PEG 1000. This process was repeated weekly in 5% increments until the protein precipitated, typically at 25% PEG 1000. Another method was used to mimic slow drying, in which drops containing protein and crystallization solution were covered with Parrafin oil, light mineral oil, or a 50:50 mixture of the two oils. The two oils allow evaporation of water from the protein drop at different rates, thereby slowly increasing the concentration of the contents of the drop.

Several attempts were also made to seed crystallization in new drops using the original crystal and either streak seeding (*10*) or microseeding (*11*) methods. For streak seeding, a cat's

whisker was dragged lightly across the surface of a crystal to capture tiny fragments of crystal (seeds). The whisker was then dragged lightly through a fresh drop containing protein and crystallization solution to deposit the seeds, which can serve as sites for the nucleation of new crystal growth. For microseeding, a small chunk of the crystal was gently broken off, and placed into 1 mL of "stabilizing solution," consisting of 0.1 M Hepes pH 7.5, 40% PEG 1000. The crystal was then fragmented by vigorous vortexing with a ceramic bead. From this solution, serial dilutions of 1:10 to $1:10^9$ were prepared in stabilizing solution. The various dilutions were used as microseed stock for screening many crystallization conditions. A typical drop contained 1 μL protein (10-60 mg/mL), 1 μL crystallization solution and ~0.2 μL microseed stock. Many of the conditions described in the paragraphs above were also screened by streak seeding and microseeding. Unfortunately, none of the conditions tested succeeded in reproducing the original crystal.

4.3.9 The class I synthases from *Sphingopyxis alaskensis* ($PhaC_{Sa}$) and *Leptothrix cholodnii* ($PhaC_{Lc}$) may be good candidates for crystallography

We have also cloned, purified, and characterized the activity of two additional class I synthases, $PhaC_{Sa}$ and $PhaC_{Lc}$, which share 38% and 56% identity with $PhaC_{Re}$ respectively. Each synthase was expressed as an N-terminally $(His)_6$-tagged protein and could be rapidly purified to >95% homogeneity (Figure 4.11, lanes 1 and 3). Neither protein required hecameg or another detergent for successful purification. $PhaC_{Sa}$ was readily concentrated to 10 mg/mL for storage, and $PhaC_{Lc}$ was concentrated to ~5 mg/mL. $PhaC_{Lc}$ was screened at 5 mg/mL in Crystal Screens I and II (96 conditions), Index Screen (96 conditions), and the $PEGR_x$ screen (48 conditions). We have also cloned, expressed and purified the class I synthase from

Magnetospirillum magneticum ($PhaC_{Mm}$) (Figure 4.11, lane 5) but it has not yet been characterized.

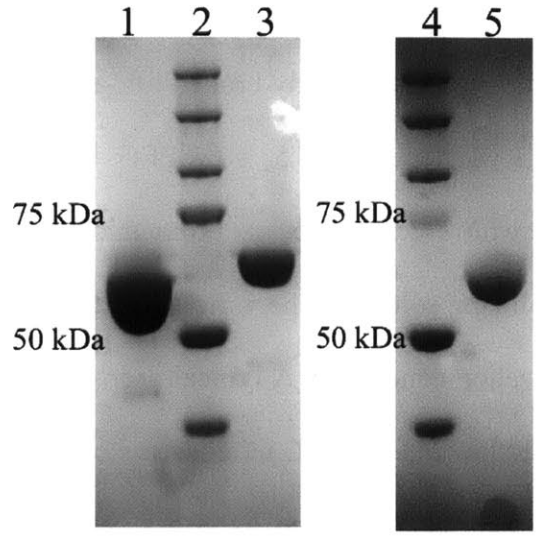

Figure 4.11 Purified class I synthases. Lane 1, 10 μg $PhaC_{Lc}$. Lane 2, molecular weight standards. Lane 3, 5 μg $PhaC_{Sa}$. Lane 4, molecular weight standards. Lane 5, 5 μg $PhaC_{Mm}$.

The specific activities of $PhaC_{Sa}$ and $PhaC_{Lc}$ at 30 ˚C were determined using the CoA release assay, and found to be 39 U/mg and 28 U/mg, respectively (Figure 4.12). The kinetics of both enzymes are similar to $PhaC_{Re}$, exhibiting lag phases in CoA release, with that for $PhaC_{Lc}$ being more pronounced than that for $PhaC_{Sa}$ (Figure 4.12). The specific activity of both enzymes was therefore determined from the linear phase of CoA release that follows the lag phase.

.

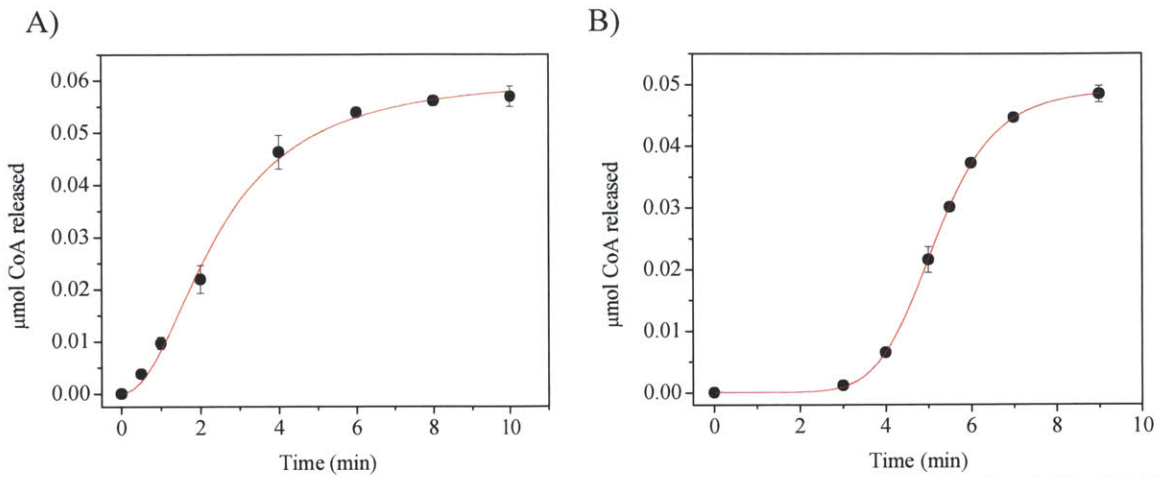

Figure 4.12 Assays of A) $PhaC_{Sa}$ and B) $PhaC_{Lc}$ at 30 °C. The assays contained 50 nM $PhaC_{Sa}$ or 100 nM $PhaC_{Lc}$ and 0.75 mM HBCoA (0.06 µmol total). The error bars are the standard deviation from the mean of three measurements. The data are fit to a sigmoidal function.

During an internship required as a member of the Biotechnology Training Grant program, I worked at Metabolix, Inc. They were interested in identifying PHB synthases that maintain enzyme activity over the daily temperature fluctuations experienced by crops in the field. To determine the temperature range over which $PhaC_{Sa}$ and $PhaC_{Lc}$ are active, assays were carried out from 10-40 °C in the case of $PhaC_{Sa}$, and 15-40 °C in the case of $PhaC_{Lc}$. The data are summarized in Table 4.11. $PhaC_{Lc}$ achieves maximum activity at 30 °C, then its activity decreases as the temperature continues to increase.

$PhaC_{Sa}$ appears to have a much broader temperature range over which it is active. *S. alaskensis* has been isolated from ocean water at 4-8 °C, and can also be cultivated in the laboratory at temperatures of up to 48 °C. These observations are consistent with the thermal stability of $PhaC_{Sa}$'s activity. This characteristic might prove to be an asset for crystallography purposes, as thermostable proteins, such as those from Thermophiles, are often amenable to crystallization. Thus far $PhaC_{Sa}$ has not been screened in crystallization trials.

Table 4.11 Specific activities of $PhaC_{Sa}$ and $PhaC_{Lc}$ from 10-40 °C.

Temperature (°C)	Specific activity (μmol/min/mg)	
	$PhaC_{Sa}$	$PhaC_{Lc}$
10	10 ± 0.7	not determined
15	16 ± 1.4	2.3 ± 0.2
20	23 ± 0.2	12 ± 0.7
25	31 ± 0.6	23 ± 0.3
30	39 ± 2.6	28 ± 0.3
35	48 ± 0.6	15 ± 2.6
40	71 ± 5.9	3.5 ± 0.6

4.3.10 Cloning of the class III synthases from *A. maxima* ($PhaEC_{Am}$), *Synechocystis* sp. PCC 6803 ($PhaEC_{Syn}$), *T. pfennigii* ($PhaEC_{Tp}$), *X. campestris* ($PhaEC_{Xc}$) and *X. oryzae* ($PhaEC_{Xo}$)

Five class III synthases were cloned and characterized to varying degrees in order to determine whether they were suitable candidates for crystallography. In the case of the synthases from *A. maxima*, *Synechocystis*, and *X. oryzae*, *phaE* and *phaC* were cloned into two separate expression vectors encoding different antibiotic resistance markers. The *phaEs* were inserted into a vector that encoded an N-terminal $(His)_6$-tag, whereas *phaCs* were untagged. In the case of the synthase from *X. campestris*, *phaEC* was inserted into a single expression vector. Finally, the synthase from *T. pfennigii* was cloned both as *phaEC* inserted into a single expression vector, and as *phaE* and *phaC* cloned into separate vectors for co-expression.

4.3.10.1 $PhaEC_{Am}$ is insoluble and has little/no activity.

Arthrospira maxima is a filamentous cyanobacterium found in tropical and subtropical lakes. $PhaE_{Am}$ shares 15% identity with $PhaE_{Av}$, and $PhaC_{Am}$ shares 56% identity with $PhaC_{Av}$. $phaE_{Am}$ was inserted into pET28a for expression with an N-terminal $(His)_6$-tag, and $phaC_{Am}$ was inserted into pET3a. The two proteins were successfully co-expressed at a ratio of ~1:1 in *E. coli* BL21(DE3)Gold cells at induction temperatures of 37 °C and 18 °C (Figure 4.13). However, SDS-PAGE analysis of the soluble and insoluble cell fractions following lysis revealed that

$PhaEC_{Am}$ is insoluble in both conditions (Figure 4.13, lanes 3 and 6). Furthermore, lysis of the cells in the presence of 0.1% n-octyl-β-D-glucopyranoside, a detergent commonly used to stabilize membrane or otherwise insoluble proteins, did not improve the solubility of $PhaEC_{Am}$ (Figure 4.13, lanes 8 and 9). Finally, the soluble and insoluble fractions were assayed for polymerization activity, but no activity was detected in either fraction. Thus, $PhaEC_{Am}$ was not pursued further as a crystallography target.

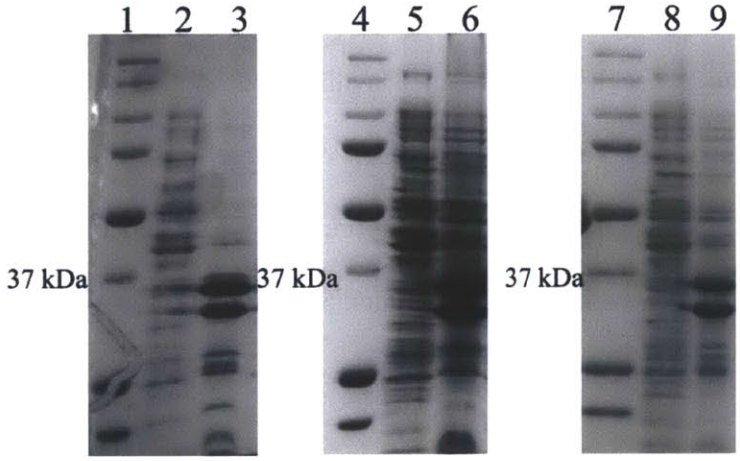

Figure 4.13 Efforts to express soluble $PhaEC_{Am}$. Lanes 1, 4 and 7, molecular weight standards. Lane 2, soluble fraction, induction at 37 ˚C. Lane 3, insoluble fraction, induction at 37 ˚C. Lane 5, soluble fraction, induction at 18 ˚C. Lane 6, insoluble fraction, induction at 18 ˚C. Lane 8, soluble fraction, induction at 18 ˚C, lysis in the presence of 0.1% octyl glucoside. Lane 9, insoluble fraction, induction at 18 ˚C, lysis in the presence of 0.1% octyl glucoside.

4.3.10.2 $PhaEC_{Syn}$ was successfully purified but precipitated extensively in crystallization trials

Synechocystis sp. PCC 6803 is a freshwater cyanobacterium. $PhaE_{Syn}$ shares 16% identity with $PhaE_{Av}$, and $PhaC_{Syn}$ shares 54% identity with $PhaC_{Av}$. *$phaE_{Syn}$* and *$phaC_{Syn}$* were successfully inserted into the pET28a and pET3a vectors, respectively, and co-expressed in *E. coli* BL21(DE3)Gold. Analysis of the protein contents of the soluble and insoluble fractions by SDS-PAGE following lysis reveals that, while both proteins are present in the soluble fraction,

there appears to be more $PhaE_{Syn}$ than $PhaC_{Syn}$ (Figure 4.14, lanes 2 and 3). $PhaEC_{Syn}$ was purified from the soluble fraction in two steps by affinity chromatography with Ni-NTA resin, followed by anion exchange chromatography with Q Sepharose resin. Following the Ni-NTA step, the protein was exchanged into 50 mM Tris pH 7.6, 10 mM NaCl, 5% glycerol by Sephadex G25 chromatography. Heavy precipitation was observed following buffer exchange, and the precipitated protein was removed by centrifugation. Following anion exchange with Q Sepharose resin, the protein was exchanged into 20 mM Hepes pH 7.5, 20 mM NaCl and concentrated. During concentration about 50% of the remaining protein was lost to precipitation. Despite the losses, ~3 mg $PhaEC_{Syn}$ per g of cells was obtained, with a specific activity of 20 U/mg, and 10% recovery of the total units. The kinetics of $PhaEC_{Syn}$ resemble those of $PhaC_{Re}$, in which a lag phase precedes the linear phase in CoA release (Figure 4.14). Purified $PhaEC_{Syn}$ was screened for crystallization at 18 °C in 150 conditions (the Index Screen and Crystal Screen I), but the protein formed dark brown precipitate in almost all of them and was thus not pursued further.

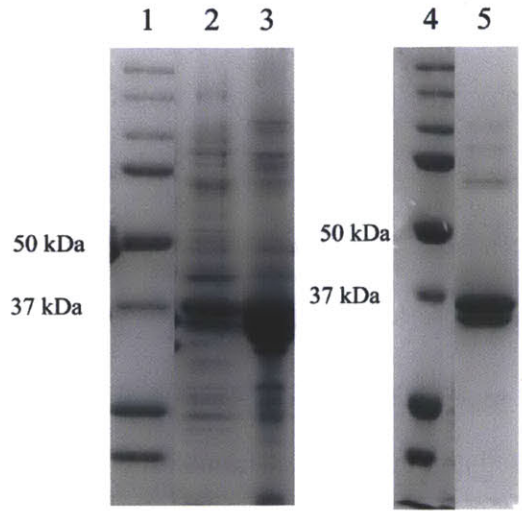

Figure 4.14 Expression and purification of PhaEC$_{Syn}$. Lane 1, molecular weight standards. Lane 2, soluble fraction post induction. Lane 3, insoluble fraction post induction. Lane 4, molecular weight standards. Lane 5, final purified protein.

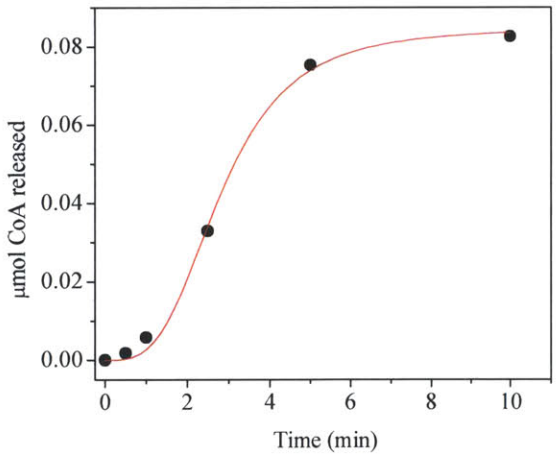

Figure 4.15 CoA release catalyzed by PhaEC$_{Syn}$. The reaction contained 100 nM PhaEC$_{Syn}$ and 0.75 mM HBCoA.

4.3.10.3 PhaEC$_{Tp}$ was successfully purified but precipitated extensively in crystallization trials

Thiococcus pfennigii is a spherical, Gram-negative purple sulfur bacterium. Its class III synthase has previously been cloned and purified by Liebergesell and coworkers (*12*). In their work, the PhaEC$_{Tp}$ construct was expressed in *Pseudomonas putida* from a single vector housing

phaEC that encoded no affinity tag. $PhaEC_{Tp}$ was purified using Procion Blue H-ERD Sepharose and hydroxyapatite anion exchange chromatography. The purified protein was a 1:1 complex of PhaE and PhaC with a specific activity of 20 U/mg at 30 °C. We initially cloned $phaEC_{Tp}$ into a single expression vector, but found that only one protein (presumably $PhaE_{Tp}$) was overexpressed in *E. coli* (not shown). We therefore inserted $phaE_{Tp}$ and $phaC_{Tp}$ separately into the pET28a and pET3a vectors, respectively, and achieved successful co-expression of both proteins at 18 °C (Figure 4.16). The cells were lysed and the soluble and insoluble fractions were separated by centrifugation and analyzed by SDS-PAGE. The soluble fraction contained some $PhaEC_{Tp}$, but the majority was insoluble (Figure 4.16, lane 3). The protein was purified by affinity chromatography using Ni-NTA resin with elution using 250 mM imidazole, followed by anion exchange using Q Sepharose resin. Following Ni-NTA chromatography, the protein that eluted from the column was concentrated to 1 mL (5 mg/mL) for buffer exchange. During concentration $PhaEC_{Tp}$ precipitated heavily and the precipitated protein was removed by centrifugation. The supernatant containing soluble protein was exchanged by dialysis at 4 °C into 50 mM tris pH 7.6, 10 mM NaCl for Q Sepharose chromatography. A contaminating band migrating just below the 75 kDa marker could not be removed (Figure 4.16, lane 5). The resulting protein was concentrated and exchanged into 20 mM Hepes pH 7.5, 20 mM NaCl and again there was extensive precipitation of $PhaEC_{Tp}$, which was removed by centrifugation, precluding its concentration to higher than ~1 mg/mL. The final protein was ~75% pure due to the contaminating band migrating just below the 75 kDa marker, which co-eluted with $PhaEC_{Tp}$ following each chromatography step. The ratio of PhaE to PhaC appeared to be 1:1 by eyeball (Figure 4.16, lane 5). $PhaEC_{Tp}$ was assayed and its specific activity was 20 U/mg, as measured from the initial linear phase (Figure 4.17). The kinetics resemble those of $PhaEC_{Av}$. $PhaEC_{Tp}$ was

screened at 1 mg/mL in Crystal Screens I and II (96 conditions), Index Screen (96 conditions), and PEG/Ion Screens I and II (96 conditions). As was the case with $PhaEC_{Syn}$, $PhaEC_{Tp}$ formed dark brown precipitate in the majority of conditions, even at very low concentration of enzyme. Thus it was not extensively pursued in further crystallization trials.

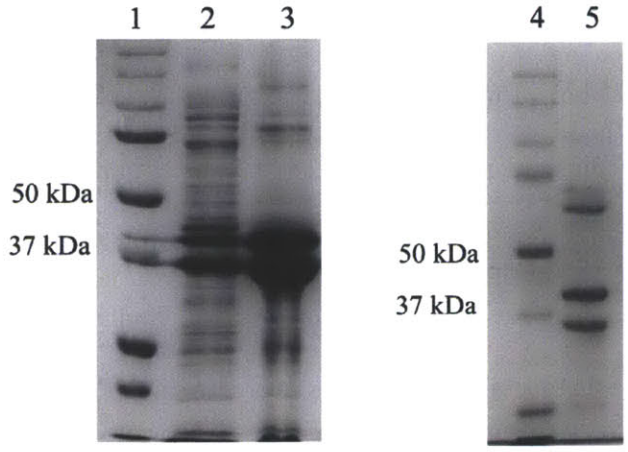

Figure 4.16 Expression and purification of $PhaEC_{Tp}$. Lane 1, molecular weight standards. Lane 2, soluble fraction with expression at 18 °C. Lane 3, insoluble fraction with expression at 18 °C. Lane 4, molecular weight standards. Lane 5, final purified protein.

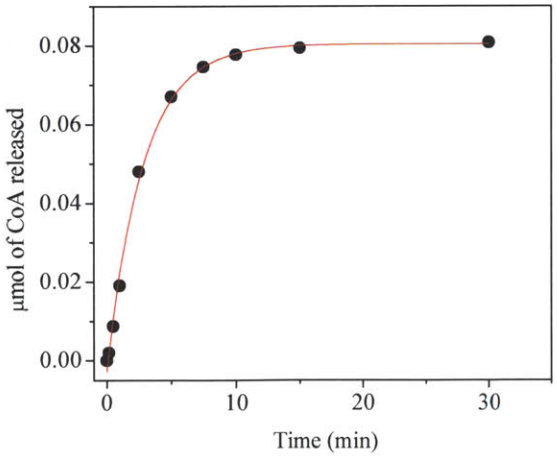

Figure 4.17 CoA release catalyzed by $PhaEC_{Tp}$. The reaction was carried out at 30 °C and contained 20 nM $PhaEC_{Tp}$ and 0.75 mM HBCoA in 20 mM Hepes pH 7.5, 20 mM NaCl.

4.3.10.4 Expression and purification of $PhaEC_{Xc}$ and $PhaEC_{Xo}$

Xanthomonas campestris and *Xanthomonas oryzae* are Gram-negative plant pathogens and are considered select agents by the US government due to their potential for causing widespread crop destruction. They contain class III synthases with PhaCs that share 57% identity with $PhaC_{Av}$, and PhaEs that share 18% identity with $PhaE_{Av}$. *$phaEC_{Xc}$* was cloned into pET52b, which encodes an N-terminal StrepII-tag on PhaE for affinity purification. $PhaEC_{Xc}$ was expressed in recombinant *E. coli* harboring the plasmid $pPhaEC_{Xc}$ at 18 °C; three bands were apparently over-expressed, one migrating just below the 37 kDa marker and two migrating just above the 50 kDa marker (Figure 4.18A, lane 3). The sequence of the plasmid was reanalyzed to confirm it was correct. It was unclear at first whether all three bands were in fact $PhaEC_{Xc}$, because the over-expression was rather weak. To determine whether the three bands co-purified, cells expressing $PhaEC_{Xo}$ were lysed and the soluble fraction was combined with Streptactin affinity resin. When the protein was eluted with desthiobiotin, analysis by SDS-PAGE revealed three distinct bands (Figure 4.18B, lane 5). To identify these bands, they were transferred to a PVDF membrane and the fastest migrating band was excised and sent for N-terminal sequencing, revealing the amino acids MKGPL, which correspond to the first five residues of $PhaC_{Xc}$. It is likely that the two slower migrating bands are $PhaE_{Xc}$ and a truncated version of $PhaE_{Xc}$. This construct was not further pursued.

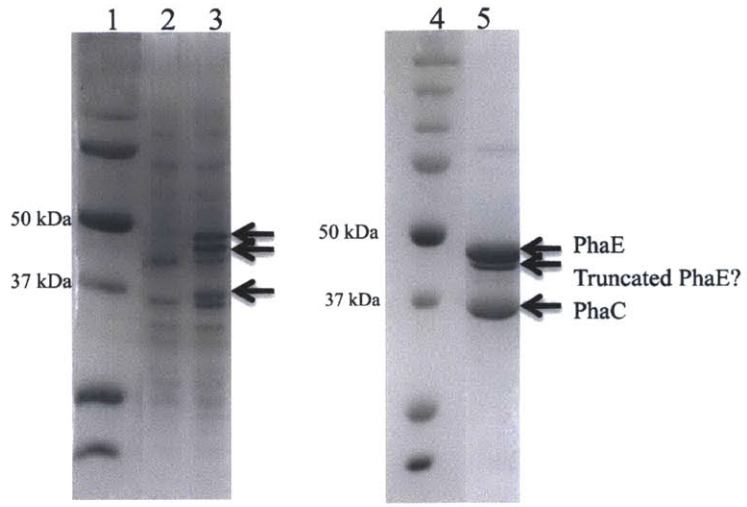

Figure 4.18 Expression and purification of $PhaEC_{Xc}$. Lane 1, molecular weight standard. Lane 2, pre-induction sample. Lane 3, post induction sample. Lane 4, molecular weight standards. Lane 5, final purified $PhaEC_{Xc}$.

$PhaEC_{Xo}$ was also expressed in recombinant *E. coli* harboring $pPhaEC_{Xo}$ at 37 °C and 18 °C, and the cells were lysed to analyze the soluble and insoluble fractions for their protein content and for activity of $PhaEC_{Xo}$ (Figure 4.19). At 37 °C, PhaE and PhaC were predominantly found in the insoluble fraction (Figure 4.19, lane 3). Decreasing the expression temperature to 18 °C, however, increased the amount of soluble protein (Figure 4.19, lane 4). Unfortunately, assays of the soluble and insoluble fractions from both expression temperatures revealed no activity, thus this protein was not pursued further for crystallography studies.

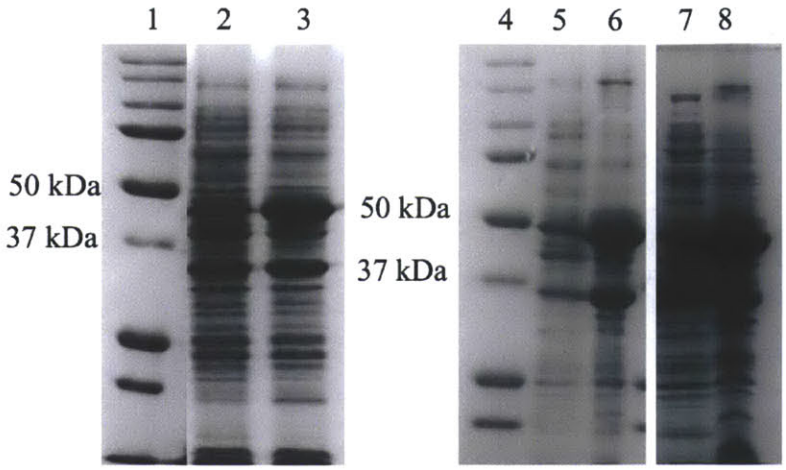

Figure 4.19 Expression and solubility of PhaEC$_{Xc}$. Lane 1, molecular weight standards. Lane 2, soluble fraction with induction at 37 ˚C. Lane 3, insoluble fraction with induction at 37 ˚C. Lane 4, molecular weight standards. Lane 5, soluble fraction with induction at 18 ˚C. Lane 6, insoluble fraction with induction at 18 ˚C. Lane 7, soluble fraction with induction at 18 ˚C and lysis in the presence of 0.1% octyl glucoside. Lane 8, insoluble fraction with induction at 18 ˚C and lysis in the presence of 0.1% octyl glucoside.

4.4 Discussion

Unfortunately we were unable to obtain crystals of a PHB synthase that were of a high enough quality to solve the X-ray structure. However, some of the observations and progress that we have made may be helpful for any future attempts to crystallize a synthase.

PhaEΔ27C$_{Av}$ and PhaEΔ35C$_{Av}$ crystallize in many conditions. In our experience, the generalization can be made that crystals of the fern/dendrite morphology, which typically form with PEG 3350 (or sometimes PEG of a different M_w) as a precipitant, never diffract. Grid screening around a condition that produces crystals of the fern/dendrite morphology has also not succeeded in producing crystals of diffraction quality. Therefore in future crystallization trials, we recommend that crystals of other crystal morphologies be given priority in terms of additional screening for diffraction quality. An additional observation is that co-crystallization with the inhibitor HBCH$_2$CoA resulted in the growth of crystals in a few conditions that did not promote

crystallization in the absence of $HBCH_2CoA$. This result suggests that the crystals were co-crystals of $PhaE\Delta27C_{Av}$ bound to $HBCH_2CoA$. Refining of these crystallization conditions by addition of osmolytes such as taurine and sarcosine resulted in the highest diffraction obtained with a class III synthase construct (4-5 Å), though, screening the diffraction of several additional crystals grown under these conditions revealed that most of the crystals diffracted to >7 Å. However the results suggest that co-crystallization with a non-covalent substrate analog such as $HBCH_2CoA$ can potentially result in higher quality crystals than those grown in the absence of a substrate analog.

The most promising result obtained was the discovery of a crystal of $PhaC_{Cc}\Delta N$ that grew during an extended incubation (~1 year), as described in section 4.3.7. Our analysis of the protein from a similar condition in the same crystallization tray suggested that the protein in this crystal was full-length (rather than a proteolytic fragment). The crystal diffracted to ~2 Å, the highest diffraction yet obtained with any PHB synthase, and a partial data set was collected. Attempts to solve the structure using molecular replacement with models generated by threading and structure prediction software were unsuccessful. This is perhaps not surprising considering the most reliable structure prediction is of the α/β hydrolase fold domain, which comprises only ~200 residues of the 589 residues in $PhaC_{Cc}\Delta N$. Attempts to reproduce the crystallization were also unsuccessful. However, the fact that a crystal of a PHB synthase diffracts to 2 Å is nonetheless a promising result, as previous efforts all resulted in crystals that diffracted no better than 7 Å.

Finally, the class I synthases $PhaC_{Sa}$ and $PhaC_{Lc}$ are worth exploring further as candidates for crystallization. They are well-behaved in solution and can be rapidly and highly purified. Furthermore, $PhaC_{Sa}$ seems to be somewhat thermally stable compared to the other synthases.

Thermal stability is a quality that makes the proteins of thermophiles attractive candidates when trying to obtain a crystal structure of a homolog to a difficult to crystallize protein of interest, and suggests that $PhaC_{Sa}$ could be amenable to crystallization.

4.5 Acknowledgement

We thank Professor Karen Allen for agreeing to collaborate with us on a difficult project and for her helpful input. We also thank Drs. Kelly Daughtry, Lorenzo Finci, Nick Denunzio and Nick Silvaggi for their assistance with screening crystals and for helpful discussions. And finally we thank Dr. Paul Hubbard for supplying us with $pPhaE\Delta27_{Av}$ and $pPhaC_{Av}$.

4.6 References

1. Jia, Y., Kappock, T. J., Frick, T., Sinskey, A. J., and Stubbe, J. (2000) Lipases provide a new mechanistic model for polyhydroxybutyrate (PHB) synthases: characterization of the functional residues in *Chromatium vinosum* PHB synthase, *Biochemistry 39*, 3927-3936.
2. Li, P., Chakraborty, S., and Stubbe, J. (2009) Detection of covalent and noncovalent intermediates in the polymerization reaction catalyzed by a C149S class III polyhydroxybutyrate synthase, *Biochemistry 48*, 9202-9211.
3. Yuan, W., Jia, Y., Tian, J., Snell, K. D., Muh, U., Sinskey, A. J., Lambalot, R. H., Walsh, C. T., and Stubbe, J. (2001) Class I and III polyhydroxyalkanoate synthases from *Ralstonia eutropha* and *Allochromatium vinosum*: characterization and substrate specificity studies, *Arch. Biochem. Biophys. 394*, 87-98.

4. Kalinin, Y., Kmetko, J., Bartnik, A., Stewart, A., Gillilan, R., Lobkovsky, E., and Thorne, R. (2005) A new sample mounting technique for room-temperature macromolecular crystallography, *J. Appl. Crystallogr. 38*, 333-339.

5. Müh, U., Sinskey, A.J., Kirby, D.P., Lane, W.S., Stubbe, J. (1999) PHA Synthase from *Chromatium vinosum*: cysteine 149 is Involved in covalent catalysis, *Biochemistry 38*, 826-837.

6. Tian, J. (2005) Mechanistic investigation of polyhydroxybutyrate (PHB) synthases and elucidation of PHB biosynthesis and degradation process in *Wautersia eutropha* H6, in *Chemistry*, p 345, Massachusetts Institute of Technology, Cambridge.

7. Bolen, D. W. (2004) Effects of naturally occurring osmolytes on protein stability and solubility: issues important in protein crystallization, *Methods (San Diego, Calif 34*, 312-322.

8. Sheldrick, G. M. (2008) A short history of SHELX, *Acta Crystallogr. D64*, 112-122.

9. Winn, M. D., Ballard, C. C., Cowtan, K. D., Dodson, E. J., Emsley, P., Evans, P. R., Keegan, R. M., Krissinel, E. B., Leslie, A. G., McCoy, A., McNicholas, S. J., Murshudov, G. N., Pannu, N. S., Potterton, E. A., Powell, H. R., Read, R. J., Vagin, A., and Wilson, K. S. (2011) Overview of the CCP4 suite and current developments, *Acta Crystallogr. D Biol. Crystallogr. 67*, 235-242.

10. Sturo, E. A., and Wilson, I. A. (1991) Applications of the streak seeding technique in protein crystallization, *J. Cryst. Growth 110*, 270-282.

11. Luft, J. R., and DeTitta, G. T. (1999) A method to produce microseed stock for use in the crystallization of biological macromolecules, *Acta Cryst. D Biol. Cryst. 55*, 988-993.

12. Liebergesell, M., Rahalkar, A., and Steinbüchel, A. (2000) Analysis of the *Thiocapsa pfennigii* polyhydroxyalkanoate synthase: subcloning, molecular characterization and generation of hybrid synthases with the corresponding *Chromatium vinosum* enzyme, *Appl. Microbiol. Biotechnol. 54*, 186-194.

Chapter 5:

Miscellaneous studies and future outlooks

5 Miscellaneous studies and future outlook

5.1 Introduction

This Chapter presents additional studies carried out during the course of this thesis. These include electron microscopy studies of the structure of the truncated construct of $PhaEC_{Av}$, PhaEΔ27C, additional *in vitro* studies with $PhaC_{Cc}\Delta N$, transmission electron microscopy (TEM) of stalked and swarmer cells of *Caulobacter crescentus*, and efforts to prepare mutant heterodimers of $PhaC_{Cc}$. These sections will be presented individually such that each topic has its own introduction, materials and methods, and results and discussion sections.

5.2 Electron microscopy (EM) investigation of the structure of a truncated mutant of $PhaEC_{Av}$

5.2.1 Introduction

Our efforts to obtain a crystal structure of class I and III synthases, detailed in Chapter 4, have not been successful for a variety of reasons. In the case of the truncated and full length constructs of the class I synthase from *C. crescentus*, we were unable to obtain crystals. In contrast, in the case of the truncated mutant of the class III synthase from *Allochromatium vinosum*, PhaEΔ27C, crystals were readily obtained in dozens of conditions, but the crystals always failed to diffract to under 7 Å.

An alternative method for structural analysis of proteins is negative staining electron microscopy, which has the benefits of not requiring crystallization of a protein of interest and also allowing the use of much lower concentrations of protein. In this method, a sample of protein is dispersed on a 70-80 nm thick carbon layer supported on an EM grid. The protein is stained, typically with uranyl acetate, then imaged with an electron microscope. The protein

particles disperse randomly across the surface of the grid, so every image captured contains protein molecules in a variety of orientations and conformational states. Computer software is then used to assist in the identification of each protein particle followed by the sorting of these various conformations into groups, which are 2-dimensional representations of the structure of the protein. The groups can then be used to reconstruct 3-dimensional structures at 10-30 Å in resolution. Thus, while this method does not provide atomic resolution, it can provide information about the overall conformation of a protein. This section presents our preliminary efforts to examine the structure of PhaEΔ27C by EM.

5.2.2 Materials and Methods

5.2.2.1 Materials

Unless otherwise stated, all chemicals were obtained from Sigma-Aldrich (St. Louis, MO) and used without further purification. Copper/rhodium grids and uranyl acetate were obtained from Electron Microscopy Sciences (Hatfield, PA).

5.2.2.2 Expression and purification of PhaEΔ27C

Expression and purification of PhaEΔ27C were carried out as described in section 4.2.3.

5.2.2.3 Preparation and imaging of EM grids and preliminary data analysis

A sheet of freshly cleaved mica was placed into a carbon evaporation chamber, and a thin (~15 nm) layer of carbon was deposited on it. The carbon film was lifted off of the mica sheets by floating them in a dish of water. Copper/rhodium grids were grasped with forceps, submerged in the dish and lifted through the floating carbon film. The grids were then glow-discharged in

the presence of amylamine in order to briefly activate the surface of the grid, in order to enhance the adsorption of sample onto the surface.

PhaEΔ27C was diluted to a final concentration of 20 μg/mL in 150 mM NH_4^+ acetate, pH 6.8. A sample of protein (5 μL) was pipetted onto the carbon surface of the grid. After 15 s, excess sample was removed by touching the corner of a Kim wipe to the edge of the grid. The grid was then stained with 1% uranyl acetate in ddH_2O for 15 s and the excess stain was blotted with a Kim wipe. Finally the grid was submerged in a dish of water and lifted through a second thin (~15 nm) carbon film to create a carbon "sandwich." The samples were imaged using an FEI Technai Spirit Transmission Electron Microscope at 80 keV at the W. M. Keck Microscopy Facility of the Whitehead Institute.

Using EMAN software for single particle analysis (*1*), 5505 particles were selected from 10 micrographs and the particles selected by the program were visually inspected to remove false positives. Selected particles were interpolated to 4.2 Å per pixel, and the particles were contained within 50-pixel boxes, about 50% larger than the particle diameters. The particles were band-pass filtered in order to retain information between 20 and 220 Å. The boxed particle images were then aligned, in order to bring particles within a particular orientation into common register, such that the class averages could be prepared. Class averages were then prepared from the aligned particles.

5.2.3 Results and Discussion

In order to obtain the typical result shown in Figure 5.1, several sample preparation variables were altered individually, including the sample concentration (5-100 μg/μL) and the staining time (5-30 s). Ultimately, the best micrographs were prepared from samples containing

20 μg/mL PhaEΔ27C with a staining time of 15 s. In Figure 5.1, the protein complexes are the bright particles, resembling flowers or coffee beans, surrounded by stain halos. In their original report of the expression and purification of $PhaEC_{Av}$, Steinbüchel and coworkers also imaged the synthase by electron microscopy (*2*). In their micrographs, they see particles that look very similar to ours, suggesting that truncation of the C-terminal 27 residues of PhaE does not dramatically change the quaternary structure. This observation is consistent with our observations that the truncated mutant retains activity. For data analysis, 5505 of these particles were selected and automatically sorted into 25 class averages (Figure 5.2). Table 5.1 indicates how many particles are sorted into each of the class averages.

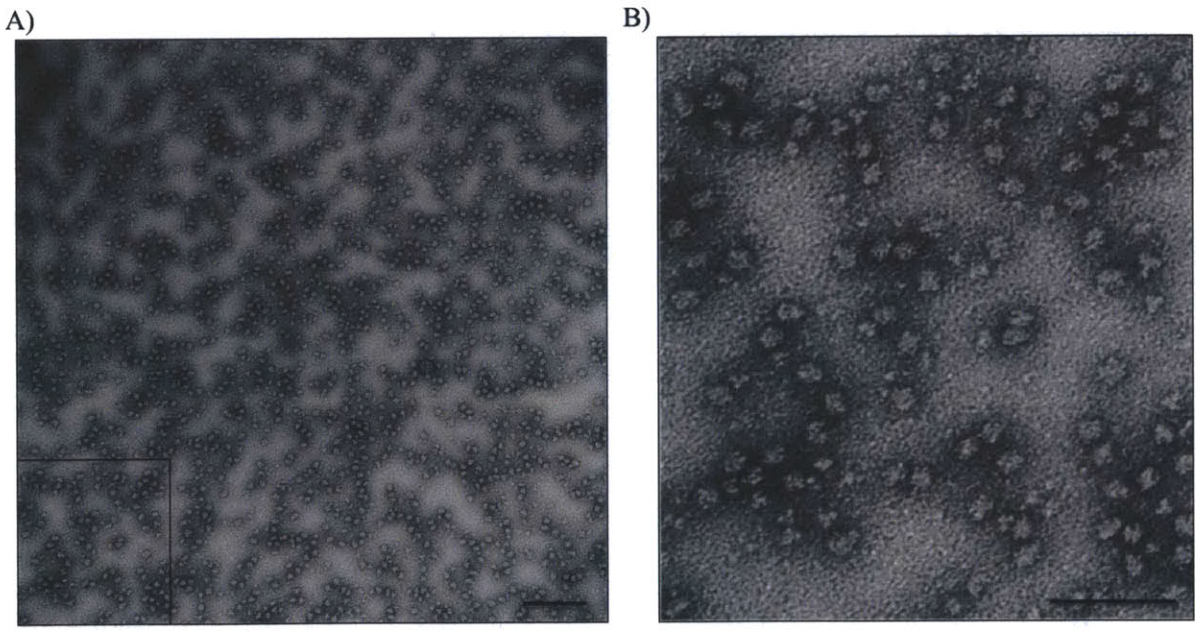

Figure 5.1 A typical electron micrograph of PhaEΔ27C. A) Electron micrograph of PhaEΔ27C. The sample was prepared by diluting PhaEΔ27C to 20 μg/mL in 150 mM NH_4^+ acetate, pH 6.8. Five μL was incubated 15 s on a copper/rhodium grid coated with carbon. The sample was stained 15 s with 1% uranyl acetate in ddH_2O. The scale bar is 150 nm B) Expansion of the boxed region in panel A. The scale bar is 75 nm.

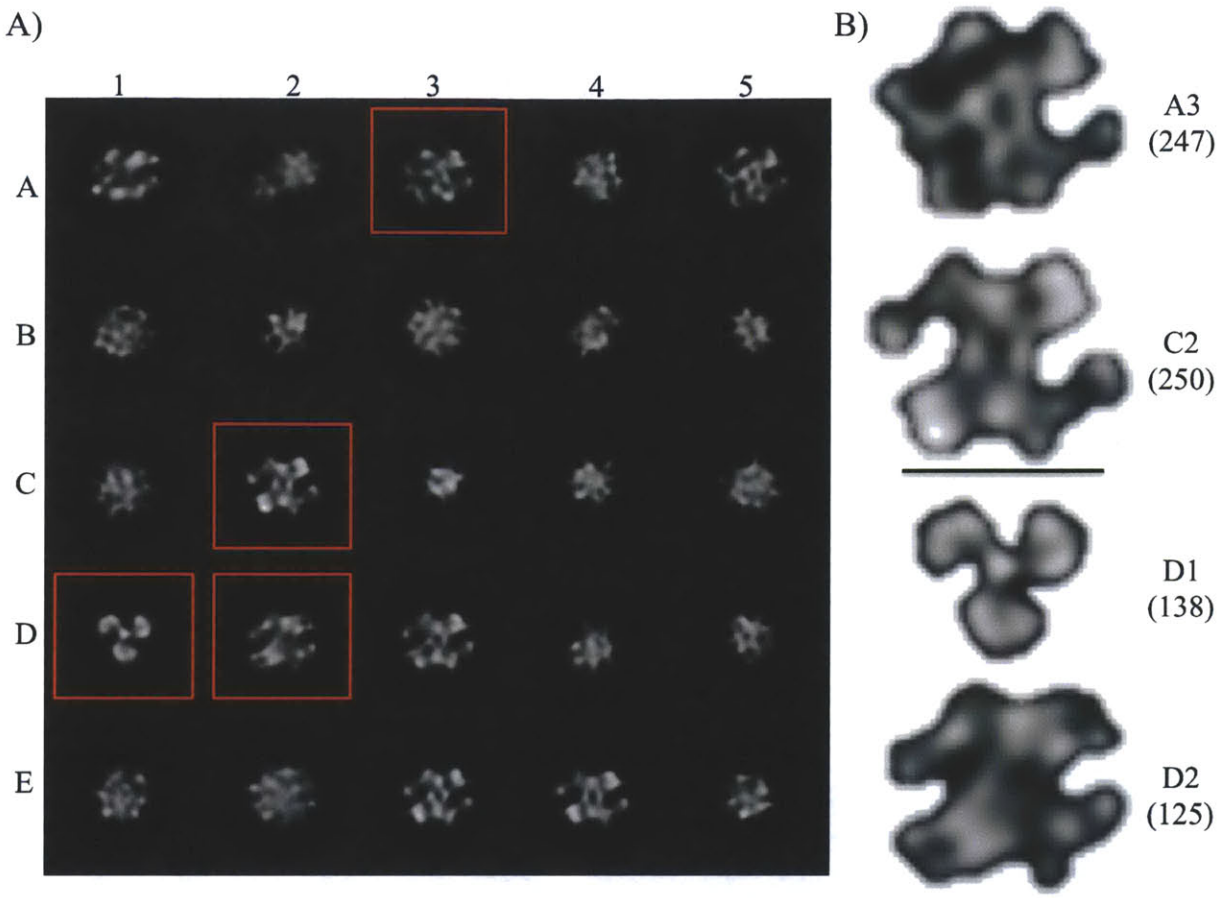

Figure 5.2 Class averages of PhaEΔ27C. A) Particles were sorted into 25 class averages. B) Enlarged class averages and the number of particles in each. The bar represents 15 nm.

Table 5.1 Number of particles sorted into each of the class averages shown in Figure 5.2.

Class average	Number of particles	Class average	Number of particles
A1	122	D1	138
A2	350	D2	125
A3	247	D3	231
A4	279	D4	192
A5	102	D5	129
B1	330	E1	300
B2	352	E2	255
B3	515	E3	235
B4	165	E4	110
B5	103	E5	345
C1	204		
C2	250		
C3	120		
C4	135		
C5	171		

Many of the class averages look similar, suggesting that if the software had been instructed to sort the particles into fewer class averages, these would have been grouped together. For example, class averages A1, A2 and A5, which contain ~10% of the total particles, represent apparently very similar structures/orientations of PhaEΔ27C. The same is true for class averages C2, D2, D3, E3 and E4, which together contain ~20% of the total particles. The remaining class averages are similar to one another and depict a globular structure that does not have any particularly distinctive features.

In Chapter 4, we presented size exclusion chromatography analysis of the quaternary structure of PhaEΔ27C, which suggested that it was a mixture of dimers and tetramers of PhaEΔ27C. PhaEΔ27 and PhaC are both ~40 kDa in M_w, and a typical 40 kDa globular protein has a diameter of ~4-5 nm. In Figure 5.2B the scale bar is 15 nm, demonstrating that the class averages tend to have diameters of ~15 nm, which would be consistent with the range of diameters expected for dimers and tetramers of PhaEΔ27C. Class average D1 is noticeably distinct from the other class averages, in particular because it has three-fold symmetry that is seemingly inconsistent with the observation of dimers and tetramers of PhaEd27Cs being the predominant quaternary structures. However, the lobes of D1 are approximately the same size as the larger lobes on class average C2 and other similar class averages (compare the upper right lobes of D1 with the upper right lobes of C2, D2, D3, E3 and E4). This suggests that D2 may be either a different orientation of a structure similar to that or C2, or it could represent a partially disassembled structure that has lost one or more subunits.

These results demonstrate that further examination of the quaternary structure of $PhaEC_{Av}$ could prove fruitful. In particular, it may be interesting to study the mutant D302A-$PhaEC_{Av}$ incubated with 5-100 equiv. of HBCoA. Previous studies carried out in our lab

demonstrated that the D302A mutant can be relatively uniformly loaded with substrate (*3*); thus, we may be able to investigate whether structural changes take place upon initiation of polymerization.

5.3 *In vitro* studies of $PhaC_{Cc}\Delta N$

5.3.1 Introduction

PhaC from *C. crescentus* is annotated incorrectly in the database as a 65 kDa protein. In Chapter 2 we present the cloning and purification of this 65 kDa construct ($PhaC_{Cc}\Delta N$) as well as a 73 kDa construct that was originally proposed by Qi and Rehm to be the relevant form *in vivo (4)*. In Chapter 2 we demonstrated that the 73 kDa construct has 50-fold higher activity *in vitro* than the 65 kDa construct. Studies presented in Chapter 4 demonstrate that the synthase is ~75 kDa *in vivo* by Western blot analysis using antibodies generated to his-tagged $PhaC_{Cc}\Delta N$. The 73 kDa construct has an 8 kDa N-terminal domain that is enriched in Ala, Lys and Pro residues. This domain has no homology to any sequences in the database and furthermore it does not have any predicted secondary structure.

In this section, we present our additional efforts to characterize $PhaC_{Cc}\Delta N$. We have characterized the quaternary structure of $PhaC_{Cc}\Delta N$, the stoichiometry of acylation with sTCoA, and the effect of priming with sTCoA on the effect of the activity of $PhaC_{Cc}\Delta N$.

5.3.2 Materials and methods

5.3.2.1 Materials

All chemicals were obtained at the highest purity available from Sigma-Aldrich (St. Louis, MO) unless otherwise specified. The compounds sTCoA was synthesized by Dr. Ping Li according to the method of Jia *et al.* (*5*).

5.3.2.2 Construction of pRBphaC_{Cc}ΔN and expression and purification of PhaC_{Cc}ΔN

The expression plasmid pRBphaC_{Cc}ΔN was constructed as described in section 2.2.2. PhaC_{Cc}ΔN was expressed and purified as described in section 2.2.3.

5.3.2.3 Reaction of PhaC_{Cc}ΔN with sTCoA: determination of the stoichiometry of acylation

The stoichiometry of acylation was measured using the DTNB assay to monitor CoA release. The reaction was carried out at 30 °C and contained in a final volume of 110 μL: 20 mM Hepes pH 7.5, 20 mM NaCl, 50 μM PhaC_{Cc}ΔN and 500 μM sTCoA. At various time points, 20 μL aliquots were withdrawn and quenched in 50 μL 10% TCA. The samples were analyzed by the discontinuous DTNB assay described in section 2.2.5.

5.3.2.4 Activity of PhaC_{Cc} and PhaC_{Cc}ΔN following acylation with sTCoA

The reaction was carried out at 30 °C. In a final volume of 110 μL, the reaction mixture contained: 20 mM Hepes pH 7.5, 20 mM NaCl, 100 nM PhaC_{Cc}ΔN and 500 μM sTCoA. After 30 s, the assay was initiated by addition of 0.76 mM HBCoA. At various time points, 20 μL aliquots were withdrawn and quenched in 50 μL ice cold 10% TCA. The samples were centrifuged 5 min at 14,000 x*g* to remove precipitated protein, and 68 μL was removed and

added to 262 μL 0.25 mM 5,5′-dithiobis-(2-nitrobenzoic acid (DTNB) in 0.5 M KH_2PO_4, pH 7.8. The reactions were incubated for 5 min and A_{412} of each sample was measured. Specific activity is calculated from the rate of the linear phase of the kinetic trace and is given in U/mg, where one unit is one μmol substrate consumed per min. Data were fit to a sigmoidal function using Equation 5.1.

Equation 5.1 $$y = \frac{Ax^n}{K^n + x^n}$$

5.3.3 Results and Discussion

5.3.3.1 Reaction of $PhaC_{Cc}\Delta N$ with sTCoA: $PhaC_{Cc}\Delta N$ is acylated with a stoichiometry of one per dimer of PhaC

To examine the stoichiometry of acylation with sTCoA, 50 μM $PhaC_{Cc}\Delta N$ was incubated with 500 μM sTCoA and the reaction was monitored by hand quenching of various time points followed by DTNB assay to evaluate CoA release. These experiments showed a burst of CoA release corresponding to 0.5 per monomer of $PhaC_{Cc}\Delta N$ (Figure 5.3). The stoichiometry of 0.5 per monomer of $PhaC_{Cc}\Delta N$ is reminiscent of the stoichiometry of $PhaC_{Re}$, suggestive of half-sites reactivity. In contrast, however, $PhaC_{Re}$ is predominantly a monomer with a small population of dimer. As reported in Chapter 2, full length $PhaC_{Cc}$ is a single oligomeric species (dimer or trimer) and its acylation with sTCoA gives a stoichiometry of one per monomer. These results suggest that the N-terminal domain of $PhaC_{Cc}$ plays a role in the stoichiometry of PHB chain synthesis that requires further study.

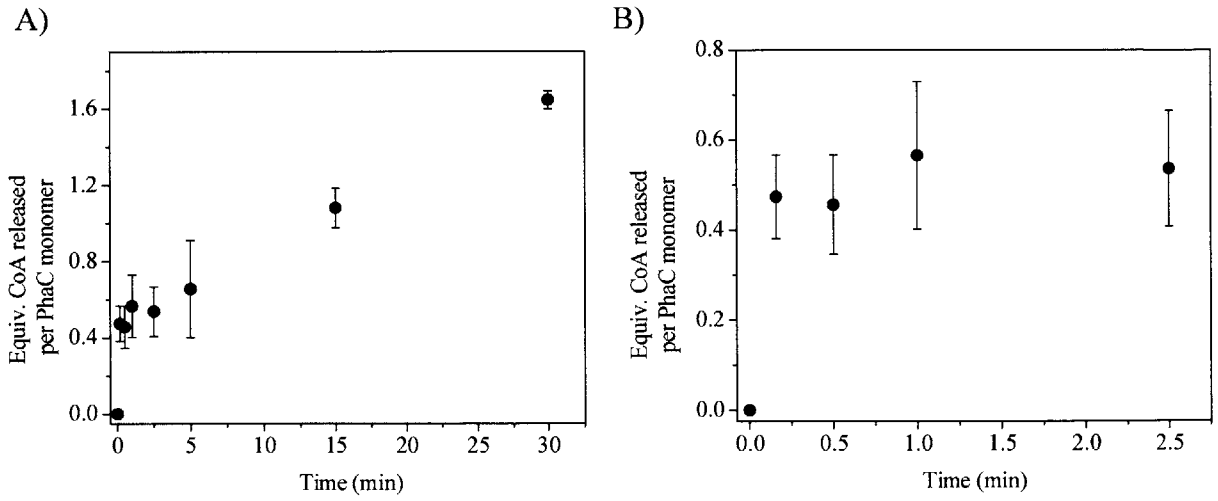

Figure 5.3 Reaction of PhaC$_{Cc}$ΔN with sTCoA. A) CoA release from acylation of PhaC$_{Cc}$ΔN with sTCoA. The reaction contained 50 μM PhaC$_{Cc}$ΔN and 500 μM sTCoA and was carried out at 30 °C. Equivalents of CoA released are given per PhaC monomer. The error bars represent the standard deviation from the mean of three experiments. B) Expansion of the first 2.5 min.

5.3.3.2 Reaction of sT-PhaC$_{Cc}$ΔN with HBCoA: priming with sTCoA increases the activity 20-fold

We next examined the effect of priming with sTCoA on the activity and on the lag phase of PhaC$_{Cc}$ΔN. Activity assays following acylation with sTCoA were carried out to determine whether sT could act as a primer for PhaC$_{Cc}$ and increase activity, as is the case with PhaC$_{Re}$. PhaC$_{Cc}$ΔN (100 nM) was incubated with 500 μM sTCoA for 30 s at 30 °C, then 1 mM HBCoA was added to initiate polymerization and the reaction was monitored by hand quenching of various time points followed by DTNB assay. The results demonstrated that the activity of PhaC$_{Cc}$ΔN is enhanced nearly 20-fold, from 1 U/mg to 18 U/mg, by priming with sTCoA, and the lag phase is eliminated or obscured (Figure 5.4). In contrast, as described in section 2.2.12, acylation with sTCoA prior to reaction with HBCoA increases the activity of full length PhaC$_{Cc}$ by only 2-fold. These results in combination with the size exclusion data that demonstrate PhaC$_{Cc}$ΔN is a mixture of monomer and dimer in solution are consistent with the proposal that

sTCoA decreases/eliminates the lag phases of $PhaC_{Re}$ and $PhaC_{Cc}\Delta N$ by shifting the monomer/dimer equilibrium in favor of dimer. However, due to the instability of sT-$Pha_{Cc}\Delta N$ (not shown) this species could not be examined by SEC.

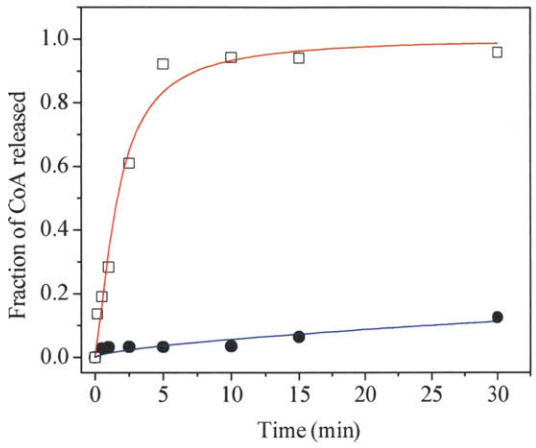

Figure 5.4 Effect of priming with sTCoA on the activity of $PhaC_{Cc}\Delta N$. The reaction contained 100 nM $PhaC_{Cc}\Delta N$ reacted with 1 mM HBCoA (●, blue) or pre-acylated with 500 μM sTCoA then chased with 1 mM HBCoA (□, red).

5.4 TEM analysis of division of granules between stalked and swarmer cells

5.4.1 Introduction

C. crescentus divides asymmetrically, with each round of division producing two distinct types of daughter cells, the stalked cell and the swarmer cell (Figure 5.5) (*6*). The stalked cell is sessile and has a single polar extension of the cytoplasm, periplasm and cell wall called the "stalk." The swarmer cell is motile and has a single polar flagellum. Asymmetric division is thought to play a role in adaptation to nutrient limited growth conditions, because motile swarmer daughter cells can disperse upon division, thus reducing competition for nutrients between daughter cells (*7*). Such nutrient-limited growth conditions, when a carbon source is abundant, are also conducive to PHB accumulation.

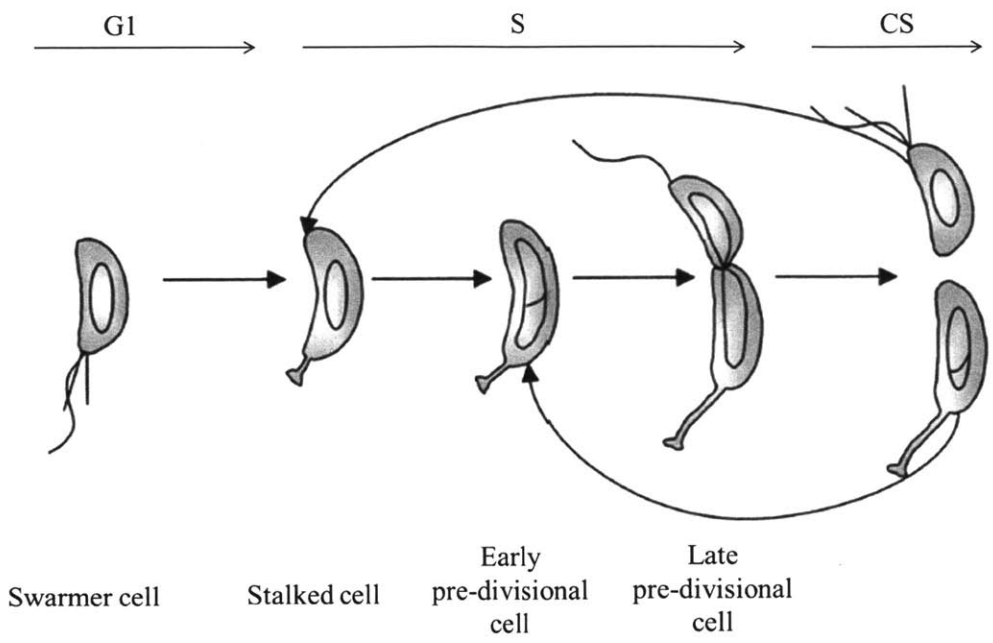

Figure 5.5 Lifecycle of *C. crescentus*. The motile swarmer cell remains in the G1 phase for a certain period of time before differentiating into a sessile stalked cell. The stalked cell is capable of DNA replication and immediately begins a round of cell division. Each stalked cell produces one stalked cell and one swarmer cell which begin the cycle anew. The different cell types have different densities, allowing their separation by density gradient centrifugation. G1, lag phase before DNA replication. S, period of new DNA synthesis. CS, cell separation. Adapted from reference (*8*).

The question of how granules are divided between cells during growth is related to the question of where granules form within the cell and how. Recent studies suggest that granules in *R. eutropha* are associated with nucleoid via the recently discovered the protein PhaM (*9, 10*). PhaM is thought to non-specifically bind nucleoid and simultaneously PHB. This proposal is attractive in that it explains how dividing cells, which are necessarily replicating and dividing nucleoid, could ensure roughly even segregation of granules between daughter cells. PhaM homologs are found in most members of the β-proteobacteria, a group that includes *R. eutropha*. However, α-proteobacteria, including *C. crescentus*, do not contain an identifiable homolog to PhaM.

We were interested in exploring the division of granules between stalked and swarmer cells in cultures of *C. crescentus* grown on nitrogen limited medium in the presence of glucose. Owing to their different densities, stalked and swarmer cells can be separated by density gradient centrifugation. Separation is most commonly done using Percoll, which is a colloidal mixture of silica particles (15-30 nm in diameter) that forms a density gradient upon centrifugation. The method is non-perturbative and is most commonly used as a technique to synchronize cultures of *C. crescentus*. Here, we have exploited this technique to separate stalked and swarmer cells at an early time point in PHB accumulation. The separate cell types were then fixed and embedded for transmission electron microscopy (TEM) to examine the distribution and localization of granules. We find that there is no difference between the two populations of cells in terms of either number or localization of granules. This result suggests that *C. crescentus* has a mechanism for dividing granules between daughter cells during division.

5.4.2 Materials and methods

5.4.2.1 Materials

All chemicals were purchased from Sigma-Aldrich (St. Louis, MO) at the highest purity available, unless otherwise noted, and used without further purification. Peptone and yeast extract were obtained from Difco (Franklin Lakes, NJ). Percoll was purchased from Fluka (Hannover, Germany). Glutaraldehyde (15% solution), OsO_4, uranyl acetate, propylene oxide, low viscosity embedding resing (LVER, containing vinyl-4-cyclohexene dioxide, diglycidyl ether polypropylene glycol, nonenyl succinic anhydride, and dimethylamino ethanol combined in proportions as per the manufacturer's protocol), flat silicone embedding molds and 200-mesh

nickel grids coated with carbon Formvar were purchased from Electron Microscopy Sciences (Hattfield, PA).

5.4.2.2 Media and growth conditions

Growths were carried out at 30 °C with shaking at 220 rpm, as described in section 3.2.2. Briefly, 50 mL PYE overnight cultures in 500 mL baffled flasks were inoculated with a single colony of *C. crescentus* and grown to saturation (~15 h, OD_{600} = 1.4). Two mL of overnight culture was used to inoculate 50 mL PYE "starter" cultures in 500 mL baffled flasks. The starter cultures were grown 4-5 h until OD_{600} = 0.15, then 20 mL was used to inoculate 500 mL PHB_p cultures in 4 L baffled flasks. The PHB_p cultures were grown 12 h until OD_{600} = 0.5, and the cells were pelleted and the stalked and swarmer cells separated be density centrifugation as described in the following section.

5.4.2.3 Separation of swarmer and stalked cells by centrifugation over a Percoll density gradient

Stalked and swarmer cells were separated over a Percoll density gradient by an adaptation from the method of Huguenel and Austin (*11*). Percoll is a colloidal mixture of silica particles (15-30 nm in diameter) that spontaneously separate to form a density gradient upon centrifugation. Stalked and swarmer cells of *C. crescentus* have densities of 1.01 g/mL and 1.07 g/mL, respectively. PHB_p cultures described in section 5.4.2.2 were pelleted by centrifugation at 4 °C for 20 min at 10,000 x*g* and the supernatant was decanted. The cells were washed by resuspension in 25 mL ice cold sterile 0.85% NaCl, then pelleted again by centrifugation and the supernatant was discarded.

The cell pellet was resuspended in 5 mL ice cold 0.85% NaCl and 5 mL ice cold Percoll and the suspension was placed in an Ultra-Clear Centrifuge Tube (14 x 89 mm) (Beckman Instruments, Palo Alto, CA). Stalked and swarmer cells were separated by centrifugation at 4 °C for 30 min at 8,000 x*g*. Stalked cells remained at the top of the gradient while swarmer cells sedimented to ~ 1 cm from the bottom of the tube. The centrifuge tube was carefully pierced with 3 mL syringes fitted with 18 ½ gauge needles, and the stalked and swarmer cells were individually withdrawn and placed in 15 mL Falcon tubes. The cell suspensions were diluted with ice cold 0.85% NaCl to a final volume of 10 mL, and the cells were pelleted by centrifugation at 4 °C for 20 min at 10,000 x*g*. The supernatant was decanted from each sample and EM samples were prepared as described in the following section.

5.4.2.4 Crotonate analysis of the PHB content of each cell type

Samples of each cell type were added to borosilicate tubes (16 mm x 125 mm) and dried overnight at 120 °C. The samples (~10-15 mg dry weight) were analyzed by the crotonate assay as described in section 3.2.8.

5.4.2.5 Transmission electron microscopy (TEM)

TEM samples were prepared as described in section 3.2.15 with minor modifications.

5.4.2.5.1 Fixation

The methods for preparation of TEM samples were adapted from (*12*). To prepare a typical sample, 25 mL of cell culture grown in PHB_p medium was combined 1:1 with 25 mL fixative containing 2% (v/v) glutaraldehyde, 3% (w/v) paraformaldehyde, 5% (w/v) sucrose in 0.1 M sodium cacodylate, pH 7.4. Samples were mixed with gentle rocking for 1 min, then

centrifuged for 10 min at 7000 x*g* at 4 °C. The cell pellets were resuspended in 10 mL fresh fixative and incubated for 1 h at 4 °C with gentle rocking. After fixation, the cell pellets were washed three times in 1 mL of 0.1 M sodium cacodylate pH 7.4 by centrifugation at 7000 x*g* at 4 °C. The cell pellets were then dislodged into 1 mL of 1% OsO_4 solution in Veronal-acetate buffer (0.24% (w/v) sodium acetate, 0.58% (w/v) sodium barbitol, 0.02 N HCl) and incubated for 1 h at RT with gentle rotation. Samples were centrifuged for 5 min at 14,000 x*g*, and the supernatant was removed. One mL Kellenberger uranyl acetate stain (0.5% uranyl acetate in Veronal acetate buffer) was then added to each sample, and the pellets were dislodged and broken apart, then incubated overnight for additional staining.

5.4.2.5.2 Dehydration

Following uranyl acetate staining, the pellets were dehydrated by incubations in increasing concentrations of ethanol. The pellets were dislodged into 1.5 mL 50% (v/v) ethanol in ddH_2O and rotated gently on a nutating mixer at RT for 10 min, then centrifuged 1 min at 14,000 x*g* and the supernatant decanted. This process was repeated with 70%, 90% and 95% ethanol, and repeated three times with 100% ethanol. The pellets were then dislodged into 1 mL of a mixture of 50% (v/v) ethanol, 50% (v/v) propylene oxide for 5 min, then 100% propylene oxide for 5 min. Finally the pellets were dislodged into 1 mL of a mixture of 50% (v/v) propylene oxide, 50% (v/v) LVER and incubated overnight at RT.

5.4.2.5.3 Embedding

The pellets were transferred into 1.5 mL 100% LVER, placed under vacuum at RT for 4 h, then exchanged into fresh 100% LVER. This process was repeated three times. After the final incubation in LVER the samples were centrifuged 1 min at 14,000 x*g* and then LVER was removed. The pellets were then placed on a clear surface (typically a plastic petri dish) and cut

into smaller pieces (~1-2 mm) using a toothpick. Several pieces of each sample were then embedded in flat silicone molds in ~250 μL fresh 100% LVER. The samples were cured for 48 h at 60 °C.

5.4.2.5.4 Sectioning and microscopy

Sectioning and imaging were carried out at the W.M. Keck Microscopy Facility at the Whitehead Institute (Cambridge, MA). Sectioning was performed by Dr. Mimi Cho. Sections (70-80 nm thick) were cut from each beam capsule using a Reichert Ultracut E Ultramicrotome equipped with a Diatome diamond knife. Sections were picked up by 200-mesh Formvar coated nickel grids. Samples were then imaged using an FEI Technai Spirit Transmission Electron Microscope at 80 kV at the W.M. Keck Microscopy Facility at the Whitehead Institute for Biomedical Research.

5.4.3 Results and Discussion

In order to examine the division of granules between stalked and swarmer cells, PHB_p cultures grown 12 h were pelleted and the two cells types were separated by density centrifugation over a Percoll gradient. The stalked and pre-divisional cells remained at the top of the gradient, while the swarmer cells settled at a band near the bottom of the gradient (Figure 5.6). There appear to be more stalked and pre-divisional cells than swarmer cells, which may be due to the fact that at the time point the cells were isolated, the cultures were actively growing and dividing, thus many cells were in the pre-divisional state. Both cell types were analyzed individually by crotonate assay and were found to contain ~3% PHB cdw, consistent with our previous measurements of cells isolated at the same time point in growth (Chapter 3). The isolated cells were then fixed, stained with uranyl acetate and embedded in LVER plastic and

EM samples were prepared. Comparison of the two cell types reveals little difference between them in terms of the number and size of granules (Figure 5.7), suggesting that the granules partition between the two daughter cells during each round of division. Furthermore, the morphology of the two cell types in Figure 5.7 is very similar. The only morphological difference between the two cell types is the presence of the flagellum on the swarmer cell and the stalk on the stalked cell. The flagellum has a diameter of ~20 nm (*6*), and the stalk has a diameter of 150-200 nm (*7, 13*). Considering that the micrographs in Figure 5.7 represent 70-80 nm slices of samples, it is not surprising that we do not see flagella in Figure 5.7A. In Figure 5.7B portions of stalks that have been imaged are indicated with black arrows, and a predivisional cell is indicated with a white arrow.

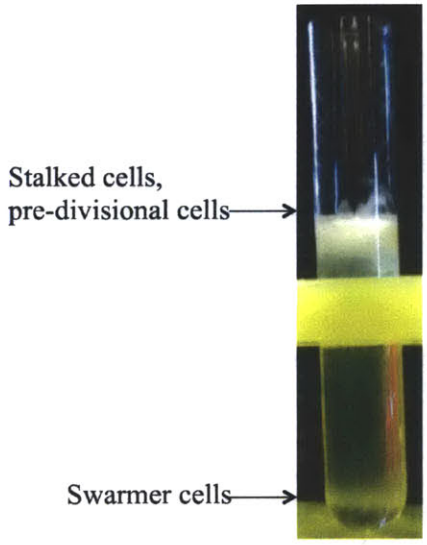

Figure 5.6 Percoll gradient separation of stalked and swarmer cells of *C. crescentus*. PHB_p cultures were grown 12 h, then the cells were pelleted, washed and applied to the top of the Percoll gradient. Following centrifugation, the two cell types were carefully pipetted from where they each had settled, and samples were prepared for electron microscopy.

PhaM homologs are only found in β-proteobacteria such as *R. europha*, and *C. crescentus* belongs to the α-proteobacteria. Because it divides asymmetrically in each round of division, *C.*

crescentus has elaborate mechanisms for generating the asymmetry, many of which are well understood (*14*). If the α-proteobacteria do in fact contain a distinct dedicated mechanism for partitioning of granules during growth, *C. crescentus* may be an ideal candidate for examining this process.

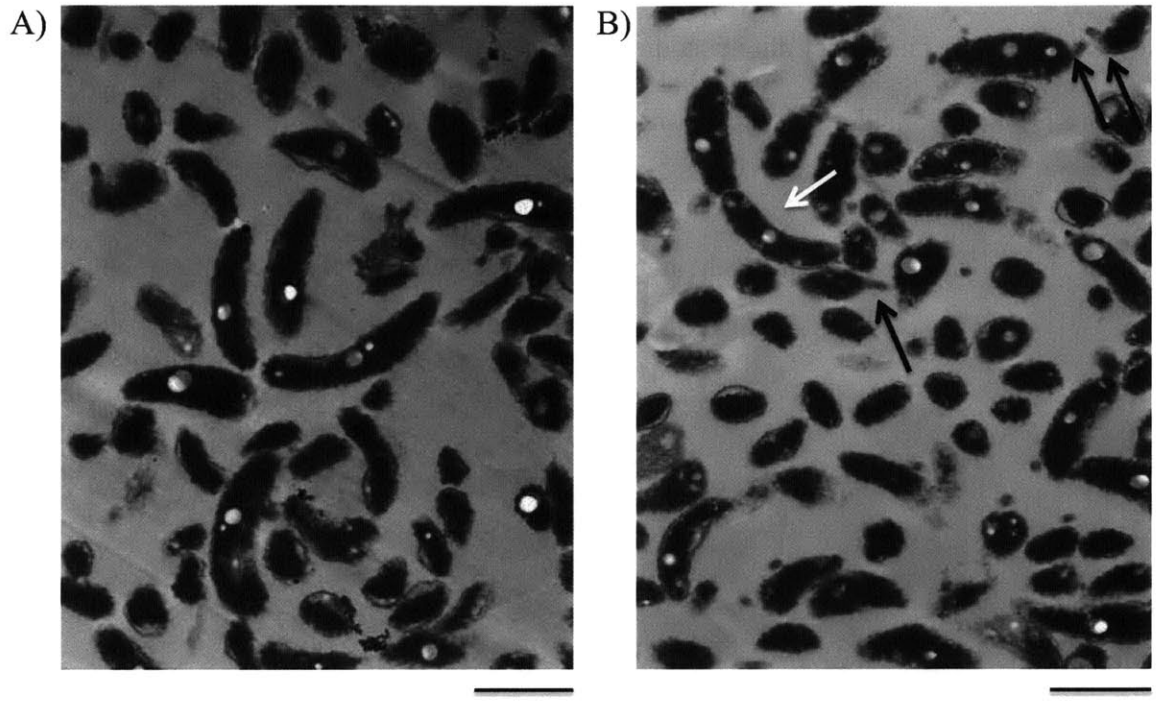

Figure 5.7 TEM of *C. crescentus* A) swarmer cells and B) stalked and pre-divisional cells grown 12 h in PHB_p medium. Both cell types contain ~3% PHB cdw.

5.5 Preparation and characterization of mutant heterodimers of $PhaC_{Cc}$

5.5.1 Introduction

Two models in Figure 5.8 for the mechanism of polymerization have been proposed based on studies conducted primarily on $PhaC_{Re}$ and $PhaEC_{Av}$. In both models, a dimer of PhaCs synthesizes a single PHB chain. This aspect of the models is based on the observations that acylation with artificial primers such as sTCoA results in a stoichiometry of labeling of 1 per dimer, and shifts the monomer-dimer equilibrium in favor of a dimer of synthases (*15, 16*). The

models differ in whether the Cys residue of both PhaC monomers is involved in catalysis, or whether the enzymes exhibit half-sites reactivity, with only a single Cys participating in catalysis. The model shown in Figure 5.8A was based on an analogy to fatty acid synthases and involves the participation of both Cys residues (*17*). In this model, there are no non-covalent intermediates, as the growing chain is passed between the two Cys residues with the addition of each HB monomer. The model shown in Figure 5.8B was is a variant on the mechanism proposed for some type III polyketide synthases (*18*). In this model, a single Cys residue synthesizes the PHB chain and after each ester bond is formed, the growing chain is transiently released from the active site Cys. The enzyme is then rapidly reacylated, releasing CoA. This model predicts that if the rate of reacylation is slowed, transient non-covalent intermediates could potentially be trapped. We have recently demonstrated the involvement of non-covalent intermediates with a mutant of the class III synthase from *Allochromatium vinosum* in which the active site Cys was mutated to Ser, C149S-PhaEC$_{Av}$. This mutant has a specific activity that is 1/2200th that of the wt enzyme. C149S-PhaEC$_{Av}$ was reacted with HBCoA and quenched at various time points, allowing trapping of the intermediates $(HB)_2CoA$ and $(HB)_3CoA$. While these findings support the mechanism shown in Figure 5.8B, a caveat remains that the Cys to Ser mutation could alter the mechanism of polymerization. Non-covalent intermediates in the reaction of a wt synthase with HBCoA have yet to be observed.

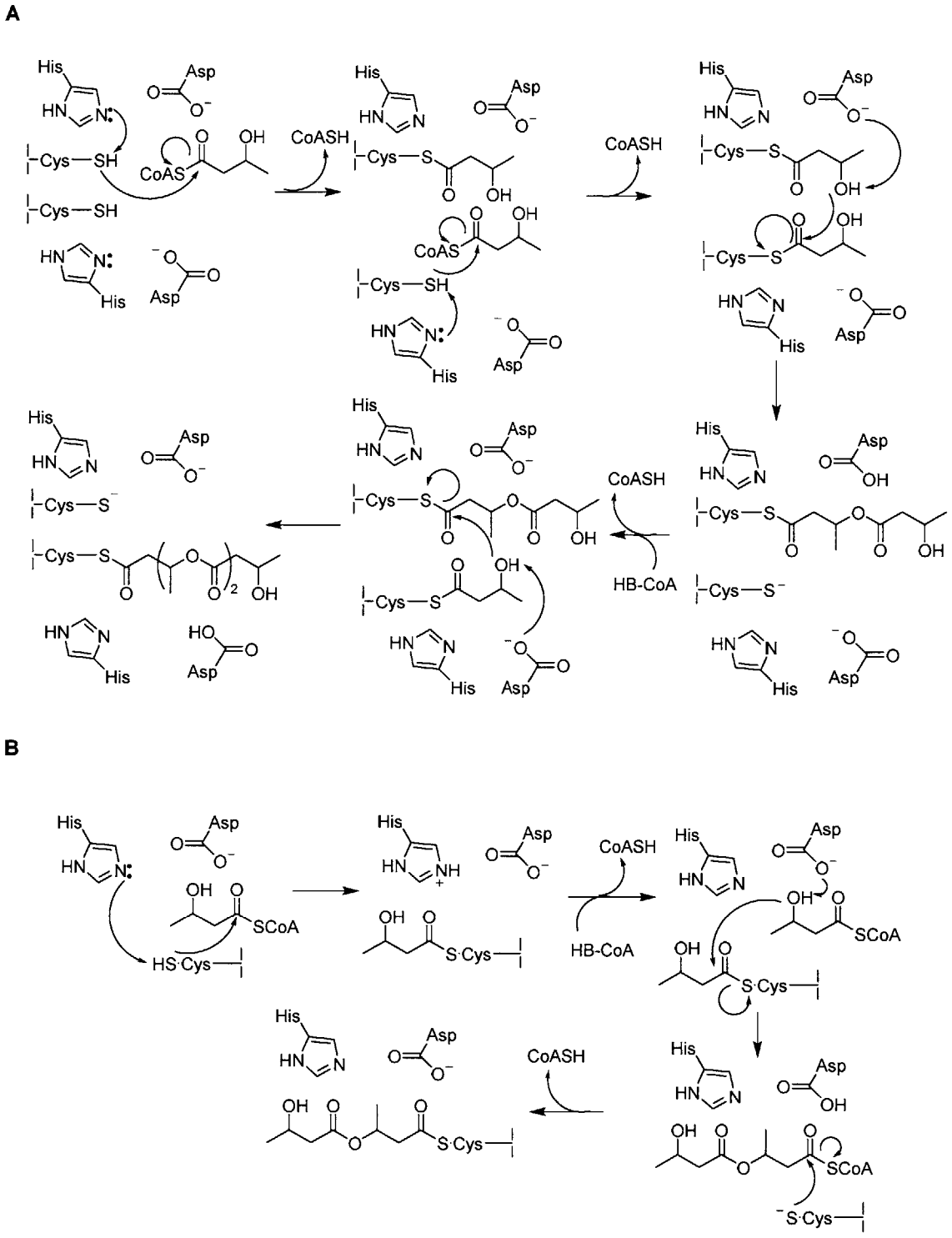

Figure 5.8 Working models for the mechanism of polymerization by PhaCs. A) Working model based off of analogy to fatty acid synthase involving the participation of Cys residues from two PhaCs. B) Working model based off of analogy to some type III polyketide synthases, involving the participation of only a single Cys residue.

In elegant experiments carried out by Smith and coworkers on mammalian fatty acid synthase, preparation of mutant heterodimers demonstrated that a mutation in one domain of one subunit can be complemented by the wt domain in the second subunit of the dimer (*19, 20*). In principle, this is the ideal experiment to distinguish between the mechanisms in Figure 5.8. In the mechanism in Figure 5.8A, one would predict that a mutant heterodimer composed of a wt subunit and a mutant subunit in which Cys is replaced with Ala would be inactive if both Cys residues are required for catalysis. Alternatively if only a single Cys participates in catalysis than the mutant heterodimer should have the same activity as the wt enzyme. The preparation of such mutant heterodimers of $PhaC_{Re}$ was reported by Goodwin and coworkers and is described in detail in Chapter 1 (section 1.3.2.6) (*21*). In their experiments, wt $PhaC_{Re}$ and mutant C319A-$PhaC_{Re}$ were combined at a stoichiometry of 1:1 under dilute conditions, which they believed promote conversion of $PhaC_{Re}$ to monomers. The exact concentration of $PhaC_{Re}$ in the "dilute" conditions is not provided, but based on the information available in the paper we can estimate that it is 3 μM. We have previously examined the dissociation of dimers of $PhaC_{Re}$ isolated by SEC into monomers, and have measured the K_D of the interconversion to be ~4 μM (*22*). Thus at 3 μM a portion of $PhaC_{Re}$ is likely still dimeric. To promote conversion to the dimeric form, they added 70% w/v fructose to the $PhaC_{Re}$ mixture, which they claimed promotes conversion to dimeric PhaC. They then compared the total units of activity of wt $PhaC_{Re}$ before and after addition formation of mutant heterodimers, and found that 50% of the total units were lost. Reassociation of wt and mutant PhaCs should occur at a rate of 1:2:1 of wt-wt to wt-mutant to mutant-mutant, thus they interpreted their results to indicate that the wt-mutant heterodimers were inactive, as predicted by the mechanism in Figure 5.8B. However, the authors have failed to consider the complicated equilibria of the monomer dimer conversion. Furthermore, we have

attempted to reproduce their studies suggesting fructose promotes dimerization, and have found that addition of fructose actually decreases the specific activity of $PhaC_{Re}$. Thus the experiments of Goodwin and coworkers were not correctly done, and they have likely misinterpreted their data.

Our observations that $PhaC_{Cc}$ is predominantly a single oligomeric state at high concentrations suggested that stable mutant heterodimers could be obtained given the appropriate isolation conditions. However, as each $PhaC_{Cc}$ is thought to make a single PHB chain on the basis of acylation studies with sTCoA (Chapter 2), these studies only address whether the active sites can function independently. We have included these experiments in this Chapter primarily to provide the experimental details, which may prove useful for future attempts to make mutant heterodimers.

5.5.2 Materials and Methods

5.5.2.1 Materials

All chemicals were purchased at the highest purity available from Sigma-Aldrich (St. Louis, MO) unless otherwise specified. Oligonucleotide primers were purchased from Integrated DNA Technologies (Coralville, IA) and are listed in Table 5.2. Restriction enzymes were purchased from New England Biolabs (Beverly, MA), GoTaq DNA polymerase and T4 DNA ligase were purchased from Promega (Fitchburg, WI), and PfuII Ultra and Pfx polymerase were purchased from Invitrogen (Carlsbad, CA). 3-*(R)*-hydroxybutyryl-CoA (HBCoA) was synthesized by Dr. Ping Li by the method of Yuan *et al.* (*23*). The plasmids used in this study are listed in Table 5.3.

5.5.2.2 Protein quantitation

PhaC concentration was determined by A_{280} (ε = 103,630 M^{-1} cm^{-1} for His_6-PhaC and 110,330 M^{-1} cm^{-1} for Strep2-PhaCs) or Bradford assay using BSA as a standard (*24*). For heterogeneous mixtures of proteins total concentration was determined by Bradford assay.

5.5.2.3 Construction of N-terminally tagged *his$_6$-phaC* and *strep2-phaCs* for expression in *E. coli*

Genomic DNA isolation and construction of the plasmid pRBhis$_6$phaC was carried out as described in section 3.2.3. For construction of pRBstrep2(HRV)phaC, *phaC* was amplified from pRBhis$_6$phaC using GoTaq polymerase and the primers phaCstrep2fw and phaCstrep2rev to insert a BamHI restriction site at the 5′ end of *phaC* and a NotI restriction site at the 3′ end of *phaC*. An annealing temperature of 55 °C and an extension temperature of 72 °C for 2 min were used. The amplified *phaC* product was digested with BamHI and NotI and inserted into pET52b (Novagen) that had been digested with the same restriction enzymes, to produce pRBstrep2(HRV)phaC. pET52b encodes the N-terminal strep2 tag and the sequence GALEVLFQGPGYQDP. The underlined portion of the sequence is an HRV 3C protease cleavage site. The portion of pRBstrep2(HRV)PhaC containing *strep2-phaC* was sequenced by the MIT Biopolymers Laboratory.

For construction of pRBstrep2phaC, *phaC* was excised from pRBhis$_6$phaC by digestion with NheI and BamHI then ligated into pET24a digested with the same restriction enzymes. A strep2 tag was then inserted by two successive rounds of mutagenesis first using the primers phaC_Insert1fw/phaC_Insert1rev to insert the first four amino acids of the strep2 tag (WSHP) followed by mutagenesis using the primers phaC_Insert2fw/phaC_Insert2rev to insert the second

four amino acids (QFEK). Mutagenesis was performed using PfuII polymerase with 1% DMSO as an additive. An annealing temperature of 55 °C and an extension temperature of 68 °C for 7 min were used. The plasmid was sequenced at the MIT Biopolymers Laboratory.

5.5.2.4 Construction of *his$_6$-phaC-C406A* and *strep2-phaC-C406A*

Attempts to generate the active site C406A mutant synthase by conventional mutagenesis methods were unsuccessful. Therefore both the His$_6$-tagged and Strep-tagged mutants were generated by the primer overlap extension method (*25*). Construction of pRBhis$_6$phaC-C406A is described in Chapter 2. For the construction of Strep2-PhaC-C406A, the 5′ region of *phaC* was amplified using *GoTaq* polymerase and the primers phaCStrep2fw and phaCC406Arev (product strepAB) and the 3′ region was amplified using GoTaq polymerase and the primers phaCC406Afw and phaCStreprev (product strepCD) (Table 5.2). phaCStrep2fw introduced a BamHI restriction site at the 5′ end of strepAB and phaCStrep2rev introduced a NotI restriction site at the 3′ end of strepCD.

The amplified PCR products were purified and the relative concentrations estimated by densitometry analysis by ethidium bromide staining in a 1% agarose gel. Based on this analysis, strepAB and strepCD were combined in a 1:1 ratio and these products then served as the templates for a second set of PCR reactions. strepAB and strepCD were amplified using *GoTaq* polymerase and the primers phaCStrep2fw and phaCStrep2rev. This PCR reaction "stitched" together the two template pieces, producing the products strepAD corresponding to *strep2-phaC-C406A*. *strep2-phaC-C406A* was subcloned into pCR2.1 TOPO by the manufacturer's protocol, then excised using the appropriate restriction enzymes. Using T4 DNA ligase, *strep2-phaC-C406A* was ligated into pET52b (Novagen) between BamHI and NotI restriction sites.

The resulting plasmid pRBstrep2(HRV)phaC-C406A was sequenced at MIT Biopolymers Laboratory and was found to contain a single base pair insertion at the site of the mutation. Therefore a final round of mutagenesis using PfuII polymerase and the primers phaCC406Afw and phaCC406Afw was carried out to remove the insertion using an annealing temperature of 55 °C and an extension temperature of 68 °C. The sequence was confirmed by sequencing at the MIT Biopolymers Laboratory.

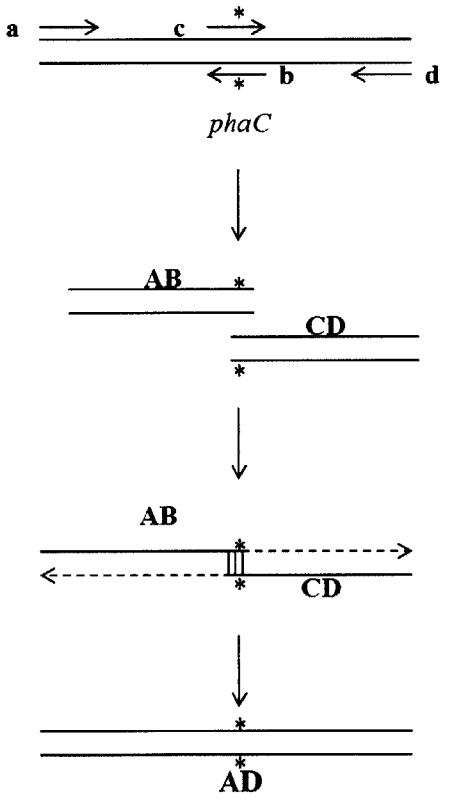

Figure 5.9 Schematic of primer overlap extension method of mutagenesis adapted from (*25*). Site-directed mutagenesis is accomplished using primers b and c, which contain the mutation (*), and primers a and d, which anneal to the 5′ and 3′ ends of the gene, respectively. The first PCR reaction produces fragments AB and CD. PCR products AB and CD, which overlap at the site of the mutation, are then used as template for the second PCR reaction. AB and CD hybridize at the site of the mutation and PCR using primers a and d generates the full length product AD.

Table 5.2 Primers used in Chapter 5.

Name	Sequence[a]
phaCStrep2fw	5′ - GGATCCTATGGCCACGGCGAAGGCCGCCCCCAAGGCTCGAA AGAAAGCCGCGAC - 3′
phaCStrep2rev	5′ - GATATAGCGGCCGCTCAGGGTTGTGACTTTACCAGCAC - 3′
phaCfw	Described in Table 2.1.
phaCrev	Described in Table 2.1.
phaC_Insert1fw	5′ - GGAGATATACATATGGCTAGCTGGAGCCACCCGATGGCC ACGGCGAAGGCCGCGCCCC - 3′
phaC_Insert1rev	5′ - GGGGCGCGGCCTTCGCCGTGGCCATCGGGTGGCTCCAGCTA GCCATATGTATATCTCC - 3′
phaC_Insert2fw	5′ - CATATGGCTAGCTGGAGCCACCCGCAGTTCGAAAAGATGG CCACGGCGAAGGCCGC - 3′
phaC_Insert2rev	5′ - GCGGCCTTCGCCGTGGCCATCTTTTCGAACTGCGGGTGGC TCCAGCTAGCCATATG - 3′

[a]Restriction sites, insertion sequences, and mutated codons are underlined.

Table 5.3 Plasmids used in Chapter 5.

Plasmid	Description	Reference
pRBstrep2(HRV)phaC	*phaC* inserted into pET52b between BamHI and NotI restriction sites; encodes N-terminal Strep2 tag (WSHPQFEK) and the linker GALEVLFQGPGYQDP, containing an HRV 3C protease site (underlined).	This work
pRBphaC$_{Cc}$	Described in Table 2.2.	This work
pRBphaC$_{Cc}$-C406A	Same as pRBhphaC with point mutation C406A.	This work
pRBstrep2(HRV)phaC-C406A	Same as pRBstrep2(HRV)phaC with point mutation C406A.	This work
pRBstrep2phaC	*phaC* inserted into pET24a; N-terminal Strep2 tag inserted by mutagenesis, no linker between *phaC* and Strep2 tag.	This work

5.5.2.5 Expression and purification of His$_6$-PhaC and His$_6$-PhaC-C406A

His$_6$-PhaC and His$_6$-PhaC-C406A were expressed and purified as described in section 2.2.3.

5.5.2.6 Expression and purification of Strep2(HRV)-PhaC, Strep2(HRV)-PhaC-C406A and Strep2PhaC

All culture medium was supplemented with 100 μg/mL ampicillin (Amp). A single colony of *E. coli* BL21(DE3) cells harboring either pRBstrep2(HRV)phaC or pRBstrep2(HRV)phaC-C406A was used to inoculate 5 mL LB culture broth. The cells were grown overnight at 37 °C. The entire culture was used to inoculate 1 L of LB in a 2.8 L baffled flask. The culture was grown to OD_{600} = 0.6 at 37 °C then the cultures were rapidly cooled to 25 °C and expression was induced with 0.4 mM IPTG. The cells were grown an additional 3-4 h at 25 °C then pelleted by centrifugation for 10 min at 3,500 x *g* at 4 °C. The cell pellets were flash frozen in liquid nitrogen and stored at -80 °C until use. A typical 1 L culture yielded 2.5 g cells.

The cell pellets were resuspended in 5 mL Strep-tactin lysis buffer (100 mM Tris, 150 mM NaCl, 1 mM EDTA pH 8.0) per g cells and lysed by two passes through the French pressure cell at 14,000 psi. The cell lysate was then centrifuged at 20,000 x *g* for 20 min to remove the insoluble cell debris. The resulting clarified extract was combined with Strep-tactin resin (IBA, GmbH, Göttingen, Germany; 0.2 mL resin per mL lysate) pre-equilibrated with Strep-tactin lysis buffer and incubated with gentle rocking for 30 min at 4 °C. The resin was then applied to a column and the flowthrough collected. The column was washed with 20 column volumes (cvs) of Buffer A, then the protein was eluted with 10 cvs Strep-tactin lysis buffer containing 1 mM desthiobiotin and the eluent was collected in fractions. The fractions containing protein were combined, concentrated and exchanged into 20 mM Hepes pH 7.5, 200 mM NaCl, 10% glycerol. Typical purifications yielded 2-3 mg of pure protein per g of cells.

5.5.2.7 Enzyme assays

Enzyme assays were carried out as described in section 2.2.5 with PhaC concentrations from 0.05 to 1 μM. When indicated, the assay mixture also contained n-octyl-β-$_D$-glucoside (0.1-1%). The specific activity is measured from the rate of the first linear phase and is given in U/mg, where a unit (U) is defined as a μmol of CoA released per min. Data are fit to equation 5.1.

5.5.2.8 Control for binding of Strep2(HRV)-PhaC to Ni-NTA resin and His_6-PhaC to Strep-tactin resin

Purified His_6-PhaC (5 μM) was prepared in 1 mL of Strep-tactin lysis buffer. Purified Strep2(HRV)-PhaC (5 μM) was prepared in 1 mL Ni-NTA lysis buffer. The solutions were then combined with the inappropriate affinity resin (0.25 mL) and incubated with gentle rocking at 4 °C for 30 min. The slurries were applied to columns (7 x 10 mm) and the flowthrough collected. The Strep-tactin resin was washed with 4 x 1 mL Strep-tactin lysis buffer and each wash fraction was collected. The Strep-tactin resin was then washed with 4 x 1 mL Strep-tactin lysis buffer containing 1 mM desthiobiotin to elute any His_6-PhaC that remained bound to the Strep-tactin resin and the elution fractions were collected. The Ni-NTA resin was washed with 4 x 1 mL Ni-NTA lysis buffer and each wash fraction was collected. The Ni-NTA resin was then washed with 4 x 1 mL Ni-NTA lysis buffer containing 250 mM imidazole to elute bound Strep2(HRV)-PhaC and the elution fractions were collected. Fifteen μL each fraction was combined with 10 μL Laemmli buffer and the fractions were analyzed by 10% SDS-PAGE.

5.5.2.9 Testing conditions for formation of His_6-PhaC/Strep2(HRV)-PhaC heterodimers by exchange of homodimers

Several conditions were tested for the dissociation of His_6-PhaC and Strep2-PhaC homodimers and reformation of heterodimers. In a final volume of 1 mL, 5 μM His_6-PhaC and Strep2-PhaC were combined in 20 mM Hepes, pH 7.5 with the following additives: 0.2-2 M NaCl; 0.2 M NaCl, 0.3% *n*-octyl-β-$_D$-glucoside; 0.2 M NaCl, 1% *n*-octyl-β-$_D$-glucoside; 2 M NaCl, 0.3% *n*-octyl-β-$_D$-glucoside; 0.2 M NaCl, 2 M urea; 0.2 M NaCl, 2-4 M guanidinium HCl; and 0.2 M NaCl, 15% 1,6-hexanediol. The solutions were incubated for 30 min-4 h at room temperature then exchanged overnight into 4 L 20 mM Hepes pH 7.5, 0.2 M NaCl by dialysis at 4 °C in Slide-a-Lyzer dialysis cassettes (0.5 - 3 mL capacity, 10,000 MWCO) (ThermoFisher Scientific, Waltham, MA). The dialysis cassettes were then transferred to 4 L Ni-NTA lysis buffer for 4 h at 4 °C. Following exchange, the solutions were combined individually with 0.25 mL Ni-NTA resin and equilibrated for 30 min at 4 °C. The slurries were then applied to columns (7 x 10 mm) and the flowthrough was collected. The columns were washed with 4 x 1 mL Ni-NTA lysis buffer and the washes were collected. The protein was eluted with 4 x 1 mL Ni-NTA lysis buffer containing 250 mM imidazole, and the elution fractions collected. Fractions (15 μL) were combined with 10 μL Laemmli buffer for analysis by 8% or 10% SDS-PAGE. The elution fractions (4 mL) were combined with 100 mL Strep-tactin lysis buffer to dilute imidazole, then concentrated to ~1 mL by filtration through a Centricon (15 mL, 30,000 MWCO) (Millipore, Billerica, MA). The reactions were again diluted with 20 mL Strep-tactin lysis buffer and concentrated to 1 mL, then combined with 0.25 mL Strep-tactin resin and incubated for 30 min at 4 °C with gentle rocking. The slurries were loaded to columns (7 x 10 mm) and the flowthrough collected. The columns were washed with 4 x 1 mL Strep-tactin lysis buffer and the washes were

collected. The columns were eluted with 4 x 1 mL Strep-tactin lysis buffer with 1 mM desthiobiotin and the fractions were collected. An aliquot (15 μL) from each fraction was combined with 10 μL Laemmli buffer and analyzed by 8% SDS-PAGE.

5.5.2.10 Preparation of His_6-PhaC/Strep2(HRV)-PhaC heterodimers on a large scale by exchange in 3 M guanidinium HCl

In a final volume of 5 mL, reaction **A** contained: 5 μM wt His_6-PhaC and 5 μM wt Strep2(HRV)-PhaC in 20 mM Hepes pH 7.5, 200 mM NaCl and 3 M guanidinium HCl. The reaction contained 3.5 mg total protein. In a final volume of 10 mL, reaction **B** contained: 5 μM wt His_6-PhaC and 5 μM Strep2(HRV)-PhaC-C406A in 20 mM Hepes pH 7.5, 200 mM NaCl and 3 M guanidinium HCl. Reaction **C** was identical to reaction **B** except that it contained 5 μM His_6-PhaC-C406A and 5 μM wt Strep2(HRV)-PhaC. The reactions contained 7 mg protein total. The solutions were incubated for 30 min at room temperature, then dialyzed overnight at 4 °C against 4 L of 20 mM Hepes pH 7.5, 200 mM NaCl to allow for reformation of dimers. The reactions were then exchanged by dialysis into Ni-NTA lysis buffer (50 mM NaH_2PO_4, 300 mM NaCl, 10 mM imidazole, pH 8.0) for 4 h at 4 °C. Following dialysis, the reactions were combined with 2.5 mL Ni-NTA resin (~1 mL for the wt reaction) and equilibrated with gentle rocking for 30 min at 4 °C, then loaded onto columns (7 mm x 30 mm) and the flowthrough collected. The columns were washed with 20 cvs lysis buffer then 10 cvsNi-NTA lysis buffer with 50 mM imidazole. The proteins were eluted with five cvs of Ni-NTA lysis buffer with 250 mM imidazole and the elution fractions were combined, concentrated and exchanged into Strep-tactin lysis buffer. The reactions were combined with 1 mL of Strep-tactin resin and equilibrated for 30 min at 4 °C with gentle rocking. The slurries were loaded onto columns (7 mm x 10 mm)

and the flowthrough was collected. The columns were washed with 20 cvs of Strep-tactin lysis buffer then eluted with five cvs of Strep-tactin lysis buffer with 1 mM desthiobiotin. The reactions were concentrated to <200 μL and assayed for activity.

5.5.2.11 Control for loss of activity of His_6-PhaC and Strep2(HRV)-PhaC in 3 M guanidinium HCl

In a final volume of 1 mL, 5 μM His_6-PhaC and 5 μM Strep2(HRV)-PhaC were incubated in two separate reactions for 30 min at room temperature in 20 mM Hepes pH 7.5, 200 mM NaCl, 3 M guanidinium HCl. The reactions were loaded into Slide-a-Lyzer dialysis cassettes (0.5 - 3 mL capacity, 10,000 MWCO) and dialyzed overnight at 4 °C against 1 L of 20 mM Hepes pH 7.5, 200 mM NaCl, and the activity was assayed and compared to the activities of fresh protein.

5.5.2.12 Western blot analysis of heterodimers with anti-His_6 and anti-Strep2 antibodies

For anti-His_6 tag Western blots, samples of reactions **B** and **C** (section 5.5.2.10) (10-1000 ng) and a standard of His_6-PhaC (200 ng) were resolved by 8% SDS-PAGE. A sample of Strep2(HRV)-PhaC (200 ng) was included to test for cross-reactivity with the anti-His_6 antibody. For anti-Strep2 tag Western blots, samples of reactions **B** and **C** (10-25 ng) and a standard curve of Strep2(HRV)-PhaC (5-50 ng) were resolved by 8% SDS-PAGE. The proteins were blotted onto a PVDF membrane (Immun-Blot, BioRad) at 4 °C for 80 min at 100 V. The blotting buffer contained 25 mM Tris, 192 mM glycine, 20% (v/v) methanol, and 0.01% SDS. The blots were blocked in 3% milk, 0.1% Tween-20 in Tris-acetate-EDTA (TAE) buffer (blocking buffer) for 30 min at room temperature. For anti-His_6 Western blots, the blots were incubated for 1 h at

room temperature with anti-His_6 antibody (Roche) conjugated to horse radish peroxidase. For anti-Strep2 Western blots, the blots were incubated for 1 h at room temperature with anti-Strep2 antibody (Qiagen) diluted 1:1000 in blocking buffer. Anti-Strep2 Western blots were then incubated 1 h at room temperature in goat anti-mouse secondary antibody conjugated to horse radish peroxidase (Abcam), used at a dilution of 1:5000. The blots were developed using SuperSignal® West Femto chemiluminescent detection reagents (Thermo Scientific) and imaged using a BioRad ChemiDoc XRS imager. Band intensities were analyzed using Quantity-One® 1-D software (BioRad).

5.5.3 Results

5.5.3.1 Expression and purification of His_6-PhaCs, Strep2(HRV)-PhaCs and Strep2-PhaC

The expression and purification of His_6-PhaC and His_6-PhaC-C406A are described in section 2.2.3. Two *strep2-phaC* constructs were cloned. Strep2(HRV)-PhaC contains an N-terminal Strep2 tag that is separated from *phaC* by a spacer that encodes an HRV 3C protease cleavage site. Purification of Strep2(HRV)-PhaC and -C406A yielded about 3 mg protein per g of cells. As with His_6-PhaC, a large portion of the synthase is contained within the insoluble fraction after cell lysis (Figure 5.10, lane 3). Expression at lower temperatures increased the fraction of synthase in the soluble fraction. The final purified protein was only ~80% pure, as judged by 10% SDS-PAGE after concentration (Figure 5.10, lane 6), likely due to extensive precipitation of Strep2(HRV)-PhaC during concentration that consequently enriched contaminating proteins. Inclusion of 10% glycerol in the storage buffer in subsequent purifications somewhat mitigated this problem. The specific activity of the preparation shown in Figure 5.10 was 35 U/mg, compared to ~50 U/mg measured for His_6-PhaC. Two additional

purifications of Strep2(HRV)-PhaC were carried out, and the final proteins had specific activities of 10 U/mg and 5 U/mg (Table 5.4). The reason for the variability in the specific activities is not known, but may be due to the tendency of the synthase to precipitate, resulting in impure protein.

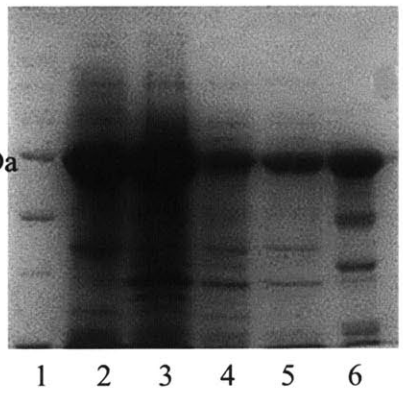

Figure 5.10 SDS-PAGE (10%) gel of Strep2(HRV)-PhaC purification steps. Lane 1, molecular weight markers. Lane 2, soluble cell-free extract. Lane 3, insoluble cell-free extract. Lane 4, Strep-tactin column flowthrough. Lane 5, Strep-tactin column wash. Lane 6, final protein.

Table 5.4 Activity table for the purification of Strep2(HRV)-PhaC.

Purification step	Volume (mL)	Protein (mg)	Activity (U^a/mg)	Total units	% yield[b]
Crude soluble extract	15	285	11	3140	100
Strep-tactin flowthrough	23	190	7.3	1360	43
Strep-tactin wash	63	38	25	950	30
Final protein	1.7	20	35[c]	710	23

[a]One unit of activity is one µmol CoA released per min.
[b]% yield is calculated based on total units in crude soluble extract.
[c]The purification table gives the results of the purification that yielded synthase with the highest specific activity.

The second *strep2-phaC* construct contained *phaC* with an N-terminal Strep2 tag with no linker. The tag was inserted by two rounds of mutagenesis and additional mutagenesis was carried out to insert either a (G_4S) or $(G_4S)_2$ linker. The purification of Strep2-PhaC with no linker was robust and yielded synthase with a specific activity of 52 U/mg (Table 5.5). This specific activity is comparable to the specific activity of His_6-PhaC (50 U/mg). Purification of

Strep2-PhaC also yielded protein that was 95% pure as judged by 8% SDS-PAGE (Figure 5.11, lane 5), and this protein was used in all subsequent experiments.

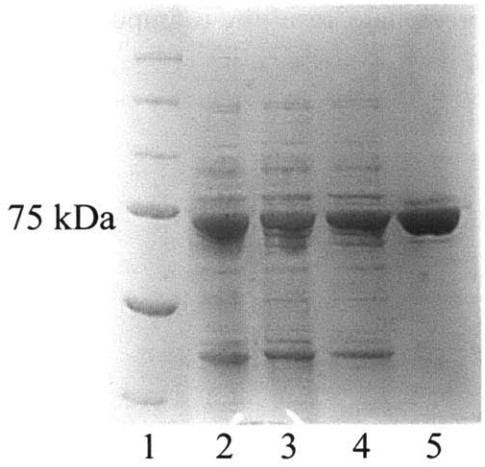

Figure 5.11 SDS-PAGE (8%) analysis of Strep2-PhaC purification steps. Lane 1, molecular weight standards. Lane 2, soluble cell-free extract. Lane 3, Strep-tactin column flowthrough. Lane 4, Strep-tactin column wash. Lane 5, final purified protein.

Table 5.5 Activity table for the purification of Strep2-PhaC.

Purification step	Volume (mL)	Protein (mg)	Activity (U[a]/mg)	Total units	% yield[b]
Crude soluble extract	21	320	8.3	2660	100
Strep-tactin flowthrough	23	280	4.7	1320	50
Strep-tactin wash	51	18	14	250	9.4
Final protein	1.5	6	52	310	12

[a]One unit of activity is one μmol CoA released per min.
[b]% yield is calculated based on total units in crude soluble extract.

5.5.3.2 Control for binding of Strep2(HRV)-PhaC to Ni-NTA resin and His_6-PhaC to Strep-tactin resin

A control was carried out to determine whether non-specific binding of His_6-PhaC and Strep2(HRV)-PhaC to the Streptactin and Ni-NTA affinity resin, respectively, occurred. The conditions in this experiment mimicked the conditions used for testing various conditions for exchange of heterodimers, as described below. His_6-PhaC mixed with Strep-tactin resin and loaded into a column is found entirely in the flowthrough and the first two wash fractions (Figure

5.12A, lanes 2-4). No protein is found in the elution fractions. When Strep2(HRV)-PhaC is mixed with Ni-NTA resin and loaded onto a column, the protein is almost entirely in the flowthrough and first two wash fractions (Figure 5.12B, lanes 2-4). A small amount of protein is present in the first elution fraction (Figure 5.12B, lane 7). Under these conditions the column was only washed with 10 mM imidazole. In scaled up exchange reactions described below, the Ni-NTA columns are washed additionally with 50 mM imidazole, which washes out the remainder of the non-specifically bound Strep2(HRV)-PhaC. These control reactions demonstrate that under the conditions used subsequently to test conditions for heterodimer formation, there is no non-specific binding to the affinity resins.

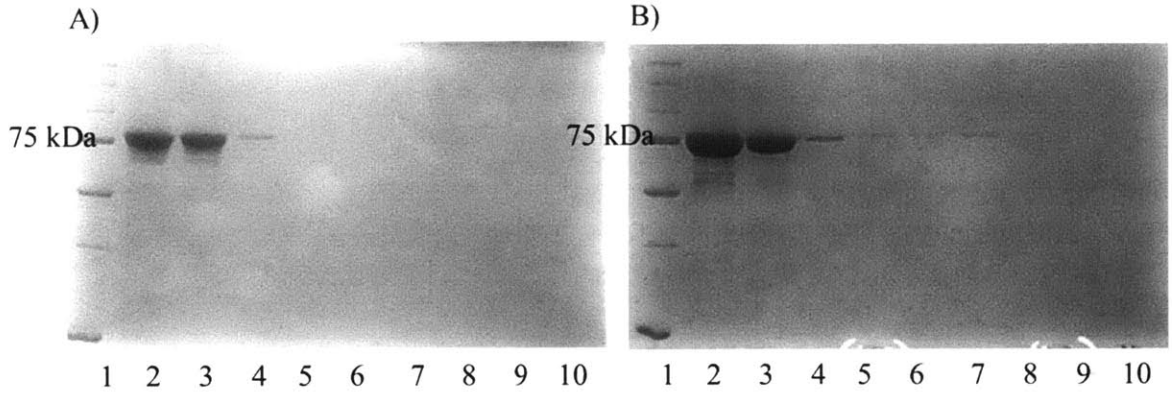

Figure 5.12 Control to test for non-specific binding of His_6-PhaCs and Strep2(HRV)-PhaCs binding to inappropriate affinity resin. A) His_6-PhaC (50 μM in 1 mL of 20 mM Hepes pH 7.5, 20 mM NaCl) was mixed with 0.2 mL of Strep-tactin resin. Lane 1, molecular weight standards. Lane 2, flowthrough from Strep-tactin resin. Lanes 3-6, 10 mM imidazole wash fractions. Lanes 7-10, elution fractions. B) Strep2(HRV)-PhaC (5 μM in 1 mL of 20 mM Hepes pH 7.5, 20 mM NaCl) was mixed with 0.2 mL of Ni-NTA resin. Lane 1, molecular weight standards. Lane 2, flowthrough from Ni-NTA column. Lanes 3-6, wash fractions. Lanes 7-10, elution fractions.

5.5.3.3 Migration of His_6-PhaCs and Strep2(HRV)-PhaCs in 8% SDS-PAGE.

His_6-PhaC and Strep2(HRV)-PhaC have molecular weights of 76,039 and 76,488 Da, respectively. We wished to determine whether the two proteins could be resolved by 8% SDS-

PAGE, as this would be the easiest way to determine whether both were present following heterodimer preparation and subsequent purification. His_6-PhaC, despite having a slightly lower molecular weight, migrates slightly higher than Strep2(HRV)-PhaC (Figure 5.13A, lanes 2-4 compared to lanes 5-7). When the two proteins are purified separately and then combined for SDS-PAGE analysis they are clearly distinguishable (Figure 5.13A, lanes 8-10). His_6-PhaC-C406A, Strep2(HRV)-PhaC and Strep2(HRV)-PhaC-C406A migrate at the same position (Figure 5.13B, lanes 3-5). Strep2-PhaC has a molecular weight of 74,829 Da and migrates more rapidly than the other PhaC constructs in 8% SDS-PAGE (Figure 5.13B, lane 6).

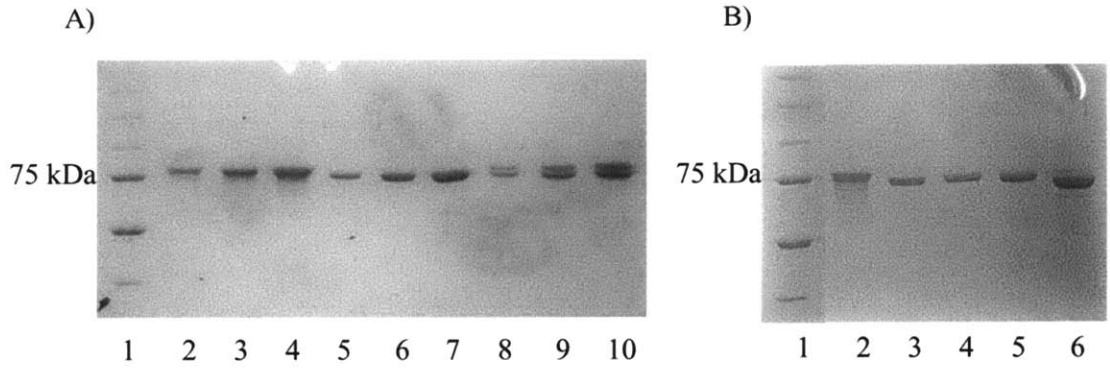

Figure 5.13 Relative migrations of His_6-PhaCs and Strep2(HRV)-PhaCs in 8% SDS-PAGE. A) Lane 1, molecular weight standards. Lanes 2-4, His_6-PhaC (1-3 μg). Lanes 5-7, Strep2(HRV)-PhaC (1-3 μg). Lanes 8-10, His_6-PhaC and Strep2(HRV)-PhaC (1-3 μg each protein). Proteins were purified separately and combined in gel sample. B) Lane 1, molecular weight standards. Lane 2, His_6-PhaC (2 μg). Lane 3, His_6-PhaC-C406A (2 μg). Lane 4, Strep2(HRV)-PhaC (2 μg). Lane 5, Strep2(HRV)-PhaC-C406A (2 μg). Lane 6, Strep2-PhaC (2 μg).

5.5.3.4 Testing conditions for formation of His_6-PhaC/Strep2(HRV)-PhaC heterodimers by exchange of homodimers

In order to find conditions that promote dissociation of PhaC dimers, several small scale reactions were carried out. His_6-PhaC and Strep2(HRV)-PhaC were incubated in 1 mL of buffered solutions containing a variety of additives.

5.5.3.4.1 Exchange in 20 mM Hepes pH 7.5, 0.2 M NaCl

His_6-PhaC and Strep2(HRV)-PhaC are stored in 20 mM Hepes pH 7.5, 200 mM NaCl. An exchange reaction between His_6-PhaC and Strep2(HRV)-PhaC was carried out in the storage buffer in order to confirm that spontaneous exchange doesn't occur, which would complicate heterodimer isolation. Figure 5.14 shows the results of this control. After purification with both affinity resins, a small amount of protein elutes from the Strep-tactin column (Figure 5.14B, lane 7). This protein migrates predominantly as a single band, but there appears to have been some degradation/proteolysis during the course of the experiment. Given that under less strenuous wash conditions (10 mM imidazole), a small amount of Strep2(HRV)-PhaC sticks to the Ni-NTA resin (Figure 5.14B), this single band is likely just Strep2-tagged synthase. As the wt PhaCs migrate at different rates, if both were present we should be able to distinguish them. There does not appear to be exchange between the His_6- and Strep2-tagged synthases in storage buffer.

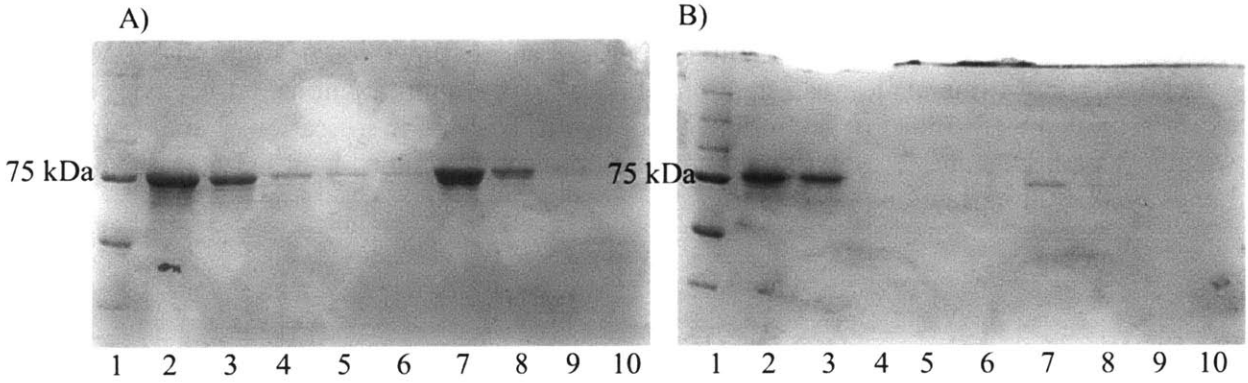

Figure 5.14 SDS-PAGE (8%) analysis of heterodimer exchange of His_6-PhaC and Strep2(HRV)-PhaC in 0.2 M NaCl. A) Analysis of Ni-NTA affinity purification of heterodimers. Lane 1, molecular weight standards. Lane 2, flowthrough from Ni-NTA column. Lanes 3-6, 10 mM imidazole wash fractions. Lanes 7-10, elution fractions. B) Analysis of Strep-tactin affinity purification of heterodimers following Ni-NTA purification. Lane 1, molecular weight standards. Lane 2, flowthrough from Strep-tactin column. Lanes 3-6, wash fractions. Lanes 7-10, elution fractions.

5.5.3.4.2 Exchange in 20 mM Hepes pH 7.5, 0.5-2 M NaCl

Three additional conditions were explored with variable concentrations of NaCl (0.5-2 M) in order to determine whether disruption of electrostatic interactions at the dimer interface could promote dissociation. In all three conditions only a single band elutes from the Strep-tactin column, again suggesting that there was no exchange between PhaCs (Figures 5.15-17B, lanes 7 and 8).

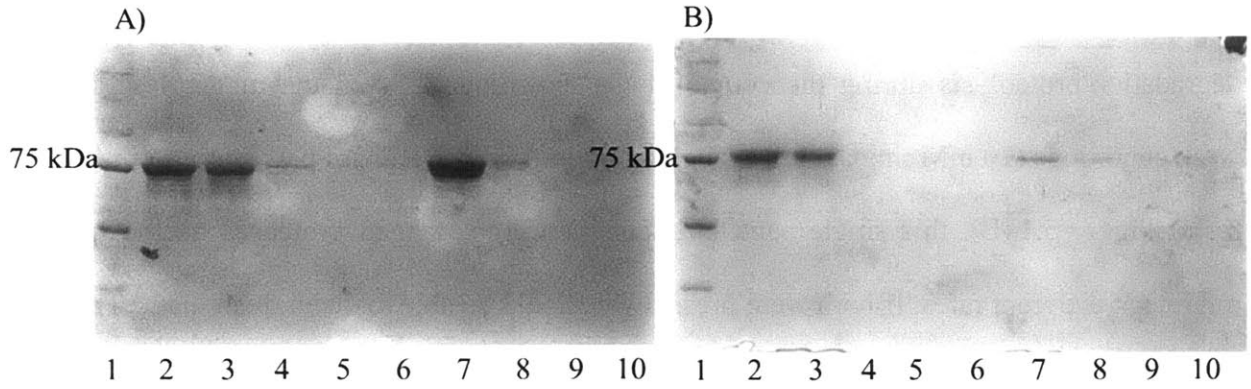

Figure 5.15 SDS-PAGE (8%) analysis of heterodimer exchange of His_6-PhaC and Strep2(HRV)-PhaC in 0.5 M NaCl. A) Analysis of Ni-NTA affinity purification of heterodimers. Lane 1, molecular weight standards. Lane 2, flowthrough from Ni-NTA column. Lanes 3-6, 10 mM imidazole wash fractions. Lanes 7-10, elution fractions. B) Analysis of Strep-tactin affinity purification of heterodimers following Ni-NTA purification. Lane 1, molecular weight standards. Lane 2, flowthrough from Strep-tactin column. Lanes 3-6, wash fractions. Lanes 7-10, elution fractions.

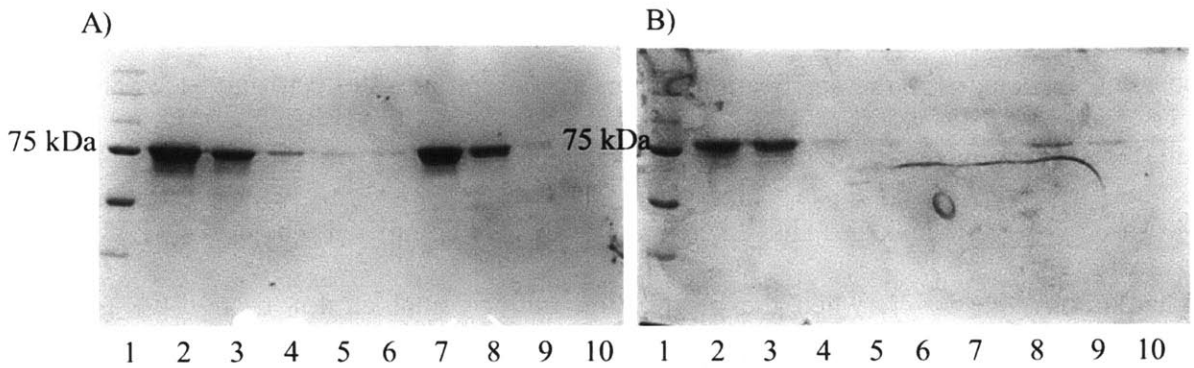

Figure 5.16 SDS-PAGE (8%) analysis of heterodimer exchange of His_6-PhaC and Strep2(HRV)-PhaC in 1 M NaCl. A) Analysis of Ni-NTA affinity purification of heterodimers. Lane 1, molecular weight standards. Lane 2, flowthrough from Ni-NTA column. Lanes 3-6, 10 mM imidazole wash fractions. Lanes 7-10, elution fractions. B) Analysis of Strep-tactin affinity purification of heterodimers following Ni-NTA purification. Lane 1, molecular weight standards. Lane 2, flowthrough from Strep-tactin column. Lanes 3-6, wash fractions. Lanes 7-10, elution fractions.

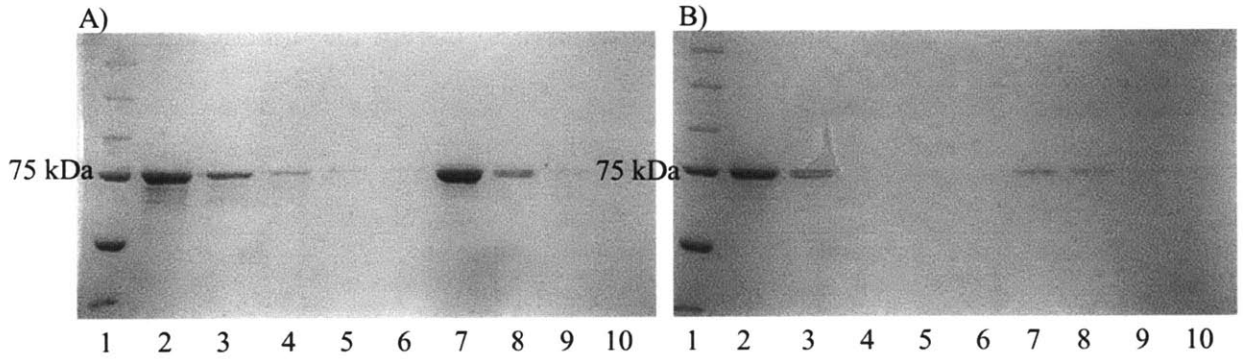

Figure 5.17 SDS-PAGE (8%) analysis of heterodimer exchange of His_6-PhaC and Strep2(HRV)-PhaC in 2 M NaCl. A) Analysis of Ni-NTA affinity purification of heterodimers. Lane 1, molecular weight standards. Lane 2, flowthrough from Ni-NTA column. Lanes 3-6, 10 mM imidazole wash fractions. Lanes 7-10, elution fractions. B) Analysis of Strep-tactin affinity purification of heterodimers following Ni-NTA purification. Lane 1, molecular weight standards. Lane 2, flowthrough from Strep-tactin column. Lanes 3-6, wash fractions. Lanes 7-10, elution fractions.

5.5.3.4.3 Exchange in 20 mM Hepes pH 7.5, 0.3-1% n-octyl-β-$_D$-glucoside

Previously, we purified the class III PHB synthase from *Xanthomonas oryzae*. This synthase, like the prototypical class III synthase from *Allochromatium vinosum*, is composed of two subunits, PhaC and PhaE, both ~40 kDa. In this construct, PhaE contained an N-terminal

His_6-tag (His_6-PhaE), whereas PhaC was untagged. In efforts to purify this synthase, n-octyl-β-$_D$-glucoside was included in the purification buffers at concentrations of 0.1% and 1%. The critical micelle concentration (cmc) of n-octyl-β-$_D$-glucoside is 0.69%. In the absence or presence of 0.1% n-octyl-β-$_D$-glucoside, His_6-PhaE and PhaC copurified by Ni-NTA affinity chromatography. However, when the purification buffer contained 1% n-octyl-β-$_D$-glucoside, His_6-PhaE and PhaC did not copurify. Under these conditions there was also no activity in the soluble cell-free extract. We took this observation to indicate that n-octyl-β-$_D$-glucoside above its cmc disrupts the interaction between PhaE and PhaC from *X. oryzae* and renders the enzyme inactive. When the concentration of n-octyl-β-$_D$-glucoside in the assay mixture for $(His)_6$-PhaC is increased from 0% to 1%, there is a steady drop in the activity (Figure 5.18). We therefore explored whether n-octyl-β-$_D$-glucoside could be used to disrupt the dimeric forms of PhaC, facilitating heterodimer formation.

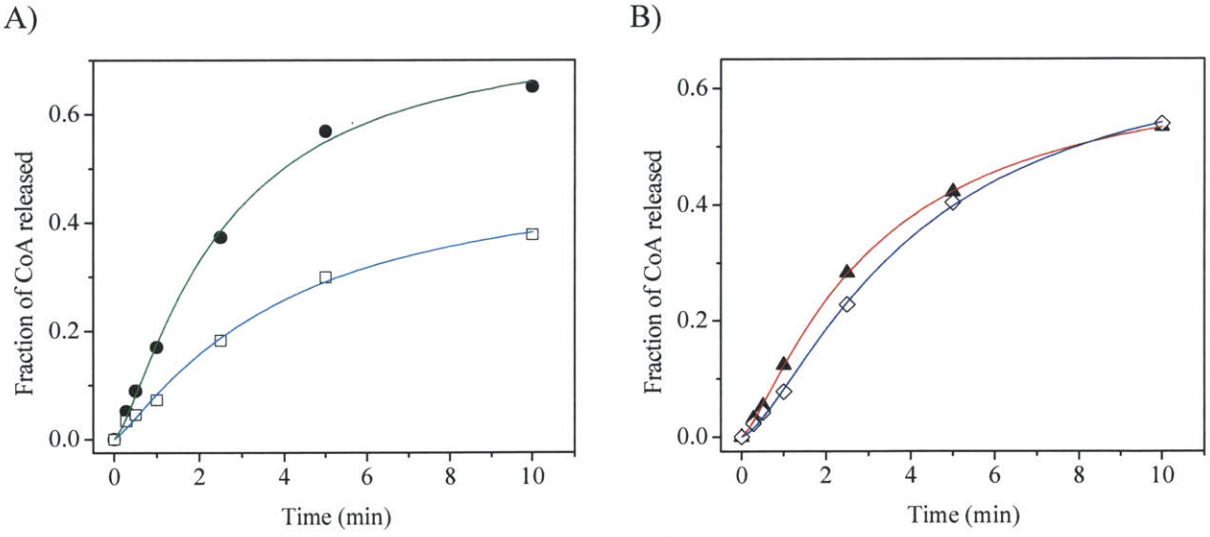

Figure 5.18 Effect of n-octyl-β-$_D$-glucoside on His_6-PhaC activity. The assays were carried out at 30 °C and contained 50 nM His_6-PhaC and 0% (●), 0.1% (□), 0.3% (▲), 0.6% (◊), or 1% (x) n-octyl-β-$_D$-glucoside.

Detergents can disrupt hydrophobic interactions at a dimer interface. We therefore also tried n-octyl-β-$_D$-glucoside in combination with 0.2 M and 2 M NaCl, the latter condition to

disrupt both hydrophobic and electrostatic interactions simultaneously. Upon incubation in 0.3% n-octyl-β-$_D$-glucoside and 2 M NaCl, the proteins precipitated extensively. However, incubation in 0.3% n-octyl-β-$_D$-glucoside or 2 M NaCl alone did not result in precipitation. In all three conditions there was no exchange (Figures 5.19-5.21, lanes 7 and 8).

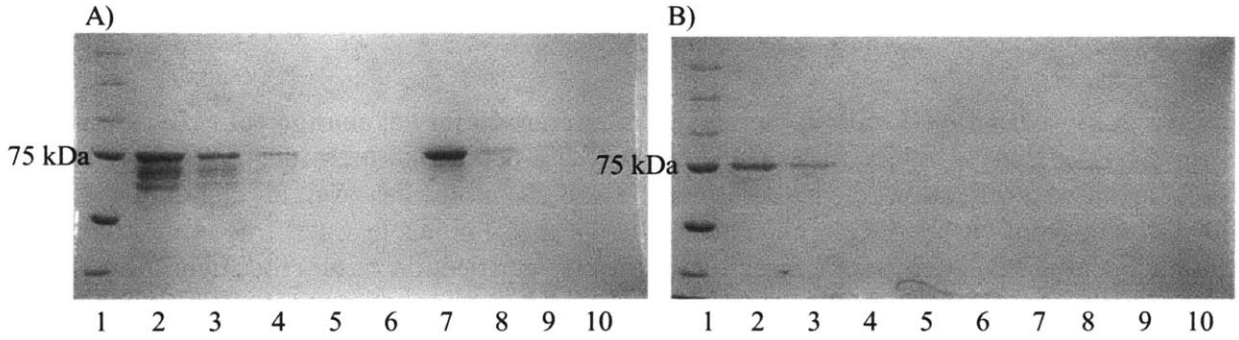

Figure 5.19 SDS-PAGE (8%) analysis of heterodimer exchange of His_6-PhaC and Strep2(HRV)-PhaC-C406A in 0.2 M NaCl, 0.3% n-octyl-β-$_D$-glucoside. A) Analysis of Ni-NTA affinity purification of heterodimers. Lane 1, molecular weight standards. Lane 2, flowthrough from Ni-NTA column. Lanes 3-6, 10 mM imidazole wash fractions. Lanes 7-10, elution fractions. B) Analysis of Strep-tactin affinity purification of heterodimers following Ni-NTA purification. Lane 1, molecular weight standards. Lane 2, flowthrough from Strep-tactin column. Lanes 3-6, wash fractions. Lanes 7-10, elution fractions.

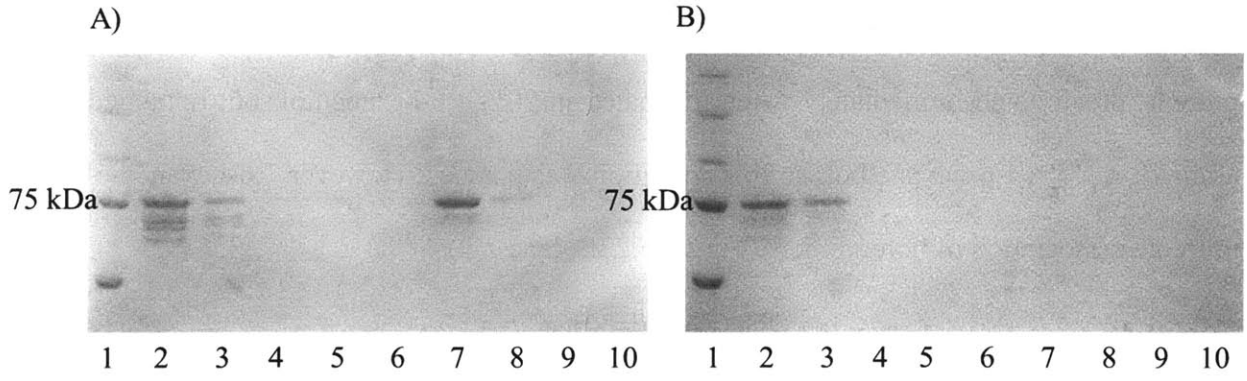

Figure 5.20 SDS-PAGE (8%) analysis of heterodimer exchange of His_6-PhaC and Strep2(HRV)-PhaC-C406A in 0.2 M NaCl, 1% n-octyl-β-$_D$-glucoside. A) Analysis of Ni-NTA affinity purification of heterodimers. Lane 1, molecular weight standards. Lane 2, flowthrough from Ni-NTA column. Lanes 3-6, 10 mM imidazole wash fractions. Lanes 7-10, elution fractions. B) Analysis of Strep-tactin affinity purification of heterodimers following Ni-NTA purification. Lane 1, molecular weight standards. Lane 2, flowthrough from Strep-tactin column. Lanes 3-6, wash fractions. Lanes 7-10, elution fractions.

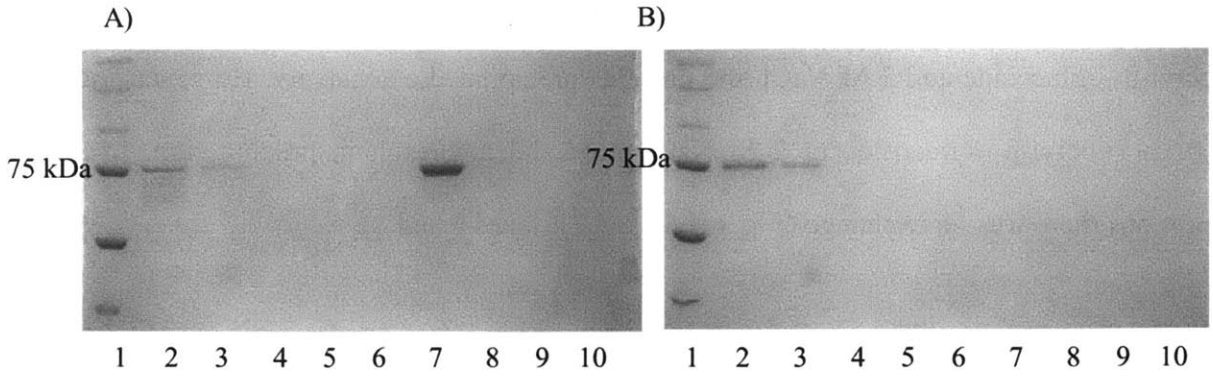

Figure 5.21 SDS-PAGE (8%) analysis of heterodimer exchange of His_6-PhaC and Strep2(HRV)-PhaC-C406A in 2 M NaCl, 0.3% n-octyl-β-D-glucoside. A) Analysis of Ni-NTA affinity purification of heterodimers. Lane 1, molecular weight standards. Lane 2, flowthrough from Ni-NTA column. Lanes 3-6, 10 mM imidazole wash fractions. Lanes 7-10, elution fractions. B) Analysis of Strep-tactin affinity purification of heterodimers following Ni-NTA purification. Lane 1, molecular weight standards. Lane 2, flowthrough from Strep-tactin column. Lanes 3-6, wash fractions. Lanes 7-10, elution fractions.

5.5.3.4.4 Exchange in 20 mM Hepes pH 7.5, 0.2 M NaCl, 15% 1,6-hexanediol.

Vargo and coworkers reported successful formation of mutant heterodimers of glutathione-S-transferase by incubation of homodimers in 15-20% 1,6-hexanediol (*26*). Therefore, His_6-PhaC and Strep2(HRV)-PhaC were incubated in 10-20% 1,6-hexanediol. The proteins precipitated immediately when incubated in 20% 1,6-hexanediol, but remained soluble after 2 h in 15% 1,6-hexanediol, so this condition was pursued. However 1,6-hexanediol did not promote dissociation of homodimers (Figure 5.22B, lane 7-9).

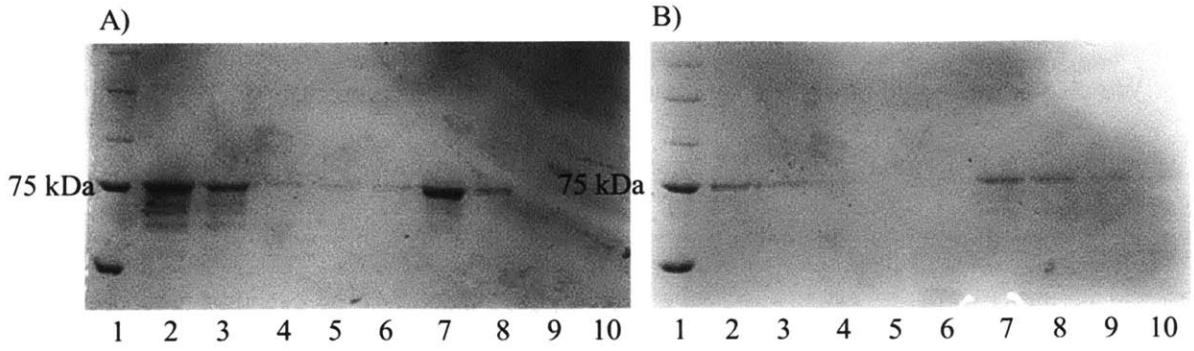

Figure 5.22 SDS-PAGE (8%) analysis of heterodimer exchange of His_6-PhaC-C406A and Strep2(HRV)-PhaC in 15% 1,6-hexanediol. A) Analysis of Ni-NTA affinity purification of heterodimers. Lane 1, molecular weight standards. Lane 2, flowthrough from Ni-NTA column. Lanes 3-6, 10 mM imidazole wash fractions. Lanes 7-10, elution fractions. B) Analysis of Strep-tactin affinity purification of heterodimers following Ni-NTA purification. Lane 1, molecular weight standards. Lane 2, flowthrough from Strep-tactin column. Lanes 3-6, wash fractions. Lanes 7-10, elution fractions.

5.5.3.4.5 Exchange in 20 mM Hepes, pH 7.5, 0.2 M NaCl, 2 M urea

Mild denaturation with 2 M urea was explored to dissociate homodimers by partial unfolding. Though there was no observable precipitation upon refolding, no exchange of heterodimers occurred (Figure 5.23B, lane 7).

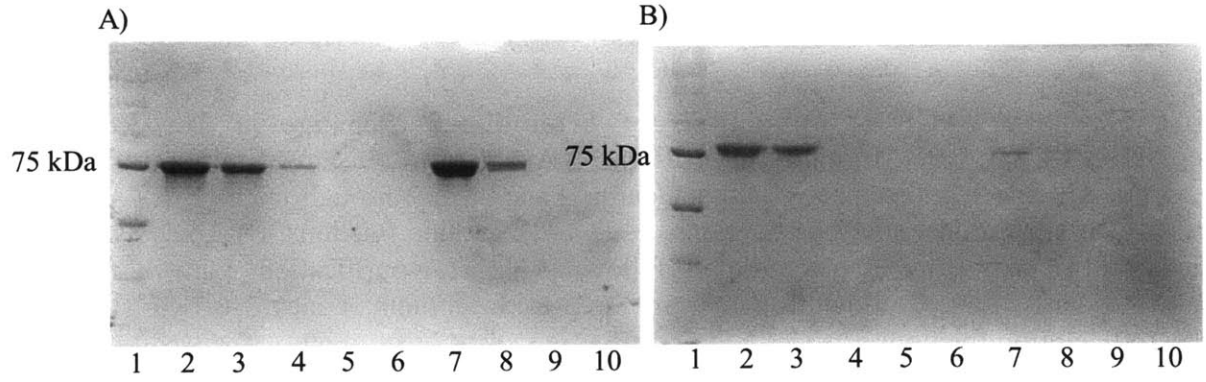

Figure 5.23 SDS-PAGE (8%) analysis of heterodimer exchange of His_6-PhaC and Strep2(HRV)-PhaC in 2 M urea. A) Analysis of Ni-NTA affinity purification of heterodimers. Lane 1, molecular weight standards. Lane 2, flowthrough from Ni-NTA column. Lanes 3-6, 10 mM imidazole wash fractions. Lanes 7-10, elution fractions. B) Analysis of Strep-tactin affinity purification of heterodimers following Ni-NTA purification. Lane 1, molecular weight standards. Lane 2, flowthrough from Strep-tactin column. Lanes 3-6, wash fractions. Lanes 7-10, elution fractions.

5.5.3.4.6 Exchange in 20 mM Hepes, pH 7.5, 0.2 M NaCl, 2-4 M guanidinium HCl

We also explored denaturation by incubation of His_6-PhaC and Strep2(HRV)-PhaC in 2-4 M guanidinium HCl. Incubation in 2 M guanidinium HCl promoted exchange of heterodimers, identified by two distinct bands in Figure 5.24B, lanes 7 and 8, but with very low yield. We speculated that the yield could be improve using harsher denaturation conditions, which might promote more dissociation of dimers into monomers. Thus 3 M and 4 M guanidinium HCl were tested. Incubation in 3 M guanidinium HCl improved the yield of heterodimers, as judged by SDS-PAGE (Figure 5.25B, lanes 7 and 8). The proteins precipitated extensively in 4 M guanidinium HCl, precluding heterodimer formation (Figure 5.26B, lanes 7 and 8). Therefore 3 M guanidinium was selected for scaling up heterodimer exchange.

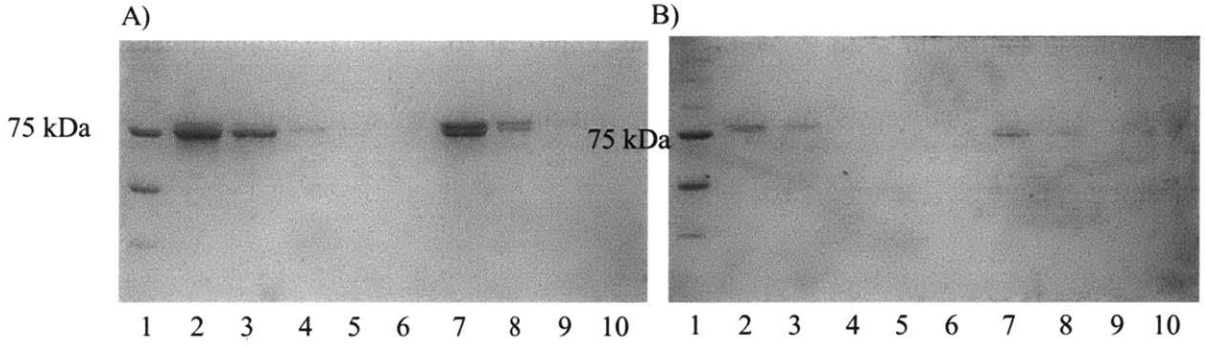

Figure 5.24 SDS-PAGE (8%) analysis of heterodimer exchange of His_6-PhaC and Strep2(HRV)-PhaC in 2 M guanidinium HCl. A) Analysis of Ni-NTA affinity purification of heterodimers. Lane 1, molecular weight standards. Lane 2, flowthrough from Ni-NTA column. Lanes 3-6, 10 mM imidazole wash fractions. Lanes 7-10, elution fractions. B) Analysis of Strep-tactin affinity purification of heterodimers following Ni-NTA purification. Lane 1, molecular weight standards. Lane 2, flowthrough from Strep-tactin column. Lanes 3-6, wash fractions. Lanes 7-10, elution fractions.

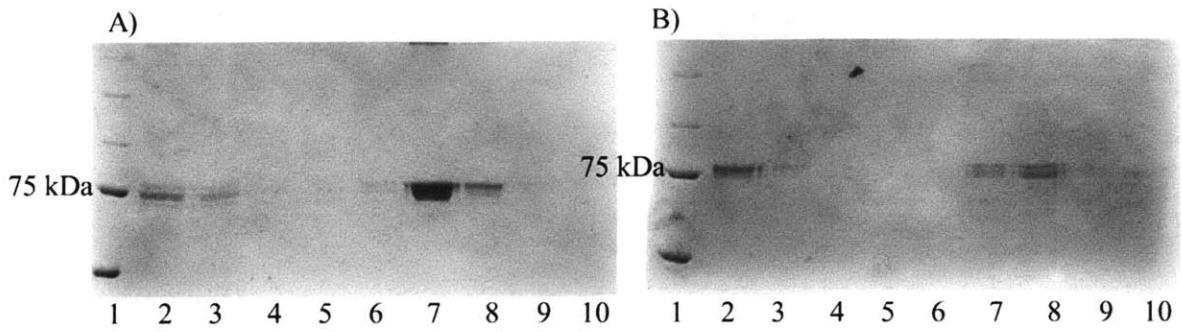

Figure 5.25 SDS-PAGE (8%) analysis of heterodimer exchange of His_6-PhaC and Strep2(HRV)-PhaC-C406A in 3 M guanidinium HCl. A) Analysis of Ni-NTA affinity purification of heterodimers. Lane 1, molecular weight standards. Lane 2, flowthrough from Ni-NTA column. Lanes 3-6, 10 mM imidazole wash fractions. Lanes 7-10, elution fractions. B) Analysis of Strep-tactin affinity purification of heterodimers following Ni-NTA purification. Lane 1, molecular weight standards. Lane 2, flowthrough from Strep-tactin column. Lanes 3-6, wash fractions. Lanes 7-10, elution fractions.

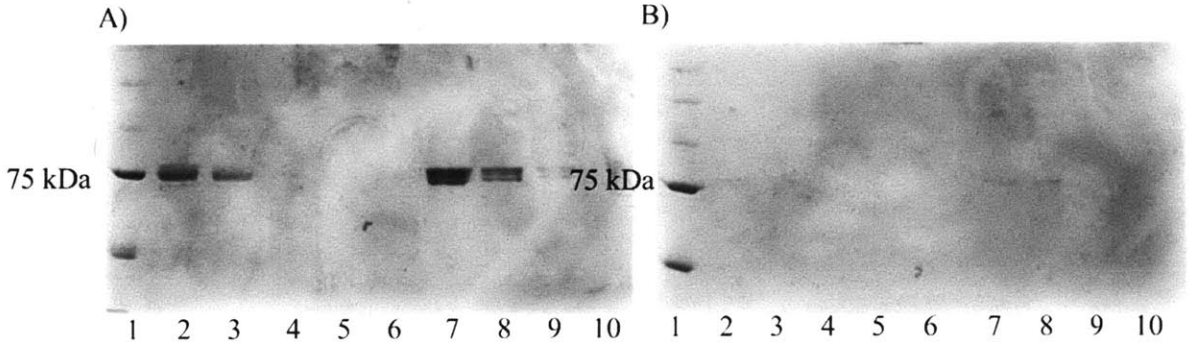

Figure 5.26 SDS-PAGE (8%) analysis of heterodimer exchange of His_6-PhaC and Strep2(HRV)-PhaC-C406A in 4 M guanidinium HCl. A) Analysis of Ni-NTA affinity purification of heterodimers. Lane 1, molecular weight standards. Lane 2, flowthrough from Ni-NTA column. Lanes 3-6, 10 mM imidazole wash fractions. Lanes 7-10, elution fractions. B) Analysis of Strep-tactin affinity purification of heterodimers following Ni-NTA purification. Lane 1, molecular weight standards. Lane 2, flowthrough from Strep-tactin column. Lanes 3-6, wash fractions. Lanes 7-10, elution fractions.

5.5.3.5 Control for loss of activity of His_6-PhaC and Strep2(HRV)-PhaC in 3 M guanidinium HCl

To control for activity loss upon incubation in 3 M guanidinium HCl, both His_6-PhaC and Strep2(HRV)-PhaC were incubated in 3 M guanidinium HCl, then dialyzed overnight into 20 mM Hepes pH 7.5, 200 mM NaCl. The enzymes were assayed, revealing that His_6-PhaC activity dropped from 50 U/mg to 20 U/mg upon incubation in 3 M guanidinium HCl, (Figure 5.27A). In contrast the activity of Strep2(HRV)-PhaC remained stable at 20 U/mg (Figure 5.27B).

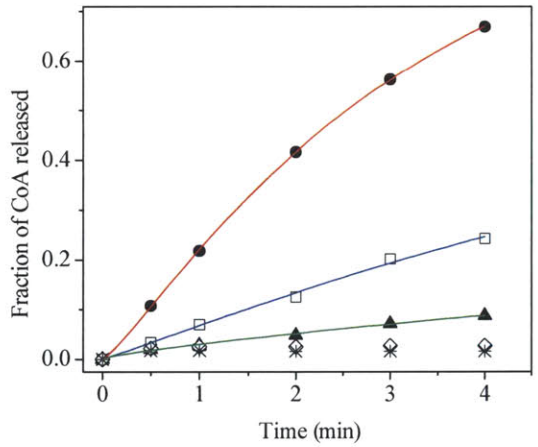

Figure 5.27 Time course of CoA release from wt His_6-PhaC and Strep2(HRV)-PhaC following incubation in 3 M guanidinium HCl. A) His_6-PhaC (25 nM) was assayed before (●) and after (□) incubation for 30 min in 3 M guanidinium HCl and overnight dialysis into 20 mM Hepes pH 7.5, 200 mM NaCl. B) Strep2(HRV)-PhaC (50 nM) was assayed before (▲) and after (◊) incubation for 30 min in 3 M guanidinium HCl and overnight dialysis into 20 mM Hepes pH 7.5, 200 mM NaCl.

5.5.3.6 Preparation and characterization of His_6-PhaC/Strep2(HRV)-PhaC heterodimers by exchange in 3 M guanidinium HCl

The encouraging results in 3 M guanidinium HCl prompted us to scale up the reaction so the specific activities of the resulting heterodimers could be determined. Reaction **A**, containing both wt His_6-PhaC and Strep2-PhaC, was carried out to assess the activity of wt-wt heterodimers for comparison with wt-mutant heterodimers, and the results are shown in Figure 5.30. Starting

from 3.5 mg of protein total, following incubation in 3 M guanidinium and dialysis in refolding buffer, 2.9 mg of protein were recovered (Table 5.6). The loss is from precipitation upon refolding as precipitated protein is observed in the dialysis cassettes. In addition, loss of protein was observed in all three reactions following dialysis. The final yield of heterodimers in reaction **A** was very low, only 7 μg, or 0.2% of starting material. Most of the protein was lost in the flowthrough and 10 mM imidazole wash fractions from the Ni-NTA column, which we expect to contain Strep2(HRV)-PhaC homodimers. There was considerably less protein in the flowthrough from the Strep-tactin resin, which we expect to contain His_6-PhaC homodimers. The results suggest that the protein lost from the 3 M guanidinium unfolding step and dialysis/refolding was primarily His_6-PhaC, which also seems to be true for all three reactions (Tables 5.6, 5.7 and 5.8), which may in part explain why the yield of heterodimer is so low. The activity of the purified His_6-PhaC/Strep2(HRV)-PhaC is only 0.93 +/- 0.1 U/mg. By 8% SDS-PAGE two bands can be clearly distinguished in the final protein sample (Figure 5.28, lane 9). The band that migrates at an apparent higher molecular weight is His_6-PhaC and the band that migrates at a lower molecular weight is Strep2(HRV)-PhaC.

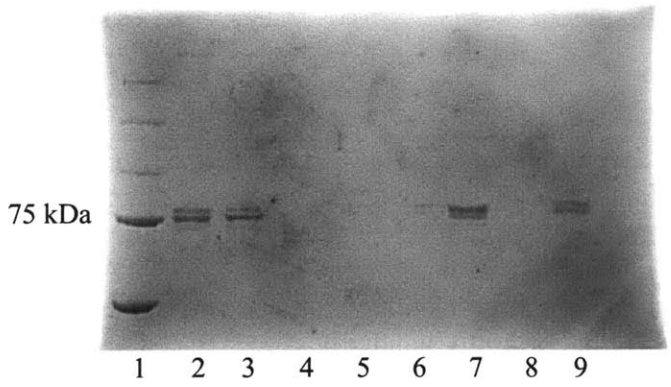

Figure 5.28 SDS-PAGE (8%) analysis of exchange of His_6-PhaC and Strep2(HRV)-PhaC in 3 M guanidinium HCl. Lane 1, molecular weight standards. Lane 2, post refolding dialysis step. Lane 3, Ni-NTA column flowthrough. Lane 4, Ni-NTA column 10 mM imidazole wash. Lane 5, Ni-NTA column 50 mM imidazole wash. Lane 6, post Ni-NTA column. Lane 7, Strep-tactin column flowthrough. Lane 8, Strep-tactin column wash. Lane 9, final protein.

Table 5.6 Activity table of preparation of His_6-PhaC/Strep2(HRV)-PhaC heterodimers (reaction A).

Purification step	Volume (mL)	Protein (mg)	Activity (U/mg)	Total units	% total activity
Post-dialysis	5	2.9	4	11	100
Ni-NTA flowthrough	5	1.5	2.9	4.4	38
Post Ni-NTA	14	1.4	2.9	4.1	36
Strep-tactin flowthrough	5	0.25	13	3.3	29
Final protein	0.065	0.007	0.93 +/- 0.1[a]	0.007	0.06

[a]The specific activity of the final protein was measured in triplicate and the error is standard deviation from the mean.

Reactions **B** and **C** were carried out with twice as much protein as was used in reaction **A**, and the yield in both reaction was ~10-fold higher than for reaction **A** (Tables 5.7 and 5.8). The specific activity of the final purified heterodimers in reaction **B** was 1.7 +/- 0.1 U/mg. The results for reactions **B** and **C** are shown in Figures 5.29 and 5.30, respectively.

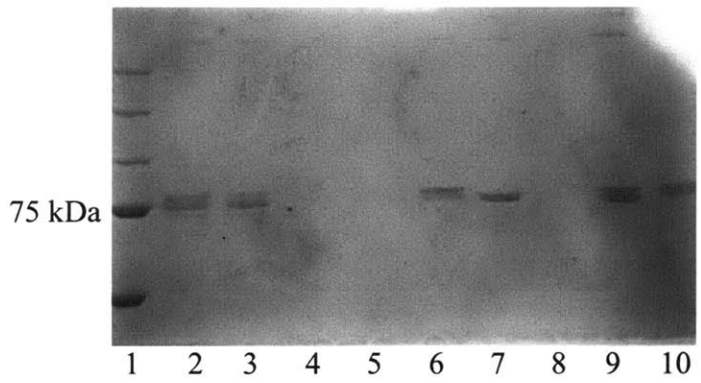

Figure 5.29 SDS-PAGE (8%) analysis of exchange of wt His_6-PhaC and Strep2(HRV)-PhaC-C406A in 3 M guanidinium HCl. Lane 1, molecular weight standards. Lane 2, post refolding dialysis step. Lane 3, Ni-NTA column flowthrough. Lane 4, Ni-NTA column 10 mM imidazole wash. Lane 5, Ni-NTA column 50 mM imidazole wash. Lane 6, post Ni-NTA column. Lane 7, Strep-tactin column flowthrough. Lane 8, Strep-tactin column wash. Lane 9, final protein. Lane 10, wt His_6-PhaC + Strep2(HRV)-PhaC-C406A standard.

Table 5.7 Activity table of preparation of His_6-PhaC/Strep2(HRV)-PhaC-C406A heterodimers (reaction B).

Purification step	Volume (mL)	Protein (mg)	Activity (U/mg)	Total units	% total activity
Post-dialysis	10	4.6	1.1	5.1	100
Ni-NTA flowthrough	10	1.4	0.2	0.28	5.5
Post Ni-NTA	14	1.8	4	7.2	140
Strep-tactin flowthrough	6.5	0.3	13	3.9	77
Final protein	0.2	0.08	1.7 +/- 0.1[a]	0.14	2.7

[a]The specific activity of the final protein was measured in triplicate and the error is standard deviation from the mean.

Finally, His_6-PhaC-C406A and Strep2(HRV)-PhaC migrate as one band and cannot be distinguished by 8% SDS-PAGE. The specific activity of the heterodimers purified from reaction **C** is 1.3 +/- 0.1 U/mg. All three heterodimers have specific activities of 1-2 U/mg, considerably lower than either of the two proteins prior to exchange. The cause of the drop in activity is not understood but may be in part due to improper re-folding following incubation in guanidinium.

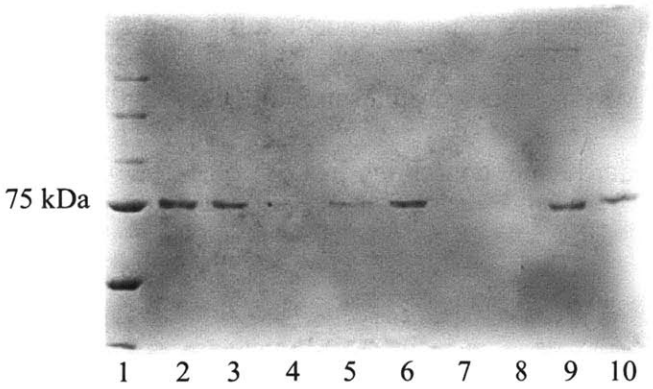

Figure 5.30 SDS-PAGE (8%) analysis of exchange of His_6-PhaC-C406A and wt Strep2(HRV)-PhaC in 3 M guanidinium. Lane 1, molecular weight standards. Lane 2, post refolding dialysis step. Lane 3, Ni-NTA column flowthrough. Lane 4, Ni-NTA column 10 mM imidazole wash. Lane 5, Ni-NTA column 50 mM imidazole wash. Lane 6, post Ni-NTA column. Lane 7, Strep-tactin column flowthrough. Lane 8, Strep-tactin column wash. Lane 9, final protein. Lane 10, His_6-PhaC-C406A + wt Strep2(HRV)-PhaC standard.

Table 5.8 Activity table of preparation of His_6-PhaC-C406A/Strep2-PhaC heterodimers (reaction C).

Purification step	Volume (mL)	Protein (mg)	Activity (U/mg)	Total units	% total activity
Post-dialysis	10	5.4	7	38	100
Ni-NTA flowthrough	9.5	3.0	7	21	56
Post Ni-NTA	15	2.0	1.1	2.3	6
Strep-tactin flowthrough	10	0.5	1.5	0.75	2.0
Final protein	0.22	0.09	1.3 +/- 0.1[a]	0.12	0.31

[a]The specific activity of the final protein was measured in triplicate and the error is standard deviation from the mean.

In reactions **B** and **C** two bands cannot be as clearly distinguished by 8% SDS-PAGE as in reaction **A**. Therefore Western blot analysis using commercially available antibodies against the His_6- and Strep2-tags was carried out. First, two standard curves were generated by Western blot using anti-Strep2 antibody against 25-200 ng of Strep2-PhaC (Figure 5.31A) and 25-200 ng of a one to one mixture of Strep2(HRV)-PhaC to His_6-PhaC (Figure 5.31B). The purpose of this control was to confirm that the standard curves were the same and therefore that the amount of Strep2(HRV)-PhaC in a mixture of the two proteins could be accurately determined. The standard are similar, thus the ng of Strep2(HRV)-PhaC present in a sample of Strep2-PhaC/His_6-PhaC heterodimer was determined using a standard curve containing just Strep2(HRV)-PhaC.

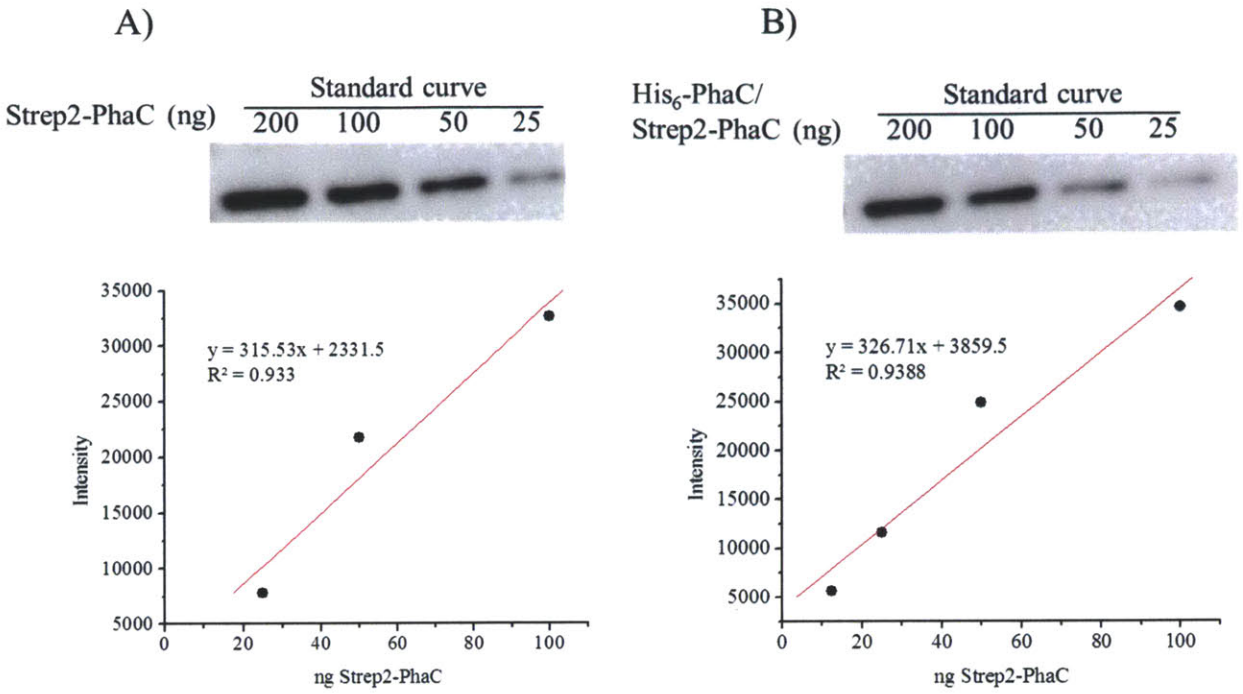

Figure 5.31 Western blot standard curves of anti-Strep2 antibody. A) Standard curve generated from 25-200 ng of Strep2(HRV)-PhaC. B) Standard curve generated from 25-200 ng of a 1:1 mixture of His_6-PhaC to Strep2(HRV)-PhaC (12.5-100 ng of each protein). The intensity in B) is plotted as a function of the ng of Strep2(HRV)-PhaC, rather than of ng of both proteins.

The amount of Strep2(HRV)-PhaC in the heterodimer products of reactions **B** and **C**, His_6-PhaC/Strep2(HRV)-PhaC-C406A and His_6-PhaC-C406A/Strep2(HRV)-PhaC was then determined using this method. A sample of reaction **B** of 10 ng total protein (as judged by Bradford assay) contains 4.9 ng of Strep2-PhaC, and a sample of 25 ng total protein contains 9.4 +/- 2.3 ng of Strep2-PhaC (Figure 5.32A). A 10 ng sample of reaction **C** contains 5 ng of Strep2-PhaC, and a 25 ng sample contains 12 +/- 0.4 ng Strep2(HRV)-PhaC (Figure 5.32B). These results are consistent with the purified heterodimers containing a nearly 1:1 ratio of His_6-PhaC to Strep2(HRV)-PhaC.

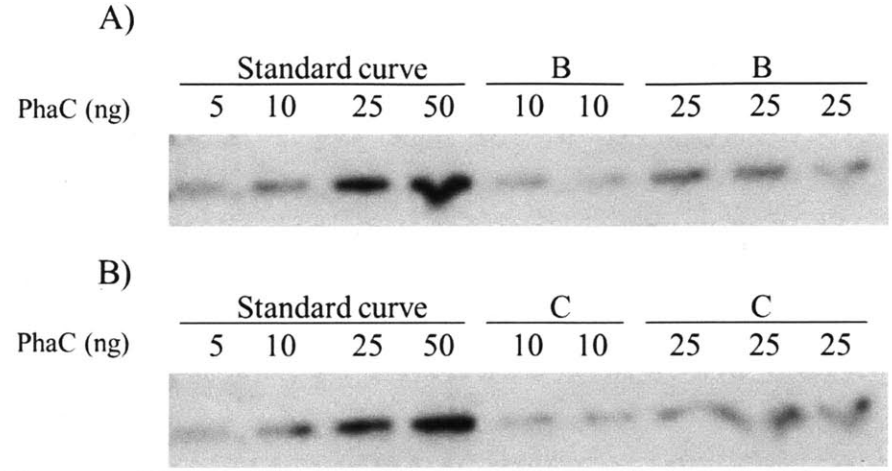

Figure 5.32 Anti-Strep2 Western blots of A) His_6-PhaC/Strep2(HRV)-PhaC-C406A (reaction B) and B) His_6-PhaC-C406A/Strep2(HRV)-PhaC (reaction C) heterodimers.

A similar analysis was carried out using anti-His_6 antibody. Initial attempts to do quantitative Western blots with anti-His_6 antibody failed. The anti-His_6 antibody must be used at a much higher concentration compared to the anti-Strep2 antibody, which led to higher background. About 10-fold more sample must be loaded to detect the presence of the tag. The results in Figure 5.33 clearly show that both reactions **B** and **C** contain His_6-PhaC and His_6-PhaC-C406A, respectively. His_6-PhaC and Strep2(HRV)-PhaC standards were also loaded to confirm that the antibody does not cross-react with the Strep2-tag or react non-specifically with PhaC. Taken together, the results from both Westerns confirm that both His_6- and Strep2-PhaCs are present in both reactions, and that Strep2-PhaC comprises about half of the total ng of protein in each sample. The assay results indicate that both mutant heterodimers have approximately the same activity as the wild type heterodimer.

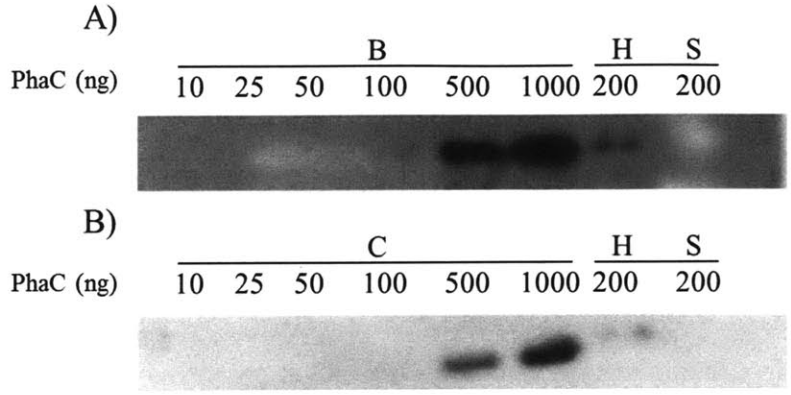

Figure 5.33 Anti-His_6 Western blots of A) His_6-PhaC/Strep2(HRV)-PhaC-C406A (reaction B) and B) His_6-PhaC-C406A/Strep2(HRV)-PhaC (reaction C) heterodimers. Ten to 1000 ng each of reactions B and C were loaded, as well as 200 ng of His_6-PhaC (H) and Strep2-PhaC (S) standards.

5.5.3.7 Discussion

This section presents our efforts to prepare and characterize mutant heterodimers of $PhaC_{Cc}$. We initially speculated that because $PhaC_{Cc}$ is entirely dimeric at high concentrations, if conditions could be identified in which it could be dissociated into monomers, then wt and mutant monomers could be mixed. To form heterodimers, the protein could then be exchanged back into conditions that promote dimerization. We thus screened a number of additives to identify one that would promote exchange of monomers to form heterodimers. However, nearly all of the additives failed to induce monomerization, with the exception of guanidinium HCl. We therefore scaled up heterodimer formation in 3 M guanidinium HCl and characterized the specific activity of the resulting protein. Unfortunately, the specific activity of the heterodimers was so low, even in the case of the wt heterodimers; thus, it was difficult to draw strong conclusions. In Chapter 2, we presented SEC studies that showed that decreasing the concentration of $PhaC_{Cc}$ induces the dissociation of dimers into monomers. Hence an alternative method for the formation of heterodimers might be to simply decrease the concentration, mix wt

and mutant monomers, and then concentrate the protein to reform dimer. This method could potentially be less perturbative to the activity of the protein compared to incubation in guanidinium HCl. Following the reformation of heterodimers, the affinity purification steps could be carried out as described in this section to remove homodimers.

Finally, it should be noted that if the stoichiometry of acylation of $PhaC_{Cc}$ with the artificial primer sTCoA presented in Chapter 2 is indicative of the stoichiometry of PHB chain synthesis, then each monomer makes one PHB chain and the mechanism in Figure 5.8A is necessarily ruled out. Thus, in the case of $PhaC_{Cc}$, at least, it seems likely that polymerization occurs via non-covalent intermediates.

5.6 Acknowledgements

We would like to thank Don Gantz at the BU School of Medicine for preliminary preparation and characterization of PhaEΔ27C by EM. We would also like to acknowledge Dr. Ed Brignole, who collaborated with us in preparing samples for electron microscopy of PhaEΔ27C, imaging grids and analyzing the data presented in this section. We would also like to thank Drs. Mimi Cho and Phillip Snyder for helpful discussions.

5.7 References

1. Ludtke, S. J., Baldwin, P. R., and Chiu, W. (1999) EMAN: semiautomated software for high-resolution single-particle reconstructions, *J. Struct. Biol. 128*, 82-97.
2. Liebergesell, M., Sonomoto, K., Madkour, M., Mayer, F., and Steinbüchel, A. (1994) Purification and characterization of the poly(hydroxyalkanoic acid) synthase from

Chromatium vinosum and localization of the enzyme at the surface of poly(hydroxyalkanoic acid) granules, *Eur. J. Biochem. 226*, 71-80.

3. Tian, J., Sinskey, A. J., and Stubbe, J. (2005) Detection of intermediates from the polymerization reaction catalyzed by a D302A mutant of class III polyhydroxyalkanoate (PHA) synthase, *Biochemistry 44*, 1495-1503.

4. Qi, Q., and Rehm, B.A. . (2001) Polyhydroxybutyrate biosynthesis in *Caulobacter crescentus*: molecular characterization of the polyhydroxybutyrate synthase., *Microbiology 147*, 3353-3358.

5. Jia, Y., Yuan, W., Wodzinska, J., Park, J., Sinskey, A.J., Stubbe, J. (2001) Mechanistic studies on class I polyhydroxybutyrate (PHB) synthase from *Ralstonia eutropha*: class I and III synthases share a similar catalytic mechanism., *Biochemistry 40*, 1011-1019.

6. Poindexter, J. S. (1981) The *Caulobacters* - ubiquitous unusual bacteria, *Microbiol. Rev. 45*, 123-179.

7. Poindexter, J. S. (1964) Biological properties and classification of *Caulobacter* group, *Bacteriol. Rev. 28*, 231-293.

8. Ausmees, N., and Jacobs-Wagner, C. (2003) Spatial and temporal control of differentiation and cell cycle progression in *Caulobacter crescentus*, *Annu. Rev. Microbiol. 57*, 225-247.

9. Cho, M., Brigham, C. J., Sinskey, A. J., and Stubbe, J. (2012) Purification of polyhydroxybutyrate synthase from its native organism, *Ralstonia eutropha*: implications for the initiation and elongation of polymer formation in vivo, *Biochemistry 51*, 2276-2288.

10. Pfeiffer, D., Wahl, A., and Jendrossek, D. (2011) Identification of a multifunctional protein, PhaM, that determines number, surface to volume ratio, subcellular localization and distribution to daughter cells of poly(3-hydroxybutyrate), PHB, granules in *Ralstonia eutropha* H16, *Mol. Microbiol. 82*, 936-951.

11. Huguenel, E. D., and Newton, A. (1984) Evidence that subcellular flagellin pools in *Caulobacter crescentus* are precursors in flagellum assembly, *J. Bacteriol. 157*, 727-732.

12. Tian, J., Sinskey, A. J., and Stubbe, J. (2005) Kinetic studies of polyhydroxybutyrate granule formation in *Wautersia eutropha* H16 by transmission electron microscopy, *J. Bacteriol. 187*, 3814-3824.

13. Briegel, A., Dias, D. P., Li, Z., Jensen, R. B., Frangakis, A. S., and Jensen, G. J. (2006) Multiple large filament bundles observed in *Caulobacter crescentus* by electron cryotomography, *Mol. Microbiol. 62*, 5-14.

14. Laub, M. T., Shapiro, L., and McAdams, H. H. (2007) Systems biology of *Caulobacter*, *Annu. Rev. Genet. 41*, 429-441.

15. Wodzinska, J., Snell, K. D., Rhomberg, A., Sinskey, A. J., Biemann, K., and Stubbe, J. (1996) Polyhydroxybutyrate synthase: evidence for covalent catalysis, *J. Amer. Chem. Soc. 118*, 6319-6320.

16. Jia, Y., Kappock, T. J., Frick, T., Sinskey, A. J., and Stubbe, J. (2000) Lipases provide a new mechanistic model for polyhydroxybutyrate (PHB) synthases: characterization of the functional residues in *Chromatium vinosum* PHB synthase, *Biochemistry 39*, 3927-3936.

17. Smith, S. (1994) The animal fatty acid synthase: one gene, one polypeptide, seven enzymes, *FASEB J. 8*, 1248-1259.

18. Austin, M. B., and Noel, J. P. (2003) The chalcone synthase superfamily of type III polyketide synthases, *Nat. Prod. Rep. 20*, 79-110.

19. Joshi, A. K., Witkowski, A., and Smith, S. (1997) Mapping of functional interactions between domains of the animal fatty acid synthase by mutant complementation *in vitro*, *Biochemistry 36*, 2316-2322.

20. Witkowski, A., Joshi, A., and Smith, S. (1996) Fatty acid synthase: *in vitro* complementation of inactive mutants, *Biochemistry 35*, 10569-10575.

21. Zhang, S. M., Kolvek, S., Lenz, R. W., and Goodwin, S. (2003) Mechanism of the polymerization reaction initiated and catalyzed by the polyhydroxybutyrate synthase of *Ralstonia eutropha*, *Biomacromolecules 4*, 504-509.

22. Tian, J. (2005) Mechanistic investigation of polyhydroxybutyrate (PHB) synthases and elucidation of PHB biosynthesis and degradation process in *Wautersia eutropha* H6, in *Chemistry*, p 345, Massachusetts Institute of Technology, Cambridge.

23. Yuan, W., Jia, Y., Tian, J., Snell, K. D., Muh, U., Sinskey, A. J., Lambalot, R. H., Walsh, C. T., and Stubbe, J. (2001) Class I and III polyhydroxyalkanoate synthases from *Ralstonia eutropha* and *Allochromatium vinosum*: characterization and substrate specificity studies, *Arch. Biochem. Biophys. 394*, 87-98.

24. Bradford, M. M. (1976) Rapid and sensitive method for quantitation of microgram quantities of protein utilizing principle of protein-dye binding, *Anal. Biochem. 72*, 248-254.

25. Heckman, K. L., and Pease, L. R. (2007) Gene splicing and mutagenesis by PCR-driven overlap extension, *Nat. Protoc. 2*, 924-932.

26. Vargo, M. A., and Colman, R. F. (2004) Heterodimers of wild-type and subunit interface mutant enzymes of glutathione S-transferase A1-1: interactive or independent active sites?, *Prot. Sci. 13*, 1586-1593.